University of Alberta

Estimation of the post-failure stiffness of rock

by

Timothy Grain Joseph ©

A thesis submitted to the Faculty of Graduate Studies and Research in partial fulfillment of the requirements for the degree of Doctor of Philosophy

in

Mining Engineering

Department of Civil and Environmental Engineering

Edmonton, Alberta
Fall, 2000

National Library of Canada

Acquisitions and Bibliographic Services

395 Wellington Street
Ottawa ON K1A 0N4
Canada

Bibliothèque nationale du Canada

Acquisitions et services bibliographiques

395, rue Wellington
Ottawa ON K1A 0N4
Canada

Your file Votre référence

Our file Notre référence

The author has granted a non-exclusive licence allowing the National Library of Canada to reproduce, loan, distribute or sell copies of this thesis in microform, paper or electronic formats.

L'auteur a accordé une licence non exclusive permettant à la Bibliothèque nationale du Canada de reproduire, prêter, distribuer ou vendre des copies de cette thèse sous la forme de microfiche/film, de reproduction sur papier ou sur format électronique.

The author retains ownership of the copyright in this thesis. Neither the thesis nor substantial extracts from it may be printed or otherwise reproduced without the author's permission.

L'auteur conserve la propriété du droit d'auteur qui protège cette thèse. Ni la thèse ni des extraits substantiels de celle-ci ne doivent être imprimés ou autrement reproduits sans son autorisation.

0-612-59605-2

Canada

University of Alberta

Library Release Form

Name of Author	Timothy Grain Joseph
Title of Thesis	Estimation of the post-failure stiffness of rock
Degree	Doctor of Philosophy
Year this degree is granted	2000

Permission is hereby granted to the University of Alberta Library to reproduce single copies of this thesis and to lend or sell such copies for private, scholarly or scientific research purposes only.

The author reserves all other publication and other rights in association with the copyright in the thesis, and except as herein before provided, neither the thesis nor any substantial portion thereof may be printed or otherwise reproduced in any material form whatever without the author's prior written permission.

8403 - 187 Street
Edmonton, AB
T5T 1H9

Date___July 20, 2000____

University of Alberta

Faculty of Graduate Studies and Research

The undersigned certify that they have read, and recommend to the Faculty of Graduate Studies and Research for acceptance, a thesis entitled "Estimation of the post-failure stiffness of rock" submitted by Timothy Grain Joseph in partial fulfillment of the requirements for the degree of Doctor of Philosophy in Mining Engineering.

Dr. K. Barron (Supervisor)

Dr. J.K. Szymanski (Co-supervisor)

Dr. N.R. Morgenstern

Dr. D.C. Sego

Dwayne Tannant
Dr. D.D. Tannant

Reg Eadie
Dr. R.L. Eadie

Dr. B. Stimpson

Date: July 17, 2000

Abstract

The phenomenon of pillar bumps in coal beds is well documented in the available literature, where the potential for a pillar bump may be estimated from the difference between local mine stiffness and post peak pillar stiffness (Pen, 1994). While the evaluation of local mine stiffness has already been well established, the post peak pillar stiffness can only be estimated through an empirical approach (Pen, 1994). Certainly, a more comprehensive approach to the evaluation of post peak stiffness would be desirable.

This research introduces the Joseph-Barron post peak criterion and its application to predicting the post peak behaviour of rock and rock structures using intact rock, rock mass, broken rock and non-intact coal data sets from the literature. Physical tests were carried out on two very different rocks, the results of which were also used to verify this criterion. The core of the approach is an effective friction concept that relates the post peak cohesive and frictional characteristics of the rock, to the strain.

For the purposes of this work, the term "effective friction" is used to describe a mathematical combination of friction and cohesion, where the apparent cohesion that maintains the integrity of the asperity height of a rough or broken surface under given confining conditions is combined with the rough surface resistance to sliding.

It has been shown that the post peak effective friction - strain behaviour is common for all states of a given rock, whether in the intact, mass, or crushed states. The same is postulated for coal, regardless of intact, non-intact or coal mass state. This behaviour has been shown to translate to a unique single post peak modulus relationship regardless of the confinement conditions. It is this post peak modulus relationship that may be employed to determine post peak stiffness values commensurate with the rock structure dimensions.

As an example of the use of this criterion in analyzing the stability of rock structures, it was applied to the consideration of post peak behaviour of pillars. The criterion was used with a commercial finite element program, and the variation of post peak modulus with pillar width to height ratio was determined. These results were compared with an approach suggested by Hoek et al. (1997), and shown to make a significant difference. The use of this criterion in consideration of pillars yields results that are compatible with Zipf's empirically established relationship (Zipf, 1999).

Dedication

For Hugh

1917 - 1992

Acknowledgement

The author wishes to acknowledge the continual support of Dr. Ken Barron, as both mentor and friend during the course of this work. Dr. Barron's guidance was both inspirational and unwavering during this period.

This project was partly funded from NSERC, University of Alberta Ph.D. Scholarship, Coal Mining Research Company Graduate Scholarship, and the CIM Coal Research Award enabling the author to complete the project in a timely fashion.

The author would also like to recognize the supervisory committee for their suggestions and positive influence over the past 4 years. In addition, Dr. Evert Hoek for this encouragement in taking on a Ph.D. project and advice as the project proceeded.

Finally, the author would like to thank his family; Laura, Jarod, Sydney, and his mother Marion for their patience, love and support.

Table of Contents

Chapter 1 **Introduction** **1**

1.1 Significance of the problem 1

1.1.1 Pillar bump potential 1

1.1.2 Application of the pillar bump concept 2

1.2 Definition of the problem 2

1.2.1 Post peak behaviour as a function of σ_3 4

1.2.2 The existence of 3 strength levels; peak, residual and base 6

1.2.3 Significance of the brittle-ductile transition point 8

1.2.4 Post peak stress-strain data 8

1.3 Previous work related to stiffness, modulus and post peak behaviour 10

1.4 Research objectives 23

Chapter 2 **Postulates, assumptions and definitions** **24**

2.1 Definition of the effective angle of friction ϕ_e for the post peak region 24

2.2 Postulates 26

2.2.1 Postulate 1 - At peak strength 26

2.2.2 Postulate 2 - Beyond peak strength 26

2.3 Assumptions 27

2.3.1 Assumption 1 - Pre-peak modulus 27

2.3.2 Assumption 2 - Peak strength relationship 27

2.3.3 Assumption 3 - Residual strength relationship 27

2.3.4 Assumption 4 - Base strength relationship 28

2.3.5 Assumption 5 - Relationship between the peak, residual and base strengths 28

2.3.6 Assumption 6 - Friction - strain functional 29

relationship
2.3.7 Assumption 7 - Friction - strain minimum at the brittle-ductile transition point 29
2.3.8 Assumption 8 - Peak strength - residual strength relationships at the brittle-ductile transition point 30
2.3.9 Assumption 9 - Post peak modulus 30
Chapter 3 The Joseph-Barron approach (applied to intact rock) 31
3.1 Determination of the Hoek-Brown strength criterion constants 31
3.2 Determination of the residual strength polynomial constants and σ_{3t} via polynomial regression analysis 32
3.3 Estimation of the residual strength polynomial constants and σ_{3t} via a linear approximation of the available residual strength data 34
3.4 Refinement of the residual strength polynomial constants D and F originally determined via a linear approximation process 36
3.5 Determination of the base angle of friction, ϕ_b 37
3.6 Determination of the effective friction - strain relationship 38
3.7 Estimate of the base strain at the brittle-ductile transition point 40
  3.7.1 Determination of ϕ_e from the available data 40
  3.7.2 Y vs e 42
  3.7.3 Estimate of the base strain 43
3.8 Determination of the post peak modulus, and its normalized form 44
3.9 Determination of the post peak stiffness 46
3.10 Variances to the Joseph-Barron approach when only peak 47

strength triaxial data is made available
3.11 Conclusion 48
Chapter 4 Intact rock - Verification of the postulates and assumptions via an example data set from the literature 49
4.1 The intact rock data set 49
4.2 Assuming that both peak and residual data are available 51
4.2.1 Determination of the peak strength criterion 51
4.2.2 Determination of the brittle-ductile transition point 52
4.2.3 Determination and refinement of the residual strength criterion 54
4.2.4 Estimation of the base angle of friction 56
4.2.5 Comparison of the peak, residual and base strength criteria 56
4.2.6 Determination of the base strain, e_b, the R, S and T constants, and the solution to the effective friction - strain polynomial 57
4.2.7 Comparison of ϕ_e-e curve with the ϕ_e-e data - verification 60
4.2.8 Reconstruction of the σ - e curves and original comparison 61
4.2.9 The normalized post peak modulus 63
4.3 Assuming that only peak data is available 64
4.3.1 Determination of the peak strength criterion 64
4.3.2 Estimation of the base angle of friction, ϕ_b 64
4.3.3 Determination of the brittle-ductile transition point confinement 65
4.3.4 Determination of the residual strength polynomial 65
4.3.5 Comparison of the peak, residual and base strength 66

criteria

4.3.6 Determination of the base strain, e_b, the R, S and T constants, and the solution to the effective friction - strain polynomial 66

4.3.7 Comparison of ϕ_e-e curve with the ϕ_e-e data - verification 68

4.3.8 Reconstruction of the σ - e curves and original comparison 69

4.3.9 The normalized post peak modulus 70

4.4 Comparison of the peak and residual data to peak data results 71

4.5 Varying the value of the base angle of friction, ϕ_b 73

4.6 Verification of postulates and assumptions using other intact rock data sets from the literature 74

4.7 Conclusions 75

Chapter 5 Verification of the postulates and assumptions through physical testing of intact rock 77

5.1 Testing program for TimKen rock and Highvale mudstone 77

5.1.1 Triaxial test 77

5.1.2 Tilt test 78

5.1.3 Triaxial slip test 80

5.1.4 Shear box test 81

5.2 TimKen rock 82

5.2.1 Triaxial test results 83

5.2.2 Tilt test results and analysis 84

5.2.3 Triaxial slip test results and analysis 84

5.2.4 Shear box test results and analysis 85

5.3 Verification of the postulates and assumptions using 86

TimKen rock

5.3.1 Assuming that the peak and residual data are available and applying the Joseph-Barron approach 86
  5.3.1a Determination of the peak strength criterion 86
  5.3.1b Determination of the brittle-ductile transition point 87
  5.3.1c Determination and refinement of the residual strength criterion 89
  5.3.1d Estimation of the base angle of friction 90
  5.3.1e Comparison of the peak, residual and base strength criteria 91
  5.3.1f Determination of the base strain, e_b and the solution to the effective friction - strain polynomial 92
  5.3.1g Comparison of ϕ_e-e curve with the ϕ_e-e data - verification 93
  5.3.1h Reconstruction of the σ - e curves and comparison with the original data 93
  5.3.1i The normalized post peak modulus 94
5.3.2 Assuming that the peak data is solely available and applying the Joseph-Barron approach 95
  5.3.2a Determination of the peak strength criterion 95
  5.3.2b Estimation of the base angle of friction from a tilt test 96
  5.3.2c Determination of the brittle-ductile transition point 96
  5.3.2d Determination of the residual strength criterion 96
  5.3.2e Comparison of the peak, residual and base strength criteria 97
  5.3.2f Determination of the base strain, e_b and the 97

solution to the effective friction - strain polynomial
5.3.2g Comparison of ϕ_e-e curve with the ϕ_e-e data - verification 98
5.3.2h Reconstruction of the σ - e curves and original comparison 100
5.3.2i The normalized post peak modulus 101
5.4 Comparison of the TimKen rock peak and residual data to peak data results 102
5.5 Highvale mudstone 104
5.5.1 Triaxial test results 104
5.5.2 Tilt test results and analysis 105
5.5.3 Triaxial slip test results and analysis 105
5.5.4 Shear box test results and analysis 106
5.6 Verification of the postulates and assumptions using Highvale mudstone 107
5.6.1 Assuming that the peak and residual data are available and applying the Joseph-Barron approach 107
5.6.1a Determination of the peak strength criterion 107
5.6.1b Determination of the brittle-ductile transition point 108
5.6.1c Determination and refinement of the residual strength criterion 110
5.6.1d Estimation of the base angle of friction 112
5.6.1e Comparison of the peak, residual and base strength criteria 113
5.6.1f Determination of the base strain, e_b and the solution to the effective friction - strain polynomial 113
5.6.1g Comparison of ϕ_e-e curve with the ϕ_e-e data 114

- verification
5.6.1h Reconstruction of the σ - e curves and comparison with the original data 115
5.6.1i The normalized post peak modulus 117
5.6.2 Assuming that the peak data is solely available and applying the Joseph-Barron approach 117
5.6.2a Determination of the peak strength criterion 117
5.6.2b Estimation of the base angle of friction from a tilt test 117
5.6.2c Determination of the brittle-ductile transition point 118
5.6.2d Determination of the residual strength criterion 118
5.6.2e Comparison of the peak, residual and base strength criteria 119
5.6.2f Determination of the base strain, e_b and the solution to the effective friction - strain polynomial 119
5.6.2g Comparison of ϕ_e-e curve with the ϕ_e-e data - verification 120
5.6.2h Reconstruction of the σ - e curves and original comparison 121
5.6.2i The normalized post peak modulus 122
5.7 Comparison of the Highvale mudstone peak and residual data to peak data results 123
5.8 Vaidity of the tilt test in defining the base angle of friction, ϕ_b 124
5.9 Conclusions 125
Chapter 6 Application of the Joseph-Barron approach to establish the post peak modulus of broken rock 127
6.1 Introduction and background 127

6.2 Postulates 128

- 6.2.1 Postulate 3 - Effective friction - strain relationship for broken rock 128
- 6.2.2 Postulate 4 - Post peak stress-strain behaviour of broken versus intact rock 128
- 6.2.3 Postulate 5 - The post peak modulus 129

6.3 Assumptions 129

- 6.3.1 Assumption 10 - Empirical relationships after Hoek et al. (1997) 129
- 6.3.2 Assumption 11 - Pre-peak broken rock deformation modulus 130
- 6.3.3 Assumption 12 - The Hoek-Brown peak strength criterion and the residual strength polynomial relationship for broken rock 133

6.4 The Joseph-Barron approach applied to broken rock - a verification of the postulates using example data sets from the available literature 134

- 6.4.1 Where triaxial data is available 135
  - 6.4.1a Determination of the Hoek-Brown strength parameters 135
  - 6.4.1b Estimation of the base angle of friction, ϕ_b 137
  - 6.4.1c Determination of the confinement at the brittle-ductile transition point 138
  - 6.4.1d Determination of the residual strength polynomial constants σ_{cr}, D and F 138
  - 6.4.1e Comparison of the intact and rock mass strength criteria 140
  - 6.4.1f Determination of e_b and the solution to the effective friction - strain polynomial 141

6.4.1g Reconstruction of the σ-e curves 143
6.4.1h Determination of the post peak modulus and stiffness 145
6.4.2 Where only the Hoek-Brown intact peak strength parameters and values for GSI taken from charts (Hoek et al., 1997) are available 146
6.4.2a Determination of the Hoek-Brown strength parameters 146
6.4.2b Estimation of the base angle of friction 146
6.4.2c Determination of the confinement at the brittle-ductile transition point 147
6.4.2d Determination of the residual strength polynomial constants σ_{cr}, D and F 147
6.4.2e Comparison of the intact and rock mass strength criteria 148
6.4.2f Determination of e_b and the solution to the effective friction - strain polynomial 149
6.4.2g Reconstruction of the σ-e curves 151
6.4.2h Determination of the post peak modulus and stiffness 152
6.4.3 Verification of the postulates and assumptions using other broken rock data sets from the literature 153
6.5 Evaluation of a crushed rock data set - crushed basalt (Hussaini, 1991) 153
6.6 Evaluation of the Panguna andesite data set (Hoek et al., 1980) 159
6.7 Conclusions 166
Chapter 7 Application of the Joseph-Barron approach to coal 168

7.1 Introduction 168
7.2 Intact coal, non-intact coal and coal mass strength properties 168
7.3 Postulates 171
- 7.3.1 Postulate 6 - Effective friction - strain relationship for coal 171
- 7.3.2 Postulate 7 - Post peak stress-strain behaviour of coal 172
- 7.3.3 Postulate 8 - The normalized coal post peak modulus 172

7.4 Assumptions 172
- 7.4.1 Assumption 13 - Estimation of the failure angle, 2θ 173

7.5 Application of the Joseph-Barron approach to coal and verification of postulates 6, 7, and 8 174
- 7.5.1 Determination of the Hoek-Brown strength criterion constants 174
- 7.5.2 Estimation of the base angle of friction, ϕ_b 176
- 7.5.3 Determination of the brittle-ductile transition point confinements 176
- 7.5.4 Determination of the residual strength polynomial constants σ_{cr}, D and F 177
- 7.5.5 Comparison of the peak, residual and base strength criteria 177
- 7.5.6 Determination of e_b and the solution to the effective friction - strain polynomial 179
- 7.5.7 Comparison of the ϕ_e - e curve with the ϕ_e - e data 180
- 7.5.8 Reconstruction of the σ-e curves for non-intact coal and the prediction of σ - e curves for intact coal and 181

coal mass

7.5.9 Determination of the post peak modulus & stiffness 183

7.6 Verification of the postulates and assumptions using other non-intact coal data sets from the literature 184

7.7 Conclusions 184

Chapter 8 Application of the Joseph-Barron post peak criterion to predicting pillar behaviour 186

8.1 Introduction 186

8.2 Triaxial strength prediction via Flac 2d and the Joseph-Barron approach 187

8.2.1 Flac 2d 187

8.2.2 Triaxial test model 188

8.3 Prediction of pillar behaviour via Flac 2d and the Joseph-Barron approach 190

8.4 Prediction of pillar behaviour via Phase 2, the Joseph-Barron approach and the approach suggested by Hoek et al. (1997) 192

8.4.1 Using the Joseph-Barron post peak criterion with Phase 2 193

8.4.2 Using the Hoek et al. (1997) approach with Phase 2 199

8.4.3 Comparison of pillar behaviour predicted by the Joseph-Barron post peak criterion and the Hoek et al. (1997) approach 200

8.5 Application of the Joseph-Barron approach to a coal mass 202

8.6 Conclusions 209

Chapter 9 Conclusions and recommendations for future work 211

9.1 The Joseph-Barron post peak criterion 211

9.2 Verified and validated original postulates and assumptions 212

9.2.1 Effective friction - strain relationship 212

9.2.2 Residual strength relationship 212
9.2.3 Post peak modulus relationship 213
9.2.4 Determination of intact or broken rock pre-peak modulus 214
9.3 Physical testing - the tilt test to determine ϕ_b 214
9.4 The Joseph-Barron post peak criterion applied to pillars 214
9.5 Recommendations for future work 215
References **217**
Appendix A **Procedure for polynomial regression analysis (after Visman et al., 1970)** **222**
Appendix B **Derivation of the post peak modulus, E_{pp}** **223**
Appendix C **General solution for the ϕ_e-e polynomial: fe = R+Se+Te^2** **227**
Appendix D **Determination of σ_{3t} when only peak data is available** **230**
Appendix E **Evaluation of a residual strength 2nd order polynomial** **231**
Appendix F **Determination of the strain at the transition point e_b** **234**
Appendix G **Solution for 2θ (after Balmer, 1952)** **235**
Appendix H **Worked intact rock data sets where peak and residual data was available** **239**
H.1 Intact high strength concrete HS15 (Ansari et al., 1998) 239
H.2 Intact marl (Farmer, 1983) 242
H.3 Intact mudstone (Farmer, 1983) 245
H.4 Intact Portland stone (Farmer, 1983) 248
H.5 Intact Saccharoidal limestone (Farmer, 1983) 251
H.6 Intact sandstone (Farmer, 1983) 254
H.7 Intact silty sandstone (Farmer, 1983) 257
H.8 Intact quartzite (Gates, 1988) 260
H.9 Intact Lac du Bonnet pink granite (Gorski et al., 1991) 263
H.10 Intact Doddington sandstone (Santarelli et al., 1989) 266

H.11 Intact Gebdykes dolomite (Santarelli et al., 1989) 269
H.12 Intact mudstone (Tao, 1991) 272

Appendix J Worked intact rock data sets where peak and residual data was available, but only peak data was used for comparison with results from appendix H 275

J.1 Intact high strength concrete HS15 (Ansari et al., 1998) 275
J.2 Intact marl (Farmer, 1983) 278
J.3 Intact mudstone (Farmer, 1983) 281
J.4 Intact Portland stone (Farmer, 1983) 284
J.5 Intact Saccharoidal limestone (Farmer, 1983) 287
J.6 Intact sandstone (Farmer, 1983) 290
J.7 Intact silty sandstone (Farmer, 1983) 293
J.8 Intact quartzite (Gates, 1988) 296
J.9 Intact Lac du Bonnet pink granite (Gorski et al., 1991) 299
J.10 Intact Doddington sandstone (Santarelli et al., 1989) 302
J.11 Intact Gebdykes dolomite (Santarelli et al., 1989) 305
J.12 Intact mudstone (Tao, 1991) 308

Appendix K Worked intact rock data sets where only peak data was available 311

K.1 Intact Berea sandstone (Aldritch, 1969) 311
K.2 Intact high strength concrete HS06 (Ansari et al., 1998) 314
K.3 Intact high strength concrete HS10 (Ansari et al., 1998) 317
K.4 Intact quartzite (Barron, 1970) 320
K.5 Intact Solenhofen limestone (Barron, 1970) 323
K.6 Intact Syenite (Barron, 1970) 326
K.7 Intact Berea sandstone (Blanton, 1981) 329
K.8 Intact charcoal granodiorite (Blanton, 1981) 332
K.9 Intact Indiana limestone (Blanton, 1981) 335
K.10 Intact Blair dolomite (Brace, 1964) 338

K.11 Intact quartzite (Chan, 1972) 341
K.12 Intact concrete (Dougill, 1985) 344
K.13 Intact Berea sandstone (Gnirk et al., 1965) 347
K.14 Intact Carthage marble (Gnirk et al., 1965) 350
K.15 Intact Danby marble (Gnirk et al., 1965) 353
K.16 Intact Hasmark dolomite (Gnirk et al., 1965) 356
K.17 Intact Indiana limestone (Gnirk et al., 1965) 359
K.18 Intact Virginia greenstone (Gnirk et al., 1965) 362
K.19 Intact Jastrzebie sandstone (Kwasniewski, 1983) 365
K.20 Intact medium grained Pinowek sandstone (Kwasniewski, 1983) 368
K.21 Intact fine grained Pinowek sandstone (Kwasniewski, 1983) 371
K.22 Intact Inada granite (Mogi, 1964) 374
K.23 Intact Nabe-ishi peridotite (Mogi, 1965) 377
K.24 Intact Orikabe diorite (Mogi, 1965) 380
K.25 Intact Shirochoba andesite (Mogi, 1964) 383
K.26 Intact Ukigane diorite (Mogi, 1964) 386
K.27 Intact carboniferous sandstone (Santarelli et al., 1989) 389
K.28 Intact Tennessee marble (Wawersik et al., 1970) 392
K.29 Intact concrete type A (Xie et al., 1995) 395
K.30 Intact concrete type B (Xie et al., 1995) 398
K.31 Intact concrete type C (Xie et al., 1995) 401
K.32 Intact tuffaceous sandstone (Yoshinaka et al., 1980) 404
Appendix L Evaluation of a residual 2nd order polynomial for broken rock 407
Appendix M Worked rock mass data sets 409
M.1 Average quality rock mass (Hoek et al., 1997) 409
M.2 Very good hard quality rock mass (Hoek et al., 1997) 412

M.3 Poor quality rock mass (Hoek et al., 1997) 415
M.4 Bilsthorpe mudstone (Hobbs, 1970) 418
M.5 Bilsthorpe silty mudstone (Hobbs, 1970) 421
M.6 Hucknall shale (Hobbs, 1970) 424
M.7 Ormonde siltstone (Hobbs, 1970) 427

Appendix N Dense crushed basalt (Hussaini, 1991) 430

Appendix P Panguna andesite (Hoek et al., 1980) 442

Appendix R Worked coal data sets 448

R.1 Pittsburgh coal (Kripakov, 1981) 448
R.2 Barnsley brights coal (Hobbs, 1964) 453
R.3 Barnsley hards coal (Hobbs, 1964) 457
R.4 Cwmtillery coal (Hobbs, 1964) 461
R.5 Deep Duffryn coal (Hobbs, 1964) 465
R.6 Linby coal (Hobbs, 1964) 469
R.7 Markham coal (Hobbs, 1964) 473
R.8 Oakdale coal (Hobbs, 1964) 477
R.9 Pentremawr coal (Hobbs, 1964) 481
R.10 Teversal coal (Hobbs, 1964) 485

Appendix S Flac 2d code for triaxial test and pillar models 489

S.1 Flac 2d input code file for a triaxial test at σ_3 = 14 MPa (after Itasca, 1995) 489
S.2 Flac 2d input code file for a pillar of W/H = 6.0 491

Appendix T Manipulation of the post peak relationships to evaluate a new pseudo elastic modulus, E_{ps} for input into Phase 2, for a known previous post peak iteration 494

Appendix U Modification of rib pillar strength to equivalent square pillar strength 496

Appendix W Modeling a pilar using Phase 2 and the Joseph-Barron post-peak criterion 497

List of Tables

Table 4.1 Silty sandstone data set interpretation from figure 4.1 50
Table 5.1 Comparison of determined base angle of friction values 125
Table 6.1 Summary of the peak strength parameters for the crushed basalt 154
Table 6.2 Summary of σ_{3t} and the residual strength polynomial parameters 154
Table 6.3 Peak strength, base strength and pre-peak modulus parameters 160
Table 6.4 σ_{3t} and residual strength polynomial parameters, σ_{cr}, D and F 161

List of Figures

Figure 1.1 Change in confinement measured across a short squat pillar, as indicated by Hoek et al. (1980) 5

Figure 1.2 Variance of pre and post peak moduli with increasing confinement from triaxial testing of rock 6

Figure 1.3 Peak, residual and base strength criteria and typical stress path for a given confinement 7

Figure 1.4 A simplified evaluation of post peak modulus, after Hoek, et al., 1997 9

Figure 1.5 Pre and post peak moduli of a rock specimen 11

Figure 1.6 Spring analogy showing machine-specimen interaction analogous to a pillar-loading system, after Brady et al., 1993 12

Figure 1.7 Post-peak unloading for soft and stiff machines, after Brady et al., 1993 13

Figure 1.8 Post peak stiffness, λ, as a function of deformation, s, (Salamon, 1970) 17

Figure 1.9 Pillar post peak stiffness field and laboratory data compiled by Pen, after Pen (1994) 21

Figure 2.1 Definition of the effective angle of friction 24

Figure 2.2 Peak, residual and base strength criteria 28

Figure 3.1 2nd order polynomial regression of residual data plotted with Hoek-Brown peak strength values to attempt to identify σ_{3t} at the brittle-ductile transition point 32

Figure 3.2 2nd order polynomial regression of residual data plotted with Hoek-Brown strength values for no identification of σ_{3t} at the brittle-ductile transition point 33

Figure 3.3 Linear regression of the available residual strength data to 34 allow identification of σ_{3t}

Figure 3.4 Modification of residual polynomial function based on lower confinement interpretation 36

Figure 3.5 Boundary conditions for the effective friction - strain 2nd order polynomial function 38

Figure 3.6 Y versus e plot to allow e_b interpretation from the slope 42

Figure 3.7 Example of an effective friction - strain function solution compared to the original data 43

Figure 3.8 Example of post peak modulus plotted against post peak strain, described by equation 3.19 45

Figure 3.9 Example of normalized post peak modulus versus post peak strain as described by equation 3.20 45

Figure 4.1 Silty sandstone data set, after Farmer (1983) 50

Figure 4.2 Linear form of the Hoek-Brown failure criterion applied to the silty sandstone data set 51

Figure 4.3 Plot of residual strength polynomial regression curve and peak strength curve with the original data to try and identify the brittle-ductile transition point 52

Figure 4.4 Evaluation of the residual strength linear approximation via linear regression of the available data 53

Figure 4.5 Residual strength polynomial and linear approximation plotted together to show error in the polynomial function at low confining pressures 54

Figure 4.6 Effect of the refinement process for the residual strength polynomial at low confining pressures 55

Figure 4.7 Comparison of peak, residual and base strength criteria in relation to zero confinement and the brittle-ductile transition point 56

Figure 4.8 Plot of Y versus e to determine the base strain 59

Figure 4.9 Correlation between the effective friction - strain polynomial and the effective friction data values 60

Figure 4.10 Comparison of the reconstructed with the actual stress-strain curves for the silty sandstone data set 62

Figure 4.11 Plot of normalized post peak modulus versus post peak strain for a range of σ_3 and σ_{pp} values 63

Figure 4.12 Comparison of peak, residual and base strength criteria in relation to zero confinement and the brittle-ductile transition point using peak data only 66

Figure 4.13 Plot of Y versus e to determine the base strain using the available peak data only 67

Figure 4.14 Correlation between the effective friction - strain polynomial and the effective friction data values using the peak data only 69

Figure 4.15 Comparison of the reconstructed with the actual stress-strain curves using the available peak data only 70

Figure 4.16 Normalized post peak modulus derived from the peak data only 71

Figure 4.17 Comparison of effective friction - strain polynomial functions with respect to data availability 72

Figure 4.18 The effect of varying the base angle of friction on the effective friction - strain function 73

Figure 5.1 Tilt test arrangement using core, after Stimpson (1981) 79

Figure 5.2 Plot of τ versus σ to evaluate the base angle of friction from triaxial slip test results 81

Figure 5.3 Shear box testing arrangement 82

Figure 5.4 TimKen rock triaxial test results 83

Figure 5.5 Triaxial slip test results for TimKen rock 84

Figure 5.6 Shear box test results for TimKen rock 85

Figure 5.7 Linear form of the Hoek-Brown failure criterion applied to TimKen rock 86
Figure 5.8 Polynomial regression of the available residual data to identify the brittle-ductile transition point 87
Figure 5.9 Linear regression of the available TimKen residual data to allow identification of σ_{3t} 88
Figure 5.10 Residual strength polynomial and linear approximation revealing error in the polynomial function 89
Figure 5.11 Modified residual strength polynomial and linear approximation post refinement process 90
Figure 5.12 Comparison of peak, residual and base strength criteria in relation to zero confinement and the brittle-ductile transition point 91
Figure 5.13 Plot of Y versus e to determine e_b 92
Figure 5.14 Correlation between effective friction - strain polynomial and effective friction data values 93
Figure 5.15 Comparison of the reconstructed with the actual stress-strain curves for the TimKen rock 94
Figure 5.16 Normalized post peak modulus versus post peak strain for the TimKen rock 95
Figure 5.17 Comparison of peak, residual and base strength criteria 97
Figure 5.18 Plot of Y versus e to determine e_b 98
Figure 5.19 Correlation between effective friction - strain polynomial and peak data effective friction values 99
Figure 5.20 Comparison of the reconstructed with the actual stress-strain curves for TimKen rock using peak data only 100
Figure 5.21 Normalized post peak modulus versus post peak strain for TimKen rock via peak data only 101
Figure 5.22 Comparison of the peak and residual to peak only 102

approaches via the effective friction polynomials

Figure 5.23 Comparison of the peak and residual to peak only (dashed) reconstructions of the original stress-strain curves 103

Figure 5.24 Highvale mudstone triaxial test results 105

Figure 5.25 Triaxial slip test results for Highvale mudstone 106

Figure 5.26 Shear box test results for Highvale mudstone 107

Figure 5.27 Linear form of the Hoek-Brown failure criterion applied to Highvale mudstone 108

Figure 5.28 Polynomial regression of the available residual data to identify the brittle-ductile transition point 109

Figure 5.29 Linear regression of the available Highvale mudstone residual data to allow identification of σ_{3t} 110

Figure 5.30 Residual strength polynomial and linear approximation revealing error in the polynomial function 111

Figure 5.31 Modified residual strength polynomial and linear approximation post refinement process 111

Figure 5.32 Comparison of peak, residual and base strength criteria in relation to zero confinement and the brittle-ductile transition point for Highvale mudstone 113

Figure 5.33 Plot of Y versus e to determine e_b 114

Figure 5.34 Correlation between effective friction - strain polynomial and effective friction data values 115

Figure 5.35 Comparison of the reconstructed with the actual stress-strain curves for the Highvale mudstone 116

Figure 5.36 Normalized post peak modulus versus post peak strain for the Highvale mudstone 116

Figure 5.37 Comparison of peak, residual and base strength criteria 118

Figure 5.38 Plot of Y versus e to determine e_b 119

Figure 5.39 Correlation between effective friction - strain polynomial 120 and peak data effective friction values

Figure 5.40 Comparison of the reconstructed with the actual stress-strain curves for Highvale mudstone using peak data 121

Figure 5.41 Normalized post peak modulus versus post peak strain data for Highvale mudstone via peak data only data 122

Figure 5.42 Comparison of the peak and residual to peak only approaches via the effective friction polynomials 123

Figure 5.43 Comparison of the peak and residual to peak only (dashed) reconstructions of the original σ-e curves 124

Figure 6.1 Comparison of equation 6.5 (solid line) to equation 6.6 (dashed line), after Bieniawski, 1984 131

Figure 6.2 Empirical plot of data after Hoek et al. (1997) to verify equation 6.8 133

Figure 6.3 Linear form of the Hoek-Brown broken rock peak strength criterion to evaluate m_b from the slope 136

Figure 6.4 Linear regression of a σ_1 versus σ_3 plot to evaluate s from the intercept 136

Figure 6.5 Comparison of broken and intact peak, residual and base strength criteria showing two transition points 140

Figure 6.6 Plot of Y versus e to determine the base strain 141

Figure 6.7 Effective friction - strain polynomial compared to the available effective friction data values for the intact rock and the rock mass 143

Figure 6.8 Comparison of reconstructed intact and broken rock stress-strain curves for a range of confining pressures 144

Figure 6.9 Plot of intact and broken rock normalized post peak modulus revealing a single function 145

Figure 6.10 Comparison of broken and intact peak, residual and base strength criteria showing two transitions 148

Figure 6.11 Plot of Y versus e to determine the base strain 149
Figure 6.12 Effective friction - strain polynomial compared to the available effective friction data values for the intact rock and rock mass 150
Figure 6.13 Comparison of reconstructed intact and broken rock stress-strain curves for a range of confinement 151
Figure 6.14 Plot of intact and broken rock normalized post peak modulus as a single function 152
Figure 6.15 Comparison of the peak, residual and base strength criteria and the available peak strength data clustered about the residual strength polynomial 154
Figure 6.16 Comparison of the peak, residual and base strength criteria, and the available peak strength data moving towards the peak strength criterion 155
Figure 6.17 Effective friction - strain polynomial for the crushed basalt 157
Figure 6.18 Reconstructed stress strain curves for all crush sizes for $\sigma_3 = 1$ MPa and $\sigma_3 = 2.5$ MPa 158
Figure 6.19 Normalized post peak modulus versus post peak strain for the crushed basalt 159
Figure 6.20 Comparison of the peak, residual and base strength criteria with respect to weathered rock mass 161
Figure 6.21 Plot of Y versus e showing scatter in data due to weathering of rock mass 162
Figure 6.22 Effective friction - strain polynomial for the Panguna andesite, indicating varying base friction angle with degree of weathering 163
Figure 6.23 Effective friction - strain plots for each individual weathered set with ϕ_b values from figure 6.24 164
Figure 6.24 Relationship between ϕ_b and RMR 164

Figure 6.25 Reconstructed stress-strain plots for a single confining pressure with varying degree of weathering 165

Figure 6.26 Plot of normalized post peak modulus versus post peak strain showing the effect of weathering on the Panguna andesite 166

Figure 7.1 Linearized Hoek-Brown plot to determine m and the uniaxial intact compressive strength, σ_c 175

Figure 7.2 Comparison of the strength criteria and non-intact coal to coal mass relationships for Cwmtillery coal 178

Figure 7.3 Comparison of the strength criteria for the intact Cwmtillery coal 179

Figure 7.4 Plot of Y versus e to determine the base strain for the Cwmtillery coal 180

Figure 7.5 Effective friction - strain polynomial derived from non-intact coal data and common for non-intact coal, intact coal and coal mass post peak interpretations 181

Figure 7.6 Reconstructed stress-strain plots for all three coal states, illustrating a common post peak relationship 182

Figure 7.7 Normalized post peak modulus versus post peak strain for the three Cwmtillery coal states 183

Figure 8.1 Comparison of Joseph-Barron to Flac 2d triaxial test models for an intact mudstone (Farmer, 1983) 189

Figure 8.2 Flac 2d pillar model output for a range of width to height ratios 190

Figure 8.3 Phase 2 pillar model elements, discretization and boundary conditions 192

Figure 8.4 Determining a pseudo elastic modulus E_{ps} 194

Figure 8.5 Translation from E_{pp} to E_{ps} for Phase 2 196

Figure 8.6 Evaluation of E_{ps} using the Hoek et al. (1997) post peak 199 approach

Figure 8.7 Comparison of the Joseph-Barron and Hoek et al. (1997) approaches to predicting pillar behaviour 201

Figure 8.8 Effect of varying post peak modulus constant A' for the Hoek et al. (1997) approach to pillar modeling 202

Figure 8.9 Predicted Pittsburgh coal mass pillar behaviour using the Joseph-Barron approach and Phase 2 software 203

Figure 8.10 Comparison of modeled to empirical coal mass square pillar strengths of varying W/H ratio 206

Figure 8.11 Comparison of post peak modulus via the Joseph-Barron approach and a coal field data empirical relationship (Zipf, 1999) 207

Figure 8.12 Plot of post failure modulus versus width to height ratio, after Zipf (1999), showing coal mass (field) and non-intact (lab) data 208

Nomenclature, symbols and abbreviations

2d	two dimensional
a	Hoek-Brown peak strength criterion exponent
a	Salamon et al. (1985) empirical pillar strength constant
b	non-intact coal specimen width
b	Salamon et al. (1985) empirical pillar strength constant
A	cross-sectional area of a pillar
A’	ratio of linear pre-peak to post peak modulus
B	intercept of the linear form of the effective friction - strain equation
c	Coulomb-Navier cohesion
C	post peak change in stress with respect to a change in strain
d	core diameter
D	2nd order residual strength polynomial constant
e	strain value taken from available data for Y versus e plot
e_1	axial strain in the direction of major principal stress
e_p	strain experienced at peak strength for a given confinement
e_{pp}	post peak strain measured from the zero strain datum
e_r	strain experienced at residual strength for a given confinement
E	pre peak modulus
E_{field}	post peak field (coal mass) modulus
E_{lab}	post peak laboratory determined (non-intact) modulus
E_{pp}	post peak modulus
$E_{pp(n)}$	normalized post peak modulus
E_{ps}	pseudo elastic post peak modulus for use with Phase 2
E_s	Young’s modulus
F	2nd order residual strength polynomial constant
FLAC	Fast Lagrangian Analysis of Continua
G	slope of the residual strength linear approximation
GSI	geological strength index
h	non-intact coal specimen size height

H	height of pillar
k	local mine stiffness, machine stiffness, spring constant,
K	base strength criterion constant
K'	unconfined compressive strength of a $1m^3$ coal specimen
k_i	local mine stiffness of the ith pillar
L	length of mining span of openings adjacent to pillars
L	length of pillars
LMS	local mine stiffness
m	Hoek-Brown parameter for intact rock
m_b	Hoek-Brown parameter for broken rock
m_{cm}	Hoek-Brown parameter for coal mass
m_{ni}	Hoek-Brown parameter for non-intact coal
M	slope of the linear form of the effective friction - strain equation
n	Salamon et al. (1985) pillar shape factor (1 for square pillars)
n	ratio of pillar length to pillar width
N	normal load during a shear box test
P	axial force applied to a specimen
P_r	axial load applied to a rock specimen
P_s	axial load of two springs in series
Q	peak stress difference, $(\sigma_{1p} - \sigma_3)$
r	polynomial regression constant as defined by Visman et al. (1970)
R	friction-strain polynomial constant
R	width to height ratio
R_o	width to height ratio cut off for "squat pillar formula"
RMR	rock mass rating
RMR_{broken}	rock mass rating for broken rock
RMR_{intact}	rock mass rating for intact rock
R-square	linear regression constant
S	friction-strain polynomial constant
s	Hoek-Brown parameter
s_{cm}	Hoek-Brown parameter for coal mass

s_{ni}	Hoek-Brown parameter for non-intact coal
s'	axial displacement of a specimen
sd	standard deviation
T	friction-strain polynomial constant
T	shear load during a shear box test
u_y	vertical deformation measured using Phase 2
W	width of pillar
w_B	width of opening adjacent to pillar along its short side
w_L	width of a cross cut adjacent to a pillar along its long side
W_m	energy released by the machine
W_o	width of opening between two pillars
W_p	width of pillar
W_s	energy absorbed by the specimen
X	linear strain variable in base strain analysis
Y	linear effective friction variable in base strain analysis
α	angle of core inclination at slip during a tilt test
α	Salamon et al. (1985) empirical pillar strength constant
β	half the internal angle of an equilateral triangle, 30°
β	Salamon et al. (1985) empirical pillar strength constant
δe_{pp}	change in post peak strain
$\delta\phi_e$	change in effective friction
$\delta\sigma_{1p}$	change in peak strength
$\delta\sigma_{1r}$	change in residual strength
$\delta\sigma_3$	change in confinement
$\delta\sigma_{pp}$	change in post peak stress
Δc	uniform perturbation closure applied to an element of a pillar
Δe	change in strain
Δe_{pp}	small change in post peak strain
$\Delta\gamma$	change in spring displacement
ΔF	change in load applied to a pillar in the post peak region

ΔH	change in height of a pillar under load in the post peak region
ΔP	change in load applied to a jack replacing an ith pillar
Δp_i	change in load on an element in the ith pillar
ΔP_r	change in load applied to a rock specimen
ΔP_s	change in load applied to a spring
Δs	change in axial displacement, virtual displacement
$\Delta\sigma_{pp}$	small change in post peak stress
Δw_r	change in work to cause displacement in a rock specimen
ΔW_s	change in work done by a spring to cause a displacement Δs
ε	Salamon et al. (1985) empirical pillar strength eccentricity factor
ϕ	Coulomb-Navier friction
ϕ_b	base angle of sliding friction
ϕ_e	effective angle of friction
ϕ_ε	effective angle of friction
ϕ_p	peak effective angle of friction
ϕ_r	residual effective angle of friction
γ	spring displacement representing machine and specimen
λ	specimen stiffness
λ_i	post peak stiffness of the ith pillar
λ_m	minimum post peak stiffness of a pillar defined by Salamon (1970)
λ_{pp}	post peak stiffness
ν	Poisson's ratio
ψ	rib pillar to square pillar strength conversion factor
σ	normal stress
σ_1	major principal stress, axial loading stress
$\sigma_{1:1}$	strength of a pillar of W/H = 1
σ_{1av}	average strength from a range of strength values
σ_{1b}	base strength
σ_{1p}	peak strength for a given confinement
σ_{1n}	corrected stress value for pseudo elastic modulus determination.

σ_{1o}	stress value returned from Phase 2 uncorrected
σ_{1r}	residual strength for a given confinement
σ_{1t}	peak strength at the brittle-ductile transition point
σ_3	minor principal stress, confining stress
σ_{3av}	average confinement from a range of confinement values
σ_{3n}	predicted confinement for the next Phase 2 iteration
σ_{3o}	confinement returned by Phase 2 for the previous iteration
σ_{3t}	confining stress at the brittle-ductile transition point
σ_c	uniaxial unconfined compressive strength
σ_{cr}	uniaxial unconfined residual strength
σ_p	average pillar strength
σ_{pp}	post peak stress
σ_{rib}	rib pillar strength
σ_R	rectangular pillar strength
σ_S	required square pillar strength
σ_v	vertical stress applied to a pillar
τ	shear stress
θ	angle made with the failure plane to the major principal stress
$^\circ$	degrees

Chapter 1

Introduction

1.1 Significance of the problem

Room and pillar and longwall mining methods that rely on pillars as part and parcel of the strata support system, particularly those employed in coal seams, have a long history of violent pillar failures. These failures may be violent in the most adverse conditions of bump-prone coal beds. The U.S. Bureau of Mines has cited numerous cases of such events over the past 50 years, where danger to the safety of workers and equipment was found to be imminent and ongoing.

With the advent and increased use of mechanized longwall mining systems replacing the more traditional room and pillar mining methods of coal fields such as those found in the Appalacian Eastern United States, the number of incidents has decreased, but the use of chain pillars in longwall mining has not negated these occurrences completely.

1.1.1 Pillar bump potential

These violent failures are known as pillar bumps and arise from the difference in stiffness between the pillar and the mining environment loading the pillar. If the pillar material is of a stiffer nature than that of the overlying or underlying strata then there is a potential for the pillar to violently explode if the overall pillar strength is exceeded.

The effect is not restricted to single pillars, but may develop into a domino effect involving adjacent pillars and in extreme cases complete collapse of the active mining area. The domino effect arises from a load shedding mechanism, where a failed pillar can no longer support its initial load and so sheds that load onto the pillars surrounding it, thus increasing their bearing requirement above the peak allowable pillar load for the adjacent pillars.

The concept of pillar bump potential arises from the work of Cook (1965) and Salamon (1970) who recognized and formulated a relationship between the local mine stiffness (LMS) and the post peak pillar stiffness, λ_{pp}. When the magnitude of the post peak pillar stiffness is greater than that of the local mine stiffness there is a potential explosive release of energy from the mine environment into the pillar causing catastrophic failure. This concept is reviewed in more detail in section 1.3.

1.1.2 Application of the pillar bump concept

The prediction of these events has been the subject of research for a number of years, with the most recent work being conducted by Pen (1994) on coal pillars. Although Pen completed work on the evaluation of local mine stiffness and incorporated this information into the numerical pillar model Mulsim NL, his prediction of pillar bump potential relied on an empirical post peak stiffness relationship derived from post peak stiffness data gleaned from the available literature. He noted in his conclusions that more work was necessary to predict the post peak stiffness directly, that would allow a more accurate evaluation of pillar bump potential.

1.2 Definition of the problem

It is necessary to define the terms "modulus" and "stiffness" as related to rock, through specifying the units commonly used to measure these properties:

i The modulus of rock, whether in the pre-peak or post-peak region of the stress-strain curve for a given value of confinement, is a change in stress for a unit change in strain. The Systeme International units of modulus are either GPa or MPa. The latter is used in this thesis.

ii The stiffness of rock, whether in the pre-peak or post-peak region of the load-deformation curve for a given value of confinement, is a change in load for a unit change in deformation. The Systeme International units of stiffness are kN/m.

As suggested by Pen (1994), the crux of the problem is one of defining the post peak pillar stiffness without having to rely on empirical relationships. The post peak pillar stiffness depends on the post peak modulus of the rock, which varies from location to location across the pillar. Thus the problem becomes one of defining the post peak stress-strain behaviour for the rock. This is complicated by the need for a generalized definition that also accounts for all possible values of confinement. It has been well established (Wagner, 1974 and Brady et al., 1993) that confinement increases from the pillar edge to the pillar core, and that the magnitude of this confinement at any location changes with increasing pillar width to height ratio. It is also well known that the slope of the post peak stress-strain relationship varies with confinement, as evidenced from triaxial tests on rock samples; hence, for any structure where strength is enhanced through confinement the post peak modulus will vary across a given cross section.

1.2.1 Post peak behaviour as a function of σ_3

It has been recognized that an evaluation of post peak stiffness for any rock, not just for coal, would aid an understanding of the post peak failure processes not only in pillars but also in stability of slopes, or any other structure excavated in rock, where strength change through confinement is of importance.

The prediction of post peak stiffness at any level of confinement for an element within a larger mass of rock depends on an understanding of the post peak portion of the stress-strain behaviour for the rock in question. Since the failure mechanism of rock fracture, whether intact rock or rock mass, is a predominantly brittle phenomenon, it is possible to restrict the scope of the problem to a region from zero confinement to that at the brittle-ductile transition point with all possible degrees of confinement spanning those limits.

From the work of Wagner (1974), Das (1986) and others it is known that overall pillar strength increases with increasing width to height ratio. Wagner (1974) found that although the perimeter of the pillar was only capable of carrying minor stresses, it did act in a lateral confining capacity, enhancing the strength of the pillar core. This is an assumption used by Wilson et al. (1972) in formulating the pillar core confinement model, and by Barron et al. (1992) in the refinement of an analytical pillar model. In other words a short squat pillar will demonstrate a higher bearing capacity than a tall thin pillar. In a short squat pillar, the confinement increases from the pillar edge towards the pillar core, increasing the overall pillar strength, as demonstrated by Hoek et al. (1980) and illustrated in figure 1.1.

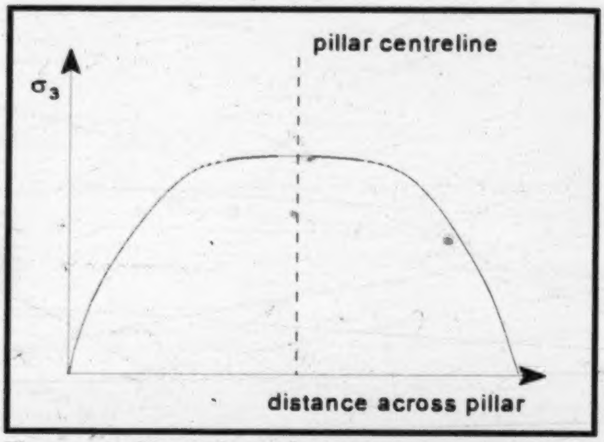

Figure 1.1: Change in confinement measured across a short squat pillar, as indicated by Hoek et al. (1980)

During failure of such a pillar, the outer most region of the pillar fails first and sheds its load onto the remnant portion (Wilson et al., 1972). The whole pillar does not fail immediately due to the increased confinement experienced by the central portion, allowing a progressively higher bearing capacity as the central core is approached.

Since the post peak modulus of rock varies with confinement and the degree of confinement varies with pillar width to height ratio, the overall post peak behaviour of the pillar will be dependent on the pillar width.

Hence, to be able to evaluate the overall post peak pillar modulus, it is necessary to understand how the post peak stress-strain curve for the rock varies with confinement. It has been established, as indicated by Brady et al., (1993) that pre-peak modulus varies with changing confining pressure as illustrated in figure 1.2 for a series of triaxial tests and in accordance with the relationship given in equation 1.1.

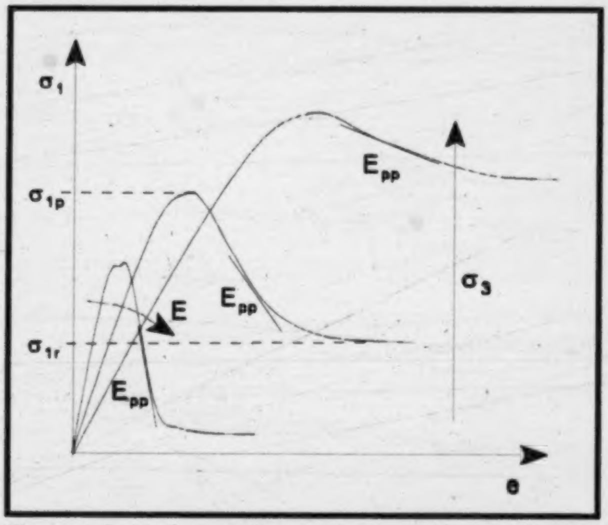

Figure 1.2: Variance of pre and post peak moduli with increasing confinement from triaxial testing of rock

$$E=\frac{\sigma_1}{e_1}-2\nu\frac{\sigma_3}{e_1} \qquad 1.1$$

However, a relationship has not been established to explain the variance of post peak modulus, E_{pp} with change in confinement, as also illustrated in figure 1.2. Estimation of this relationship is made possible by the Joseph-Barron post peak criterion as established during the course of this research.

1.2.2 The existence of 3 strength levels; peak, residual and base

In evaluating the behaviour of rock in the post peak region it is necessary to understand what is happening in the physical sense. For an intact rock specimen at peak strength, σ_{1p} for a given confinement, σ_3 fracture through the specimen will take place. At that instant a rough fracture surface is formed. Motion along the rough surface ensues with some fracture and crushing of the rough asperities until a stable residual strength, σ_{1r} is established. For any further increase in strain the applied stress remains constant at the residual value, σ_{1r} as indicated in figure 1.2. Figure 1.3 illustrates the increase of peak, residual and base strength with confining pressure. For any given confinement, the post peak stress path from peak to residual and conceptually to base strength is shown.

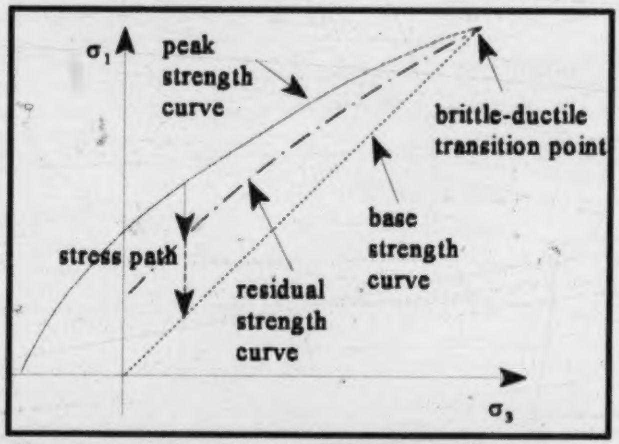
σ_1
peak strength curve
brittle-ductile transition point
base strength curve
stress path
residual strength curve
σ_3

Figure 1.3: Peak, residual and base strength criteria and typical stress path for a given confinement.

As the confinement is increased both the peak and residual strength also increase and the roughness of the asperities decreases. Conceptually, if the asperities were ground to a smooth surface, a base strength would be realized that would be lower than any residual strength corresponding to a given confinement. However, base strength is only achieved at the brittle-ductile transition point, where it is equal to the peak and residual strengths.

1.2.3 Significance of the brittle-ductile transition point

At the brittle-ductile transition point the confinement is sufficient to realize a residual strength that is equal to both the peak strength and the base strength, since at this degree of confinement all of the asperities shear and crush, leaving a smooth surface. Above the brittle-ductile confinement, the rock behaves in a ductile manner. For the purposes of this research, due to the brittle nature of the rock fracture under investigation, the brittle-ductile transition point was taken as the upper limit of study.

1.2.4 Post peak stress-strain data

The available literature contains relatively few complete stress-strain curves for rock, although those that are documented, particularly for studies on man-made materials such as concrete, provide good data for a wide range of confining pressures. The sparsity of complete stress-strain curves obtained via triaxial strength testing echoes the difficulty of the physical testing of rock. The main problem is the efficiency in holding a confining pressure constant on a specimen while completing the post-peak portion of the stress-strain curve, without rupturing the membrane in such devices as the Hoek-Franklin cell used for triaxial testing of rock at high confinement. For this reason, most triaxial tests are terminated at or just beyond the peak strength and are not continued to the residual strength. Hence, there is a very large quantity of solely peak strength data in the literature.

Hoek et al. (1997) suggested an evaluation approach for the post-peak stress-strain curve and hence the post-peak modulus by classifying the rock under investigation into one of three types, as illustrated in figure 1.4:

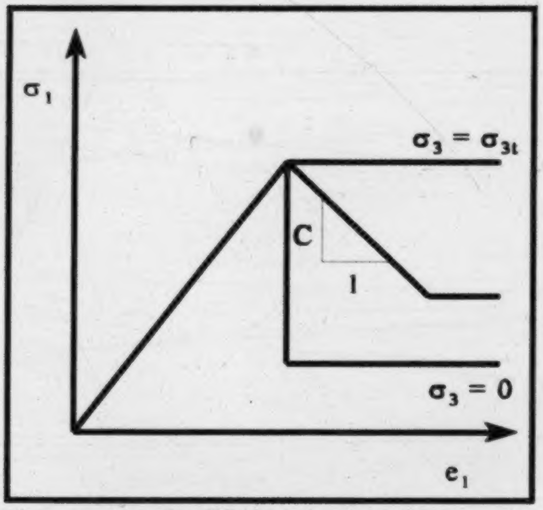

Figure 1.4: A simplified evaluation of post-peak modulus, after Hoek et al., (1997).

i At zero confinement the post peak strength abruptly decreases with virtually no additional strain.

ii At the brittle-ductile transition point the strength remains constant as the strain increases.

iii At any confinement between the two extremes, the drop in post-peak strength with respect to strain is a constant, C.

The selection of the constant C is somewhat arbitrary, and assumes a linear post-peak relationship. From observation of the available post-peak stress-strain trends, as illustrated in figure 1.2, this is certainly not the case. The constant C, described by Hoek et al. (1997), is a linear approximation of the non-linear post-peak modulus, E_{pp} suggested from the evidence of triaxial tests. The research conducted by the author aims to establish a more accurate non-linear estimate of the post-peak modulus that ties in with the reported triaxial test post-peak evidence.

1.3 Previous work related to post-peak behaviour

When evaluating the behaviour of rock pillars or elements of pillars, there are several moduli or stiffnesses that need to be considered, figure 1.5:

i The pre-peak stiffness is an elastic stiffness that is defined as the increase in load per unit of elastic deformation, usually in units of kN/m. This is directly proportional to Young's modulus E_s, which is the slope of the straight line portion of the pre peak stress-strain curve.

ii The post peak pillar stiffness is a function of the degree of fracturing and crushing along the fracture planes resulting from failure. The post peak stiffness, λ_{pp}, is defined as the decrease in load per unit of post peak deformation. This is directly proportional to the post peak modulus, E_{pp}, which is the slope of the of the post peak portion of the stress-strain curve at the point of interest.

iii To evaluate the stability of a pillar under load, the relative stiffness of pillar and loading environment must be considered (Pen, 1994). The stiffness of the loading system is known as the local mine stiffness (LMS), k. LMS is defined as the load required to cause a unit of deformation of the loaded pillar.

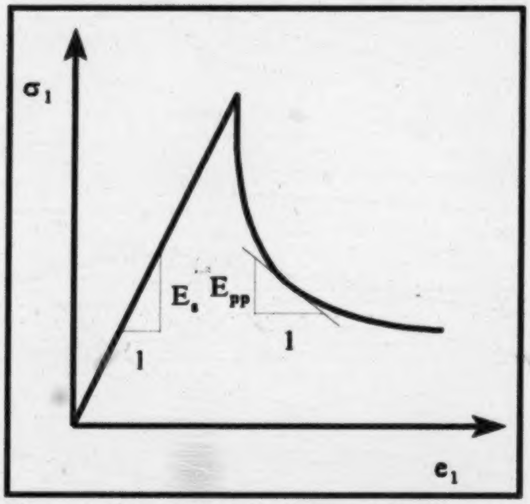

Figure 1.5: Pre and post peak moduli of a rock specimen.

The relationship between the stiffness of a pillar in the pre and post peak regions and the stiffness of the loading system (LMS) was introduced by Cook (1965), described in detail by Salamon (1970) and validated by Starfield et al. (1968), Ozbay (1989) and Pen (1994) through variations in the perturbation process. The perturbation process is described later in this section in some detail.

The work of Cook and Salamon draws on an analogy to the stiff or soft characteristics of a testing machine relative to a specimen under load in the machine, in terms of the stiffness of a series of springs describing the pillar-loading system scenario.

Figure 1.6 shows the loading and unloading of a specimen and machine.

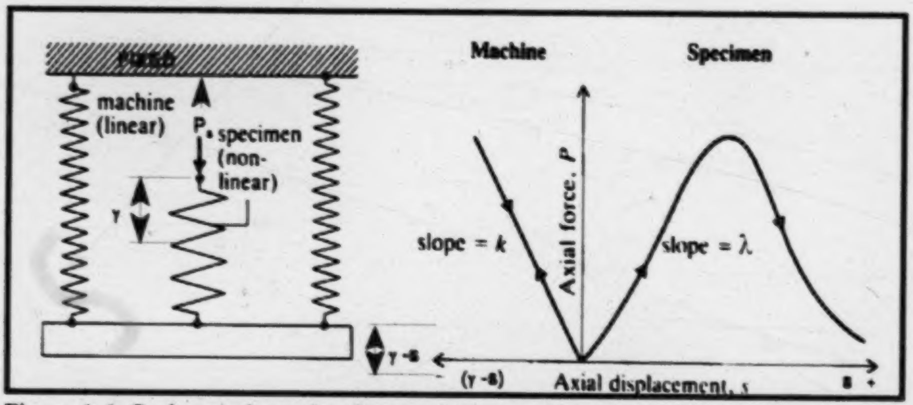

Figure 1.6: Spring analogy showing machine-specimen interaction analogous to a pillar-loading system, after Brady et al., (1993).

As the specimen is loaded its representative spring is compressed elastically while the testing machine springs are extended elastically. Beyond the point of failure in the specimen, the testing machine unloads elastically in a linear fashion along the reverse path as loading took place, since the stiffness characteristics of the testing machine have not changed. However, the stiffness characteristics of the specimen spring have changed as it becomes damaged. This has the effect that the spring can no longer resist the load at peak and either deforms slowly to a state of equilibrium, or fails rapidly due to the rate of energy release from the machine.

Figure 1.7 illustrates the specimen/loading machine analogy in terms of the energy released after failure of the specimen. If the machine has a stiffness less than the specimen being tested (a soft machine), then during unloading the energy stored and released by the machine, W_m, is greater than can be absorbed by the specimen, W_s, and violent failure of the specimen ensues. If the machine has a stiffness greater than the specimen being tested (stiff machine), then during unloading the energy released by the machine, W_m, is less than can be absorbed by the specimen, W_s, and gentle failure will follow, as energy must be added to drive the fracture process in the rock; (Brady et al., 1993).

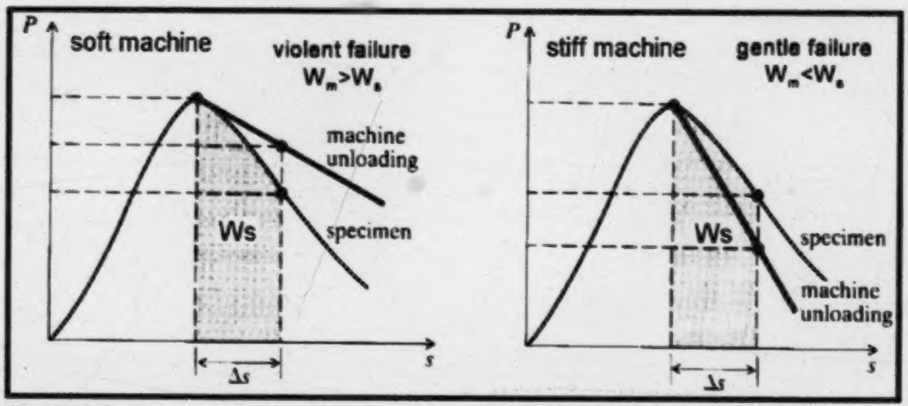
P
soft machine
violent failure
W_m>W_s
machine unloading
specimen
Ws
Δs
s
P
stiff machine
gentle failure
W_m<W_s
specimen
machine unloading
Ws
Δs
s

Figure 1.7: Post-peak unloading for soft and stiff machines, after Brady et al., (1993).

It is the concept of a gently failing system that is highly desirable in pillar reliant mining methods, as the violent failure scenario is one of unstable pillars resulting in pillar bumps. That is, when the LMS or machine stiffness, k, is less than the post peak pillar stiffness or specimen stiffness, λ_{pp}, then violent failure is likely.

Following from the initial work of Cook, (1965), Starfield and Fairhurst, (1968) suggested that the stability of pillar workings could be tested via a comparative analogy to machine stiffness, which they termed the "local mine stiffness" (LMS). LMS being the stiffness of the mine at the vicinity of a pillar of interest. The method applied, termed the "perturbation method", considered that the local mine stiffness could be determined by replacing the ith pillar in an array of pillars by an imaginary jack. For an incremental change in load applied by the jack, ΔP, the corresponding jack displacement, Δs is used to determine the local mine stiffness, LMS = $\Delta P/\Delta s$.

The theory was put into practice by Starfield et al. (1972), and later by Ozbay (1989), who established two different perturbation methods using both laboratory specimens and pillars in the field, that confirmed the validity of the approaches. The first approach perturbed the ith pillar by a unit displacement and monitored the change in load. The second approach perturbed the ith pillar by increasing the reaction load of the jack replacing the pillar and monitored the change in displacement relative to the loading strata and the pillar jack.

Around the same time that Starfield was developing the perturbation method, Salamon (1970) formulated the mathematical relationships that arose out of the initial work of Cook (1965), and defined the conditions for stable and unstable pillar workings, which he confirmed would fail in either a controlled or uncontrolled manner respectively. Salamon's theoretical formulation was reasoned as follows:

A specimen in a loading frame, figure 1.6, can be modeled as two sets of springs, representing the loading frame and a specimen, respectively. The combination is then subjected to an axial load, P_s. During loading, both ends of the specimen spring move downwards. If the spring upper end displacement, γ represents the machine and the specimen and the spring lower end displacement, $(\gamma - s)$ represents the machine alone, where s is the displacement of the specimen alone, then by Hooke's law:

$$P_s = k(\gamma - s) \qquad 1.2$$

Where k is the spring constant and P_s is the compressive load. Equation 1.2 is then a description of the machine reaction due to the applied load.

If the load-displacement relationship for the rock specimen, characteristic of the post peak failure region is known to be equation 1.3:

$$P_r=f(s) \tag{1.3}$$

Then the load applied to the rock and the load applied to the testing frame must be equal, equation 1.4:

$$f(s)=k(\gamma-s) \tag{1.4}$$

Equation 1.4 may be considered stable if no additional energy is supplied to the specimen by the machine, that is $\Delta\gamma = 0$.

The same expression may also be described in terms of virtual work, where the equilibrium remains unchanged if the work done by the spring, ΔW_s, during a virtual displacement, Δs, is less than the work required to produce the same displacement in the rock, ΔW_r:

$$\Delta W_r-\Delta W_s>0 \tag{1.5}$$

If the work done by the spring on the rock, during the virtual displacement is:

$$\Delta W_s=(P+\frac{1}{2}\Delta P_s)\Delta s \tag{1.6}$$

And the work required to deform the rock further is:

$$\Delta W_r=(P+\frac{1}{2}\Delta P_r)\Delta s \tag{1.7}$$

And if $\Delta\gamma = 0$, then:

$$\Delta P_s = k(0 - \Delta s) = -k\Delta s \tag{1.8}$$

$$\Delta P_r = f'(s)\Delta s = \lambda_{pp}\Delta s \tag{1.9}$$

Where λ_{pp} is the post peak stiffness, which is equivalent to the post peak slope of the load-deformation curve for the specimen.

Combining equations 1.4 through 1.9 yields the condition for stability in the system:

$$\frac{1}{2}(k + \lambda_{pp})\Delta s^2 > 0 \tag{1.10}$$

$$(k + \lambda_{pp}) > 0 \tag{1.11}$$

If the load-deformation curve pertaining to the ith pillar in an array of identical pillars describes the LMS of the pillar, k_i and the post failure stiffness of the pillar, λ_i then in accordance with load-deformation plot in figure 1.6:

i Prior to peak load, both k_i and λ_i are positive, equation 1.11 holds and the system is stable.

ii In the post peak region, if $k_i < |\lambda_i|$, then equation 1.11 is violated, and the pillar will fail violently, that is the local mine stiffness is less than the post peak pillar stiffness, which is analogous to the soft machine scenario, figure 1.7.

iii If $k_i > |\lambda_i|$ in the post peak region, then equation 1.11 holds and the pillar will fail gently, that is the local mine stiffness is greater than the post peak pillar stiffness, which is analogous to the stiff machine, figure 1.7.

It can be concluded from Salamon's work that pillar stability is controlled by the peak strength of the pillar, σ_p, the post-peak stiffness of the pillar, λ_i, and the local mine stiffness, k_i. If the peak strength of the pillar is exceeded, the relative stiffness of the system, $(k_i + \lambda_i)$, will dictate whether the pillar will fail violently, causing a pillar bump, or gently in a controlled manner, figure 1.8.

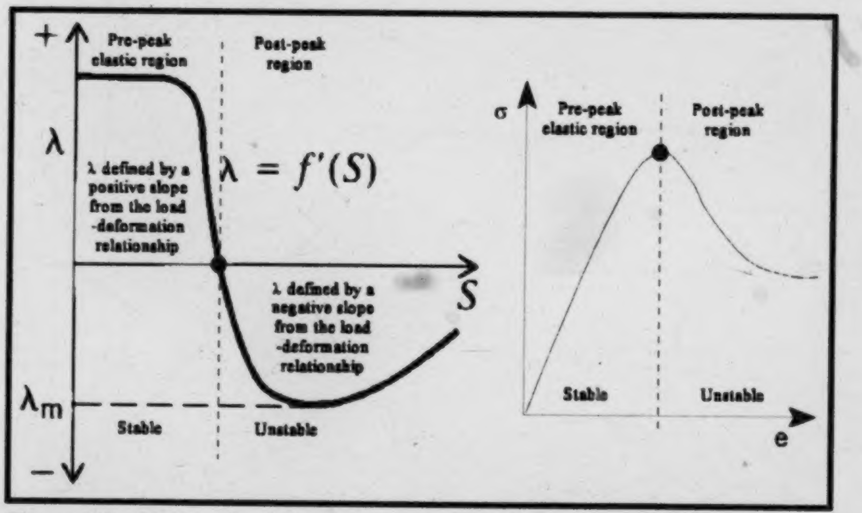
+
Pre-peak elastic region
Post-peak region
λ
λ defined by a positive slope from the load -deformation relationship
λ = f′(S)
S
λ defined by a negative slope from the load -deformation relationship
λm
Stable
Unstable
−
σ
Pre-peak elastic region
Post-peak region
Stable
Unstable
e

Figure 1.8: Post peak stiffness, λ, as a function of deformation, s, after Salamon, (1970)

Ozbay (1989) used a displacement discontinuity program to perform parametric studies on two dimensional rib pillar-panel configurations. This was in part follow up work to that of Brady et al., (1980), who used a direct formulation of a two dimensional boundary element method to determine local mine stiffnesses and pillar stiffnesses in the elastic range, to subsequently establish that the local mine stiffness increases with a decrease of W_o/W_p ratio; where W_o is the width of an opening immediately adjacent to the pillar of interest, and W_p is the width of the pillar. Brady et al., (1980) assumed that the average of the convergence across the pillar was representative of the elastic local mine stiffness. They showed that the postulate of Salamon, (1970), equation 1.11, was closely approximated for stratiform orebodies.

Ozbay (1989) determined stiffness through a variation on the Starfield perturbation process, akin to that later used by Pen (1994). He applied a uniformly distributed displacement disturbance across the entire width of the pillar, and concluded that if the extraction ratio were kept constant, then the local mine stiffness would increase proportional to the change in L/H ratio, where L was the mining span of the openings adjacent to the pillar under investigation, and H is the height of the pillar. This was shown to hold if the number of pillars in the layout in any one direction was greater than 5. He also noted that the strata stiffness decreased with an increasing number of pillars in the layout.

In 1994 Pen evaluated the potential for pillar bumps in chain pillar design for longwall mining panels. This work was based on the evaluation and comparison of the local mine stiffness, k, with an estimation of the post peak pillar stiffness, λ. He employed Salamon's pillar bump hypothesis (Salamon, 1970) to compare these two parameters, such that the condition for stability in equation 1.11 held.

Through the use of the boundary element model, MULSIM/NL (Zipf, 1992) modified by Pen (1994) to incorporate the Ozbay's displacement perturbation process (Ozbay, 1989), Pen was able to estimate the potential of a pillar bump occurring for a given unit of perturbation across an entire pillar via measuring the associated change in load conditions to establish LMS and comparing to an empirical value of post peak stiffness.

MULSIM was developed as a boundary element approach and employed to evaluate the LMS, after the initial work of Pariseau, (1981), and Kripakov et al., (1983), who performed investigative work on pillar loading. Zipf (1992) made several adaptations which resulted in the development of MULSIM/NL, a three dimensional displacement discontinuity boundary element model, which was specifically designed to simulate and analyze stresses and displacements of tabular multiple coal seams in elastic homogeneous rock.

The calculation of local mine stiffness within MULSIM/NL was achieved by Zipf by incorporating Starfield's perturbation method, (Starfield et al, 1972). He chose to perturb a single element in a pillar, which was already in an equilibrium state, thus facilitating a displacement. He then assumed that the resulting load change on the element divided by this elemental perturbation was the local mine stiffness.

Pen's modification, (Pen, 1994), of MULSIM/NL took Zipf's premise of local mine stiffness, but instead of perturbing a unit deformation for a single element and measuring the associated change in load for that element, he perturbed every element across the pillar by the same constant deformation, as per the method suggested by Ozbay (1989) and then measured the individual load changes at those elements across the cross section of the pillar. This gave a non-uniform cross sectional loading change for the pillar, which better matched the actual change in loading conditions of a given mining environment.

Working from the definitions laid down by Starfield et al. (1972), Pen (1994) defined the local mine stiffness in terms of units of modulus, equation 1.12:

$$LMS = \frac{\sum_{i=1}^{i=n} \frac{\Delta p_i}{A}}{\frac{\Delta c}{H}} \qquad 1.12$$

Where LMS is the local mine stiffness of a pillar comprising elements summed from 1 to n., Δc is the uniform perturbation closure applied to each of the elements across the pillar, Δp_i is the load change associated with each of the representative elements across the pillar, H is the pillar height, and A is the pillar cross-sectional area.

To compare the post-peak pillar stiffness to LMS, Pen (1994) devised an empirical relationship from post-failure pillar stiffness data collated from the available literature, to establish the post failure pillar stiffness, λ_{pp}, for his coal pillar models. Pen (1994) reviewed the literature and compiled post-failure pillar stiffness data, for variable W_p/H pillar ratios, from a number of sources. The researchers in these sources measured both small and large specimens, both in the laboratory and in the field; including Das (1986), Seedsman et al. (1991), van Heerden (1975), Wagner (1974), Wang et al. (1976), Iannachionne (1988), and Crouch et al. (1973).

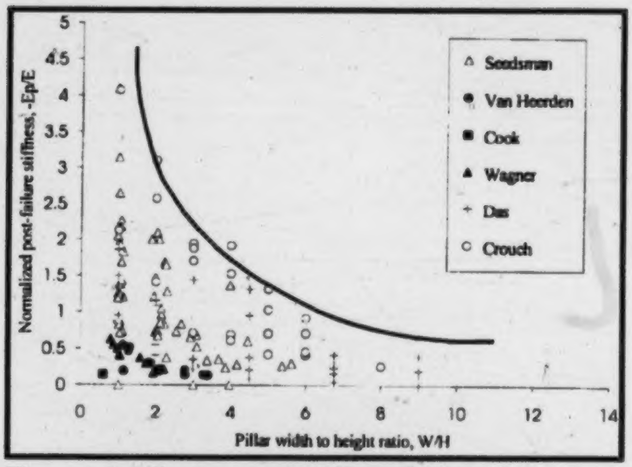

Figure 1.8: Pillar post peak stiffness field and laboratory data compiled by Pen, after Pen (1994).

He plotted the data as normalized post failure stiffness (E_{pp}/E_s), figure 1.8, where E_{pp} is the post failure modulus, and E_s is Young's elastic modulus, against W_p/H ratio; and arrived at the following empirical relationship, which he incorporated into the MULSIM/NL model.

$$\frac{E_{pp}}{E_s} = 5.98243[\frac{W_p}{H}]^{1.1976} \qquad 1.13$$

The local mine stiffness for the pillars was thus compared to an empirically derived post peak pillar stiffness (Pen, 1994). Pen used this knowledge to suggest an application to control pillar bumps and improve chain pillar design in longwall mining, under bump-prone coal bed conditions.

To avoid pillar bumps, Pen re-iterated the same concept as previously suggested by Cook (1965), Cook et al., (1966), Salamon (1970), Ozbay (1989), and others, that the local mine stiffness should be greater than the post-failure stiffness of the pillar; thus effecting the stiff machine scenario, and allowing gentle failure to occur.

1.4 Research objectives

As can be seen from this review of previous work, there is a need to better determine the post peak stiffness of rock structures such as pillars. To be able to do this, it is necessary to have a good understanding of the post peak stress-strain behaviour for both intact rock and rock masses. The objectives for this work are therefore as follows:

Phase 1: To develop a means of estimating the post failure modulus of intact rock from data obtained from triaxial tests on intact specimens.

Phase 2: To extend the concepts developed in phase 1 to allow the estimation of the post failure modulus of a rock mass from triaxial tests on intact rock together with a knowledge of the geological strength index (GSI), (Hoek et al., 1997).

Phase 3: To illustrate the use of post peak modulus evaluation in assessing the stability of rock structures, such as pillars.

Chapter 2

Definitions, postulates and assumptions

2.1 Definition of the effective angle of friction, ϕ_e for the post peak region

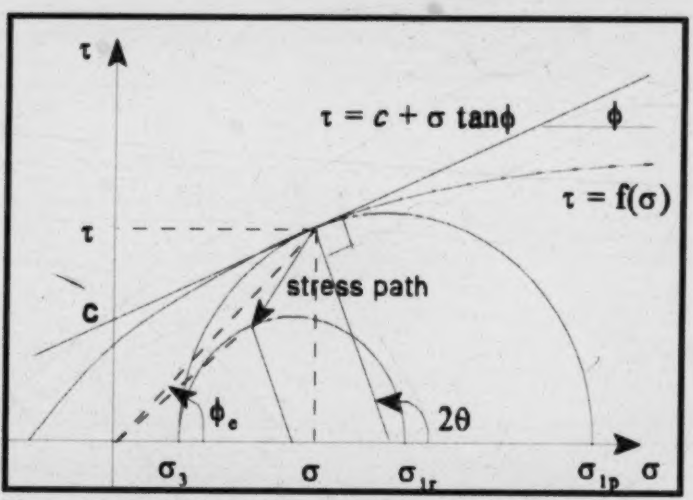

Figure 2.1: Definition of the effective angle of friction

Figure 2.1 shows a general failure criterion, where τ is the shear strength of the material and σ is the normal stress applied to the material mobilizing that shear strength. Thus in general:

$$\tau = f(\sigma) \qquad 2.1$$

NOTE: The term "effective angle of friction, ϕ_e," defined in figure 2.1 is a mathematical expression that combines the traditional Coulomb-Navier parameters of friction, ϕ and cohesion, c as described by the relationship; $\tau = c + \sigma \tan\phi$, into one parameter. The "effective angle of friction" term used here is not the same as the traditional soil mechanics term, which for example describes the effect of reduced friction due to pore pressure effects.

The effective angle of friction, ϕ_e, as defined in figure 2.1, allows any strength in the post peak region between peak strength, σ_{1p}, and residual strength, σ_{1r}, for a given value of confinement, σ_3 to be stated by a family of failure envelopes whose post-peak locus describes the stress path as indicated in the illustration, such that in general

$$\phi_e = \tan^{-1}[\frac{\tau}{\sigma}] \qquad 2.2$$

At σ_{1p}, $\phi_e = \phi_p$ and at σ_{1r}, $\phi_e = \phi_r$ for a given value of confinement, σ_3, where σ_{1p} is the peak strength and σ_{1r} is the residual strength.

At the instant prior to peak failure, where $\phi_e = \phi_p$, this represents a measure of both internal friction and cohesion, and the strain experienced is e_p.

At the instant after failure at peak strength, σ_{1p}, the strain remains the same, but a rough surface has now been formed, and the effective angle of friction is now a measure of two components of shear resistance:

i	Frictional resistance to sliding on the rough surface
ii	An apparent cohesional resistance representative of the strength of the rough surface asperities.

As failure continues, the apparent cohesion reduces as the asperities are sheared, resulting in a reduced roughness, and a correspondingly reduced frictional resistance. As the roughness reduces the sliding angle of friction also reduces. That is, the effective angle of friction is a measure of how the combination of these two components change.

For any given confining pressure, σ_3 when the residual strength, σ_{1r}, is reached, there is no further drop in apparent cohesion due to shearing of the asperities, and the resistance is due solely to friction on a rough surface. The strain experienced at this point is e_r. The surface of reduced roughness still has a resistance greater than that defined by the base strength of the material, σ_{1b}

At the brittle-ductile transition point, (σ_{1t}, σ_{3t}), all the asperities have been sheared off, and the effective angle of friction is then equivalent to the base angle of sliding friction for that material, ϕ_b.

2.2 Postulates

2.2.1 Postulate 1 - At peak strength

At peak strength, immediately before failure, the strain e_p is known. At the instant after failure, a failure plane is formed with an effective angle of friction, ϕ_{ep}, and the strain remains at e_p. **It is postulated that** the peak strain is a functional relationship of the peak effective angle of friction.

$$\phi_p = f(e_p) \tag{2.3}$$

2.2.2 Postulate 2 - Beyond peak strength

At any point in the post peak region, prior to and including the residual strength, the strain is **postulated** as being described by the same functional relationship.

$$\phi_e = f(e_{pp}) \tag{2.4}$$

2.3 Assumptions

2.3.1 Assumption 1 - Pre-peak modulus

It is assumed that the pre-peak modulus, E is defined as the straight line relationship defined by the peak σ_{1p}, e_p values, such that:

$$E=\frac{\sigma_{1p}}{e_p} \tag{2.5}$$

2.3.2 Assumption 2 - Peak strength relationship

It is assumed that the peak strength is governed by the Hoek-Brown failure criterion, (Hoek et al, 1980):

$$\sigma_{1p}=\sigma_3+[m\sigma_c\sigma_3+s\sigma_c^2]^{1/2} \tag{2.6}$$

Where m and s are constants and σ_c is the uniaxial unconfined compressive strength of the rock.

2.3.3 Assumption 3 - Residual strength relationship

It is assumed that the residual strength is described by a 2nd order polynomial criterion:

$$\sigma_{1r}=D\sigma_3^2+F\sigma_3+\sigma_{cr} \tag{2.7}$$

Where D and F are constants and σ_{cr} is the unconfined residual strength.

2.3.4 Assumption 4 - Base strength relationship

It is assumed that the base strength, σ_{1b} is described by the Coulomb-Navier rearrangement:

$$\sigma_{1b}=K\sigma_3=\frac{(1+\sin\phi_b)}{(1-\sin\phi_b)}\sigma_3 \qquad 2.8$$

Where K is the σ_{1b} - σ_3 base strength relationship, and ϕ_b is the base angle of friction.

2.3.5 Assumption 5 - Relationship between the peak, residual and base strengths

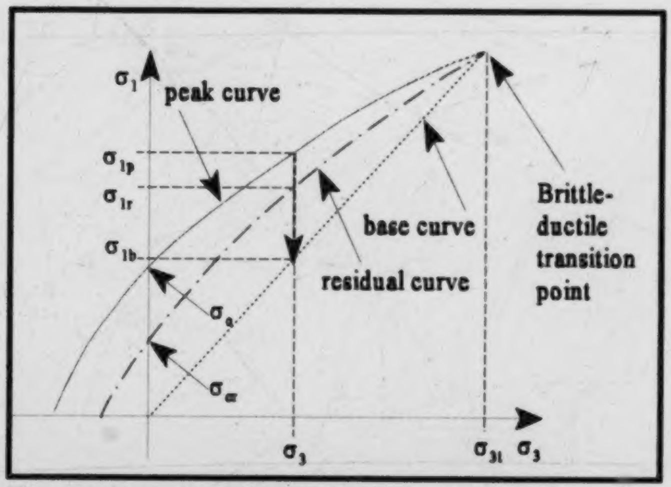
σ_1
peak curve
σ_{1p}
σ_{1r}
σ_{1b}
base curve
residual curve
Brittle-ductile transition point
σ_c
σ_{cr}
σ_3
σ_{3t}
σ_3

Figure 2.2: Peak, residual and base strength criteria

It is assumed, as illustrated in figure 2.2, that:

i At zero confinement, $\sigma_{1p} = \sigma_c$, $\sigma_{1r} = \sigma_{cr}$, and $\sigma_{1b} = 0$

ii At the brittle-ductile transition confinement, $\sigma_{1p} = \sigma_{1r} = \sigma_{1b}$

2.3.6 Assumption 6 - Friction - strain functional relationship

The functional relationship outlined by the postulates is assumed to be given by a 2nd order polynomial. The polynomial form was chosen as being the simplest function that gave a reasonable fit to all the available data, (see chapters 4 and 5).

$$\phi_e = R + Se_{pp} + Te_{pp}^2 \qquad 2.9$$

Where R, S and T are constants for a given rock type, and e_{pp} is measured from the zero strain datum.

2.3.7 Assumption 7 - Friction - strain minimum at the brittle-ductile transition point

It is assumed that the ϕ_e polynomial, equation 2.9, exhibits a minimum corresponding to the base strain, e_b, at the brittle-ductile transition point, $(\sigma_{1t}, \sigma_{3t})$.

$$\frac{\delta\phi_e}{\delta e_{pp}} = 0 \qquad 2.10$$

This arises from the fact that at the brittle-ductile transition point, the confinement is sufficient that an applied stress to cause motion along the fracture plane will only encounter a base friction resistance, since all of the asperities have been eroded to a smooth surface. Thus for any further increase in strain under those conditions, the frictional resistance will be constant. So the change in frictional response for any given change in strain will be zero. The strain accumulated at the point of brittle-ductile transition must therefore be the base strain, e_b.

If equation 2.10 is applied to equation 2.9, the result is

$$\frac{\delta\phi_e}{\delta e_{pp}}=S+2Te_{pp}=0 \qquad 2.11$$

Or

$$e_b=\frac{-S}{2T} \qquad 2.12$$

2.3.8 Assumption 8 - Peak strength - residual strength relationships at the brittle ductile transition point

At the transition point, (σ_{1t}, σ_{3t}), the peak, σ_{1p} and residual, σ_{1r} strengths are equal, as explained in section 2.3.5. Further, the slopes of the functions describing σ_{1p} and σ_{1r} are also equal at the brittle-ductile transition point.

$$\sigma_{1p}=\sigma_{1r}=\sigma_{1b} \qquad \frac{\delta\sigma_{1p}}{\delta\sigma_3}=\frac{\delta\sigma_{1r}}{\delta\sigma_3} \qquad 2.13$$

2.3.9 Assumption 9 - Post peak modulus

The post peak modulus is defined as the slope of the post peak stress-strain curve

$$E_{pp}=\frac{\delta\sigma_{pp}}{\delta e_{pp}} \qquad 2.14$$

Where $\delta\sigma_{pp}$ is a change post peak stress corresponding to a change in post peak strain, δe_{pp}.

Chapter 3

The Joseph-Barron approach (applied to intact rock)

The Joseph-Barron approach relies on certain data being available. The minimum requirement is peak data from a number of triaxial tests including values for σ_3, σ_{1p} and e_p, and a value for the base angle of friction, ϕ_b obtained from a tilt test. The optimum requirement would be the complete stress-strain information from a number of triaxial tests including values for σ_3, σ_{1p}, e_p, σ_{1r}, and e_r, from which a more accurate value for the base angle of friction may be calculated without resorting to a tilt test. There are therefore two cases of analysis via the Joseph-Barron approach, dependent on the availability of data:

i Peak and residual data approach

ii Peak data and base friction approach

For the purposes of this discussion, case i is assumed. Divergence from the procedure for case ii is described in section 3.10.

3.1 Determination of the Hoek-Brown strength criterion constants

The Hoek-Brown constants, m and σ_c are determined via a re-arrangement of the Hoek-Brown peak strength criterion, equation 2.6, into a linear form and solving for the slope and intercept where s = 1 for intact rock (Hoek et al, 1980):

$$(\sigma_{1p}-\sigma_3)^2 = m\sigma_c\sigma_3 + s\sigma_c^2 \qquad 3.1$$

Where the slope = $m\sigma_c$ and the intercept = $s\sigma_c^2$.

3.2 Determination of the residual strength polynomial constants and σ_{3t} via polynomial regression analysis

The order in which the residual strength polynomial constants D and F, equation 2.7, and the brittle-ductile confining pressure, σ_{3t} are determined depends on the availability of sufficient triaxial test data in proximity to the brittle-ductile transition point.

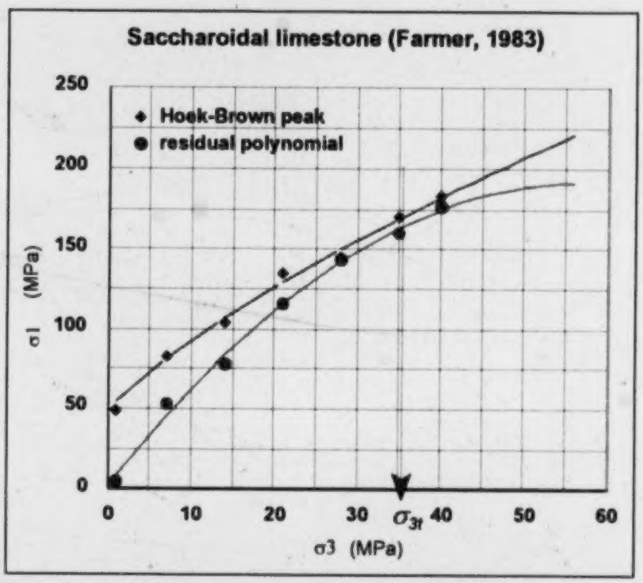

Figure 3.1: 2nd order polynomial regression of residual data plotted with Hoek-Brown peak strength values to attempt to identify σ_{3t} at the brittle-ductile transition point

If the available triaxial test data spans a range of σ_3 from unconfined to the brittle-ductile transition point, then it is more likely that a 2nd order polynomial regression of the available residual data (Visman et al., 1970) plotted with the Hoek-Brown peak strength criterion versus σ_3 will yield a brittle-ductile transition point and hence a value for σ_{3t}. Figure 3.1 illustrates a reasonable brittle-ductile transition point identification. The polynomial regression in this case yielded values for D, F and σ_{cr} directly as demonstrated in appendix A. Conversely, figure 3.2 illustrates a case with data far removed from the brittle-ductile transition point, such that the transition is not identifiable.

In the case where D, F and σ_{cr} are identified through a 2nd order polynomial regression, σ_{3t} is alternatively defined by equating the Hoek-Brown peak strength criterion, where m, σ_c and s are known, to the 2nd order residual polynomial and solving for σ_{3t}. A spreadsheet is necessary for this solution, as the combination of two 2nd order equations requires a quartic determination.

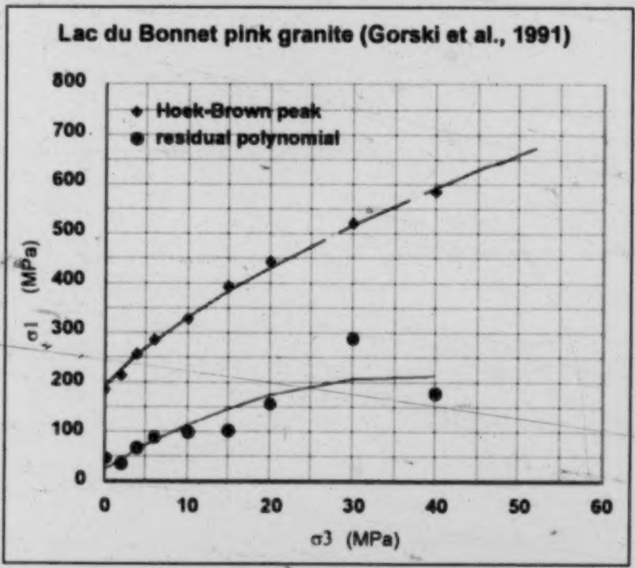

Figure 3.2: 2nd order polynomial of residual data plotted with Hoek-Brown strength values for no identification of σ_{3t} at the brittle-ductile transition point.

3.3 Estimation of the residual strength polynomial constants and σ_{3t} via a linear approximation of the available residual strength data

If a brittle-ductile transition point is not identified through polynomial regression, then the determined values of D, F and σ_{cr} by this method, appendix A, may not be relied on, and an alternative approach must be employed.

In such a case, a linear regression of the available residual strength data, figure 3.3, allows a direct evaluation of σ_{cr} at zero confinement, and an approximation of σ_{3t} when the linear form is equated with the peak strength criterion at the instance of brittle-ductile transition. The linear residual strength criterion is expressed as:

$$\sigma_{1r}=\sigma_{cr}+G\sigma_3 \qquad 3.2$$

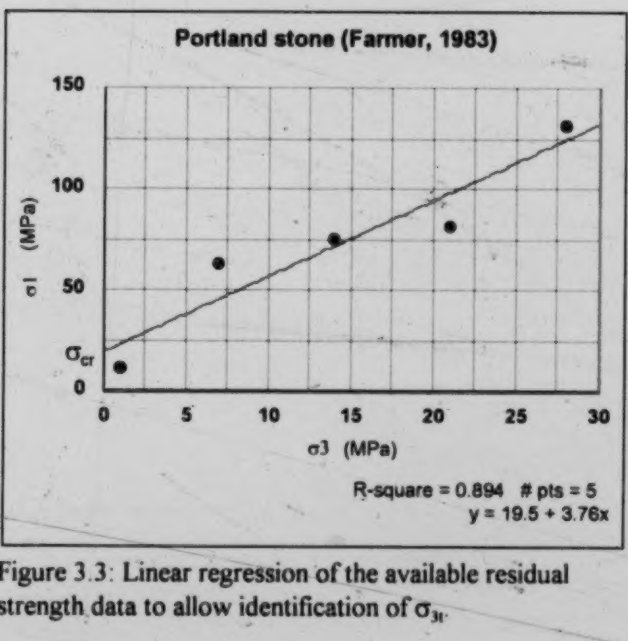

Figure 3.3: Linear regression of the available residual strength data to allow identification of σ_{3t}.

Equating 2.6 and 3.2, allows a linear approximation for σ_{3t}:

$$\sigma_{3t}+[m\sigma_c\sigma_{3t}+s\sigma_c^2]^{1/2}=G\sigma_{3t}+\sigma_{cr}$$

$$(G-1)^2\sigma_{3t}^2+(2\sigma_{cr}(G-1)-m\sigma_c)\sigma_{3t}+\sigma_{cr}{}^2-s\sigma_c^2=0$$

$$\sigma_{3t}=\frac{-(2\sigma_{cr}(G-1)-m\sigma_c)+\sqrt{(2\sigma_{cr}(G-1)-m\sigma_c)^2-4(G-1)^2(\sigma_{cr}^2-s\sigma_c^2)}}{2(G-1)^2} \qquad 3.3$$

Having employed the linear approximation process to identify a value for σ_{3t}, the residual polynomial constants D and F may be determined while keeping the values of σ_{3t} and σ_{cr} as fixed end points for the polynomial function. The evaluation is carried out at the brittle-ductile transition point where the peak and residual strength values are identical, $\sigma_{1p} = \sigma_{1r}$ and the slopes of their respective functions are also identical, equation 2.13. Appendix E provides a step by step solution for D and F culminating in equations 3.4 and 3.5 respectively.

$$D=\frac{1}{\sigma_{3t}^2}[\sigma_{cr}-[m\sigma_c\sigma_{3t}+s\sigma_c^2]^{1/2}+\frac{m\sigma_c\sigma_{3t}}{2[m\sigma_c\sigma_{3t}+s\sigma_c^2]^{1/2}}] \qquad 3.4$$

$$F=1-\frac{m\sigma_c}{2[m\sigma_c\sigma_{3t}+s\sigma_c^2]^{1/2}}-\frac{2}{\sigma_{3t}}[\sigma_{cr}-[m\sigma_c\sigma_{3t}+s\sigma_c^2]^{1/2}] \qquad 3.5$$

By back substitution into the 2nd order residual polynomial form

$$\sigma_{1r}=\frac{\sigma_3}{\sigma_{3t}}([\frac{\sigma_3}{\sigma_{3t}}-1][\sigma_{cr}-[m\sigma_c\sigma_{3t}+s\sigma_c^2]^{1/2}+\frac{m\sigma_c\sigma_{3t}}{2[m\sigma_c\sigma_{3t}+s\sigma_c^2]^{1/2}}]-\sigma_{cr}+[m\sigma_c\sigma_{3t}+s\sigma_c^2]^{1/2})+\sigma_3+\sigma_{cr}$$

3.4 Refinement of the residual strength polynomial constants D and F originally determined via a linear approximation process

In most reported cases for rock, triaxial data results tend to be closer to zero confinement than to the brittle-ductile transition confining pressure, due to the difficulty in maintaining sufficiently high confining pressures closer to the transition point. In these cases a linear approximation to the available data provides a reasonable regression value, often greater than 0.95.

Since the polynomial constant values of D and F are based on the linear approximation constant G, an iterative optimization process can be performed to enhance the residual curve at the higher unreported values of σ_3.

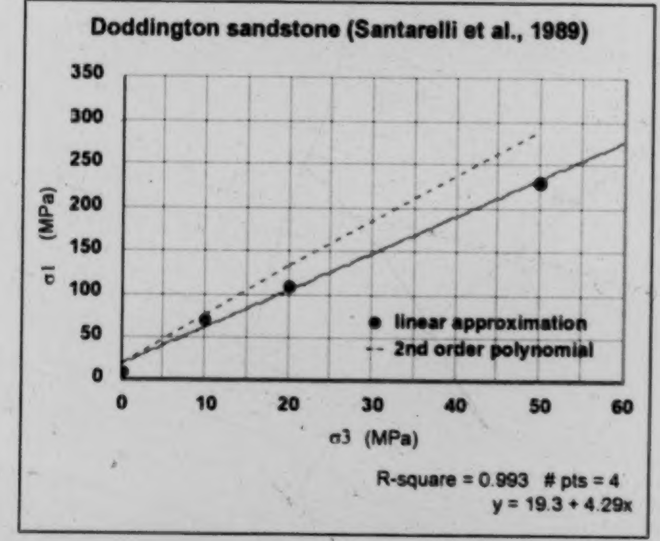

Figure 3.4: Modification of residual polynomial function based on lower confinement linear interpretation.

By plotting σ_{1r} determined via the residual polynomial together with the σ_{1r} determined via the linear approximation versus σ_3, using a spreadsheet, such that any variation in G automatically varies D, F and σ_{3t} accordingly, the linear relation and the polynomial curve can be brought together, as illustrated in figure 3.4. This provides an agreement between the approximation and assumed function for residual strength at low confining pressures, and allows a better estimate of what is occurring at higher confinement. For this process σ_{cr}, σ_c, m and s are held constant.

3.5 Determination of the base angle of friction, ϕ_b

Given a value for σ_{3t}, the base angle of friction, ϕ_b can be determined, since the peak strength, σ_{1p}, equation 2.6 and the base strength, σ_{1b}, equation 2.8 command the same value, (σ_{3t}, σ_{1t}) at the brittle-ductile transition point. Hence, equating equations 2.6 and 2.8:

$$\sigma_{1t}=\sigma_{1p}=\sigma_{3t}+[m\sigma_c\sigma_{3t}+s\sigma_c^2]^{1/2}=\sigma_{1b}=\frac{1+\sin\phi_b}{1-\sin\phi_b}\sigma_{3t} \qquad 3.6$$

Re-arranging and letting $Q = (m\sigma_c\sigma_{3t} + s\sigma_c^2)^{1/2}$

$$Q=\sigma_{3t}[\frac{1+\sin\phi_b}{1-\sin\phi_b}-1]=\sigma_{3t}\frac{(1+\sin\phi_b)-(1-\sin\phi_b)}{1-\sin\phi_b}=\sigma_{3t}\frac{2\sin\phi_b}{1-\sin\phi_b}$$

$$Q-Q\sin\phi_b=2\sigma_{3t}\sin\phi_b$$

$$\phi_b=\sin^{-1}[\frac{Q}{2\sigma_{3t}+Q}]=\sin^{-1}[\frac{(m\sigma_c\sigma_{3t}+s\sigma_c^2)^{1/2}}{2\sigma_{3t}+(m\sigma_c\sigma_{3t}+s\sigma_c^2)^{1/2}}] \qquad 3.7$$

3.6 Determination of the effective friction - strain relationship

The effective friction, ϕ_e - post peak strain, e_{pp} relationship introduced as equation 2.9 in section 2.3.6 is bounded by conditions that restrict its applicability to the region of confinement between unconfined and the brittle-ductile transition point. Thus the general expression in 2.9 can be rewritten:

$$\phi_e = R + Se_{pp} + Te_{pp}^2 \qquad 2.9$$

$$\phi_p = R + Se_p + Te_p^2 \qquad 3.8$$

$$\phi_b = R + Se_b + Te_b^2 \qquad 3.9$$

Figure 3.5 illustrates the boundary conditions applied to generalized form of the 2nd order polynomial effective friction - strain relationship.

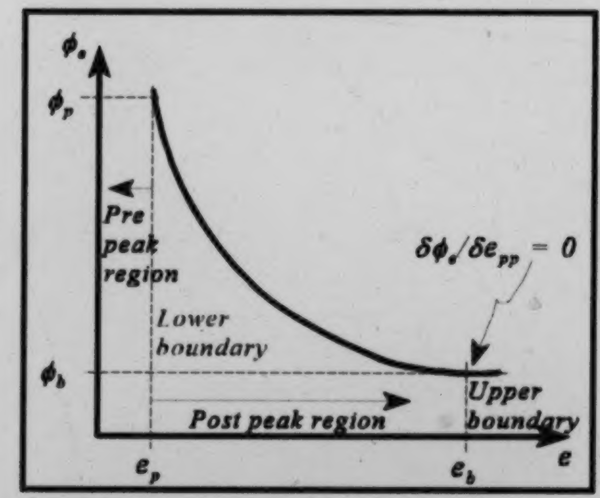
ϕ_e
ϕ_p
Pre peak region
$\delta\phi_e/\delta e_{pp} = 0$
Lower boundary
ϕ_b
Upper boundary
Post peak region
e_p
e_b
e

Figure 3.5: Boundary conditions for the effective friction - strain 2nd order polynomial function

In the unconfined state at peak strength, σ_{1p} a fracture plane forms with an effective angle of friction ϕ_p corresponding to an amount of strain, e_p. This is represented by the lower boundary condition imposed on equation 2.9, as expressed by equation 3.8 and illustrated in figure 3.5

At the brittle-ductile transition point (σ_{3t}, σ_{1t}) the fracture plane is now a smooth basal surface with an effective angle of friction ϕ_b corresponding to an amount of strain, e_b. This is represented by the upper boundary condition imposed on equation 2.9, as expressed by equation 3.9 and illustrated in figure 3.5

It has been shown in section 2.3.7 that there is a minimum with respect to the friction - strain function, since beyond the brittle-ductile transition point there is no further decrease in effective friction for any further increase in strain beyond e_b. That is for any strain greater than e_b, ϕ_b is a constant, as shown in figure 3.5. This allows the minimum to yield a value for e_b as in equation 2.12:

$$e_b = \frac{-S}{2T} \tag{2.12}$$

Appendix C solves equations 3.8, 3.9 and 2.12 simultaneously for the polynomial constants R, S and T, equations 3.12, 3.11 and 3.10 respectively,

$$T = \frac{(\phi_p - \phi_b)}{(e_b - e_p)^2} \tag{3.10}$$

$$S = -2e_b \frac{(\phi_p - \phi_b)}{(e_b - e_p)^2} \tag{3.11}$$

$$R=\phi_b+e_b^2\frac{(\phi_p-\phi_b)}{(e_b-e_p)^2} \qquad 3.12$$

and the general solution for the effective friction - strain polynomial 3.13.

$$\frac{(\phi_e-\phi_b)}{(\phi_p-\phi_b)}=\frac{(e_b-e_{pp})^2}{(e_b-e_p)^2} \qquad 3.13$$

3.7 Estimate of the base strain at the brittle-ductile transition point

As previously stated in 2.3.7, the base strain, e_b can be determined from the minimum condition at the brittle-ductile transition point. However, use of the available strength and strain data can be made to provide a graphical evaluation of e_b directly, appendix F.

3.7.1 Determination of ϕ_e from the available data

Equation 2.2 can be expanded in terms of σ_3, σ_1 and 2θ via the Mohr-Coulomb τ and σ relationships, where σ_1 may be either peak or residual strength provided that the associated strain e_p or e_r respectively is noted.

2θ is described after the work of Balmer (1952), appendix G, equation 3.14, and will remain constant once the fracture plane has been formed at peak strength. This allows the use of the same 2θ to evaluate peak and residual effective frictions for a given value of σ_3. It also follows that the value of 2θ determined at peak strength must be valid for any value of effective friction in the post peak region lying between peak and residual. This is illustrated in figure 2.1.

$$2\theta = 2\tan^{-1}\left[\sqrt{\frac{\delta\sigma_1}{\delta\sigma_3}}\right] \tag{3.14}$$

When the differential of σ_1 with respect to σ_3 is applied to the Hoek-Brown peak strength criterion the following result is obtained:

$$\frac{\delta\sigma_1}{\delta\sigma_3} = 1 + \frac{m\sigma_c}{2(m\sigma_c\sigma_3 + s\sigma_c^2)^{1/2}} \tag{3.15}$$

The effective angle of friction for any strength condition in the post peak region has been previously defined as:

$$\phi_e = \tan^{-1}\left[\frac{\tau}{\sigma}\right] \tag{2.2}$$

From the geometry of Mohr's circle, figure 2.1, equation 2.2 can be redefined:

$$\phi_e = \tan^{-1}\left[\frac{(\sigma_{pp} - \sigma_3)\sin 2\theta}{(\sigma_{pp} + \sigma_3) + (\sigma_{pp} - \sigma_3)\cos 2\theta}\right] \tag{3.16}$$

Where σ_{pp} is any value of post-peak stress including both peak and residual strengths for a given value of σ_3. This relationship may then be applied to the available peak and residual strength data gleaned from triaxial tests. Each value of ϕ_e determined by this method should be paired with its corresponding strain measurement from the available data. In this format a value for e_b may be determined..

3.7.2 Y vs e

The effective friction - strain relationship, equation 3.13, can be manipulated into a linear form, Y = MX + B, where X is the strain variable, e at the point of interest, M is the slope and B the intercept of the function. This manipulation is provided in appendix F, where the linear form is:

$$Y=\sqrt{\frac{(\phi_e-\phi_b)}{(\phi_p-\phi_b)}}=\frac{-e_{pp}}{(e_b-e_p)}+\frac{e_b}{(e_b-e_p)} \qquad 3.17$$

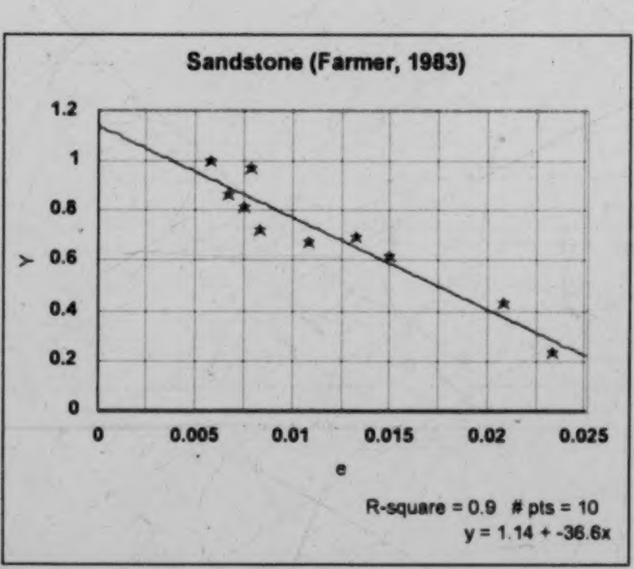

Figure 3.6: Y versus e plot to allow e_b interpretation from the slope.

Where the peak effective friction, ϕ_p and peak strain, e_p are taken as the unconfined lower boundary limit values, figure 3.5, at $\sigma_3 = 0$; and the base friction, ϕ_b has previously been determined in section 3.5, equation 3.7. An example plot of this graphical interpretation process is illustrated in figure 3.6.

3.7.3 Estimate of the base strain

A measurement of the Y versus e slope through linear regression, figure 3.6, allows the best evaluation of e_b, since the linear regression process averages the available data.

$$e_b = \frac{-1}{M} + e_p \qquad 3.18$$

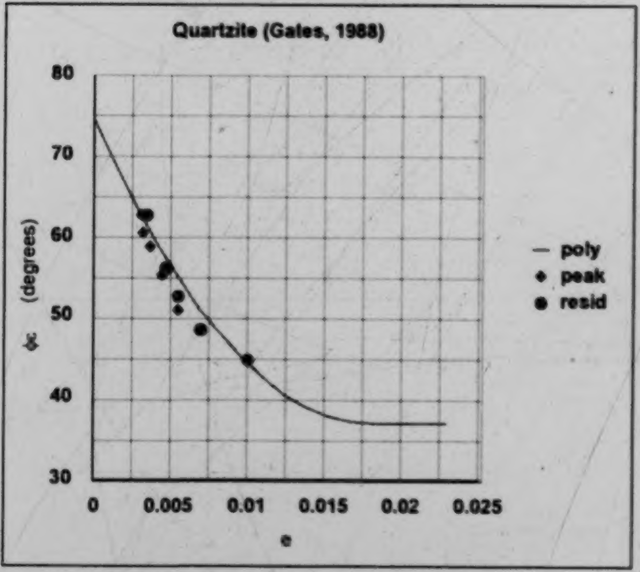

Figure 3.7: Example of an effective friction - strain function solution compared to the original data.

Once all constants are known; e_b, e_p, ϕ_b and ϕ_p; values for R, S, and T, equations 3.12, 3.11 and 3.10 respectively can be determined, and an solution for the effective friction - strain relationship, equation 3.13, figure 3.7, established.

3.8 Determination of the post peak modulus, and its normalized form

The post peak modulus, E_{pp} has been defined in equation 2.14 as the change in post peak stress for a given change in post peak strain:

$$E_{pp}=\frac{\delta\sigma_{pp}}{\delta e_{pp}} \qquad 2.14$$

Appendix B shows the derviation of the function in terms of quantities already defined resulting in the expression:

$$E_{pp}=\frac{\sin 2\theta}{\sin^2\phi_e}\frac{(\sigma_{pp}-\sigma_3)^2}{\sigma_3}\frac{(\phi_e-\phi_b)}{(e_{pp}-e_b)} \qquad 3.19$$

An example of the function is plotted in figure 3.8, showing the stepwise nature of the function with varying confinement.

The normalized form of the post peak modulus, $E_{pp(n)}$ allows a smooth continuous curve relation when plotted against post peak strain, e_{pp}, figure 3.9.

$$E_{pp(n)}=\frac{E_{pp}}{(\sigma_{pp}-\sigma_3)}=\frac{\sin 2\theta}{\sin^2\phi_e}\frac{(\sigma_{pp}-\sigma_3)}{\sigma_3}\frac{(\phi_e-\phi_b)}{(e_{pp}-e_b)} \qquad 3.20$$

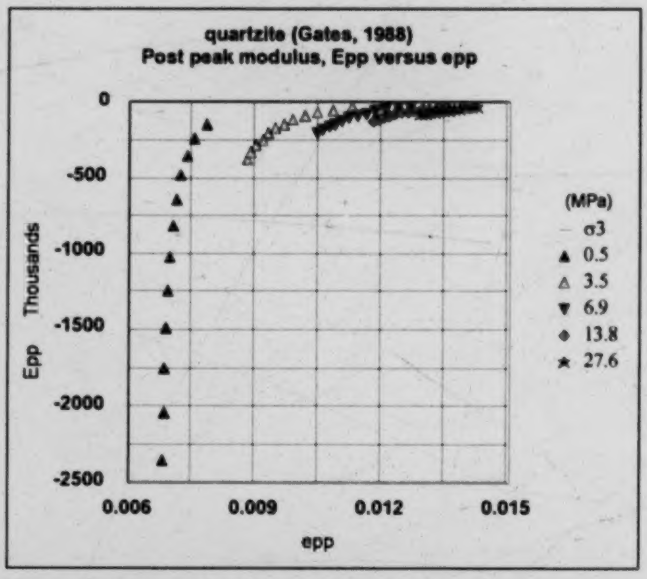

Figure 3.8: Example of post peak modulus plotted against post peak strain, described by equation 3.19

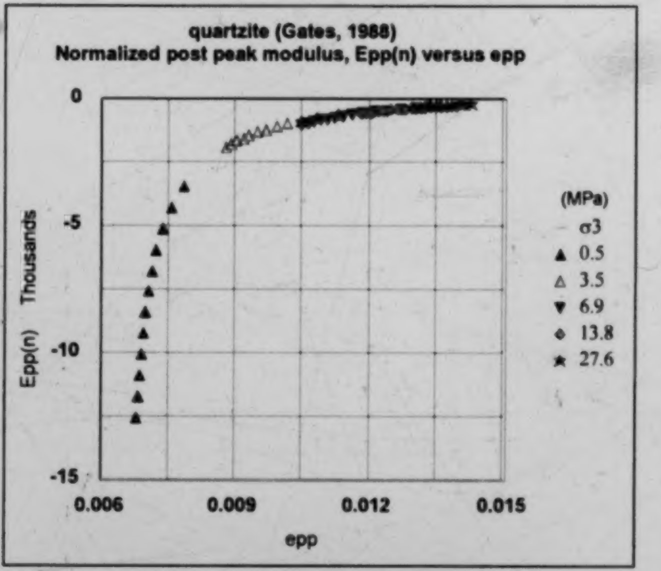

Figure 3.9: Example of normalized post peak modulus versus post peak strain as described by equation 3.20

3.9 Determination of the post peak stiffness

The post peak stiffness, k_{pp}, can be expressed in terms of the post peak modulus, E_{pp}, and the dimensions of the rock sample or pillar under investigation; cross-sectional area, A and height, H, for any degree of confinement, σ_3.

For a change in applied load, ΔF per unit change in height of a pillar, ΔH:

$$k_{pp} = \frac{\Delta F}{\Delta H} \qquad \text{kN/m} \qquad 3.21$$

But from equation 2.14:

$$E_{pp} = \frac{\delta\sigma_{pp}}{\delta e_{pp}} \qquad \text{GPa} \qquad 2.14$$

Where $\delta\sigma_{pp} = \Delta F/A$ and $\delta e_{pp} = \Delta H/H$. Therefore:

$$E_{pp} = \frac{\Delta F(H)}{\Delta H(A)} \qquad 3.22$$

Substituting 3.21 into 3.22 and re-arranging, an expression for k_{pp} is obtained:

$$k_{pp} = \frac{E_{pp}A}{H} \qquad 3.23$$

3.10 Variances to the Joseph-Barron approach when only peak strength triaxial data is available

As mentioned at the beginning of this chapter, in the absence of residual data it is not possible to determine a brittle-ductile transition point without first evaluating a base angle of friction. This has been successfully done using a simple tilt test on core samples (Stimpson, 1981) and will be discussed in chapter 5. Other methods of obtaining base angles of friction include the triaxial slip test and shear box test and are more complex in approach. They have been used to verify the applicability of the tilt test, as reported in chapter 5.

Given that the Hoek-Brown constants have been determined, since only peak data is required for that analysis, appendix D outlines the approach for determining the brittle-ductile transition confinement, σ_{3t}, via assumption 8 (section 2.3.8) where $\sigma_{1p} = \sigma_{1b}$ at the brittle-ductile transition point. The outcome is a positive root solution of a quadratic form yielding:

$$\sigma_{3t} = \frac{m\sigma_c + \sqrt{m^2\sigma_c^2 + 4(K-1)^2 s\sigma_c^2}}{2(K-1)^2} \qquad 3.24$$

Once σ_{3t} has been determined, the solutions for the residual strength polynomial, the effective friction - strain polynomial, and the post peak modulus are determined as outlined previously, with the following additional assumption.

Due to the absence of residual data, it is not possible to graphically estimate a value for the residual strength at zero confinement, σ_{cr}, as was conducted in section 3.3. Consequently, it is assumed that the residual strength, σ_{cr} is 20% of the uniaxial unconfined compressive strength, σ_c evaluated through the Hoek-Brown analysis, section 3.1. The choice of 20% is arbitrary. Variance of σ_{cr} values from 5% to 50% of σ_c revealed that there is a negligible effect on the determined value of the σ_{3t} boundary, as a result of varying the $\sigma_3 = 0$ boundary condition.

Again due to the absence of residual data to provide a linear approximation, the refinement process described in section 3.4 is not possible. However, as will be shown in chapters 4 and 5, the use of peak data only has little effect on the overall outcome of the analysis procedure.

3.11 Conclusion

The Joseph-Barron approach provides a means of quantifying the post peak behaviour via simply measured quantities. By keeping the choice of post peak function simple, as employed with 2nd order polynomial functions, the ease of use via a spreadsheet format makes this approach a useful partner to the triaxial testing process. Application and verification of this procedure follows in chapters 4 and 5.

Chapter 4

Intact rock - Verification of the postulates and assumptions via an example data set from the literature

4.1 The intact rock data set

The data set was selected on the following criteria:

i Both peak and residual strength and strain data were available to allow both the peak and residual data analysis and the peak data only analysis for comparison of the two approaches.

ii The available data were spread over a reasonable span of the range from zero to brittle-ductile transition confinement, but not necessarily to the latter confinement boundary.

iii The data were available in the form of stress-strain plots to allow comparison with the calculated/predicted stress-strain plots.

iv A value for the base angle of friction was available or calculable to allow the peak only data analysis.

The author identified 12 such data sets in the literature, of which a silty sandstone (Farmer, 1983) was selected for demonstration purposes. The other 11 data sets are provided for both the peak and residual analysis and peak only analysis in appendices H and J respectively.

Figure 4.1 shows the silty sandstone data set used. The peak strength values are clearly defined, however the residual strength values are a little more difficult to define due to the fluctuations in the residual region, particularly at the higher confining pressures. In those cases, the residual strength point was taken as the intersection of a best fit line passing through the residual region with a best fit line through the post peak region. The interpretation of the stress and strain values read from figure 4.1 are reported in table 4.1.

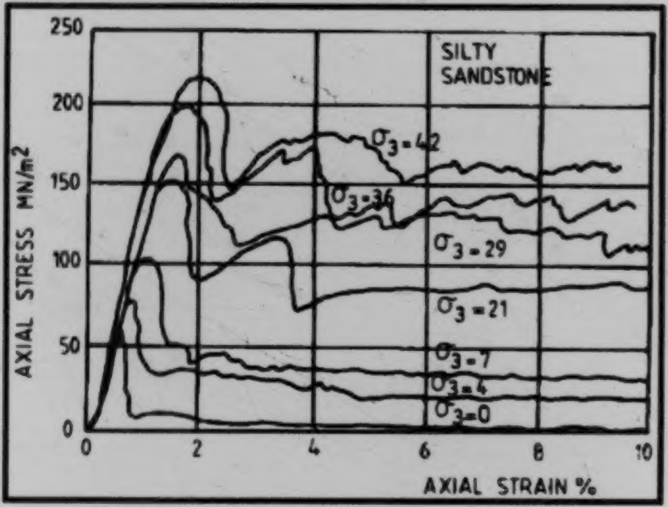

Figure 4.1: Silty sandstone data set, after Farmer (1983)

σ_3	σ_{1p}	σ_{1r}	e_p	e_r
(MPa)	(MPa)	(MPa)	(strain)	(strain)
0	64	9	0.006	0.009
4	81	35	0.008	0.013
7	108	42	0.01	0.018
21	151	93	0.015	0.019
29	172	116	0.016	0.026
36	202	142	0.017	0.023
42	221	154	0.019	0.025

Table 4.1: Silty sandstone data set interpretation from figure 4.1

4.2 Assuming that both peak and residual data are available

4.2.1 Determination of the peak strength criterion

The Hoek-Brown peak strength criterion (Hoek et al., 1980) was rearranged into the linear form, equation 3.1, and the peak strength and confinement data from table 4.1 used to create the plot in figure 4.2.

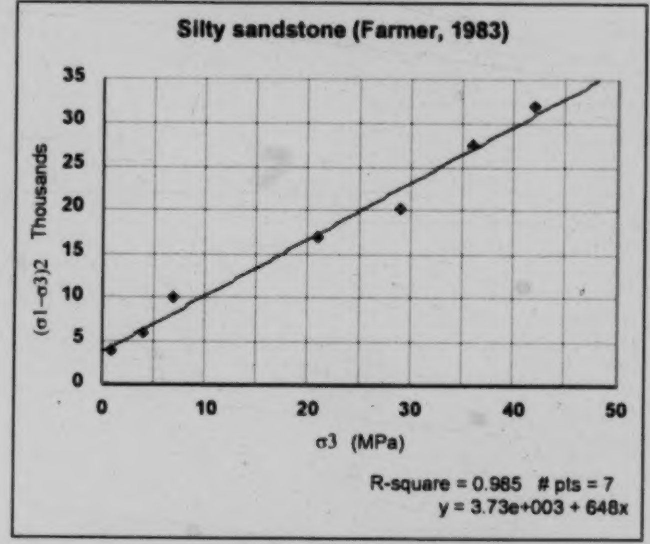

Figure 4.2: Linear form of the Hoek-Brown failure criterion applied to the silty sandstone data set.

The slope and the intercept were used to calculate the Hoek constant m and σ_c assuming that s = 1 for intact rock:

$$\sigma_c = \{\text{intercept}/s\}^{1/2} = \{3730/1\}^{1/2} = 61 \text{ MPa}$$

$$m = \text{slope}/\sigma_c = 648/61 = 10.6$$

or $$\sigma_{1p} = \sigma_3 + \{648\,\sigma_3 + 3730\}^{1/2} \qquad 4.1$$

4.2.2 Determination of the brittle-ductile transition point

Analysis of the σ_{1r} versus σ_3 data via polynomial regression (Visman, 1970) allowed an initial determination of the residual strength polynomial constants, D, F and σ_{cr} in equation 2.7, yielding:

$$\sigma_{1r} = -0.026\,\sigma_3^2 + 4.5\,\sigma_3 + 10.5 \text{ MPa} \qquad 4.2$$

Equations 4.1 and 4.2 were plotted together, but failed to identify a value for the brittle ductile transition point, (σ_{1t}, σ_{3t}), figure 4.3.

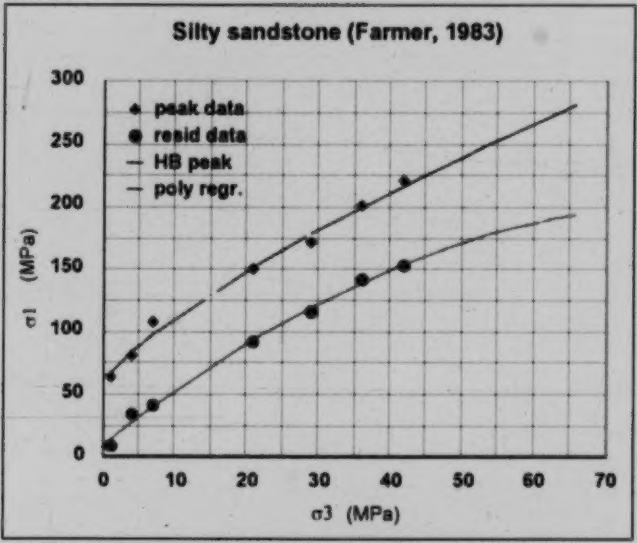

Figure 4.3: Plot of residual strength polynomial regression curve and peak strength curve with the original data to try and identify the brittle-ductile transition point.

From a review of figure 4.1 it can be seen that the data represents a range at confining pressures much lower than that required for brittle-ductile transition, thus the plot in figure 4.3 contains insufficient data points at high enough confinement to identify the brittle-ductile transition by the polynomial regression method. In addition, the values of the residual polynomial constants in equation 4.2 are not reliable, and the approximation approach for the brittle-ductile transition point, section 3.3, must be employed.

The σ_{1r} versus σ_3 data were plotted directly, figure 4.4, and a linear regression applied to determine the linear constants G and σ_{cr} in equation 3.2, equation 4.3.

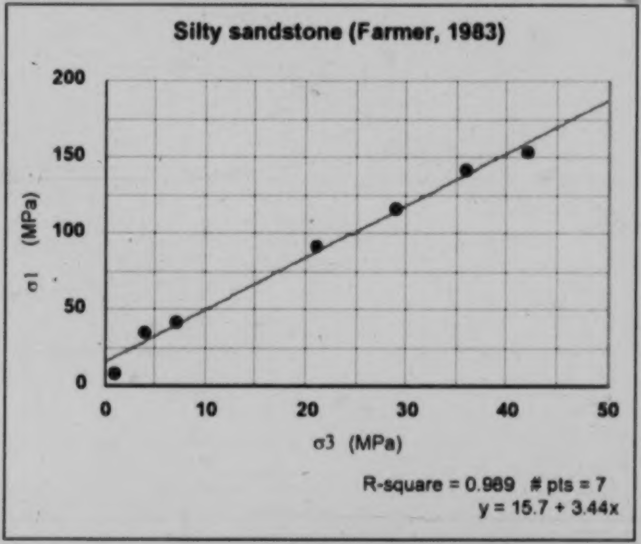

Figure 4.4: Evaluation of the residual strength linear approximation via linear regression of the available data.

$$\sigma_{1r} = 3.44\ \sigma_3 + 15.7\ \text{MPa} \qquad 4.3$$

Equating equations 4.1 and 4.3 according to the peak strength residual strength equality condition at the brittle-ductile transition confinement, assumption

8, section 2.3.8, allows the initial estimation of σ_{3t} as per equation 3.3.

$$\sigma_{3t} = 102 \text{ MPa}$$

4.2.3 Determination and refinement of the residual strength criterion

Fixing the value of σ_{3t} and retaining the value of σ_{cr} at σ_{cr} = 15.7 MPa, the values of the residual strength polynomial constants, D and F, can be re-calculated according to equations 3.4 and 3.5 respectively. This results in a new residual strength polynomial:

$$\sigma_{1r} = -0.012\,\sigma_3^2 + 4.7\,\sigma_3 + 15.7 \text{ MPa} \qquad 4.4$$

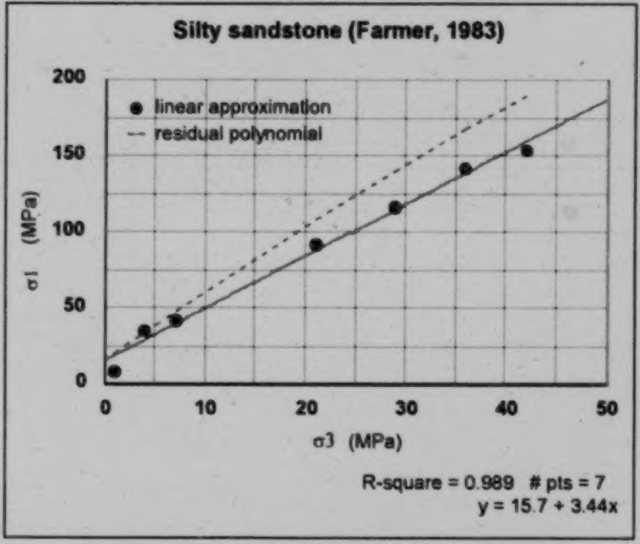

Figure 4.5: Residual strength polynomial and linear approximation plotted together to show error in the polynomial function at low confining pressures.

If equation 4.4 is plotted with the linear approximation in figure 4.4, then a visual error at the lower confining pressures where the original residual strength data was available becomes apparent, as illustrated in figure 4.5.

Using a spreadsheet connection, so that changes in the linear approximation are reflected by changes in the value of σ_{3t} and the residual strength polynomial, the iterative optimization refinement process outlined in section 3.4 can be put into practice. This allows the linear and polynomial residual strength criteria to agree at low confinement, in the region of available residual strength data, figure 4.6:

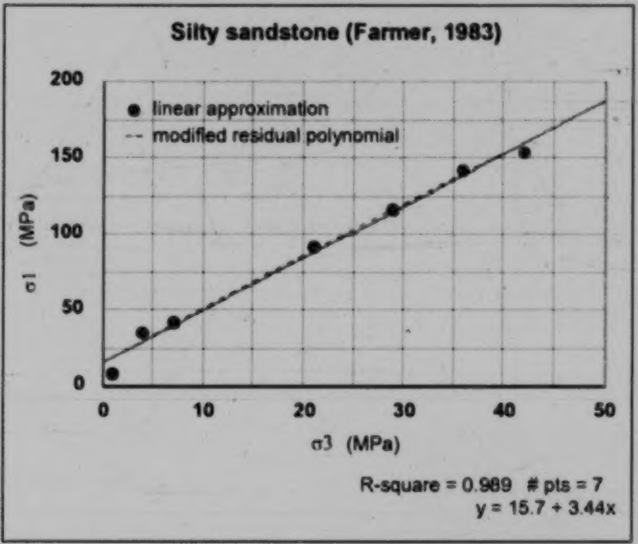

Figure 4.6: Effect of the refinement process for the residual strength polynomial at low confining pressures.

Consequently, σ_{3t} = 199 MPa and equation 4.4 becomes:

$$\sigma_{1r} = -0.004\,\sigma_3^2 + 3.6\,\sigma_3 + 15.7 \text{ MPa} \qquad 4.5$$

4.2.4 Estimation of the base angle of friction

Given that the confining pressure at the brittle-ductile transition point is known, σ_{3t}, the base angle of friction, ϕ_b, can be determined by equation 3.7:

$$\phi_b = 28.5^\circ$$

This allows a determination of the base strength criteria, as defined by equation 2.8, resulting in:

$$\sigma_{1b} = 2.8\,\sigma_3 \qquad 4.6$$

4.2.5 Comparison of the peak, residual and base strength criteria

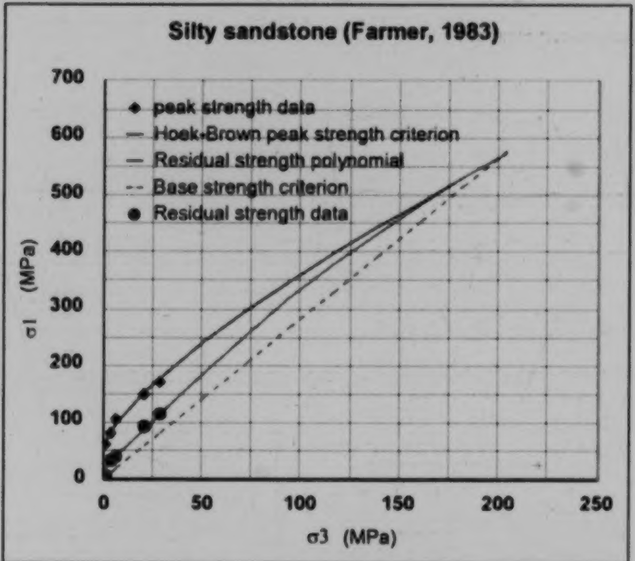

Figure 4.7: Comparison of peak, residual and base strength criteria in relation to zero confinement and the brittle-ductile transition point.

Figure 4.7 shows the graphical relation between the peak, residual and base strength criteria. For any σ_3 between zero and the brittle-ductile transition, there is a transition from peak to residual strength, that can be represented by an effective friction. At residual strength sufficient sliding roughness is retained along the plane of failure, such that there is a measure of roughness from residual to base strength. Only at the brittle-ductile transition point confinement, σ_{3t}, are the peak, residual and base strengths the same value, σ_{1t}.

The values of the peak and residual strength at zero confinement define the unconfined uniaxial compressive strength, σ_c and residual strength, σ_{cr} respectively.

4.2.6 Determination of the base strain, e_b, the R, S, and T constants, and the solution to the effective friction - strain polynomial

The general solution of the effective friction - strain polynomial is given by equation 3.13:

$$\frac{(\phi_e-\phi_b)}{(\phi_p-\phi_b)}=\frac{(e_b-e_{pp})^2}{(e_b-e_p)^2} \qquad 3.13$$

Which can be re-arranged into a linear form of Y versus e, as described in section 3.7.2:

$$Y=\sqrt{\frac{(\phi_e-\phi_b)}{(\phi_p-\phi_b)}}=\frac{-e}{(e_b-e_p)}+\frac{e_b}{(e_b-e_p)} \qquad 3.17$$

Where e is the available peak and residual strain variable, table 4.1, and ϕ_e can be determined for the corresponding available peak and residual strength data, table 4.1, via equation 3.16:

$$\phi_e = \tan^{-1}\left[\frac{(\sigma_{pp}-\sigma_3)\sin 2\theta}{(\sigma_{pp}+\sigma_3)+(\sigma_{pp}-\sigma_3)\cos 2\theta}\right] \qquad 3.16$$

Where σ_{pp} can be either the peak or residual strength variable and 2θ is given by the combination of equations 3.14 and 3.15, equation 4.7:

$$2\theta = 2\tan^{-1}\sqrt{1+\frac{m\sigma_c}{2(m\sigma_c\sigma_3+s\sigma_c^2)^{1/2}}} \qquad 4.7$$

In expression 3.17, ϕ_p and e_p are the effective friction and strain values under unconfined conditions, representing the maximum effective friction and the minimum strain of the post peak region as illustrated in figure 3.5. These values remain constant. The value of ϕ_b was previously determined in section 4.2.4 and also remains constant.

$\phi_p = 65°$

$e_p = 0.006$

$\phi_b = 28.5°$

A plot of Y versus e, figure 4.8, allows the base strain to be determined from the slope of the linear regression using equation 3.18.

$$e_b = -1/M + e_p = 1/28.3 + 0.0058 = 0.04$$

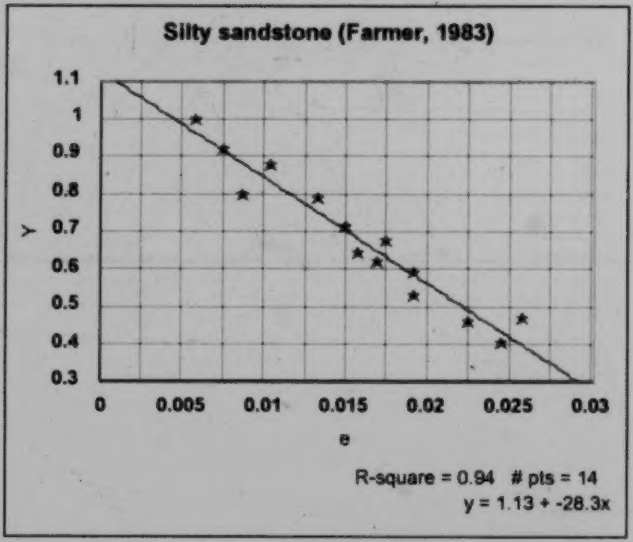

Figure 4.8: Plot of Y versus e to determine the base strain

Once all the constants in equation 3.13 have been determined, the values of the effective friction - strain polynomial constants, R, S and T, equation 2.9, can be determined via equations 3.12, 3.11 and 3.10 respectively:

$R = 79^\circ$
$S = -2430\ ^\circ/\text{strain}$
$T = 29600\ ^\circ/\text{strain}^2$

Therefore the exact solution for the effective friction - strain polynomial for the silty sandstone data set becomes:

$$\phi_e = 79 - 2430\, e_{pp} + 29600\, e_{pp}^2 \qquad 4.8$$

4.2.7 Comparison of ϕ_e-e curve with the ϕ_e-e data - verification

A plot of the effective friction values determined from the available data via equation 3.16 against the corresponding available strain data and the effective friction-strain polynomial shows that there is good agreement between the derived function and the available data, figure 4.9:

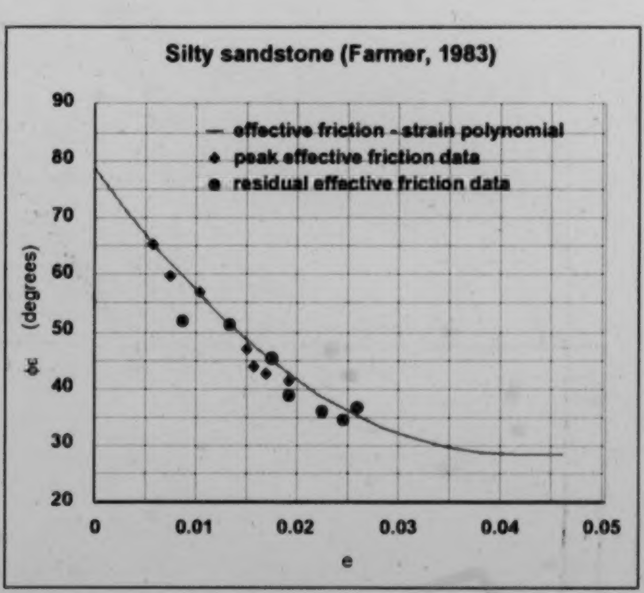

Figure 4.9: Correlation between the effective friction - strain polynomial and the effective friction data values

This correlation verifies postulates 1 and 2. **There exists a functional relationship between effective friction and post peak strain, and that relationship holds for all values between peak and residual strength regardless of the confinement imposed on the rock.**

If it is considered that the degree of fracturing in the post peak region is a function of the applied confinement, σ_3, then for an incremental increase in confinement, the range of peak to residual strengths for the respective confinements will overlap and the effective frictions will overlap, but all will lie on the curve. Therefore, all strains in the post peak region, not just those at peak and residual strength, at varying degrees of effective friction will lie on the same curve.

Once defined, the effective friction - strain relationship allows the prediction of the effective friction for any given amount of post peak strain, e_{pp}.

4.2.8 Reconstruction of the σ - e curves and original comparison

Given that the peak strength, residual strength and effective friction - strain exact solutions for the rock under investigation are known, equations 4.1, 4.5 and 4.8 respectively, and given expressions for ϕ_e, equation 3.6 and 2θ, equation 4.7, for any σ_3 between zero and the brittle-ductile transition point, a post peak stress-strain plot can be created. The following is a step by step process provided as a guideline:

i Select a value of σ_3 between zero and the brittle-ductile transition.

ii Calculate a value for σ_{1p} from equation 4.1.

iii Determine a value for 2θ from equation 4.7.

iv Calculate a value of σ_{1r} from equation 4.5.

v Divide the range from σ_{1p} to σ_{1r} into equal increments of σ_{pp}.

vi For each incremented value determine a value of ϕ_e from equation 3.16.

vii For each value of ϕ_e solve equation 4.8 for e_{pp}.

viii Plot the post peak stress strain plot from σ_{pp} versus e_{pp}.

The same set of confining pressures reported in the original data set, (Farmer, 1983), were used to create the predicted stress-strain curves which were compared to the original curve set in figure 4.1, as illustrated in figure 4.10.

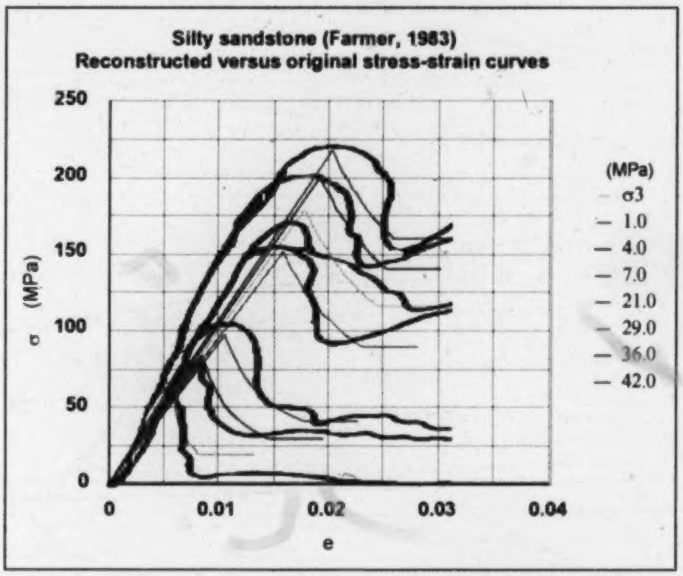

Figure 4.10: Comparison of the reconstructed with the actual stress strain curves for the silty sandstone data set.

Since the Joseph-Barron approach does not look at the pre-peak region, but solely the post peak region from peak to residual strength, the pre-peak regions are not of prime importance in the comparison. However, it has been assumed in section 2.3.1 that the pre-peak region behaves according to the modulus expression, equation 2.5.

The post peak portions of the predicted stress-strain curves appear to match the original data curves well, thus verifying the approach.

4.2.9 The normalized post peak modulus

The normalized post peak modulus, $E_{pp(n)}$, as described in equation 3.20 has been plotted in figure 4.11 as a function of post peak strain, e_{pp}.

$$E_{pp(n)} = \frac{E_{pp}}{(\sigma_{pp}-\sigma_3)} = \frac{\sin 2\theta}{\sin^2\phi_e}\frac{(\sigma_{pp}-\sigma_3)}{\sigma_3}\frac{(\phi_e-\phi_b)}{(e_{pp}-e_b)} \qquad 3.20$$

The values of the constants ϕ_b and e_b are known, and all other parameters in equation 3.20 are discernable for a given value of σ_3 and a selected value of σ_{pp}.

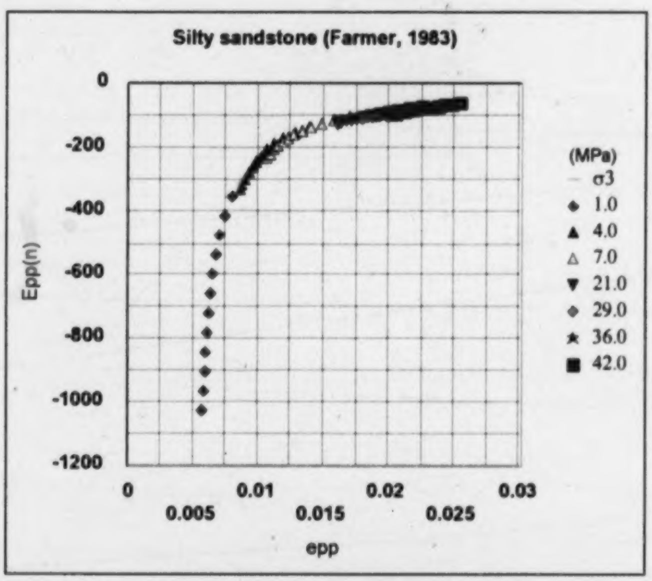

Figure 4.11: Plot of normalized post peak modulus versus post peak strain for a range of σ_3 and σ_{pp} values

As can be seen from figure 4.11, regardless of the choice of σ_{pp} between the determined values of σ_{1p} and σ_{1r} associated with a given value of σ_3, there exists a continuous relationship between $E_{pp(n)}$ and e_{pp}.

4.3 Assuming that only peak data is available

4.3.1 Determination of the peak strength criterion

The peak strength criterion evaluation is conducted in exactly the same fashion as in section 4.2.1, resulting in equation 4.1:

$$\sigma_{1p} = \sigma_3 + \{648\,\sigma_3 + 3730\}^{1/2} \qquad 4.1$$

4.3.2 Estimation of the base angle of friction, ϕ_b

Since no residual data is available in this case, it is not possible to calculate the brittle-ductile transition point without first knowing the base angle of friction, ϕ_b, which can be evaluated by one of several methods as mentioned in section 3.10.

To allow a direct comparison of all other parameters involved in the Joseph-Barron approach, the base angle of friction has been set for this verification at the same value estimated in section 4.2.4, resulting in the base strength criterion, equation 4.6. Section 4.5 discusses the effect of varying the base angle of friction.

$$\phi_b = 28.5^{\circ}$$

$$\sigma_{1b} = 2.8\,\sigma_3 \qquad 4.6$$

4.3.3 Determination of the brittle-ductile transition point confinement

The brittle-ductile transition point confinement, σ_{3t}, is found by equating equations 4.1 and 4.6 in accordance with assumption 8, section 2.3.8, resulting in the solution to equation 3.24, equation 4.9:

$$\sigma_{3t} = \frac{648 + \sqrt{648^2 + 4(2.83-1)^2 3730}}{2(2.83-1)^2} \qquad 4.9$$

$$\sigma_{3t} = 199 \text{ MPa}$$

The value of σ_{3t}, as would be expected since both the peak and base strength criteria are the same as used in section 4.3, is the same quantity determined from the available peak and residual data Joseph-Barron approach.

4.3.4 Determination of the residual strength polynomial

The residual strength polynomial constants, D and F are evaluated using equations 3.4 and 3.5, as conducted in section 4.2.3. However, due to the absence of residual strength data from which to evaluate σ_{cr}, an approximation at 20% σ_c is assumed as per the discussion in section 3.10. The resulting residual strength polynomial differs only via the choice of σ_{cr}, and its corresponding effects on the determination of D and F, equation 4.10:

$$\sigma_{cr} = 0.2(61) = 12.2 \text{ MPa}$$

$$\sigma_{1r} = -0.004\,\sigma_3^2 + 3.7\,\sigma_3 + 12.2 \text{ MPa} \qquad 4.10$$

4.3.5 Comparison of the peak, residual and base strength criteria

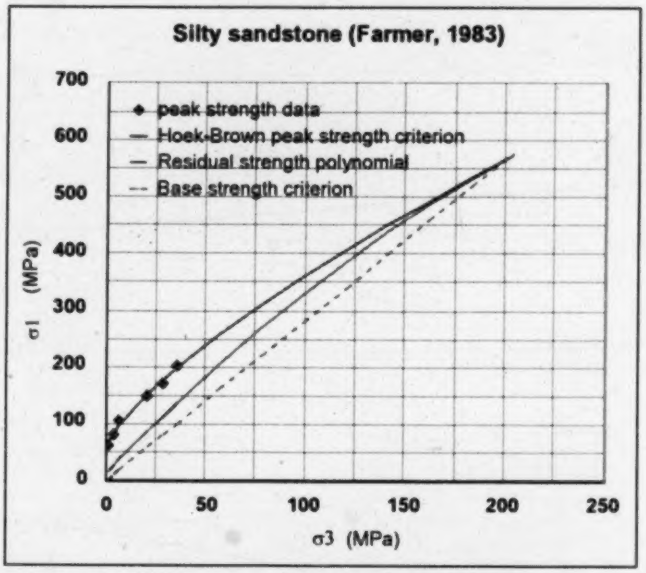

Figure 4.12: Comparison of peak, residual and base strength criteria in relation to zero confinement and the brittle ductile transition point using peak data only

The comparison of the peak data only evaluated strength criteria, illustrated in figure 4.12 provides an equally viable set of criteria, as illustrated in figure 4.7 for the peak and residual data approach.

4.3.6 Determination of the base strain, e_b, the R, S, and T constants, and the solution to the effective friction - strain polynomial

The base strain, R, S and T constants, and ϕ_e - e_{pp} polynomial are evaluated by the same approach described in section 4.2.6. The values of ϕ_p and e_p are still available since these are peak values, and ϕ_b is known:

$$\phi_p = 65°$$
$$e_p = 0.006$$
$$\phi_b = 28.5°$$

The plot of Y versus e is different since the previous evaluation in figure 4.8 included the residual data, which is no longer available. Figure 4.13 illustrates the Y versus e plot using the peak data only, which allows a slightly different base strain to be determined from the slope of the linear regression using equation 3.18.

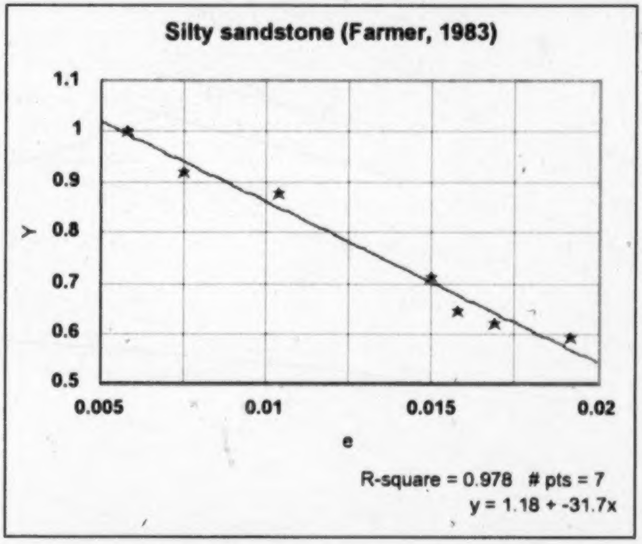

Figure 4.13: Plot of Y versus e to determine the base strain using the available peak data only.

$$e_b = -1/M + e_p = 1/31.7 + 0.006 = 0.04$$

(The same as $e_b = 0.04$ in the previous analysis)

The values of R, S and T are evaluated as before from equations 3.12, 3.11 and 3.10 respectively, leading to a solution of the effective friction - strain polynomial, equation 4.11.

$R = 80^\circ$

$S = -2770\ ^\circ/\text{strain}$

$T = 37100\ ^\circ/\text{strain}^2$

Therefore the exact solution for the effective friction - strain polynomial for the silty sandstone data set becomes:

$$\phi_e = 80 - 2770\, e_{pp} + 37100\, e_{pp}^{\ 2} \qquad 4.11$$

This function is compared with that for the peak and residual data availability case in section 4.4.

4.3.7 Comparison of ϕ_e-e curve with the ϕ_e-e data - verification

As found for the peak and residual data case, section 4.2.7, a plot of the effective friction determined from the peak data via equation 3.16 against the corresponding peak strain data, and the effective friction polynomial, equation 4.11, shows good agreement between the derived function and the available data. This is illustrated in figure 4.14.

Once again it can be said that the correlation verifies postulates 1 and 2. There exists a functional relationship between effective friction and post peak strain, and the relationship holds for all values of peak strength regardless of the confinement imposed on the rock.

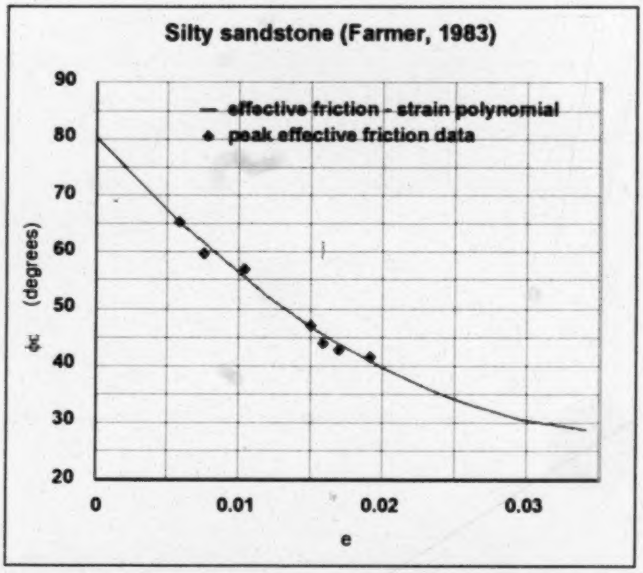

Figure 4.14: Correlation between the effective friction strain polynomial and the effective friction data values using the peak data only.

4.3.8 Reconstruction of the σ - e curves and original comparison

The procedure introduced in section 4.2.8 is used to reconstruct the stress-strain curves to compare with the triaxial test data output, figure 4.1, with the following two changes:

iv Calculate a value of σ_{1r} from equation 4.10.
vii For each value of ϕ_e solve equation 4.11 for e_{pp}

Figure 4.15 shows the comparison of the original data curves with the reconstructed stress-strain curves derived from the available peak data only.

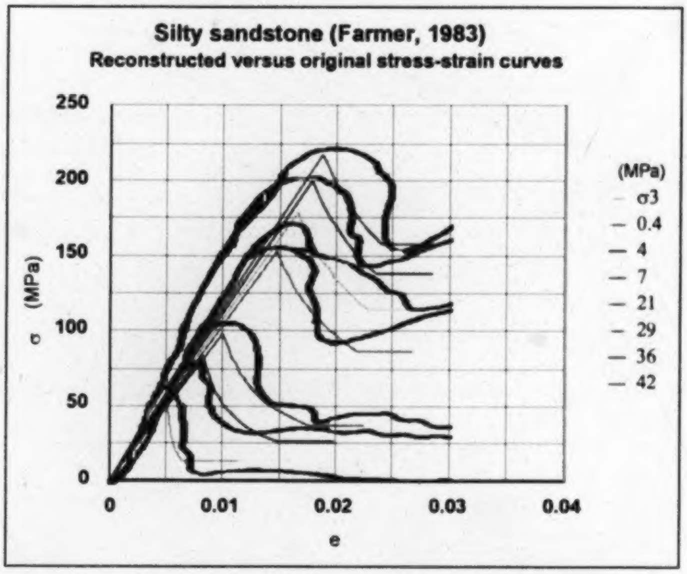

Figure 4.15: Comparison of the reconstructed with the actual stress-strain curves using the available peak data only.

4.3.9 The normalized post peak modulus

The normalized post peak modulus, $E_{pp(n)}$ is determined using equation 3.20 and plotted as a function of e_{pp} in figure 4.16. When compared to figure 4.11 which illustrates the plot of $E_{pp(n)}$ versus e_{pp} for the peak and residual data availability, it is evident that there is little difference between the two functions.

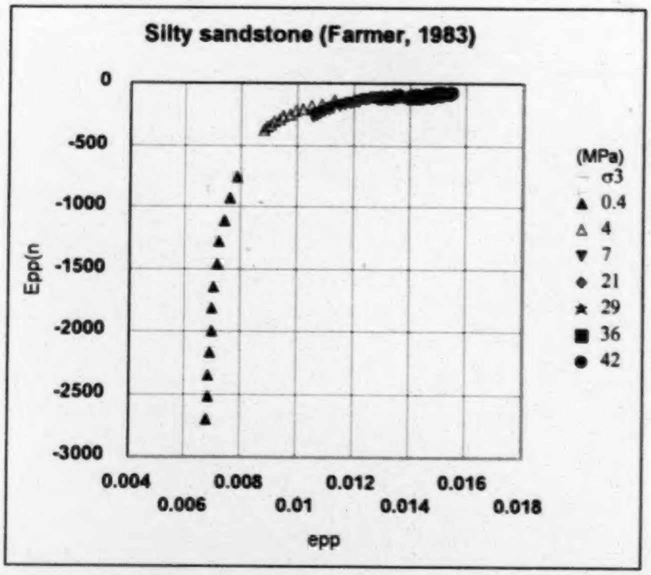

Figure 4.16: Normalized post peak modulus derived from the peak data only.

4.4 Comparison of the peak and residual data to peak data results

Since the major difference between the two approaches is dependent on the availability of peak and residual data, the effective friction - strain function is the most affected. This is due to the procedure for evaluating the base strain that provides the upper boundary limit at the brittle-ductile transition point, which relies on the maximum number of data points for increased accuracy, evident by the number of data points used in section 4.2.6 versus section 4.3.6.

Consequently, differences in the reconstructed stress-strain curves, sections 4.2.8 and 4.3.8, and the normalized post peak modulus curves, sections 4.2.9 and 4.3.9 are the result of the differences seen in the effective friction - strain curves of the two data sets used. Figure 4.17 shows a comparison of figure 4.9 and figure 4.14.

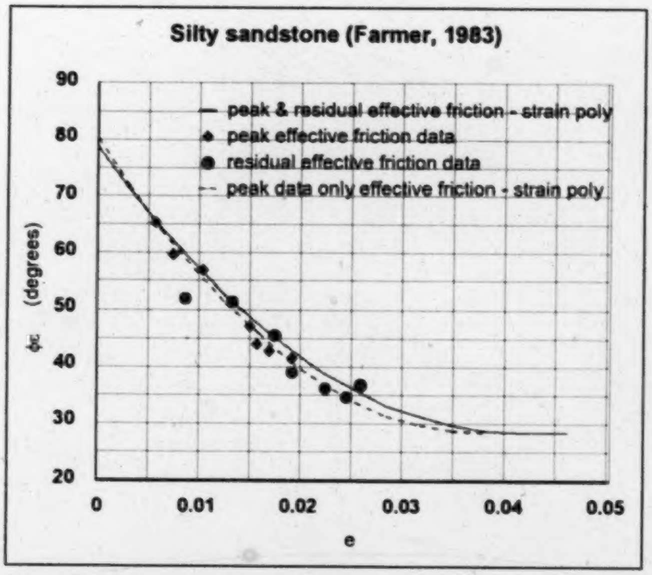

Figure 4.17: Comparison of effective friction - strain polynomial functions with respect to data availability

As visually expressed in figure 4.17, there is little difference between the two outcomes with respect to data availability, which suggests that it is not necessary to gather residual strength data to be able to evaluate the behaviour of the post peak region. A proviso for this is the need for a careful evaluation of the base angle of friction to allow the analysis to proceed.

The question then arises as to the sensitivity of the base angle of friction in evaluating the post peak region. If a technique such as the tilt test, which is a simplified method of determining the base angle of friction (Stimpson, 1981), is used then the value of ϕ_b may be coarse. Section 4.5 addresses this issue by looking at varying the base angle of friction by several degrees either side of the calculated value.

4.5 Varying the value of the base angle of friction, ϕ_b

The value of ϕ_b was varied by 8 degrees, in 2 degree increments, either side of the calculated value of 28.5°, and the effective friction - strain function plotted in each case, figure 4.18.

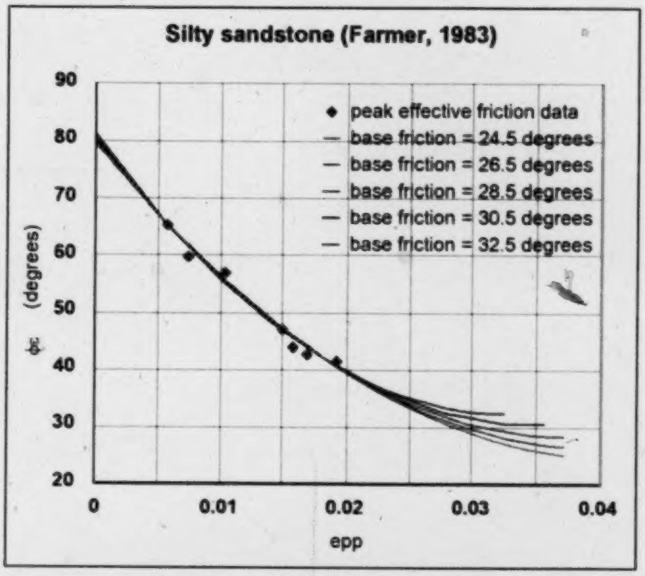

Figure 4.18: The effect of varying the base angle of friction on the effective friction - strain function.

The plot in figure 4.18 shows that there is negligible difference due to varying the base angle of friction in the region where the data is available. However, as the brittle-ductile transition point is approached, where in this case the silty sandstone had insufficient peak data available, there is some divergence of the respective functions.

It is apparent from figure 4.18 that a small error of one or two degrees in the evaluation of the base angle of friction does not seem to greatly alter the effective friction - strain function in its description of the post peak region.

4.6 Verification of postulates and assumptions using other intact rock data sets from the literature

As previously stated in section 4.1, 11 additional data sets that contain both peak and residual data have been worked in a similar fashion to the set described in this chapter. The results of both peak and residual analysis, and peak only analysis, on these data sets are summarized in appendices H and J respectively. In addition, appendix K contains a further 32 worked data sets where only peak data was available.

It is interesting to note the differences between appendices H and J, where the effect of peak and residual data being available can be compared to the outcome if only peak data is used. In appendix H it can be seen that interpretation of the residual strength, and particularly the strain at which the residual strength commences is made difficult by the fluctuations recorded in the post peak region. Whether these fluctuations are due to the effects of equipment or human error during the course of triaxial testing is unknown, but certainly there appears to be less control in data collection in the post peak region compared to that in the region up to peak strength.

The effective friction - strain plots show differences between the effective friction and strain values determined from the recorded and interpreted data compared to the effective friction - strain polynomial. It will be noted that, when comparing the peak and residual data reconstructions (appendix H) with peak only data reconstructions (appendix J), for many of the rocks the latter curves are displaced somewhat to higher strain values (e.g. marl, appendices H2 and J2), which better reflect the original strain data. These differences are primarily due to the difficulty in defining accurately the residual strains from the original data curves. Where well defined residual strains are available from the original data this problem does not arise, e.g. mudstone (appendices H3 and J3).

If, as shown in appendix J, only the peak data is used, there is a much better correlation between the effective friction - strain polynomial and the effective friction data points, resulting in a better reconstruction and correlation with the original stress-strain plots. This leads to a tentative conclusion that poorly collected residual strain data may in fact do more harm than good.

Since the peak data only approach in section 4.3 and appendix J provides a good reconstruction of the post peak region of the stress-strain curves, the notion arises as to whether it is necessary to gather residual data to define the post peak region. This is confirmed by data cases where both the peak and residual and peak data approaches compare well, such as the mudstone example (Farmer, 1983), appendices H.3 and J.3.

Certainly, if a good evaluation of the base angle of friction can be made easily, then the peak only data approach would be more reliable, due to the difficulty in evaluating residual data, particularly in a triaxial testing environment.

4.7 Conclusions

Each set of triaxial data taken from the available literature, regardless of the availability of peak and/or residual data was successfully used to define a post peak effective friction - strain relationship and a reconstruction of the post peak stress-strain data.

It may be concluded that the postulates and assumptions made in chapter 2 have been verified and validated for all 44 data sets from intact rock taken from the literature, and reported in appendices H, J and K.

Further verification will be reported in chapter 5 using data from tests carried out by the author on two materials of very different properties.

Chapter 5

Verification of the postulates and assumptions through physical testing of intact rock

5.1 Testing program for TimKen rock and Highvale mudstone

Two very different rock types were selected to verify the postulates and assumptions in chapter 2. TimKen is a manmade material whose composition and manufacture were devised by the author, and which will be discussed in greater detail in section 5.2. Highvale mudstone is a natural rock extracted from the Highvale coal mining operation West of Edmonton, Alberta. This rock was located 35 m below surface, 3 m below the lowest coal seam, and is thought to have been deposited by glacial activity. The Highvale mudstone is generally of a higher strength than the sedimentary layers above the coal seams or partings, but is highly susceptible to weathering.

5.1.1 Triaxial test

Triaxial testing was conducted on two different core sizes, dictated by the size of the available Hoek-Franklin triaxial confinement cells, (Hoek et al, 1968):

i	TimKen rock	BX size = 1.625" diameter core
ii	Highvale mudstone	EX size = 0.8125" diameter core

Testing of the Highvale mudstone was conducted using the smallest core size possible, due to the high strength of the rock which required very high confining pressures to approach the brittle-ductile transition point.

Once recording of the sample dimensions had been made, triaxial testing was conducted in accordance with the ISRM standards, whereby the applied confinement pressure was built up in small stages in conjunction with the applied axial pressure, to the confinement set for the test. Testing proceeded in all cases using a MTS loading frame fitted with a 600,000 lb load cell in stroke control mode. The restricting factor in testing was the system for applying confining pressure to the Hoek-Franklin cell, which had an upper reliable limit of 42 MPa. From peak to residual strength the applied confinement pressure was kept constant through manual adjustment. Once residual strength was achieved and held constant the test was stopped, and the confining pressure bled to zero matching the applied axial pressure to avoid ringing of the specimen.

The data was recorded on a plotter as load versus deformation and transferred to a spreadsheet manually for interpretation as stress-strain data, thereby taking the dimensions of the specimen into account. The stiffness of the testing frame was recorded as 11.6×10^5 kN/m.

Unconfined uniaxial compression tests were also conducted on the samples in accordance with ISRM standards to provide zero confinement data for each rock type, which were analyzed with the triaxial data.

5.1.2 Tilt test

Tilt tests were conducted on core samples to establish the base angle of friction for the two different rock types. The BX and NX core sizes corresponding to TimKen and Highvale mudstone as described in section 5.1.1 were used. The approach used by Stimpson (1981) was employed where one core was allowed to just slide on two other touching cores of the same diameter, such that the angle of inclination of the core, α with the horizontal could be measured, figure 5.1.

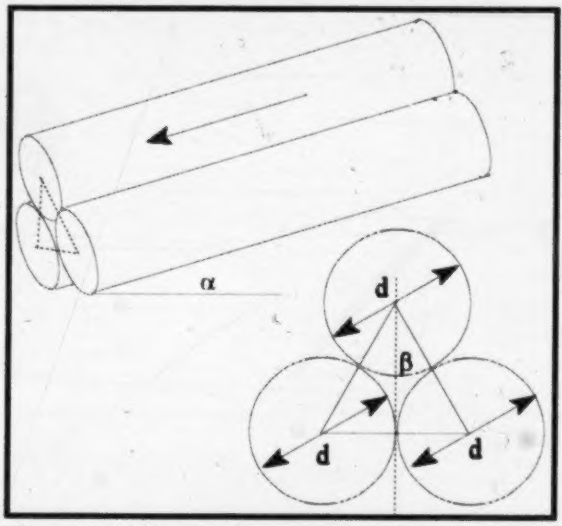

Figure 5.1: Tilt test arrangement using core, after Stimpson, (1981).

The core surfaces were as drilled with only loose material and dust being removed with a soft brush and air.

For each set of three cores, the uppermost core was used for three tests having been rotated to a fresh surface for each test. The core positions were interchanged so that a total of 9 tests were performed on each set of three cores.

Stimpson showed that the base angle of sliding friction could be calculated by taking into account the angle made by a line passing through the core centres of any two of three touching cores with the vertical, such that:

$$\phi_b = \tan^{-1}[\sec(\beta)\tan(\alpha)] \qquad 5.1$$

Where β is half the angle of the internal equilateral triangle made by the centres of three touching cores of equal diameter, d, figure 5.1, that is $\beta = 30^{o}$. Therefore equation 5.1 becomes equation 5.2:

$$\phi_b=\tan^{-1}[1.155\tan(\alpha)] \qquad 5.2$$

To verify the tilt test, two other methods of establishing the base angle of friction were used; the triaxial slip test and the shear box test.

5.1.3 Triaxial slip test

The triaxial slip test was conducted in the same fashion as the triaxial test, with the exception that each core sample tested was pre-cut at an angle of approximately 30^{o} to the major principal axis, although this angle could be arbitrary. The angle was recorded since it was needed for the analysis of ϕ_b. The surfaces of the cut were ground and polished to remove any saw tooth imprints that might adversely affect the base friction evaluation. Again the BX and EX core sizes were used.

Once peak strength, indicated by slip, had been achieved then the test was paused, the peak strength and confinement recorded and the confinement increased to a higher value. The test was then resumed until slip occurred for the new value of confinement. The test allowed several data points to be collected for each sample.

The base angle of friction was determined from the slope of a plot of shear stress, τ versus normal stress σ, figure 5.2, where τ, equation 5.3 and σ, equation 5.4 were determined from the values of the peak strength, σ_1, confinement, σ_3 and the angle made with the major principal stress, θ recorded.

$$\tau = \frac{(\sigma_1 - \sigma_3)}{2}\sin(2\theta) \qquad 5.3$$

$$\sigma = \frac{(\sigma_1 + \sigma_3)}{2} + \frac{(\sigma_1 - \sigma_3)}{2}\cos(2\theta) \qquad 5.4$$

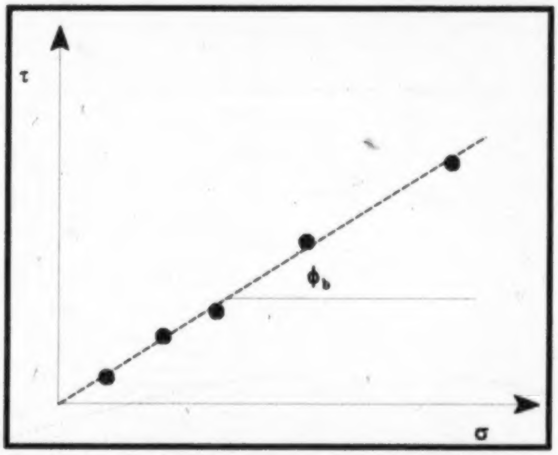

Figure 5.2: Plot of τ versus σ to evaluate the base angle of friction from triaxial slip test results

5.1.4 Shear box test

The shear box test was conducted on pieces of core cut perpendicular to the cylindrical axis and mounted in a shear box. Varying normal loads, N were applied to the box, and the applied shear load, T necessary to cause motion of the two halves measured in each case, figure 5.3. As with the triaxial slip test, the two halves of core were ground and polished to remove any saw tooth effects that might adversely affect the base friction evaluation. To maximize the contact surface for this test an NX core size, 2.125" diameter, was used for both the TimKen and Highvale mudstone samples.

A plot of T versus N, similar to the τ - σ plot for the triaxial slip test, allowed an evaluation of the base angle of friction for the rock.

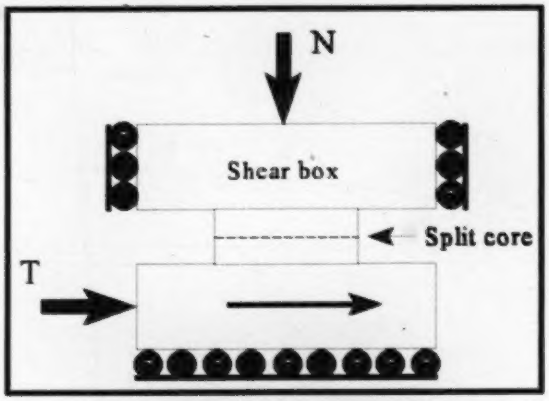

Figure 5.3: Shear box testing arrangement

5.2 TimKen rock

TimKen rock is a manmade material consisting of the following constituent proportions by volume:

i 21.4 % Portland cement
ii 53.6% dolomite size 20 sand
iii 25.0% water

The constituents were mixed to a smooth slurry and poured into a 16" x 16" x 6" mold. An initial setting time of 24 hours ensured that a sufficiently stable structure could be turned out of the mold. The resulting block of material was dried and cured under constant temperature and airflow conditions for one year, with bi-monthly turning of the block to ensure even drying and curing. After one year the block was cored to provide the appropriate size and number of samples required to perform the tests outlined in section 5.1. The cores were then dried under the same constant temperature and airflow drying conditions for a further month. Four such blocks were prepared and cored for testing.

5.2.1 Triaxial test results

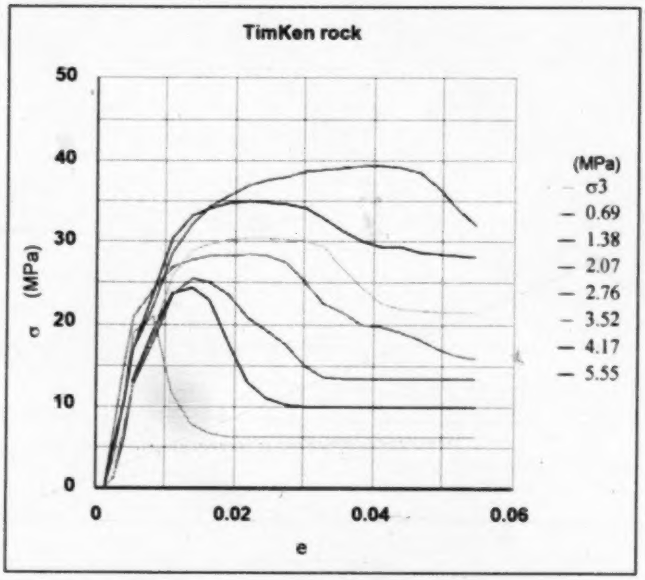

Figure 5.4: TimKen rock triaxial test results

Figure 5.4 shows the triaxial test data output for TimKen rock for a range of confining pressures spanning the range from zero to brittle-ductile confinement.

5.2.2 Tilt test results and analysis

144 tilt tests were performed on 21 cores, rotating any set of three randomly chosen cores, so that the slip angle, α was measured for each core in the set of three. The base angle of friction, ϕ_b was determined using equation 5.2 in each case and an average and standard deviation determined:

$$\phi_b = 38.4^\circ$$
$$sd = 0.6^\circ$$

5.2.3 Triaxial slip test results and analysis

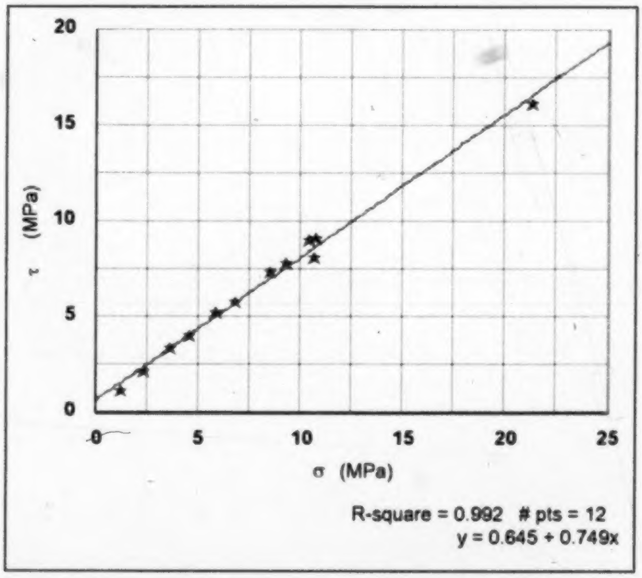

Figure 5.5: Triaxial slip test results for TimKen rock

The triaxial slip test was conducted 12 times using 3 samples. The major and minor principal stresses recorded via peak load and confining pressure in each case were used to determine the shear and normal stresses, τ and σ respectively. These were plotted as illustrated in figure 5.5. The base angle of friction was then determined via the slope of the plot:

$$\phi_b = \tan^{-1}\{\text{slope}\} = \tan^{-1}\{0.749\} = 36.8°$$

5.2.4 Shear box test results and analysis

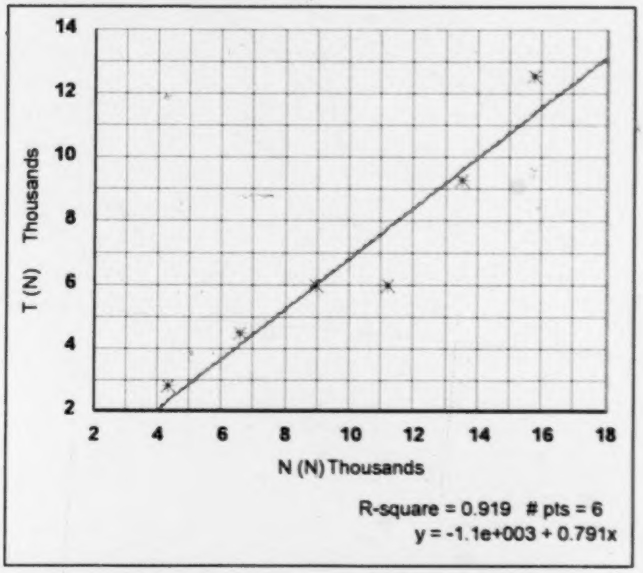

Figure 5.6: Shear box test results for TimKen rock

The shear box test was carried out on 6 different samples at 6 different normal loads. The shear load, T to cause motion along the surface between the two halves of core, figure 5.3, was plotted against the normal load, N, as shown in figure 5.6. As with the triaxial slip test, the base angle of friction was determined from the slope of the plot:

$$\phi_b = \tan^{-1}\{\text{slope}\} = \tan^{-1}\{0.791\} = 38.3^{\circ}$$

5.3 Verification of the postulates and assumptions using TimKen rock

As carried out in chapter 4, the data has been treated in two ways. The first looks at all the available triaxial data, while the second uses only the peak data. Following, in section 5.4, a direct comparison is made of the two approaches.

5.3.1 Assuming that the peak and residual data are available and applying the Joseph-Barron approach

5.3.1a Determination of the peak strength criterion

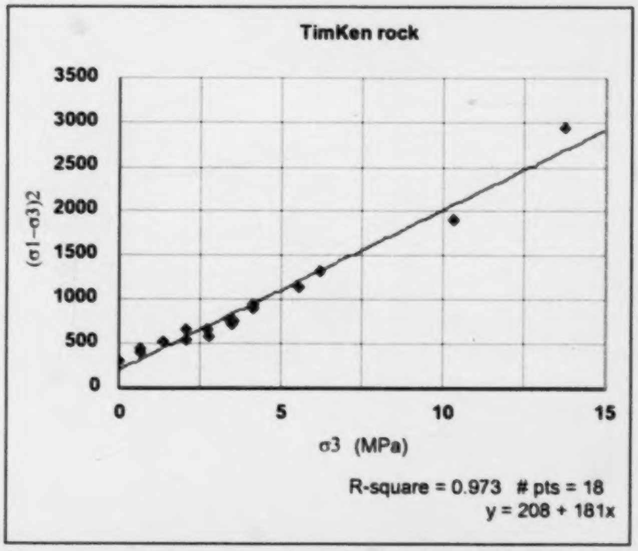

Figure 5.7: Linear form of the Hoek-Brown failure criterion applied to TimKen rock.

The peak strength criterion was determined from the available peak strength data, as per section 3.1, and as illustrated in figure 5.7. The slope and the intercept from figure 5.7 were used to calculate the Hoek constant m and σ_c assuming that s = 1 for intact rock, and define the peak strength criterion, equation 5.5.

$$\sigma_c = \{\text{intercept/s}\}^{1/2} = \{208/1\}^{1/2} = 14.4 \text{ MPa}$$

$$m = \text{slope}/\sigma_c = 181/14.42 = 12.6$$

and $$\sigma_{1_p} = \sigma_3 + \{181\, \sigma_3 + 208\}^{1/2} \qquad 5.5$$

5.3.1b Determination of the brittle-ductile transition point

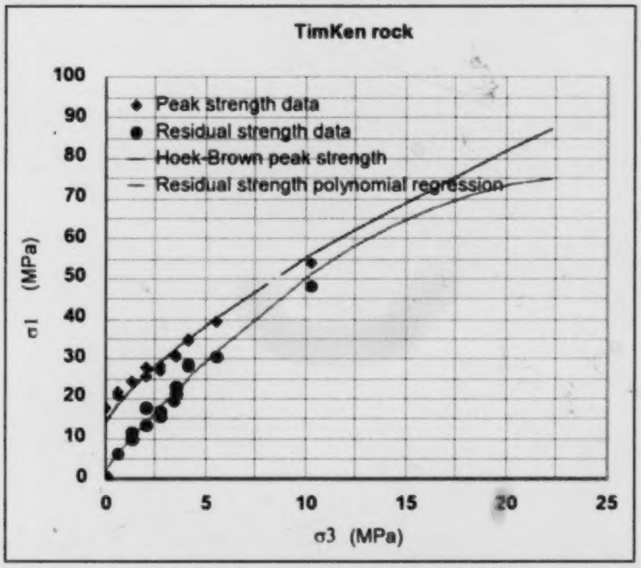

Figure 5.8: Polynomial regression of the available residual data to identify the brittle-ductile transition point.

A polynomial regression analysis of the available residual data, as outlined in section 3.2, did not provide an identifiable brittle-ductile transition point when plotted with the peak strength criterion, equation 5.5, although a sense of the brittle-ductile confinement was identified between 10 and 20 MPa, figure 5.8.

The linear approximation process, described in section 3.3 was carried out providing a linear approximation to the residual strength as shown in figure 5.9 and equation 5.6.

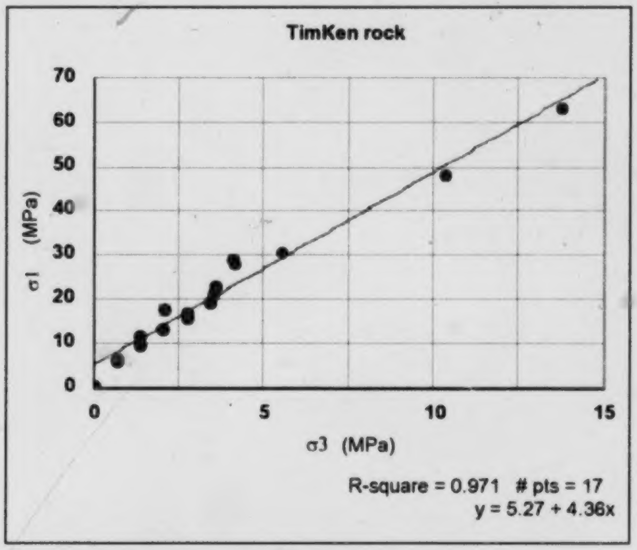

Figure 5.9: Linear regression of the available TimKen residual data to allow identification of σ_{3t}

$$\sigma_{1r} = 4.36\,\sigma_3 + 5.27 \text{ MPa} \qquad 5.6$$

Equating equations 5.5 and 5.6 according to assumption 8, section 2.3.8, allowed the determination of σ_{3t} as per equation 3.3.

$$\sigma_{3t} = 14.0 \text{ MPa}$$

5.3.1c Determination and refinement of the residual strength criterion

The residual strength polynomial constants, D and F were determined according to equations 3.4 and 3.5 respectively, assuming σ_{cr} = 5.3 MPa from the linear approximation, equation 5.6, resulting in the residual strength polynomial, equation 5.7.

$$\sigma_{1r} = -0.12\,\sigma_3^2 + 6.0\,\sigma_3 + 5.3 \text{ MPa} \qquad 5.7$$

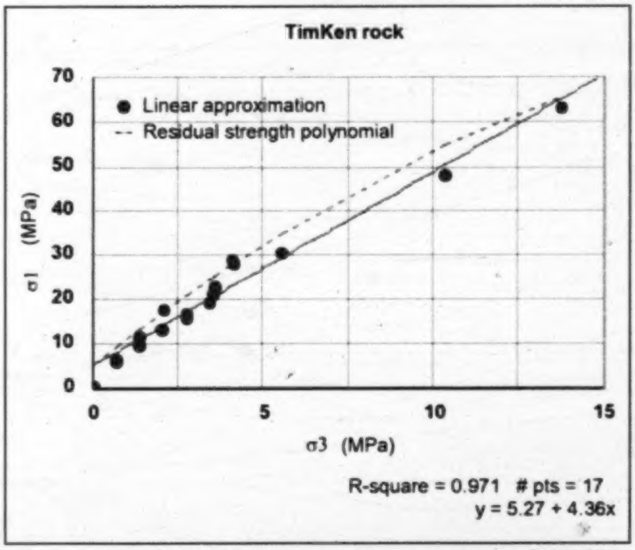

Figure 5.10: Residual strength polynomial and linear approximation revealing error in the polynomial function

The error in the residual strength polynomial was visible when plotted with the linear approximation, figure 5.10, which when refined to figure 5.11 allowed new values for σ_{3t} and the residual strength polynomial to be determined, equation 5.8.

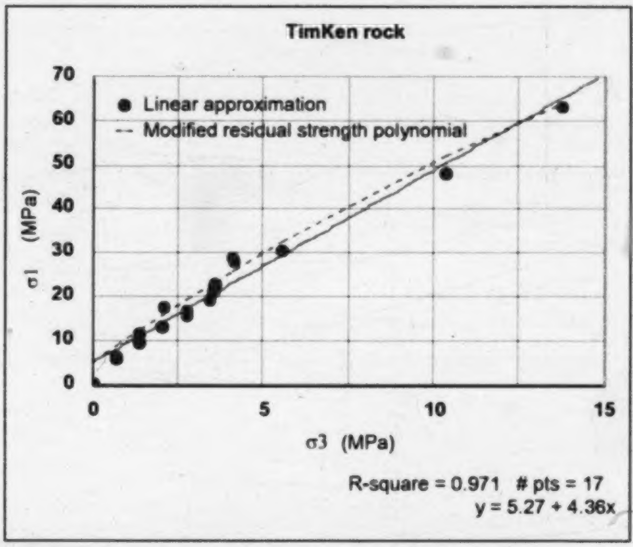

Figure 5.11: **Modified** residual strength polynomial and linear approximation post refinement process.

$$\sigma_{3t} = 19.0 \text{ MPa}$$

$$\sigma_{1r} = -0.07\,\sigma_3^2 + 5.3\,\sigma_3 + 5.3 \text{ MPa} \qquad 5.8$$

5.3.1d Estimation of the base angle of friction

The base angle of friction was determined via equation 3.7, given that σ_{3t} has been calculated:

$$\phi_b = 37.9^\circ$$

When compared to the values for ϕ_b determined via the tilt test, triaxial slip test and the shear box test, 38.4°, 36.8° and 38.3° respectively, not only did this value seem reasonable, but the value determined by the tilt test compared well with all other values and was hence validated.

The base strength criterion, defined by equation 2.8 and using the calculated value of ϕ_b becomes equation 5.9:

$$\sigma_{1b} = 4.2\,\sigma_3 \qquad 5.9$$

5.3.1e Comparison of the peak, residual and base strength criteria

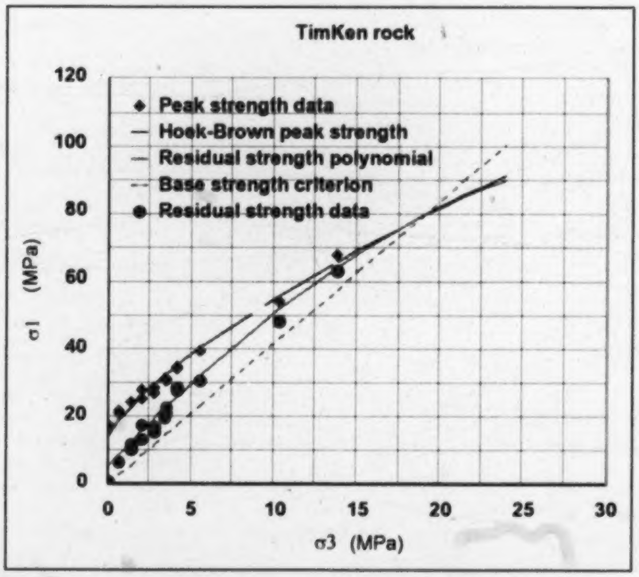

Figure 5.12: Comparison of peak, residual and base strength criteria in relation to zero confinement and the brittle-ductile transition point.

Figure 5.12 shows that the peak residual and base strength criteria behave in a manner suggested by the available data and show the relationship between peak, residual and base strength as discussed in section 4.2.5.

5.3.1f Determination of the base strain, e_b, and the solution to the effective friction - strain polynomial

The base strain, e_b was determined as per the procedural example in section 4.2.6, via the slope of the Y versus e plot, figure 5.13.

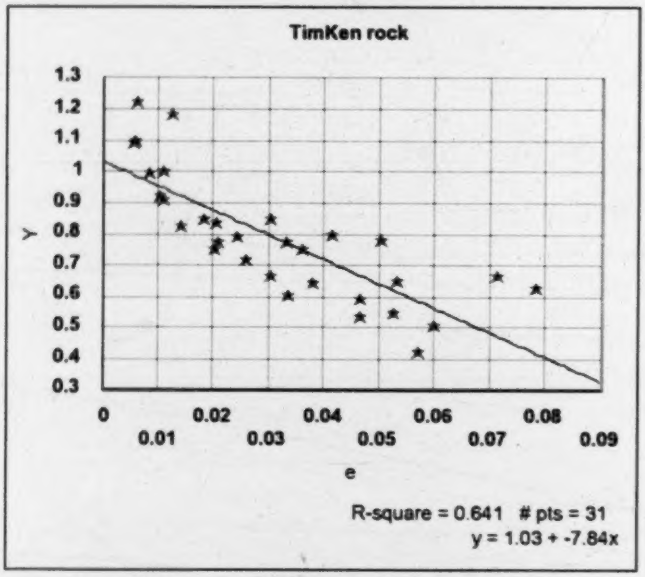

Figure 5.13: Plot of Y versus e to determine e_b

$$e_b = -1/M + e_p = 1/7.84 + 0.01 = 0.14$$

The solution to the effective friction - strain polynomial, equation 5.10, was found via calculating R, S, and T, equations 3.12, 3.11 and 3.10 respectively, given that $\phi_p = 59.1°$ and $e_p = 0.01$ when $\sigma_3 = 0$.

$$\phi_e = 63 - 361\ e_{pp} + 1300\ e_{pp}^2 \qquad 5.10$$

5.3.1g Comparison of ϕ_e-e curve with the ϕ_e-e data - verification

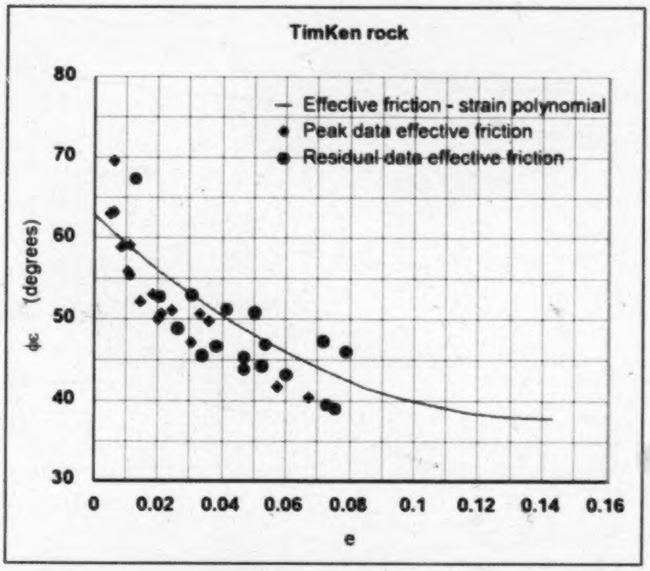

Figure 5.14: Correlation between effective friction - strain polynomial and effective friction data values

Figure 5.14 shows a reasonable correlation between the data and effective friction polynomial function, verifying postulates 1 and 2.

5.3.1h Reconstruction of the σ-e curves and comparison with the original data

The stress-strain curves were reconstructed using the procedure described in section 4.2.8, and compared with the original data curves from figure 5.4. This is illustrated in figure 5.15.

The strain differences seen in figure 5.15 are a reflection of the scatter in the interpretation of the residual strains, as also evident in figure 5.14.

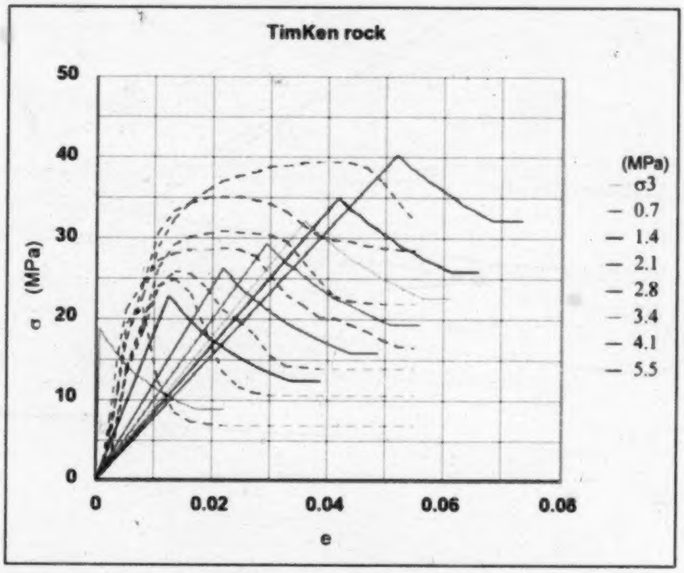

Figure 5.15: Comparison of the reconstructed with the actual stress-strain curves for the TimKen rock.

5.3.1i The normalized post peak modulus

Figure 5.16 shows the normalized post peak modulus determined from equation 3.20 for the TimKen data set.

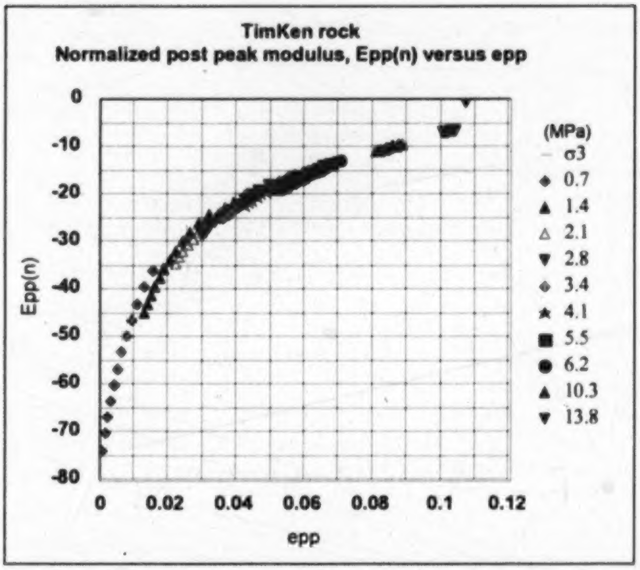

Figure 5.16: Normalized post peak modulus versus post peak strain for the TimKen rock.

5.3.2 Assuming that only the peak data is available and applying the Joseph-Barron approach

5.3.2a Determination of the peak strength criterion

The peak strength criterion is the same as determined in section 5.3.1a, equation 5.5, since only peak strength data was used in either case.

$$\sigma_{1p} = \sigma_3 + \{181\ \sigma_3 + 208\}^{1/2} \qquad 5.5$$

5.3.2b Estimation of the base angle of friction from a tilt test

The base angle of friction was taken as the value determined by the tilt test, which compared well with the triaxial slip test and the shear box test, as mentioned in section 5.3.1d, and allowing the determination of the base strength criterion, equation 5.11.

$$\phi_b = 38.4°$$

$$\sigma_{1b} = 4.3\ \sigma_3 \qquad 5.11$$

5.3.2c Determination of the brittle-ductile transition point

The brittle ductile transition point confining pressure, σ_{3t} was determined by the procedure outlined in section 3.10, using equation 3.24 arising out of equating equations 5.5 and 5.11, resulting in:

$$\sigma_{3t} = 18.0\ \text{MPa}$$

5.3.2d Determination of the residual strength criterion

The residual strength polynomial was determined as per the procedure followed in section 5.3.1c taking σ_{cr} as 20% of σ_c and thus yielding equation 5.12.

$$\sigma_{1r} = -0.09\ \sigma_3^2 + 5.7\ \sigma_3 + 2.9\ \text{MPa} \qquad 5.12$$

5.3.2e Comparison of the peak, residual and base strength criteria

Figure 5.17 illustrates the relationship between the three strength criteria, which compares equally well to the version in figure 5.12 where peak and residual data were used.

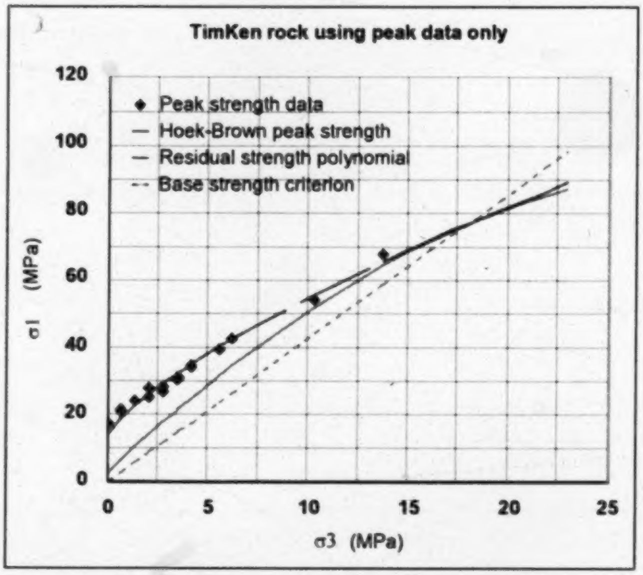

Figure 5.17: Comparison of peak, residual and base strength criteria.

5.3.2f Determination of the base strain, e_b and the solution to the effective friction - strain polynomial

The base strain calculation procedure was carried out as described in section 4.2.6, with the exception that only peak data effective friction values were used. Figure 5.18 shows the Y versus e linear plot giving a slope for determining e_b.

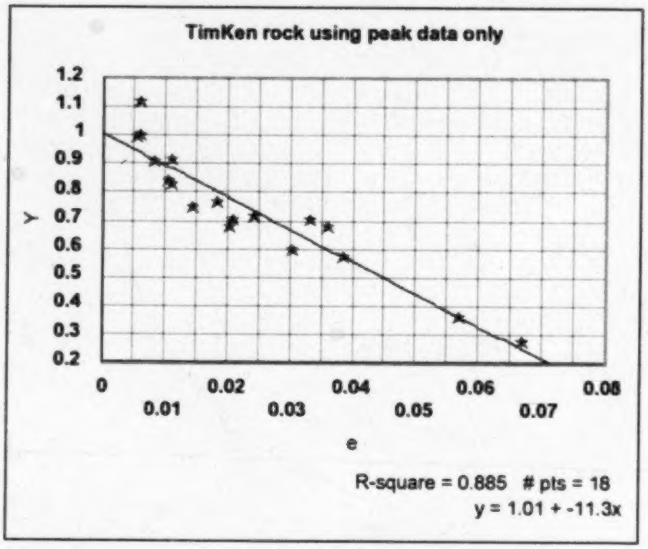

Figure 5.18: Plot of Y versus e to determine e_b.

$$e_b = -1/M + e_p = 1/11.3 + 0.01 = 0.095$$

This value is lower than that determined using the peak and residual data option, where $e_b = 0.14$.

The solution to the effective friction - strain polynomial was determined as equation 5.13, given the same values for ϕ_p and e_p as in section 5.3.1f.

$$\phi_e = 67 - 600\, e_{pp} + 3190\, e_{pp}^2 \qquad 5.13$$

5.3.2g Comparison of ϕ_e-e curve with the ϕ_e-e data - verification

Figure 5.19 shows the effective friction - strain polynomial plotted with the peak data effective friction values. When compared to figure 5.14, where both peak and residual data were employed, the polynomial function in figure 5.19 is equally valid with respect to the available data. The peak only data option seems to provide a closer correlation of the polynomial with the data points, indicating that the residual data gathered during triaxial testing may not have been as accurate as that of the peak data, evident from the degree of scatter associated with the residual data. When compared to the lower strength rock data drawn from the literature, such as the marl (Farmer, 1983), appendices H.2 and J.2, or the Gebdykes dolomite (Santarelli et al., 1989), appendices H.11, and J.11, this observation is not unreasonable.

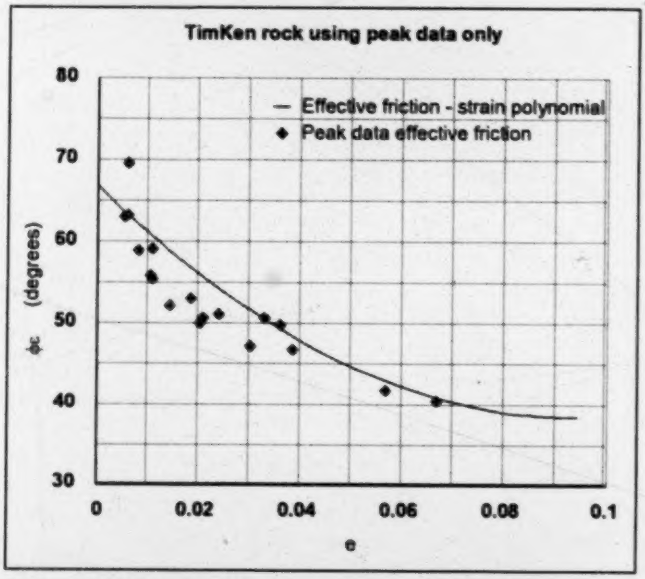

Figure 5.19: Correlation between effective friction - strain polynomial and peak data effective friction values.

Figure 5.19 shows an equally reasonable correlation between the polynomial and the data points, as found with figure 5.14, thus verifying postulates 1 and 2.

5.3.2h Reconstruction of the σ - e curves and original comparison

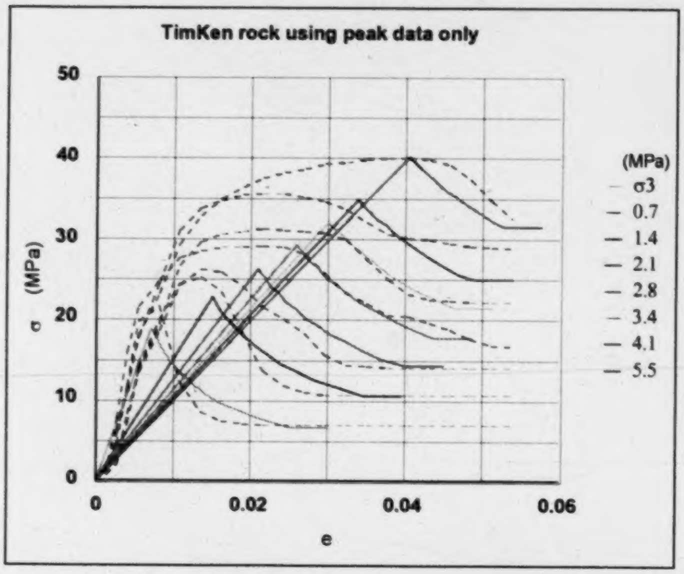

Figure 5.20: Comparison of the reconstructed with the actual stress-strain curves for TimKen rock using peak data only.

Comparing figures 5.20 and 5.15 and the corresponding effective friction-strain figures 5.19 and 5.14, it can be seen that using solely the peak data allows for a better reconstruction of the stress-strain curves in the post peak region. The largest difference between the two approaches being the adverse effect of including poorly interpreted residual strain data. This reinforces the fact that it is very difficult to interpret the amount of strain experienced when residual strength is achieved from a triaxial test stress-strain plot, due to the shallow erratic curvature of the post peak region tail.

Figure 5.20 does validate the Joseph-Barron approach and emphasizes the fact that it may only be necessary to collect peak strength and strain data.

5.3.2i The normalized post peak modulus

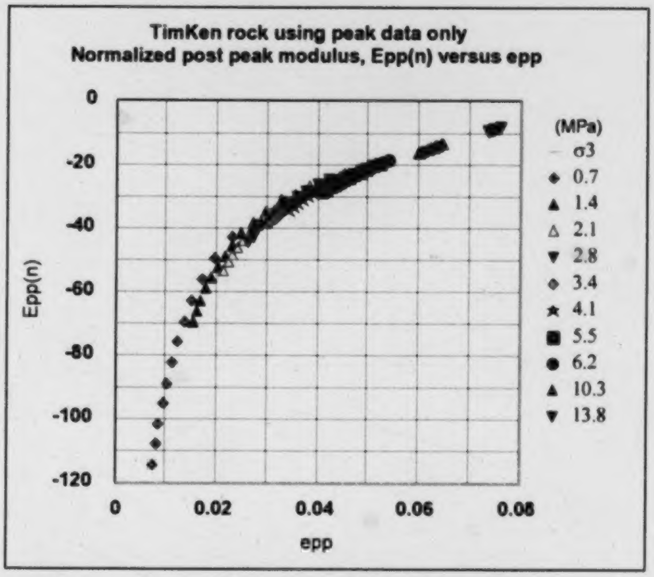

Figure 5.21: Normalized post peak modulus versus post peak strain data for TimKen rock via peak data only.

Comparing figure 5.21 to that for the peak and residual data, figure 5.16, both curves are virtually the same. This similarity suggests that despite the differences between the effective friction - strain and stress-strain plots discussed in the preceding 2 sections, the slope of the post peak curves change very little, regardless of the accuracy of the strain recordings of the residual data. If the slopes of the post peak curves in figures 5.20 and 5.15 are reviewed it will be seen that it is hard to distinguish them unless a very large plot scale is employed. This is more clearly seen in figure 5.23.

5.4 Comparison of the TimKen rock peak and residual data to peak data results

During the course of the previous section, 5.3.2, where the peak data was solely used, comparisons were made with section 5.3.1 at each stage of the Joseph-Barron approach. Figures 5.22 and 5.23 show a comparison of the peak and residual to peak only approaches in terms of the effective friction - strain and stress-strain plots respectively. In each case the peak only curves are shown as dashed lines.

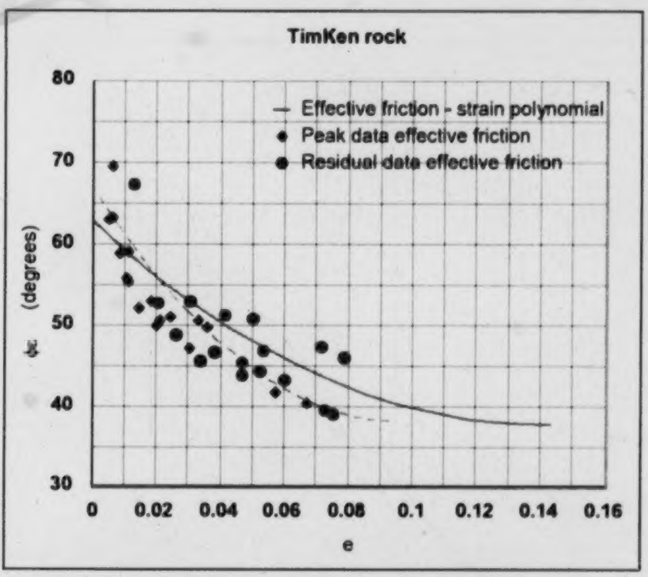

Figure 5.22: Comparison of the peak and residual to peak only approaches via the effective friction polynomials.

Figure 5.22 reveals that the dashed peak only polynomial line passes through the peak and residual data more effectively than the polynomial curve determined from the peak and residual data. This is due to the outlying residual data points which cause the peak and residual function to overestimate the effective friction.

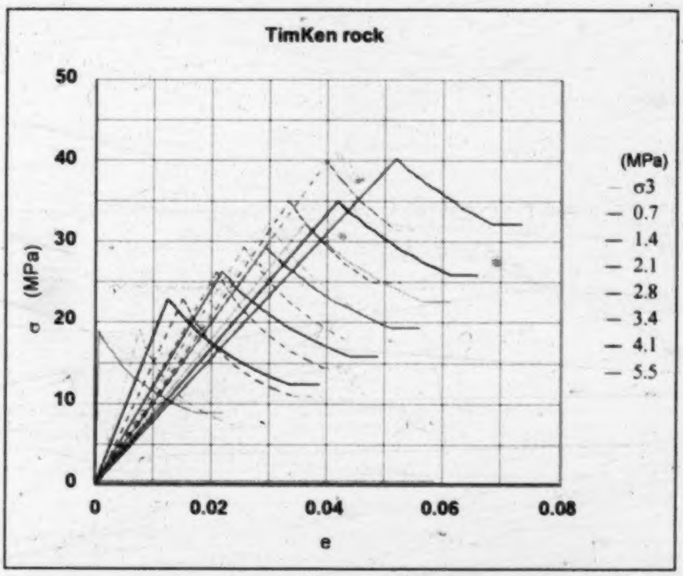

Figure 5.23: Comparison of the peak and residual to peak only (dashed) reconstructions of the original stress-strain curves.

As discussed in section 5.3.2i, the curvature of the post peak regions in both the peak and residual and peak only cases are similar, particularly at the higher confinements. The strain differences between the two sets, caused by the large scatter in the residual data points in figure 5.22 is made apparent here by the effect on the peak and residual strain values. Despite this, the peak and residual strength values match very well. This continues to suggest that the difference between the two sets of curves is the interpretation of the effective friction - strain polynomial.

Having investigated the effective friction - strain behaviour of the post peak region of a weak strength rock, attention is turned to a rock of much greater strength, where it was only possible to carry out triaxial testing at the lower values of confining pressure with respect to the brittle-ductile transition point.

5.5 Highvale mudstone

As mentioned in section 5.1, the Highvale mudstone is a natural rock of local origin. It consists of a fine grained matrix of particle size less than 0.1 mm, which classifies the grains in the silt range, and has a cement containing a large clay fraction. During coring of the rock to gain core samples for testing it became evident that although the rock was hard enough to warrant water for cooling of the core barrel, water would very quickly cause the clay cement to soften, thus changing the behaviour of the material from one of rock to clay. This high susceptibility to water necessitated a much slower coring program with higher air pressures for core bit cooling, than had been employed for the TimKen rock. Consequently, great care was taken to ensure that the rock was dry and remained dry during the course of testing.

5.5.1 Triaxial test results

Figure 5.23 shows the triaxial test data recorded for a range of confining pressures. Due to the high strength of the rock, indicated by the measured uniaxial compressive strength of 93 MPa compared to 18 MPa for the TimKen rock, the confinement required to reach the brittle-ductile transition point would be much greater than possible with the confinement system available. This is seen by the difference in peak to residual strength values achieved with a maximum possible confining pressure of 41 MPa. As will be seen the confinement necessary to achieve brittle-ductile transition for the Highvale mudstone is 350 MPa.

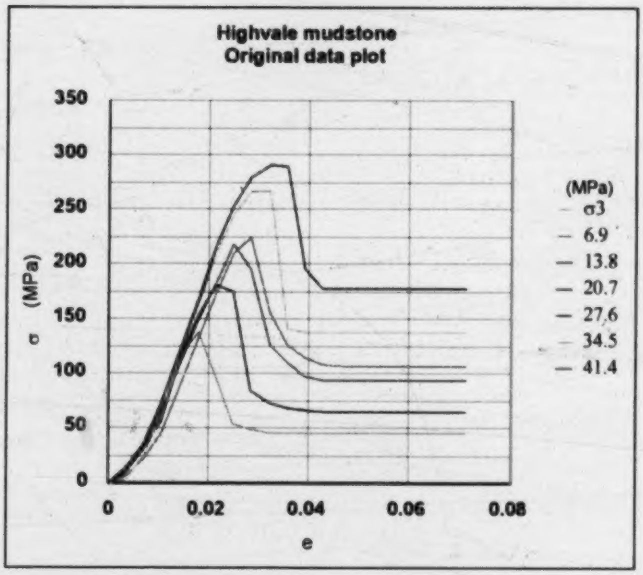

Figure 5.24: Highvale mudstone triaxial test results

5.5.2 Tilt test results and analysis

30 tilt tests were performed on various randomly chosen permutations of 15 cores. The base angle of friction, ϕ_b was determined via equation 5.2 for each recording, with the average and standard deviation found to be:

$$\phi_b = 28.5°$$
$$sd = 0.7°$$

5.5.3 Triaxial slip test results and analysis

The triaxial slip test was conducted 10 times using 3 samples. The correspondingly determined values of τ and σ from each test were plotted as shown in figure 5.25 to allow determination of ϕ_b from the slope of the graph.

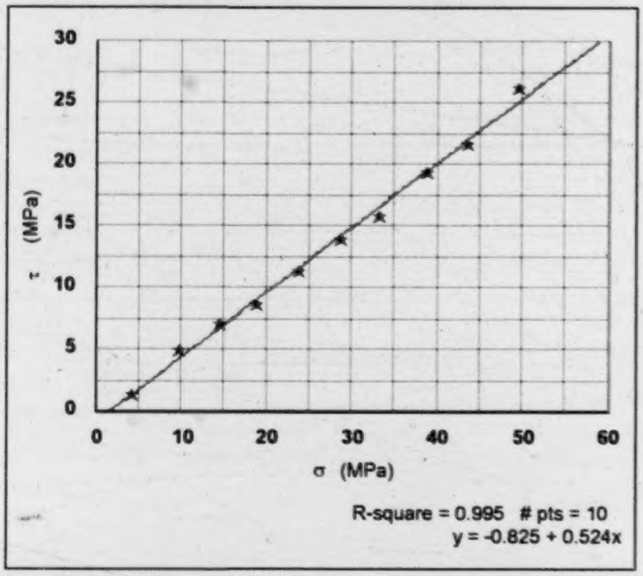

Figure 5.25: Triaxial slip test results for Highvale mudstone.

$$\phi_b = \tan^{-1}\{\text{slope}\} = \tan^{-1}\{0.524\} = 27.7^{\circ}$$

5.5.4 Shear box test results and analysis

The shear box test was carried out on 6 different samples at 6 different normal loads. Figure 5.26 shows the shear load measured, T versus normal load, N to allow determination of ϕ_b from the slope of the graph.

$$\phi_b = \tan^{-1}\{\text{slope}\} = \tan^{-1}\{0.552\} = 28.9^{\circ}$$

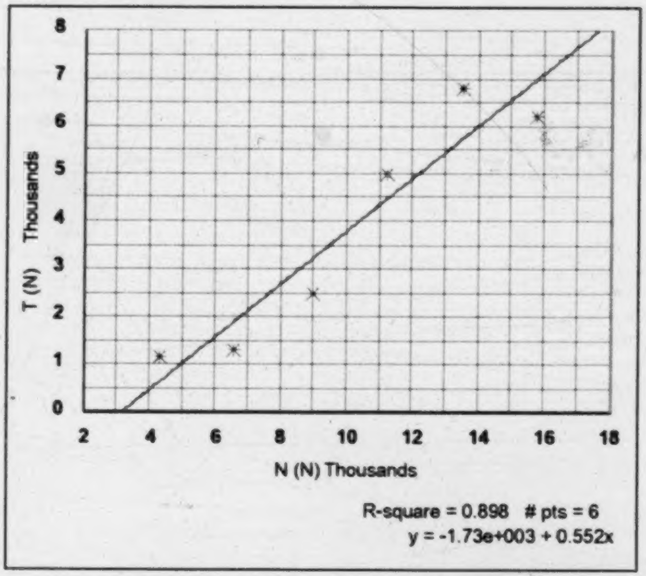

Figure 5.26: Shear box test results for Highvale mudstone.

5.6 Verification of the postulates and assumptions using Highvale mudstone

As was carried out for TimKen rock, the peak and residual data Joseph-Barron approach is looked at first, followed by the case using peak data only. Again, as in section 5.4, a direct comparison of the two approaches is made in section 5.7.

5.6.1 Assuming that the peak and residual data are available and applying the Joseph-Barron approach

5.6.1a Determination of the peak strength criterion

As before, section 3.1, the Hoek-Brown peak strength criterion constant m and σ_c were determined assuming the Hoek-Brown constant s = 1 for intact rock.

Figure 5.27 shows the linear regression of the linear form of the Hoek-Brown failure criterion applied to the Highvale mudstone, allowing the exact solution of the peak strength criterion, equation 5.14.

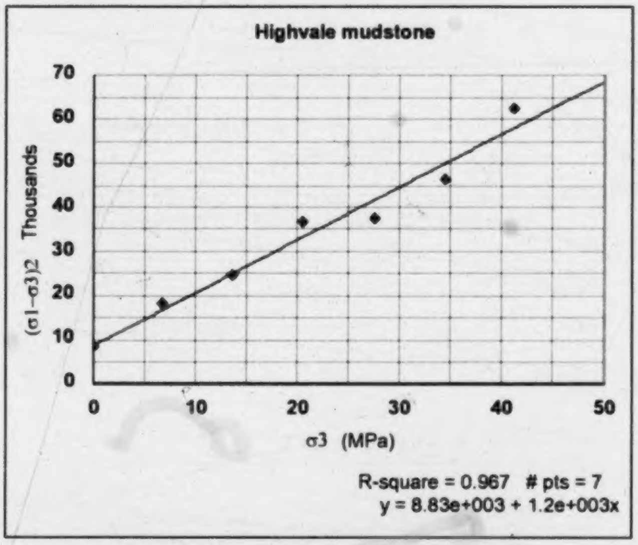

Figure 5.27: Linear form of the Hoek-Brown failure criterion applied to Highvale mudstone.

$\sigma_c = \{\text{intercept}/s\}^{1/2} = \{8830/1\}^{1/2} = 94$ MPa

$m = \text{slope}/\sigma_c = 1200/93.97 = 12.8$

and $$\sigma_{1p} = \sigma_3 + \{1200\,\sigma_3 + 8830\}^{1/2} \qquad 5.14$$

5.6.1b Determination of the brittle-ductile transition point

As was found for the TimKen rock, figure 5.8, a polynomial regression analysis of the available residual data did not identify a brittle-ductile transition point when plotted with the Hoek-Brown failure criterion, equation 5.14, as shown in figure 5.28. In this case it was not possible to even hazard a guess at the brittle-ductile confining pressure due to the absence of any available data within reasonable proximity to the brittle-ductile transition point.

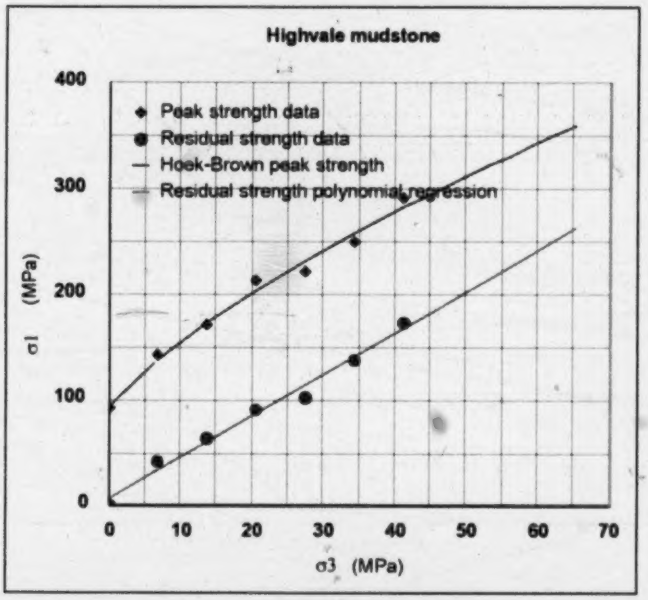

Figure 5.28: Polynomial regression of the available residual data to identify the brittle-ductile transition point

The linear approximation process, as outlined in section 3.3, was employed as illustrated in figure 5.29, allowing the determination of σ_{3t} via the equating of equation 5.15 to 5.14 using assumption 8, section 2.3.8.

$$\sigma_{1r} = 3.89\,\sigma_3 + 6.88 \text{ MPa} \qquad 5.15$$

$$\sigma_{3t} = 146 \text{ MPa}$$

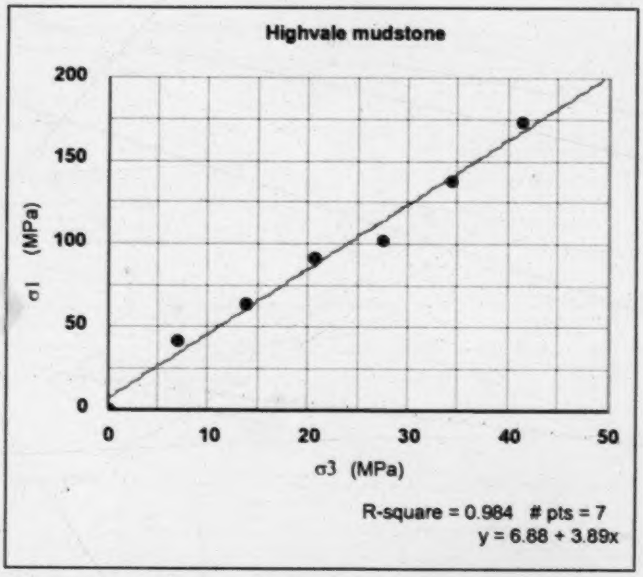

Figure 5.29: Linear regression of the available Highvale mudstone residual data to allow identification of σ_{3t}.

5.6.1c Determination and refinement of the residual strength criterion

The residual strength polynomial constants, D and F were determined as before assuming $\sigma_{cr} = 6.9$ MPa from equation 5.15, allowing an initial, pre-refinement residual strength polynomial, equation 5.16 to be stated:

$$\sigma_{1r} = -0.01\,\sigma_3^2 + 5.4\,\sigma_3 + 6.9 \text{ MPa} \qquad 5.16$$

The error in the residual strength polynomial compared to the linear approximation for the Highvale mudstone is much greater than that experienced for the TimKen rock, figure 5.10, as shown in figure 5.30.

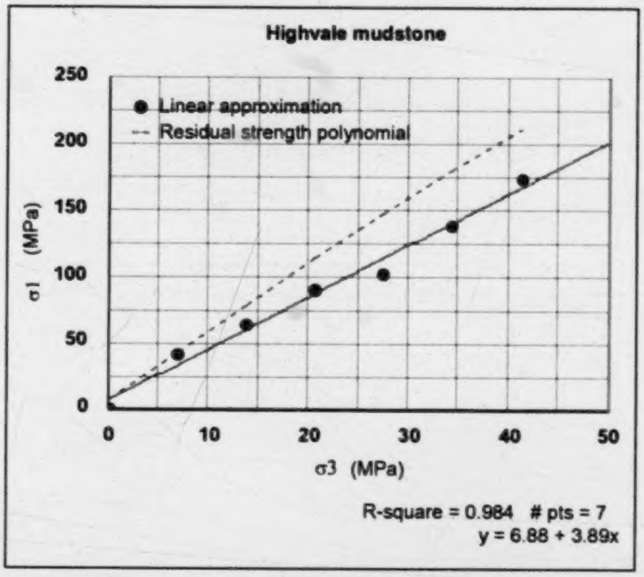

Figure 5.30: Residual strength polynomial and linear approximation revealing error in the polynomial function.

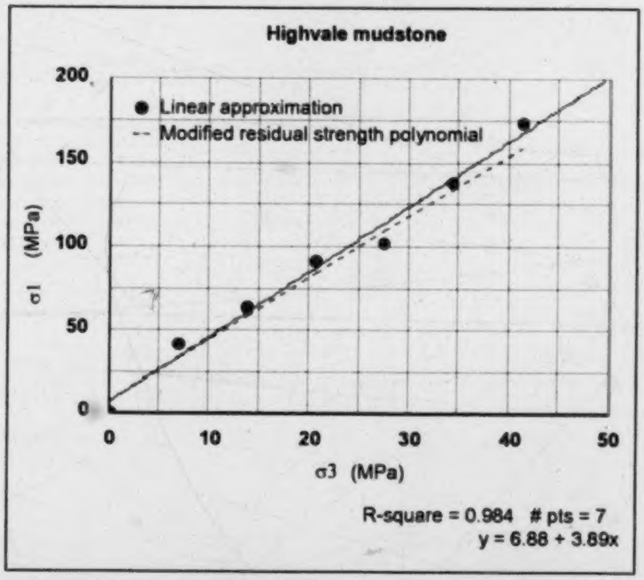

Figure 5.31: Modified residual strength polynomial and linear approximation post refinement process.

In the Highvale mudstone case the polynomial function appears linear in figure 5.30. This is due to the low confinement region of the data collected compared to the brittle-ductile transition point confinement. By adjusting the slope of the linear approximation in figure 5.31, the residual strength polynomial, equation 5.17 and the brittle-ductile confining pressure are refined.

$$\sigma_{1r} = -0.003\,\sigma_3^2 + 3.8\,\sigma_3 + 6.9 \text{ MPa} \qquad 5.17$$

$$\sigma_{3t} = 350 \text{ MPa}$$

5.6.1d Estimation of the base angle of friction

The base angle of friction was determined from equation 3.7 to be:

$$\phi_b = 28.9^\circ$$

When compared to the values for ϕ_b determined via the tilt test, triaxial slip test and the shear box test, 28.5°, 27.7° and 28.9° respectively, not only is the calculated value reasonable, but the value of ϕ_b determined by the tilt test is comparable with all other values determined. This confirms the validity of the tilt test.

The base strength criterion, defined by equation 2.8, and given the value of ϕ_b calculated, is equation 5.18.

$$\sigma_{1r} = 2.9\,\sigma_3 \qquad 5.18$$

5.6.1e Comparison of the peak, residual and base strength criteria

Figure 5.32 illustrates the comparison of the three strength criteria defined by equations 5.14, 5.17 and 5.18. As found with the Timken rock, the appropriate relationships discussed in section 4.2.5 continue to hold.

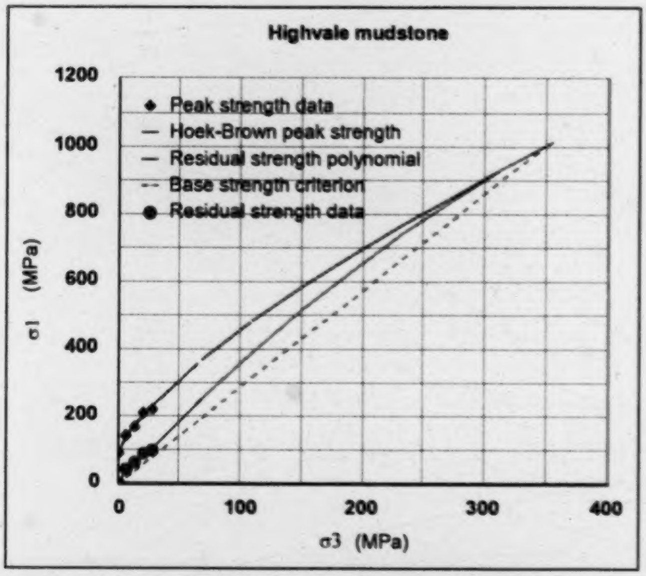

Figure 5.32: Comparison of peak, residual and base strength criteria in relation to zero confinement and the brittle-ductile transition point for Highvale mudstone.

5.6.1f Determination of the base strain, e_b and the solution to the effective friction - strain polynomial

The base strain, e_b was determined as before according to section 4.2.6. The plot of Y versus e, figure 5.33, gives a slope to determine e_b for Highvale mudstone.

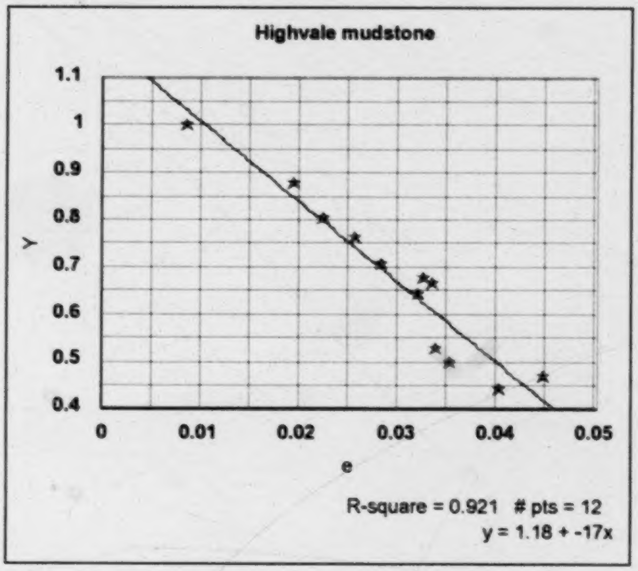

Figure 5.33: Plot of Y versus e to determine e_b

$$e_b = -1/M + e_p = 1/17 + 0.009 = 0.07$$

R, S and T were evaluated as before using equations 3.12, 3.11 and 3.10 respectively, and the effective friction - strain polynomial determined as equation 5.19, given that $\phi_p = 70°$ and $e_p = 0.009$ when $\sigma_3 = 0$.

$$\phi_e = 83 - 1590\, e_{pp} + 11800\, e_{pp}^2 \qquad 5.19$$

5.6.1g Comparison of ϕ_e-e curve with the ϕ_e-e data - verification

Figure 5.34 shows a good correlation between the effective friction - strain data and the polynomial determined in equation 5.19. The agreement verifies postulates 1 and 2.

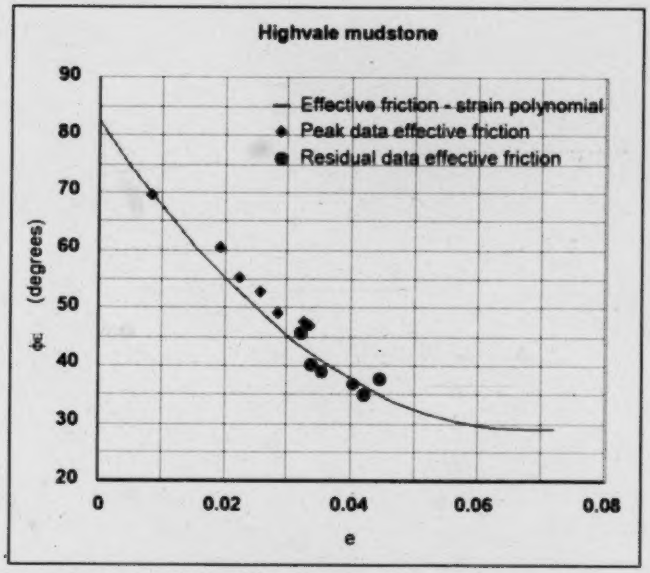

Figure 5.34: Correlation between the effective friction - strain polynomial and the effective friction data values.

5.6.1h Reconstruction of the σ - e curves and comparison with the original data

The stress-strain curves were reconstructed in figure 5.35 using the procedure from section 4.2.8 and compared in the same plot with the original data curves from figure 5.24. The original stress-strain curves are shown as dashed lines.

Despite the sparsity of available data in the case of the Highvale mudstone, the close clustering of data in figure 5.34 about the effective friction - strain polynomial allowed an accurate reconstruction of the stress-strain plots.

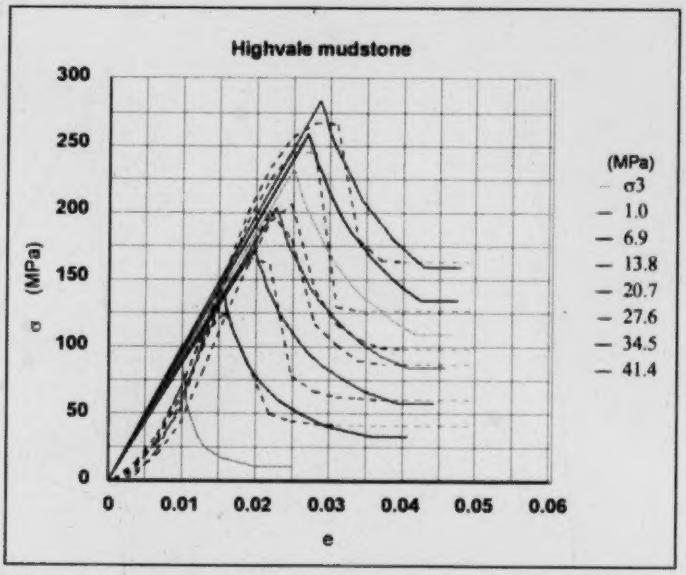

Figure 5.35: Comparison of the reconstructed with the actual stress-strain curves for the Highvale mudstone.

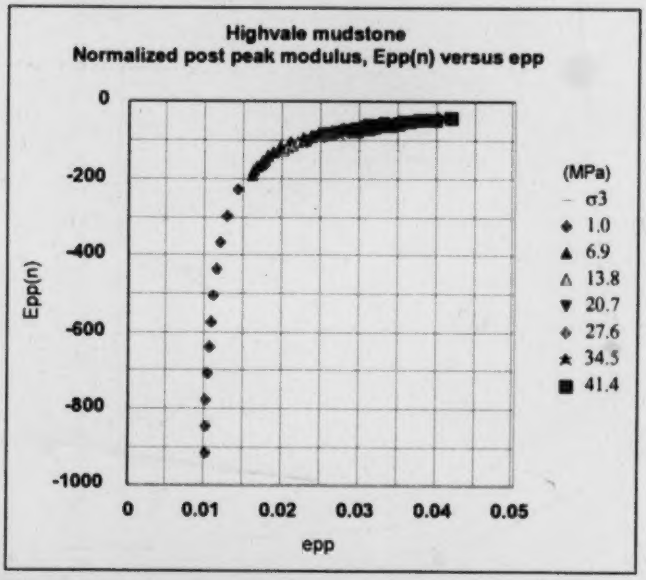

Figure 5.36: Normalized post peak modulus versus post peak strain for the Highvale mudstone.

5.6.1i The normalized post peak modulus

Figure 5.36 shows the normalized post peak modulus determined from equation 3.20 for the Highvale mudstone.

5.6.2 Assuming that only the peak data is available and applying the Joseph-Barron approach

5.6.2a Determination of the peak strength criterion

The peak strength criterion is the same as determined in section 5.6.1a, equation 5.14.

$$\sigma_{1p} = \sigma_3 + \{1200\ \sigma_3 + 8830\}^{1/2} \qquad 5.14$$

5.6.2b Estimation of the base angle of friction from a tilt test

The base angle of friction was taken as the value determined by the tilt test, which compared well with all values measured or determined as mentioned in section 5.6.1d. The base strength criterion was evaluated from this value, equation 5.20.

$$\phi_b = 28.5^\circ$$

$$\sigma_{1b} = 2.8\ \sigma_3 \qquad 5.20$$

5.6.2c Determination of the brittle-ductile transition point

The procedure in section 3.10, employing equation 3.24 via equations 5.14 and 5.20 allowed the determination of the brittle-ductile transition confinement:

$$\sigma_{3t} = 370 \text{ MPa}$$

5.6.2d Determination of the residual strength criterion

The residual strength polynomial was determined using the approach followed in section 5.6.1c, taking σ_{cr} as 20% of σ_c, resulting in equation 5.21.

$$\sigma_{1r} = -0.002\,\sigma_3^2 + 3.7\,\sigma_3 + 18.8 \text{ MPa} \qquad 5.21$$

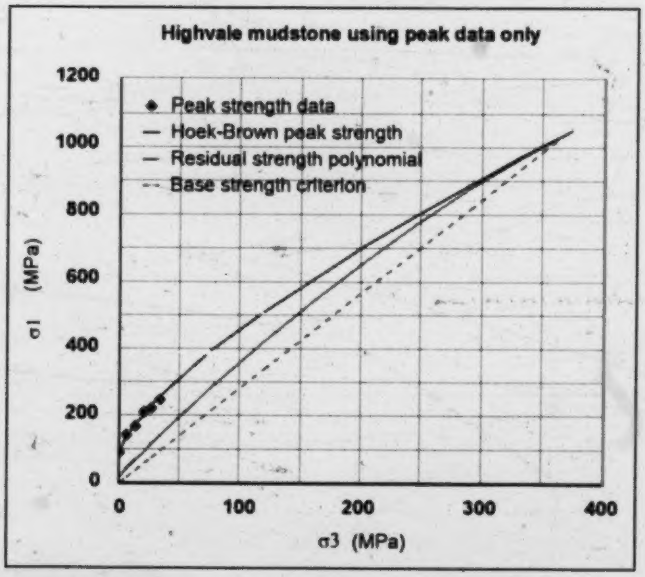

Figure 5.37: Comparison of peak, residual and base strength criteria.

5.6.2e Comparison of the peak, residual and base strength criteria

Figure 5.37 shows the relationship between the three strength criteria. These compare well with the peak and residual data approach version, figure 5.32.

5.6.2f Determination of the base strain, e_b and the solution to the effective friction - strain polynomial

The base strain calculation procedure in section 4.2.6 was followed, but only using the available peak data effective friction values. Figure 5.33 shows the Y versus e plot used to determine e_b from the slope.

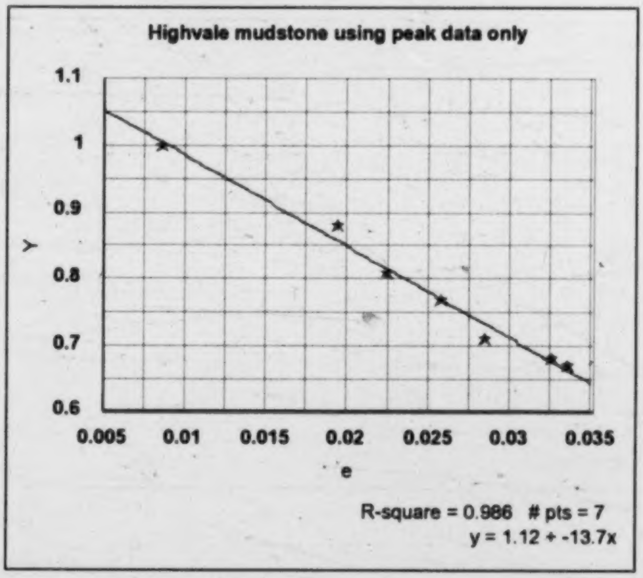

Figure 5.38: Plot of Y versus e to determine e_b

$$e_b = -1/M + e_p = 1/13.7 + 0.009 = 0.08$$

The solution to the effective friction - strain polynomial was found to be equation 5.22 given the same values for ϕ_p and e_p as in section 5.6.1f.

$$\phi_e = 80 - 1270\, e_{pp} + 7760\, e_{pp}^2 \qquad 5.22$$

5.6.2g Comparison of ϕ_e-e curve with the ϕ_e-e data - verification

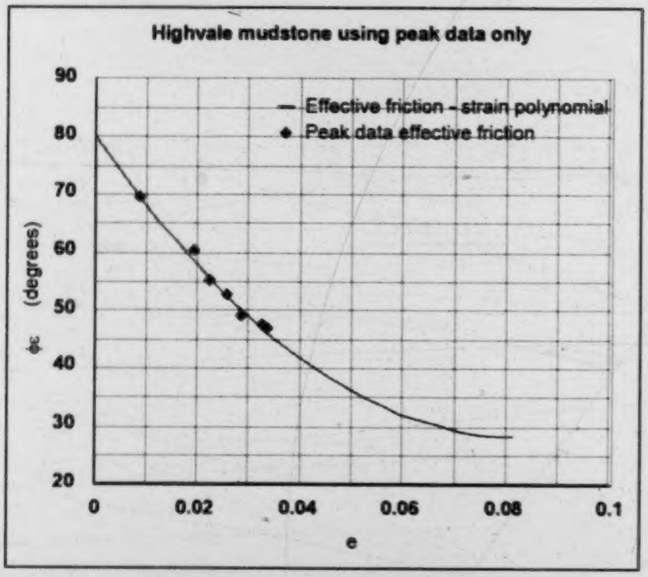

Figure 5.39: Correlation between effective friction - strain polynomial and peak data effective friction values.

As good a correlation between the effective friction - strain polynomial is seen for the peak only data approach, figure 5.39, as was seen in figure 5.34 where the peak and residual data was used. In this case the correlation gives a tight grouping of the peak data effective friction values to the polynomial. On reviewing figure 5.34, the residual data still gives some scatter around the polynomial, whereas the peak data is much closer.

5.6.2h Reconstruction of the σ - e curves and original comparison

Again the procedure in section 4.2.8 was followed to reconstruct the stress-strain curves which have been plotted in figure 5.40 with the original curves from figure 5.24. The original curves are shown as dashed lines.

As was found in figure 5.35 previously, there is an equally good correlation between the reconstructed and original stress-strain curves.

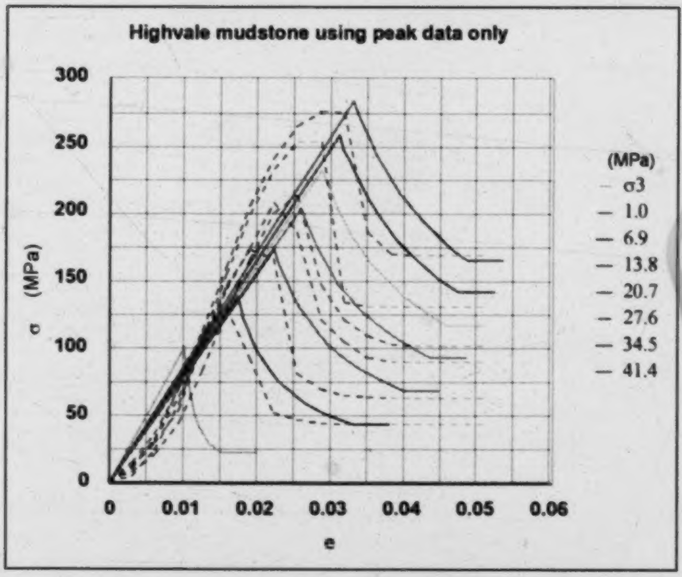

Figure 5.40: Comparison of the reconstructed with the actual stress-strain curves for Highvale mudstone using peak data.

5.6.2i The normalized post peak modulus

As was done with the TimKen rock, section 5.3.2i, comparing figure 5.41 to figure 5.36 reveals that both curves are virtually the same.

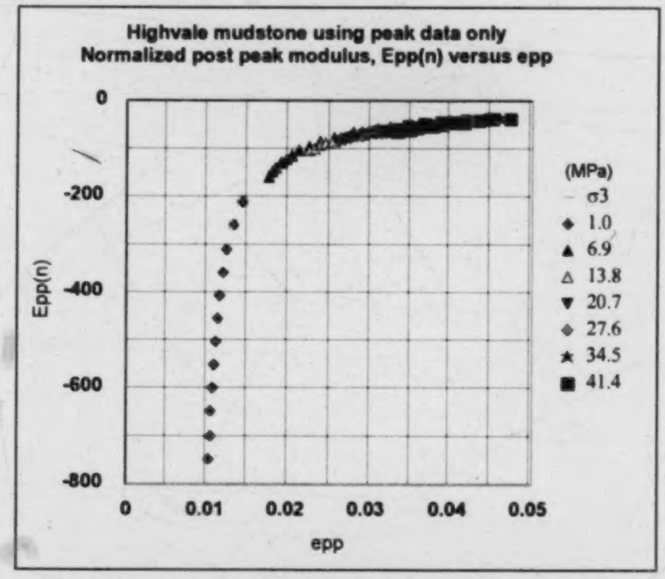

Figure 5.41: Normalized post peak modulus versus post peak strain data for Highvale mudstone via peak only data.

Again, this suggests that any differences between the peak and residual and peak only approaches become small with respect to the slope of the post peak region, as evidenced by figures 5.41 and 5.36.

5.7 Comparison of the Highvale mudstone peak and residual data to peak data results

Figures 5.42 and 5.43 compare the peak and residual to peak only approaches in terms of the effective friction - strain and stress-strain plots respectively. As in section 5.4, the peak only option is shown as dashed lines.

Again, as with the TimKen rock, the Highvale mudstone shows equally good output from the peak only option as for the peak and residual approach. This validates the use of peak only data rather than relying on the collection of peak and residual triaxial data, which is less reliable and more costly than the collection of peak triaxial data alone.

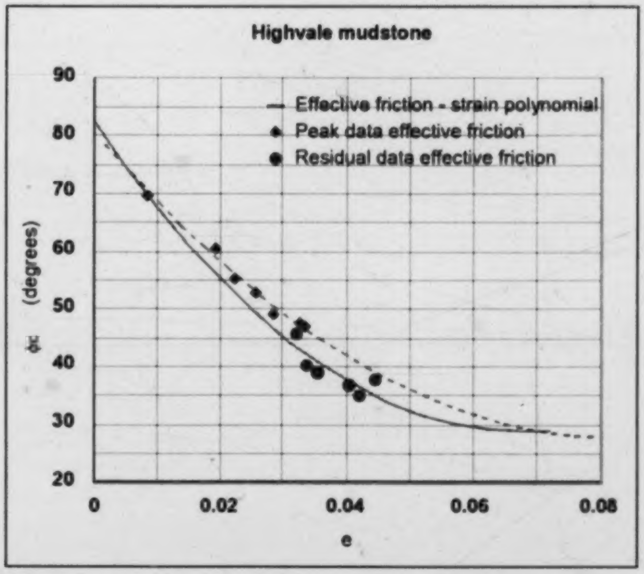

Figure 5.42: Comparison of the peak and residual to peak only approaches via the effective friction polynomials.

In both figures 5.42 and 5.43, each of the approaches used are equally good in their outcome of stress-strain reconstruction and matching to the available data employed in each case.

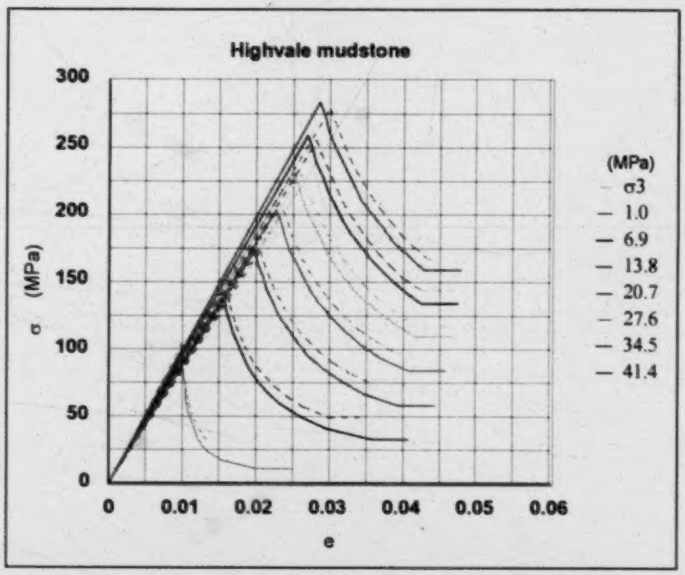

Figure 5.43: Comparison of the peak and residual to the peak only (dashed) reconstructions of the original σ-e curves.

5.8 Validity of the tilt test in defining the base angle of friction, ϕ_b

The tilt test results for both the TimKen rock and Highvale mudstone have been compared with those from the triaxial slip test and shear box test and found to be comparable, table 5.1.

In addition, the values for ϕ_b calculated from the peak and residual data approach, also reported in table 5.1, are comparable with the tilt test values. It can thus be concluded that the tilt test is a valid approach for determining the base angle of friction, ϕ_b.

	tilt test	triaxial slip test	shear box test	peak and residual calculation
TimKen rock	38.4	36.8	38.3	37.9
Highvale mudstone	28.5	27.7	28.9	28.9

Table 5.1: Comparison of determined base angle of friction values.

5.9 Conclusions

The postulates and assumptions made in chapter 2 have been verified through the physical testing of two intact rocks; TimKen rock and Highvale mudstone.

In particular, the residual strength polynomial is a valid residual strength criterion for interpreting the available residual strength data and predicting the behaviour of residual behaviour where data is not available. The effective friction - strain polynomial is a valid function for interpreting post peak stress-strain behaviour by allowing reconstruction of the post peak stress-strain curves. The post peak modulus relationship validly describes the post peak behaviour of intact rock.

Both the peak and residual data approach and the peak only data approach have been shown to provide similar results, allowing equally good predictions of the effective friction - strain, stress-strain and post peak modulus behaviour of the two rocks investigated.

The tilt test as an approach for the determination of the base angle of friction,

ϕ_b has been validated through comparison with the values from the triaxial slip test and shear box test, and with the value calculated from peak and residual data.

It is not necessary to rely on the gathering of residual triaxial data in addition to peak triaxial data, since the post peak region may be evaluated with merely the latter set and an evaluation of the base angle of friction by a simple tilt test.

The peak only data Joseph-Barron approach is a valid means of evaluating the post peak modulus and reconstructing the stress-strain curves.

Chapter 6

Application of the Joseph-Barron approach to establish the post peak modulus of broken rock

6.1 Introduction and background

In this chapter, the term "broken rock" is used to describe both rock that is damaged (i.e. non-intact), for example the rock mass data sets reported by Hobbs (1970), and where the rock is completely broken (i.e. comprised of reformed crushed material), for example the crushed rock data set reported by Hussaini (1991). In both cases the value of the Hoek-Brown constant, s is less than unity.

The available literature reveals little work previously carried out on the post-peak region for any rock, whether intact or broken. Some empirical work has been carried out by Hoek et al. (1997) using the concepts of geological strength index, GSI, representing the fractured nature of the rock akin to rock mass rating, RMR, and a knowledge of the intact rock Hoek-Brown peak strength criterion to predict post peak behaviour. However, to do this Hoek et al. assumed that the post peak region can be approximated by linear relationships as illustrated in figure 1.2.

Hobbs (1970) conducted triaxial testing on 4 broken rocks drilled from the roof of coal seams in the U.K., and Hussaini (1991) on 5 sizes of crushed basalt, providing several fully reported data sets at peak strength in each case. But, in each of these cases the aim was to investigate the behaviour to peak strength only, with no consideration of the post peak region.

Hoek et al. (1980) and Jaeger (1970) reported on the Panguna andesite rock mass at 5 degrees of weathering, and Hoek et al. (1997) report on 3 additional rock masses described only as very good, average or very poor in quality.

Apart from those listed above, the author was unable to locate any further broken rock data sufficient to perform an example analysis. In fact the 8 data sets reported by Hoek et al., 1980 and 1997 provide only a pre-peak modulus, a base angle of friction and the Hoek-Brown peak strength criterion constants, m_b and s, where m_b is the m value applied to broken rock, with no actual triaxial data being reported.

6.2 Postulates

The original postulates outlined in section 2.2 still hold, plus the following:

6.2.1 Postulate 3 - Effective friction - strain relationship for broken rock

At any point in the post peak region for broken rock, prior to and including the residual strength for that broken rock it is postulated that the same effective friction - strain relationship postulated in section 2.2 holds both for intact and broken rock of the same material.

$$\phi_e = f(e_{pp}) \tag{2.4}$$

6.2.2 Postulate 4 - Post peak stress-strain behaviour of broken versus intact rock

It is postulated that the peak stress and strain for broken rock at a given confinement, σ_3, describes a point that lies on the post peak stress-strain curve of the intact rock under the same confinement conditions. The shape of the post peak stress-strain curve for the broken rock is identical to that of the intact rock post peak stress-strain curve. The broken rock curve passes through the residual stress-strain point for the intact rock, becoming constant at a residual strength that is less than the intact residual strength.

6.2.3 Postulate 5 - The post peak modulus

It is postulated that the normalized post peak modulus for the intact rock and the broken rock follow same relationship.

6.3 Assumptions

The assumptions 1 through 9 outlined in section 2.3 remain valid. The Hoek-Brown peak strength criterion, equation 2.6 must however be put into a form appropriate for use with rock mass, equation 6.1, (Hoek et al., 1997).

$$\sigma_{1p}=\sigma_3+\sigma_c[m_b\frac{\sigma_3}{\sigma_c}+s]^a \tag{6.1}$$

Where a is the Hoek-Brown exponent which has a value of ½ for intact rock, m_b and s are the Hoek-Brown broken rock empirical constants and s is less than unity assumed for intact rock.

6.3.1 Assumption 10 - Empirical relationships after Hoek et al. (1997)

Hoek et al. provide charts in their paper that allow a determination of the RMR or GSI parameters, where GSI = RMR - 5. The following empirical relationships described in the same paper allow an estimation of the peak strength criterion when no triaxial peak strength data is available:

$$m_b = m \ \exp[\frac{GSI - 100}{28}] \qquad 6.2$$

If GSI > 25 then a = ½ and

$$s = \exp[\frac{GSI - 100}{9}] \qquad 6.3$$

If GSI < 25 (poor quality rock mass) then s = 0 and

$$a = 0.65 - \frac{GSI}{200} \qquad 6.4$$

6.3.2 Assumption 11 - Pre-peak broken rock deformation modulus

Bieniawski (1978) suggested an empirical relationship between RMR and in-situ modulus of deformation based on gathered data, equation 6.5. Serafim et al. (1983) proposed a modified version to predict pre-peak deformation modulus, equation 6.6 when RMR is less than 60. A comparison of the two functions is made in figure 6.1, after Bieniawski (1984), showing the direction change at RMR = 60.

$$E_{m(broken)} = (2RMR_{broken} - 100) \ GPa \qquad 6.5$$

$$E_{m(broken)} = 10^{[\frac{RMR_{broken} - 10}{40}]} \ GPa \qquad 6.6$$

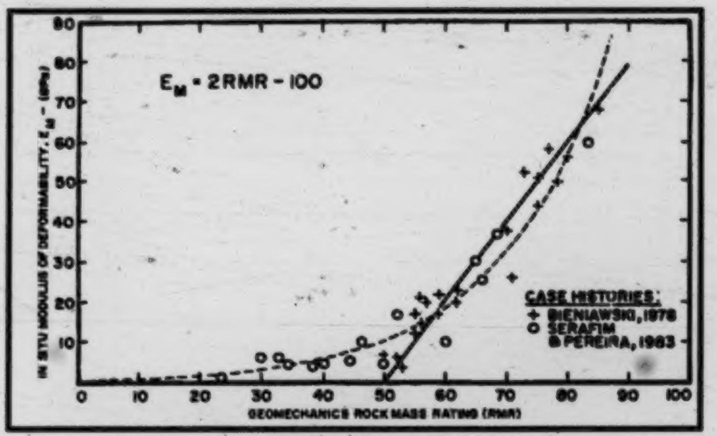

Figure 6.1: Comparison of equation 6.5 (solid line) to equation 6.6 (dashed line), after Bieniawski, 1984.

Hoek et al. (1997) suggested that the Serafim et al. form, equation 6.6 worked well except when the uniaxial compressive strength, σ_c is less than 100 MPa. They modified the Serafim et al. form for such cases, as given in equation 6.7. Once again, as with the work of Bieniawski and Serafim et al., equation 6.7 was devised by Hoek et al. on an empirical basis.

$$E_{m(broken)} = \sqrt{\frac{\sigma_c}{100}}\, 10^{\left|\frac{RMR_{broken}}{40}\right|}\ GPa \qquad 6.7$$

It is therefore assumed that if the intact uniaxial compressive strength, σ_c of the rock is less than 100 MPa, then the broken rock pre-peak modulus, $E_{m(broken)}$ is given by equation 6.7. If σ_c is greater than 100 MPa and RMR is greater than 60, then $E_{m(broken)}$ is given by equation 6.5. If σ_c is greater than 100 MPa and RMR is less than 60, then $E_{m(broken)}$ is given by equation 6.6.

To be able to verify the postulates via the Joseph-Barron approach it is necessary to be able to establish the strain at peak strength for a given value of σ_3 for both the intact and broken material. If, as is the case with the Panguna andesite and the generalized rock mass data sets reported in the literature, Hoek et al. (1980) and Hoek et al. (1997) respectively, where no strain data is directly available, the strain data at peak strength must be generated from a knowledge of the pre-peak modulus, and using equation 2.5.

$$E=\frac{\sigma_{1p}}{e_p} \qquad 2.5$$

If no pre-peak intact modulus is reported, then one must be assumed to be able to further the analysis. The author took the available data from Hoek et al., 1997, where the broken pre-peak moduli were given, and used equation 6.5 to generate intact pre-peak moduli values. The data gave the empirical relationship in equation 6.8, as illustrated in figure 6.2.

$$Log_{10}[\frac{E_{m(broken)}}{E_{m(intact)}}]=2.85[\frac{RMR_{broken}}{RMR_{intact}}-1] \qquad 6.8$$

It is assumed that in cases where triaxial data is unavailable for a range of confinements, but there is sufficient data to discern RMR for both intact and broken rock, and also a pre- peak modulus for the broken material from an appropriate choice of either equations 6.5, 6.6 or 6.7, then the intact rock pre-peak modulus may be obtained via this empirical relationship, equation 6.8. The strain at peak may then be determined using equation 2.5.

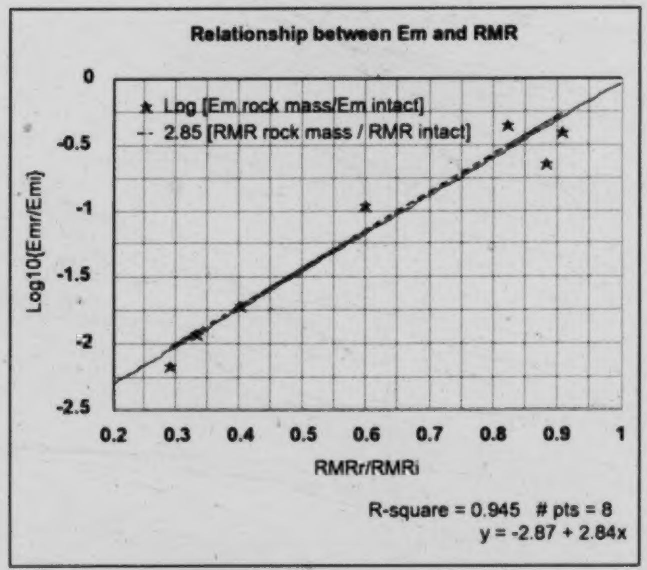

Figure 6.2: Empirical plot of data after Hoek et al. (1997) to verify equation 6.8.

6.3.3 Assumption 12 - The Hoek-Brown peak strength criterion and the residual strength polynomial relationship for broken rock

When rock is broken it will exhibit broken behaviour as opposed to intact behaviour. When intact rock becomes broken for a given confinement and peak load, then beyond the peak strength it follows a broken behaviour. When broken rock is subjected to a given confinement and loaded to peak strength, then beyond peak strength it continues to exhibit broken behaviour.

Broken rock no longer permits the use of a Hoek-Brown parameter value of $s = 1$, but $s < 1$ dependent on the degree of fragmentation of the broken rock. A Hoek-Brown peak strength criterion with a value of $s < 1$ describes the peak strength of broken rock for a given confinement. The residual strength polynomial, equation

2.7, also describes a strength of broken rock for a given confinement.

If broken rock is considered in the unconfined state, then at peak strength the effective friction holding the broken rock together is overcome. Since there is no confinement holding the rock together then the roughness of the broken surfaces are not reduced and the effective friction experienced at peak remains constant. In other words the peak strength and the residual strength are the same at $\sigma_3 = 0$. It is therefore assumed that the peak strength and the residual strength for the broken rock are described by the same function at not only the brittle-ductile transition point, ($\sigma_3 = \sigma_{3t}$), but also in the unconfined state, ($\sigma_3 = 0$), equation 6.9.

$$\sigma_{1p} = \sigma_{1r} = \sigma_{cr} \qquad \text{when } \sigma_3 = 0 \qquad 6.9$$

6.4 The Joseph-Barron approach applied to broken rock - a verification of the postulates using example data sets from the available literature

There are two cases arising from the available data reported in the literature. The Joseph-Barron approach for cases i and ii are outlined using sample data sets in sections 6.4.1 and 6.4.2 respectively, allowing verification of the postulates and assumptions concurrently.

i Triaxial peak strength and strain data for a number of confining pressures is available for both the intact and broken rock.

ii No triaxial data is available, but the Hoek-Brown intact peak strength parameters and a geological description of the rock are available.

6.4.1 Where triaxial data is available

An Ormonde siltstone data set (Hobbs, 1970) was selected to verify the postulates as applied to broken rock. Appendix M.7 provides a summary of the available intact triaxial data, rock mass triaxial data, and the subsequent analysis.

If triaxial data is available for both the intact and broken rock then two analyses may be conducted concurrently to allow a comparison between the intact and broken relationships. The intact analysis would follow the procedures laid out in chapter 3, while that for the broken rock is outlined below.

It should be noted that no broken rock residual strength triaxial data was found in the literature. This is understandable considering the difficulty in gaining intact rock residual data via triaxial testing as discussed in chapters 4 and 5. Consequently, the Joseph-Barron analysis described below is akin to the peak only intact data option.

6.4.1a Determination of the Hoek-Brown strength parameters

To enable the values of m_b and s to be determined, since $s < 1$, two plots must be constructed. One, as described in section 3.1, using the linear rearrangement of the Hoek-Brown peak strength criterion, equation 6.1; the second plot being a direct plot of σ_{1p} versus σ_3.

Figure 6.3 shows that the slope of the function allows the determination of m_b given that the uniaxial intact compressive strength σ_c is known, as per section 3.1. Figure 6.4 illustrates the determination of s via the intercept at $\sigma_3 = 0$, equation 6.10, again given that σ_c is known.

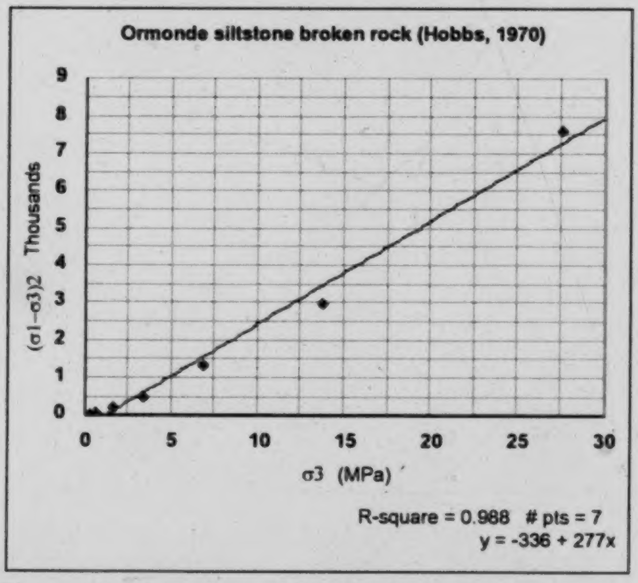

Figure 6.3: Linear form of the Hoek-Brown broken rock peak strength criterion to evaluate m_b from the slope.

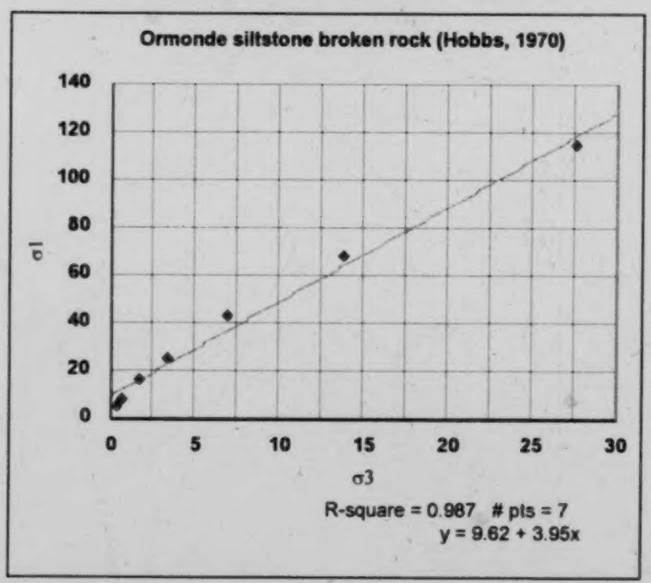

Figure 6.4: Linear regression of a σ_1 versus σ_3 plot to evaluate s from the intercept.

$$\sigma_{1p}=\sigma_3+\sigma_c[m_b\frac{\sigma_3}{\sigma_c}+s]^a \tag{6.1}$$

When $\sigma_3 = 0$:

$$s=[\frac{intercept}{\sigma_c}]^{\frac{1}{a}} \tag{6.10}$$

Where a = ½, except for very poor rock (GSI < 25) when s = 0 and a is given by equation 6.4.

For the Ormonde siltstone example:

Intact rock: $m = 9.6$, $s = 1$, $\sigma_c = 65$ MPa

Rock mass: $m_b = 4.3$, $s = 0.02$, $\sigma_c = 65$ MPa

6.4.1b Estimation of the base angle of friction, ϕ_b

Since the base angle of friction and hence the base strength criterion, equation 2.8, are the same for both the intact and broken rock, ϕ_b may be determined from a tilt test on cores of the intact rock or by one of the other methods described in chapter 5; or by a knowledge of similar rock behaviour from the literature. In the case of the Ormonde siltstone, the base angle of friction was assumed from a plot of shear stress versus normal stress provided in the literature, and found to be:

$$\phi_b = 30^\circ$$

6.4.1c Determination of the confinement at the brittle-ductile transition point

The confinement at the brittle-ductile transition point, σ_{3t}, is determined by equating equation 6.1 with equation 2.8, according to assumption 8, section 2.3.8. The resulting confinement values at the brittle-ductile transition point for the Ormonde siltstone were determined to be:

Intact rock: $\sigma_{3t} = 163$ MPa
Rock mass: $\sigma_{3t} = 70$ MPa

6.4.1d Determination of the residual strength polynomial constants σ_{cr}, D and F

The residual strength polynomial constants D and F are determined given that σ_{3t} and σ_{cr} are known, by equating the respective strengths and the slopes of equations 6.1 and 2.7 at the brittle-ductile transition point according to assumption 8, section 2.3.8, equations 2.13.

The uniaxial residual strength of the broken rock, σ_{cr} is determined via assumption 12, equation 6.9, such that by equating equations 6.1 and 2.7 when $\sigma_3 = 0$, equation 6.11 is defined:

$$\sigma_{cr} = \sigma_c s^a \tag{6.11}$$

Appendix L provides the detailed derivation of D and F for broken rock resulting in equations 6.12 and 6.13:

$$D=\frac{1}{\sigma_{3t}^{2}}[\sigma_{cr}-[m_b\frac{\sigma_{3t}}{\sigma_c}+s]^{a}+am_b\sigma_{3t}[m_b\frac{\sigma_{3t}}{\sigma_c}+s]^{a-1}] \qquad 6.12$$

$$F=1-am_b[m_b\frac{\sigma_{3t}}{\sigma_c}+s]^{a-1}-\frac{2}{\sigma_{3t}}[\sigma_{cr}-[m_b\frac{\sigma_{3t}}{\sigma_c}+s]^{a}] \qquad 6.13$$

The Ormonde siltstone example provided the following residual strength polynomial parameters:

Intact rock: $D = -0.006$, $F = 3.9$, $\sigma_{cr} = 13$ MPa
Rock mass: $D = -0.013$, $F = 3.7$, $\sigma_{cr} = 9.6$ MPa

In summary, the solutions to the peak, residual, and base strength criteria for the Ormonde siltstone data set were determined for the intact rock and rock mass as given below:

Intact rock: $\sigma_{1p} = \sigma_3 + 65\{0.15\sigma_3 + 1\}^{1/2}$ MPa
$\sigma_{1r} = -0.006\sigma_3^2 + 3.9\sigma_3 + 13$ MPa
$\sigma_{1b} = 3\ \sigma_3$ MPa

Rock mass: $\sigma_{1p} = \sigma_3 + 65\{0.07\ \sigma_3 + 0.02\}^{1/2}$ MPa
$\sigma_{1r} = -0.013\sigma_3^2 + 3.7\sigma_3 + 9.6$ MPa
$\sigma_{1b} = 3\ \sigma_3$ MPa

6.4.1e Comparison of the intact and rock mass strength criteria

Once the peak, and residual strength criteria have been evaluated for both broken and intact rock a comparison can be made by plotting them with the base strength criterion.

The broken rock will have a different brittle-ductile transition point than that of the intact rock, occurring at a lower value of confinement, but both transition points will lie on the base strength curve since the base angle of friction remains the same for intact and broken rock. This is illustrated in figure 6.5.

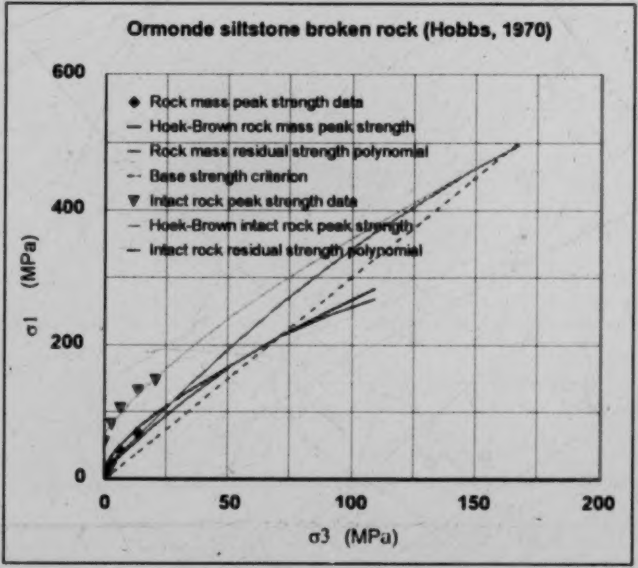

Figure 6.5: Comparison of broken and intact peak, residual and base strength criteria showing two transition points.

6.4.1f Determination of e_b and the solution to the effective friction - strain polynomial

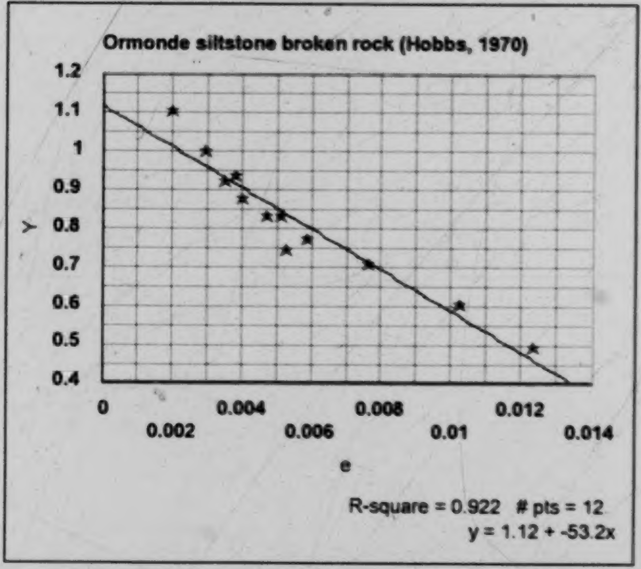

Figure 6.6: Plot of Y versus e to determine the base strain.

The procedure outlined in section 3.7 remains valid for determining the base strain, e_b, with the following change. Despite the fact that both the Hoek-Brown rock mass peak strength criterion and the rock mass residual strength polynomial both describe the broken rock behaviour, it is the derivative of the residual strength with respect to the confining pressure, equation 6.14 that is used rather than the peak strength with respect to confining pressure, equation 3.15, for the rock mass data.

$$\frac{\delta\sigma_1}{\delta\sigma_3}=2D\sigma_3+F \qquad 6.14$$

$$2\theta=2\tan^{-1}\sqrt{2D\sigma_3+F} \qquad 6.15$$

This allows the value of 2θ, equation 6.15, to be derived from equation 3.14, which in turn allows the evaluation of the effective friction data values, equation 3.16, necessary to determine values of Y, equation 3.17 for the Y versus e plot, figure 6.6, where the strain values, e are taken from the available data.

It should be borne in mind that the intact rock data values of 2θ, and subsequently ϕ_e, are still determined using the derivative of the peak strength with respect to confining pressure as previously defined by equation 3.15. All values of ϕ_e for given values of e, irrespective of intact rock or rock mass data source may be used to determine values of Y and plotted as per figure 6.6. The value of e_b was found as:

$$e_b = 0.02$$

As shown in figure 6.6, for the Ormonde siltstone example, all data points are clustered about the linear regression, indicating that regardless of fractured nature of a given rock, there exists a single effective friction function. This is seen more clearly in the comparison plot of effective friction polynomial versus effective friction data, figure 6.7.

The values of R, S and T are evaluated as before for the intact rock using equations 3.12, 3.11 and 3.10 respectively, giving the solution to equation 2.9. The Ormonde siltstone example results in a single effective friction - strain polynomial which describes the post peak behaviour of both the intact rock and the rock mass, as indicated below and in figure 6.7.

$$\phi_e = 71 - 3750\, e_{pp} + 86300\, e_{pp}^{\,2}$$

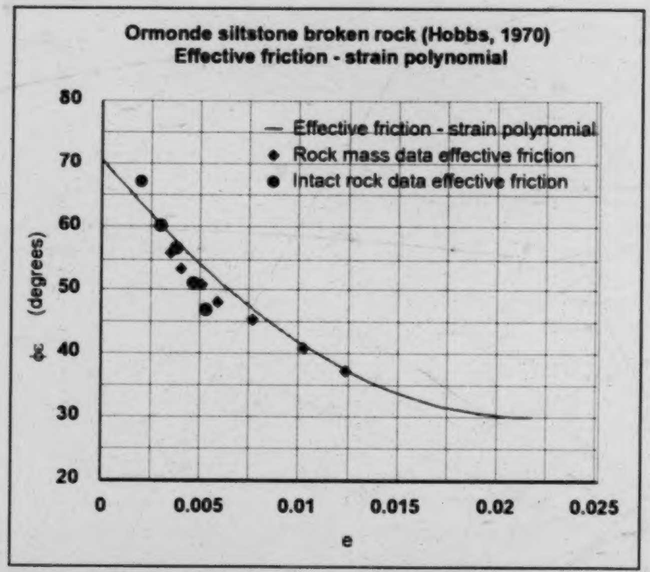

Figure 6.7: Effective friction strain polynomial compared to the available effective friction data values for the intact rock and the rock mass.

6.4.1g Reconstruction of the σ-e curves

The stress-strain reconstruction procedure is the same as outlined in section 4.2.8, with the appropriate changes according to section 6.4.1 as follows:

i Select a value of σ_3 between zero and the brittle-ductile transition.

ii Calculate a value for σ_{1p} from equation 6.1.

iii Determine a value for 2θ from equation 6.15.

iv Calculate a value of σ_{1r} from equation 2.7 using equations 6.11, 6.12 and 6.13.

v Divide the range from σ_{1p} to σ_{1r} into equal increments of σ_{pp}.

vi For each incremented value determine a value of ϕ_e from equation 3.16.

vii For each value of ϕ_e solve the exact solution to equation 2.9 for e_{pp}.

viii Plot the post peak stress strain plot from σ_{pp} versus e_{pp}.

If intact data is available, then the same procedure as outlined in section 4.2.8 should be followed. Both the intact rock and rock mass reconstructed stress-strain curves should be plotted together to show the relationship between intact and broken rock, as illustrated by the Ormonde siltstone example in figure 6.8.

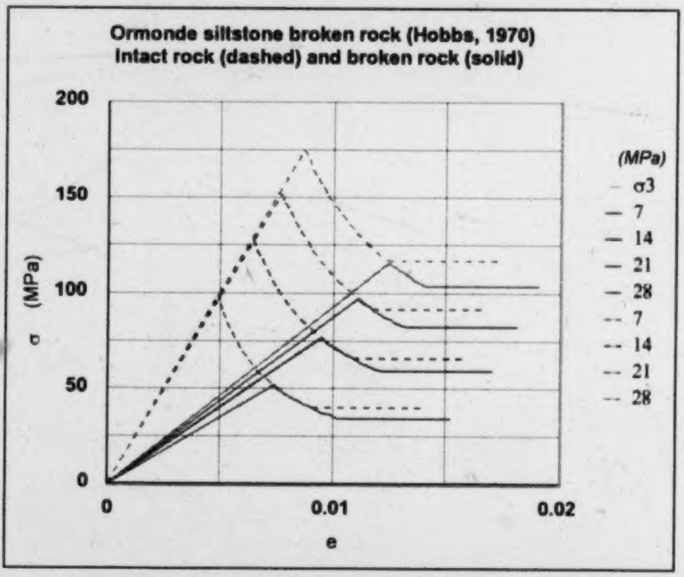

Figure 6.8: Comparison of reconstructed intact and broken rock stress-strain curves for a range of confining pressures.

Figure 6.8 clearly shows that the post peak curve in all confinement cases is the same function for both the intact rock and rock mass. The peak and residual strengths of the intact and broken rock for a given confinement all lie on the same post peak curve. The residual strength breaks away from the post peak curve when that value is reached for a given confinement, after which the rock strains in a ductile manner.

6.4.1h Determination of the post peak modulus and stiffness

The post peak modulus and post peak stiffness are evaluated using the same procedure already outlined in sections 3.8 and 3.9 respectively. Figure 6.9 illustrates the normalized post peak modulus for the Ormonde siltstone, with points for both the intact and broken rock. Regardless of the confinement there is a single post peak modulus function for the intact and broken rock.

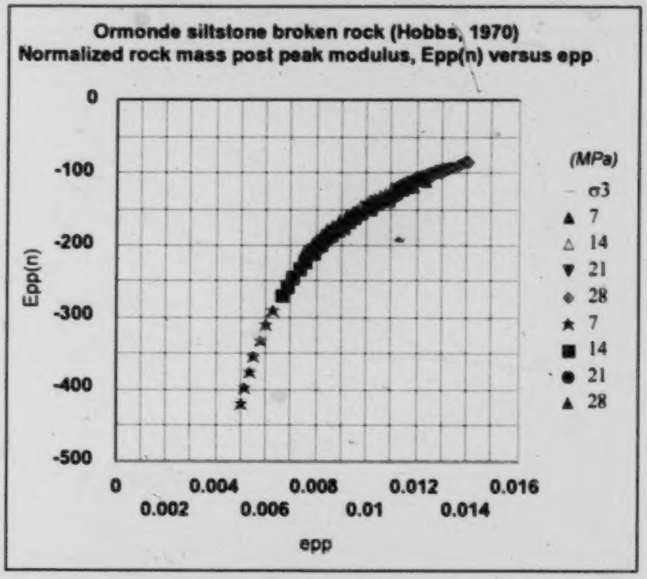

Figure 6.9: Plot of intact and broken rock normalized post peak modulus revealing a single function.

6.4.2 Where only the Hoek-Brown intact peak strength parameters and values of GSI taken from charts (Hoek et al., 1997) are available

An average quality rock mass (Hoek et al., 1997) was selected to verify the postulates as applied to broken rock for the option where no triaxial data is available. Appendix M.1 provides a summary of the data provided from the data set example and the subsequent analysis.

6.4.2a Determination of the Hoek-Brown strength parameters

Knowledge of the intact rock peak strength parameters, m and σ_c as provided in the average quality rock mass data set, together with a means of evaluating the geological strength index, GSI, allowed a determination of the broken rock peak strength parameters, m_b, a and s. Where equations 6.2, 6.3 and 6.4 were used to evaluate these values for the average quality rock mass:

Intact rock: $m = 12$, $s = 1$, $\sigma_c = 80$ MPa
Rock mass: $m_b = 2$, $s = 0.004$, $a = 0.5$

6.4.2b Estimation of the base angle of friction

The base angle of friction in the case of the average quality data set was taken as the Mohr-Coulomb effective friction value provided in the literature. If the value had not been given, then one of the alternative methods mentioned previously could be employed.

$$\phi_b = 33°$$

6.4.2c Determination of the confinement at the brittle-ductile transition point

The confinement at the brittle-ductile transition point, σ_{3t} was determined by the same approach outlined in section 6.4.1c. The values determined for the example data set were found to be:

Intact rock: $\sigma_{3t} = 174\text{MPa}$

Rock mass: $\sigma_{3t} = 28$ MPa

6.4.2d Determination of the residual strength polynomial constants, σ_{cr}, D and F

The residual strength polynomial constants were evaluated as before using equations 6.11, 6.12 and 6.13 as outlined in section 6.4.1d.

Intact rock: $D = -0.007$, $F = 4.5$, $\sigma_{cr} = 16$ MPa

Rock mass: $D = -0.04$, $F = 4.2$, $\sigma_{cr} = 5$ MPa

In summary, the exact solutions to the peak, residual, and base strength criteria for the average quality rock mass data set were determined for the intact rock and rock mass as given below:

Intact rock: $\sigma_{1p} = \sigma_3 + 80\{0.15\sigma_3 + 1\}^{1/2}$ MPa

$\sigma_{1r} = -0.007\sigma_3^2 + 4.5\sigma_3 + 16$ MPa

$\sigma_{1b} = 3.4\sigma_3$ MPa

Rock mass: $\sigma_{1p} = \sigma_3 + 80\{0.025\sigma_3 + 0.004\}^{1/2}$ MPa

$\sigma_{1r} = -0.04\sigma_3^2 + 4.2\sigma_3 + 5$ MPa

$\sigma_{1b} = 3.4\sigma_3$ MPa

6.4.2e Comparison of the intact and rock mass strength criteria

As was carried out in section 6.4.1e, the respective strength criteria were compared for both the intact rock and rock mass as illustrated in figure 6.10. Again, as before, the two transition points coincide with the base strength criterion.

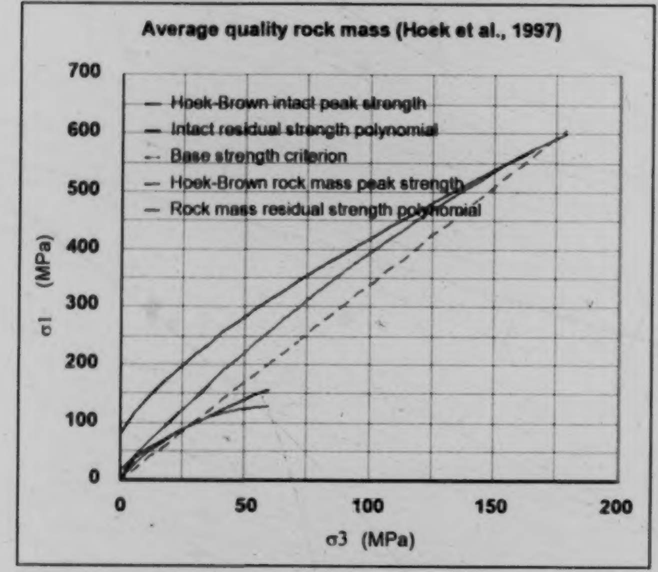

Figure 6.10: Comparison of broken and intact peak, residual and base strength criteria showing two transitions.

6.4.2f Determination of e_b and the solution to the effective friction - strain polynomial

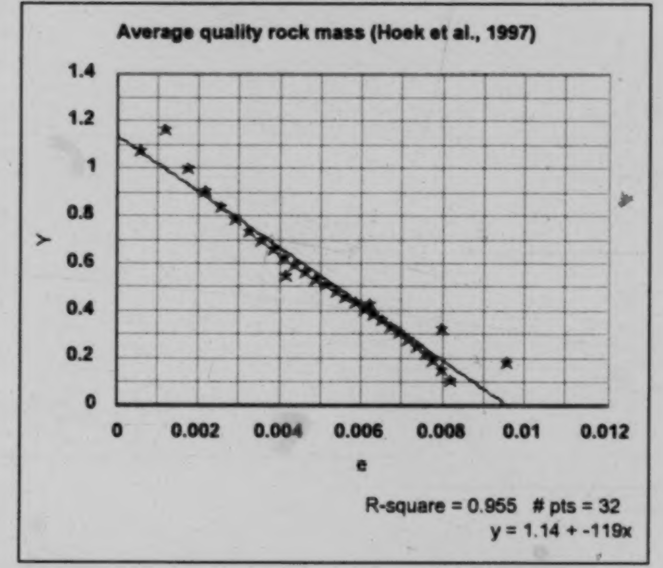

Figure 6.11: Plot of Y versus e to determine the base strain.

Since the original data set provided no strain data, then the strain data was generated using a knowledge of pre-peak moduli. The rock mass pre-peak modulus, $E_{m(broken)}$ was provided in the literature, and the intact rock pre-peak modulus was determined using equation 6.8.

The RMR_{intact} value for use in this empirical relationship was determined using Bieniawski's rock mass rating system (Hoek et al., 1980), where the only adverse effect was the uniaxial compressive strength, which yielded $RMR_{intact} = 92$. The RMR_{broken} value was found from the simple relationship given by Hoek et al. (1997) between GSI and RMR, equation 6.16, and determined to be $RMR_{broken} = 55$, for GSI = 50.

$$GSI = RMR - 5 \qquad 6.16$$

The procedure outlined in section 6.4.1f remained the same for evaluating the effective friction values for use in the Y versus e plot, figure 6.11. The value of e_b for the average quality rock mass was found to be:

$$e_b = 0.01$$

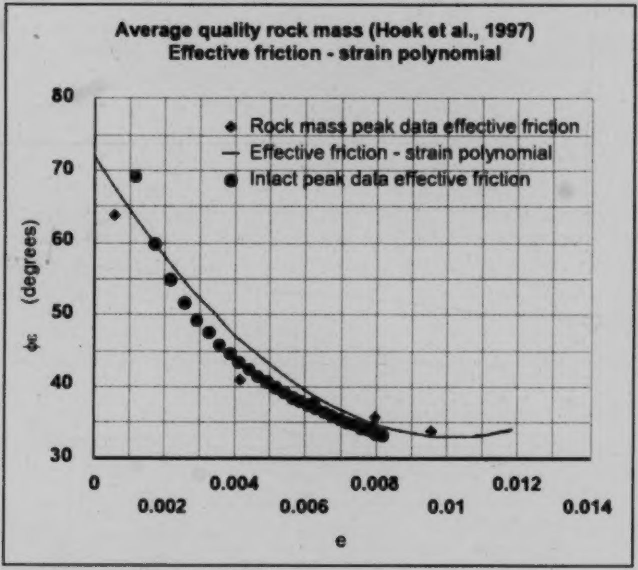

Figure 6.12: Effective friction - strain polynomial compared to the available effective friction data for the intact rock and rock mass.

The values of the R, S and T constants in the effective friction - strain polynomial were determined as outlined in section 6.4.1f providing the solution to the effective friction - strain polynomial for the average quality rock mass:

$$\phi_e = 72 - 7700\, e_{pp} + 380000\, e_{pp}^2$$

The plot of the effective friction - strain polynomial is shown above in figure 6.12. Once again, as illustrated it can be seen that there is a single post peak effective friction function that satisfies the available data.

6.4.2g Reconstruction of the σ-e curves

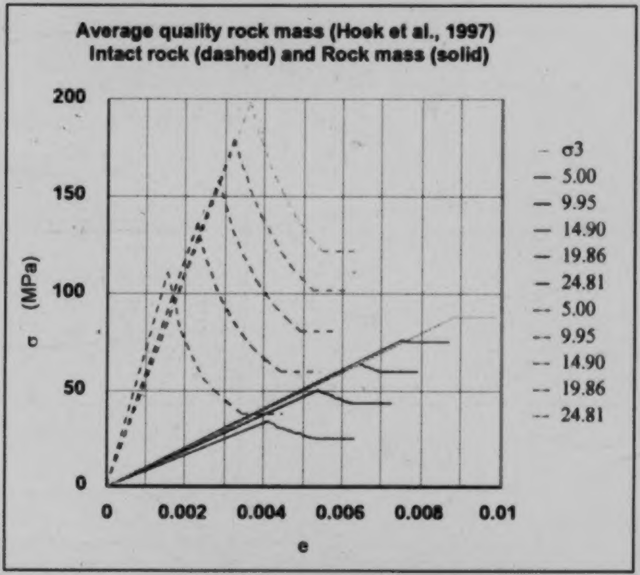

Figure 6.13: Comparison of reconstructed intact and broken rock stress-strain curves for a range of confinement

The same procedure as outlined in section 6.4.1g was used to generate the stress-strain curves for the intact rock and rock mass, as illustrated in figure 6.13. This verifies that for any given confining pressure, the post peak curve is the same function for both intact rock and rock mass. As mentioned in section 6.4.1g, the residual strength breaks away from the post peak curve when that value is reached for a given confinement, after which the rock strains in a ductile manner.

6.4.2h Determination of the post peak modulus and stiffness

The procedure outlined in sections 3.8 and 3.9 remains valid for the determination of post peak modulus and stiffness respectively. Figure 6.14 shows the normalized post peak modulus for the average quality rock mass example, again illustrating that regardless of confining pressure there is a single post peak modulus function for both the intact rock and rock mass.

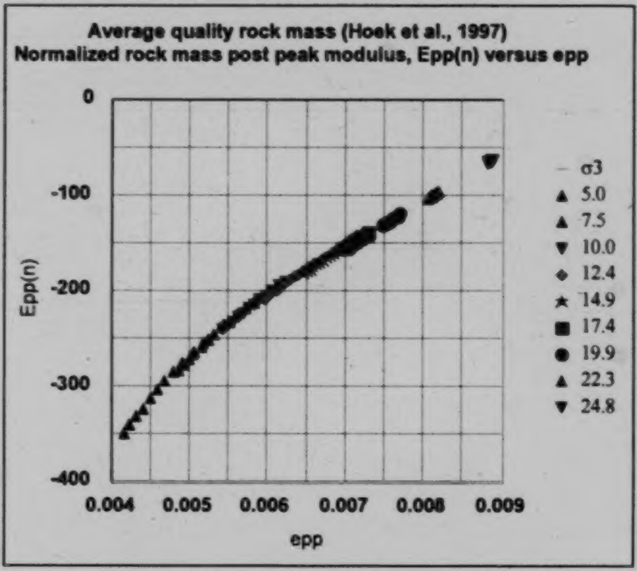

Figure 6.14: Plot of intact and broken rock normalized post peak modulus as a single function.

6.4.3 Verification of the postulates and assumptions using other broken rock data sets from the literature

Five additional data sets in addition to the two sets in sections 6.4.1 and 6.4.2, comprising the total available rock mass data sets, have been worked in a similar fashion and summarized in appendix M. In all cases the postulates and assumptions have been verified as discussed in section 6.4.4. In addition, appendices N and M contain two further data sets, a crushed basalt (Hussaini, 1991) and the Panguna andesite (Hoek et al., 1980) respectively. These two sets have been worked and also verify the postulates and assumptions, but have been treated seperately in sections 6.5 and 6.6 respectively as special cases.

6.5 Evaluation of a crushed rock data set - crushed basalt (Hussaini, 1991)

The crushed basalt data set (Hussaini, 1991) as provided in appendix N comprises of 5 sets of triaxial data with each set being conducted on a different crush size. The varying crush size can be considered as a variance of the rock mass rating, RMR of the same rock. With this in mind the data set has been worked in accordance with the triaxial data set approach to broken rock as outlined in section 6.4.1. The summary of the calculations is provided in appendix N. Treating each crush size separately, the Hoek-Brown peak strength parameters were shown to vary with crush size as shown in table 6.1.

Assuming a value for the base angle of friction at $\phi_b = 33°$, since none was given in the paper by Hussaini (1991), the brittle-ductile transition point confining pressure and the residual strength polynomial parameters were also shown to vary with crush size as shown in table 6.2.

	6.3 mm crush	12.7 mm crush	25.4 mm crush	50.8 mm crush	76.2 mm crush
σ_c (MPa)	172	172	172	172	172
m_b	0.16	0.18	0.20	0.23	0.26
s	0.00005	0.00005	0.0001	0.00012	0.00013

Table 6.1: Summary of the peak strength parameters for the crushed basalt.

	6.3 mm crush	12.7 mm crush	25.4 mm crush	50.8 mm crush	76.2 mm crush
σ_{3t} (MPa)	4.8	5.5	6.2	6.9	7.9
σ_{cr} (MPa)	1.2	1.3	1.8	1.9	2.0
D	-0.2	-0.17	-0.15	-0.14	-0.12
F	4.1	4.1	4.0	4.1	4.1

Table 6.2: Summary of σ_{3t} and the residual strength polynomial parameters.

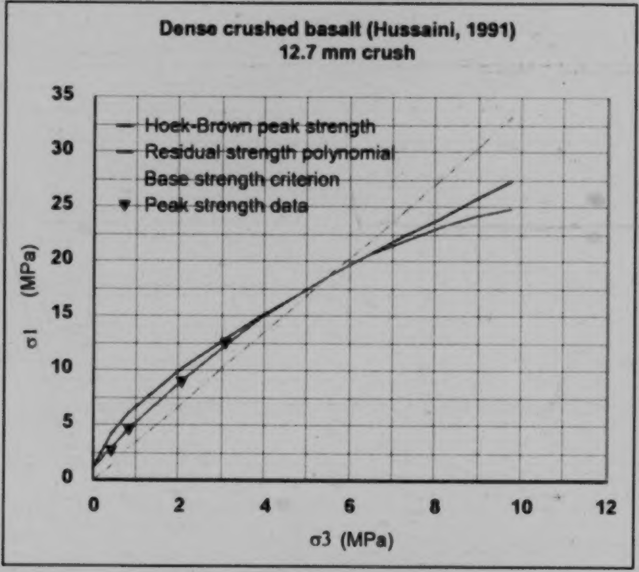

Figure 6.15: Comparison of the peak, residual and base strength criteria and the available peak strength data clustered about the residual strength polynomial.

The comparison of the peak, residual, and base strength criteria arising from the parameters given above showed the appropriate relationships with respect to crush size, as provided in appendix N. It was interesting to note that the available peak strength data points agreed more with the residual strength criterion rather than the peak strength criterion, particularly for the smaller crush sizes, as echoed in figure 6.15. However, as the particle size increases and the confinement increases, there appears to be a trend where the available peak strength data moves more towards the behaviour of the peak strength criterion, as shown in figure 6.16.

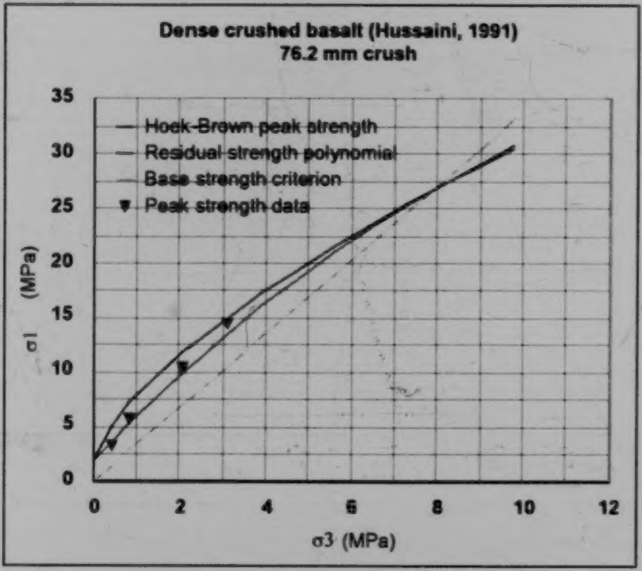

Figure 6.16: Comparison of the peak, residual and base strength criteria, and the available peak strength data moving towards the peak strength criterion.

This suggests that in the case of broken rock, although a peak strength criterion adequately satisfies the necessity of identifying a brittle-ductile transition point, the residual strength polynomial is a better descriptor of the available broken rock peak strength data at low confinement and small crush size.

In the case of intact rock it was clearly seen that the peak strength criterion provided a good representation of the available intact rock peak strength data, appendices, H, J, and K, and the residual strength polynomial provided a good representation of the available residual strength data.

However, once the intact rock had exceeded the peak strength at peak strain, the rock no longer obeyed the intact peak strength criterion. If the rock were reloaded to a new peak strength, having previously been fractured, then the new peak strength would be less than the intact rock peak strength, where the new peak strength would be dependent on the roughness and strength of the rough asperities of the broken surface. There might be some crushing of the asperities (an overcoming of material cohesion) depending on the level of confinement, but for the most part the new peak strength would be dominated by the surface roughness, amounting to an effective friction. This agrees with the definition of effective friction provided in section 2.1.

The crushed rock can be considered as a large number of broken surfaces such that as a whole the rock sample behaves more in a residual strength fashion at low confining pressures, with sliding over many rough surfaces, rather than breaking the cohesion of the material to smooth the surfaces of the crushed particle surface asperities, as evident at the higher confining pressures and larger crush size.

Taking all the data together for determining a base strain and the effective friction - strain polynomial parameters, the Y versus e plot, appendix N, showed that all the data clustered around a single function and allowed a single effective friction -

strain polynomial function to be defined as shown in figure 6.17, where the base strain, $e_b = 0.3$. The high value of base strain is indicative of a highly crushed material, such that considerable deformation is possible for relatively small loads.

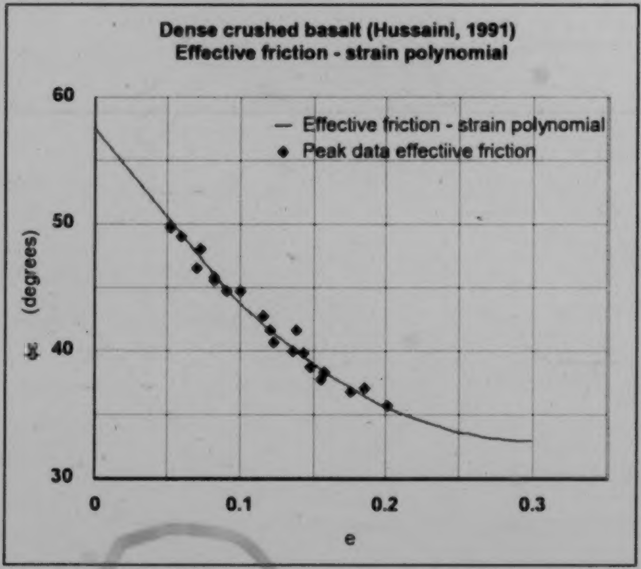

Figure 6.17: Effective friction - strain polynomial for the crushed basalt.

Figure 6.18 shows the reconstructed stress-strain curves for the complete range of crush sizes for 2 randomly selected confining pressures, within the range of the smallest crush size brittle-ductile transition point confining pressure.

Regardless of crush size, the post peak function is the same for a given confining pressure. The peak and residual strengths decrease with decreasing crush size and the residual strength departs the post peak function in the same fashion as previously discussed in sections 6.4.1g and 6.4.2g.

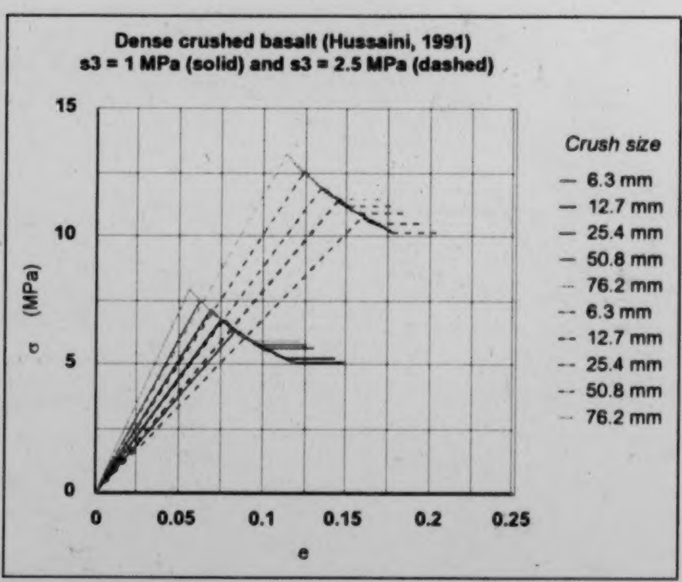

Figure 6.18: Reconstructed stress-strain curves for all crush sizes for $\sigma_3 = 1$ MPa and $\sigma_3 = 2.5$ MPa.

It can thus be concluded that regardless of RMR for a given rock, the post-peak relationship is the same for a given confinement, and that both peak and residual strengths decrease with decreasing RMR for a given confinement.

If the normalized post peak modulus is plotted against post peak strain, figure 6.19, then regardless of confinement or RMR, there exists a single normalized function for the post peak modulus.

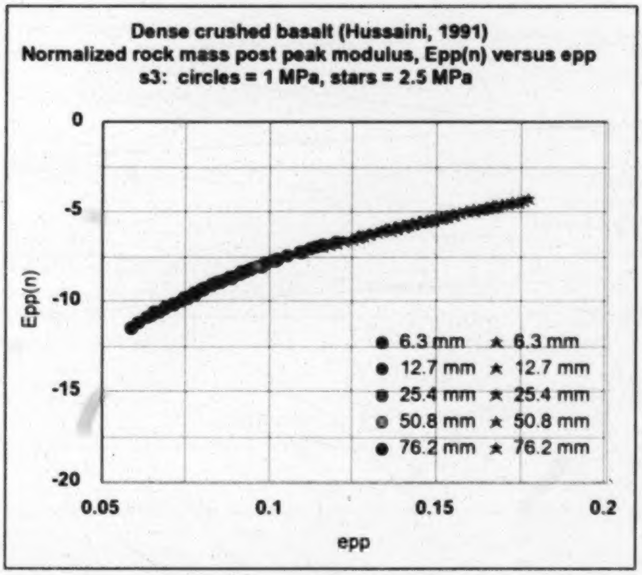

Figure 6.19: Normalized post-peak modulus versus post-peak strain for the crushed basalt.

6.6 Evaluation of the Panguna andesite data set (Hoek et al., 1980)

The Panguna andesite data set (Hoek et al., 1980) as provided in appendix P is made up of $RMR_{(broken)}$, m and σ_c values, which were used to generate the rock mass values of GSI, m_b, s, a and $E_{m(broken)}$, as indicated in table 6.3. Note that the values of s reported here were determined from equation 6.3 and differ from those reported by Hoek et al. (1980). Hoek et al. Regarded σ_c as intact and constant regardless of the weathered state of the Panguna andesite. However, with weathering the σ_c value may change. For the purposes of this analysis, σ_c is assumed constant.

The analysis of the data was carried out initially using a common base friction, ϕ_b of 22°, which was later changed for varying base friction values dependent on the degree of weathering, as was later indicated by the effective friction - strain plot. The GSI value was determined using equation 6.16. The Hoek-Brown peak strength parameters; m_b, s and a were determined using equations 6.2, 6.3 and 6.4 respectively.

			Degree of weathering			
	Undisturbed	Recompacted	Fresh/sl.	Moderate	High	Intact
RMR_{broken}	46	28	26	18	8	97
GSI	41	23	21	13	3	92
σ_c (MPa)	265	265	265	265	265	265
ϕ_b (deg.)	22	22	18	18	10	45
m_b	0.28	0.12	0.04	0.03	0.01	18.9
s	0.015	0.0061	0.0021	0.0016	0.0006	1
a	0.5	0.54	0.55	0.59	0.64	0.5
$E_{m(broken)}$	7940	2820	2510	1590	890	94000

Table 6.3: Peak strength, base strength and pre-peak modulus parameters

To enable the generation of strain data, the values for $E_{m(broken)}$ were determined using the appropriate equation from section 6.3.2, and the $E_{m(intact)}$ values were determined using the empirical relationship, equation 6.8.

The base strength criterion was determined using the initial assumed value for $\phi_b = 22^\circ$. The residual strength polynomial in each case was determined as per section 6.4.1d. Its parameters are summarized with the brittle-ductile confinement in table 6.4.

			Degree of weathering			
	Undisturbed	Recompacted	Fresh/slight	Moderate	High	Intact
σ_{3t} (MPa)	62.5	24.8	15.4	9.2	7.5	226
σ_{cr} (MPa)	32.1	17.3	9.2	6.1	2.4	53
D	-0.003	-0.004	-0.003	-0.002	-0.0009	-0.01
F	1.9	1.6	1.3	1.3	1.1	8.0

Table 6.4: σ_{3t} and residual strength polynomial parameters, σ_{cr}, D and F.

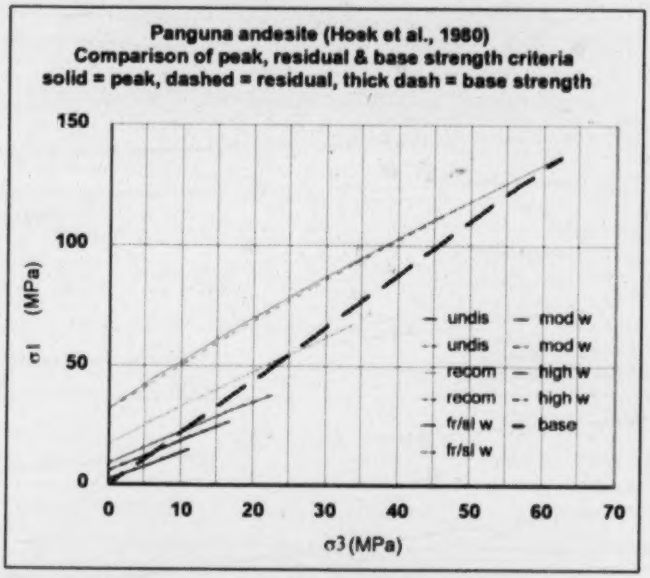

Figure 6.20: Comparison of the peak, residual and base strength criteria with respect to weathered rock mass.

Figure 6.20 shows the comparison of the peak, residual and base strength criteria, as derived from the parameters in tables 6.3 and 6.4. As was found with the crushed basalt in section 6.5, the Panguna andesite seems to vary its peak and residual strength behaviour as a function of changing RMR, as would be reflected with a variance in weathered characteristic.

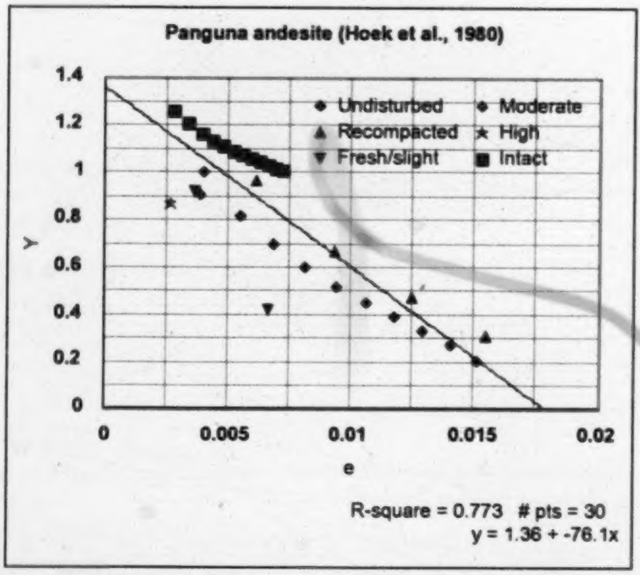

Figure 6.21: Plot of Y versus e showing scatter in data due to weathering of rock mass.

Taking the entire group of data, regardless of degree of weathering and plotting as Y versus e to determine e_b, R, S and T, as laid out in appendix P, figure 6.21 revealed that with increased levels of weathering the data tended to have lower values of Y. The more diverse nature of the data is reflected by the lower regression number of 0.77, than experienced with earlier Y versus e plots. A value for e_b was determined at $e_b = 0.015$, which is achieved at the base angle of friction in figure 6.22.

Plotting the solution for the effective friction - strain polynomial for the constants R, S and T given in appendix P, and comparing it to the effective friction data, as illustrated in figure 6.22, revealed that the base angle of friction appeared to become lower with increasing levels of weathering, and that the intact rock indicated a higher base angle of friction than originally assumed at 22°.

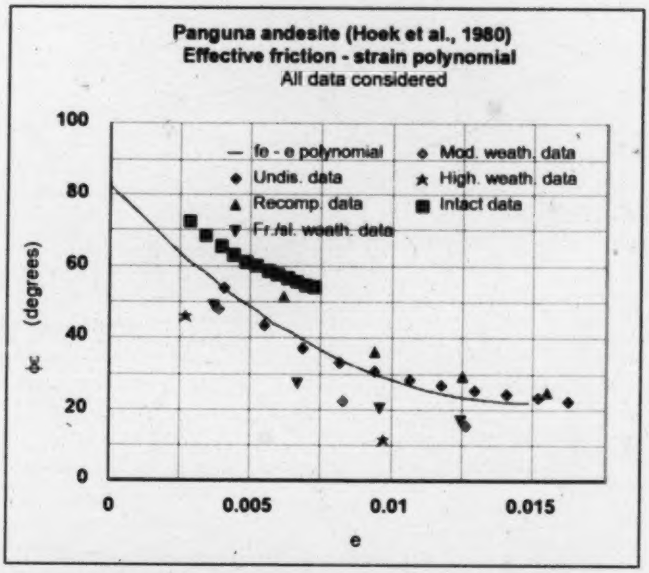

Figure 6.22: Effective friction - strain polynomial for the Panguna andesite, indicating varying base friction angle with degree of weathering.

Due to the varying ϕ_b values with weathering, independent values of ϕ_b were estimated from figure 6.22 and the Y versus e plots re-worked for each degree of weathering. Figure 6.23 indicates that ϕ_b is a function of weathering, and since the degree of weathering can be expressed in terms of RMR (Hoek et al., 1980), then a plot of ϕ_b versus RMR indicated that there is a definite correlation between ϕ_b and degree of weathering, figure 6.24, for the Panguna andesite rock mass.

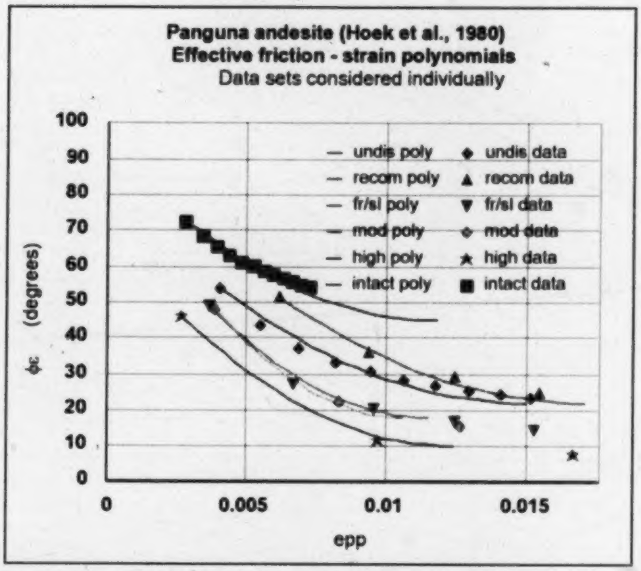

Figure 6.23: Effective friction - strain plots for each individual weathered set with ϕ_b values from figure 6.24.

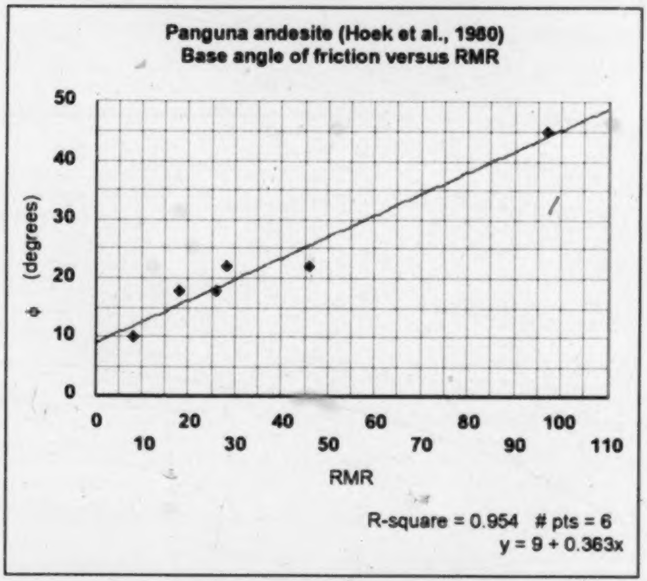

Figure 6.24: Relationship between ϕ_b and RMR.

The reconstructed stress-strain curves for a constant level of confinement are shown in figure 6.25 for both weathered and unweathered rock masses. It appears that there are several post peak relationships for a given confinement rather than just the one relationship as seen with previous examples. This seems to be due to the variance in ϕ_b that occurs with increasing levels of weathering.

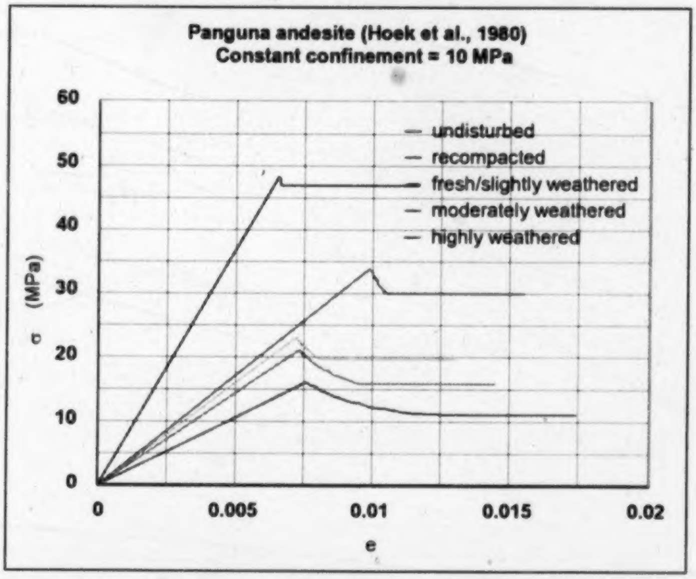

Figure 6.25: Reconstructed stress-strain plots for a single confining pressure with varying degree of weathering.

The effect seen in figure 6.25 carries over to the evaluation of normalized post peak modulus, as shown in figure 6.26.

It can therefore be concluded that since the effect of weathering changes the base angle of friction of the rock, in other words it changes a physical property of the rock, then the Joseph-Barron approach may be used in conjunction with a ϕ_b - RMR rock specific empirical function, such as illustrated in figure 6.24.

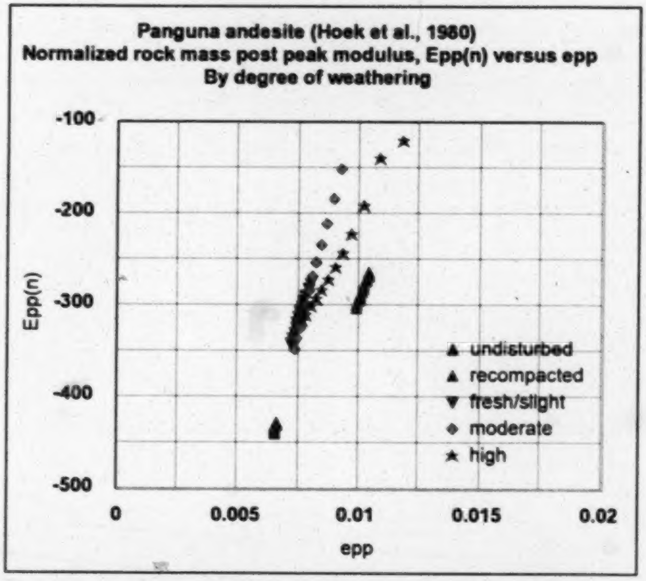

Figure 6.26: Plot of normalized post peak modulus versus post peak strain showing the effect of weathering on the Panguna andesite.

6.7 Conclusions

For each of the 8 sets of data taken from the available literature and reported in sections 6.1 through 6.5 and appendices M and N, post peak effective friction - strain relationships and reconstruction of the post peak stress-strain data was conducted successfully for both the intact and broken rock. This showed that in each case a common relationship exists for the post peak region with respect to a given confinement, that can be normalized to a single post peak modulus function by rock type. The only exception is the Panguna andesite, reported in appendix P and section 6.6, which was affected by a changing base angle of friction due to weathering.

It may be concluded that the postulates and assumptions in chapter 2 and chapter 6 have been verified and validated for all non-weathered data sets investigated in this chapter. Of particular note:

i There is a single effective friction - strain relationship that applies to both intact and broken rock.

ii The post peak stress-strain behaviour for both the intact and broken rock is the same relationship for a given confinement.

iii The post peak modulus relationship is the same for both intact and broken rock.

Thus, by gathering information from intact rock samples of manageable size, it is possible to estimate the rock mass post peak relationships.

Chapter 7

Application of the Joseph-Barron approach to coal

7.1 Introduction

As was found for broken rock, there are only a few coal data sets in the available literature that contain sufficient triaxial strength and strain data for a range of confining pressures, that permit analysis via the Joseph-Barron approach. Ten sets of data were identified as providing sufficient data for analysis, reported by Kripakov (1981) and Hobbs (1964). These data sets consist entirely of triaxial test results conducted on laboratory-sized samples. The laboratory specimen sizes, as suggested by Barron et al. (1992a), do not fall into either the category of intact coal or coal mass, but lie somewhere between the two. Consequently, a size classification termed "non-intact" is used to describe these test sizes, and the methodology outlined by Barron et al. (1992a) employed to allow an evaluation of the intact coal and coal mass behaviour from the non-intact coal behaviour.

7.2 Intact coal, non-intact coal and coal mass strength properties

It has been well documented in the literature that the strength of laboratory-sized coal specimens is highly dependent on the size and shape of the specimens. This sensitivity to specimen size and shape is thought to be a clear, indirect indication that the specimens contain discontinuities causing strength variations. Consequently, in the size range represented by laboratory sized specimens such as those reported by Kripakov (1981) and Hobbs (1964), the coal cannot be regarded as intact and thus the Hoek-Brown parameter s cannot be unity.

Hoek et al. (1982), in discussing comments by Bieniawski et al. (1982) stated that the variance in the Hoek-Brown parameter m for coal did not allow m to be considered a constant for that rock type. Hoek et al. stated that:

> *"....The most likely explanation for this unexpectedly wide range in m values was that the specimens were not truly intact and the assumption that s = 1 was not justified."*

Tao (1991) and Barron et al. (1992a) assumed that laboratory size coal specimens could not be considered intact, resulting in the development of an approach to estimate both the intact and coal mass strength properties from tests on non-intact coal specimens. From this work, a general expression, in Hoek-Brown form, was derived for coal strength, equation 7.1:

$$\sigma_1 = \sigma_3 + \{sm\sigma_c\sigma_3 + s\sigma_c^2\}^{1/2} \qquad 7.1$$

Where σ_c is the uniaxial compressive strength of the intact coal, m is the intact Hoek-Brown m parameter, and the Hoek-Brown s parameter is a function of the triaxial test specimen width, b and height, h. Tao (1991) and Barron et al. (1992a) showed that s could be approximated by one of three empirically derived relationships:

i If $b^{1/2}/h > 8.784$ and $b < 0.013$ m then the coal specimen can be considered intact and $s = 1$.

ii If $0.784 < b^{1/2}/h < 8.784$ and $0.013 < b < 1.625$ m then the coal strength depends on size and the non-intact value of s, denoted by s_{ni} is approximated by equation 7.2:

$$s_{ni} = \{0.086 + 0.104[b^{1/2}/h]\}^2 \qquad 7.2$$

ii If $b^{1/2}/h < 0.784$ or $b > 1.026$, then the coal specimen can be considered to approximate the coal mass, and the strength is no longer size or shape dependent. In this case $s = 0.028$.

Where b and h are in metres.

For example, suppose a suite of triaxial tests are performed for coal specimens in the size range defined by case ii. The specimen dimensions, b and h in units of metres are known and so s may be determined from equation 7.2. If σ_1 and σ_3 are the triaxial data pairs obtained from laboratory scale tests, then a regression analysis of $\{\sigma_1 - \sigma_3\}^2/s_{ni}$ versus σ_3 can be carried out on a linear re-arrangement of equation 7.1, as given by equation 7.3.

$$\frac{(\sigma_1-\sigma_3)^2}{s_{ni}} = m\sigma_c\sigma_3+\sigma_c^2 \qquad 7.3$$

The intercept and the slope of the linear regression allow the determination of the intact coal uniaxial compressive strength, σ_c and the Hoek-Brown m parameter.

Having determined the intact coal values for σ_c and m, the non-intact value for m, denoted m_{ni}, is determined from a comparison of equation 7.1 with equation 2.6, revealing equation 7.4:

$$m_{ni} = m\, s_{ni} \qquad 7.4$$

Similarly for the coal mass, given that s = 0.028, the coal mass value for m, denoted by m_{cm} is evaluated via equation 7.5:

$$m_{cm} = 0.028\ m \qquad 7.5$$

This allows the respective Hoek-Brown peak strength criteria for non-intact coal, intact coal and coal mass to be evaluated from the non-intact available data, equations 7.6, 7.7 and 7.8 respectively.

Non-intact coal: $\sigma_1 = \sigma_3 + \{m_m\sigma_c\sigma_3 + s_m\sigma_c^2\}^{1/2}$ 7.6

Intact coal: $\sigma_1 = \sigma_3 + \{m\sigma_c\sigma_3 + s\sigma_c^2\}^{1/2}$ 7.7

Coal mass: $\sigma_1 = \sigma_3 + \{m_{cm}\sigma_c\sigma_3 + 0.028\sigma_c^2\}^{1/2}$ 7.8

7.3 Postulates

The postulates already outlined in sections 2.2 and 6.2 remain valid, plus the addition of the following:

7.3.1 Postulate 6 - Effective friction - strain relationship for coal

At any point in the post peak region, prior to and including the residual strength it is postulated that same the effective friction - strain relationship postulated in section 2.2 holds for non-intact coal, intact coal and coal mass of the same coal type.

$$\phi_e = f(e_{pp}) \qquad 2.4$$

7.3.2 Postulate 7 - Post peak stress-strain behaviour of coal

It is postulated that the peak and residual stress and strain values for non-intact coal, intact coal and coal mass for a given confinement, σ_3, describe points that lie on a common post peak stress-strain relationship for similar confinement conditions. The shape of the post peak stress-strain curve for the non-intact coal is identical to that of the intact coal which is also identical to that of the coal mass.

The residual strength values for the intact coal, non-intact coal and coal mass break away from the common post peak stress-strain relationship and thereafter remain constant for an incremental increase in strain.

7.3.3 Postulate 8 - The normalized coal post peak modulus

It is postulated that the normalized post peak modulus for the intact coal, non-intact coal and coal mass follow the same relationship.

7.4 Assumptions

Assumptions 1 through 9 outlined in section 2.3 remain valid for intact coal, non-intact coal and coal mass. The Hoek-Brown peak strength criterion, equation 2.6 has been adapted for application to non-intact coal, intact coal and coal mass, as described in section 7.2 by equations 7.6, 7.7 and 7.8 respectively. Assumption 12 from section 6.3.3 remains valid for non-intact coal and coal mass, since both may be described as broken in nature.

7.4.1 Assumption 13 - Estimation of the failure angle, 2θ

When dealing with the transition from intact rock peak to residual strength it has been stated in section 3.7.1 that the angle of the failure plane, 2θ remains constant. This premise has been shown to be applicable for both intact and broken rock respectively in all previous examples and continues to be considered applicable for intact coal, non-intact coal and coal mass. For intact rock the value of 2θ is determined via the derivative of the peak strength criterion with respect to σ_3, equations 3.14 and 3.15.

It was also shown in section 6.4.1.f that the 2θ value for broken rock may be determined via the derivative of the residual strength polynomial with respect to σ_3 since broken rock behaves more closely to residual than peak strength behaviour. 2θ in this case is given by equations 6.14 and 6.15.

In all of the above cases, data was available for the intact rock and the broken rock. But when only non-intact coal data is available, what value of 2θ is appropriate to use for the intact coal and coal mass relationships for which there is no data?

It is assumed that the value of 2θ determined via the non-intact coal residual strength polynomial, determined from the available data, remains the same for both the intact coal and the coal mass for a given value of σ_3. It is not derived from the derivative of the intact coal peak strength criterion nor the coal mass residual strength polynomial since both these relationships are indirectly derived from the non-intact coal data. It is assumed that a more accurate evaluation of the relationship between intact coal, non-intact coal and coal mass is achieved by evaluating 2θ from the source non-intact coal data residual strength polynomial relationship.

7.5 Application of the Joseph-Barron approach to coal and verification of postulates 6, 7 and 8

As mentioned in section 7.1, the triaxial data reported in the literature is dominated by laboratory manageable specimen sizes that fall between the intact and coal mass definitions.

The author identified one data set where both peak and residual strength and strain data were reported (Kripakov, 1981) and nine data sets where peak strength data and pre-peak moduli were reported (Hobbs, 1964). All data sets were reported for coal specimen size identified as case ii of section 7.2 establishing the data as being non-intact coal. These ten data sets have been worked to verify the postulates and assumptions and are provided in appendix R.

An example data set from the available literature has been used to demonstrate the Joseph-Barron approach as applied to coal. This analysis follows the procedure laid out in chapter 3 and chapter 6, depending on whether the intact coal or non-intact coal and coal mass are being analyzed respectively. The data set reported by Hobbs (1964) describes triaxial measurements made on non-intact coal specimens extracted from the Cwmtillery coal mine, Wales.

7.5.1 Determination of the Hoek-Brown strength criterion constants

The coal specimen dimensions were provided as b = 0.025 m and h = 0.051 m. Following the procedure described in section 7.2, the non-intact coal (case ii) was evaluated for the specimen size. Using equation 7.2 the Hoek-Brown non-intact coal strength parameter, s_{ni} was determined to be 0.17. The linearized form of the generalized Hoek-Brown peak coal strength criterion, equation 7.3 allowed a plot of $(\sigma_1 - \sigma_3)^2/s_{ni}$ versus σ_3, figure 7.1, to yield the intact coal parameters, $\sigma_c = 60$ MPa and $m = 22$.

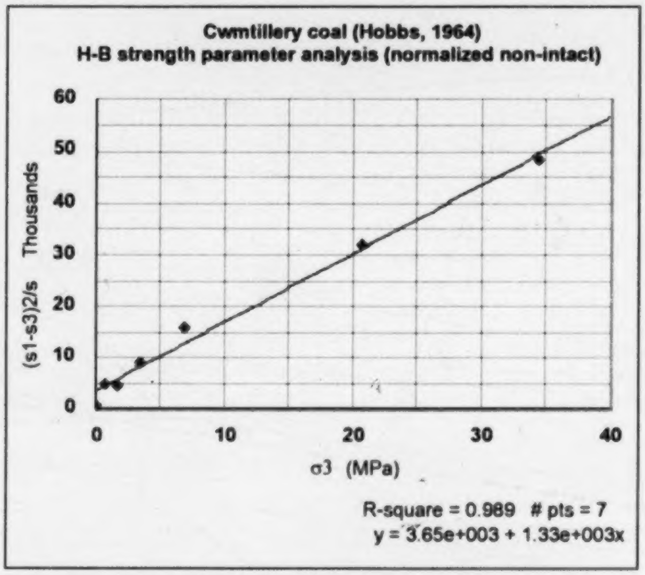

Figure 7.1: Linearized Hoek-Brown plot to determine m and the uniaxial intact compressive strength, σ_c.

Using equations 7.4 and 7.5 the non-intact coal and coal mass m values were found to be $m_{ni} = 3.7$ and $m_{cm} = 0.6$ respectively. This allowed the definition of the non-intact coal, intact coal and coal mass Hoek-Brown peak strength criteria as given by equations 7.6, 7.7 and 7.8 respectively, resulting in equations 7.9, 7.10 and 7.11:

Non-intact coal: $\sigma_{1p} = \sigma_3 + \{226\sigma_3 + 621\}^{1/2}$ MPa 7.9

Intact coal: $\sigma_{1p} = \sigma_3 + \{1330\sigma_3 + 3650\}^{1/2}$ MPa 7.10

Coal mass: $$\sigma_{1p} = \sigma_3 + \{37\sigma_3 + 102\}^{1/2} \text{ MPa} \qquad 7.11$$

7.5.2 Estimation of the base angle of friction, ϕ_b

Since no indication of a base angle of friction was reported with the Cwmtillery coal data set, as was the case for all the data sets reported by Hobbs (1964), a base angle of friction was assumed at $\phi_b = 33°$. This value was applied to most of the data sets since a variance in ϕ_b from the actual value was shown to have a minor overall effect as illustrated in section 4.5.

This allowed a base strength criterion, equation 7.12 to be evaluated from equation 2.8; the base strength criterion being common to all three coal states.

$$\sigma_{1b} = 3.4\,\sigma_3 \qquad 7.12$$

7.5.3 Determination of the brittle-ductile transition point confinements

The brittle ductile confinement for each of the three coal states was evaluated by equating equation 7.12 to equations 7.9, 7.10 and 7.11 respectively, according to assumption 8, section 2.3.8.

	σ_{3t}
Non-intact coal:	42 MPa
Intact coal:	235 MPa
Coal mass:	8.6 MPa

7.5.4 Determination of the residual strength polynomial constants σ_{cr}, D and F

In the case of the intact coal, the residual uniaxial compressive strength was estimated at 20% of the uniaxial compressive strength. The non-intact coal and coal mass residual uniaxial compressive strengths were determined using equation 6.11 in accordance with assumption 12. In all cases the value of the Hoek-Brown exponent, a, was taken as 0.5.

Having determined the values of σ_{cr} for all 3 coal states and knowing the values of σ_{3t} for all three coal states from section 7.5.3, the values of D and F for each coal state were determined using equations 3.4 and 3.5 for the intact coal, and equations 6.12 and 6.13 for the non-intact coal and coal mass. This allowed the residual strength polynomials, equations 7.13, 7.14 and 7.15 to be stated.

Non-intact coal: $\sigma_{1r} = -0.02\sigma_3^2 + 3.5\sigma_3 + 25$ MPa 7.13

Intact coal: $\sigma_{1r} = -0.04\sigma_3^2 + 2.5\sigma_3 + 10$ MPa 7.14

Coal mass: $\sigma_{1r} = -0.005\sigma_3^2 + 4.5\sigma_3 + 12$ MPa 7.15

7.5.5 Comparison of the peak residual and base strength criteria

Figure 7.2 shows the comparison of the three strength criteria for the non-intact coal and the coal mass, while the intact coal is shown separately in figure 7.3 due to the increase in strength scale for the intact coal relations compared to the non-intact coal or coal mass.

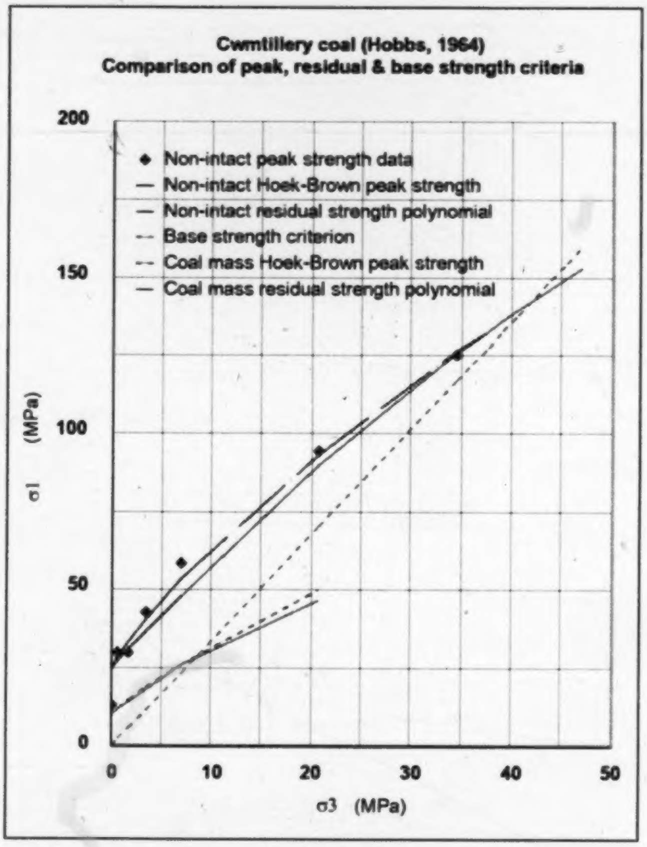

Figure 7.2: Comparison of the strength criteria and non-intact coal to coal mass relationships for Cwmtillery coal.

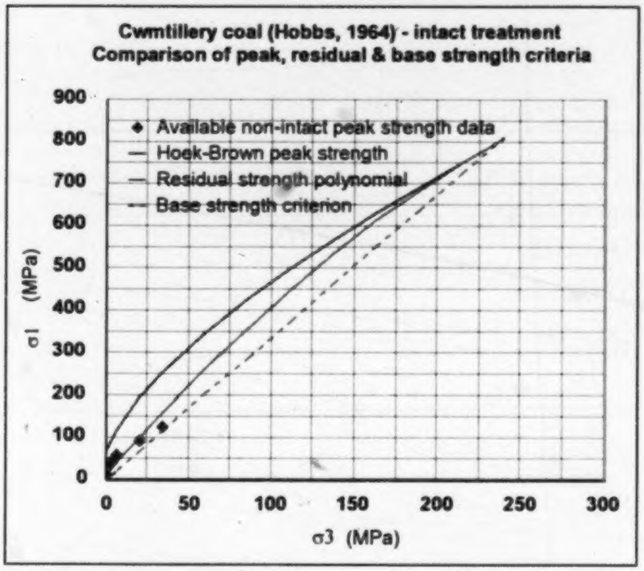

Figure 7.3: Comparison of the strength criteria for the intact Cwmtillery coal.

7.5.6 Determination of e_b and the solution to the effective friction - strain polynomial

Since only non-intact coal strength and strain data were available, only non-intact coal effective friction and strain values were used to evaluate the effective friction strain polynomial via the determination of e_b using the linearized Y versus e form, figure 7.4 and equations 3.17 and 3.18, and the polynomial constant equations 3.12, 3.11 and 3.10 for R, S and T respectively.

In order to evaluate the effective friction values from the available data, the value of 2θ was determined using equation 6.15, since the non-intact coal is considered to be essentially broken.

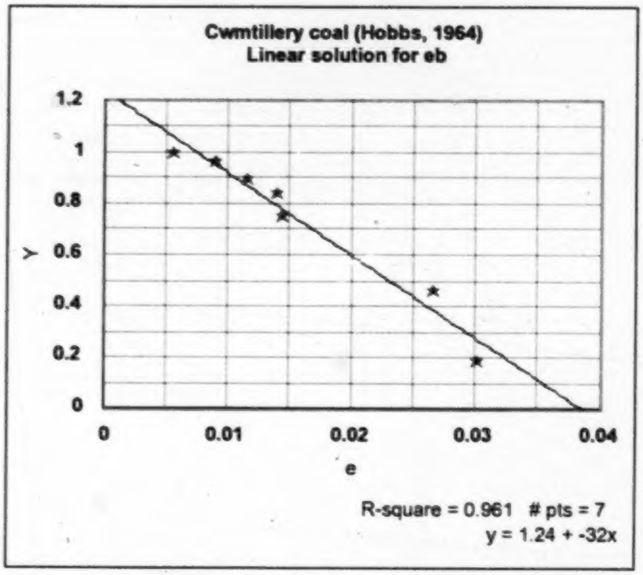

Figure 7.4: Plot of Y versus e to determine the base strain for the Cwmtillery coal.

This allowed an evaluation of the base strain from the slope at $e_b = 0.04$, and the solution to the effective friction - strain polynomial as given in equation 7.16:

$$\phi_e = 72 - 2130e_{pp} + 28900e_{pp}^2 \qquad 7.16$$

7.5.7 Comparison of the ϕ_e - e curve with the ϕ_e - e data

Figure 7.5 shows a correlation between the effective friction - strain polynomial and the effective friction data, verifying postulates 1 and 2.

It is this function that is assumed to be common for non-intact coal, intact coal and coal mass, as defined by postulate 6.

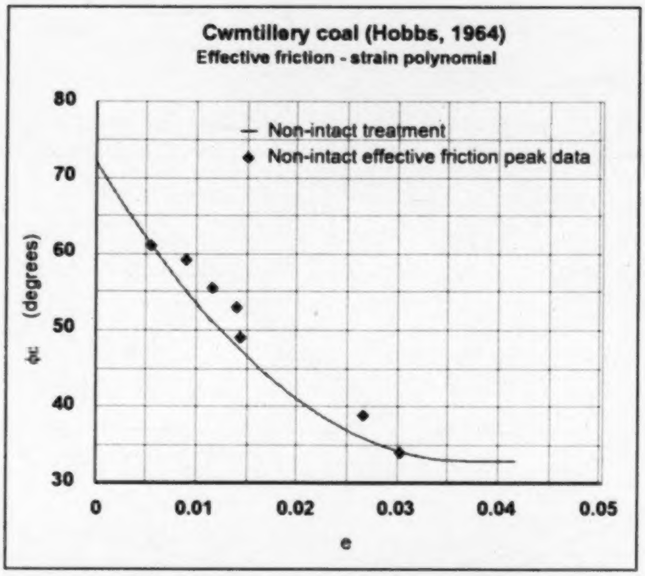

Figure 7.5: Effective friction - strain polynomial derived from non-intact coal data and common for non-intact coal, intact coal and coal mass post peak interpretations.

7.5.8 Reconstruction of the σ - e curves for non-intact coal, and the prediction of σ - e curves for intact coal and coal mass

A procedure similar to that followed in sections 4.2.8 and 6.4.1g and given below, resulted in the stress-strain reconstruction of all 3 coal states, as illustrated in figure 7.6. It is clear from this figure that the post peak relationship is common to all 3 coal states. Together with the evidence given in section 7.5.7, this verifies postulates 6 and 7.

i To allow a comparison between non-intact coal, intact coal and coal mass, select a value of σ_3 between zero and the coal mass brittle-ductile transition confinement.

ii Calculate a value for σ_{1_p} for all 3 coal states from equations 7.9, 7.10 and 7.11.

iii Determine a value for 2θ from the derivative of equation 7.13 with respect to σ_3 as per assumption 13 and equation 3.14.

iv Calculate a value of σ_{1_r} for all 3 coal states from equations 7.13, 7.14 and 7.15.

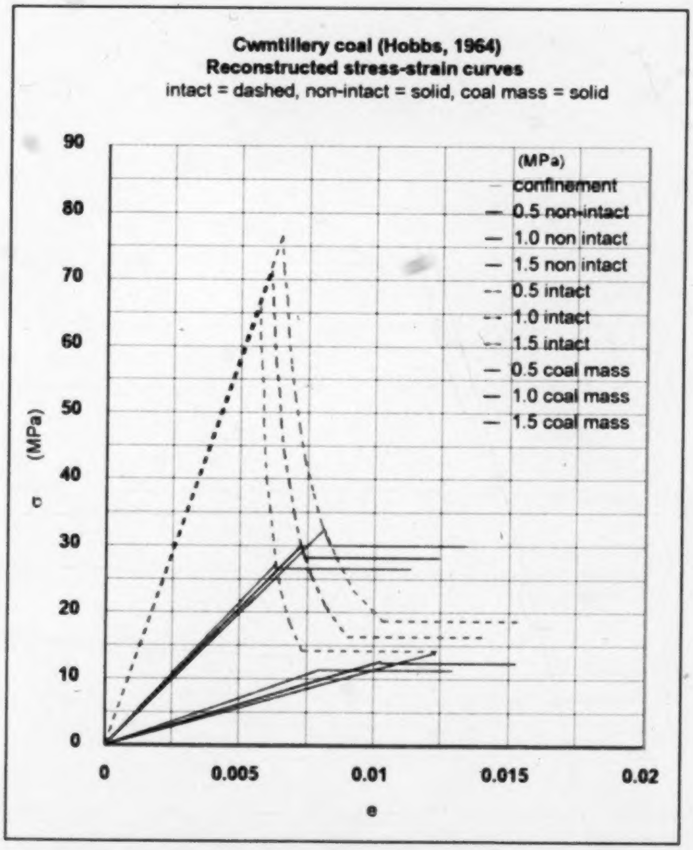

Figure 7.6: Reconstructed stress-strain plots for all three coal states, illustrating a common post peak relationship.

v Divide the range from σ_{1p} to σ_{1r} into equal increments of σ_{pp} for each of the 3 coal states.

vi For each incremented value for each coal state determine a value of ϕ_e from equation 3.16.

vii For each value of ϕ_e solve for e_{pp} using equation 7.16.

viii Plot the post peak stress strain plot from σ_{pp} versus e_{pp} for each coal state and compare.

7.5.9 Determination of the post peak modulus and stiffness

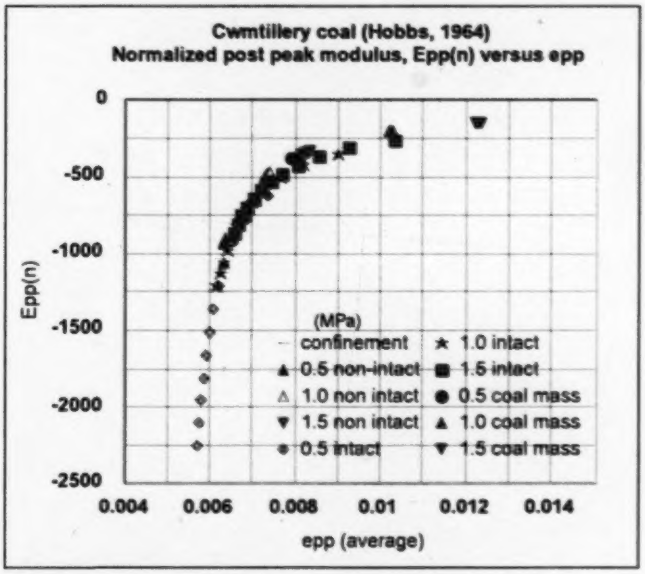

Figure 7.7: Normalized post peak modulus versus post peak strain for the three Cwmtillery coal states.

The post peak modulus and post peak stiffness are evaluated using the same procedure outlined in sections 3.8 and 3.9 respectively. Figure 7.7 shows the normalized post peak modulus for the Cwmtillery coal, with points for intact coal, non-intact coal and coal mass. Regardless of the confinement there is a single post peak modulus function for all 3 coal states. This verifies postulate 8.

7.6 Verification of the postulates and assumptions using other non-intact coal data sets from the literature

Appendix R contains nine worked data sets in addition to the Cwmtillery coal example given in section 7.5. Eight of these sets provide non-intact coal peak strength data only. The Pittsburgh coal data set (Kripakov, 1981), appendix R.1, also contains residual strength data, which allowed a determination of the base angle of friction rather than an assumption being made, and a refinement of the residual strength polynomial relationship, as was performed for the intact rock data where both peak and residual data were available, chapters 3 and 4.

In all worked cases summarized in appendix R, the postulates and assumptions outlined in sections 7.3 and 7.4 respectively were verified.

7.7 Conclusions

For each of the 10 sets of data taken from the available literature and reported in sections 7.5, 7.6 and appendix R, the post peak effective friction - strain relationships and reconstruction of the post peak stress-strain data was conducted successfully for the intact coal, non-intact coal and coal mass. As was found for broken rock and intact rock, in each coal case a common relationship exists for the post peak region with respect to a given confinement, that can be normalized to a single post peak modulus function by coal type.

It may be concluded that the postulates and assumptions in chapter 2, chapter 6 and chapter 7 have been verified and validated for all the non-intact coal data sets investigated in this chapter. This has allowed intact coal and coal mass relationships to be constructed, but there is no intact coal or coal mass data to validate those reconstructions. However, it has been shown that:

i There is a single effective friction - strain relationship that applies to non-intact coal, intact coal and coal mass.

ii The post peak stress-strain behaviour for non-intact coal, intact coal and coal mass is the same relationship for a given confinement.

iii The post peak modulus relationship is the same for non-intact coal, intact coal and coal mass.

Thus, by gathering information from laboratory manageable non-intact coal specimens, it is possible to estimate the intact coal and coal mass post peak relationships.

It should be noted that when triaxial tests are carried out on laboratory sized coal specimens, they should not be considered intact ($s = 1$), but should be assumed to be non-intact ($s < 1$). In this case s is approximated from the specimen dimensions given by Barron et al. (1992a) and iterated in section 7.2.

Chapter 8

Application of the Joseph-Barron post peak criterion to predicting pillar behaviour

8.1 Introduction

Having verified the postulates and assumptions that govern the Joseph-Barron post peak criterion in the previous chapters for intact rock, rock mass and non-intact coal, this chapter illustrates the application of the procedure to the prediction of post peak pillar behaviour. This has been carried out for an intact mudstone (Farmer, 1983), and for a coal mass whose properties were derived from non-intact Pittsburgh coal data (Kripakov, 1983).

Two popular commercially available software packages were employed; Flac 2d (Itasca Consulting Group Inc., 1995) and Phase 2 (Rocscience, 1999). The former was used to verify the Joseph-Barron approach through mimicking a triaxial test, but as will be shown was unable to provide output commensurate with expected pillar behaviour. The latter software was used successfully to illustrate post-peak pillar behaviour prediction, with a comparison of the Joseph-Barron post peak criterion with an existing post-peak approach suggested by Hoek et al. (1997).

The pillar peak strength, σ_p and post peak modulus, E_{ppp} output for the mudstone and coal mass pillars with respect to pillar width to height ratio, W/H is compared with various empirical pillar strength formulae, in particular the "squat pillar formula" after Salamon et al., (1985), and empirical expressions for post peak modulus derived from post peak pillar moduli reported in the literature compiled by Pen (1994) and Zipf (1999).

8.2 Triaxial strength prediction via Flac 2d and the Joseph-Barron approach

To allow the application of the Joseph-Barron approach to pillars to be compared with currently widely used commercially available software, it was first necessary to validate the Joseph-Barron approach by comparison with the chosen software package through a simple model. Since spreadsheets had been used successfully as a tool for illustrating the Joseph-Barron approach and comparing it to the original reported triaxial test results, triaxial test models for various values of σ_3 were run using the software package and compared to the Joseph-Barron model spreadsheet output, which had already been successfully validated by the original data.

8.2.1 Flac 2d

The software initially selected for comparison with the Joseph-Barron model was Flac 2d, version 3.3, due to its availability and popularity, evident by its frequent use, as reported in the geotechnical literature..

Flac is an acronym for "Fast Lagrangian analysis of continua". Flac 2d is described in the version 3.3 user's manual (Itasca, 1995) as being a two dimensional explicit finite difference program capable of simulating the behaviour of rock or soil. It is comparable with finite element methods in its performance, as element matrices in Flac 2d are the same as those for constant strain triangle formats in finite element approaches. However, Flac 2d uses an explicit solution method rather than an implicit solution method found in most finite element approaches. This allows a faster solution when using non-linear constitutive relationships than is possible with finite element methods. An implicit approach requires that element matrices be constantly stored and updated, the explicit approach does not require storage of matrices. This has made Flac 2d a popular package in terms of computer capacity requirements and speed of calculation.

When using Flac 2d, the structure of interest is represented by a grid of elements in the shape of the structure which are given material properties commensurate with the material making up the structure. The structure is given boundary restraints and is subjected to applied forces appropriate with those that the structure of interest might experience. Each of the elements in the structure behaves according to a specified constitutive model, which may be selected from a choice of preset relations or by a user specified model via a built-in progamming language named "Fish". Modeling takes place in either plane strain, plane stress, or axisymmetric modes, the latter being useful for modeling triaxial tests and pillars.

To compare the Joseph-Barron approach with Flac 2d, the Flac 2d built-in strain softening constitutive model was selected. This model was noted as having been widely used for the modeling of rock structures by a number of authors.

8.2.2 Triaxial test model

Appendix S.1 provides the Flac 2d triaxial test input code file for the intact mudstone with a confinement of 14 MPa. The output from Flac 2d was compared with the output from the Joseph-Barron triaxial test model for a number of confining pressures in figure 8.1. In all cases there is a good agreement between the peak and residual strengths for the two model sets.

A comparison with original mudstone data in appendix H.3 shows that the post peak curves for the Flac 2d strain softening approach do not fit the measured data as well as those for the Joseph-Barron approach.

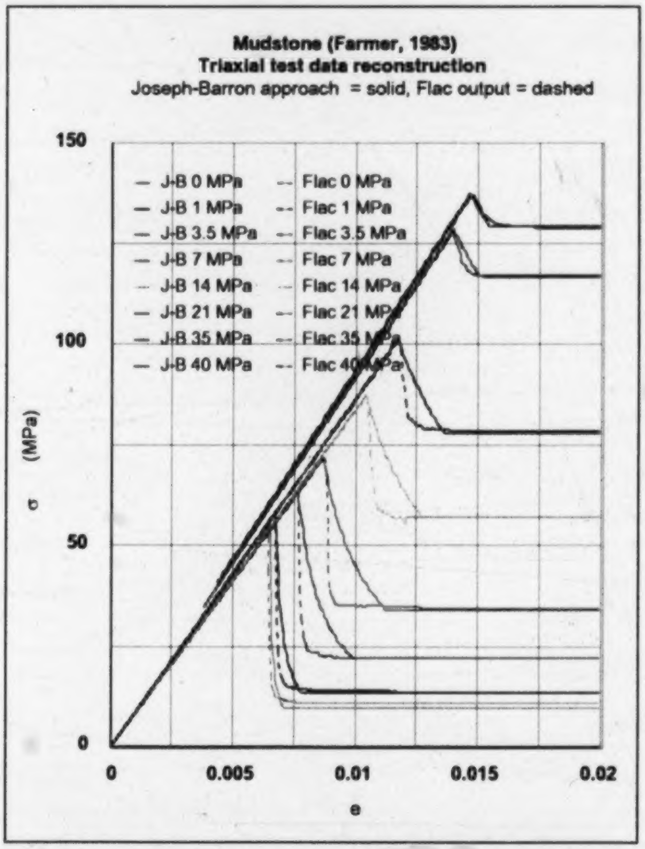

Figure 8.1: Comparison of Joseph-Barron to Flac 2d triaxial test models for an intact mudstone (Farmer, 1983).

This suggests that the Flac 2d strain softening model does not provide as accurate a reconstruction of the post peak region as the Joseph-Barron approach, but nevertheless there is a good correlation between the two methods.

8.3 Prediction of pillar behaviour via Flac 2d and the Joseph-Barron approach

Having shown a reasonable correlation between the Joseph-Barron approach and the Flac 2d strain softening approach, the same Flac 2d constitutive model was used to produce average pillar strength versus average pillar strain estimates for varying width to height ratios between 0.25 and 8.0.

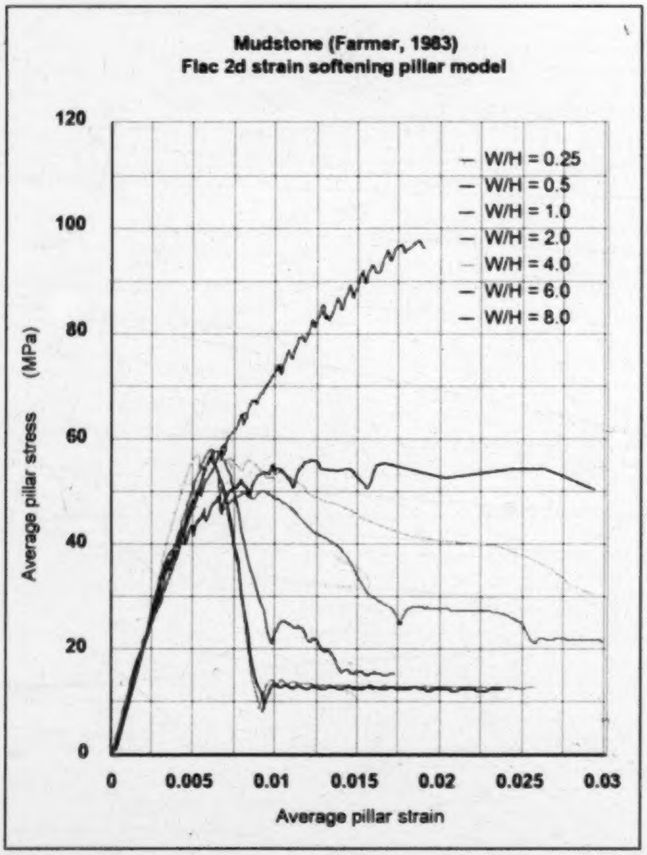

Figure 8.2: Flac 2d pillar model output for a range of width to height ratios.

An example of the Flac 2d pillar model input file code used for a width to height ratio of 6.0 is provided in appendix S.2. The output for the range of width to height ratios is plotted in figure 8.2.

It is well documented that pillar strength increases with increasing width to height ratio. That is, the wider the pillar, the higher the bearing capacity of the pillar. Figure 8.2 shows that for width to height ratios of 6 and below, the Flac 2d output indicates no increase in pillar strength with increasing width to height ratio. Since this is not possible, the author spent considerable time on this issue, but to no avail.

It was therefore tentatively concluded that Flac 2d does not take into account the change in confinement across a pillar that would lead to an increase in overall pillar strength with increasing width to height ratio. Instead, Flac 2d appeared to see the overall pillar as unconfined, and treated it as a uniaxial compression test. This certainly would account for the peak strength, for width to height ratios up to W/H = 6, being the same as the uniaxial intact compressive strength of the mudstone, at σ_c = 56 MPa. It is not known why the strength for W/H = 8 continued increasing, with no indication of a definite peak value.

The author attempted to write code using the Fish programming language to allow the Joseph-Barron post peak criterion to be incorporated into Flac 2d as a user defined constitutive model, but was unsuccessful. The author was unable to get this to work satisfactorily; consequently Flac 2d was abandoned for the pillar modeling portion of this research after 6 months.

8.4 Prediction of pillar behaviour via Phase 2, the Joseph-Barron approach and the approach suggested by Hoek et al. (1997)

The Phase 2 finite element modeling software package (Rocscience 1999) is a windows-based application with a graphic interface that permits the user to visually model and vary structures under load and deformation conditions. The finite element modeling process uses constant strain triangles and solves the stiffness matrices arising from the applied boundary conditions and applied deformations implicitly for the elements making up the structure, where each element in the structure has been designated a set of material properties. The package is restricted by only allowing 10 different material properties to be designated, which means that for a model pillar between roof and floor strata, given that one set of material properties must be designated for the roof and floor material, this leaves merely 9 sets of material properties for the pillar itself. This translates to a pillar composed of 9 elements, as illustrated in figure 8.3.

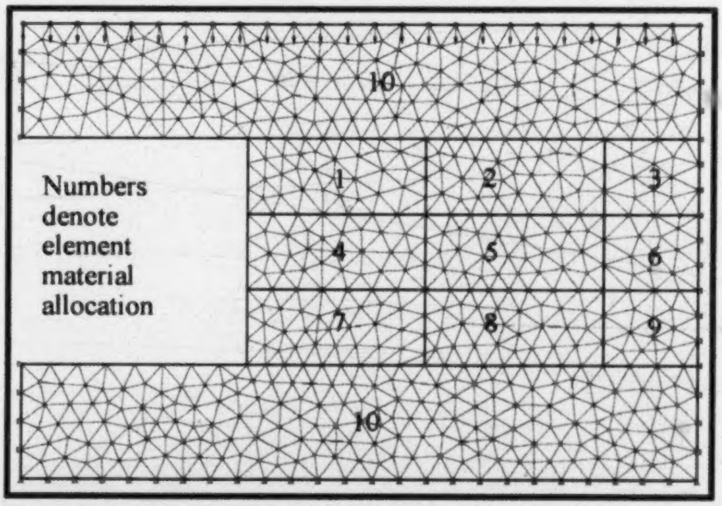

Figure 8.3: Phase 2 pillar model elements, discretization and boundary conditions

If a pillar is modeled under plane strain conditions, then half a rib pillar can be modeled with 9 elements. It should be borne in mind however that with increasing width to height ratio the size of the elements will increase, thus making the analysis coarser.

8.4.1 Using the Joseph-Barron post peak criterion with Phase 2

The author designed a spreadsheet to allow the Joseph-Barron approach to determine a new set of material properties for each incremental increase in deformation experienced by the pillar being modeled by Phase 2. Since Phase 2 was run elastically, the post peak moduli determined by the Joseph-Barron approach for each of the 9 elements in the Phase 2 pillar model were transformed into pseudo elastic moduli, E_{ps}, as illustrated in figure 8.4 and described below in point form.

For simplicity, it was previously assumed that the pre-peak elastic modulus was defined according to assumption 1, section 2.3.1, equation 2.5. However, Phase 2 uses elastic modulus, E according to its true definition, taking into account confinement as per equation 8.1, where ν is Poisson's ratio.

$$E=\frac{\sigma_1}{e_1}-2\nu\frac{\sigma_3}{e_1} \qquad 8.1$$

In equation 8.1, the pseudo modulus used by Phase 2 is given by $E = E_{ps}$ for any value of elastic moduli, whether pre-peak or post peak. The simplified pre-peak modulus used by the Joseph-Barron approach when $e_1 < e_p$ is given by the σ_1/e_1 expression in equation 8.1.

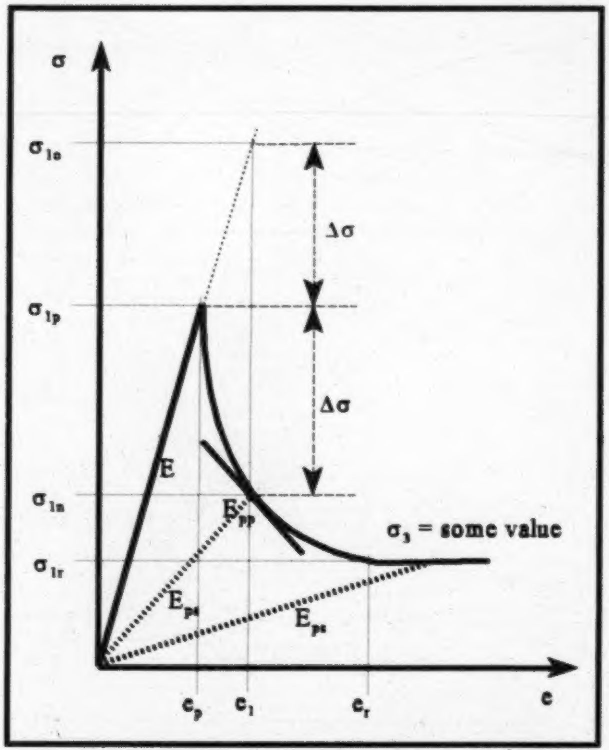

Figure 8.4: Determining a pseudo elastic modulus E_{ps}.

For the first Phase 2 iteration, each element is given the same initial elastic modulus, defined by the unconfined uniaxial compressive strength of the pillar material, as per assumption 1.

i For a given average value of σ_3 returned by Phase 2 for any element within the pillar structure having undergone an incremental increase in overall pillar deformation, values of peak and residual strength, σ_{1p} and σ_{1r} are determined from equations 2.6 and 2.7 respectively. Given values for σ_3, σ_{1p} and σ_{1r}, values of 2θ, and consequently ϕ_p and ϕ_r are then evaluated from equations 3.14, and 3.16 respectively. Using the ϕ_e-e relationship for the pillar material, equation 3.13, values for e_p and e_r are finally evaluated.

ii For a given value of e_1 returned by Phase 2 for the same element, the following is applied for the pre-peak and the region beyond e_r:

a If $e_1 < e_p$ then the elastic modulus, E returned to Phase 2 for the next iteration is defined by equation 8.1, where the term σ_1/e_1 is a constant defined by the slope of the pre-peak curve for the unconfined uniaxial compression of the pillar material, according to assumption 1.

b If $e_1 > e_r$, then a pseudo elastic modulus, $E = E_{ps}$ is returned to Phase 2 for the next iteration as defined by equation 8.1, where the term σ_1/e_1 is given by σ_{1r}/e_1, recognizing that the modulus will still decrease for increasing strain in the post residual region even though the residual strength of the element remains constant at σ_{1r} for a given value of σ_3.

It should be kept in mind that for elements within the pillar structure that have already reached the region beyond e_r, an increase in confinement will result in an increase in residual strength, even though that element is in a post e_r state.

iii For the post peak region where $e_p < e_1 < e_r$, there are two possible scenarios. The first is where the peak strength, σ_{1p} is initially exceeded requiring that the post peak criterion be invoked for the first time. The second is where the previous calculation has been conducted under post peak conditions.

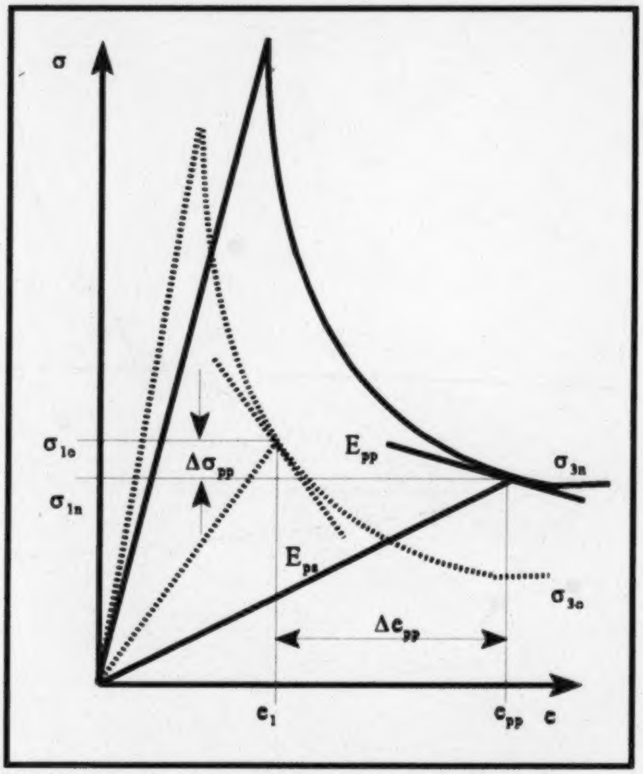

Figure 8.5: Translation from E_{pp} to E_{ps} for Phase 2

a Figure 8.4 illustrates an exaggeration of the condition where the peak strength is first exceeded. In this situation the over-estimation of σ_{1o} is corrected to σ_{1n}, by an assumed equilateral amount $\Delta\sigma = \sigma_{1n} - \sigma_{1p} = \sigma_{1p} - \sigma_{1o}$ due to a small increment of strain, $\Delta e = e_1 - e_p$. The pseudo elastic modulus, E_{ps} returned to Phase 2 is then given by equation 8.1, where the σ_1/e_1 term is determined as σ_{1n}/e_1 such that:

$$\frac{\sigma_{1n}}{e_1}=\frac{[2\sigma_{1p}-\sigma_{1o}]}{e_1} \qquad 8.2$$

b Figure 8.5 illustrates an exaggerated geometry of the transition between two known steps (dashed lines) in the post peak region giving rise to a new pseudo elastic modulus, E_{ps} for the next iteration.

The terms, σ_{1o}, σ_{3o} and e_1 are returned by Phase 2 at the end of the previous iteration, allowing new values of σ_{1n} and σ_{3n} to be calculated for the next iteration. It is assumed that the strain increment for the next iteration is the same as the strain increment for the previous iteration, that is Δe = a constant, and is therefore known. It is further assumed that the post peak modulus, E_{pp} for the next iteration can be calculated from the ratio of the differences of the stress and strain values for the previous and next iterations, that is equation 8.3:

$$E_{pp}=\frac{\sigma_{1n}-\sigma_{1o}}{\Delta e_{pp}} \qquad 8.3$$

The new pseudo elastic post peak modulus, E_{ps} required for Phase 2 to perform the next iteration is determined once a value for σ_{1n}, has been found. To facilitate this process, equation 3.16 is expanded using the trigonometric double angle identities and subsequently re-arranged into the form given by equation 8.4.

$$\sigma_{pp}=\sigma_3\tan\theta\frac{(1+\tan\phi_e\tan\theta)}{(\tan\theta-\tan\phi_e)} \qquad 8.4$$

The post peak modulus relationship, equation 3.19 may then be rewritten by expressing E_{pp} as equation 2.14 directly and replacing the σ_{pp} terms by equation 8.4, resulting in equation 8.5. The detailed manipulation is provided in appendix T.

$$\Delta\sigma_{pp}=2\Delta e_{pp}\sigma_3\frac{\tan\theta}{\cos^2\phi_e}\frac{(\phi_b-\phi_e)}{(e_b-e_{pp})}\frac{(\tan^2\theta+1)}{(\tan\theta-\tan\phi_e)^2} \qquad 8.5$$

An expression for the new confinement, σ_{3n} is achieved by equating equations 8.5 and 8.4 given that $\Delta\sigma_{pp} = \sigma_{1n} - \sigma_{1o}$ from equation 8.3, such that $\sigma_{pp} = \sigma_{1n}$ and $\sigma_3 = \sigma_{3n}$, where σ_{1n} and σ_{3n} are the values of strength and confinement for the next iteration and σ_{1o} is the strength returned by Phase 2 for the previous iteration. This results in equation 8.6.

$$\sigma_{3n}=\sigma_{1o}\frac{1-\dfrac{\tan\phi_e}{\tan\theta}}{[1+\tan\theta\tan\phi_e-2\dfrac{\Delta e_{pp}}{\cos^2\phi_e}\dfrac{(\phi_b-\phi_e)}{(e_b-e_{pp})}\dfrac{(\tan^2\theta+1)}{(\tan\theta-\tan\phi_e)}]} \qquad 8.6$$

The new strength, σ_{1n} is found by back substitution into equation 8.3. This is used to return a new estimate of pseudo elastic post peak modulus, E_{ps} as given by equation 8.7.

$$E_{ps}=\frac{\sigma_{1n}}{e_{pp}}-2\nu\frac{\sigma_{3n}}{e_{pp}} \qquad 8.7$$

8.4.2 Using the Hoek et al. (1997) approach with Phase 2

Figure 1.2 illustrates the Hoek et al. (1997) approach to post-peak behaviour. Since the Joseph-Barron post-peak criterion is a strain softening constitutive model, the Hoek et al. (1997) option iii, section 1.2.4, was used as an alternative comparative model. The post-peak slope was held constant, enabling a pseudo elastic post peak modulus to be determined and returned to Phase 2 for the next iteration, as illustrated in figure 8.6, where E is the elastic pre-peak modulus, and E_{pp} is the post-peak modulus which is related to the pre-peak modulus via a constant, A'.

From the geometry of figure 8.6 the pseudo elastic modulus, E_{ps} to be returned to Phase 2 for the next iteration is determined from the known values of E, A', σ_{pp}, σ_{1p}, σ_3 and e_{pp} as given by equation 8.8.

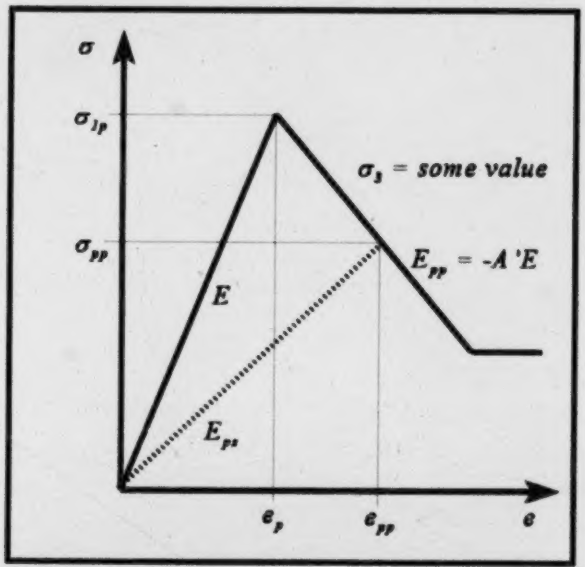

Figure 8.6: Evaluation of E_{ps} using the Hoek et al. (1997) post peak approach.

$$E_{ps} = \frac{A' E \sigma_{pp}}{\sigma_{1p}(1 + A') - \sigma_{pp}} - 2\nu \frac{\sigma_3}{e_{pp}} \qquad 8.8$$

The pre-peak region elastic modulus and the post e_r region pseudo elastic modulus are dealt with in the same manner as for the Joseph-Barron approach. To enable a direct comparison of the effect of the post-peak region on the post peak pillar behaviour for the Joseph-Barron and Hoek et al. (1997) approaches, the same residual strength criterion was used for both cases, defined by the residual strength polynomial, equation 2.7.

8.4.3 Comparison of pillar behaviour predicted by the Joseph-Barron post peak criterion and the Hoek et al. (1997) approach

Appendix W provides an example and description of the steps used in applying the Joseph-Barron approach to model a pillar using Phase 2.

Figure 8.7 shows the output from Phase 2 using the Joseph-Barron post peak criterion and the Hoek et al. (1997) approach for a range of width to height ratios for a mudstone (Farmer, 1983). The post-peak modulus for the Hoek et al approach was held constant at A' = 0.5. In each case for width to height ratios greater than 0.5, the Joseph-Barron approach predicts greater pillar strengths. This shows that the Joseph-Barron approach does make a significant difference in predicting pillar behaviour compared to the Hoek et al. approach, which stems purely from the post peak treatment process, since all other strength criteria used were common to the two approaches.

To check whether the choice of post peak modulus constant, A', for the Hoek et al. (1997) approach contributed to the large difference between the Joseph-Barron and Hoek et al. approaches, the value of A' was varied ± 0.25. The results are plotted in figure 8.8 indicating that the choice of post peak modulus if held constant makes little difference on the outcome of the Hoek et al. (1997) approach.

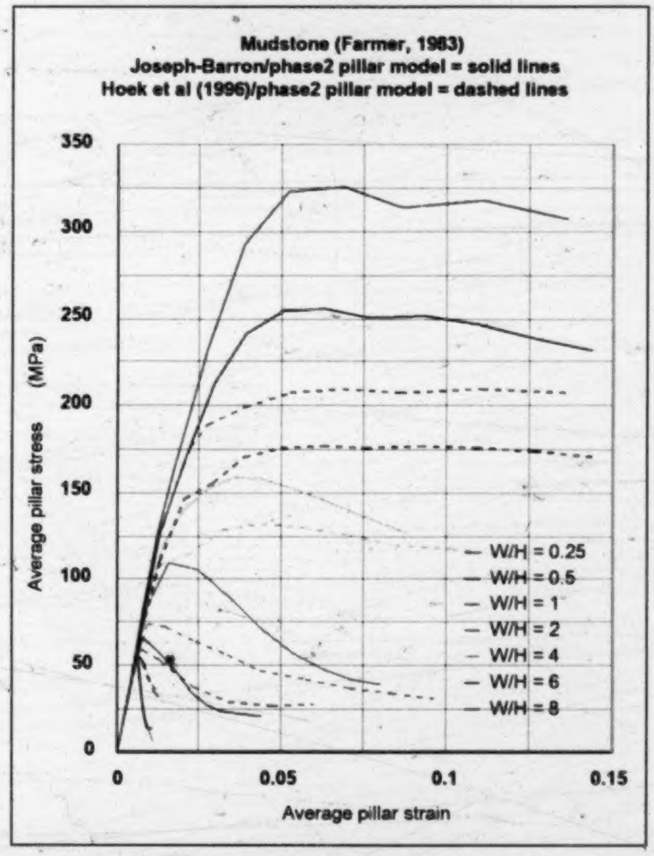

Figure 8.7: Comparison of the Joseph-Barron and Hoek et al. (1997) approaches to predicting pillar behaviour.

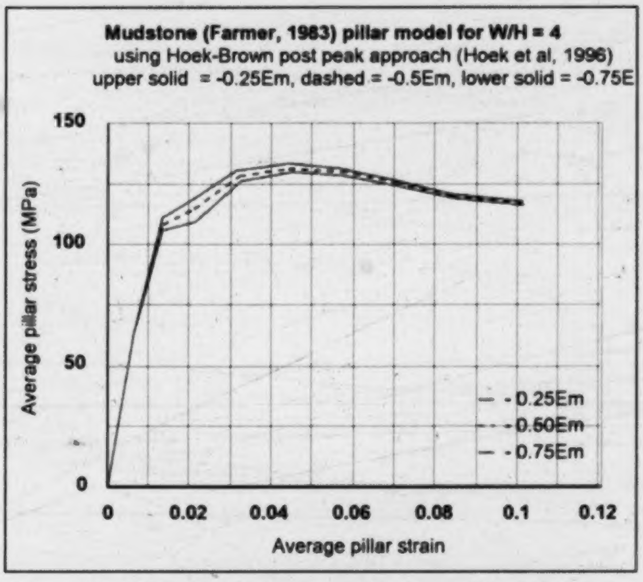

Figure 8.8: Effect of varying post peak modulus constant, A' for the Hoek et al. (1997) approach to pillar modeling.

8.5 Application of the Joseph-Barron approach to a coal mass

The Pittsburgh non-intact coal data set (Kripakov, 1981) was used to predict material properties for the coal mass in appendix R.1. These properties have been used to predict the behaviour of coal pillars of varying width to height ratio using the Joseph-Barron post peak criterion and Phase 2 software. The same procedure as explained in section 8.3.1 was employed to interface the Joseph-Barron approach with Phase 2.

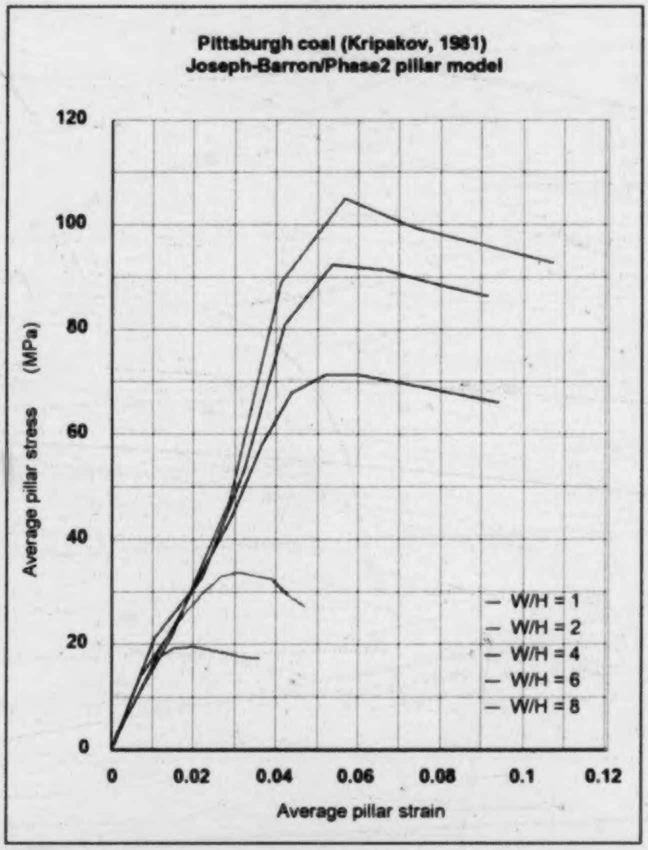

Figure 8.9: Predicted Pittsburgh coal mass pillar behaviour using the Joseph-Barron approach and Phase 2 software.

Figure 8.9 shows the output for various width to height ratios from 1 to 8. The peak strengths with respect to width to height ratio were compared with the well known and widely used empirical coal pillar strength relationships of:

i Bieniawski (1968), equation 8.9:

$$\sigma_p = \sigma_{1:1}[0.64 + 0.36\frac{W}{H}] \qquad 8.9$$

ii Obert et al. (1967), equation 8.10:

$$\sigma_p = \sigma_{1:1}[0.778 + 0.222\frac{W}{H}] \qquad 8.10$$

iii Salamon et al. (1967), equation 8.11:

$$\sigma_p = K'\frac{W^{0.46}}{H^{0.66}} \qquad 8.11$$

iv Salamon et al. (1985), equations 8.12 and 8.13:

If W/H < 4 then:

$$\sigma_p = nK'\frac{HR + w_L}{nHR + w_L}H^{\alpha - \beta}R^{\beta} \qquad 8.12$$

If W/H $\geq$ 4 then, the "squat pillar formula":

$$\sigma_p = nK'\frac{HR + w_L}{nHR + w_L}R^{2a}H^{3a}R_o^{b}[\frac{b}{\epsilon}[(\frac{R}{R_o})^{\epsilon} - 1] + 1] \qquad 8.13$$

Where for coal:

σ_p = average pillar strength in MPa.

$\sigma_{1:1}$ = peak strength of a W/H=1 pillar in MPa.

K' = strength of a 1 m^3 pillar in MPa.

n = 1, indicating square pillars.

R = width to height ratio, W/H.

w_L = width of the adjacent cross-cut to the pillar in metres.

α = a constant = -0.66

β = a constant = 0.46

R_o = transition W/H ratio between equations 8.12 and 8.13 = 4.

a = a constant = $(\alpha + \beta)/3$ = -0.0667

b = a constant = $(\beta - 2\alpha)/3$ = 0.5933

ε = an eccentricity constant = 2.5

The empirical pillar strength formulae outlined above in equations 8.9 through 8.13 were based on square pillars, whilst the Joseph-Barron applied using Phase 2 in plane strain mode yielded results for two-dimensional pillars, regarded as rib pillars. To enable a comparison to be made between empirical and modeled results, the output from Phase 2 was converted into equivalent square pillar results via the procedure outlined in appendix U, resulting in equation 8.14

$$\sigma_S = \sigma_{rib}\frac{(W+w_L)}{W} = \psi\sigma_{rib} \qquad 8.14$$

Where W = pillar width.

w_L = width of adjacent cross-cut along the length of the pillar.

σ_S = the required square pillar strength.

σ_{rib} = the Joseph-Barron/Phase 2 determined rib pillar strength.

and $\psi = (W + w_L)/W$.

Figure 8.10 shows the plot comparing the Joseph-Barron approach output converted to equivalent square pillar strength values with the empirical strengths determined from equations 8.9 through 8.13. It reveals a good agreement between the modeled and empirical strength results.

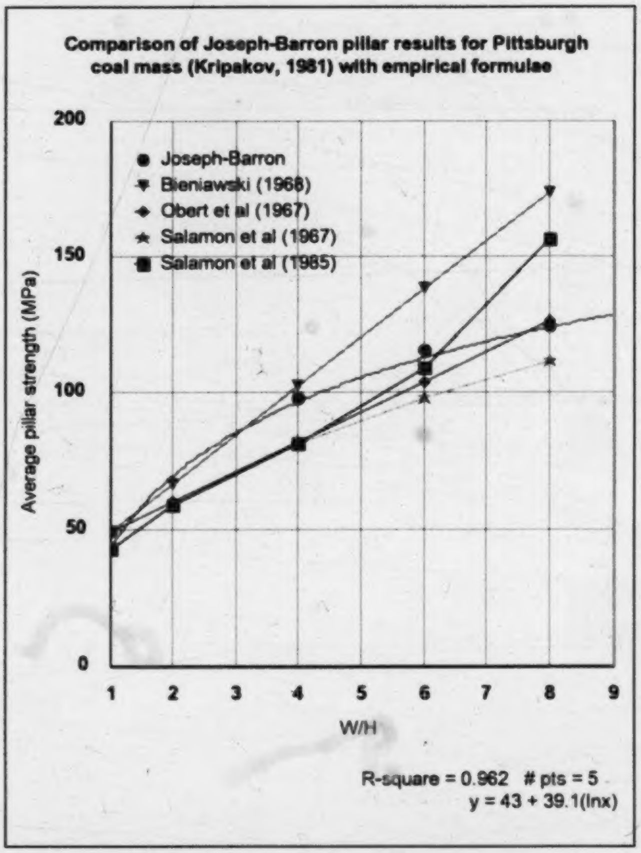

Figure 8.10: Comparison of modeled to empirical coal mass square pillar strengths of varying W/H ratio.

A determination of the post-peak modulus, and from that the post-peak stiffness, section 3.9 has been the concluding aim of this research. Pen (1994) compiled an empirical post peak modulus relationship for coal with respect to width to height ratio from values reported in the literature, equation 1.12; however, this relationship was largely based on non-intact coal data. Zipf (1999) compiled two coal empirical post peak modulus relationships, one for laboratory test coal specimens which would be appropriate for non-intact coal, the other for coal field data gleaned from the literature. It is this latter relationship, equation 8.15 that has been used in comparison with the Pittsburgh coal mass model results using the Joseph-Barron post peak criterion in figure 8.10.

$$E_{field} = -\frac{1750}{[\frac{W}{H}]} + 437 \qquad 8.15$$

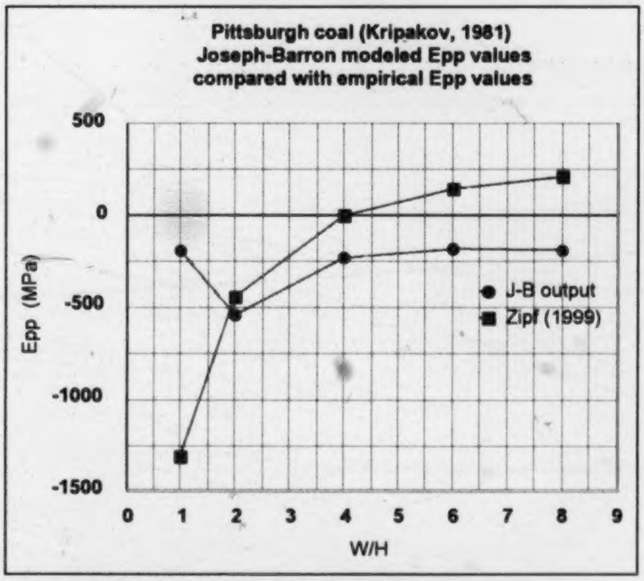

Figure 8.11: Comparison of post peak modulus via the Joseph-Barron approach and a coal field data empirical relationship (Zipf, 1999).

Figure 8.11 shows a good agreement between the Joseph-Barron approach and the Zipf empirical relationship. The Zipf relationship does yield values greater than zero for width to height ratios greater than 4. On inspection of his empirical plot as reproduced in figure 8.12 (Zipf, 1999), the relationship stated in equation 8.15 is skewed by 3 out of a total 24 data points.

The skewed Joseph-Barron data point in figure 8.11 for W/H=1 was due to the coarse nature of the pillar model (only 9 elements), which resulted in failure across the 3 mid height elements before failure of either the roof or floor pillar edge elements. A progressive failure of elements from the pillar edge to the pillar core was evident for all other W/H ratios greater than 1 modeled which provided post-peak data more in line with Zipf's findings reflected in figure 8.11.

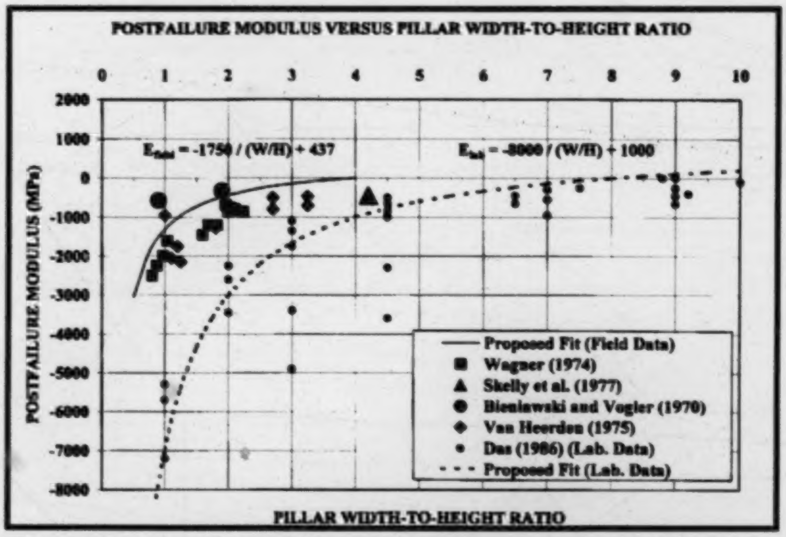

Figure 8.12: Plot of post failure modulus versus width to height ratio, after Zipf (1999), showing coal mass (field) and non-intact (lab) data.

This skewing of the resulting empirical relationship would account for predicted post peak modulus values greater than zero for width to height ratios greater than 4 in figure 8.11. Without the skew, the curves in figure 8.11 would become still closer in correlation.

8.6 Conclusions

The Joseph-Barron approach has been successfully used to model pillars for two very different rocks, an intact mudstone (Farmer, 1983) and a coal mass estimated from non-intact coal (Kripakov, 1981).

Due to popularity, evident from a wide reporting of use in the available literature, two software packages were selected for modeling triaxial testing and pillar behaviour; Flac 2d produced by Itasca (1995) and Phase 2 from Rocscience (1999).

In the case of the intact mudstone, a comparison of modeling triaxial tests using the Joseph-Barron approach and Flac 2d respectively indicated almost identical peak and residual strengths. The Joseph-Barron approach however provided a closer reconstruction of the post-peak stress-strain curves with respect to the original measured data as provided in appendix R.1.

An attempt to model pillars using Flac 2d revealed that Flac 2d appears unable to cope with changing confinement conditions for each element in the pillar structure, for each iteration step of the finite difference analysis procedure. In fact Flac 2d appears to treat pillars as unconfined uniaxial test specimens, such that the strength of pillars are the same regardless of the width to height ratio. For this reason, Flac 2d was abandoned as a pillar modeling software package.

Phase 2 was used successfully to model pillars of varying width to height ratio for the intact mudstone, where the Joseph-Barron approach was compared to a linear post-peak behaviour approach suggested by Hoek et al. (1997). The pre-peak and post e_r behaviour conditions were held constant for the two scenarios, allowing a direct comparison of the approaches due solely to the post-peak behaviour relationships suggested by each approach. In all width to height ratio cases greater than unity the Joseph-Barron approach showed greater pillar strengths than those achieved via the Hoek et al. approach. In other words, the Joseph-Barron approach does make a significant difference to the currently accepted approaches.

It was noted that a drawback of using Phase 2 as the analysis medium was the inability to dynamically update the material properties of elements as the analysis proceeded. A total of 10 sets of material properties could only be specified for any one iteration, meaning that the number of pillar elements was restricted to 9 plus one set of material properties for the roof and floor rock. Consequently, with increasing width to height ratio the individual element size increased, leading to a coarser set of strength and deformation results. The Phase 2 software was however the only commercial package available that was capable of multiple material property input.

Pittsburgh coal mass pillars of varying width to height ratio were modeled using Phase 2 with the Joseph-Barron approach defining the material properties for each iteration. The resulting average pillar strengths with respect to width to height ratio were compared with a number of empirical formulae. This indicated a good agreement, verifying that then Joseph-Barron approach predicts coal pillar strength of the same magnitude as suggested by the empirical coal pillar strength relationships.

The post peak moduli for the Joseph-Barron predicted pillar behaviour stress-strain curves were compared with a field (coal mass) empirical relationship derived by Zipf (1999) from the available literature with respect to width to height ratio. This showed that the Joseph-Barron approach provides a good prediction of post peak modulus for pillars.

Chapter 9

Conclusions and recommendations for future work

9.1 The Joseph-Barron post peak strength criterion

A post-peak strength criterion postulated as an effective friction - strain function has been verified and validated for intact rock, rock mass, crushed rock and non-intact coal. In addition it has been shown that non-intact coal behaviour may be used to define coal mass and intact coal behaviour.

It has been shown that for the same rock type, the intact rock and rock mass forms obey the same post-peak behavioural relationship, whether in terms of effective friction or post-peak modulus. It has also been shown that the same logic may be applied to intact coal, non-intact coal and the coal mass, although no complete coal data sets were available to verify this latter postulate.

However, a word of caution should be introduced here. The effective friction - strain function could conceivably be dependent on the stress path. For pillars, where generally there is an increase in load, the function is acceptable. However, in a case where load may decrease or cycle, the validity of the function has not been proved.

The Joseph-Barron post-peak strength criterion provides a means of evaluating the post-peak modulus of rock or coal in any state, whether in sample form, pillars and potentially to other rock structures under any set of confinement conditions. Through a simple transformation involving say pillar dimensions, the post-peak stiffness is then easily evaluated.

Due to the restriction on the number of different materials and therefore number of elements, that may be specified in the commercial finite element modeling software that was available to the author, the evaluation of rock structure behaviour using the Joseph-Barron post peak criterion is somewhat coarse. Nevertheless, it has been shown that the Joseph-Barron post peak criterion makes a significant difference when compared with current practices.

9.2 Verified and validated original postulates and assumptions

A number of original postulates and assumptions have been verified and validated during the course of this research, which have been shown to be applicable to any rock or coal material, regardless of whether intact, non-intact or broken in nature.

9.2.1 Effective friction - strain relationship

The effective friction - strain relationship, $\phi_e = f(e_{pp})$ which is the core of the Joseph-Barron post peak criterion is well represented by a 2nd order polynomial of the general form $\phi_e = R + Se_{pp} + Te_{pp}^2$, equation 2.9, and whose exact solution is given by equation 3.13:

$$\frac{(\phi_e - \phi_b)}{(\phi_p - \phi_b)} = \frac{(e_b - e_{pp})^2}{(e_b - e_p)^2} \qquad 3.13$$

9.2.2 Residual strength relationship

The residual strength criterion, equation 2.7 used in conjunction with the Hoek-Brown peak strength criterion, equation 2.6, is given by a 2nd order polynomial, and has been shown to adequately represent any set of available residual strength data.

Its general form, equation 2.7 and values for the polynomial constants D and F, equations 3.4 and 3.5 are given by:

$$\sigma_{1r}=D\sigma_3^2+F\sigma_3+\sigma_{cr} \tag{2.7}$$

$$D=\frac{1}{\sigma_{3t}^2}[\sigma_{cr}-[m\sigma_c\sigma_{3t}+s\sigma_c^2]^{1/2}+\frac{m\sigma_c\sigma_{3t}}{2[m\sigma_c\sigma_{3t}+s\sigma_c^2]^{1/2}}] \tag{3.4}$$

$$F=1-\frac{m\sigma_c}{2[m\sigma_c\sigma_{3t}+s\sigma_c^2]^{1/2}}-\frac{2}{\sigma_{3t}}[\sigma_{cr}-[m\sigma_c\sigma_{3t}+s\sigma_c^2]^{1/2}] \tag{3.5}$$

For s = 1, when peak and residual data are available, σ_{cr} is determined by a regression of the residual strength data. If only peak data is available , σ_{cr} is assumed to be 20% of σ_c. However, when the Hoek-Brown constant, s is less than unity, that is for broken rock, then the residual compressive strength may be determined by equation 6.11:

$$\sigma_{cr}=\sigma_c s^{\,a} \tag{6.11}$$

9.2.3 Post peak modulus relationship

The post-peak modulus arising from the effective friction - strain relationship and defined by equation 2.14 is given by the solution, equation 3.19, which in its normalized form, equation 3.20, provides a single function regardless of confinement for any rock or coal state, whether intact, non-intact or broken.

$$E_{pp} = \frac{\sin 2\theta}{\sin^2\phi_e}\frac{(\sigma_{pp}-\sigma_3)^2}{\sigma_3}\frac{(\phi_e-\phi_b)}{(e_{pp}-e_b)} \qquad 3.19$$

9.2.4 Determination of intact or broken rock pre-peak modulus

An empirical relationship was derived from the available intact and broken pre-peak modulus and RMR data for rock, resulting in a relationship between the aforementioned parameters, given by equation 6.8:

$$Log_{10}[\frac{E_{m(broken)}}{E_{m(intact)}}]=2.85[\frac{RMR_{broken}}{RMR_{intact}}-1] \qquad 6.8$$

9.3 Physical testing - the tilt test to determine ϕ_b

Through physical testing the tilt test devised by Stimpson (1981) was verified by comparison with triaxial slip and shear box tests as being a valid means of determining the base angle of friction, ϕ_b. This is a simple, quick test that requires very little sample preparation beyond rock coring.

9.4 The Joseph-Barron post peak criterion applied to pillars

The Joseph-Barron post peak criterion was used successfully to model pillars in both intact rock and a coal mass. The approach was shown to provide significantly different pillar strengths and post peak pillar moduli than those achieved using the Hoek et al (1997) approach.

The coal mass pillar strengths with respect to width to height ratio compared well with those determined from a number of empirical relationships. The variations of the coal mass pillar post peak moduli with width to height ratio were compared to an empirical relation devised by Zipf (1999) and shown to be similar.

The fact that the coal mass material properties were determined from non-intact data and still produced pillar strengths and post peak moduli similar to those from empirical relationships devised from coal mass field data sets, provides indirect evidence that there is a common post peak relationship for intact coal, non-intact coal and the coal mass.

9.5 Recommendations for future work

Recommendations for future work centre on the application and integration of the Joseph-Barron post-peak criterion into software applications.

From the use of commercially available finite element packages such as Phase 2, there is obviously a need for modeling software capable of giving each element in a given structure its own set of material properties, where those material properties can be updated dynamically. This would allow much smaller incremental steps, and many times the number of elements than employed during the course of this work, leading to a more accurate determination of rock structure behaviour.

Pen (1994) recommended that a means of determining post-peak pillar stiffness should be investigated for incorporation into the MULSIM/NL longwall chain pillar model, where he had conducted work establishing the prediction of local mine stiffness. The difference between the local mine stiffness and the post peak pillar stiffness allows an evaluation of pillar bump potential, as discussed in chapter 1. Given that this research has accomplished a method of determining post-peak pillar stiffness, the next step here would be to incorporate the Joseph-Barron post-peak criterion into the MULSIM/NL model.

In addition to rock structures such as pillars, the is a potential for the Joseph-Barron post-peak criterion to be applied to rock structures other than pillars, such as rock around openings or broken rock confined within a slope. In consideration of other structures, it would be necessary to determine whether the Joseph-Barron approach is stress path dependent.

As was shown in chapter 6, there arises a question as to the applicability of the Joseph-Barron approach to weathered material. It is suggested that there is some merit is investigating the phenomenon of varying base angle of friction as a function of weathering and the implications on the Joseph-Barron post-peak criterion.

Having analyzed broken and crushed rock in chapter 6, there is a potential application of the Joseph-Barron to finely divided soils, such as cohesionless sands and soils containing textural structure.

References

Aldritch, M.J., 1969, Pore pressure effects on Berea sandstone subjected to experimental deformation, Geological Society of America Bulletin, **80**, 1577 - 1586.

Ansari, F., and Li, Q., 1998, High-strength concrete subjected to triaxial compression, ACI Materials Journal, **95**, 6, pp 747 - 755.

Balmer, G., 1952, A general solution for Mohr's envelope, American Society for Testing and Materials, **52**, pp 1260 - 1271.

Barron, K., 1970, The fracture of brittle rocks around mine excavations, Ph.D. thesis, University of London.

Barron, K., and Pen, Y., 1992, A revised model for coal pillars, U.S.B.M. IC 9315, pp 144 - 157.

Barron, K., and Tao, Y., 1992a, Influence of specimen size and shape on the strength of coal, Proceedings of the Workshop on Coal Pillar Mechanics and Design, U.S. Bureau of Mines, I.C. 9315, pp 5 - 24.

Bieniawski, Z.T., 1968, In-situ strength and deformation characteristics of coal, Engineering Geology, **2**, pp 325 - 335.

Bieniawski, Z.T., 1978, The geomechanics classification in rock engineering applications, Proceedings of the 4th International Congress on Rock Mechanics, ISRM, Montreux, **2**, pp 41 - 48.

Bieniawski, Z.T., 1984, Rock mechanics design in mining and tunneling, Balkema Publishers, Rotterdam.

Bieniawski, Z.T., and Bauer, J., 1982, Discussion: "Empirical strength criterion for rock masses", Journal of the Geotechnical Engineering Division, ASCE, April, pp 670 - 672.

Blanton, T.L., 1981, Effect of strain rates from 10^{-2} to 10 sec^{-1} in triaxial compression tests on three rocks, International Journal of Rock Mechanics and Geomechanics Abstracts, **18**, pp 47 - 62.

Brace, W.F., 1964, Brittle fracture of rocks, Proceedings of the International Conference on State of Stress in the Earth's Crust, pp 111 - 174, Elsevier, New York.

Brady, B.H.G., and Brown, E.T., 1980, Energy changes and stability in underground mining: Design applications of boundary element methods, Transactions of the Institute of

Mining and Metallurgy, **90**, pp A61 - A68.

Brady, B.H.G., and Brown, E.T., 1993, Rock Mechanics for Underground Mining, 2nd Edition, Chapman & Hall Publishers.

Chan, S.S.M., Crocker, T.J., and Wardell, G.G., 1972, Engineering properties of rocks and rock masses in the deep mines of the Cour d'Alene mining district, Idaho, Transactions of the Society of Mining Engineers of AIME, **252**, 353 - 361.

Cook, N.G.W., 1965, A note on rockbursts considered as a problem of stability, Journal of the South African Institute of Mining and Metallurgy, **65**, pp 437 - 446.

Cook, N.G.W., Hoek, E., Pretorius, J.P.G., Ortlepp, W.D., and Salamon, M.D.G., 1966, Rock mechanics applied to the study of rockbursts, Journal of the South African Institute of Mining and Metallurgy, **66**, 10, pp 435 - 528.

Crouch, S.L., and Fairhurst, C., 1973, The mechanics of coal mine bumps and the interaction between coal pillars, mine roof and floor, U.S.B.M. H0101778.

Das, M.D., 1986, Influence of width/height ratio on post-failure behaviour, International Journal of Mining and Geological Engineering, **4**, pp 79 - 87.

Dougill, J.W., 1985, Constitutive relations for concrete and rock: Applications and extensions of elasticity and plasticity theory, Mechanics of Geomaterials: Rocks, Concrete, Soils, **3**, pp 21 - 46, John Wiley & Sons.

Farmer, I., 1983, Engineering behaviour of rocks, Chapman Hall, London.

Gates, D.J., 1988, A microscopic model for stress-strain relations in rock - part II. Triaxial compressive stress, International Journal of Rock Mechanics and Geomechanics Abstracts, **25**, 6, pp 403 - 410.

Gnirk, P.F., and Cheatham, J.B., 1965, An experimental study of single bit tooth penetration into dry rock at confining pressures of 0 - 5000 psi, Journal of Society of Petroleum Engineers, **5**, pp 117 - 130.

Gorski, B., and Lau, J.S.O., 1991, The post failure behaviour of the Lac du Bonnet pink granite, CANMET Divisional Report MRL 91-103(TR).

Hobbs, D.W., 1964, The strength and strain characteristics of coal in triaxial compression, Journal of Geology, **72**, pp 214 - 231.

Hobbs, D.W., 1970, The behaviour of broken rock under triaxial compression, International Journal of Rock Mechanics and Mining Science, 7, pp 125 - 148.

Hoek, E., and Brown, E.T., 1980, Underground Excavations in Rock, Chapman & Hall, London.

Hoek, E., and Brown, E.T., 1982, Discussion: "Empirical strength criterion for rock masses", Journal of the Geotechnical Engineering Division, ASCE, April, pp 672 - 673.

Hoek, E., and Brown, E.T., 1997, Practical estimates of rock mass strength, International Journal of Rock Mechanics and Mining Sciences & Geomechanics Abstracts, **34**, 8, pp 1165-1186.

Hoek, E., and Franklin, J.A., 1968, A simple triaxial cell for field and laboratory testing of rock, Transactions of the Institute of Mining and Metallurgy, 77, pp A22-6.

Hussaini, M.A., 1991, Effect of particle size and strain on the strength of crushed rock, Proceedings of the 5th ISRM Congress on Rock Mechanics, pp E239 - E243.

Iannacchione, A.T., 1988, Numerical simulation of coal pillar loading with the aid of a strain-softening finite difference model, Rock Mechanics as a Guide for Efficient Utilization of Natural Resources, Balkema Publishers.

Itasca Consulting Group Inc., 1995, Fast Langrangian Analysis of Continua, version 3.3, volume I: User's Manual.

Jaeger, J.C., 1970, The behaviour of closely jointed rock, Proceedings of the 11th Symposium on Rock Mechanics, AIME, pp 57 - 68, Berkeley.

Kripakov, N.P., 1981, Analysis of pillar stability in steeply pitching seams using the finite element method, U.S. Bureau of Mines, R.I. 8579.

Kripakov, N.P., and Melvin, M.T., 1983, A computer procedure to simulate progressive rock failure around coal mine entries, Proceedings of the 1st Conference on the Use of Computers in the Coal Industry, Morgantown, 56, pp 487 - 502.

Kwasniewski, M.A., 1983, Deformational and strength properties of the three structural varieties of carboniferous sandstones, 5th International Congress on Rock Mechanics, ISRM, **1**, A105 - A115, Balkema Publishers.

Mogi, K., 1964, Compression tests on dry rock sample, Bulletin of the Earthquake Research Institute, **42**, pp 491 - 514.

Mogi, K., 1965, Deformation and fracture of rocks under confining pressure (2)

Elasticity and plasticity of some rocks, Bulletin of the Earthquake Research Institute, **43**, pp 349 - 379.

Obert, L., and Duvall, W.I., 1967, Rock Mechanics and Design of Structures in Rock, pp 542 - 545, John Wiley & Sons, New York.

Ozbay, M.U., 1989, The stability and design of yield pillars located at shallow and moderate depths, Journal of the South African Institute of Mining and Metallurgy, **89(3)**, pp 73 - 79.

Pariseau, W.G., 1981, Limit design of mine pillars under uncertainty, Proceedings of the 16th U.S. Symposium on Rock Mechanics, University of Minnesota, pp 287 - 301.

Pen, Y., 1994, Chain pillar design for longwall mining in bump-prone seams, Ph.D. Thesis, Dept. of Mining, Metallurgical and Petroleum Engineering, University of Alberta.

Rocscience, 1999, Phase 2 Finite Element Model online manual.

Salamon, M.G.G., and Munroe, A.H., 1967, A study of the strength of coal pillars, Journal of the South African Institute of Mining and Metallurgy, **68**, pp 55 - 67.

Salamon, M.D.G., 1970, Stability, instability, and the design of pillar workings, International Journal of Rock Mechanics and Mining Sciences, 7, pp 613 - 631.

Salamon, M.D.G., and Wagner, H., 1985, Practical experiences in the design of coal pillars, Safety in Mines Research, Proceedings of the 21st International Conference on Rock Mechanics, Sydney, October 21 - 25, pp 3 - 9.

Santarelli, F.J., and Brown, E.T., 1989, Failure of three sedimentary rocks in triaxial and hollow cylinder compression tests, International Journal of Rock Mechanics and Geomechanics Abstracts, **26**, 5, pp 401 - 413.

Seedsman, R.W., and Hornby, P., 1991, Controlled and uncontrolled pillar collapse, NERDDC End of Grant Report, Project No. 1440.

Serafim J.L., and Pereira, J.P., 1983, Consideration of the geomechanical classification of Bieniawski, Proceedings of the International Symposium on Engineering Geology and Underground Construction, Lisbon, **1**, II, pp 33 - 44.

Starfield, A.M., and Crouch, S.L., 1972, Elastic analysis of single seam extraction, Proceedings of the 13th U.S. Symposium on Rock Mechanics, pp 421 - 439.

Starfield, A.M., and Fairhurst, C., 1968, How high speed computers advance design of practical mine pillar systems, Engineering and Mining Journal, **5**, pp 78 - 84.

Stimpson, B., 1981, A suggested technique for determining the basic friction angle of rock surfaces using core, International Journal of Rock Mechanics and Mining Science and Geomechanics Abstracts, **18**, 1, pp 88 - 95.

Tao, Y., 1991, Influence of specimen size and shape on the strength of coal, M.Sc. thesis, University of Alberta.

Van Heerden, W.L., 1975, In situ complete stress-strain characteristics of large coal specimens, Journal of the South African Institute of Mining and Metallurgy, pp 207 - 217.

Visman, J., and Picard, J.L., 1970, Guide to Engineering Statistics, Metals Reduction and Energy Centre, Department of Energy, Mines and Resources, Mines Branch, IC233.

Wagner, H., 1974, Determination of complete load deformation characteristics of coal pillars, Proceedings of the 3rd International Congress on Rock Mechanics, I.S.R.M., Denver, CO., National Academy of Sciences, **II-B**, pp 1076 - 1082.

Wang, F.D., Skelly, W.A., and Wolgamott, J., 1976, In-situ coal pillar strength study, U.S. Bureau of Mines contract report number H0242022.

Wawersik, W.R., and Fairhurst, C., 1970, A study of brittle rock fracture in laboratory compression experiments, International Journal of Rock Mechanics and Mining Science, 7, pp 561 - 575.

Wilson, A.H., and Ashwin, D.P., 1972, Research into the determination of pillar size, Part 1: An hypothesis concerning pillar stability, The Mining Engineer, **131**, pp 409 - 417.

Xie, J., Elwi, A.E., and MacGregor, J.G., 1995, Mechanical properties of three high strength concretes containing silica fume, ACI Materials Journal, **92**, 2, pp 135 - 145.

Yoshinaka, R., and Yamabe, T., 1980, Strength criterion of rocks, soils and foundations, Japan Society of Soil Mechanics and Foundation Engineering, **20**, pp 113 - 126.

Zipf, R.K., 1992, Analysis of stable and unstable pillar failure using a local mine stiffness method, U.S.B.M. IC9315, pp 128 - 143.

Zipf, R.K., 1999, Using a post failure stability criterion in pillar design, Proceedings of the 2nd International Workshop on Coal Pillar Mechanics and Design, NIOSH IC 9448, pp 181 - 192.

Appendix A

Procedure for polynomial regression analysis (after Visman et al., 1970)

To correlate a given set of data to a 2nd order polynomial of the form:

$$\sigma_{1r}=D\sigma_3^2+F\sigma_3+\sigma_{cr}$$

Employing the procedure laid down by Visman et al. (1970), the constants D, F and σ_{cr} are given by:

$$D=\frac{\Sigma([\sigma_3-\sigma_{3av}]^2[\sigma_{1r}-\sigma_{1rav}])\Sigma([\sigma_3-\sigma_{3av}][\sigma_{1r}-\sigma_{1rav}])\Sigma([\sigma_3-\sigma_{3av}]^3)}{\Sigma([\sigma_3-\sigma_{3av}]^4)\Sigma([\sigma_3-\sigma_{3av}]^2)-\frac{[\Sigma([\sigma_3-\sigma_{3av}]^2)]^3}{n}-[\Sigma([\sigma_3-\sigma_{3av}]^3)]^2}$$

$$F=\frac{\Sigma([\sigma_3-\sigma_{3av}][\sigma_{1r}-\sigma_{1rav}])-D\Sigma([\sigma_3-\sigma_{3av}]^3)}{\Sigma([\sigma_3-\sigma_{3av}]^2}-2D\sigma_{3av}$$

$$\sigma_{cr}=\frac{-D\Sigma([\sigma_3-\sigma_{3av}]^2)}{n}-\frac{\Sigma([\sigma_3-\sigma_{3av}][\sigma_{1r}-\sigma_{1rav}])-D\Sigma([\sigma_3-\sigma_{3av}]^3)}{\Sigma([\sigma_3-\sigma_{3av}]^2}\sigma_{3av}+D\sigma_{3av}^2+\sigma_{1rav}$$

Where n is the number of data points available, and σ_{1rav} and σ_{3av} are the mean values of the available data.

The correlation coefficient, r^2, indicating the confidence in the outcome for a given set of data is given by:

$$r^2=1-\frac{\Sigma(\sigma_{1r,data}-\sigma_{1r,calc})^2}{\Sigma(\sigma_{1r,data}-\sigma_{1rav,data})^2}=1-\frac{\Sigma(\sigma_{1r}-[D\sigma_3^2+F\sigma_3+\sigma_{cr}])^2}{\Sigma(\sigma_{1r}-\sigma_{1rav})^2}$$

Appendix B

Derivation of the post peak modulus, E_{pp}

The post peak modulus, E_{pp}, is defined as the slope of the post peak portion of the stress-strain curve, at any point. It can be seen that the post peak modulus decreases in magnitude when proceeding from peak to residual strength for a given confinement, σ_3. As the brittle-ductile transition point confinement is approached, E_{pp} approaches zero.

$$E_{pp}=\frac{\delta\sigma_{pp}}{\delta e_{pp}} \tag{2.14}$$

The change of stress with respect to strain which describes the slope of the post peak portion of the stress-strain curve is not a simple differentiable form, but can be made easier to solve via a product of two differentials.

$$\frac{\delta\sigma_{pp}}{\delta e_{pp}}=\left(\frac{\delta\phi_e}{\delta e_{pp}}\right)\left(\frac{\delta\sigma_{pp}}{\delta\phi_e}\right)$$

Evaluation of $\delta\phi_e/\delta e_{pp}$

$$\frac{(\phi_e-\phi_b)}{(\phi_p-\phi_b)}=\frac{(e_b-e_{pp})^2}{(e_b-e_p)^2} \tag{3.13}$$

$$\frac{\delta\phi_e}{\delta e_{pp}}=-2\frac{(\phi_p-\phi_b)}{(e_b-e_p)^2}(e_b-e_{pp})$$

But from the general ϕ_e - e equation:

$$\frac{(\phi_p-\phi_b)}{(e_b-e_p)^2}(e_b-e_{pp})=\frac{-(\phi_e-\phi_b)}{(e_{pp}-e_b)}$$

Therefore

$$\frac{\delta\phi_e}{\delta e_{pp}}=2\frac{(\phi_e-\phi_b)}{(e_{pp}-e_b)} \qquad \text{B-1}$$

Evaluation of $\delta\sigma_{pp}/\delta\phi_e$

$$\tan\phi_e=\frac{\tau}{\sigma}=\frac{(\sigma_{pp}-\sigma_3)\sin2\theta}{(\sigma_{pp}+\sigma_3)+(\sigma_{pp}-\sigma_3)\cos2\theta} \qquad 2.2$$

Rearranging gives:

$$\tan\phi_e[(\sigma_{pp}+\sigma_3)+(\sigma_{pp}-\sigma_3)\cos2\theta]=(\sigma_{pp}-\sigma_3)\sin2\theta$$

$$\sigma_{pp}=\sigma_3\frac{[\tan\phi_e(\cos2\theta-1)-\sin2\theta]}{[\tan\phi_e(1+\cos2\theta)-\sin2\theta]}$$

Differentiating σ_{pp} with respect to ϕ_e

$$\frac{\delta\sigma_{pp}}{\delta\phi_e}[\tan\phi_e(1+\cos2\theta)-\sin2\theta]+\sigma_{pp}\sec^2\phi_e(1+\cos2\theta)=-\sigma_3\sec^2\phi_e(1-\cos2\theta)$$

$$\frac{\delta\sigma_{pp}}{\delta\phi_e}=-\sec^2\phi_e\frac{[\sigma_{pp}(1+\cos2\theta)+\sigma_3(1-\cos2\theta)]}{[\tan\phi_e(1+\cos2\theta)-\sin2\theta]} \qquad \text{B-2}$$

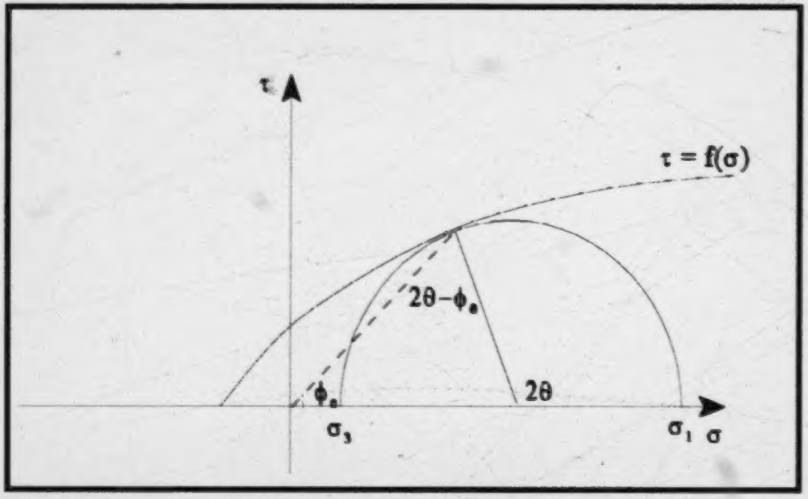

Figure B-1 Relationship between 2θ and ϕ_e via Mohr's circle

But from Mohr's circle, figure B-1, and employing the sine law

$$\frac{(\sigma_{pp}+\sigma_3)}{\sin(2\theta-\phi_e)}=\frac{(\sigma_{pp}-\sigma_3)}{\sin\phi_e}$$

But $\sin(2\theta - \phi_e) = \sin 2\theta \cos \phi_e - \cos 2\theta \sin \phi_e$, hence:

$$\frac{(\sigma_{pp}+\sigma_3)}{(\sigma_{pp}-\sigma_3)}=\frac{\sin 2\theta}{\tan\phi_e}-\cos 2\theta \qquad \text{B-3}$$

Substituting for sin 2θ in B-2 with B-3

$$\frac{\delta\sigma_{pp}}{\delta\phi_e}=-\sec^2\phi_e\frac{[\sigma_{pp}(1+\cos 2\theta)+\sigma_3(1-\cos 2\theta)]}{[\tan\phi_e(1+\cos 2\theta)-\tan\phi_e[\frac{(\sigma_{pp}+\sigma_3)}{(\sigma_{pp}-\sigma_3)}+\cos 2\theta]]}$$

$$\frac{\delta\sigma_{pp}}{\delta\phi_e} = -\sec^2\phi_e \frac{[\sigma_{pp}(1+\cos 2\theta)+\sigma_3(1-\cos 2\theta)]}{\tan\phi_e(1-\frac{(\sigma_{pp}+\sigma_3)}{(\sigma_{pp}-\sigma_3)})}$$

$$\frac{\delta\sigma_{pp}}{\delta\phi_e} = (\sigma_{pp}-\sigma_3)\sec^2\phi_e \frac{[(\sigma_{pp}+\sigma_3)+(\sigma_{pp}-\sigma_3)\cos 2\theta]}{2\sigma_3\tan\phi_e} \qquad \text{B-4}$$

Substituting cos 2θ in B-4 with B-3

$$\frac{\delta\sigma_{pp}}{\delta\phi_e} = (\sigma_{pp}-\sigma_3)\sec^2\phi_e \frac{(\sigma_{pp}+\sigma_3)+(\sigma_{pp}-\sigma_3)[\frac{\sin 2\theta}{\tan\phi_e}-\frac{(\sigma_{pp}+\sigma_3)}{(\sigma_{pp}-\sigma_3)}}{2\sigma_3\tan\phi_e}$$

$$\frac{\delta\sigma_{pp}}{\delta\phi_e} = \frac{(\sigma_{pp}-\sigma_3)^2\sec^2\phi_e\sin 2\theta}{2\sigma_3\tan^2\phi_e} = \frac{(\sigma_{pp}-\sigma_3)^2\sin 2\theta}{2\sigma_3\sin^2\phi_e} \qquad \text{B-5}$$

E_{pp} is given by the product

$$E_{pp} = \frac{\delta\sigma_{pp}}{\delta e_{pp}} = (\frac{\delta\phi_e}{\delta e_{pp}})(\frac{\delta\sigma_{pp}}{\delta\phi_e})$$

From B-1 and B-5

$$E_{pp} = \frac{\sin 2\theta}{\sin^2\phi_e}\frac{(\sigma_{pp}-\sigma_3)^2}{\sigma_3}\frac{(\phi_e-\phi_b)}{(e_{pp}-e_b)} \qquad 3.19$$

Appendix C

General solution for the ϕ_e-e polynomial: $\phi_e = R + Se + Te^2$

A second order polynomial of the form

$$\phi_e = R + Se_{pp} + Te_{pp}^2 \qquad 2.9$$

was chosen as the simplest mathematical expression which best describes the relationship between the effective friction, ϕ_e, for any given total strain, e_{pp}, in the post peak region between peak and base strength. It should be borne in mind that this expression is only applicable between these two strength boundaries, and has no physical meaning outside of these parameters.

At peak uniaxial strength, $\sigma_p = \sigma_c$, the peak effective friction, ϕ_p, corresponding to a given amount of strain experienced at peak strength, e_p, is defined, such that

$$\phi_p = R + Se_p + Te_p^2 \qquad 3.8$$

Similarly, at the brittle-ductile transition point, where the base strength of the material is realized, $\sigma_b = \sigma_{lt}$, the base friction, ϕ_b, corresponding to a given amount of strain, e_b, is defined, such that

$$\phi_b = R + Se_b + Te_b^2 \qquad 3.9$$

Due to the mathematical nature of a second order polynomial, we know that there exists a minimum or maximum value. In the instance of the above function, a minimum exists where there is no change in the frictional response for a corresponding change in strain. This also defines the base friction, ϕ_b, corresponding to a base strain, e_b. In other words, defined by the differential of the base friction relationship:

$$\frac{\delta\phi}{\delta e}=S+2Te_b=0$$

$$S=-2Te_b \qquad 2.12$$

If ϕ_p, e_p, ϕ_b, e_b are known from an examination of the available data then it is possible to solve for the polynomial constants R, S, and T, from simultaneous equations.

Subtracting 3.8 from 3.9 and substituting for S from 2.12

$$(\phi_b-\phi_p)=S(e_b-e_p)+T(e_b^2-e_p^2)$$

$$(\phi_b-\phi_p)=-2Te_b(e_b-e_p)+T(e_b^2-e_p^2)$$

$$(\phi_b-\phi_p)=T(-2e_b^2+2e_be_p+e_b^2-e_p^2)$$

$$(\phi_p-\phi_b)=T(e_b^2-2e_be_p+e_p^2)=T(e_b-e_p)^2$$

$$T=\frac{(\phi_p-\phi_b)}{(e_b-e_p)^2} \qquad 3.10$$

Substituting 3.10 back into 2.12

$$S=-2e_b\frac{(\phi_p-\phi_b)}{(e_b-e_p)^2} \qquad 3.11$$

Substituting 3.10 and 3.11 back into 3.9

$$R=\phi_b+2e_b^2\frac{(\phi_p-\phi_b)}{(e_b-e_p)^2}-e_b^2\frac{(\phi_p-\phi_b)}{(e_b-e_p)^2}$$

$$R=\phi_b+e_b^2\frac{(\phi_p-\phi_b)}{(e_b-e_p)^2} \qquad 3.12$$

Substituting for R, S, and T, 3.10, 3.11, and 3.12 into 2.9, yields the general form of the polynomial

$$\phi_e=\phi_b+e_b^2\frac{(\phi_p-\phi_b)}{(e_b-e_p)^2}-2e_be_{pp}\frac{(\phi_p-\phi_b)}{(e_b-e_p)^2}+e_{pp}^2\frac{(\phi_p-\phi_b)}{(e_b-e_p)^2}$$

$$\frac{(\phi_e-\phi_b)}{(\phi_p-\phi_b)}(e_b-e_p)^2=e_b^2-2e_be_{pp}+e_{pp}^2=(e_b-e_{pp})^2$$

$$\frac{(\phi_e-\phi_b)}{(\phi_p-\phi_b)}=\frac{(e_b-e_{pp})^2}{(e_b-e_p)^2} \qquad 3.13$$

Appendix D

Determination of σ_{3t} when only peak data is available

If no residual strength data is available, then the minimum additional requirement to allow solution for the brittle-ductile point and inherently σ_{3t} is a knowledge of the base angle of friction, ϕ_b for the rock in question. This may be achieved via a simple tilt test as described by Stimpson (1981), or by comparison with rocks of similar origin from experience, or as may be described in the available literature.

At the brittle-ductile transition point the base strength and the peak strength command the same value, $(\sigma_{3t}, \sigma_{1t})$, that is

$$\sigma_{1t}=\sigma_{1p}=\sigma_{3t}+[m\sigma_c\sigma_{3t}+s\sigma_c^2]^{1/2}=\sigma_{1b}=\frac{1+\sin\phi_b}{1-\sin\phi_b}\sigma_{3t}=K\sigma_{3t}$$

Re-arranging into a quadratic form

$$(K-1)^2\sigma_{3t}^2-m\sigma_c\sigma_{3t}-s\sigma_c^2=0$$

Then σ_{3t} can be expressed as the positive root solution

$$\sigma_{3t}=\frac{m\sigma_c+\sqrt{m^2\sigma_c^2+4(K-1)^2s\sigma_c^2}}{2(K-1)^2} \qquad 3.24$$

σ_{1t} is determined by back substitution into either the base strength or peak strength criterion, as above.

Appendix E

Evaluation of a residual strength 2nd order polynomial

If the brittle-ductile transition point is known and it is assumed that the residual strength and the peak strength command the same value, σ_{1t} at σ_{3t} then for a 2nd order residual polynomial

$$\sigma_{1r} = D\sigma_3^2 + F\sigma_3 + \sigma_{cr}$$

$$\sigma_{1p} = \sigma_3 + [m\sigma_c\sigma_3 + s\sigma_c^2]^{1/2}$$

$$\sigma_{1t} = \sigma_{1p} = \sigma_{3t} + [m\sigma_c\sigma_{3t} + s\sigma_c^2]^{1/2} = \sigma_{1r} = D\sigma_{3t}^2 + F\sigma_{3t} + \sigma_{cr}$$

Where D and F are unknown constants. σ_{cr} is taken as the intercept value from the linear residual strength approximation if peak and residual data are known, or 20% of the unconfined uniaxial compressive strength if only peak data is available. The 20% proportion seems to approximate the value if both peak and residual data were available. This proportion appears reasonably insensitive and may range from 5% to 50% of the unconfined uniaxial compressive strength with little adverse effect on the outcome.

Letting $Q = (m\sigma_c\sigma_{3t} + s\sigma_c^2)^{1/2}$ and re-arranging in terms of F

$$F = 1 + \frac{[Q - \sigma_{cr}]}{\sigma_{3t}} - D\sigma_{3t} \qquad \text{E-1}$$

It is also assumed that the slopes of both the peak and residual strength criteria at the brittle-ductile transition point are the same.

$$\frac{\delta\sigma_{1p}}{\delta\sigma_{3t}} = 1 + \frac{m\sigma_c}{2[m\sigma_c\sigma_{3t} + s\sigma_c^2]^{1/2}} = \frac{\delta\sigma_{1r}}{\delta\sigma_{3t}} = 2D\sigma_{3t} + F$$

Again letting $Q = (m\sigma_c\sigma_{3t} + s\sigma_c^2)^{1/2}$ and re-arranging in terms of F

$$F = 1 + \frac{m\sigma_c}{2Q} - 2D\sigma_{3t} \qquad \text{E-2}$$

Equating E-1 and E-2 and solving for D

$$1 + \frac{[Q - \sigma_{cr}]}{\sigma_{3t}} - D\sigma_{3t} = 1 + \frac{m\sigma_c}{2Q} - 2D\sigma_{3t}$$

$$\frac{[Q - \sigma_{cr}]}{\sigma_{3t}} + D\sigma_{3t} = \frac{m\sigma_c}{2Q}$$

$$D = \frac{1}{\sigma_{3t}^2}[\sigma_{cr} - Q + \frac{m\sigma_c\sigma_{3t}}{2Q}]$$

$$D = \frac{1}{\sigma_{3t}^2}[\sigma_{cr} - [m\sigma_c\sigma_{3t} + s\sigma_c^2]^{1/2} + \frac{m\sigma_c\sigma_{3t}}{2[m\sigma_c\sigma_{3t} + s\sigma_c^2]^{1/2}}] \qquad 3.4$$

Substituting 3.4 back into E-2

$$F = 1 - \frac{m\sigma_c}{2Q} - \frac{2}{\sigma_{3t}}[\sigma_{cr} - Q]$$

$$F=1-\frac{m\sigma_c}{2[m\sigma_c\sigma_{3t}+s\sigma_c^2]^{1/2}}-\frac{2}{\sigma_{3t}}[\sigma_{cr}-[m\sigma_c\sigma_{3t}+s\sigma_c^2]^{1/2}] \qquad 3.5$$

Substituting 3.4 and 3.5 back into the residual strength criterion

$$\sigma_{1r}=[\frac{1}{\sigma_{3t}^2}[\sigma_{cr}-Q+\frac{m\sigma_c\sigma_{3t}}{2Q}]]\sigma_3^2+[1-\frac{m\sigma_c}{2Q}-\frac{2}{\sigma_{3t}}[\sigma_{cr}-Q]]\sigma_3+\sigma_{cr}$$

$$\sigma_{1r}=\frac{\sigma_3}{\sigma_{3t}}([\frac{\sigma_3}{\sigma_{3t}}-1][\sigma_{cr}-Q+\frac{m\sigma_c\sigma_{3t}}{2Q}]-\sigma_{cr}+Q)+\sigma_3+\sigma_{cr} \qquad \text{E-5}$$

$$\sigma_{1r}=\frac{\sigma_3}{\sigma_{3t}}([\frac{\sigma_3}{\sigma_{3t}}-1][\sigma_{cr}-[m\sigma_c\sigma_{3t}+s\sigma_c^2]^{1/2}+\frac{m\sigma_c\sigma_{3t}}{2[m\sigma_c\sigma_{3t}+s\sigma_c^2]^{1/2}}]-\sigma_{cr}+[m\sigma_c\sigma_{3t}+s\sigma_c^2]^{1/2})+\sigma_3+\sigma_{cr}$$

Appendix F

Determination of the strain at the transition point e_b

Appendix C provides the general solution for the effective friction - strain polynomial, equation 3.13:

$$\frac{(\phi_e-\phi_b)}{(\phi_p-\phi_b)}=\frac{(e_b-e_{pp})^2}{(e_b-e_p)^2} \qquad 3.13$$

This equation can be re-arranged into a linear form Y = MX + B

$$Y=\sqrt{\frac{(\phi_e-\phi_b)}{(\phi_p-\phi_b)}}=\frac{-e}{(e_b-e_p)}+\frac{e_b}{(e_b-e_p)} \qquad 3.17$$

Where the Y variable is the square root term, which depends on the calculated value of ϕ_e, the X variable is the strain e, which replaces e_{pp} in equation 3.13 and represents the available peak and/or residual strain data, the linear slope is M and the intercept with the Y axis is B

$$slope=M=\frac{-1}{(e_b-e_p)} \qquad intercept=B=\frac{e_b}{(e_b-e_p)}$$

It is better to determine e_b from the slope, since it is based on an averaging of all the data points involved, whereas if determined from the intercept it is highly influenced by a single adverse data point. Thus using a rearrangement of the slope equation, the base strain is realized:

$$e_b=\frac{-1}{M}+e_p \qquad 3.18$$

Appendix G

Solution for 2θ, (after Balmer, 1952)

Balmer, (1952), provided a solution for the shear, τ, and normal, σ, stresses at the formation of a failure plane through intact material, in terms of the major, σ_1, and minor, σ_3, principal stresses, via the geometric solution of Mohr's envelope.

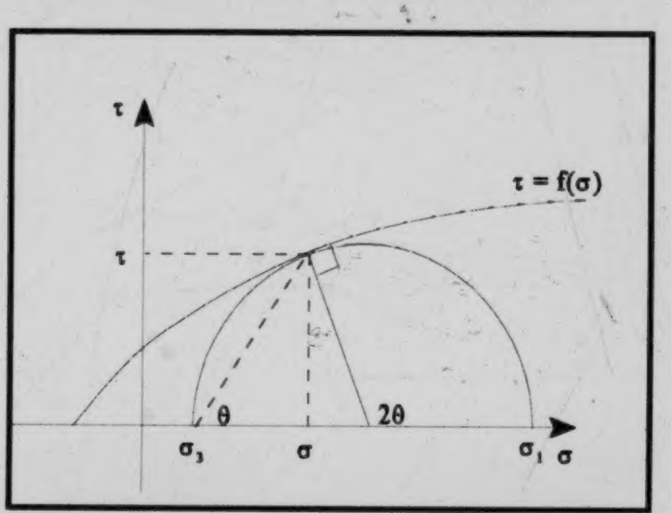

Figure G1: General analytic solution for Mohr's envelope, after Balmer (1952)

The general equation of a circle with centre (h, k) and radius r is given by:

$$(x - h)^2 + (y - k)^2 = r^2 \qquad \text{G-1}$$

For a Mohr circle, as illustrated in figure G1, the following substitutions are made

$$x = \sigma \qquad y = \tau$$

$$r = \frac{(\sigma_1 - \sigma_3)}{2}$$

Where the horizontal offset, h, at the centre of the Mohr circle is given by:

$$h=\frac{(\sigma_1+\sigma_3)}{2}$$

And the vertical offset, k, at the centre of the Mohr circle is zero, due to bisection of the circle by the horizontal σ axis.

Given these definitions, the general form of the Mohr circle is given as:

$$[\sigma-\frac{\sigma_1+\sigma_3}{2}]^2+\tau^2=[\frac{\sigma_1-\sigma_3}{2}]^2 \qquad \text{G-2}$$

By determining the partial derivative of σ_1 with respect to σ_3 it is possible to derive expressions for τ and σ in terms of σ_1 and σ_3.

Rearranging equation G-2:

$$[2\sigma-(\sigma_1+\sigma_3)]^2+4\tau^2=(\sigma_1-\sigma_3)^2$$

Expanding terms:

$$4\sigma^2-4\sigma(\sigma_1+\sigma_3)+(\sigma_1+\sigma_3)^2+4\tau^2=\sigma_1^2-2\sigma_1\sigma_3+\sigma_3^2$$

$$4\sigma^2-4\sigma\sigma_1-4\sigma\sigma_3+\sigma_1^2+2\sigma_1\sigma_3+\sigma_3^2+4\tau^2=\sigma_1^2-2\sigma_1\sigma_3+\sigma_3^2$$

$$\sigma^2-\sigma\sigma_1-\sigma\sigma_3+\sigma_1\sigma_3+\tau^2=0 \qquad \text{G-3}$$

Differentiating σ_1 in G-3 implicitly with respect to σ_3:

$$-\sigma\frac{\delta\sigma_1}{\delta\sigma_3}-\sigma+\sigma_3\frac{\delta\sigma_1}{\delta\sigma_3}+\sigma_1=0$$

$$-\sigma[1+\frac{\delta\sigma_1}{\delta\sigma_3}]+\sigma_3\frac{\delta\sigma_1}{\delta\sigma_3}+\sigma_1=0$$

$$-\sigma[1+\frac{\delta\sigma_1}{\delta\sigma_3}]+\sigma_3\frac{\delta\sigma_1}{\delta\sigma_3}+\sigma_3+\sigma_1-\sigma_3=0$$

$$-\sigma[1+\frac{\delta\sigma_1}{\delta\sigma_3}]+\sigma_3[1+\frac{\delta\sigma_1}{\delta\sigma_3}]+(\sigma_1-\sigma_3)=0$$

$$\sigma-\sigma_3=\frac{(\sigma_1-\sigma_3)}{(1+\frac{\delta\sigma_1}{\delta\sigma_3})} \qquad \text{G-4}$$

Re-arranging G-3:

$$\tau^2=-\sigma^2+\sigma\sigma_1+\sigma\sigma_3-\sigma_1\sigma_3$$

$$\tau^2=-\sigma^2+2\sigma\sigma_3-\sigma_3^2+\sigma\sigma_1-\sigma\sigma_3+\sigma_3^2-\sigma_1\sigma_3$$

$$\tau^2=-(\sigma^2+2\sigma\sigma_3+\sigma_3^2)+\sigma(\sigma_1-\sigma_3)+\sigma_3(\sigma_3-\sigma_1)$$

$$\tau^2=-(\sigma-\sigma_3)^2+\sigma(\sigma_1-\sigma_3)-\sigma_3(\sigma_1-\sigma_3)$$

$$\tau^2=-(\sigma-\sigma_3)^2+(\sigma_1-\sigma_3)(\sigma-\sigma_3)$$

Substituting $(\sigma - \sigma_3)$ with (4):

$$\tau^2=\frac{-(\sigma_1-\sigma_3)^2}{(1+\frac{\delta\sigma_1}{\delta\sigma_3})^2}+\frac{(\sigma_1-\sigma_3)^2}{(1+\frac{\delta\sigma_1}{\delta\sigma_3})}$$

$$\tau^2=\frac{(\sigma_1-\sigma_3)^2}{(1+\frac{\delta\sigma_1}{\delta\sigma_3})^2}[-1+1+\frac{\delta\sigma_1}{\delta\sigma_3}]$$

$$\tau=\frac{(\sigma_1-\sigma_3)}{(1+\frac{\delta\sigma_1}{\delta\sigma_3})}\sqrt{\frac{\delta\sigma_1}{\delta\sigma_3}} \qquad \text{G-5}$$

From geometry, 2θ is defined in figure G1 as

$$2\theta=2\tan^{-1}[\frac{\tau}{\sigma-\sigma_3}] \qquad \text{G-6}$$

That is:

$$2\theta=2\tan^{-1}[\frac{\frac{(\sigma_1-\sigma_3)}{(1+\frac{\delta\sigma_1}{\delta\sigma_3})}\sqrt{\frac{\delta\sigma_1}{\delta\sigma_3}}}{\frac{(\sigma_1-\sigma_3)}{(1+\frac{\delta\sigma_1}{\delta\sigma_3})}}] \qquad \text{G-7}$$

Which reduces to:

$$2\theta=2\tan^{-1}[\sqrt{\frac{\delta\sigma_1}{\delta\sigma_3}}] \qquad 3.14$$

Appendix H

Worked intact rock data sets where peak and residual data was available

Appendix H.1

Intact high strength concrete HS15 (Ansari et al., 1998)

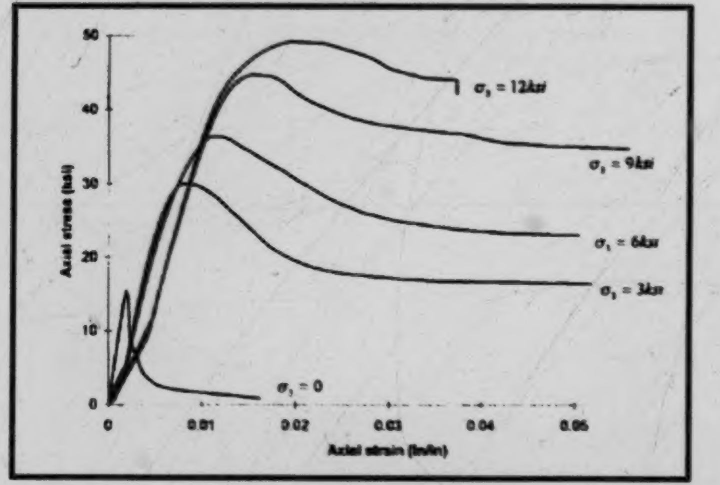

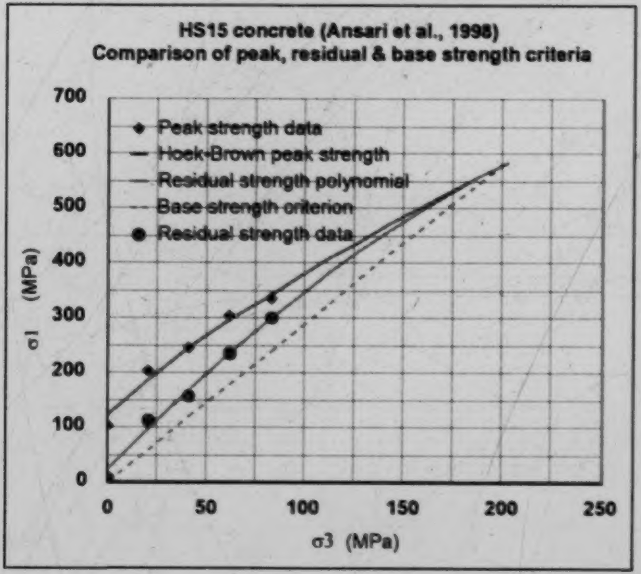

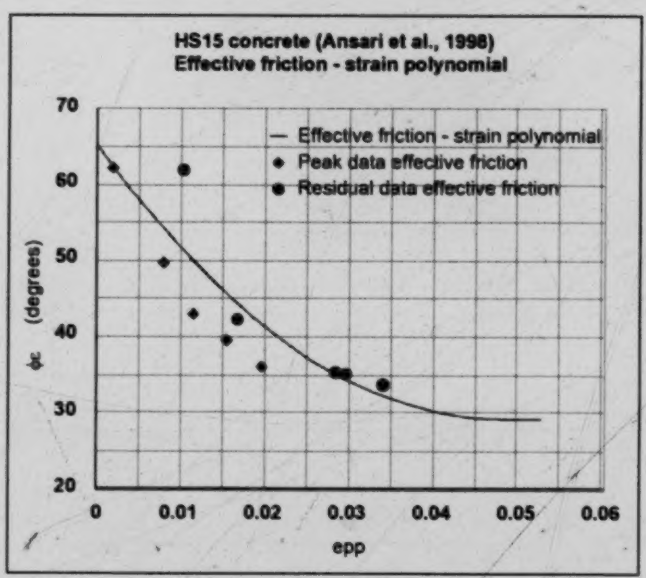
HS15 concrete (Ansari et al., 1998)
Effective friction - strain polynomial
Effective friction - strain polynomial
Peak data effective friction
Residual data effective friction
φc (degrees)
70
60
50
40
30
20
0
0.01
0.02
0.03
0.04
0.05
0.06
epp

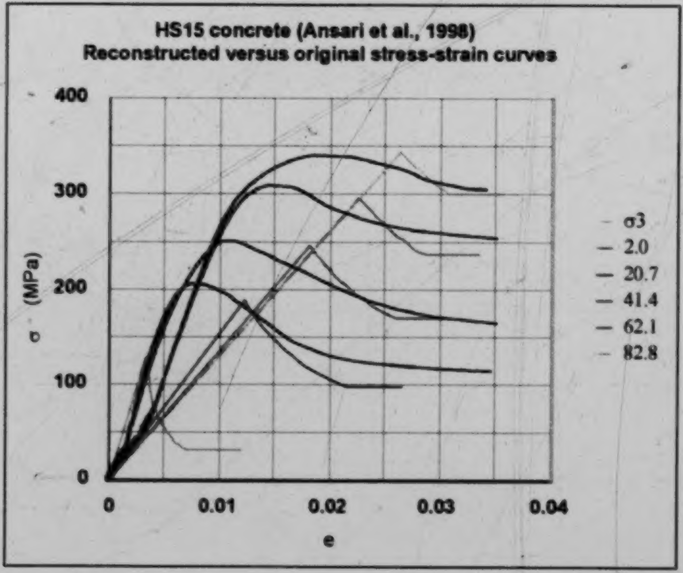
HS15 concrete (Ansari et al., 1998)
Reconstructed versus original stress-strain curves
σ (MPa)
400
300
200
100
0
0
0.01
0.02
0.03
0.04
e
σ3
2.0
20.7
41.4
62.1
82.8

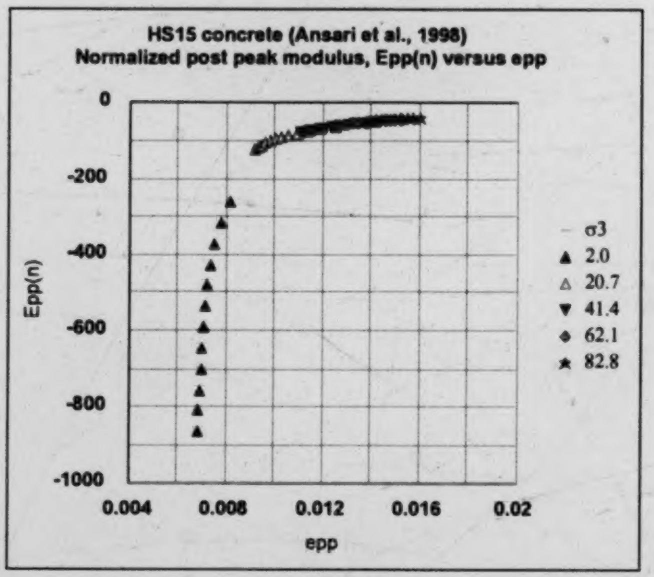

Criterion	Parameters			
Hoek-Brown peak strength	m	σ_c (MPa)	s	a
$\sigma_{1p} = \sigma_3 + \sigma_c\{m\sigma_3/\sigma_c + s\}^a$	5.2	124	1	0.5
Residual strength	D	F	σ_{cr} (M[illegible])	
$\sigma_{1r} = D\sigma_3^2 + F\sigma_3 + \sigma_{cr}$	-0.005	3.7	25	
Base strength & transition point	ϕ_b (deg.)	σ_{3t} (MPa)	σ_{1t} (MPa)	
$\sigma_{1b} = \{(1+\sin\phi_b)/(1-\sin\phi_b)\}\sigma_3$	29	199	578	
Friction-strain and base strain	R (deg.)	S	T	e_b
$\phi_e = R + Se_{pp} + Te_{pp}^2$	65	-1500	15700	0.05

Appendix H.2

Intact marl (Farmer, 1983)

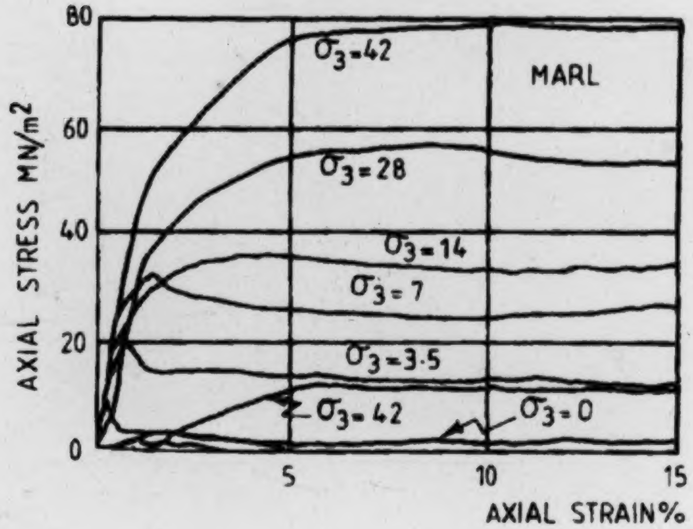

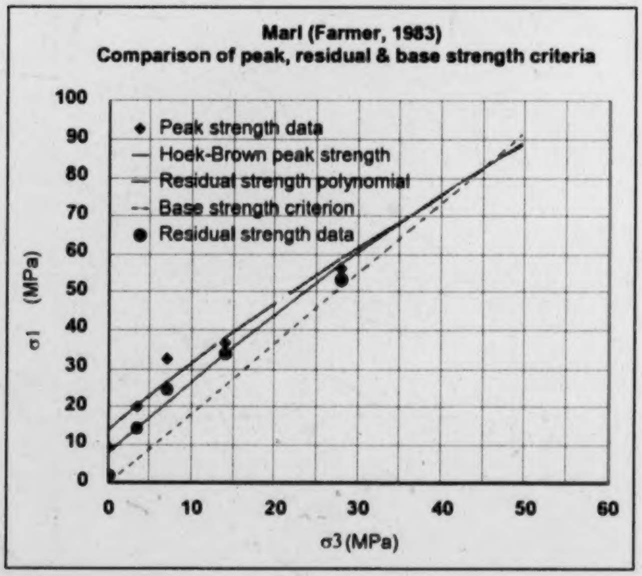

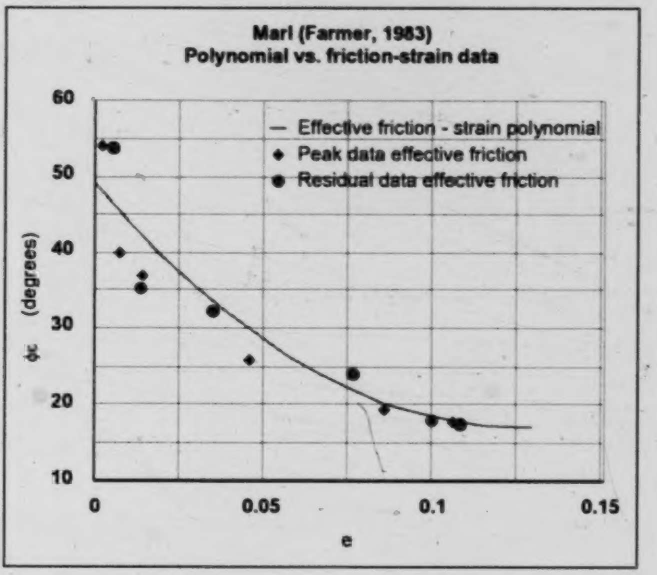
Marl (Farmer, 1983)
Polynomial vs. friction-strain data
60
50
40
30
20
10
φc (degrees)
0
0.05
0.1
0.15
e
— Effective friction - strain polynomial
◆ Peak data effective friction
● Residual data effective friction

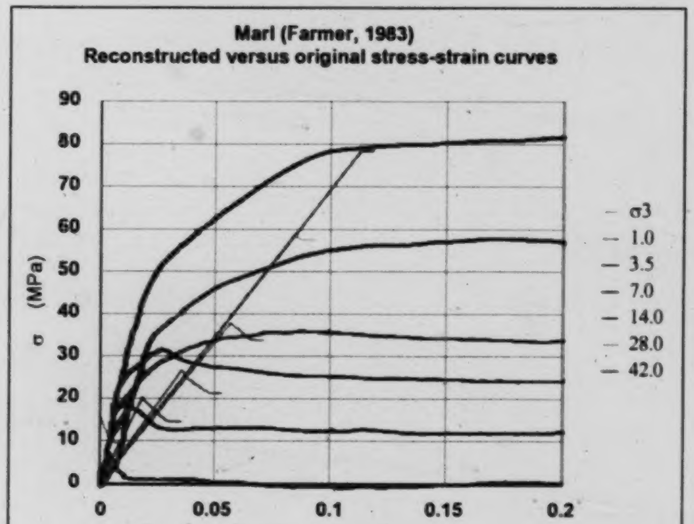
Marl (Farmer, 1983)
Reconstructed versus original stress-strain curves
90
80
70
60
50
40
30
20
10
0
σ (MPa)
0
0.05
0.1
0.15
0.2
e
σ3
1.0
3.5
7.0
14.0
28.0
42.0

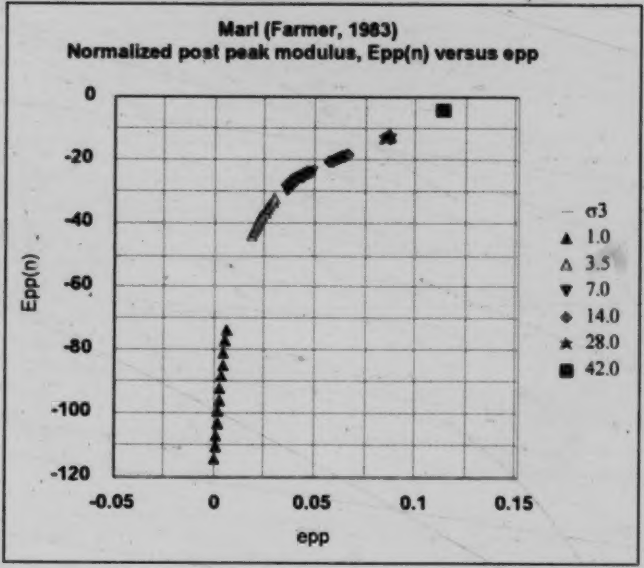

Criterion	Parameters			
Hoek-Brown peak strength	m	σ_c (MPa)	s	a
$\sigma_{1p} = \sigma_3 + \sigma_c\{m\sigma_3/\sigma_c + s\}^a$	1.9	14	1	0.5
Residual strength	D	F	σ_{cr} (MPa)	
$\sigma_{1r} = D\sigma_3^2 + F\sigma_3 + \sigma_{cr}$	-0.007	2.0	8	
Base strength & transition point	ϕ_b (deg.)	σ_{3t} (MPa)	σ_{1t} (MPa)	
$\sigma_{1b} = \{(1+\sin\phi_b)/(1-\sin\phi_b)\}\sigma_3$	17	45	82	
Friction-strain and base strain	R (deg.)	S	T	e_b
$\phi_e = R + Se_{pp} + Te_{pp}^2$	49	-520	2070	0.12

Appendix H.3

Intact mudstone (Farmer, 1983)

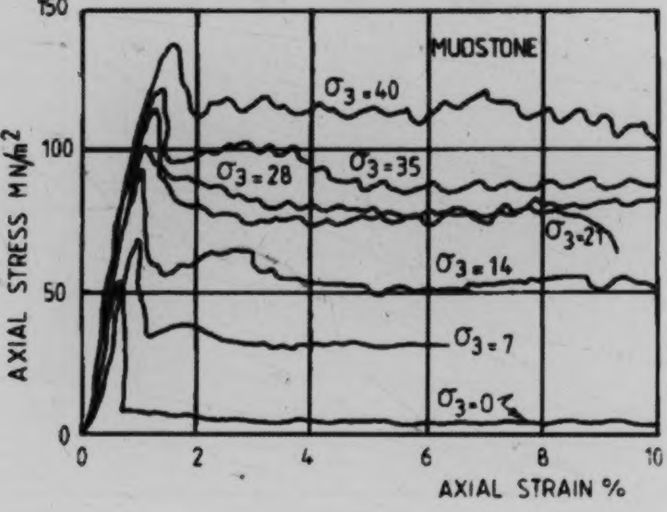

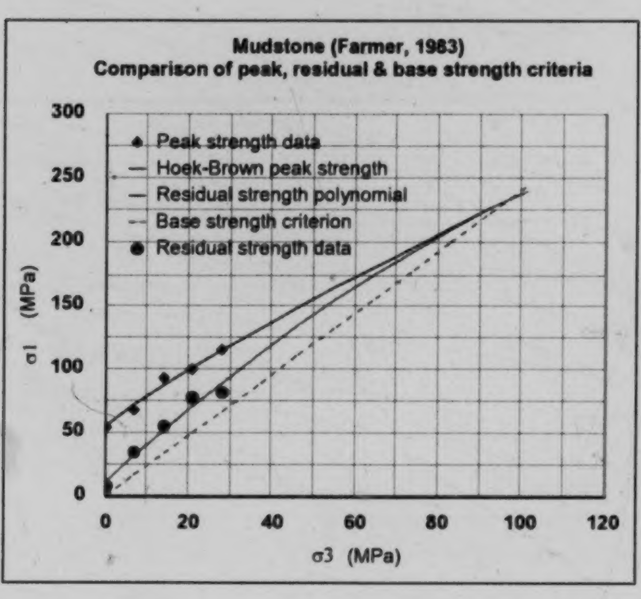

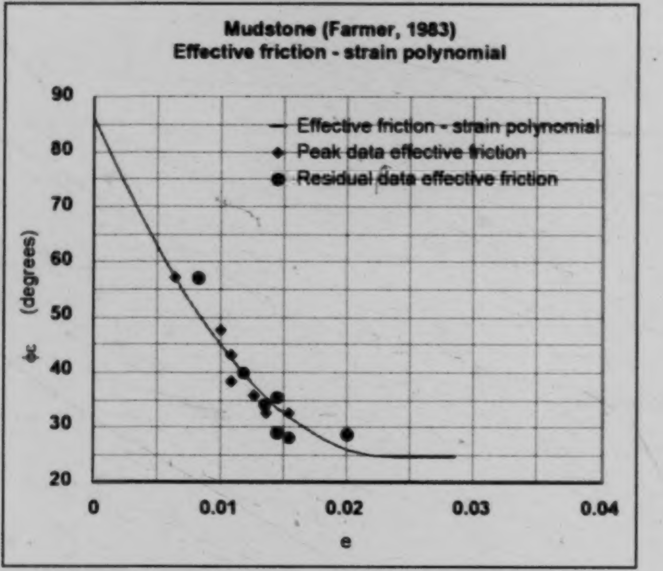
Mudstone (Farmer, 1983)
Effective friction - strain polynomial
90
80
70
60
50
40
30
20
φc (degrees)
0
0.01
0.02
0.03
0.04
e
Effective friction - strain polynomial
Peak data effective friction
Residual data effective friction

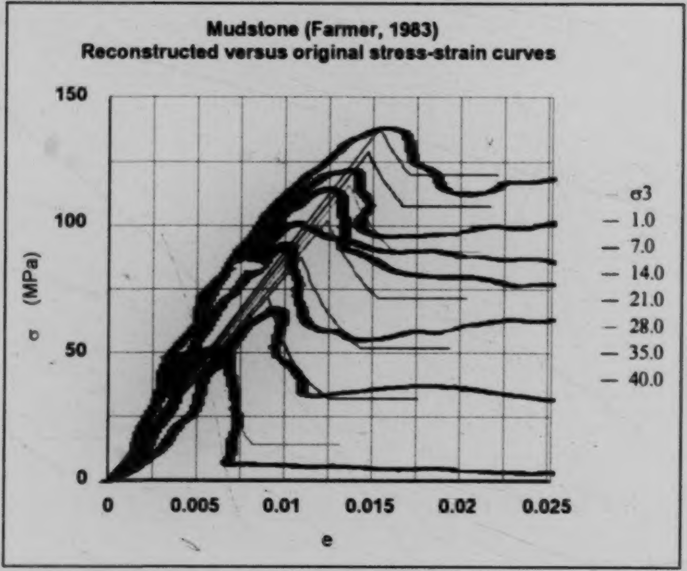
Mudstone (Farmer, 1983)
Reconstructed versus original stress-strain curves
150
100
50
0
σ (MPa)
0
0.005
0.01
0.015
0.02
0.025
e
σ3
1.0
7.0
14.0
21.0
28.0
35.0
40.0

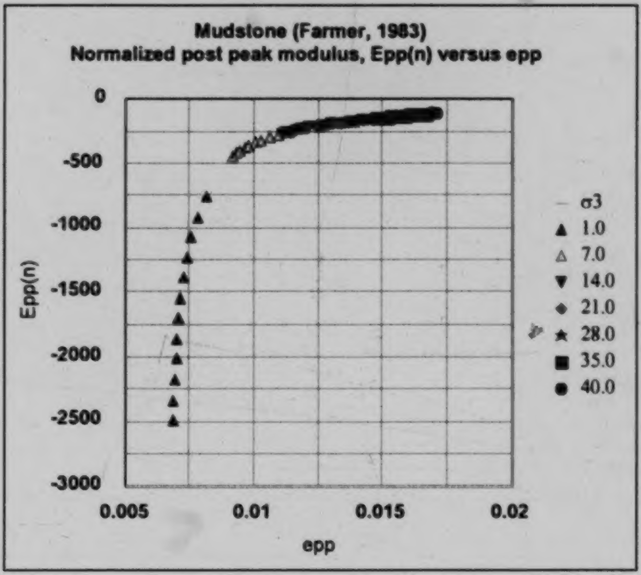

Criterion	Parameters			
Hoek-Brown peak strength	m	σ_c (MPa)	s	a
$\sigma_{1p} = \sigma_3 + \sigma_c\{m\sigma_3/\sigma_c + s\}^a$	2.9	56	1	0.5
Residual strength	D	F	σ_{cr} (MPa)	
$\sigma_{1r} = D\sigma_3^2 + F\sigma_3 + \sigma_{cr}$	-0.007	3.0	11	
Base strength & transition point	ϕ_b (deg.)	σ_{3t} (MPa)	σ_{1t} (MPa)	
$\sigma_{1b} = \{(1+\sin\phi_b)/(1-\sin\phi_b)\}\sigma_3$	24.5	97	234	
Friction-strain and base strain	R (deg.)	S	T	e_b
$\phi_c = R + Se_{pp} + Te_{pp}^2$	86	-5240	111000	0.024

Appendix H.4

Intact Portland stone (Farmer, 1983)

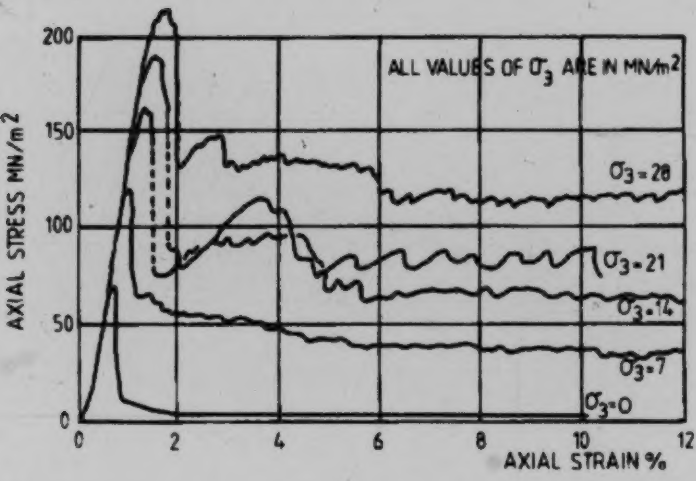

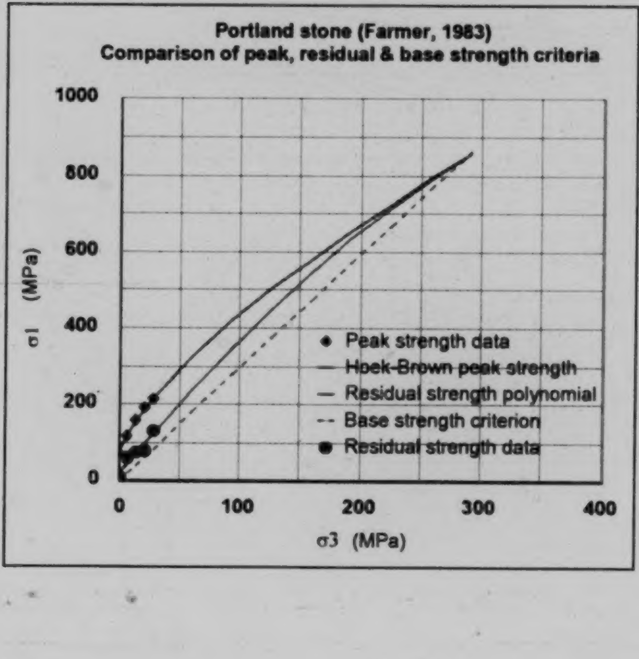

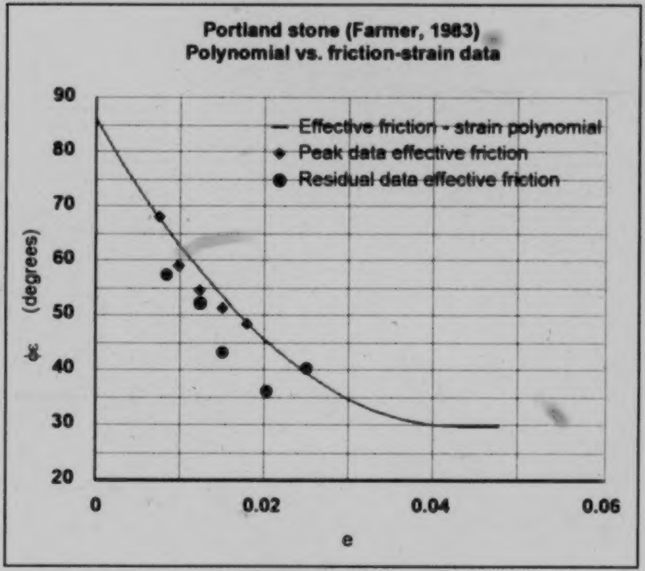

Portland stone (Farmer, 1983)
Polynomial vs. friction-strain data

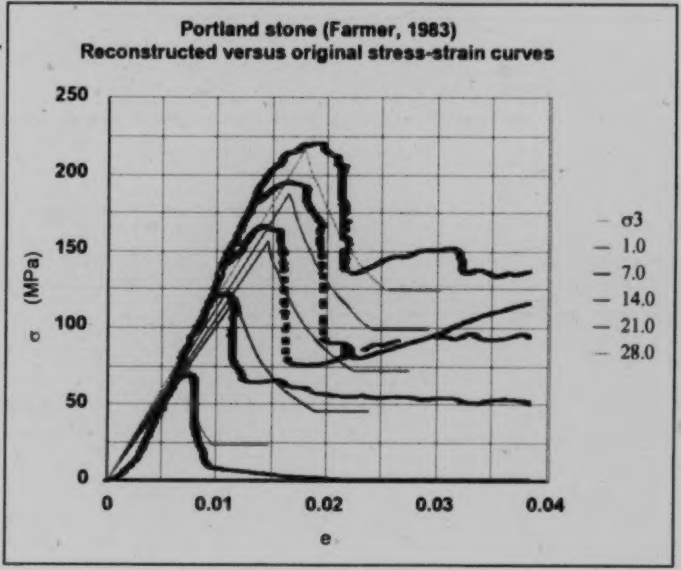

Portland stone (Farmer, 1983)
Reconstructed versus original stress-strain curves

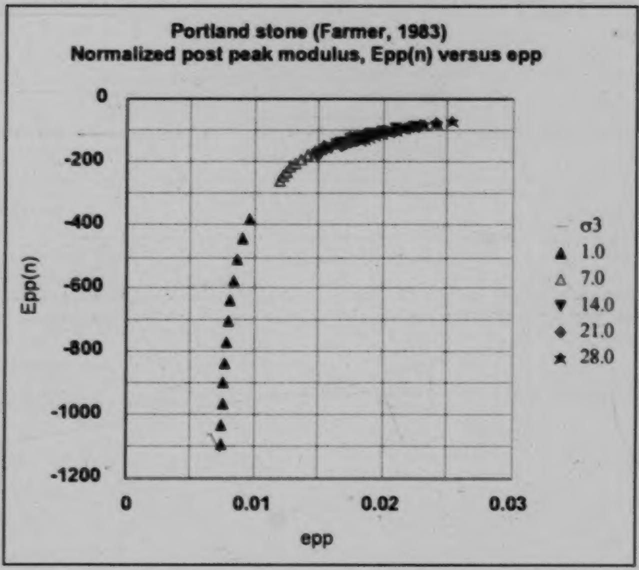

Criterion	Parameters			
Hoek-Brown peak strength $\sigma_{1p} = \sigma_3 + \sigma_c\{m\sigma_3/\sigma_c + s\}^a$	m 15.2	σ_c (MPa) 71.5	s 1	a 0.5
Residual strength $\sigma_{1r} = D\sigma_3^2 + F\sigma_3 + \sigma_{cr}$	D -0.003	F 3.8	σ_{cr} (MPa) 19.5	
Base strength & transition point $\sigma_{1b} = \{(1+\sin\phi_b)/(1-\sin\phi_b)\}\sigma_3$	ϕ_b (deg.) 30	σ_{3t} (MPa) 286	σ_{1t} (MPa) 850	
Friction-strain and base strain $\phi_e = R + Se_{pp} + Te_{pp}^2$	R (deg.) 86	S -2640	T 30800	e_b 0.043

Appendix H.5

Intact Saccharoidal limestone (Farmer, 1983)

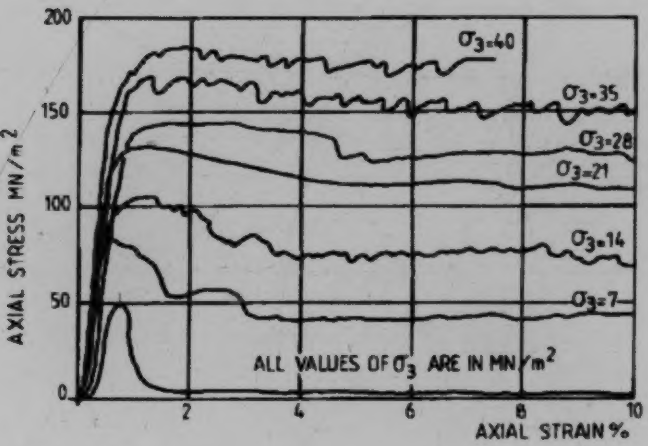

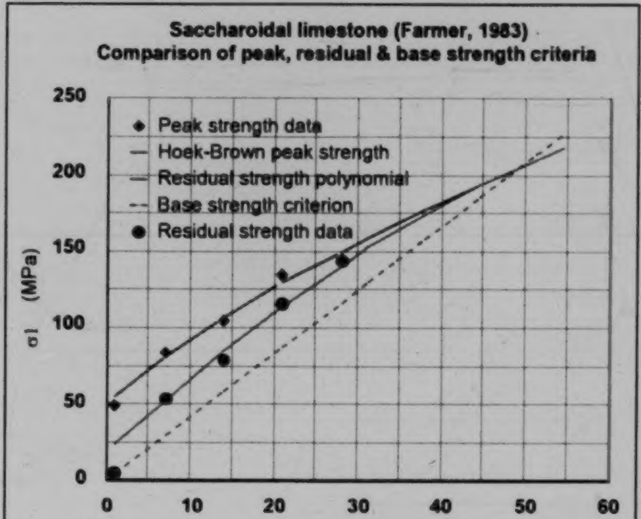

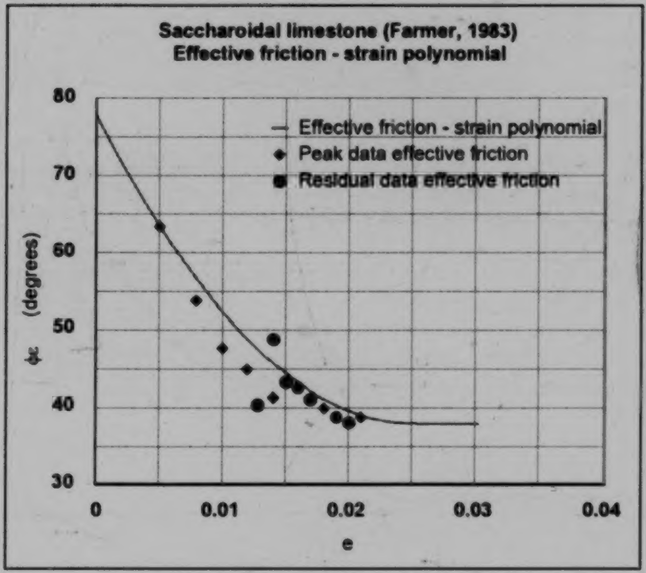
Saccharoidal limestone (Farmer, 1983)
Effective friction - strain polynomial
80
70
60
50
40
30
ϕc (degrees)
0
0.01
0.02
0.03
0.04
e
Effective friction - strain polynomial
Peak data effective friction
Residual data effective friction

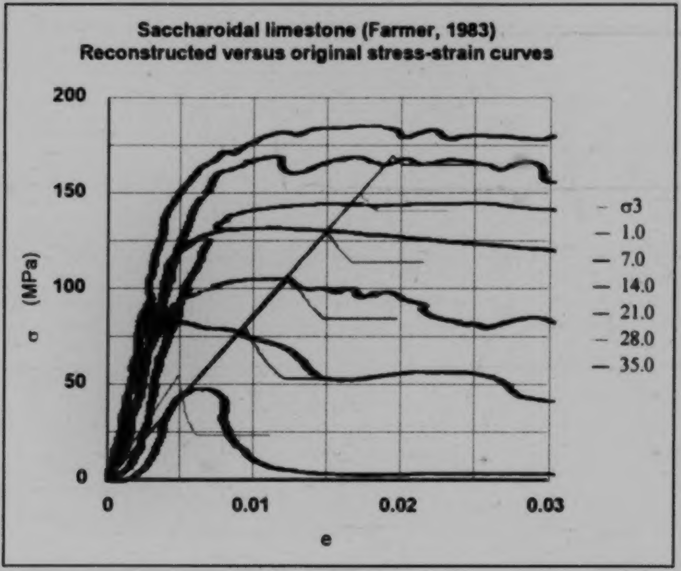
Saccharoidal limestone (Farmer, 1983)
Reconstructed versus original stress-strain curves
200
150
100
50
0
σ (MPa)
0
0.01
0.02
0.03
e
σ3
1.0
7.0
14.0
21.0
28.0
35.0

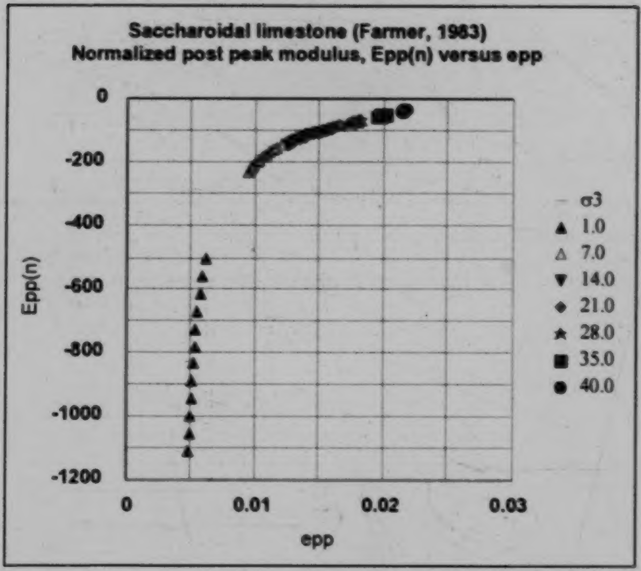

Criterion	Parameters			
Hoek-Brown peak strength	m	σ_c (MPa)	s	a
$\sigma_{1p} = \sigma_3 + \sigma_c\{m\sigma_3/\sigma_c + s\}^a$	9.0	50	1	0.5
Residual strength	D	F	σ_{cr} (MPa)	
$\sigma_{1r} = D\sigma_3^2 + F\sigma_3 + \sigma_{cr}$	-0.03	5.2	18	
Base strength & transition point	ϕ_b (deg.)	σ_{3t} (MPa)	σ_{1t} (MPa)	
$\sigma_{1b} = \{(1+\sin\phi_b)/(1-\sin\phi_b)\}\sigma_3$	38	50	206	
Friction-strain and base strain	R (deg.)	S	T	e_b
$\phi_e = R + Se_{pp} + Te_{pp}^2$	78	-3170	62800	0.025

Appendix H.6

Intact sandstone (Farmer, 1983)

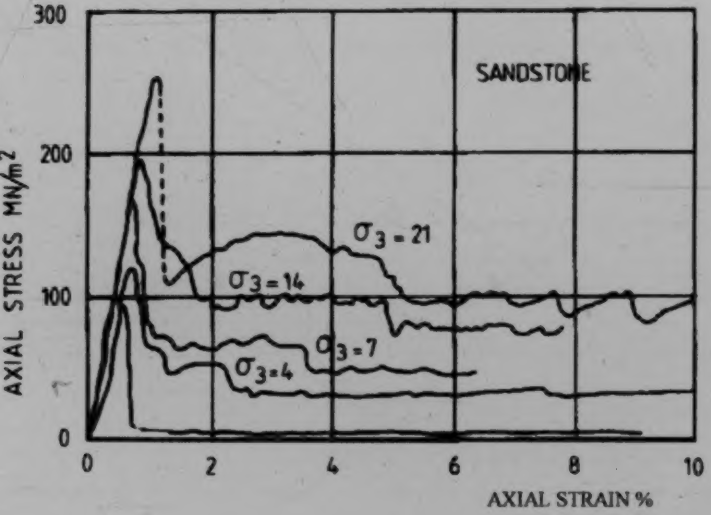

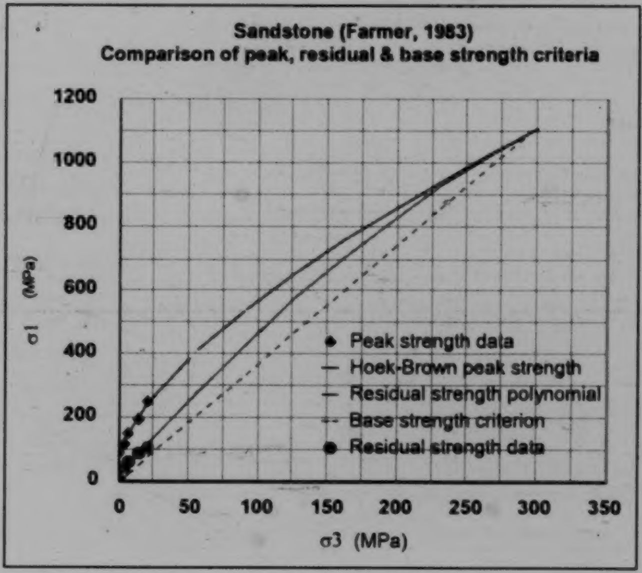

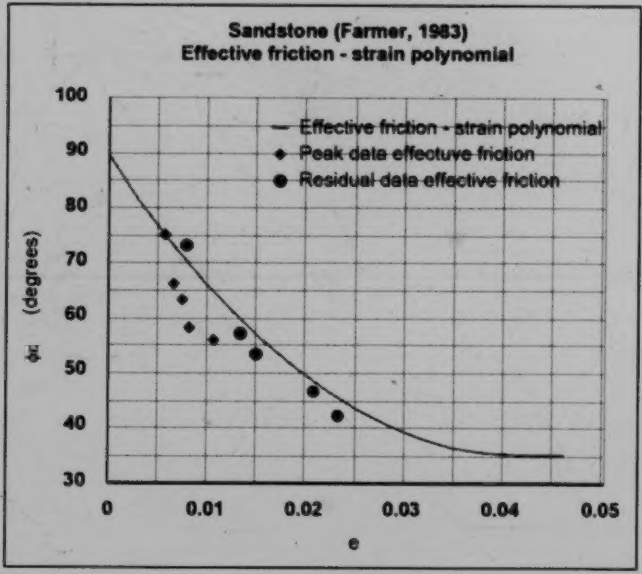
Sandstone (Farmer, 1983)
Effective friction - strain polynomial
100
90
80
70
60
50
40
30
φc (degrees)
0
0.01
0.02
0.03
0.04
0.05
e
Effective friction - strain polynomial
Peak data effectuve friction
Residual data effective friction

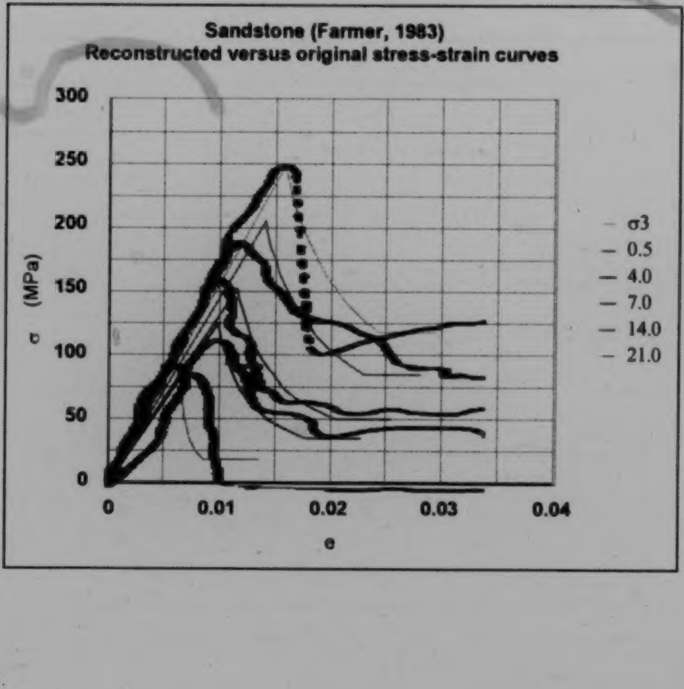
Sandstone (Farmer, 1983)
Reconstructed versus original stress-strain curves
300
250
200
150
100
50
0
σ (MPa)
0
0.01
0.02
0.03
0.04
e
σ3
0.5
4.0
7.0
14.0
21.0

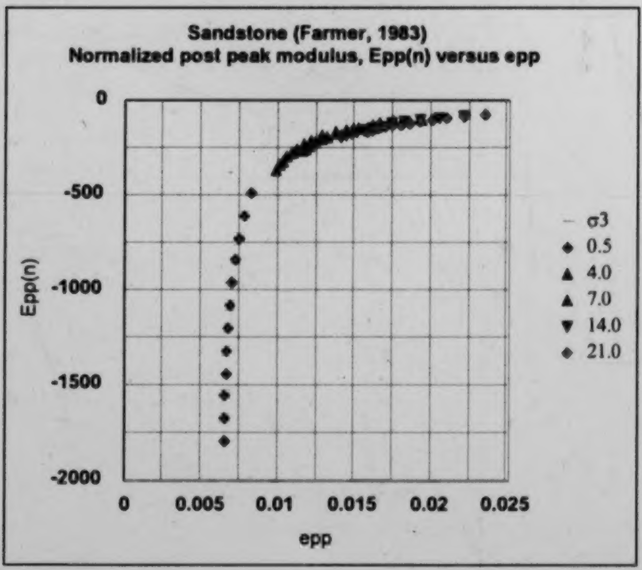

Criterion	Parameters			
Hoek-Brown peak strength	m	σ_c (MPa)	s	a
$\sigma_{1p} = \sigma_3 + \sigma_c\{m\sigma_3/\sigma_c + s\}^a$	27.7	78	1	0.5
Residual strength	D	F	σ_{cr} (MPa)	
$\sigma_{1r} = D\sigma_3^2 + F\sigma_3 + \sigma_{cr}$	-0.005	5.0	16	
Base strength & transition point	ϕ_b (deg.)	σ_{3t} (MPa)	σ_{1t} (MPa)	
$\sigma_{1b} = \{(1+\sin\phi_b)/(1-\sin\phi_b)\}\sigma_3$	35	296	1100	
Friction-strain and base strain	R (deg.)	S	T	e_b
$\phi_c = R + Se_{pp} + Te_{pp}^2$	89	-2630	31900	0.04

Appendix H.7

Intact silty sandstone (Farmer, 1983)

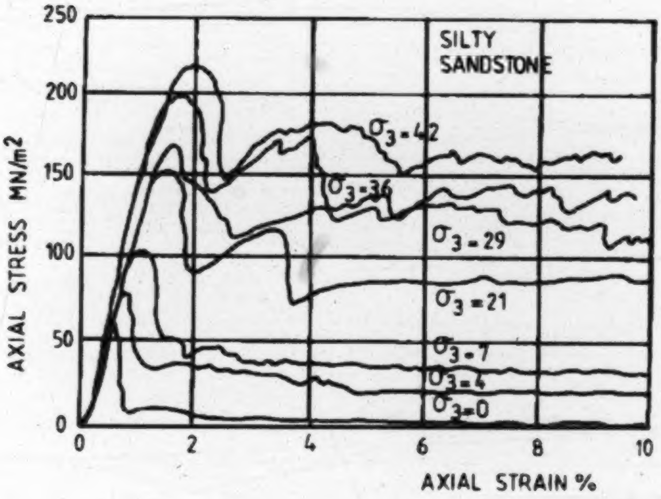

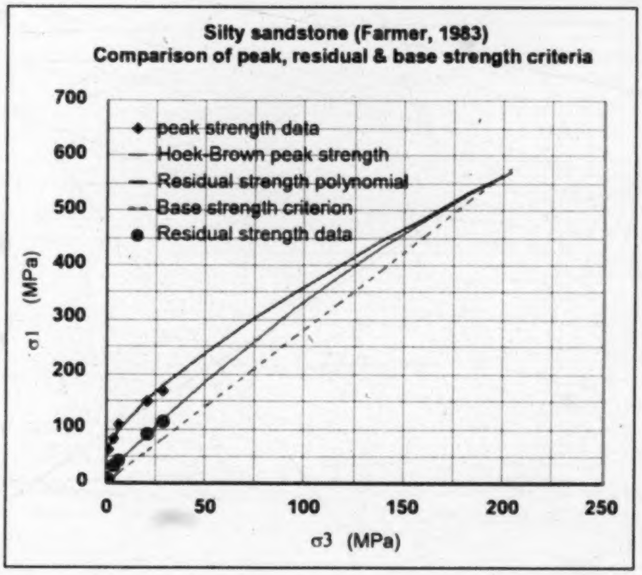

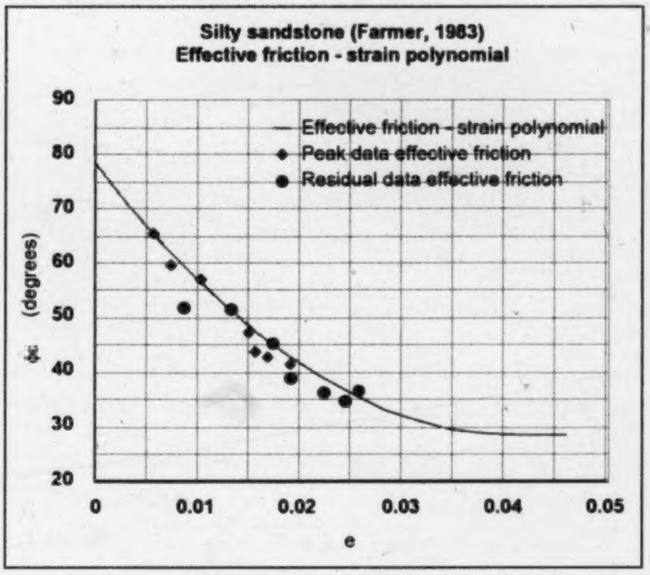
Silty sandstone (Farmer, 1983)
Effective friction - strain polynomial
90
80
70
60
50
40
30
20
φc (degrees)
0
0.01
0.02
0.03
0.04
0.05
e
Effective friction - strain polynomial
Peak data effective friction
Residual data effective friction

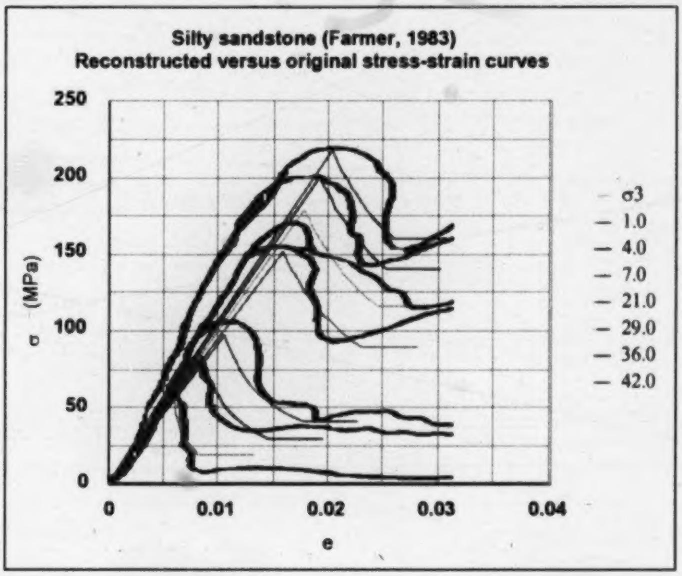
Silty sandstone (Farmer, 1983)
Reconstructed versus original stress-strain curves
250
200
150
100
50
0
σ (MPa)
0
0.01
0.02
0.03
0.04
e
σ3
1.0
4.0
7.0
21.0
29.0
36.0
42.0

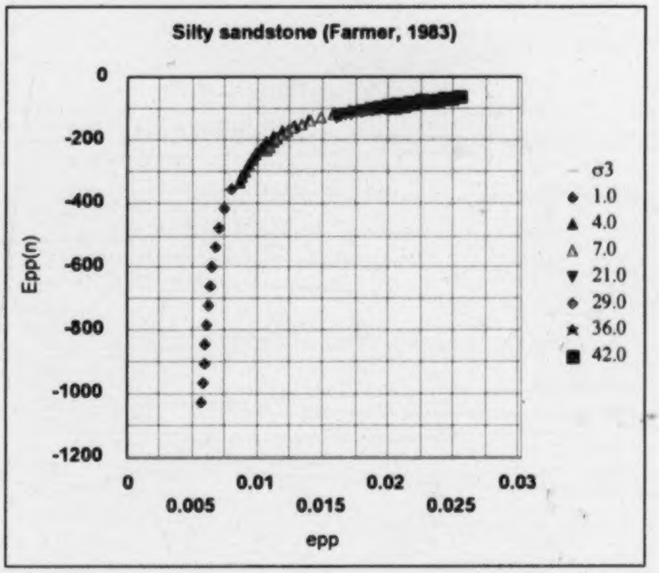

Criterion	Parameters			
Hoek-Brown peak strength	m	σ_c (MPa)	s	a
$\sigma_{1p} = \sigma_3 + \sigma_c\{m\sigma_3/\sigma_c + s\}^a$	10.6	61	1	0.5
Residual strength	D	F	σ_{cr} (MPa)	
$\sigma_{1r} = D\sigma_3^2 + F\sigma_3 + \sigma_{cr}$	-0.004	3.6	16	
Base strength & transition point	ϕ_b (deg.)	σ_{3t} (MPa)	σ_{1t} (MPa)	
$\sigma_{1b} = \{(1+\sin\phi_b)/(1-\sin\phi_b)\}\sigma_3$	28.5	200	564	
Friction-strain and base strain	R (deg.)	S	T	e_b
$\phi_e = R + Se_{pp} + Te_{pp}^2$	79	-2430	29600	0.04

Appendix H.8

Intact quartzite (Gates, 1988)

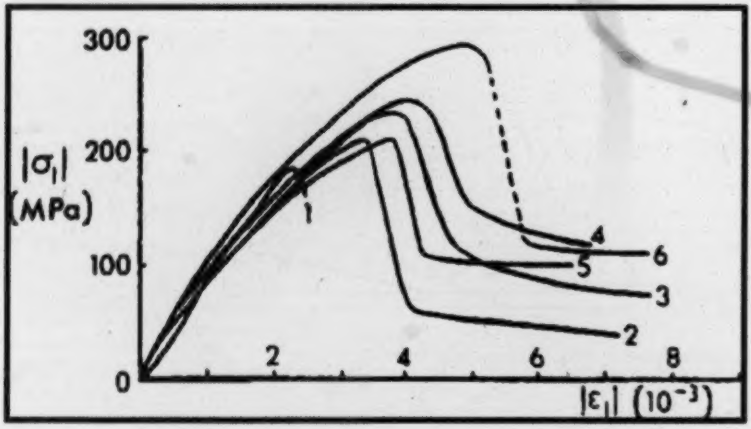

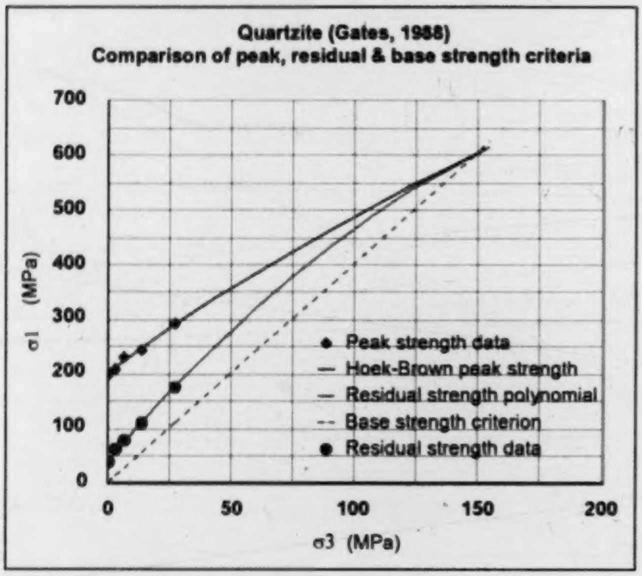

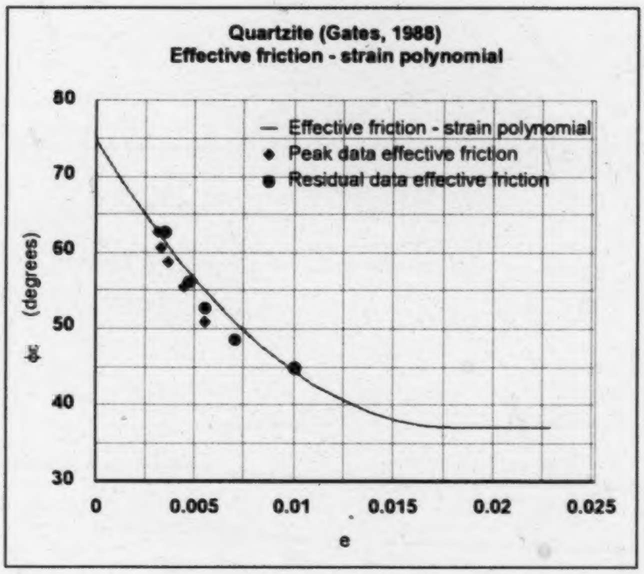
Quartzite (Gates, 1988)
Effective friction - strain polynomial
Effective friction - strain polynomial
Peak data effective friction
Residual data effective friction
φc (degrees)
80
70
60
50
40
30
0
0.005
0.01
0.015
0.02
0.025
e

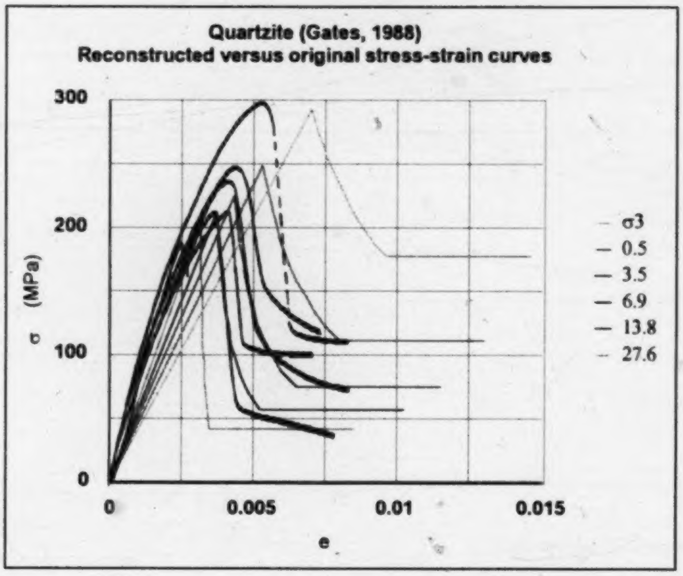
Quartzite (Gates, 1988)
Reconstructed versus original stress-strain curves
σ (MPa)
300
200
100
0
0
0.005
0.01
0.015
e
σ3
0.5
3.5
6.9
13.8
27.6

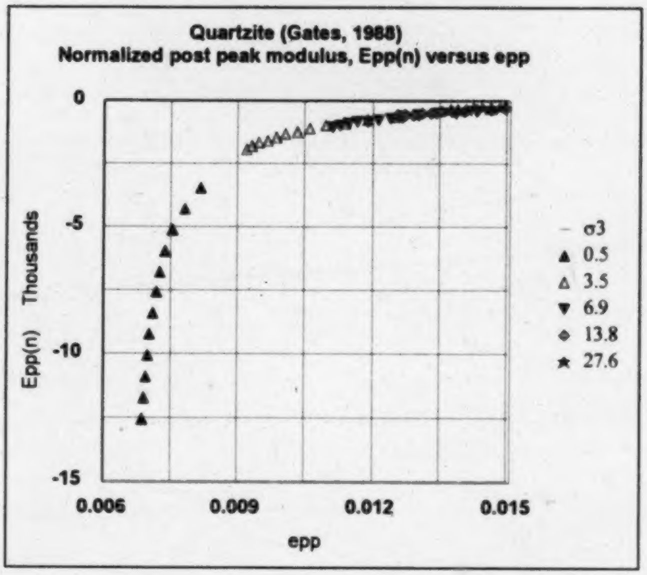

Criterion	Parameters			
Hoek-Brown peak strength	m	σ_c (MPa)	s	a
$\sigma_{1p} = \sigma_3 + \sigma_c\{m\sigma_3/\sigma_c + s\}^a$	5.6	200	1	0.5
Residual strength	D	F	σ_{cr} (MPa)	
$\sigma_{1r} = D\sigma_3^2 + F\sigma_3 + \sigma_{cr}$	-0.01	5.3	40	
Base strength & transition point	ϕ_b (deg.)	σ_{3t} (MPa)	σ_{1t} (MPa)	
$\sigma_{1b} = \{(1+\sin\phi_b)/(1-\sin\phi_b)\}\sigma_3$	37	150	605	
Friction-strain and base strain	R (deg.)	S	T	e_b
$\phi_e = R + Se_{pp} + Te_{pp}^2$	75	-4200	117000	0.018

Appendix H.9

Intact Lac du Bonnet pink granite (Gorski et al., 1991)

σ_3 data (MPa)	σ_{1p} data (MPa)	σ_{1r} data (MPa)	e_p data (strain)	e_r data (strain)
0.01	186	46.25	0.0032	0.0029
2	216	39	0.0038	0.0055
4	257	69	0.0044	0.0070
6	285	90	0.0050	0.0075
10	328	102	0.0054	0.0067
15	393	105	0.0063	0.0092
20	443	158	0.0070	0.0098
30	520	291	0.0082	0.0090
40	586	179	0.0090	0.0140
60	700	377	0.0105	0.0107

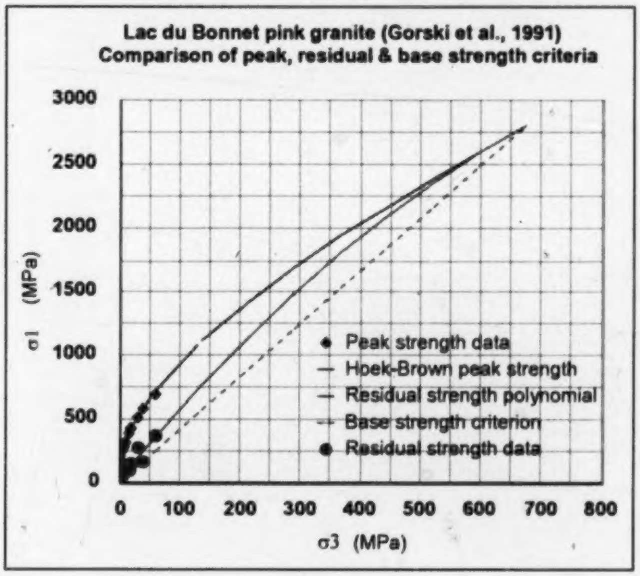

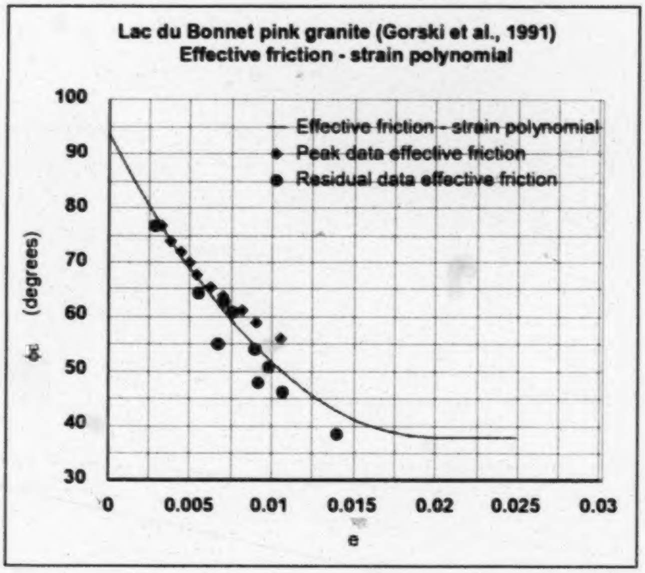
Lac du Bonnet pink granite (Gorski et al., 1991)
Effective friction - strain polynomial
100
90
80
70
60
50
40
30
ϕi (degrees)
0
0.005
0.01
0.015
0.02
0.025
0.03
e
Effective friction - strain polynomial
Peak data effective friction
Residual data effective friction

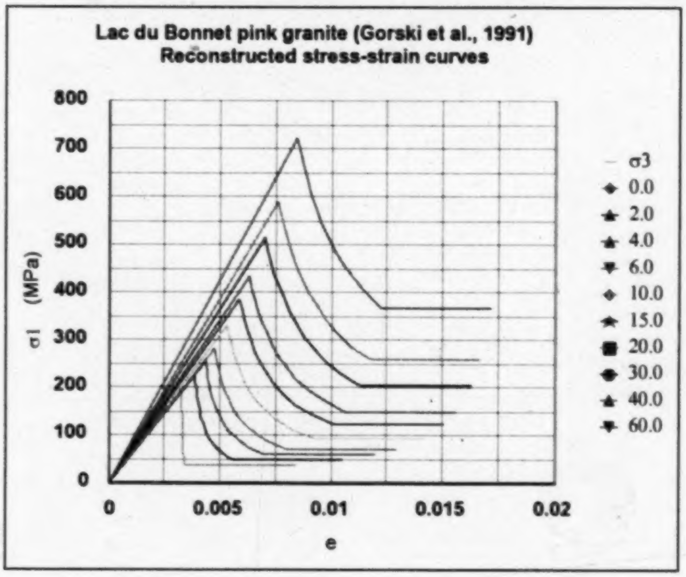
Lac du Bonnet pink granite (Gorski et al., 1991)
Reconstructed stress-strain curves
800
700
600
500
400
300
200
100
0
σ1 (MPa)
0
0.005
0.01
0.015
0.02
e
σ3
0.0
2.0
4.0
6.0
10.0
15.0
20.0
30.0
40.0
60.0

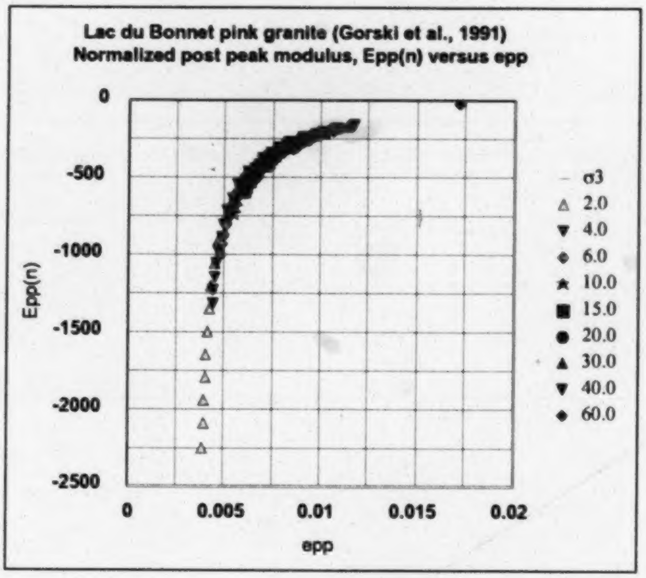

Criterion	Parameters			
Hoek-Brown peak strength	m	σ_c (MPa)	s	a
$\sigma_{1p} = \sigma_3 + \sigma_c\{m\sigma_3/\sigma_c + s\}^a$	35.0	192	1	0.5
Residual strength	D	F	σ_{cr} (MPa)	
$\sigma_{1r} = D\sigma_3^2 + F\sigma_3 + \sigma_{cr}$	-0.002	5.7	38	
Base strength & transition point	ϕ_b (deg.)	σ_{3t} (MPa)	σ_{1t} (MPa)	
$\sigma_{1b} = \{(1+\sin\phi_b)/(1-\sin\phi_b)\}\sigma_3$	38	670	2800	
Friction-strain and base strain	R (deg.)	S	T	e_b
$\phi_e = R + Se_{pp} + Te_{pp}^2$	93.5	-5590	141000	0.02

Appendix H.10

Intact Doddington sandstone (Santarelli et al., 1989)

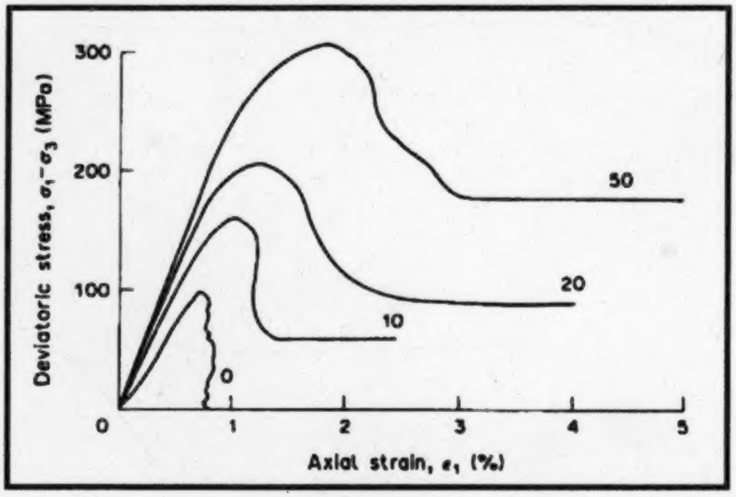

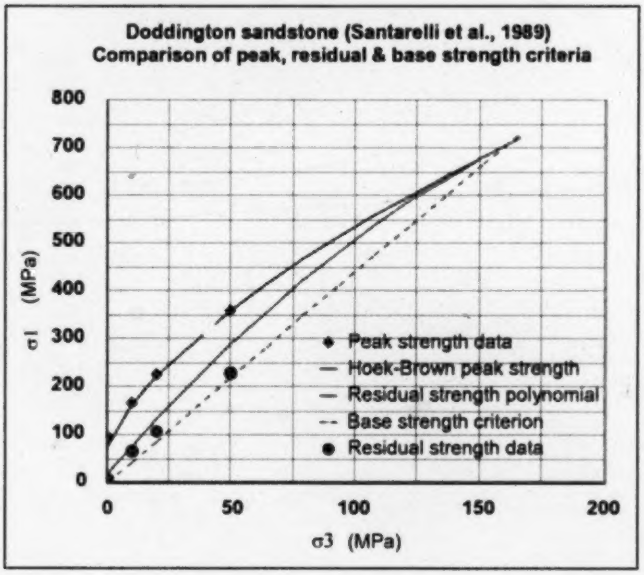

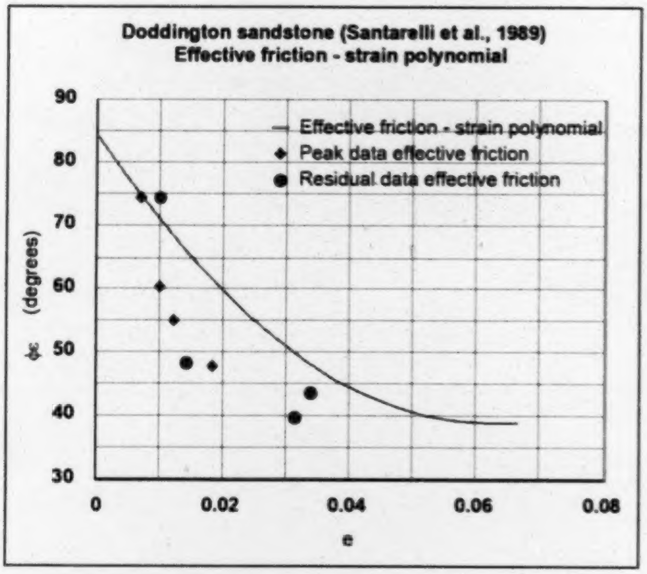

Doddington sandstone (Santarelli et al., 1989)
Effective friction - strain polynomial

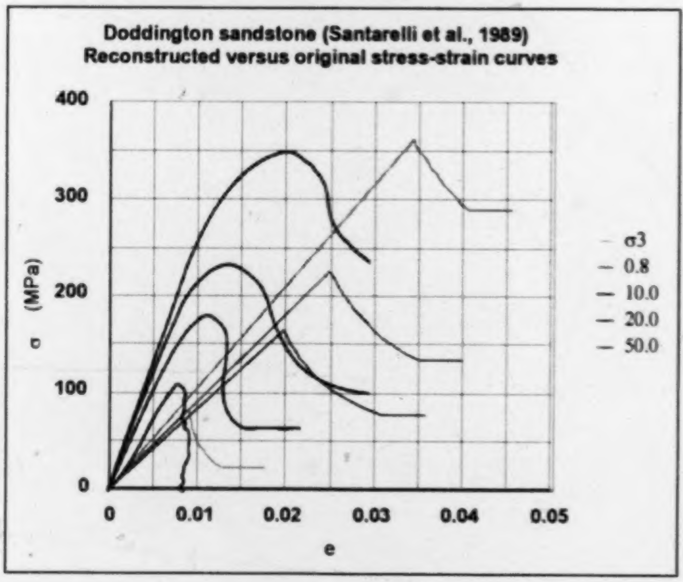

Doddington sandstone (Santarelli et al., 1989)
Reconstructed versus original stress-strain curves

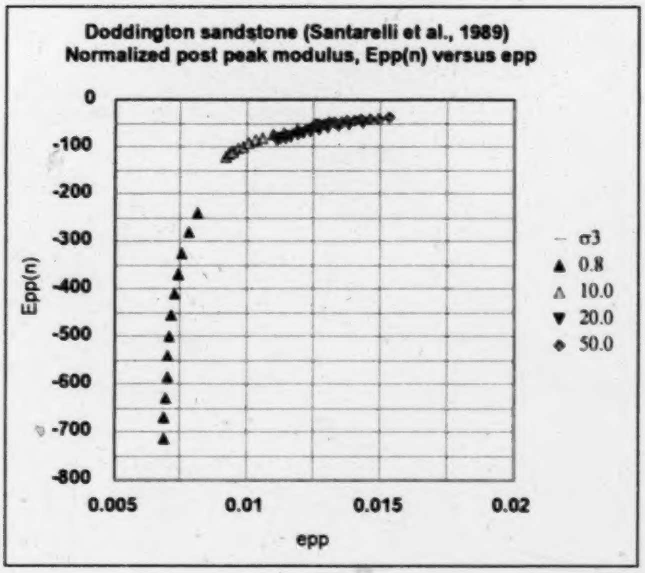

Criterion	Parameters			
Hoek-Brown peak strength	m	σ_c (MPa)	s	a
$\sigma_{1p} = \sigma_3 + \sigma_c\{m\sigma_3/\sigma_c + s\}^a$	25.0	74	1	0.5
Residual strength	D	F	σ_{cr} (MPa)	
$\sigma_{1r} = D\sigma_3^2 + F\sigma_3 + \sigma_{cr}$	-0.003	4.4	19	
Base strength & transition point	ϕ_b (deg.)	σ_{3t} (MPa)	σ_{1t} (MPa)	
$\sigma_{1b} = \{(1+\sin\phi_b)/(1-\sin\phi_b)\}\sigma_3$	33	334	1120	
Friction-strain and base strain	R (deg.)	S	T	e_b
$\phi_e = R + Se_{pp} + Te_{pp}^2$	86	-1750	14200	0.06

Appendix H.11

Intact Gebdykes dolomite (Santarelli et al., 1989)

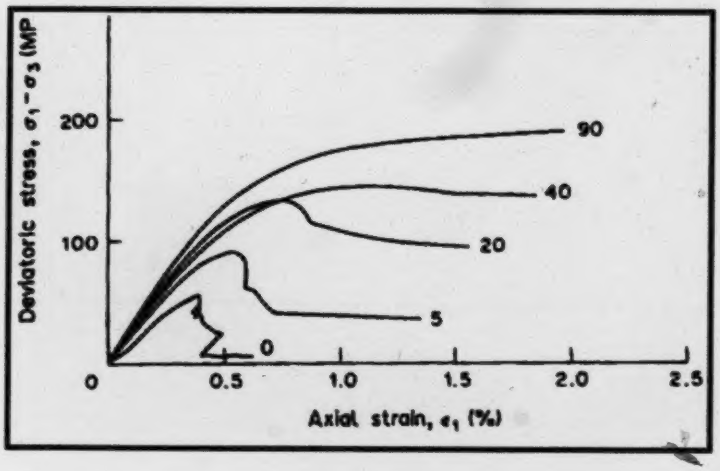

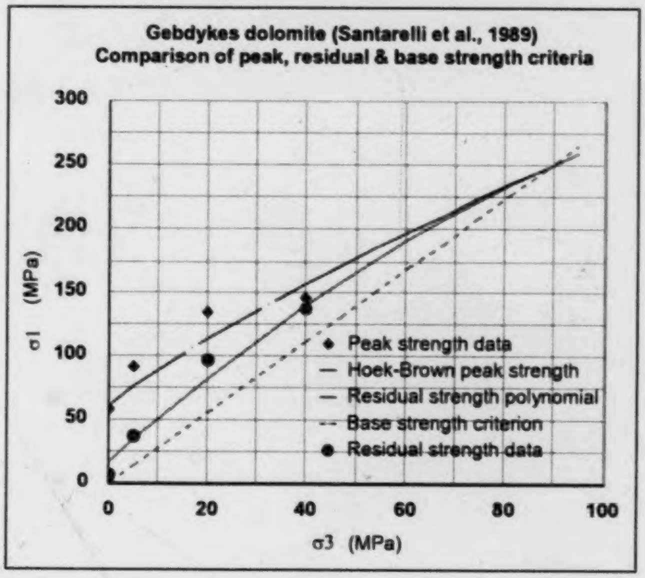

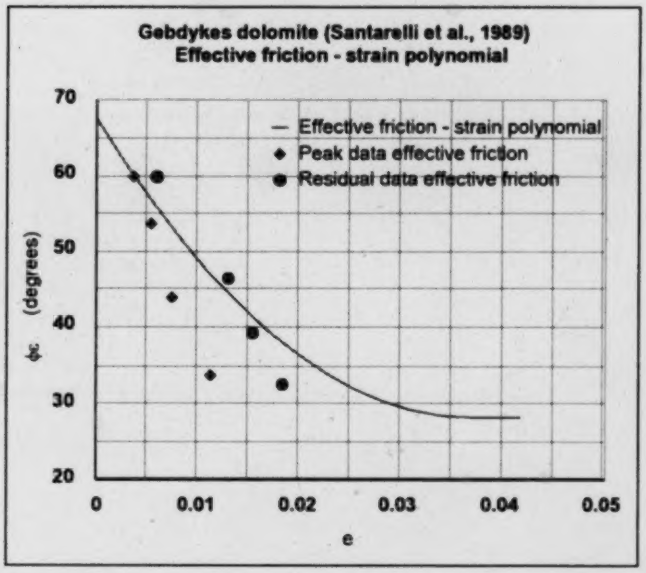
Gebdykes dolomite (Santarelli et al., 1989)
Effective friction - strain polynomial
70
60
50
40
30
20
φc (degrees)
0
0.01
0.02
0.03
0.04
0.05
e
Effective friction - strain polynomial
Peak data effective friction
Residual data effective friction

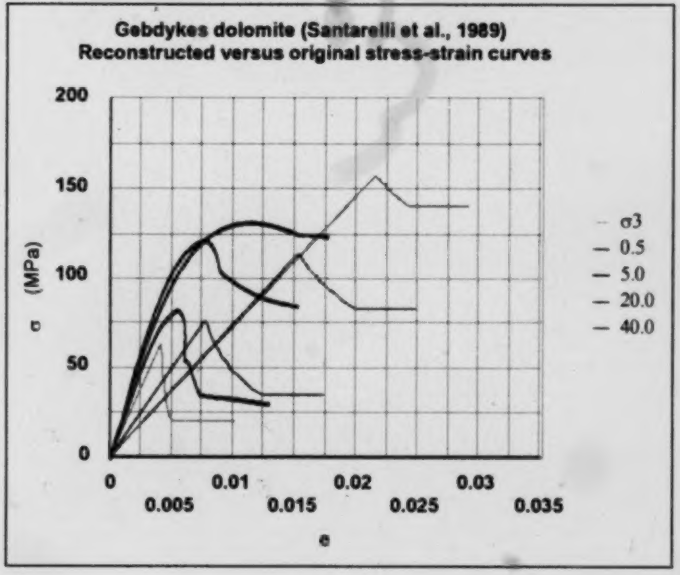
Gebdykes dolomite (Santarelli et al., 1989)
Reconstructed versus original stress-strain curves
200
150
100
50
0
σ (MPa)
0
0.005
0.01
0.015
0.02
0.025
0.03
0.035
e
σ3
0.5
5.0
20.0
40.0

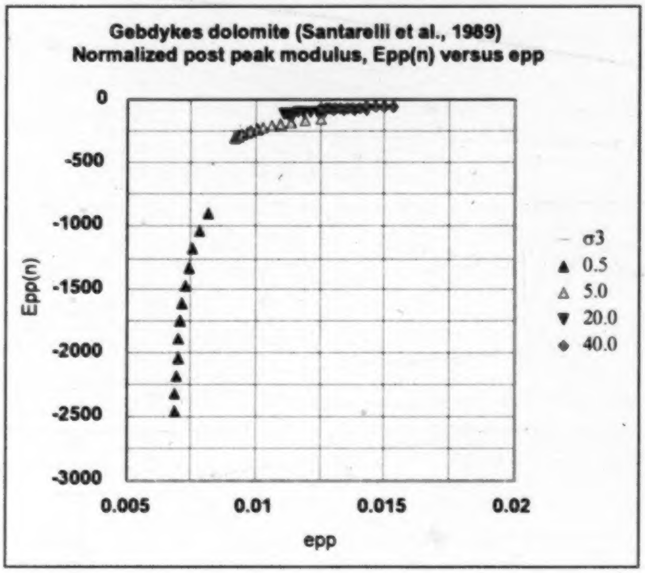

Criterion	Parameters			
Hoek-Brown peak strength	m	σ_c (MPa)	s	a
$\sigma_{1p} = \sigma_3 + \sigma_c\{m\sigma_3/\sigma_c + s\}^a$	4.0	62	1	0.5
Residual strength	D	F	σ_{cr} (MPa)	
$\sigma_{1r} = D\sigma_3^2 + F\sigma_3 + \sigma_{cr}$	-0.009	3.4	18	
Base strength & transition point	ϕ_b (deg.)	σ_{3t} (MPa)	σ_{1t} (MPa)	
$\sigma_{1b} = \{(1+\sin\phi_b)/(1-\sin\phi_b)\}\sigma_3$	28	90	252	
Friction-strain and base strain	R (deg.)	S	T	e_b
$\phi_e = R + Se_{pp} + Te_{pp}^2$	67.5	-2120	28700	0.037

Appendix H.12

Intact mudstone (Tao, 1991)

123 peak strength and strain data points and 123 residual strength data points, but no residual strain data points recorded by Tao.

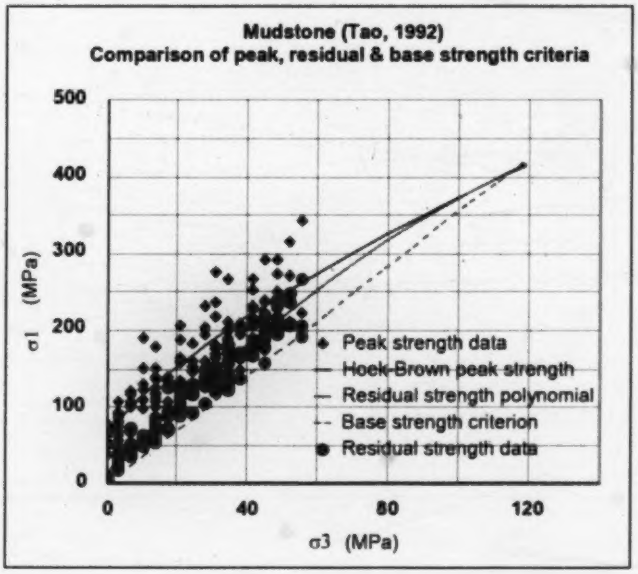

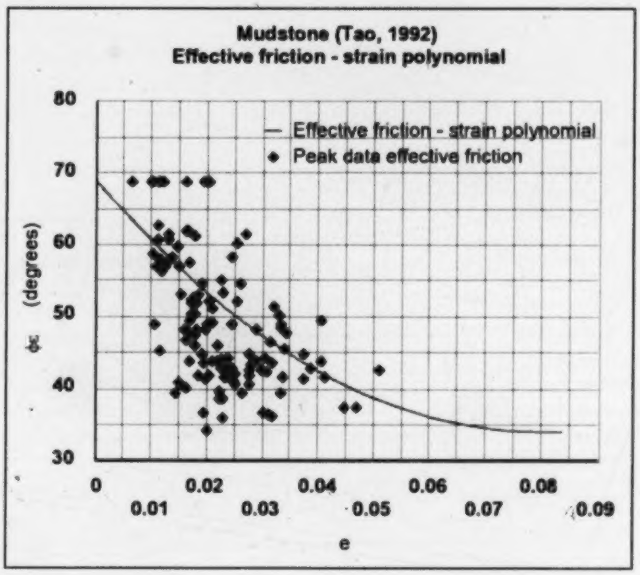
Mudstone (Tao, 1992)
Effective friction - strain polynomial
Effective friction - strain polynomial
Peak data effective friction
φc (degrees)
80
70
60
50
40
30
0
0.01
0.02
0.03
0.04
0.05
0.06
0.07
0.08
0.09
e

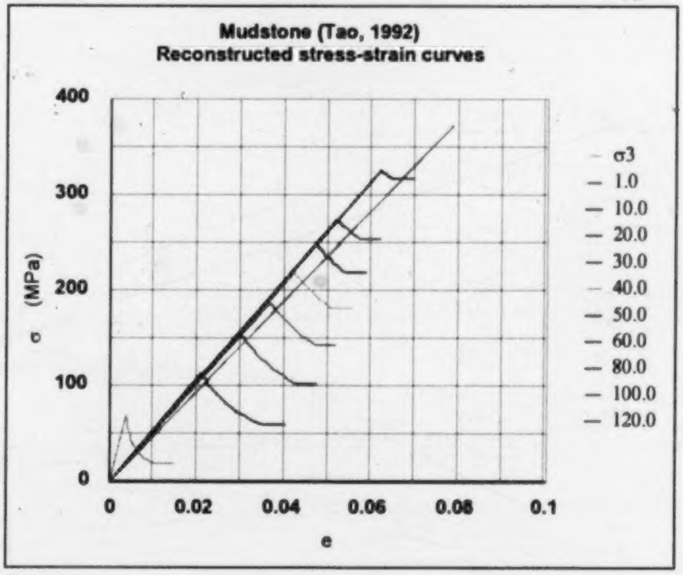
Mudstone (Tao, 1992)
Reconstructed stress-strain curves
σ (MPa)
400
300
200
100
0
0
0.02
0.04
0.06
0.08
0.1
e
σ3
1.0
10.0
20.0
30.0
40.0
50.0
60.0
80.0
100.0
120.0

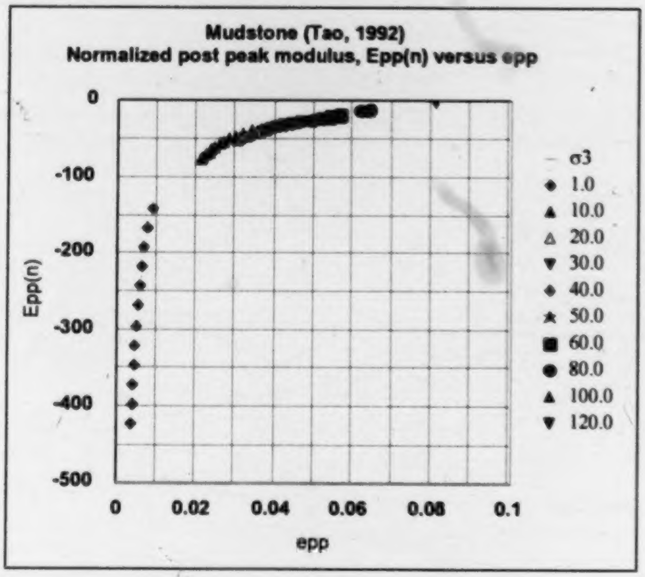

Criterion	Parameters			
Hoek-Brown peak strength	m	σ_c (MPa)	s	a
$\sigma_{1p} = \sigma_3 + \sigma_c\{m\sigma_3/\sigma_c + s\}^a$	11.4	62	1	0.5
Residual strength	D	F	σ_{cr} (MPa)	
$\sigma_{1r} = D\sigma_3^2 + F\sigma_3 + \sigma_{cr}$	-0.01	4.6	15	
Base strength & transition point	ϕ_b (deg.)	σ_{3t} (MPa)	σ_{1t} (MPa)	
$\sigma_{1b} = \{(1+\sin\phi_b)/(1-\sin\phi_b)\}\sigma_3$	34	114	406	
Friction-strain and base strain	R (deg.)	S	T	e_b
$\phi_c = R + Se_{pp} + Te_{pp}^2$	69	-883	5610	0.08

Appendix J

Worked intact rock data sets where peak and residual data was available, but only peak data was used for comparison with results from appendix H

Appendix J.1

Intact high strength concrete HS15 (Ansari et al., 1998)

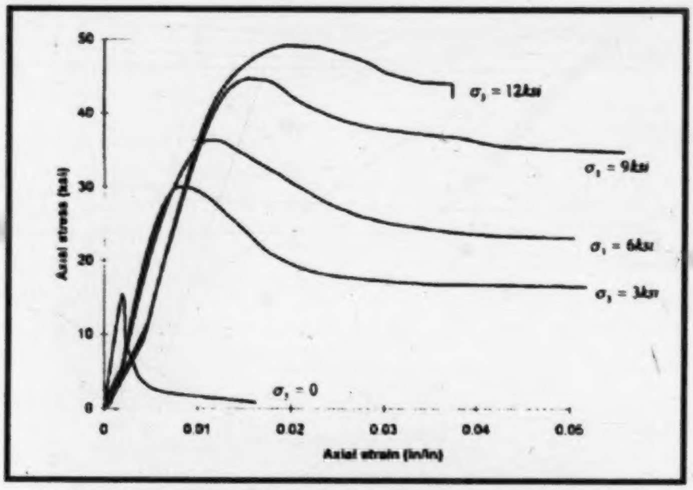

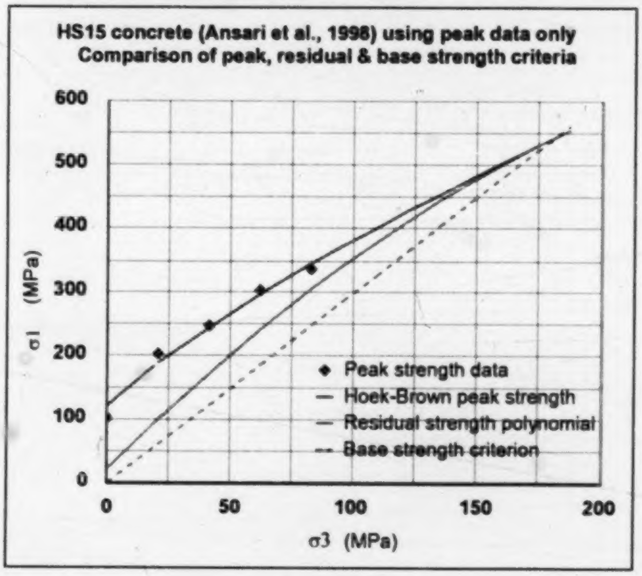

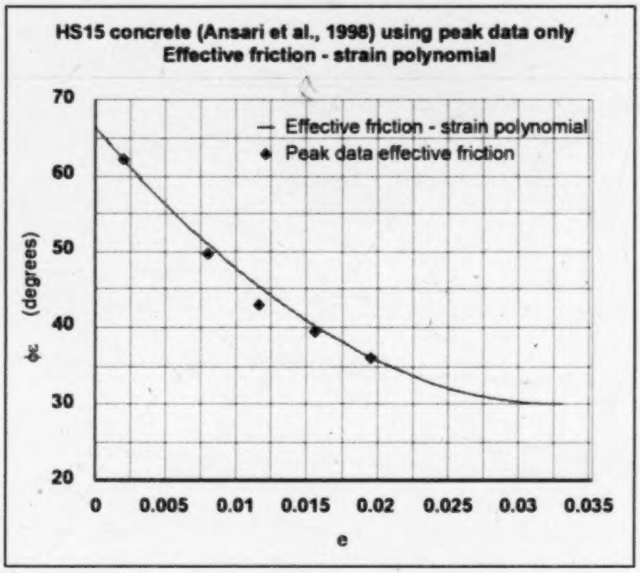

HS15 concrete (Ansari et al., 1998) using peak data only
Effective friction - strain polynomial

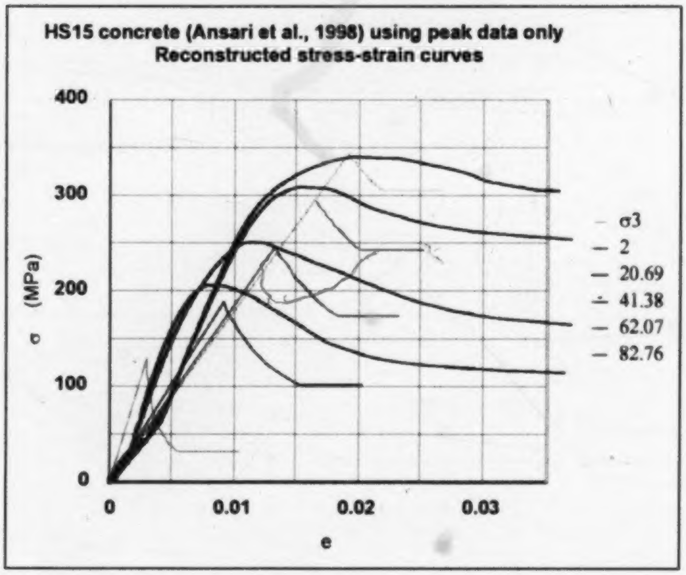

HS15 concrete (Ansari et al., 1998) using peak data only
Reconstructed stress-strain curves

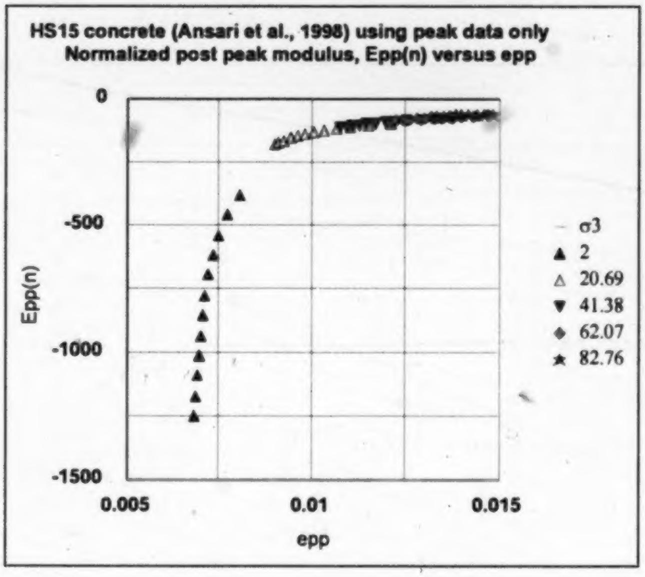

Criterion	Parameters			
Hoek-Brown peak strength	m	σ_c (MPa)	s	a
$\sigma_{1p} = \sigma_3 + \sigma_c\{m\sigma_3/\sigma_c + s\}^a$	5.2	124	1	0.5
Residual strength	D	F	σ_{cr} (MPa)	
$\sigma_{1r} = D\sigma_3^2 + F\sigma_3 + \sigma_{cr}$	-0.005	3.8	25	
Base strength & transition point	ϕ_b (deg.)	σ_{3t} (MPa)	σ_{1t} (MPa)	
$\sigma_{1b} = \{(1+\sin\phi_b)/(1-\sin\phi_b)\}\sigma_3$	30	182	547	
Friction-strain and base strain	R (deg.)	S	T	e_b
$\phi_c = R + Se_{pp} + Te_{pp}^2$	66.5	-2210	33400	0.03

Appendix J.2

Intact marl (Farmer, 1983) using peak data only

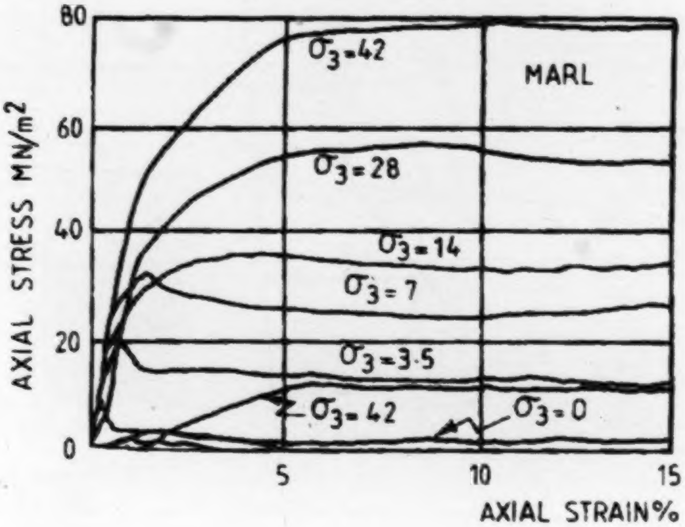

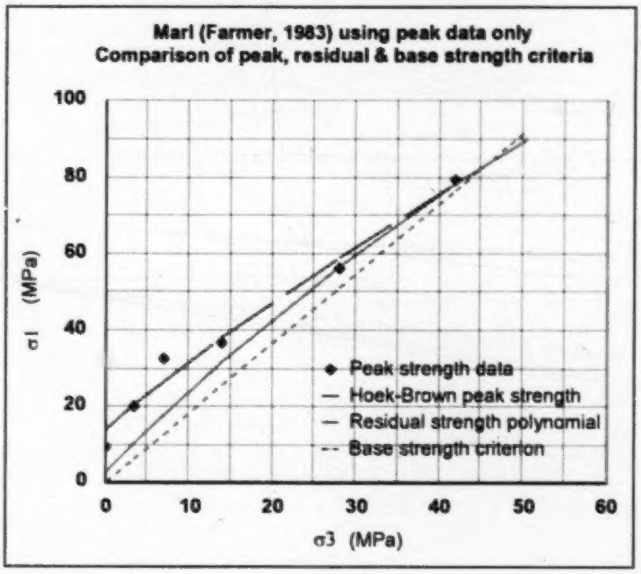

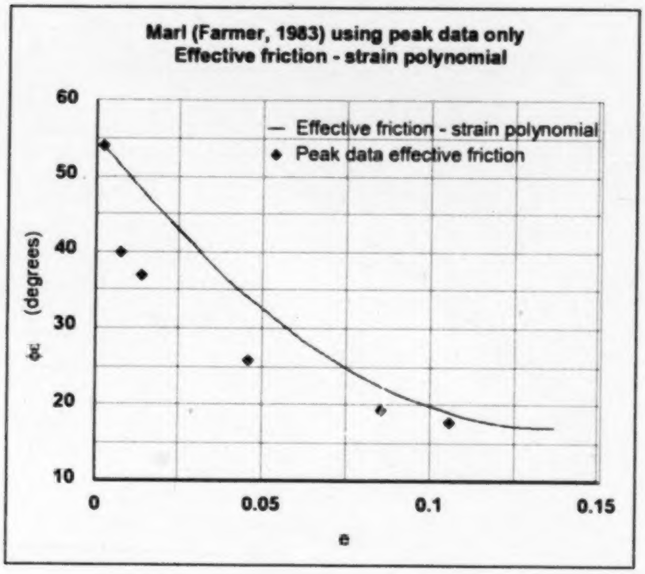
Marl (Farmer, 1983) using peak data only
Effective friction - strain polynomial
— Effective friction - strain polynomial
◆ Peak data effective friction
φc (degrees)
60
50
40
30
20
10
0
0.05
0.1
0.15
e

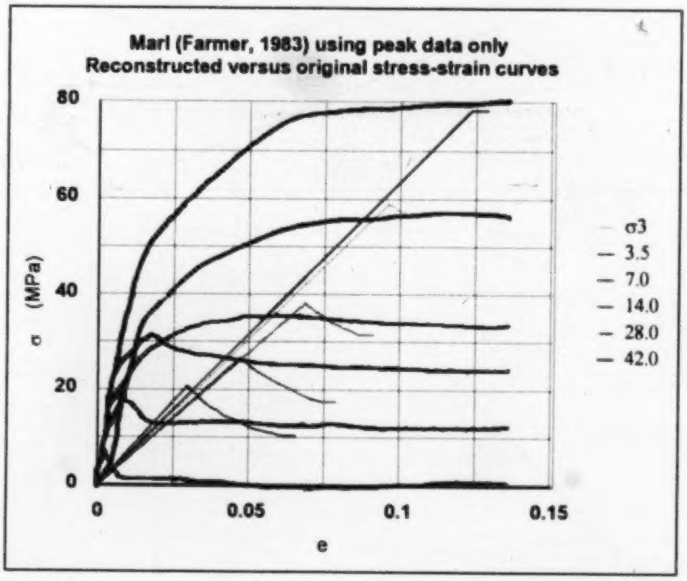
Marl (Farmer, 1983) using peak data only
Reconstructed versus original stress-strain curves
σ (MPa)
80
60
40
20
0
0
0.05
0.1
0.15
e
σ3
— 3.5
— 7.0
— 14.0
— 28.0
— 42.0

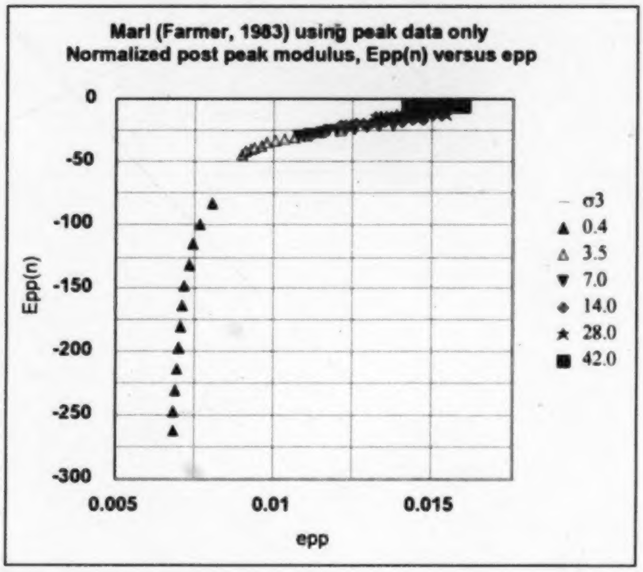

Criterion	Parameters			
Hoek-Brown peak strength	m	σ_c (MPa)	s	a
$\sigma_{1p} = \sigma_3 + \sigma_c\{m\sigma_3/\sigma_c + s\}^a$	1.9	14	1	0.5
Residual strength	D	F	σ_{cr} (MPa)	
$\sigma_{1r} = D\sigma_3^2 + F\sigma_3 + \sigma_{cr}$	-0.009	2.2	3	
Base strength & transition point	ϕ_b (deg.)	σ_{3t} (MPa)	σ_{1t} (MPa)	
$\sigma_{1b} = \{(1+\sin\phi_b)/(1-\sin\phi_b)\}\sigma_3$	17	46	83	
Friction-strain and base strain	R (deg.)	S	T	e_b
$\phi_e = R + Se_{pp} + Te_{pp}^2$	43	-464	2040	0.114

Appendix J.3

Intact mudstone (Farmer, 1983) using peak data only

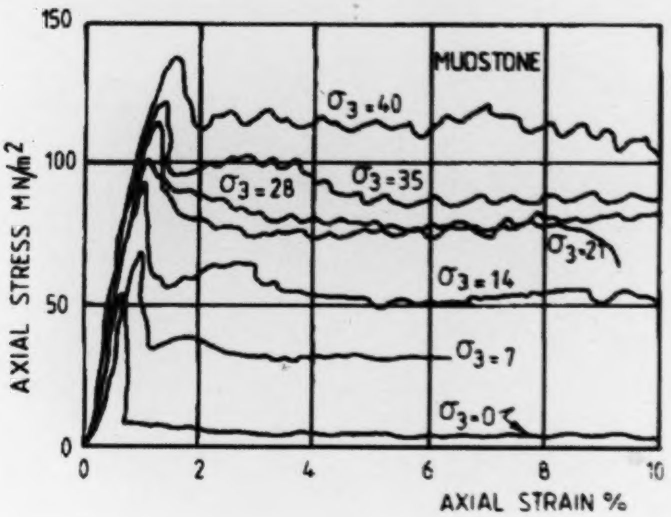

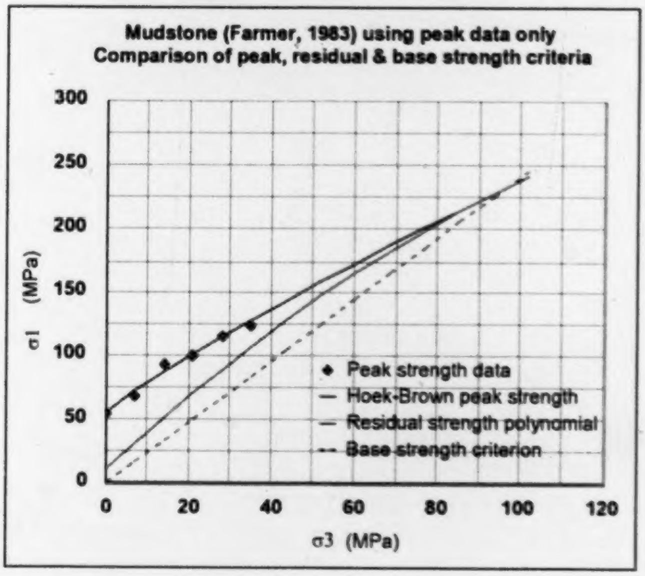

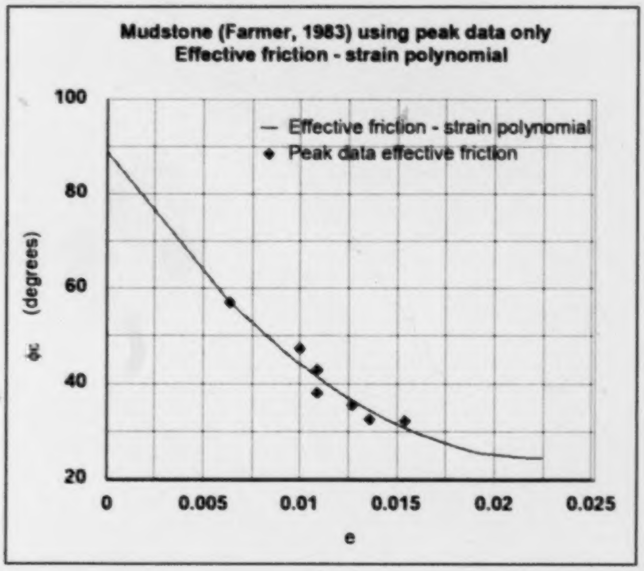

Mudstone (Farmer, 1983) using peak data only
Effective friction - strain polynomial

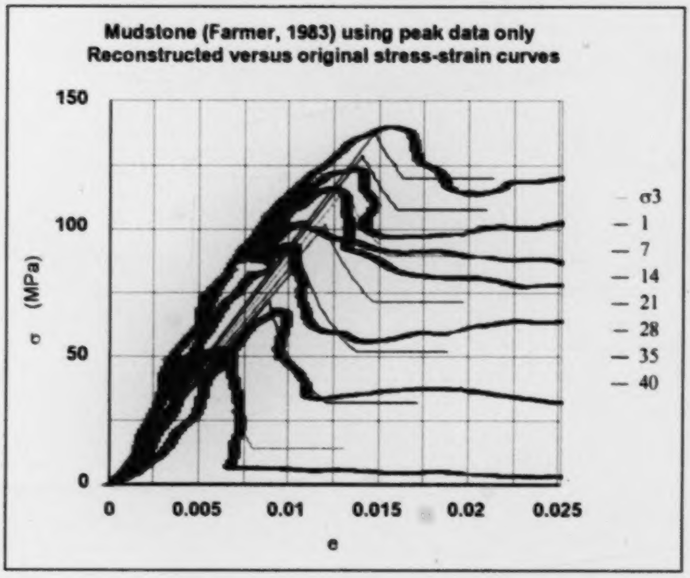

Mudstone (Farmer, 1983) using peak data only
Reconstructed versus original stress-strain curves

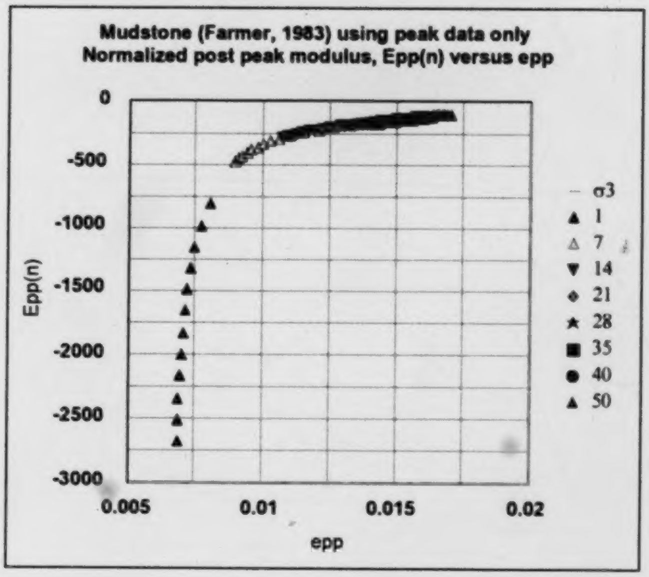

Mudstone (Farmer, 1983) using peak data only
Normalized post peak modulus, Epp(n) versus epp

Criterion	Parameters			
Hoek-Brown peak strength	m	σ_c (MPa)	s	a
$\sigma_{1p} = \sigma_3 + \sigma_c\{m\sigma_3/\sigma_c + s\}^a$	2.9	56	1	0.5
Residual strength	D	F	σ_{cr} (MPa)	
$\sigma_{1r} = D\sigma_3^2 + F\sigma_3 + \sigma_{cr}$	-0.007	3.0	11	
Base strength & transition point	ϕ_b (deg.)	σ_{3t} (MPa)	σ_{1t} (MPa)	
$\sigma_{1b} = \{(1+\sin\phi_b)/(1-\sin\phi_b)\}\sigma_3$	24.5	97	234	
Friction-strain and base strain	R (deg.)	S	T	e_b
$\phi_c = R + Se_{pp} + Te_{pp}^2$	89	-5740	128000	0.022

Appendix J.4

Intact portland stone (Farmer, 1983) using peak data only

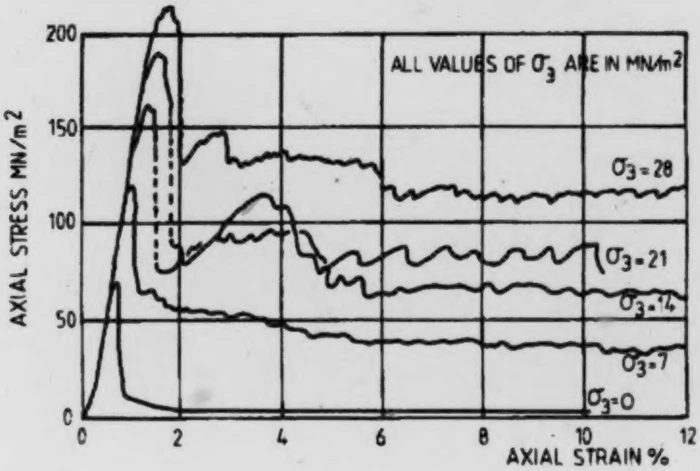

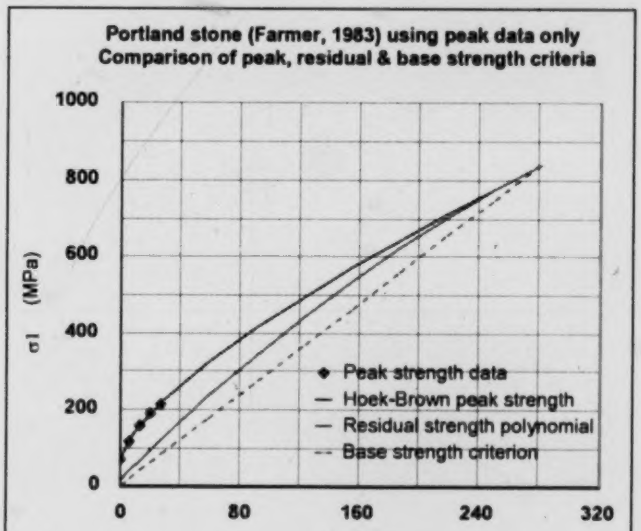

Portland stone (Farmer, 1983) using peak data only
Comparison of peak, residual & base strength criteria

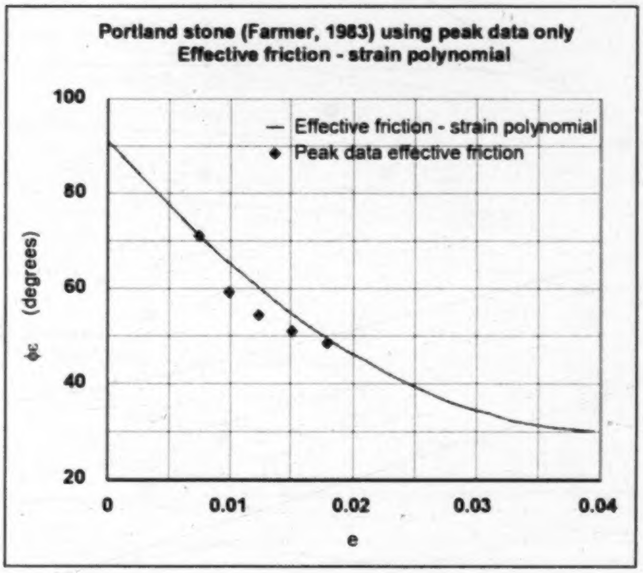

Portland stone (Farmer, 1983) using peak data only
Effective friction - strain polynomial

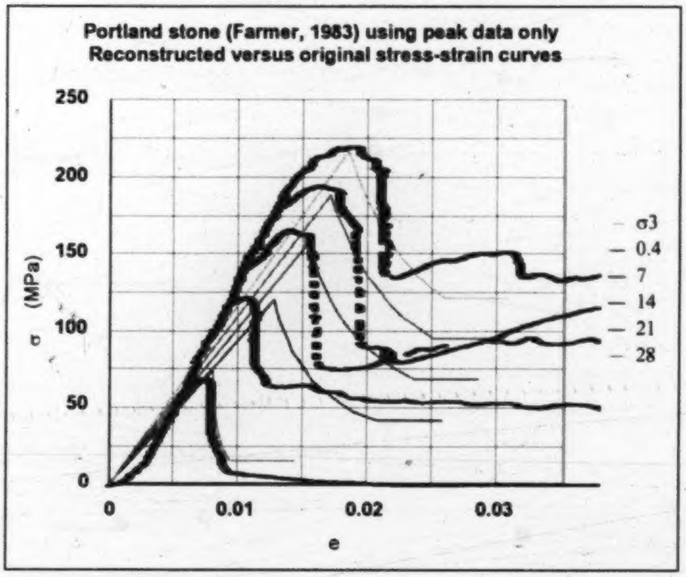

Portland stone (Farmer, 1983) using peak data only
Reconstructed versus original stress-strain curves

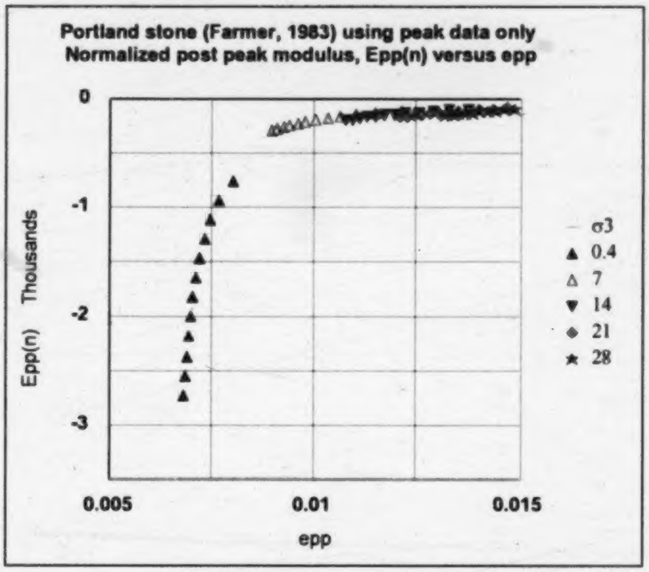

Criterion	Parameters			
Hoek-Brown peak strength	m	σ_c (MPa)	s	a
$\sigma_{1p} = \sigma_3 + \sigma_c\{m\sigma_3/\sigma_c + s\}^a$	15.3	71.5	1	0.5
Residual strength	D	F	σ_{cr} (MPa)	
$\sigma_{1r} = D\sigma_3^2 + F\sigma_3 + \sigma_{cr}$	-0.003	3.9	14	
Base strength & transition point	ϕ_b (deg.)	σ_{3t} (MPa)	σ_{1t} (MPa)	
$\sigma_{1b} = \{(1+\sin\phi_b)/(1-\sin\phi_b)\}\sigma_3$	30	277	831	
Friction-strain and base strain	R (deg.)	S	T	e_b
$\phi_e = R + Se_{pp} + Te_{pp}^2$	91	-2970	35800	0.04

Appendix J.5

Intact saccharoidal limestone (Farmer, 1983) using peak data only

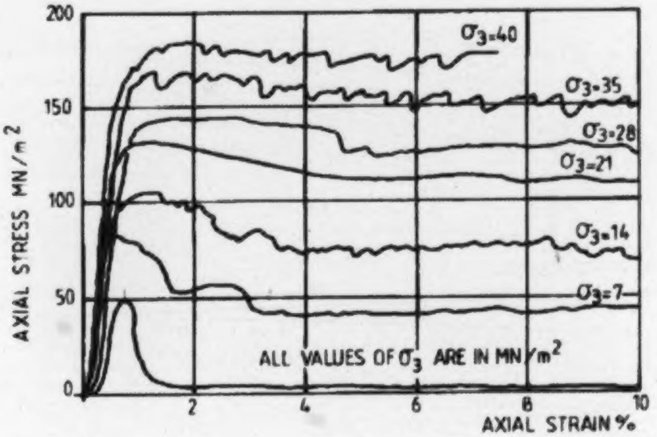

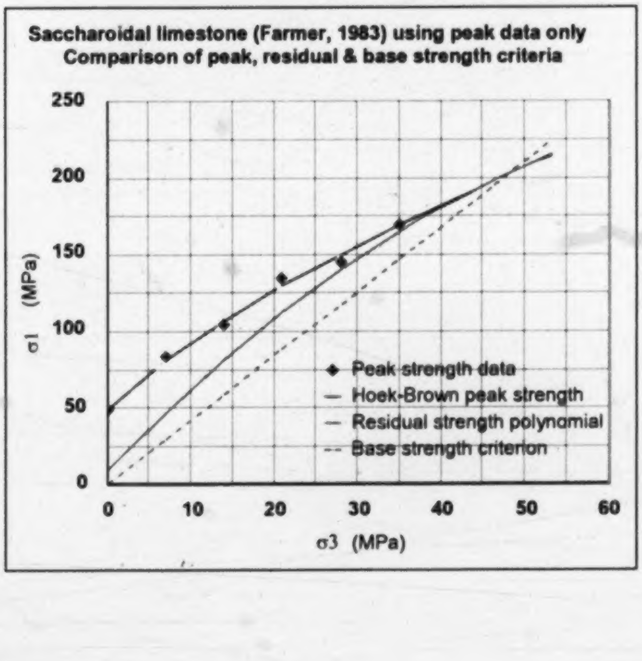
Saccharoidal limestone (Farmer, 1983) using peak data only
Comparison of peak, residual & base strength criteria

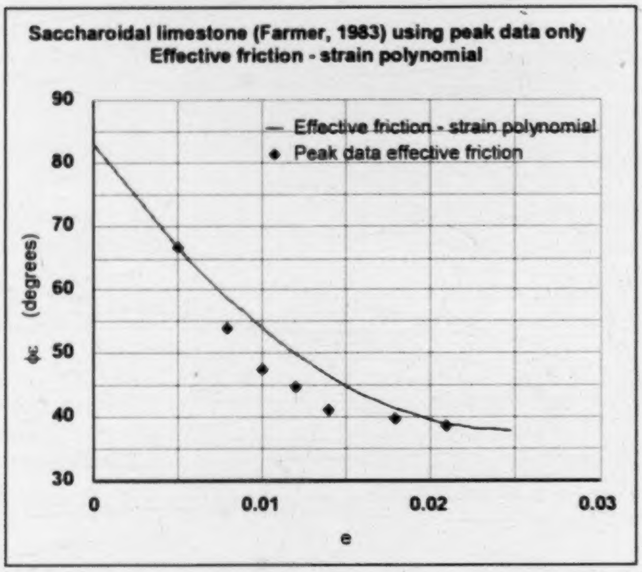
Saccharoidal limestone (Farmer, 1983) using peak data only
Effective friction - strain polynomial
90
80
70
60
50
40
30
ϕc (degrees)
— Effective friction - strain polynomial
◆ Peak data effective friction
0
0.01
0.02
0.03
e

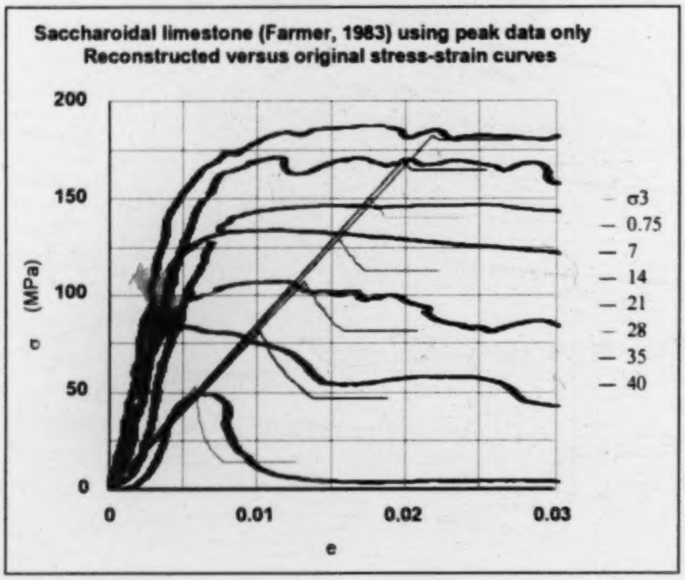
Saccharoidal limestone (Farmer, 1983) using peak data only
Reconstructed versus original stress-strain curves
200
150
100
50
0
σ (MPa)
0
0.01
0.02
0.03
e
σ3
0.75
7
14
21
28
35
40

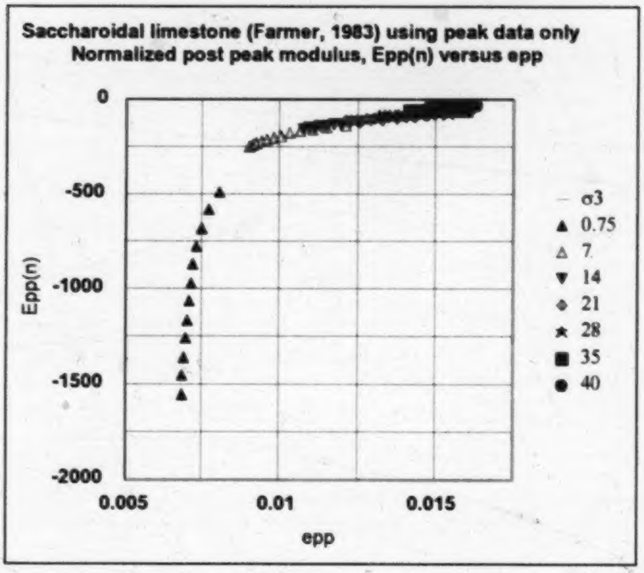

Criterion	Parameters			
Hoek-Brown peak strength	m	σ_c (MPa)	s	a
$\sigma_{1p} = \sigma_3 + \sigma_c\{m\sigma_3/\sigma_c + s\}^a$	9.0	50	1	0.5
Residual strength	D	F	σ_{cr} (MPa)	
$\sigma_{1r} = D\sigma_3^2 + F\sigma_3 + \sigma_{cr}$	-0.03	5.6	10	
Base strength & transition point	ϕ_b (deg.)	σ_{3t} (MPa)	σ_{1t} (MPa)	
$\sigma_{1b} = \{(1+\sin\phi_b)/(1-\sin\phi_b)\}\sigma_3$	38	48	204	
Friction-strain and base strain	R (deg.)	S	T	e_b
$\phi_c = R + Se_{pp} + Te_{pp}^2$	83	-3640	73300	0.025

Appendix J.6

Intact sandstone (Farmer, 1983) using peak data only

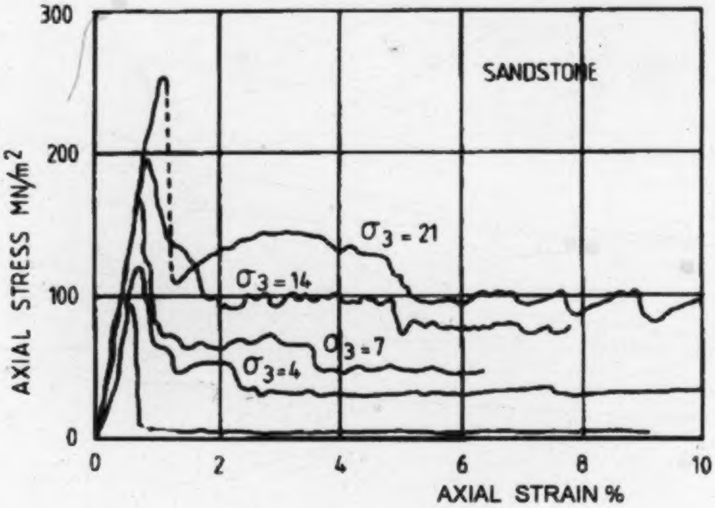

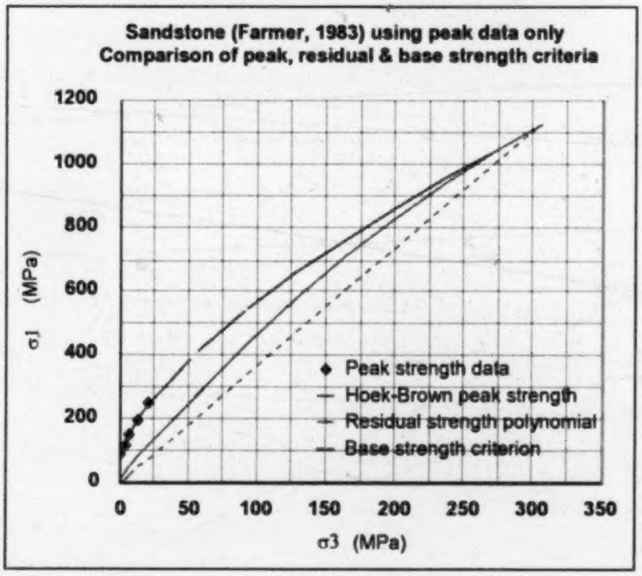

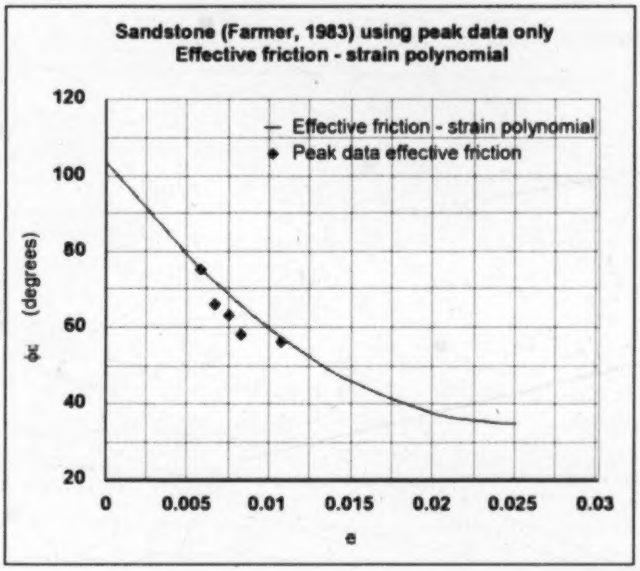
Sandstone (Farmer, 1983) using peak data only
Effective friction - strain polynomial

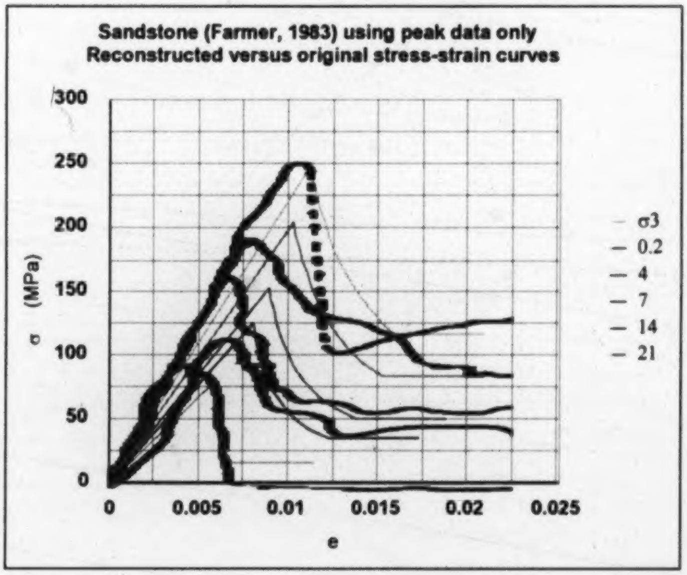
Sandstone (Farmer, 1983) using peak data only
Reconstructed versus original stress-strain curves

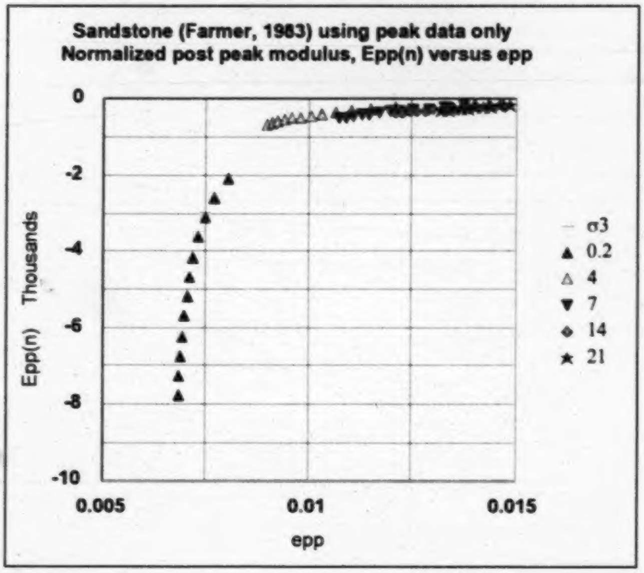

Criterion	Parameters			
Hoek-Brown peak strength	m	σ_c (MPa)	s	a
$\sigma_{1p} = \sigma_3 + \sigma_c\{m\sigma_3/\sigma_c + s\}^a$	27.7	78	1	0.5
Residual strength	D	F	σ_{cr} (MPa)	
$\sigma_{1r} = D\sigma_3^2 + F\sigma_3 + \sigma_{cr}$	-0.004	4.9	16	
Base strength & transition point	ϕ_b (deg.)	σ_{3t} (MPa)	σ_{1t} (MPa)	
$\sigma_{1b} = \{(1+\sin\phi_b)/(1-\sin\phi_b)\}\sigma_3$	35	303	1120	
Friction-strain and base strain	R (deg.)	S	T	e_b
$\phi_e = R + Se_{pp} + Te_{pp}^2$	103	-5450	109000	0.025

Appendix J.7

Intact silty sandstone (Farmer, 1983) using peak data only

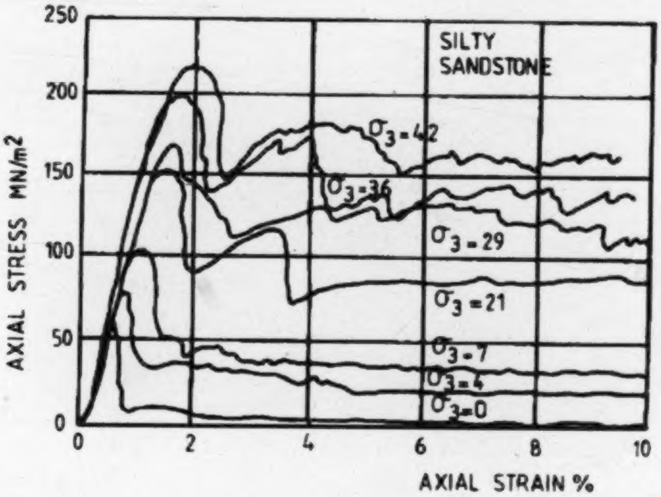

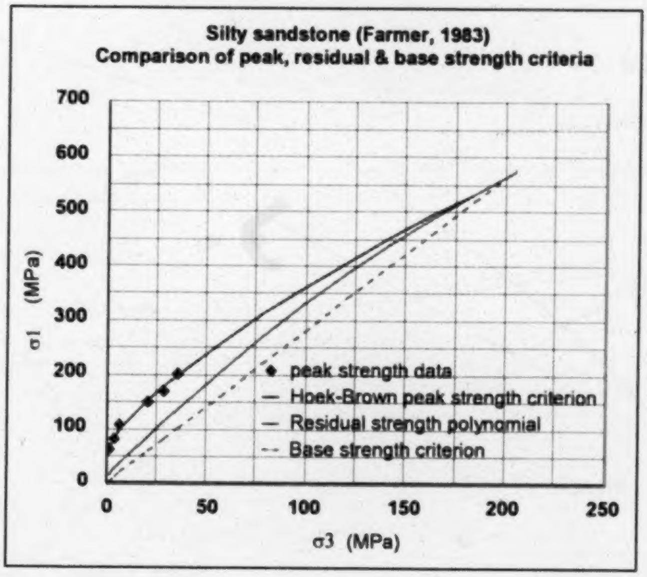

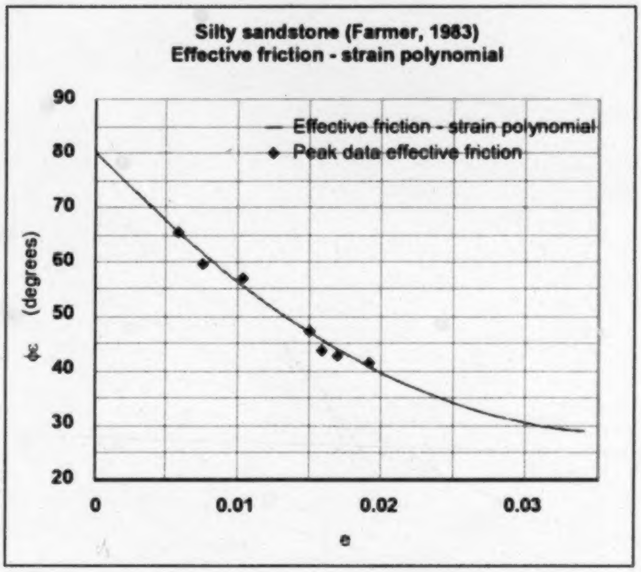

Silty sandstone (Farmer, 1983)
Effective friction - strain polynomial

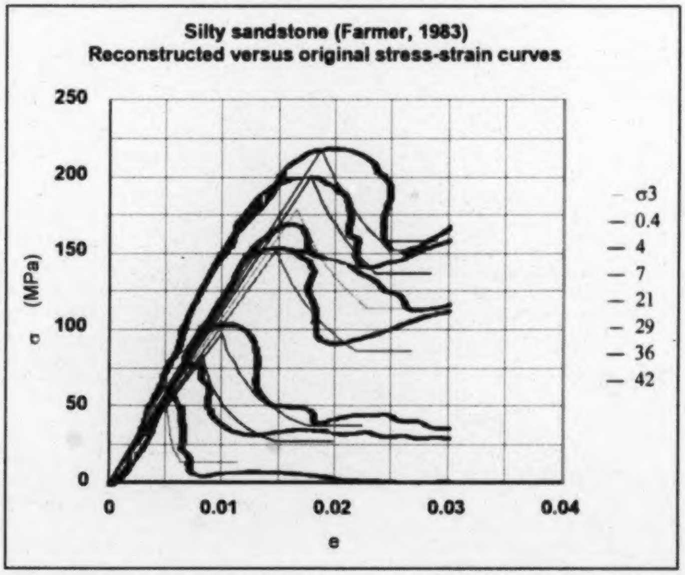

Silty sandstone (Farmer, 1983)
Reconstructed versus original stress-strain curves

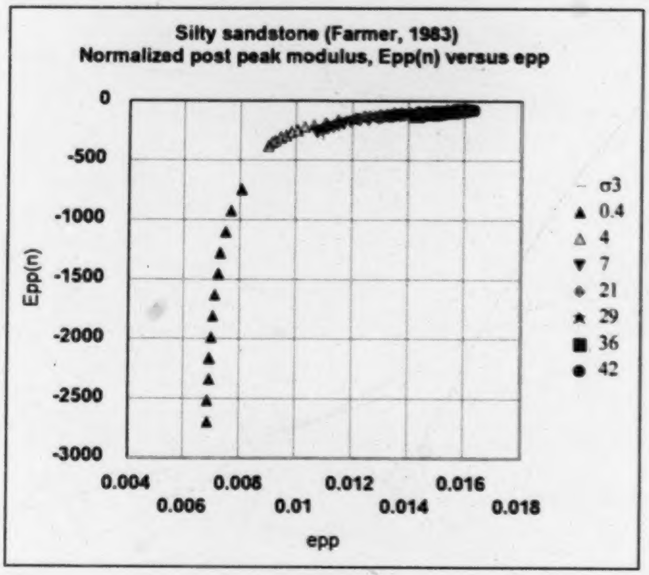

Criterion	Parameters			
Hoek-Brown peak strength	m	σ_c (MPa)	s	a
$\sigma_{1p} = \sigma_3 + \sigma_c\{m\sigma_3/\sigma_c + s\}^a$	10.6	61	1	0.5
Residual strength	D	F	σ_{cr} (MPa)	
$\sigma_{1r} = D\sigma_3^2 + F\sigma_3 + \sigma_{cr}$	-0.004	3.6	12	
Base strength & transition point	ϕ_b (deg.)	σ_{3t} (MPa)	σ_{1t} (MPa)	
$\sigma_{1b} = \{(1+\sin\phi_b)/(1-\sin\phi_b)\}\sigma_3$	28.5	200	565	
Friction-strain and base strain	R (deg.)	S	T	e_b
$\phi_c = R + Se_{pp} + Te_{pp}^2$	80	-2770	37100	0.04

Appendix J.8

Intact quartzite (Gates, 1988) using peak data only

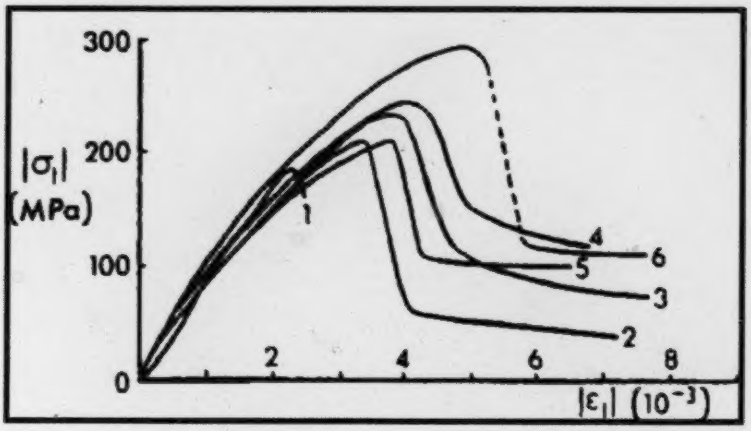

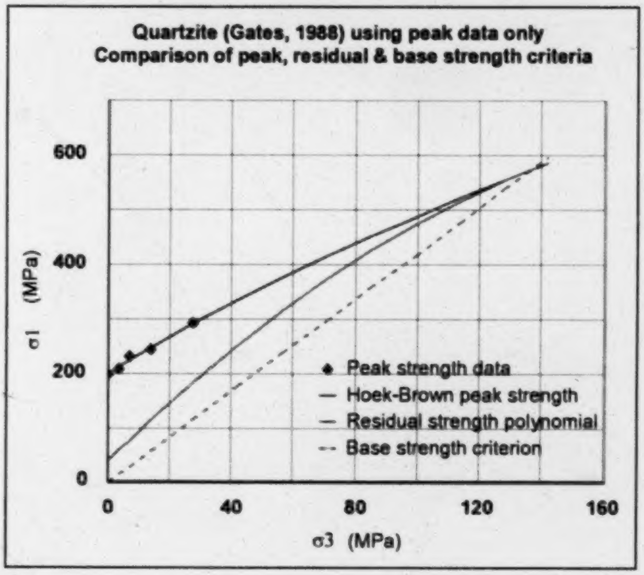

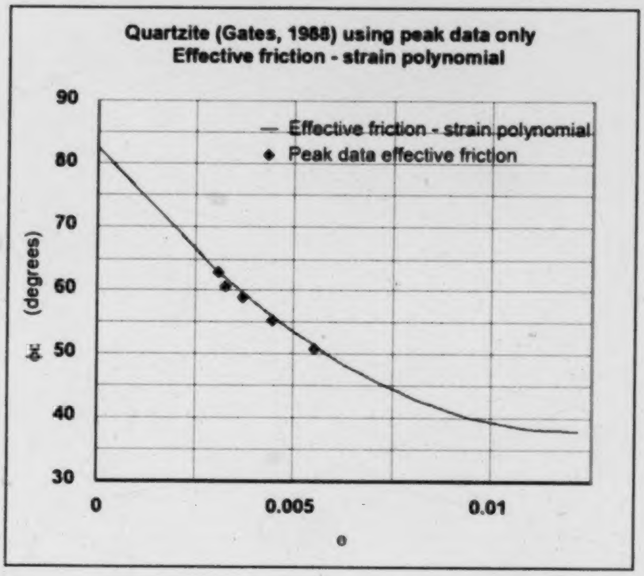
Quartzite (Gates, 1988) using peak data only
Effective friction - strain polynomial
Effective friction - strain polynomial
Peak data effective friction
90
80
70
60
50
40
30
φc (degrees)
0
0.005
0.01
e

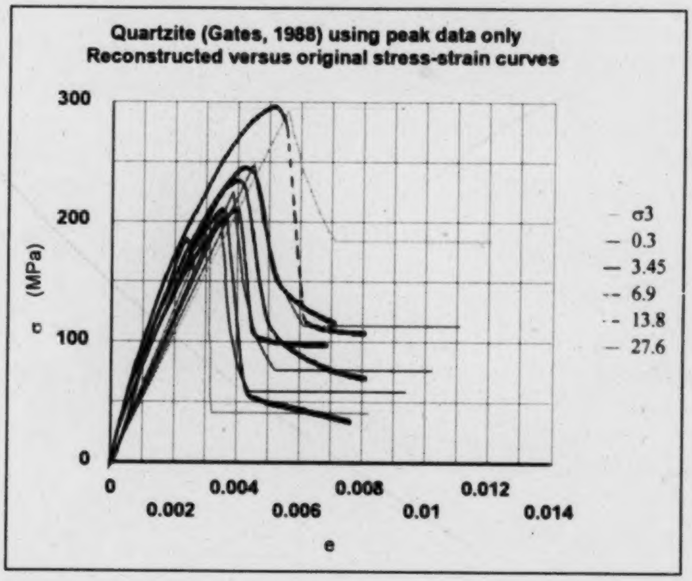
Quartzite (Gates, 1988) using peak data only
Reconstructed versus original stress-strain curves
300
200
100
0
σ (MPa)
0
0.002
0.004
0.006
0.008
0.01
0.012
0.014
e
σ3
0.3
3.45
6.9
13.8
27.6

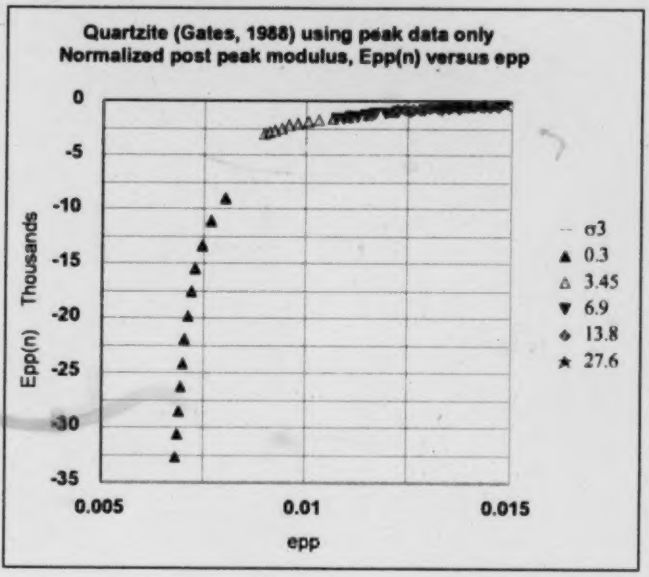

Criterion	Parameters			
Hoek-Brown peak strength	m	σ_c (MPa)	s	a
$\sigma_{1p} = \sigma_3 + \sigma_c\{m\sigma_3/\sigma_c + s\}^a$	5.6	200	1	0.5
Residual strength	D	F	σ_{cr} (MPa)	
$\sigma_{1r} = D\sigma_3^2 + F\sigma_3 + \sigma_{cr}$	-0.01	5.6	40	
Base strength & transition point	ϕ_b (deg.)	σ_{3t} (MPa)	σ_{1t} (MPa)	
$\sigma_{1b} = \{(1+\sin\phi_b)/(1-\sin\phi_b)\}\sigma_3$	38	137	578	
Friction-strain and base strain	R (deg.)	S	T	e_b
$\phi_c = R + Se_{pp} + Te_{pp}^2$	83	-7330	300600	0.012

Appendix J.9

Intact Lac du Bonnet pink granite (Gorski et al., 1991) using peak data only

σ_3 data (MPa)	σ_{1p} data (MPa)	σ_{1r} data (MPa)	e_p data (strain)	e_r data (strain)
0.01	186	46	0.003	0.003
2	216	39	0.004	0.006
4	257	69	0.004	0.007
6	285	90	0.005	0.008
10	328	102	0.005	0.007
15	393	105	0.006	0.009
20	443	158	0.007	0.010
30	520	291	0.008	0.009
40	586	179	0.009	0.014
60	700	377	0.011	0.011

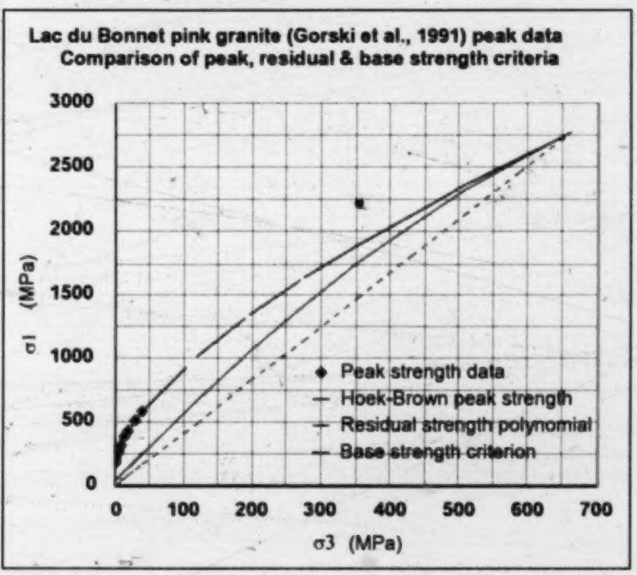

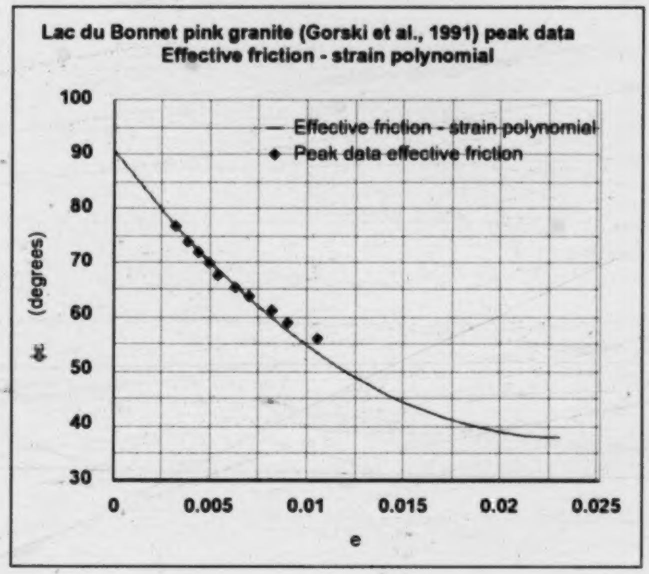
Lac du Bonnet pink granite (Gorski et al., 1991) peak data
Effective friction - strain polynomial
Effective friction - strain polynomial
Peak data effective friction
φ (degrees)
100
90
80
70
60
50
40
30
0
0.005
0.01
0.015
0.02
0.025
e

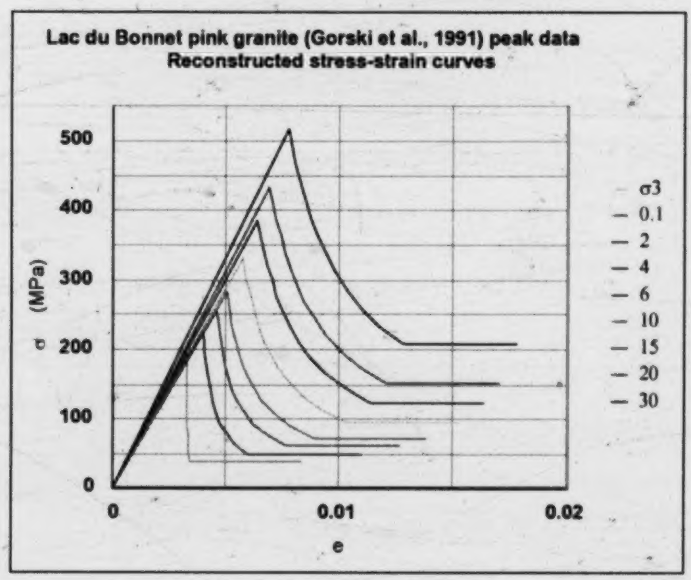
Lac du Bonnet pink granite (Gorski et al., 1991) peak data
Reconstructed stress-strain curves
σ (MPa)
500
400
300
200
100
0
0
0.01
0.02
e
σ3
0.1
2
4
6
10
15
20
30

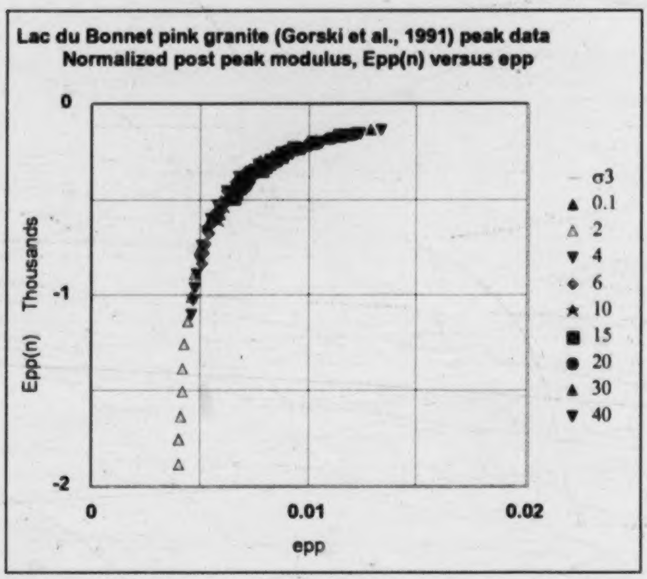

Criterion	Parameters			
Hoek-Brown peak strength	m	σ_c (MPa)	s	a
$\sigma_{1p} = \sigma_3 + \sigma_c\{m\sigma_3/\sigma_c + s\}^a$	34.9	192	1	0.5
Residual strength	D	F	σ_{cr} (MPa)	
$\sigma_{1r} = D\sigma_3^2 + F\sigma_3 + \sigma_{cr}$	-0.002	5.7	38	
Base strength & transition point	ϕ_b (deg.)	σ_{3t} (MPa)	σ_{1t} (MPa)	
$\sigma_{1b} = \{(1+\sin\phi_b)/(1-\sin\phi_b)\}\sigma_3$	38	658	2770	
Friction-strain and base strain	R (deg.)	S	T	e_b
$\phi_e = R + Se_{pp} + Te_{pp}^2$	91	-4560	98700	0.023

Appendix J.10

Intact Doddington sandstone (Santarelli et al., 1989) using peak data only

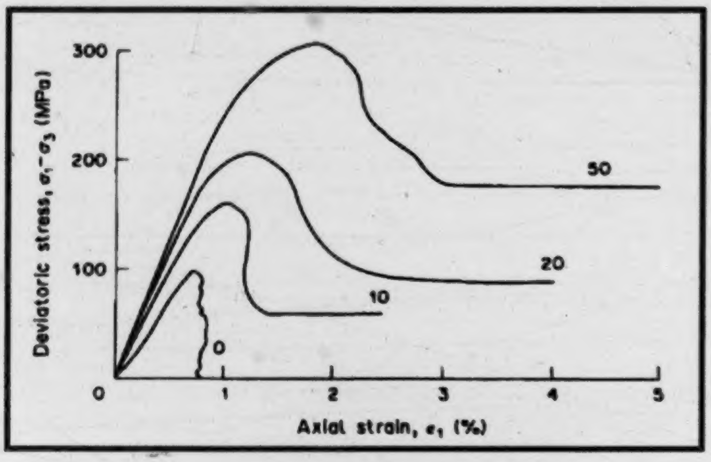

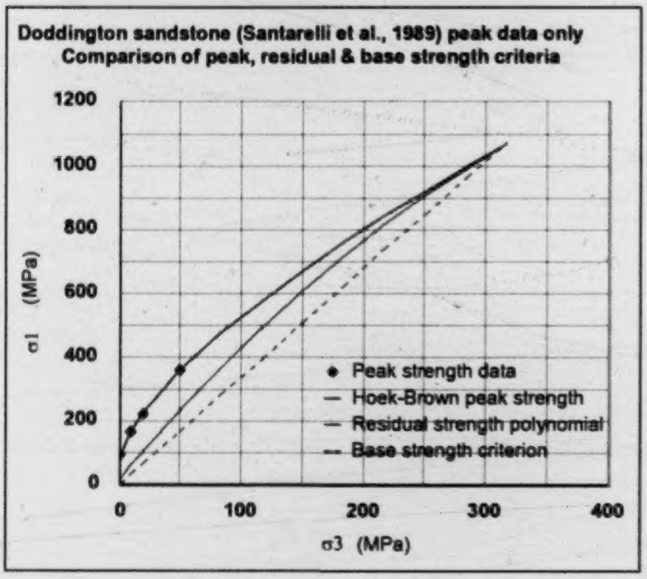
Doddington sandstone (Santarelli et al., 1989) peak data only
Comparison of peak, residual & base strength criteria

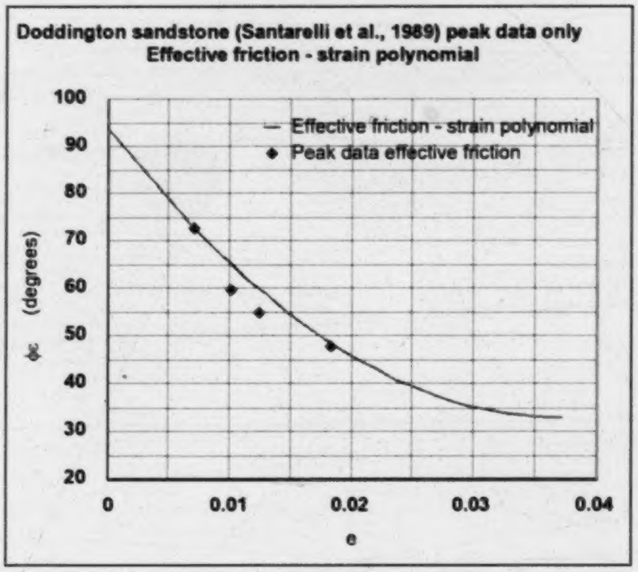

Doddington sandstone (Santarelli et al., 1989) peak data only
Effective friction - strain polynomial

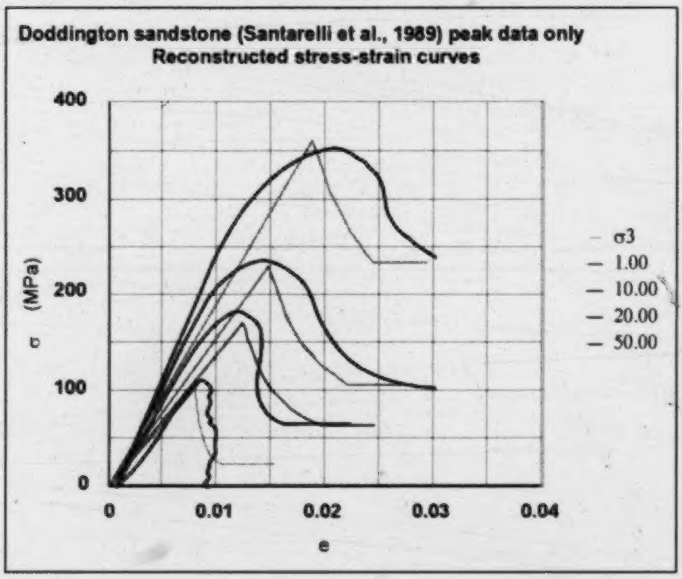

Doddington sandstone (Santarelli et al., 1989) peak data only
Reconstructed stress-strain curves

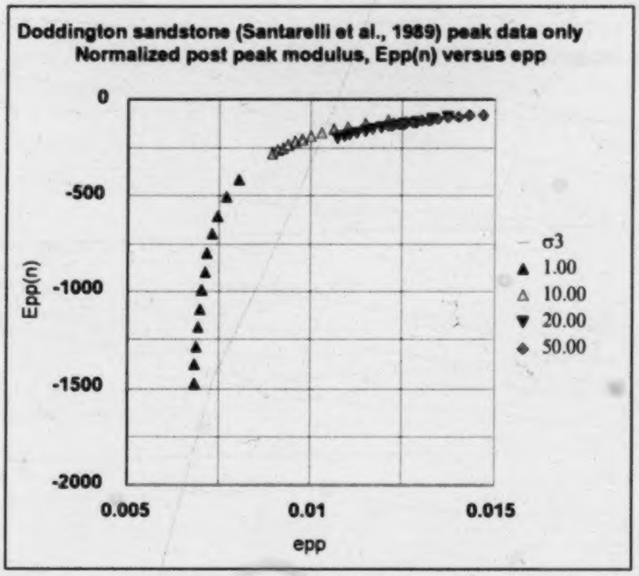

Criterion	Parameters			
Hoek-Brown peak strength	m	σ_c (MPa)	s	a
$\sigma_{1p} = \sigma_3 + \sigma_c\{m\sigma_3/\sigma_c + s\}^a$	19.2	92	1	0.5
Residual strength	D	F	σ_{cr} (MPa)	
$\sigma_{1r} = D\sigma_3^2 + F\sigma_3 + \sigma_{cr}$	-0.004	4.5	18	
Base strength & transition point	ϕ_b (deg.)	σ_{3t} (MPa)	σ_{1t} (MPa)	
$\sigma_{1b} = \{(1+\sin\phi_b)/(1-\sin\phi_b)\}\sigma_3$	33	312	1060	
Friction-strain and base strain	R (deg.)	S	T	e_b
$\phi_e = R + Se_{pp} + Te_{pp}^2$	94	-3260	43700	0.04

Appendix J.11

Intact Gebdykes dolomite (Santarelli et al., 1989) using peak data only

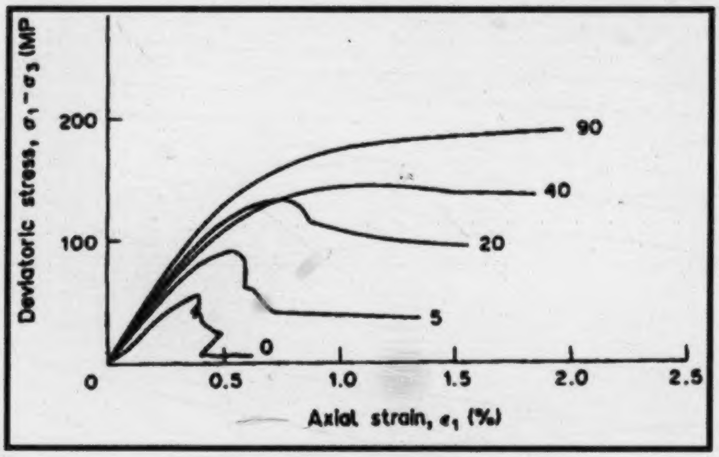

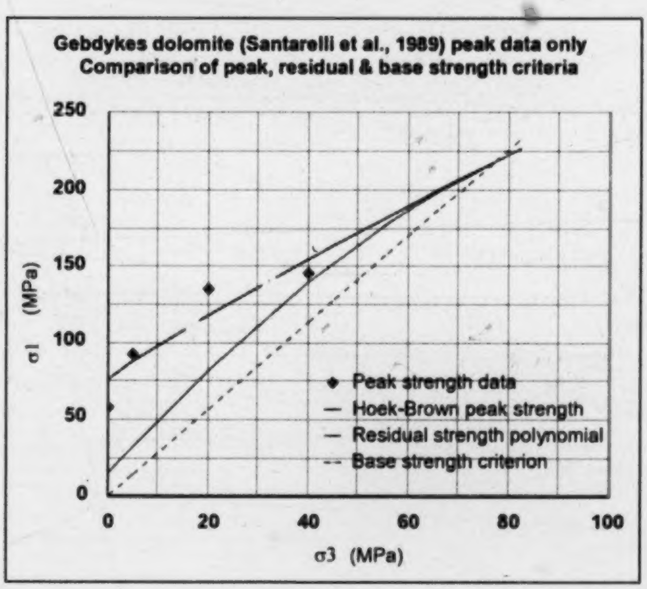

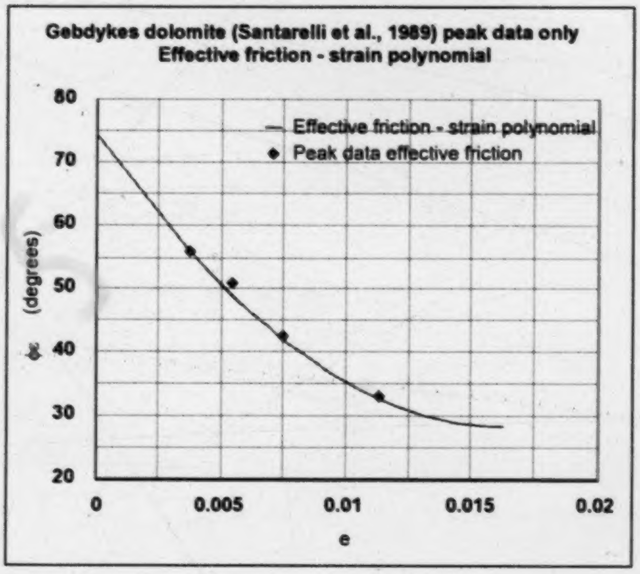
Gebdykes dolomite (Santarelli et al., 1989) peak data only
Effective friction - strain polynomial

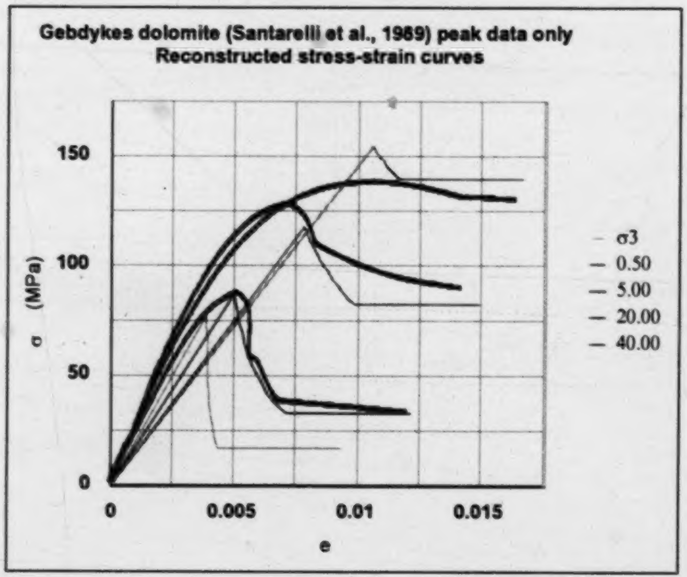
Gebdykes dolomite (Santarelli et al., 1989) peak data only
Reconstructed stress-strain curves

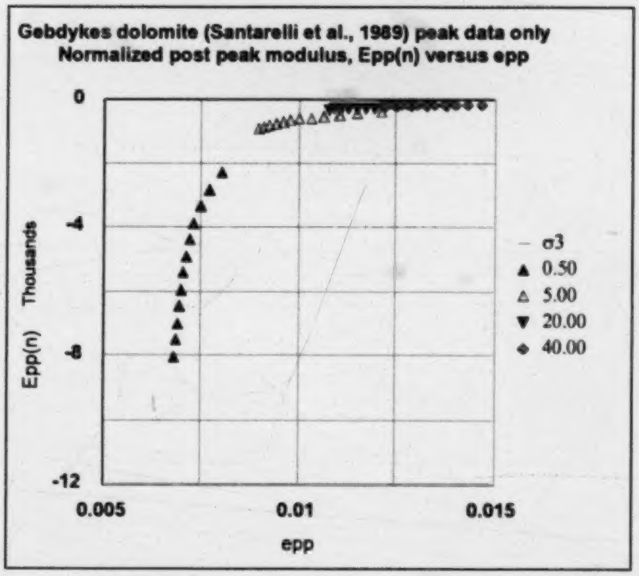

Criterion	Parameters			
Hoek-Brown peak strength	m	σ_c (MPa)	s	a
$\sigma_{1p} = \sigma_3 + \sigma_c\{m\sigma_3/\sigma_c + s\}^a$	2.4	77	1	0.5
Residual strength	D	F	σ_{cr} (MPa)	
$\sigma_{1r} = D\sigma_3^2 + F\sigma_3 + \sigma_{cr}$	-0.01	3.6	15	
Base strength & transition point	ϕ_b (deg.)	σ_{3t} (MPa)	σ_{1t} (MPa)	
$\sigma_{1b} = \{(1+\sin\phi_b)/(1-\sin\phi_b)\}\sigma_3$	28.5	78	219	
Friction-strain and base strain	R (deg.)	S	T	e_b
$\phi_e = R + Se_{pp} + Te_{pp}^2$	75	-5660	174000	0.02

Appendix J.12

Intact mudstone (Tao, 1991) using peak data only

123 peak strength and strain data points recorded by Tao.

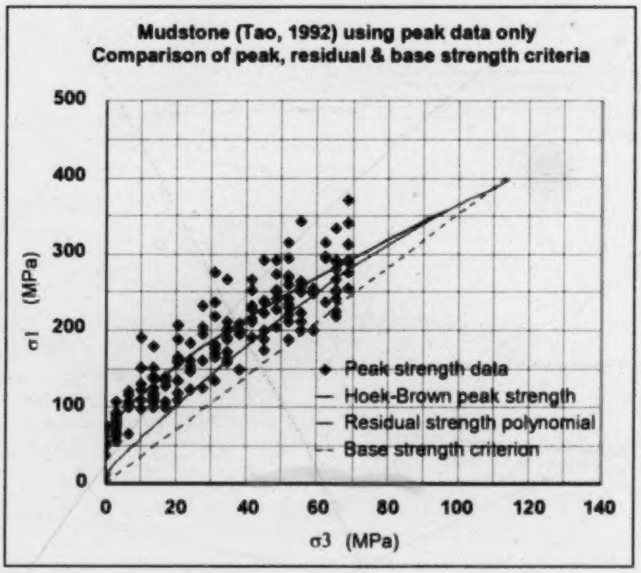

8

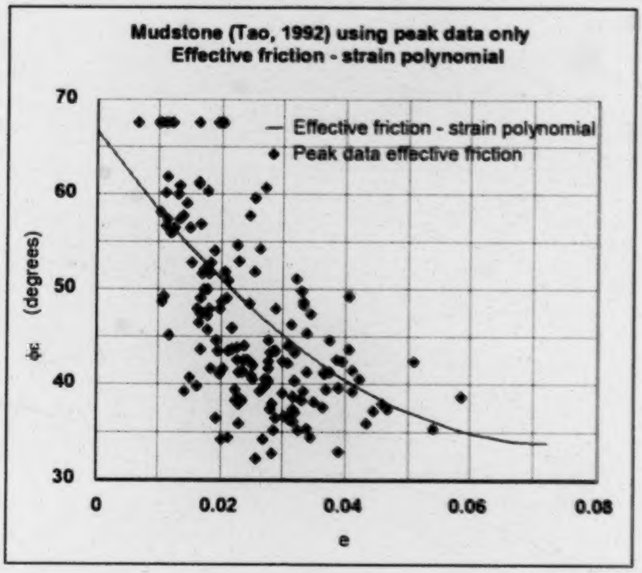
Mudstone (Tao, 1992) using peak data only
Effective friction - strain polynomial
Effective friction - strain polynomial
Peak data effective friction
φc (degrees)
70
60
50
40
30
0
0.02
0.04
0.06
0.08
e

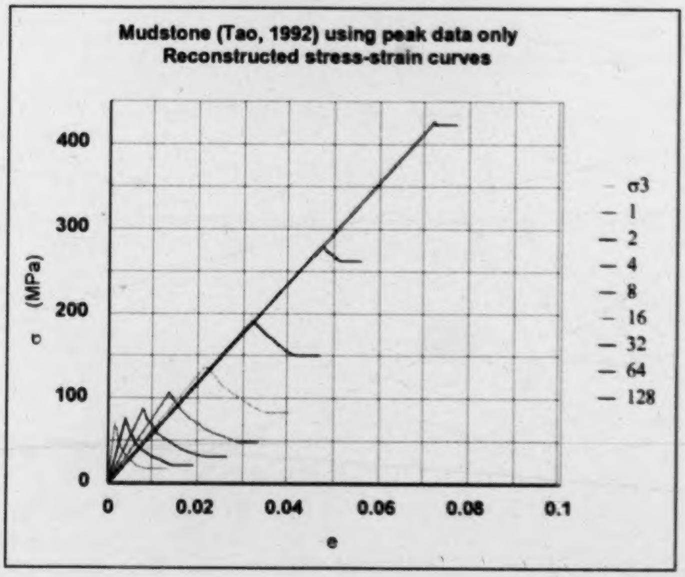
Mudstone (Tao, 1992) using peak data only
Reconstructed stress-strain curves
σ (MPa)
400
300
200
100
0
0
0.02
0.04
0.06
0.08
0.1
e
σ3
1
2
4
8
16
32
64
128

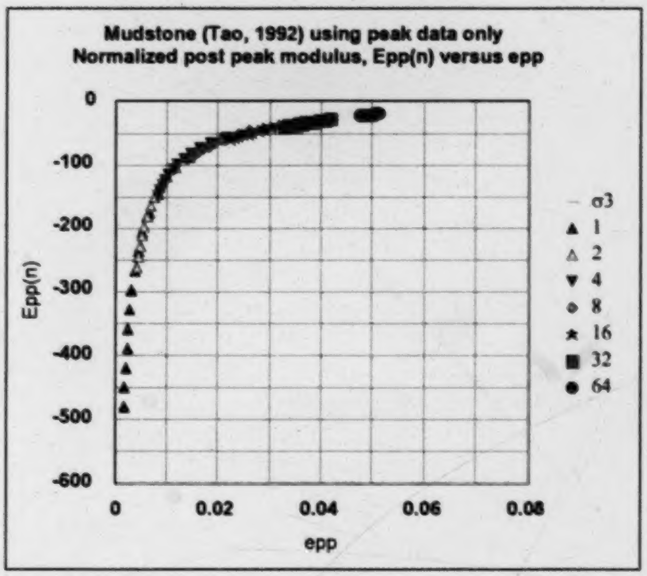

Criterion	Parameters			
Hoek-Brown peak strength	m	σ_c (MPa)	s	a
$\sigma_{1p} = \sigma_3 + \sigma_c\{m\sigma_3/\sigma_c + s\}^a$	9.9	67	1	0.5
Residual strength	D	F	σ_{cr} (MPa)	
$\sigma_{1r} = D\sigma_3^2 + F\sigma_3 + \sigma_{cr}$	-0.01	4.6	13	
Base strength & transition point	ϕ_b (deg.)	σ_{3t} (MPa)	σ_{1t} (MPa)	
$\sigma_{1b} = \{(1+\sin\phi_b)/(1-\sin\phi_b)\}\sigma_3$	34	110	388	
Friction-strain and base strain	R (deg.)	S	T	e_b
$\phi_c = R + Se_{pp} + Te_{pp}^2$	67	-907	6270	0.07

Appendix K

Worked intact rock data sets where only peak data was available

Appendix K.1

Intact berea sandstone (Aldritch, 1969)

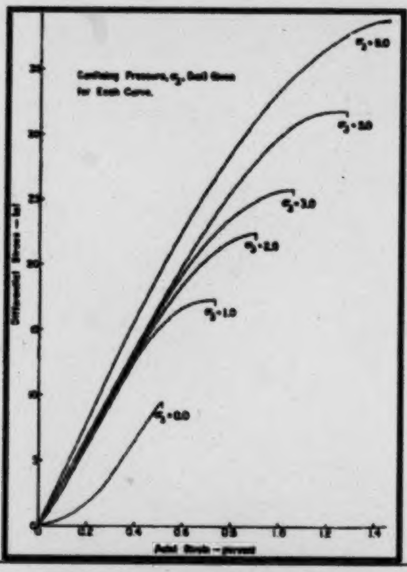

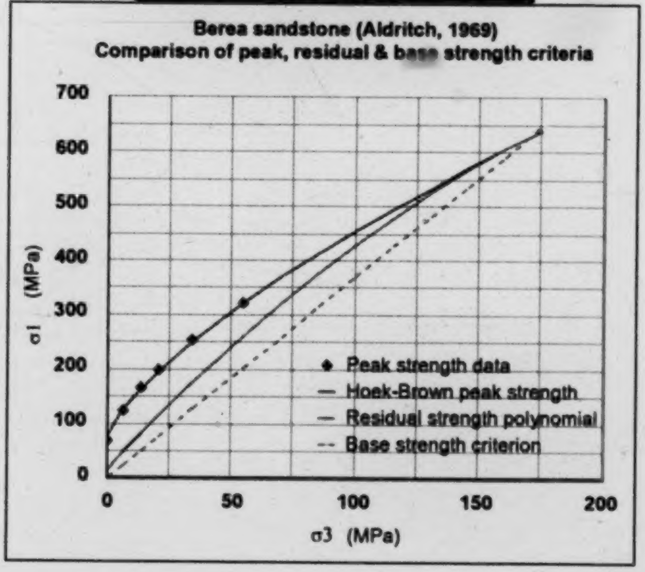

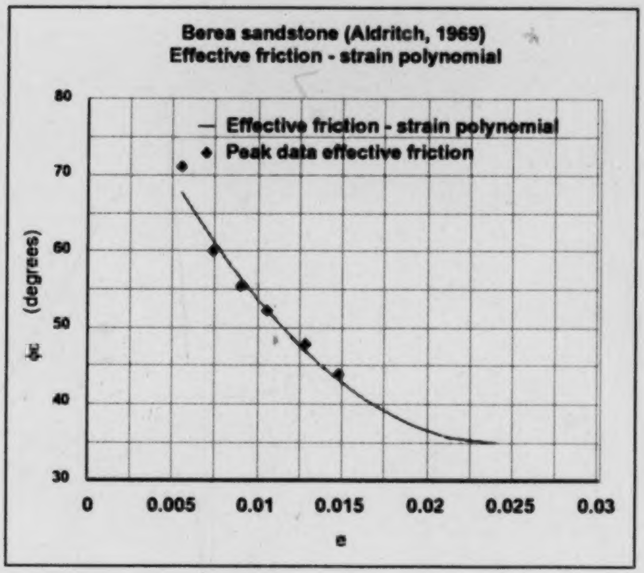
Berea sandstone (Aldritch, 1969)
Effective friction - strain polynomial

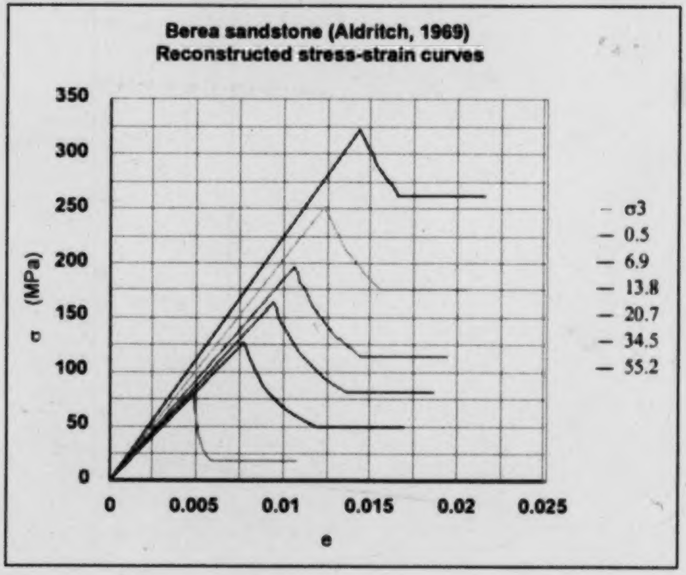
Berea sandstone (Aldritch, 1969)
Reconstructed stress-strain curves

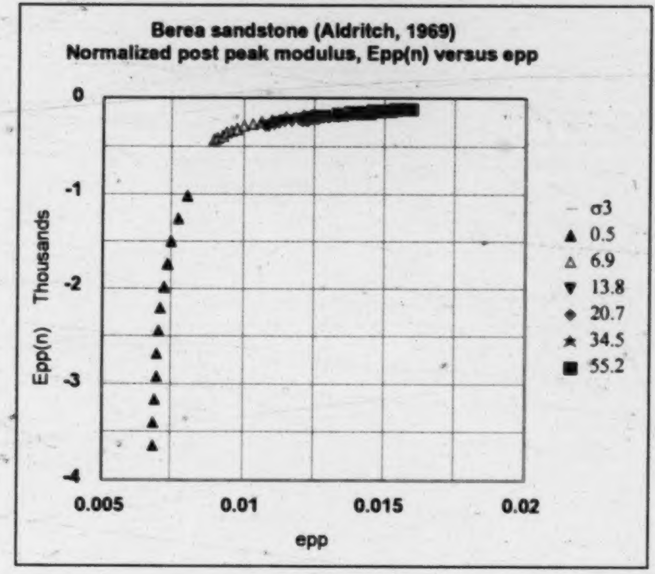

Criterion	Parameters			
Hoek-Brown peak strength	m	σ_c (MPa)	s	a
$\sigma_{1p} = \sigma_3 + \sigma_c\{m\sigma_3/\sigma_c + s\}^a$	15.4	78	1	0.5
Residual strength	D	F	σ_{cr} (MPa)	
$\sigma_{1r} = D\sigma_3^2 + F\sigma_3 + \sigma_{cr}$	-0.008	4.9	16	
Base strength & transition point	ϕ_b (deg.)	σ_{3t} (MPa)	σ_{1t} (MPa)	
$\sigma_{1b} = \{(1+\sin\phi_b)/(1-\sin\phi_b)\}\sigma_3$	35	171	630	
Friction-strain and base strain	R (deg.)	S	T	e_b
$\phi_e = R + Se_{pp} + Te_{pp}^2$	90	-4560	95000	0.024

Appendix K.2

Intact high strength concrete HS06 (Ansari et al., 1998)

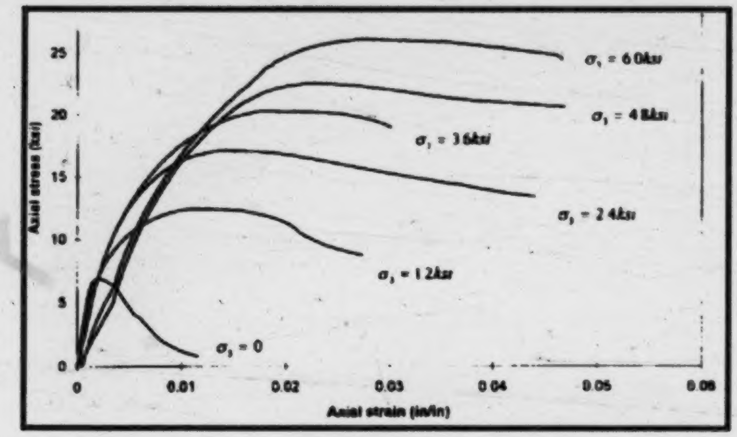

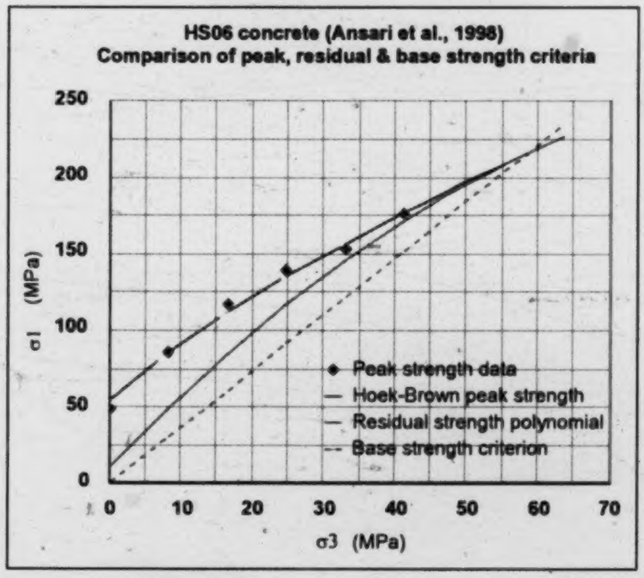

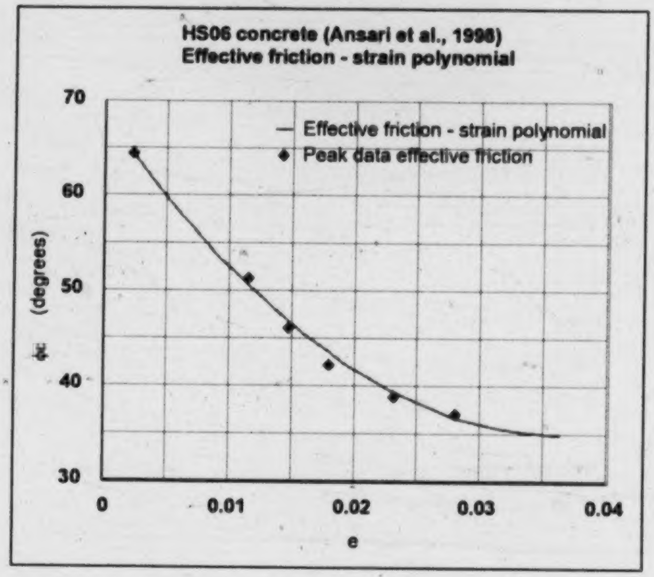
HS06 concrete (Ansari et al., 1998)
Effective friction - strain polynomial
70
60
50
40
30
φc (degrees)
0
0.01
0.02
0.03
0.04
e
Effective friction - strain polynomial
Peak data effective friction

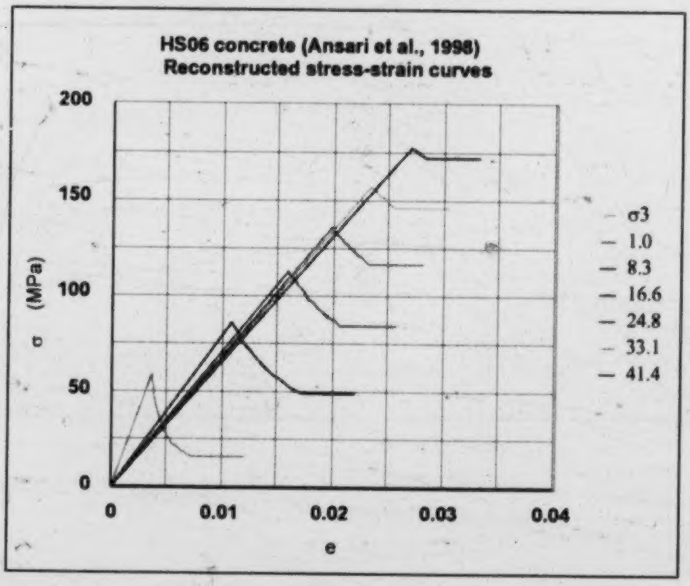
HS06 concrete (Ansari et al., 1998)
Reconstructed stress-strain curves
200
150
100
50
0
σ (MPa)
0
0.01
0.02
0.03
0.04
e
σ3
1.0
8.3
16.6
24.8
33.1
41.4

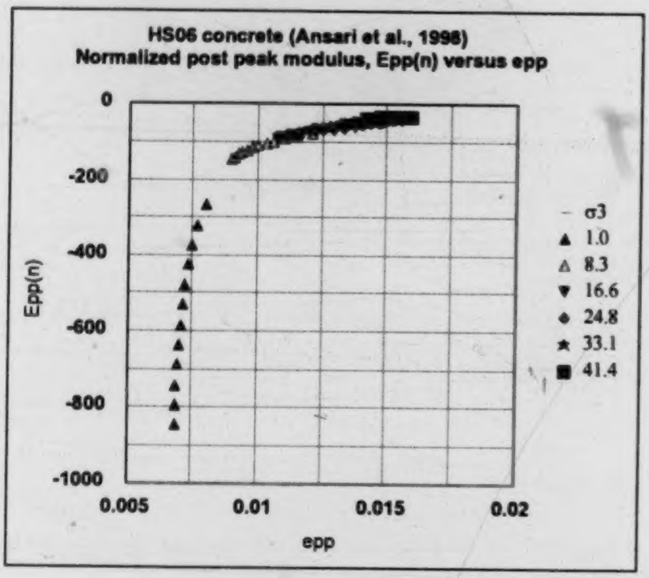

Criterion	Parameters			
Hoek-Brown peak strength	m	σ_c (MPa)	s	a
$\sigma_{1p} = \sigma_3 + \sigma_c\{m\sigma_3/\sigma_c + s\}^a$	6.8	55	1	0.5
Residual strength	D	F	σ_{cr} (MPa)	
$\sigma_{1r} = D\sigma_3^2 + F\sigma_3 + \sigma_{cr}$	-0.02	4.8	11	
Base strength & transition point	ϕ_b (deg.)	σ_{3t} (MPa)	σ_{1t} (MPa)	
$\sigma_{1b} = \{(1+\sin\phi_b)/(1-\sin\phi_b)\}\sigma_3$	35	59	217	
Friction-strain and base strain	R (deg.)	S	T	e_b
$\phi_e = R + Se_{pp} + Te_{pp}^2$	68	-1830	25100	0.04

Appendix K.3

Intact high strength concrete HS10 (Ansari et al., 1998)

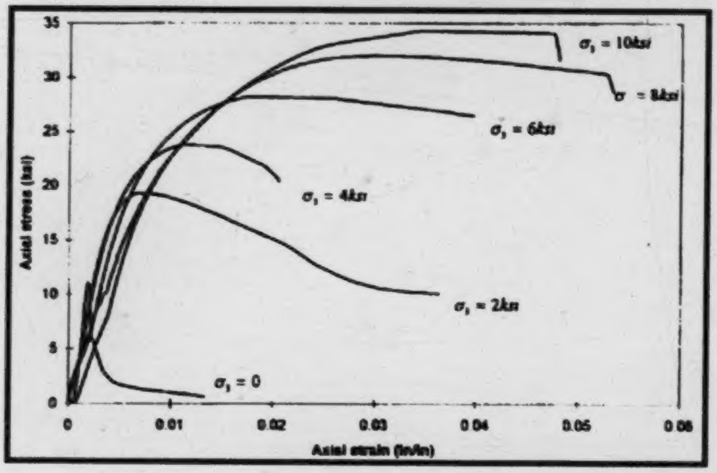

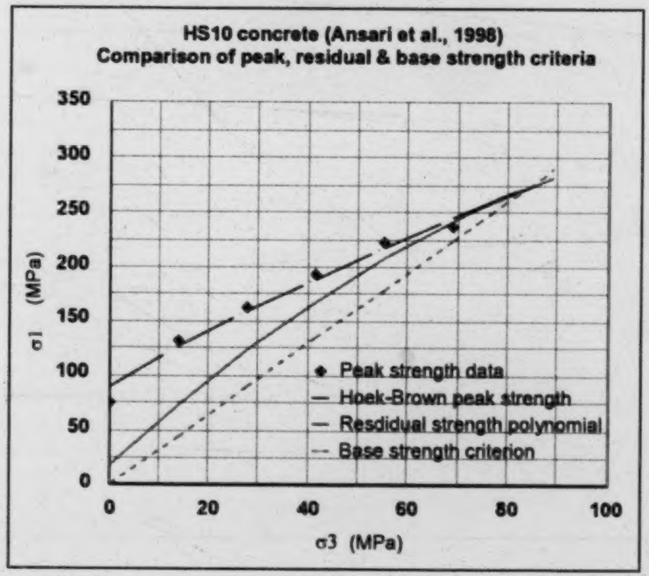

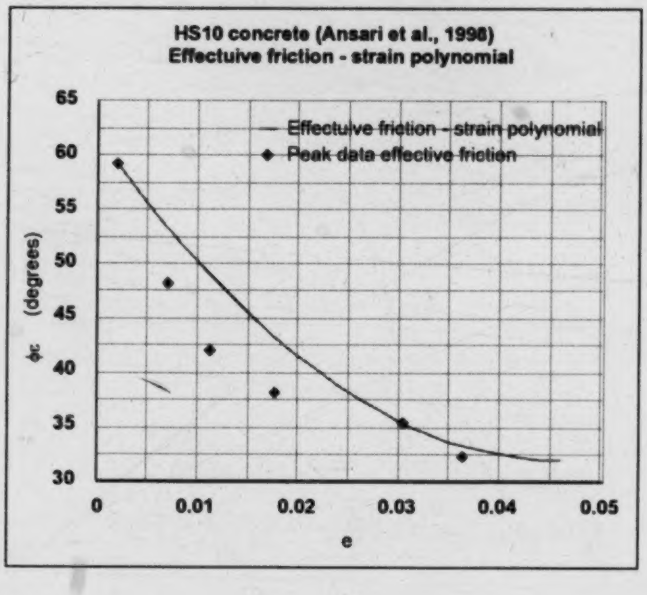

HS10 concrete (Ansari et al., 1998)
Effectuive friction - strain polynomial

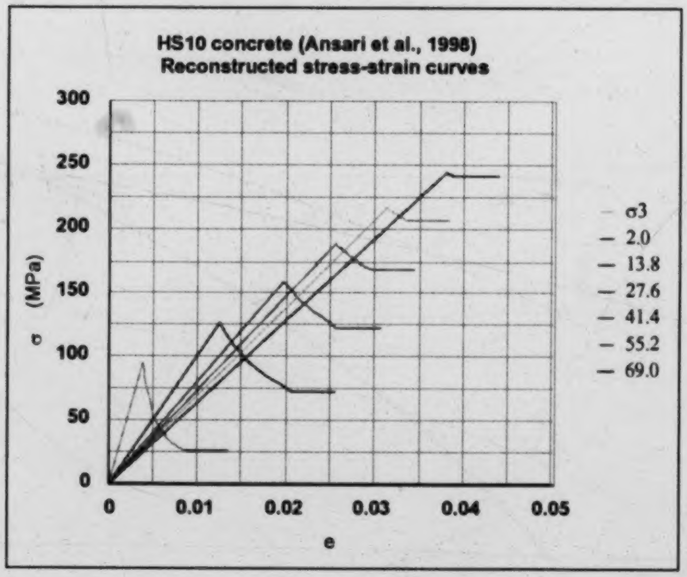

HS10 concrete (Ansari et al., 1998)
Reconstructed stress-strain curves

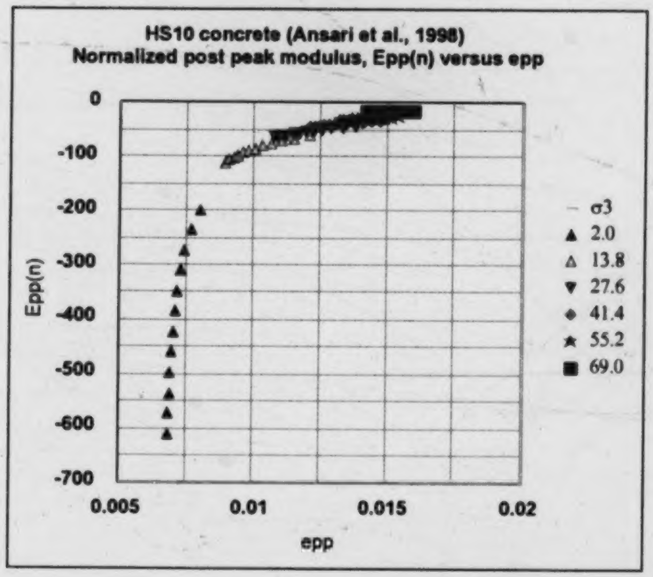

Criterion	Parameters			
Hoek-Brown peak strength	m	σ_c (MPa)	s	a
$\sigma_{1p} = \sigma_3 + \sigma_c\{m\sigma_3/\sigma_c + s\}^a$	3.7	90	1	0.5
Residual strength	D	F	σ_{cr} (MPa)	
$\sigma_{1r} = D\sigma_3^2 + F\sigma_3 + \sigma_{cr}$	-0.01	4.2	18	
Base strength & transition point	ϕ_b (deg.)	σ_{3t} (MPa)	σ_{1t} (MPa)	
$\sigma_{1b} = \{(1+\sin\phi_b)/(1-\sin\phi_b)\}\sigma_3$	32	84	274	
Friction-strain and base strain	R (deg.)	S	T	e_b
$\phi_e = R + Se_{pp} + Te_{pp}^2$	62	-1290	14100	0.05

Appendix K.4

Intact quartzite (Barron, 1970)

σ_3 data	σ_{1p} data	e_p data
(MPa)	(MPa)	(strain)
0	256	0.0028
6.9	344	0.0039
13.8	407	0.0049
20.7	441	0.0048
27.6	478	0.0056
34.5	530	0.0059

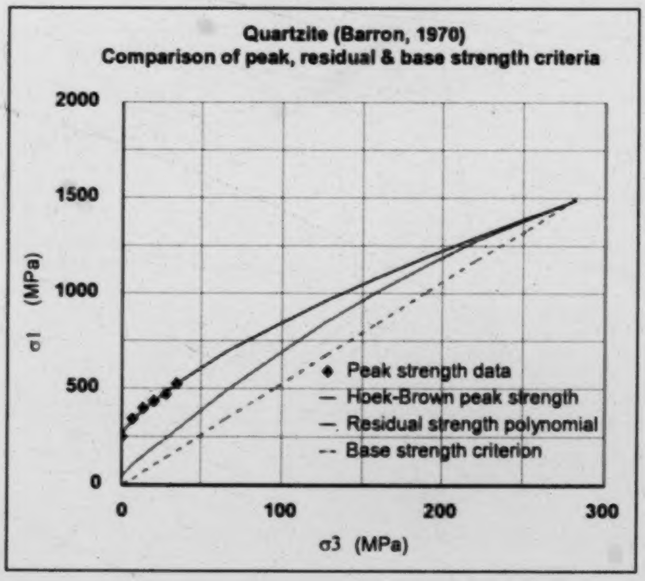

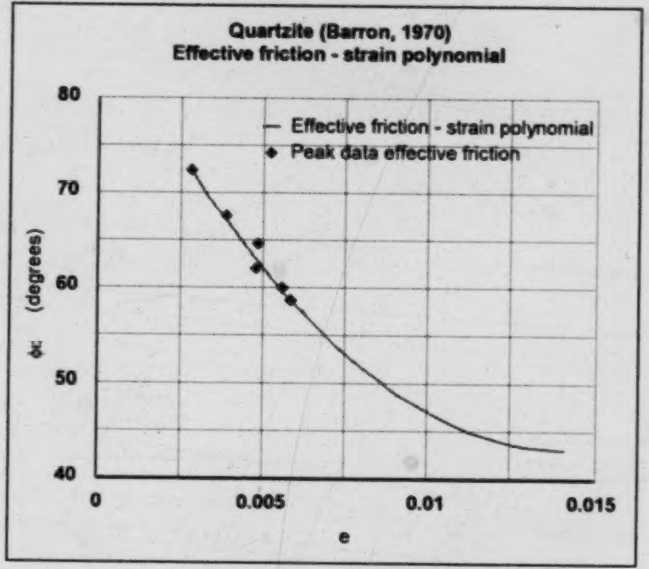

Quartzite (Barron, 1970)
Effective friction - strain polynomial

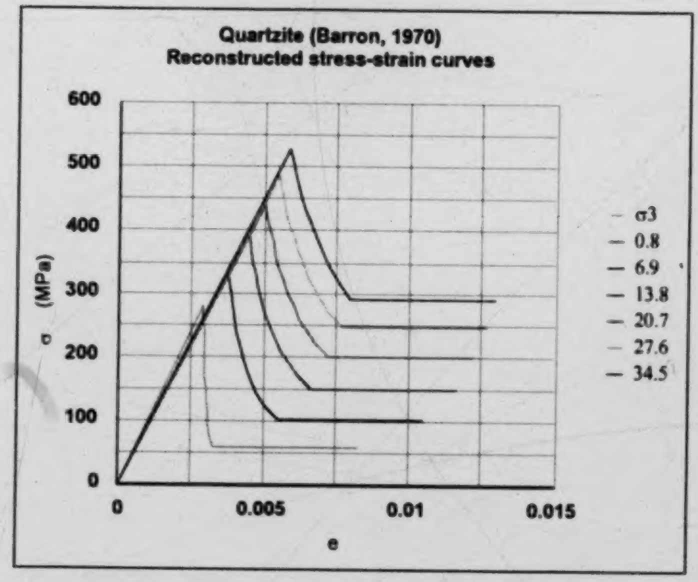

Quartzite (Barron, 1970)
Reconstructed stress-strain curves

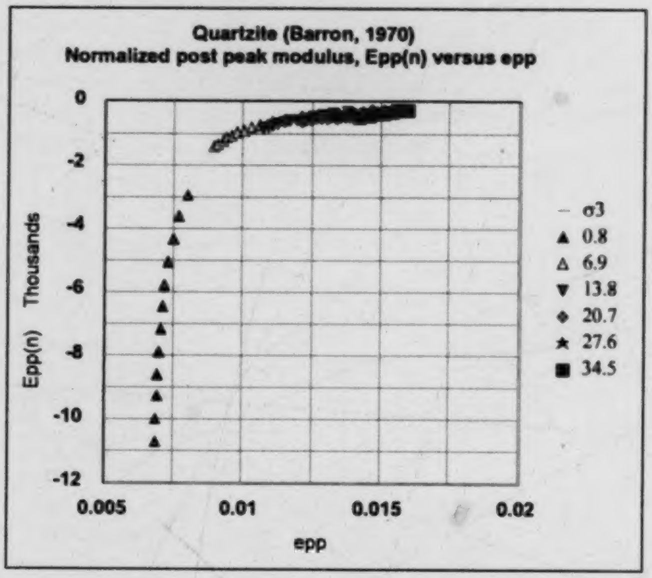

Criterion	Parameters			
Hoek-Brown peak strength	m	σ_c (MPa)	s	a
$\sigma_{1p} = \sigma_3 + \sigma_c\{m\sigma_3/\sigma_c + s\}^a$	18.0	274	1	0.5
Residual strength	D	F	σ_{cr} (MPa)	
$\sigma_{1r} = D\sigma_3^2 + F\sigma_3 + \sigma_{cr}$	-0.008	7.2	55	
Base strength & transition point	ϕ_b (deg.)	σ_{3t} (MPa)	σ_{1t} (MPa)	
$\sigma_{1b} = \{(1+\sin\phi_b)/(1-\sin\phi_b)\}\sigma_3$	43	278	1480	
Friction-strain and base strain	R (deg.)	S	T	e_b
$\phi_e = R + Se_{pp} + Te_{pp}^2$	89	-6450	228000	0.014

Appendix K.5

Intact Solenhofen limestone (Barron, 1970)

σ_3 data (MPa)	σ_{1p} data (MPa)	e_p data (strain)
0	183	0.0035
6.9	222	0.0039
13.8	236	0.0044
20.7	263	0.0049
27.6	277	0.0050
34.5	295	0.0050

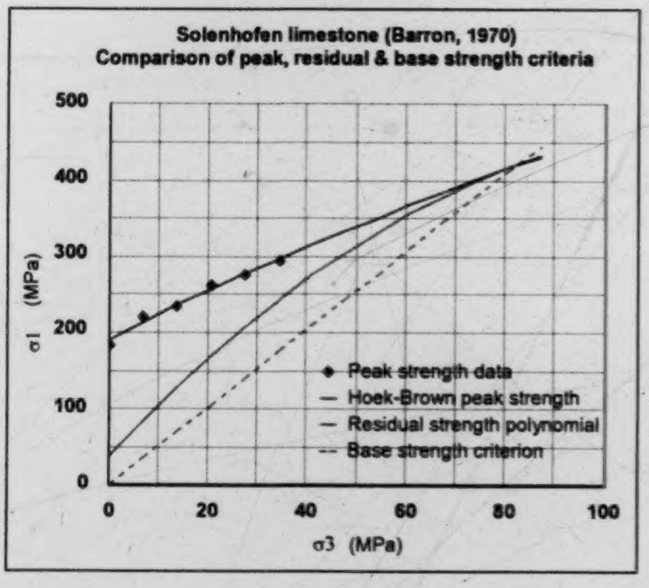

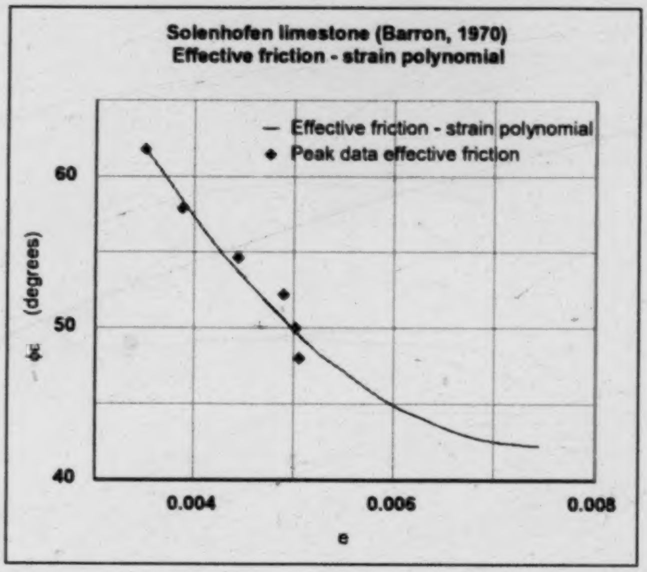
Solenhofen limestone (Barron, 1970)
Effective friction - strain polynomial
Effective friction - strain polynomial
Peak data effective friction
ϕc (degrees)
60
50
40
0.004
0.006
0.008
e

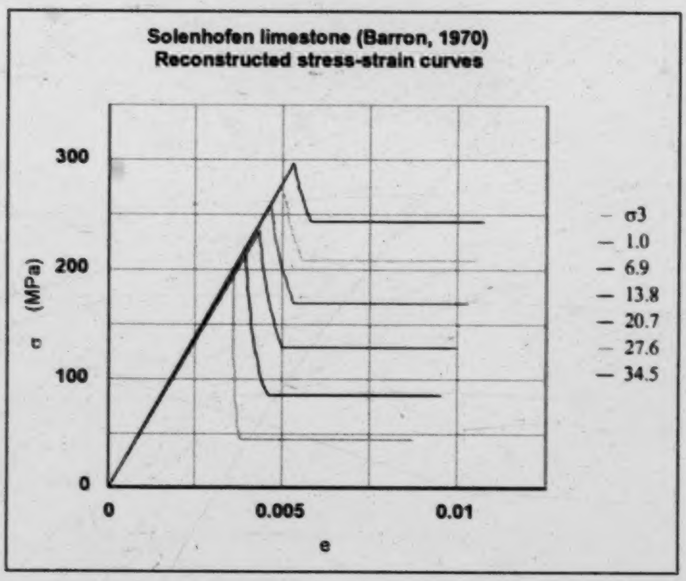
Solenhofen limestone (Barron, 1970)
Reconstructed stress-strain curves
σ (MPa)
300
200
100
0
0
0.005
0.01
e
σ3
1.0
6.9
13.8
20.7
27.6
34.5

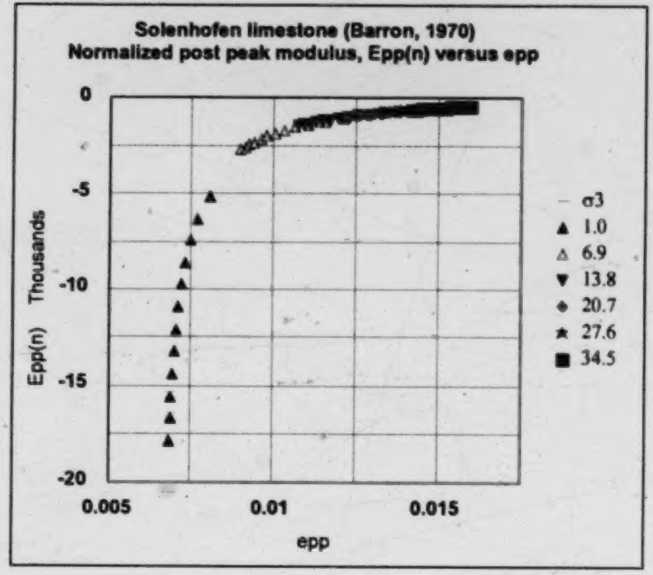

Criterion	Parameters			
Hoek-Brown peak strength	m	σ_c (MPa)	s	a
$\sigma_{1p} = \sigma_3 + \sigma_c\{m\sigma_3/\sigma_c + s\}^a$	5.0	191	1	0.5
Residual strength	D	F	σ_{cr} (MPa)	
$\sigma_{1r} = D\sigma_3^2 + F\sigma_3 + \sigma_{cr}$	-0.03	6.9	38	
Base strength & transition point	ϕ_b (deg.)	σ_{3t} (MPa)	σ_{1t} (MPa)	
$\sigma_{1b} = \{(1+\sin\phi_b)/(1-\sin\phi_b)\}\sigma_3$	42	82	421	
Friction-strain and base strain	R (deg.)	S	T	e_b
$\phi_e = R + Se_{pp} + Te_{pp}^2$	112	-18700	1250000	0.008

Appendix K.6

Intact syenite (Barron, 1970)

σ_3 data	σ_{1p} data	e_p data
(MPa)	(MPa)	(strain)
0	229	0.0032
6.9	336	0.0048
13.8	408	0.0063
20.7	468	0.0068
27.6	525	0.0079
34.5	565	0.0083

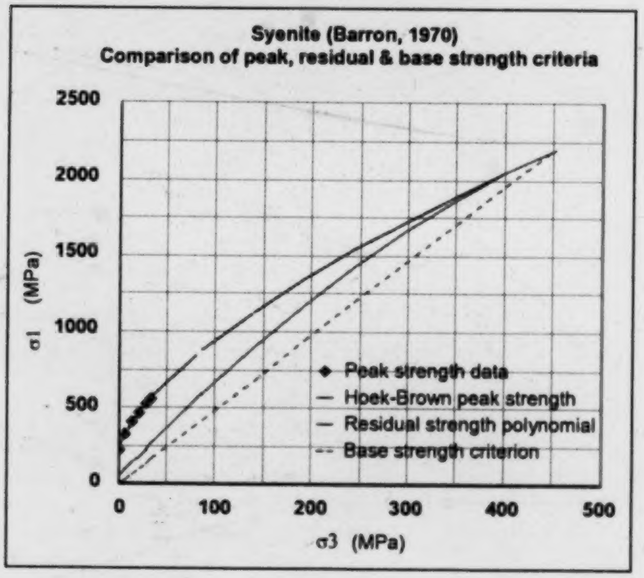

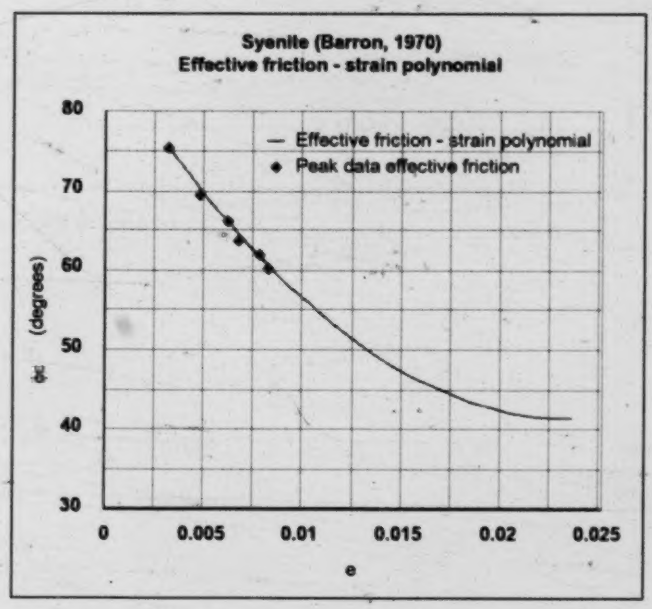
Syenite (Barron, 1970)
Effective friction - strain polynomial
80
70
60
50
40
30
φc (degrees)
0
0.005
0.01
0.015
0.02
0.025
e
Effective friction - strain polynomial
Peak data effective friction

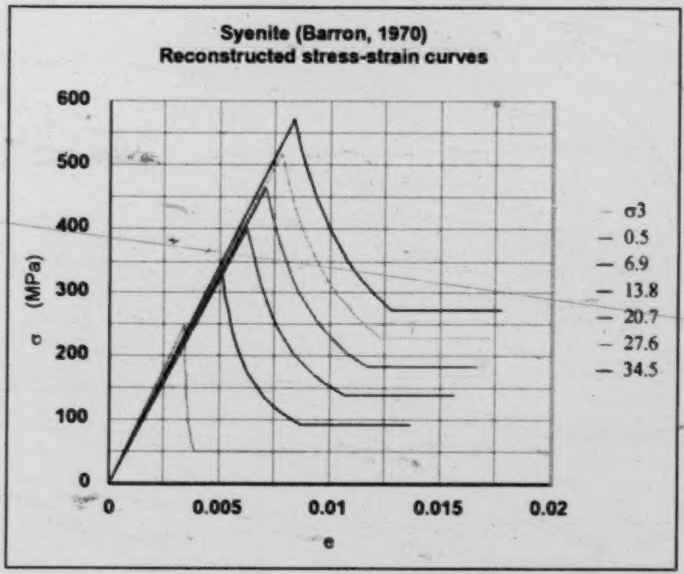
Syenite (Barron, 1970)
Reconstructed stress-strain curves
600
500
400
300
200
100
0
σ (MPa)
0
0.005
0.01
0.015
0.02
e
σ3
0.5
6.9
13.8
20.7
27.6
34.5

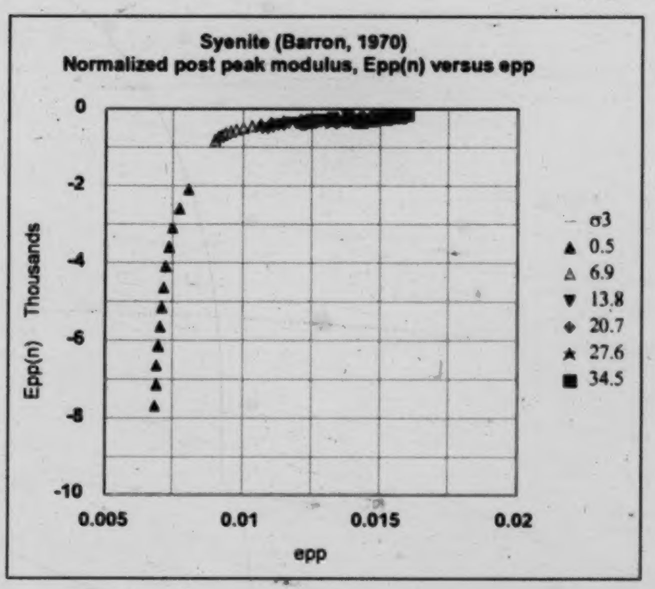

Criterion	Parameters			
Hoek-Brown peak strength	m	σ_c (MPa)	s	a
$\sigma_{1p} = \sigma_3 + \sigma_c\{m\sigma_3/\sigma_c + s\}^a$	27.4	244	1	0.5
Residual strength	D	F	σ_{cr} (MPa)	
$\sigma_{1r} = D\sigma_3^2 + F\sigma_3 + \sigma_{cr}$	-0.004	6.7	49	
Base strength & transition point	ϕ_b (deg.)	σ_{3t} (MPa)	σ_{1t} (MPa)	
$\sigma_{1b} = \{(1+\sin\phi_b)/(1-\sin\phi_b)\}\sigma_3$	41	449	2200	
Friction-strain and base strain	R (deg.)	S	T	e_b
$\phi_c = R + Se_{pp} + Te_{pp}^2$	87	-3870	82000	0.024

Appendix K.7

Intact berea sandstone (Blanton, 1981)

σ_3 data	σ_{1p} data	e_p data
(MPa)	(MPa)	(strain)
0	80	0.004
50	274	0.013
62.5	332	0.016
75	345	0.015
87.5	371	0.017
100	380	0.017

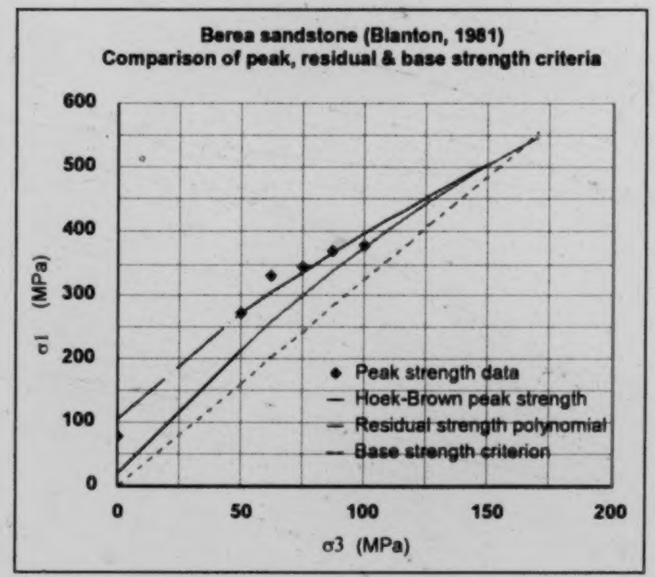

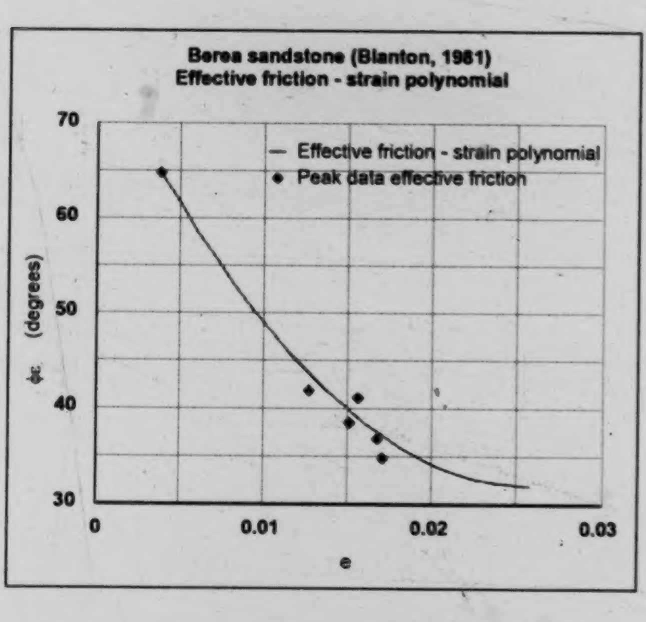
Berea sandstone (Blanton, 1981)
Effective friction - strain polynomial
Effective friction - strain polynomial
Peak data effective friction
φc (degrees)
70
60
50
40
30
0
0.01
0.02
0.03
e

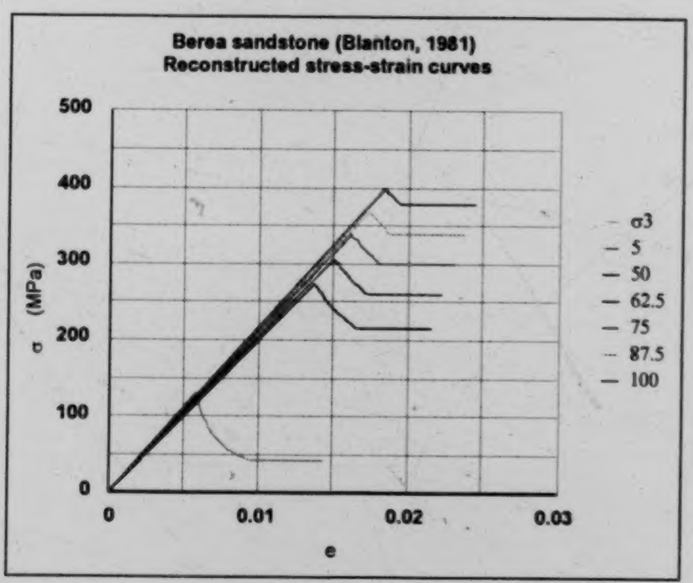
Berea sandstone (Blanton, 1981)
Reconstructed stress-strain curves
σ (MPa)
500
400
300
200
100
0
0
0.01
0.02
0.03
e
σ3
5
50
62.5
75
87.5
100

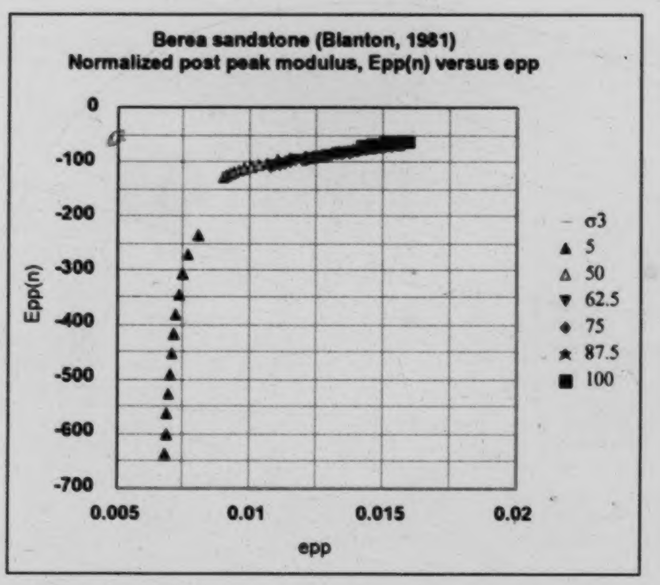

Criterion	Parameters			
Hoek-Brown peak strength	m	σ_c (MPa)	s	a
$\sigma_{1p} = \sigma_3 + \sigma_c\{m\sigma_3/\sigma_c + s\}^a$	7.1	108	1	0.5
Residual strength	D	F	σ_{cr} (MPa)	
$\sigma_{1r} = D\sigma_3^2 + F\sigma_3 + \sigma_{cr}$	-0.007	4.2	22	
Base strength & transition point	ϕ_b (deg.)	σ_{3t} (MPa)	σ_{1t} (MPa)	
$\sigma_{1b} = \{(1+\sin\phi_b)/(1-\sin\phi_b)\}\sigma_3$	32	166	539	
Friction-strain and base strain	R (deg.)	S	T	e_b
$\phi_c = R + Se_{pp} + Te_{pp}^2$	77	-3510	67800	0.03

Appendix K.8

Intact charcoal granodiorite (Blanton, 1981)

σ_3 data	σ_{1p} data	e_p data
(MPa)	(MPa)	(strain)
0	320	0.005
50	690	0.017
250	1320	0.021
450	1750	0.027

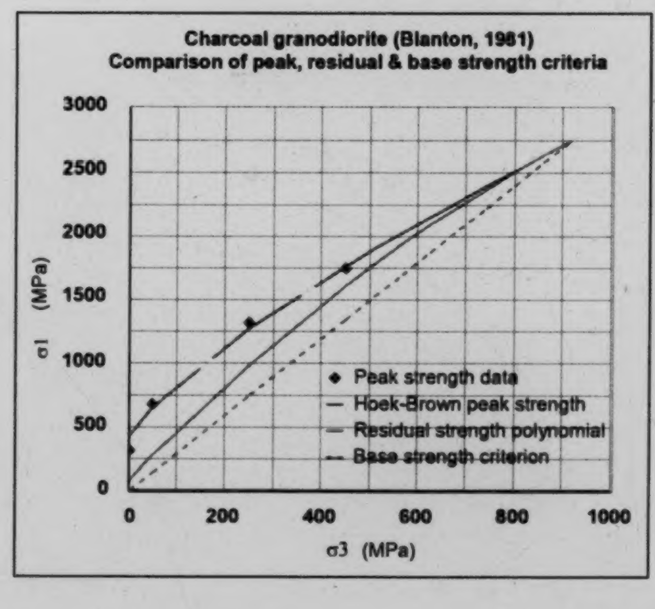

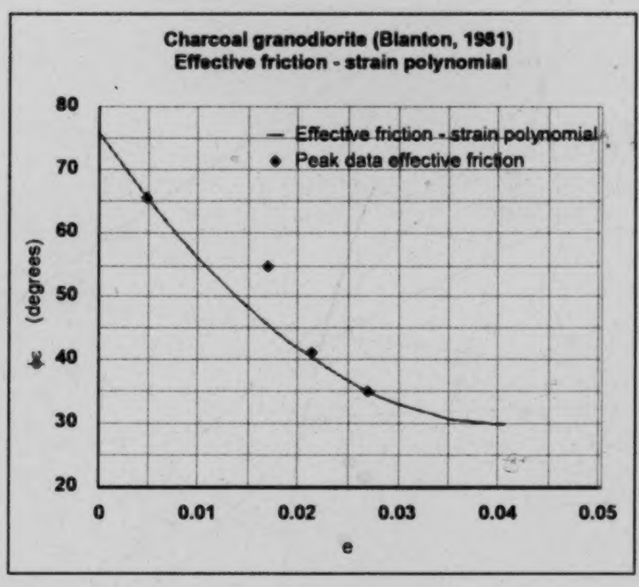
Charcoal granodiorite (Blanton, 1981)
Effective friction - strain polynomial
Effective friction - strain polynomial
Peak data effective friction
ϕc (degrees)
80
70
60
50
40
30
20
0
0.01
0.02
0.03
0.04
0.05
e

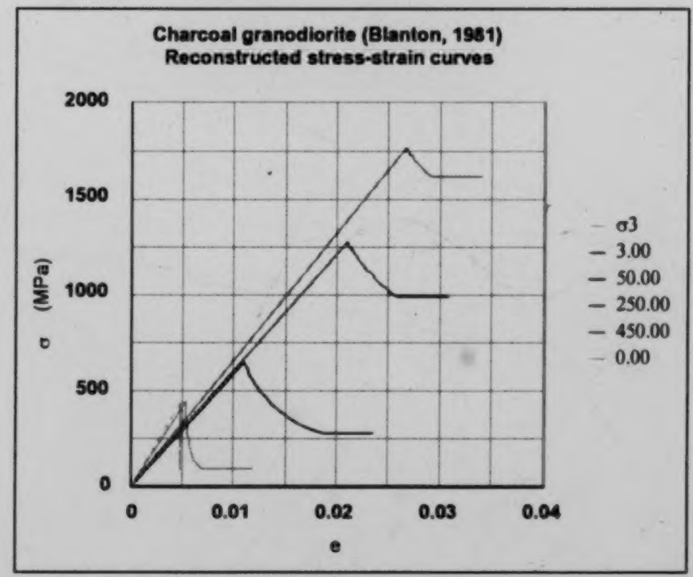
Charcoal granodiorite (Blanton, 1981)
Reconstructed stress-strain curves
σ (MPa)
2000
1500
1000
500
0
0
0.01
0.02
0.03
0.04
e
σ3
3.00
50.00
250.00
450.00
0.00

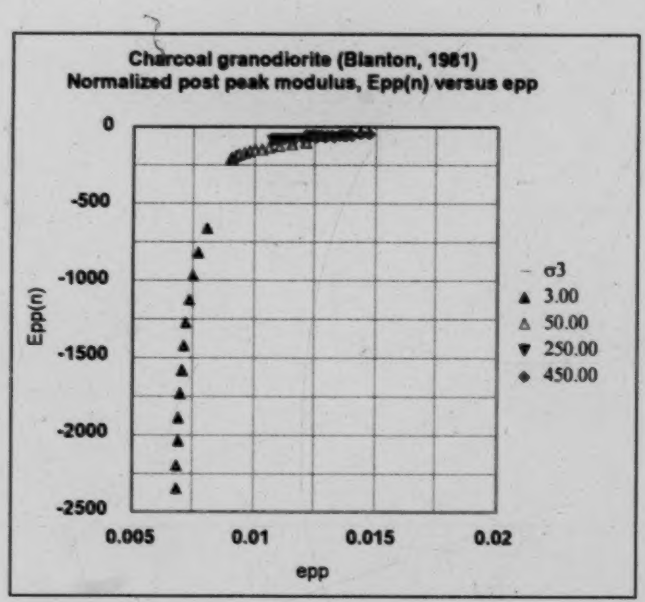

Charcoal granodiorite (Blanton, 1981)
Normalized post peak modulus, Epp(n) versus epp

Criterion	Parameters			
Hoek-Brown peak strength	m	σ_c (MPa)	s	a
$\sigma_{1p} = \sigma_3 + \sigma_c\{m\sigma_3/\sigma_c + s\}^a$	7.9	434	1	0.5
Residual strength	D	F	σ_{cr} (MPa)	
$\sigma_{1r} = D\sigma_3^2 + F\sigma_3 + \sigma_{cr}$	-0.001	3.9	87	
Base strength & transition point	ϕ_b (deg.)	σ_{3t} (MPa)	σ_{1t} (MPa)	
$\sigma_{1b} = \{(1+\sin\phi_b)/(1-\sin\phi_b)\}\sigma_3$	30	912	2730	
Friction-strain and base strain	R (deg.)	S	T	e_b
$\phi_e = R + Se_{pp} + Te_{pp}^2$	76	-2270	27900	0.04

Appendix K.9

Intact Indiana limestone (Blanton, 1981)

σ_3 data	σ_{1p} data	e_p data
(MPa)	(MPa)	(strain)
0	79	0.003
5	104	0.004
10	75	0.005
15	128	0.004
20	135	0.006
25	165	0.008
50	174	0.010

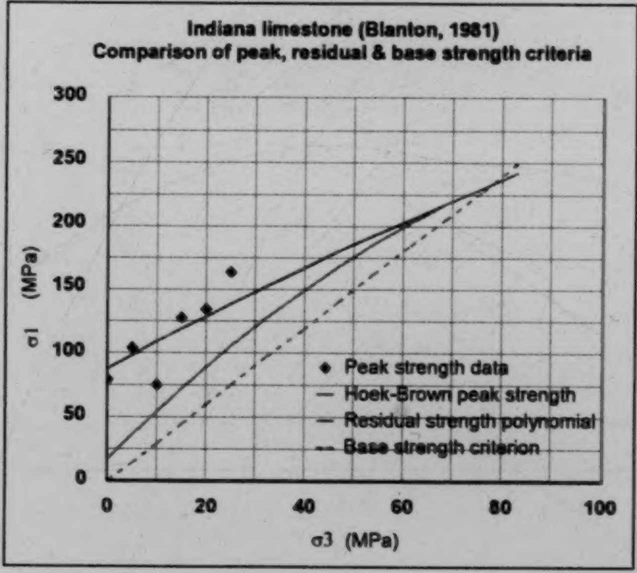

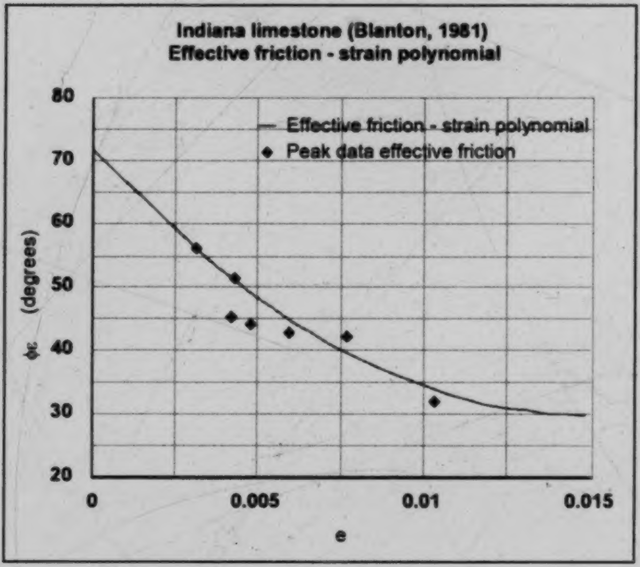

Indiana limestone (Blanton, 1981)
Effective friction - strain polynomial

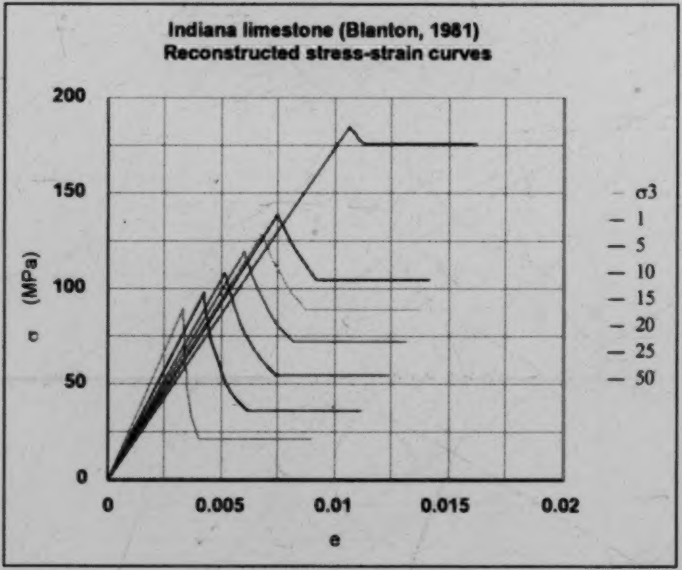

Indiana limestone (Blanton, 1981)
Reconstructed stress-strain curves

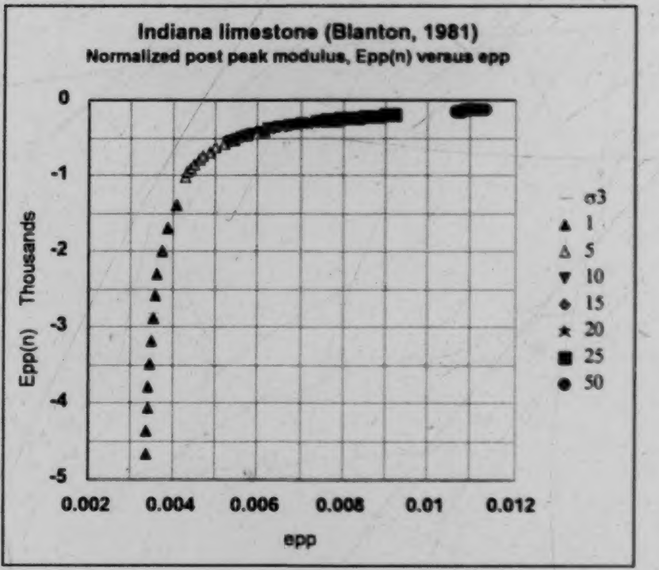

Criterion	Parameters			
Hoek-Brown peak strength	m	σ_c (MPa)	s	a
$\sigma_{1p} = \sigma_3 + \sigma_c\{m\sigma_3/\sigma_c + s\}^a$	2.4	88	1	0.5
Residual strength	D	F	σ_{cr} (MPa)	
$\sigma_{1r} = D\sigma_3^2 + F\sigma_3 + \sigma_{cr}$	-0.014	3.9	18	
Base strength & transition point	ϕ_b (deg.)	σ_{3t} (MPa)	σ_{1t} (MPa)	
$\sigma_{1b} = \{(1+\sin\phi_b)/(1-\sin\phi_b)\}\sigma_3$	30	78	234	
Friction-strain and base strain	R (deg.)	S	T	e_b
$\phi_e = R + Se_{pp} + Te_{pp}^2$	72	-5630	189000	0.015

Appendix K.10

Intact Blair dolomite (Brace, 1964)

σ_3 data	σ_{1p} data	e_p data
(MPa)	(MPa)	(strain)
46	826	0.009
94	1020	0.013
115	1060	0.017
157	1130	0.013
184	1240	0.013
273	1370	0.013
349	1470	0.03

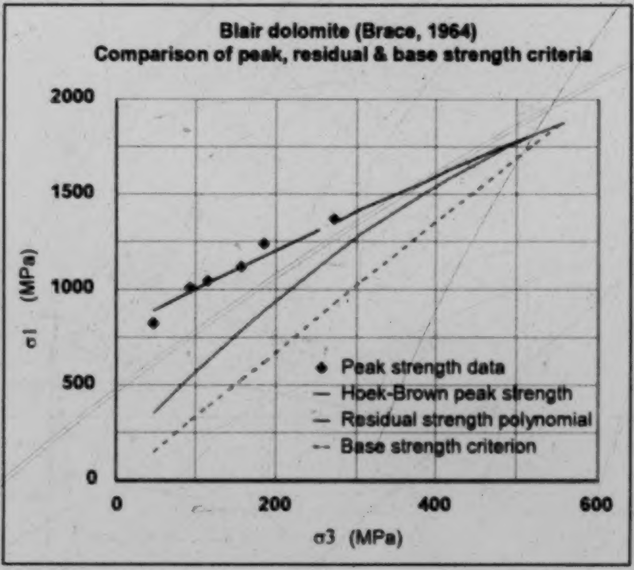

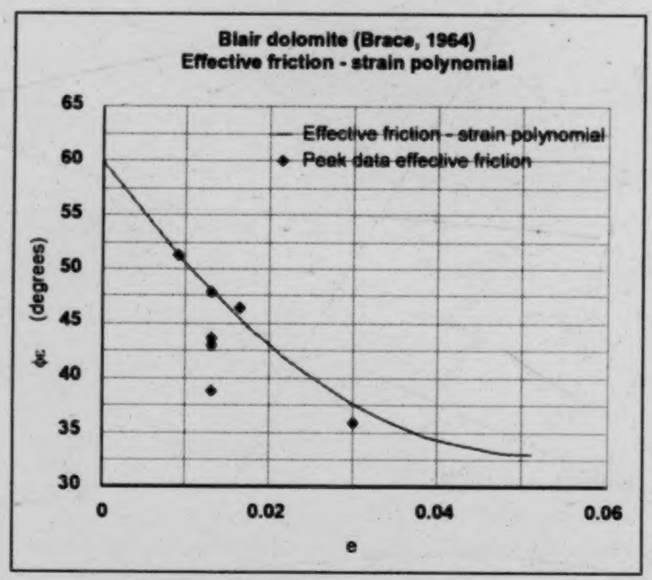
Blair dolomite (Brace, 1964)
Effective friction - strain polynomial

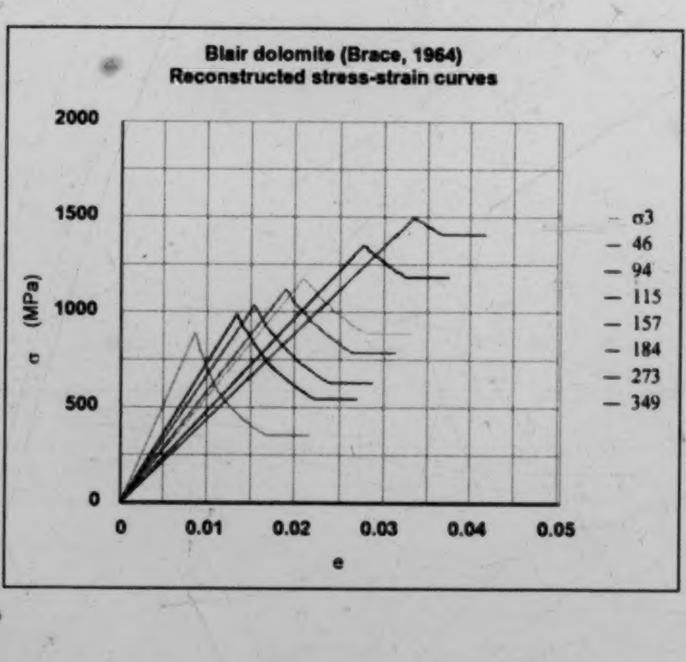
Blair dolomite (Brace, 1964)
Reconstructed stress-strain curves

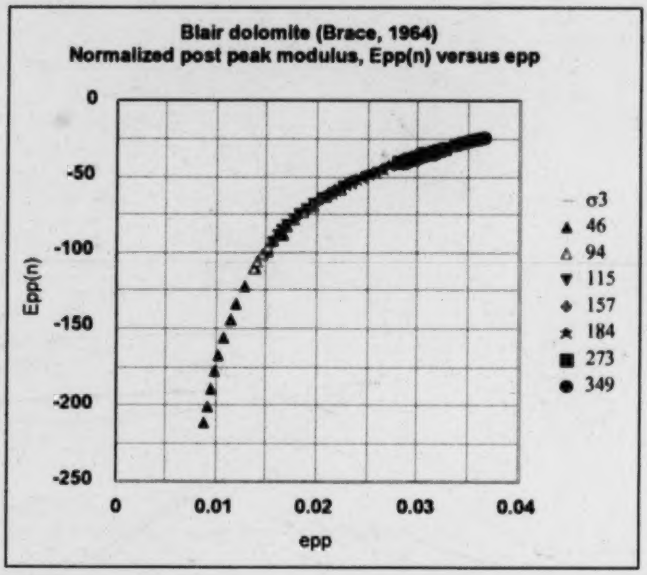

Criterion	Parameters			
Hoek-Brown peak strength	m	σ_c (MPa)	s	a
$\sigma_{1p} = \sigma_3 + \sigma_c\{m\sigma_3/\sigma_c + s\}^a$	2.6	791	1	0.5
Residual strength	D	F	σ_{cr} (MPa)	
$\sigma_{1r} = D\sigma_3^2 + F\sigma_3 + \sigma_{cr}$	-0.002	4.4	157	
Base strength & transition point	ϕ_b (deg.)	σ_{3t} (MPa)	σ_{1t} (MPa)	
$\sigma_{1b} = \{(1+\sin\phi_b)/(1-\sin\phi_b)\}\sigma_3$	33	554	1880	
Friction-strain and base strain	R (deg.)	S	T	e_b
$\phi_e = R + Se_{pp} + Te_{pp}^2$	60	-1050	10200	0.05

Appendix K.11

Intact quartzite (Chan et al., 1972)

σ_3 data	σ_{1p} data	e_p data
(MPa)	(MPa)	(strain)
0	224	0.0038
10.3	265	0.0045
13.8	321	0.0055
27.6	420	0.0072

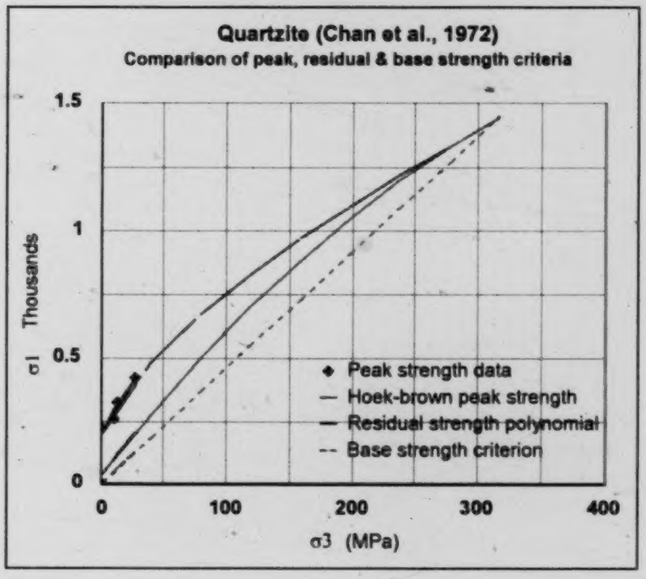

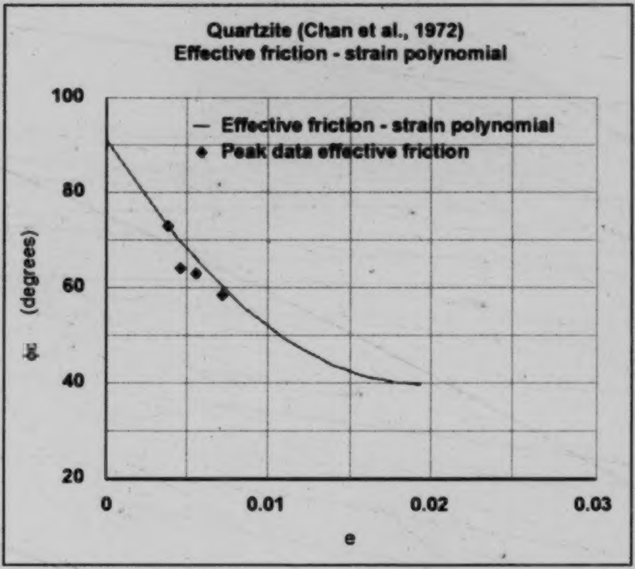
Quartzite (Chan et al., 1972)
Effective friction - strain polynomial
— Effective friction - strain polynomial
◆ Peak data effective friction
φc (degrees)
100
80
60
40
20
0
0.01
0.02
0.03
e

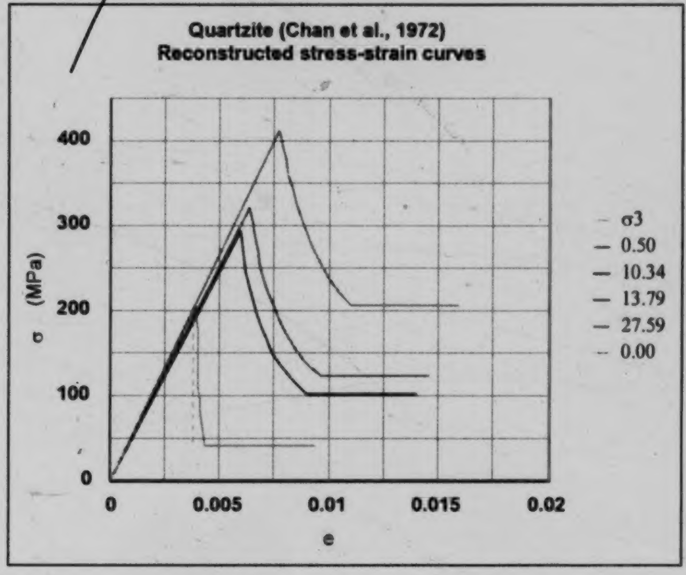
Quartzite (Chan et al., 1972)
Reconstructed stress-strain curves
σ (MPa)
400
300
200
100
0
0
0.005
0.01
0.015
0.02
e
σ3
0.50
10.34
13.79
27.59
0.00

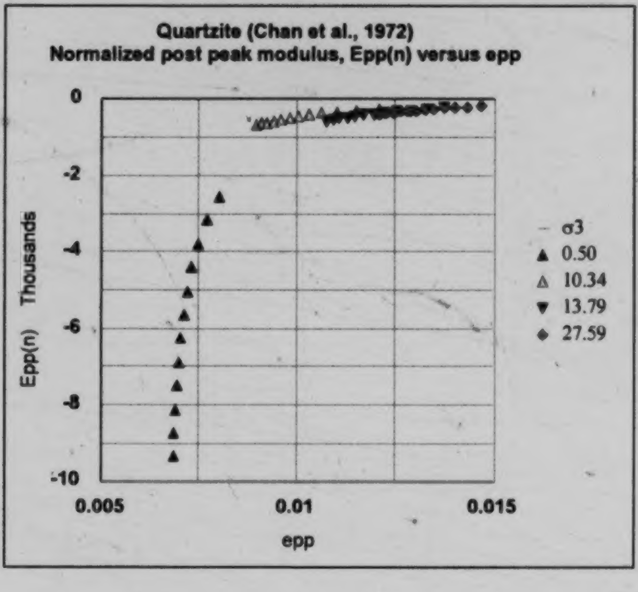

Criterion	Parameters			
Hoek-Brown peak strength	m	σ_c (MPa)	s	a
$\sigma_{1p} = \sigma_3 + \sigma_c\{m\sigma_3/\sigma_c + s\}^a$	19.	201	1	0.5
Residual strength	D	F	σ_{cr} (MPa)	
$\sigma_{1r} = D\sigma_3^2 + F\sigma_3 + \sigma_{cr}$	-0.006	6.2	10	
Base strength & transition point	ϕ_b (deg.)	σ_{3t} (MPa)	σ_{1t} (MPa)	
$\sigma_{1b} = \{(1+\sin\phi_b)/(1-\sin\phi_b)\}\sigma_3$	40	312	1430	
Friction-strain and base strain	R (deg.)	S	T	e_b
$\phi_e = R + Se_{pp} + Te_{pp}^2$	91	-5280	136000	0.02

Appendix K.12

Intact concrete (Dougill, 1985)

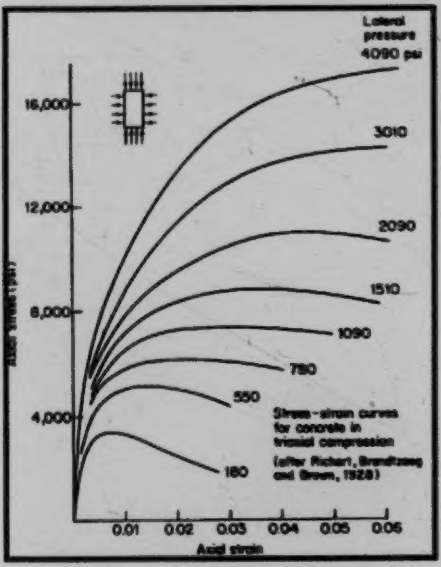

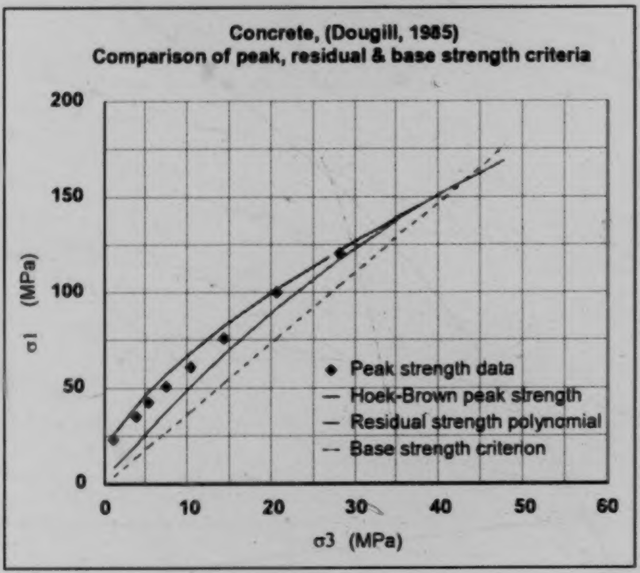

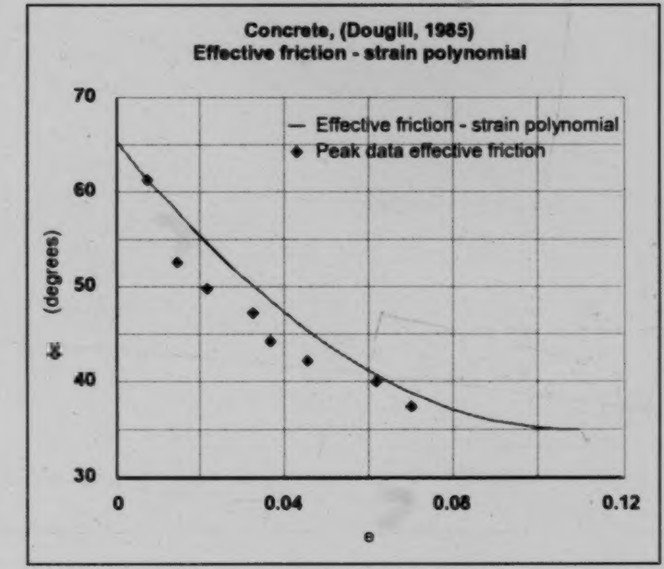
Concrete, (Dougill, 1985)
Effective friction - strain polynomial
70
60
50
40
30
φ (degrees)
— Effective friction - strain polynomial
◆ Peak data effective friction
0
0.04
0.08
0.12
e

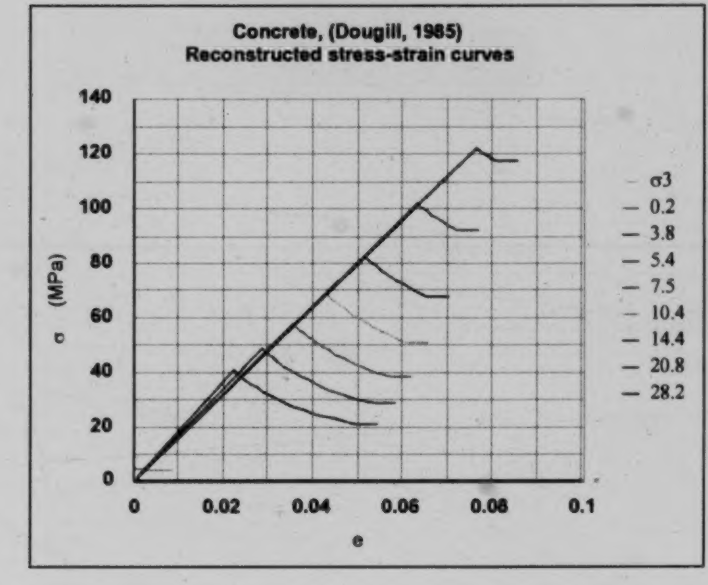
Concrete, (Dougill, 1985)
Reconstructed stress-strain curves
140
120
100
80
60
40
20
0
σ (MPa)
0
0.02
0.04
0.06
0.08
0.1
e
σ3
— 0.2
— 3.8
— 5.4
— 7.5
— 10.4
— 14.4
— 20.8
— 28.2

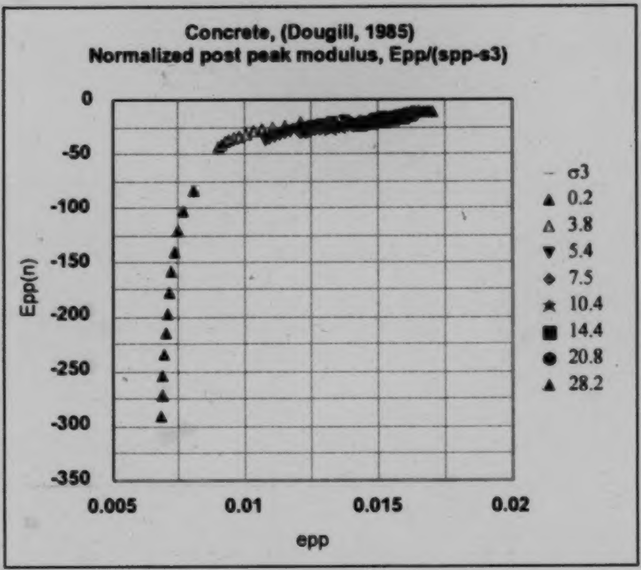

Criterion	Parameters			
Hoek-Brown peak strength	m	σ_c (MPa)	s	a
$\sigma_{1p} = \sigma_3 + \sigma_c\{m\sigma_3/\sigma_c + s\}^a$	20.0	15	1	0.5
Residual strength	D	F	σ_{cr} (MPa)	
$\sigma_{1r} = D\sigma_3^2 + F\sigma_3 + \sigma_{cr}$	-0.03	4.9	3	
Base strength & transition point	ϕ_b (deg.)	σ_{3t} (MPa)	σ_{1t} (MPa)	
$\sigma_{1b} = \{(1+\sin\phi_b)/(1-\sin\phi_b)\}\sigma_3$	35	43	159	
Friction-strain and base strain	R (deg.)	S	T	e_b
$\phi_c = R + Se_{pp} + Te_{pp}^2$	65.5	-556	2540	0.11

Appendix K.13

Intact berea sandstone (Gnirk et al., 1965)

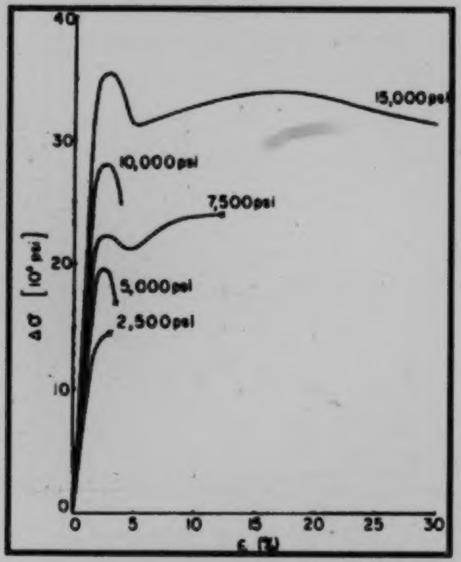

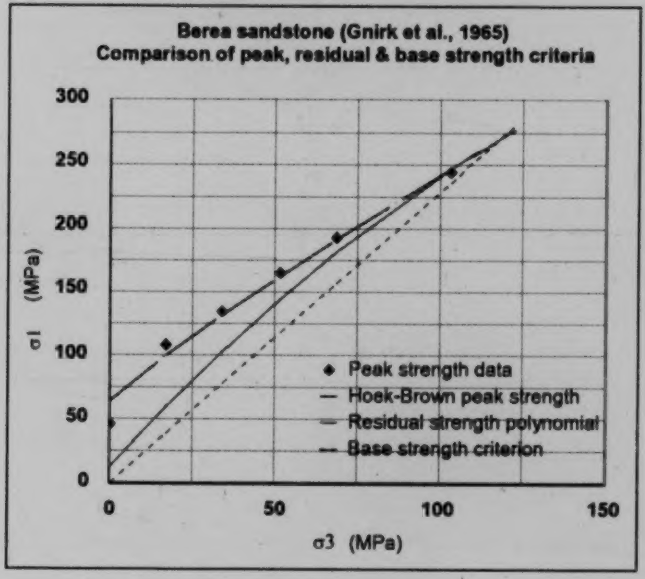

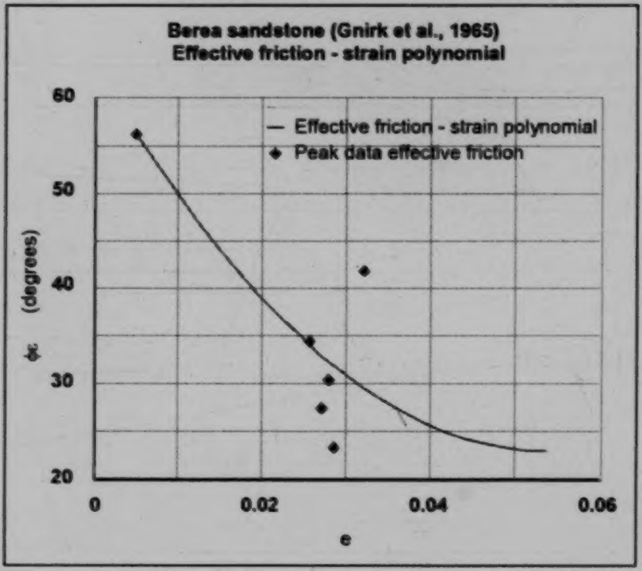
Berea sandstone (Gnirk et al., 1965)
Effective friction - strain polynomial

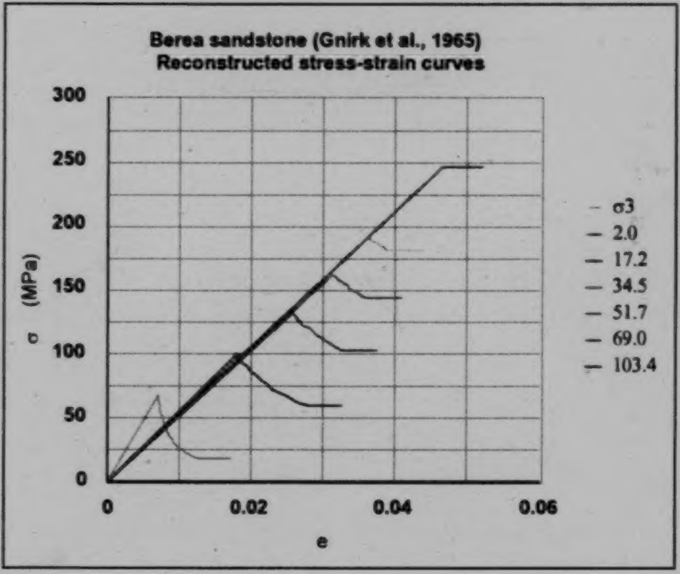
Berea sandstone (Gnirk et al., 1965)
Reconstructed stress-strain curves

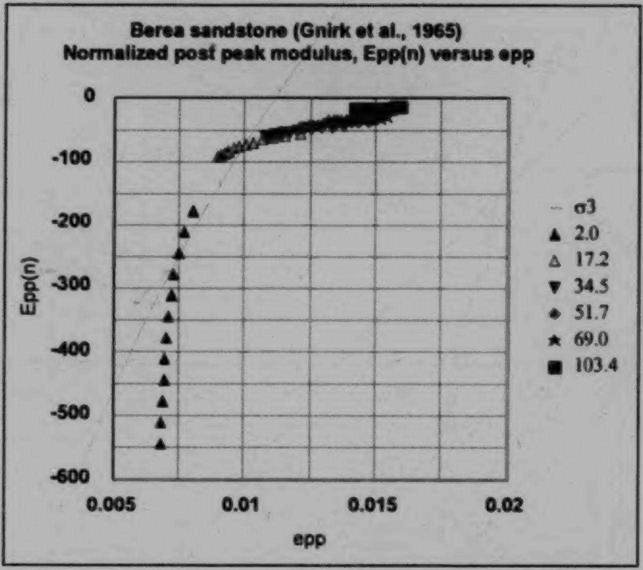

Criterion	Parameters			
Hoek-Brown peak strength	m	σ_c (MPa)	s	a
$\sigma_{1p} = \sigma_3 + \sigma_c\{m\sigma_3/\sigma_c + s\}^a$	2.5	64	1	0.5
Residual strength	D	F	σ_{cr} (MPa)	
$\sigma_{1r} = D\sigma_3^2 + F\sigma_3 + \sigma_{cr}$	-0.006	2.8	13	
Base strength & transition point	ϕ_b (deg.)	σ_{3t} (MPa)	σ_{1t} (MPa)	
$\sigma_{1b} = \{(1+\sin\phi_b)/(1-\sin\phi_b)\}\sigma_3$	23	118	270	
Friction-strain and base strain	R (deg.)	S	T	e_b
$\phi_e = R + Se_{pp} + Te_{pp}^2$	63	-1500	14000	0.05

Appendix K.14

Intact Carthage marble (Gnirk et al., 1965)

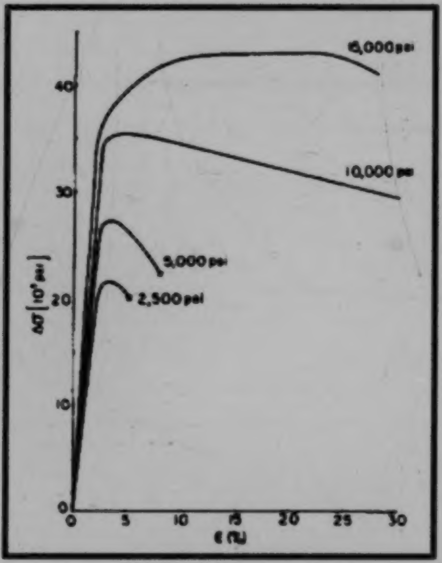

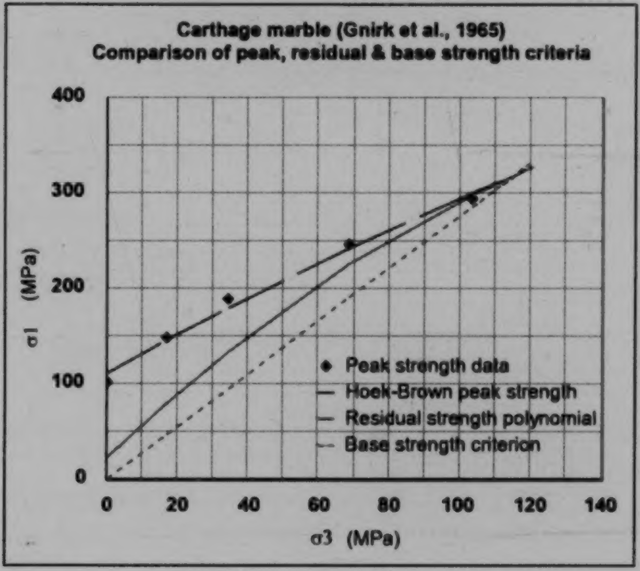
Carthage marble (Gnirk et al., 1965)
Comparison of peak, residual & base strength criteria

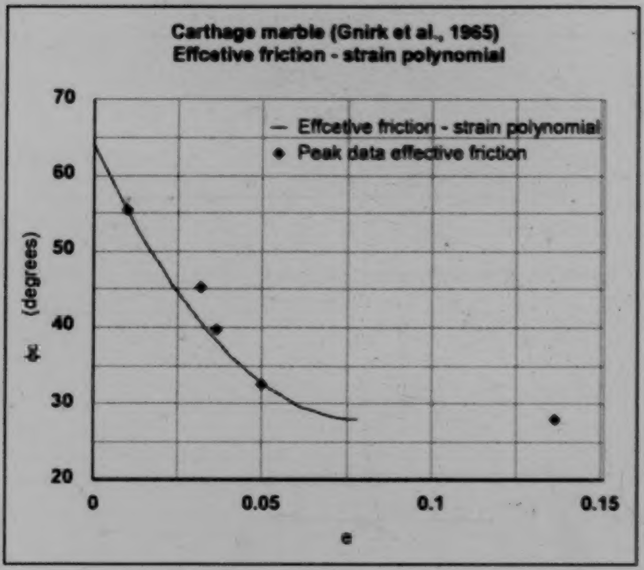
Carthage marble (Gnirk et al., 1965)
Effcetive friction - strain polynomial
Effcetive friction - strain polynomial
Peak data effective friction
70
60
50
40
30
20
φc (degrees)
0
0.05
0.1
0.15
e

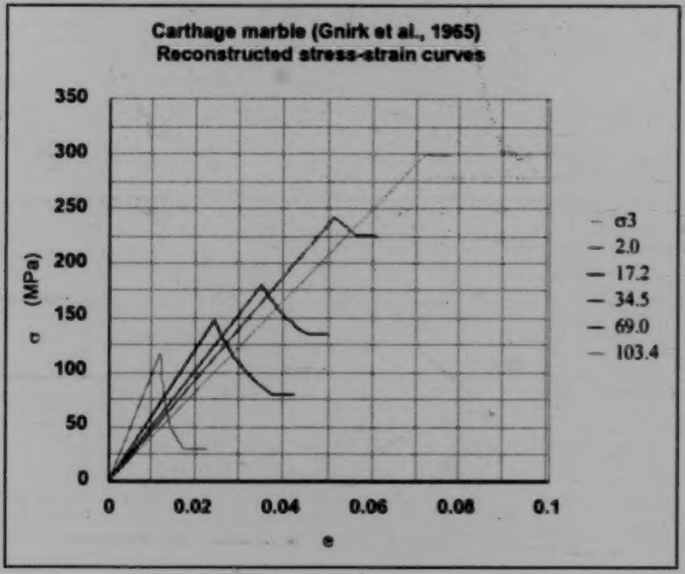
Carthage marble (Gnirk et al., 1965)
Reconstructed stress-strain curves
350
300
250
200
150
100
50
0
σ (MPa)
0
0.02
0.04
0.06
0.08
0.1
e
σ3
2.0
17.2
34.5
69.0
103.4

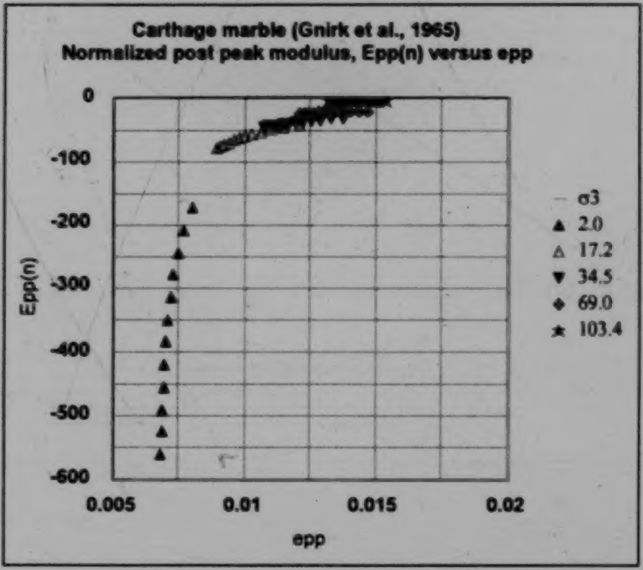

Criterion	Parameters			
Hoek-Brown peak strength	m	σ_c (MPa)	s	a
$\sigma_{1p} = \sigma_3 + \sigma_c\{m\sigma_3/\sigma_c + s\}^a$	2.3	113	1	0.5
Residual strength	D	F	σ_{cr} (MPa)	
$\sigma_{1r} = D\sigma_3^2 + F\sigma_3 + \sigma_{cr}$	-0.008	3.5	23	
Base strength & transition point	ϕ_b (deg.)	σ_{3t} (MPa)	σ_{1t} (MPa)	
$\sigma_{1b} = \{(1+\sin\phi_b)/(1-\sin\phi_b)\}\sigma_3$	28	116	321	
Friction-strain and base strain	R (deg.)	S	T	e_b
$\phi_e = R + Se_{pp} + Te_{pp}^2$	64	-921	5870	0.08

Appendix K.15

Intact Danby marble (Gnirk et al., 1965)

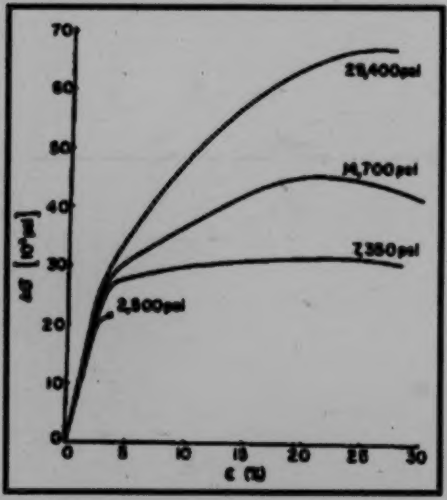

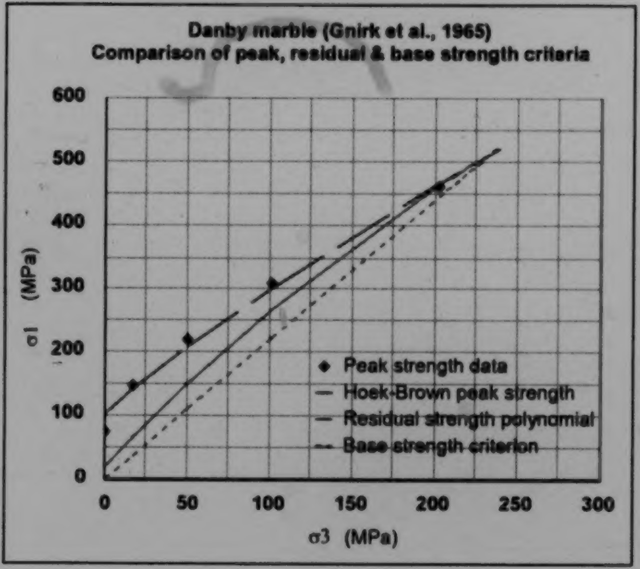

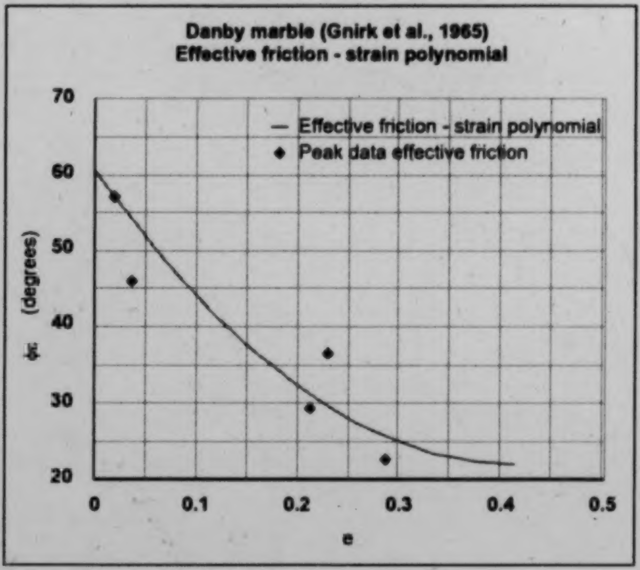

Danby marble (Gnirk et al., 1965)
Effective friction - strain polynomial

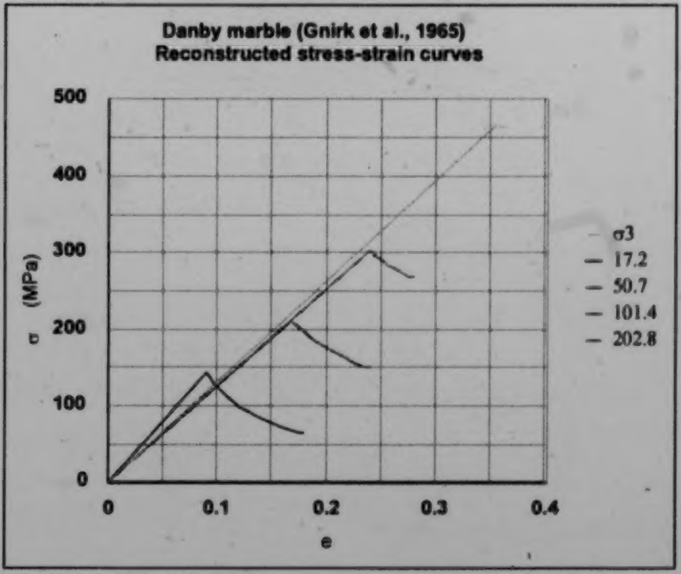

Danby marble (Gnirk et al., 1965)
Reconstructed stress-strain curves

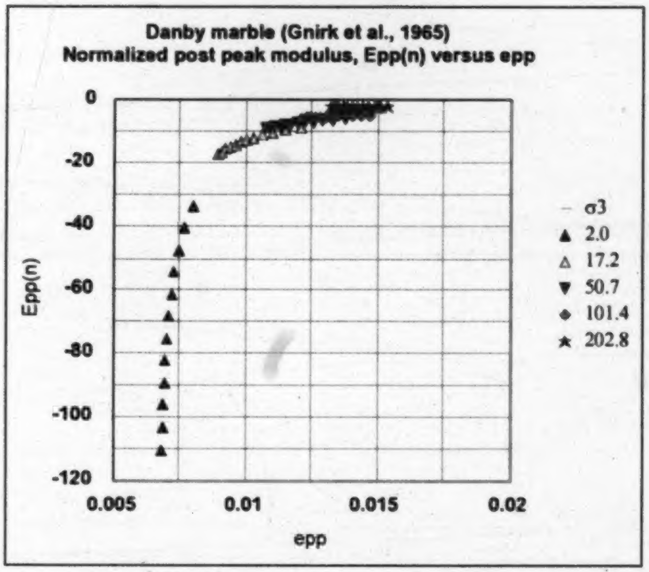

Criterion	Parameters			
Hoek-Brown peak strength	m	σ_c (MPa)	s	a
$\sigma_{1p} = \sigma_3 + \sigma_c\{m\sigma_3/\sigma_c + s\}^a$	2.8	105	1	0.5
Residual strength	D	F	σ_{cr} (MPa)	
$\sigma_{1r} = D\sigma_3^2 + F\sigma_3 + \sigma_{cr}$	-0.003	2.7	21	
Base strength & transition point	ϕ_b (deg.)	σ_{3t} (MPa)	σ_{1t} (MPa)	
$\sigma_{1b} = \{(1+\sin\phi_b)/(1-\sin\phi_b)\}\sigma_3$	22	235	516	
Friction-strain and base strain	R (deg.)	S	T	e_b
$\phi_e = R + Se_{pp} + Te_{pp}^2$	61	-186	224	0.42

Appendix K.16

Intact Hasmark dolomite (Gnirk et al., 1965)

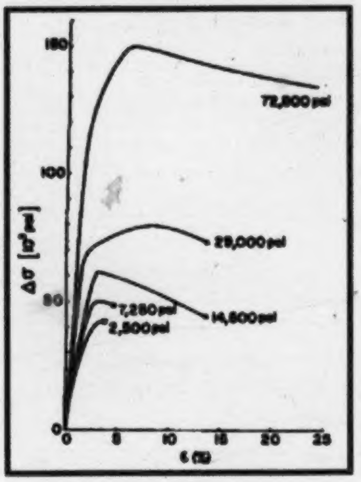

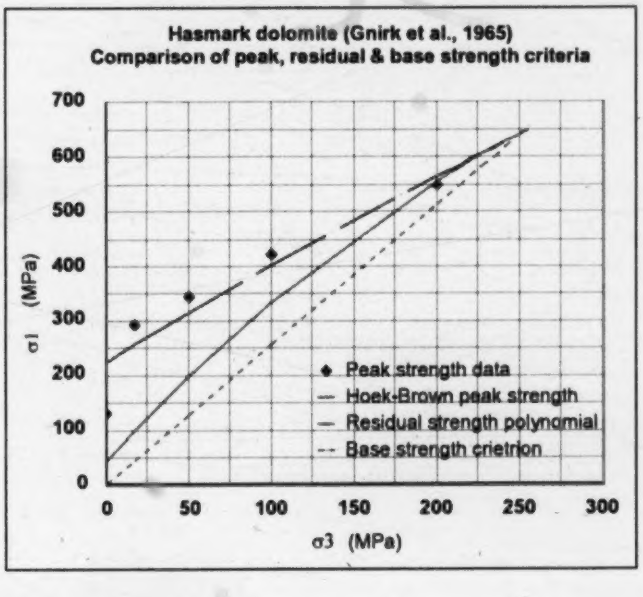

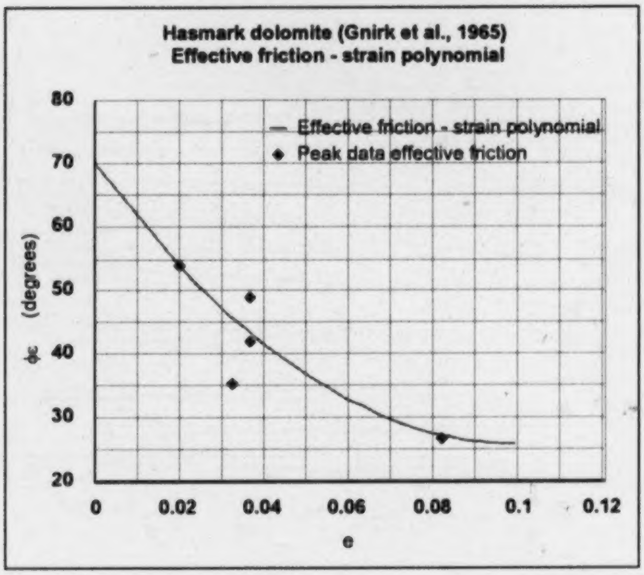
Hasmark dolomite (Gnirk et al., 1965)
Effective friction - strain polynomial
Effective friction - strain polynomial
Peak data effective friction
φc (degrees)
80
70
60
50
40
30
20
0
0.02
0.04
0.06
0.08
0.1
0.12
e

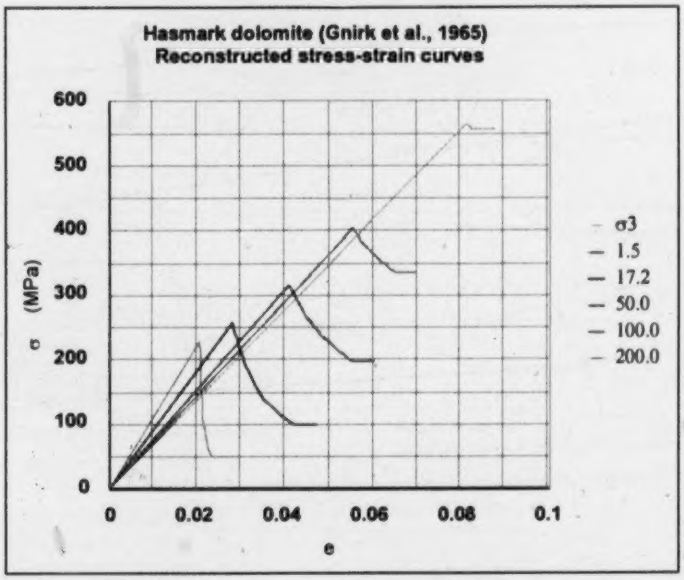
Hasmark dolomite (Gnirk et al., 1965)
Reconstructed stress-strain curves
σ (MPa)
600
500
400
300
200
100
0
0
0.02
0.04
0.06
0.08
0.1
e
σ3
1.5
17.2
50.0
100.0
200.0

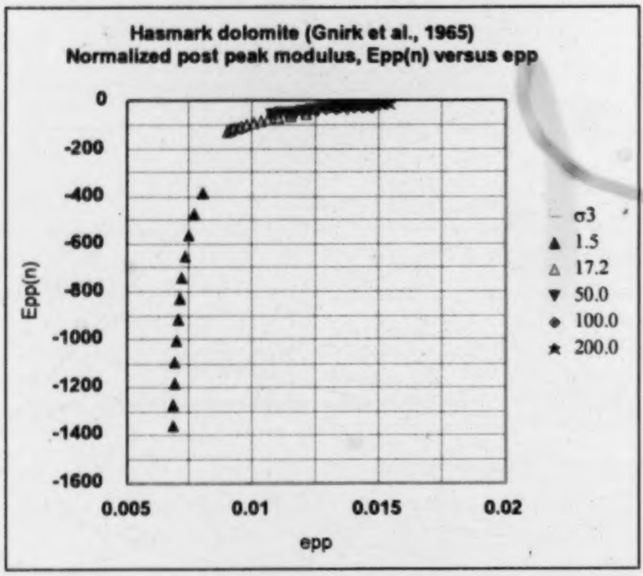

Criterion	Parameters			
Hoek-Brown peak strength	m	σ_c (MPa)	s	a
$\sigma_{1p} = \sigma_3 + \sigma_c\{m\sigma_3/\sigma_c + s\}^a$	1.8	226	1	0.5
Residual strength	D	F	σ_{cr} (MPa)	
$\sigma_{1r} = D\sigma_3^2 + F\sigma_3 + \sigma_{cr}$	-0.003	3.2	45	
Base strength & transition point	ϕ_b (deg.)	σ_{3t} (MPa)	σ_{1t} (MPa)	
$\sigma_{1b} = \{(1+\sin\phi_b)/(1-\sin\phi_b)\}\sigma_3$	26	251	644	
Friction-strain and base strain	R (deg.)	S	T	e_b
$\phi_e = R + Se_{pp} + Te_{pp}^2$	70	-886	4460	0.1

Appendix K.17

Intact Indiana limestone (Gnirk et al., 1965)

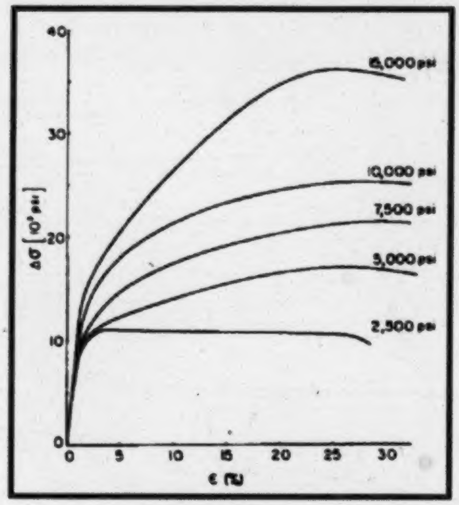

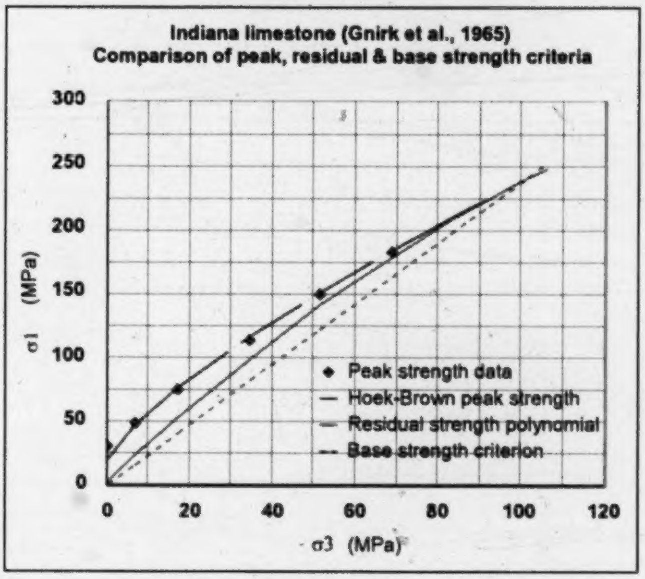

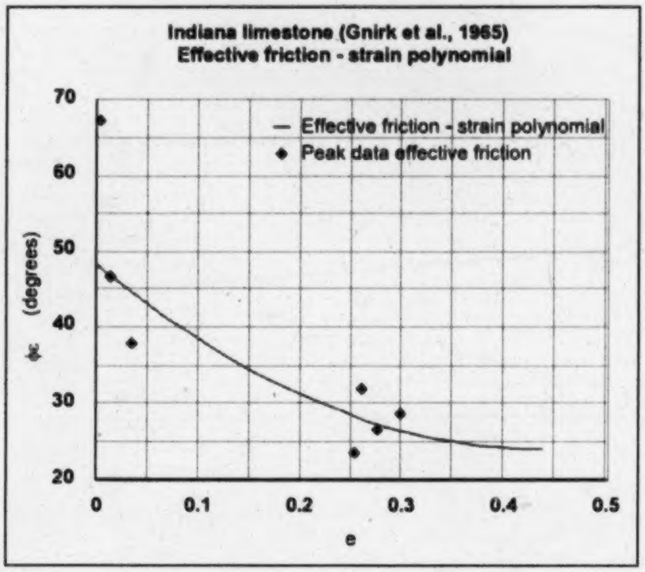
Indiana limestone (Gnirk et al., 1965)
Effective friction - strain polynomial
70
60
50
40
30
20
φc (degrees)
0
0.1
0.2
0.3
0.4
0.5
e
— Effective friction - strain polynomial
◆ Peak data effective friction

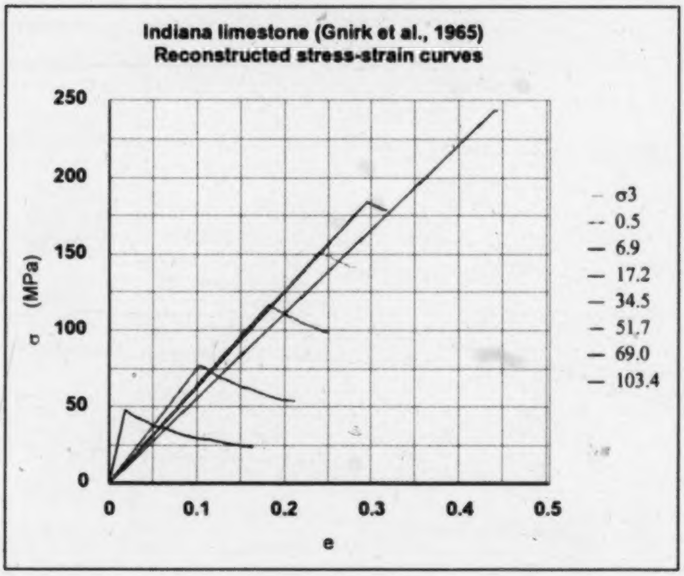
Indiana limestone (Gnirk et al., 1965)
Reconstructed stress-strain curves
250
200
150
100
50
0
σ (MPa)
0
0.1
0.2
0.3
0.4
0.5
e
σ3
0.5
6.9
17.2
34.5
51.7
69.0
103.4

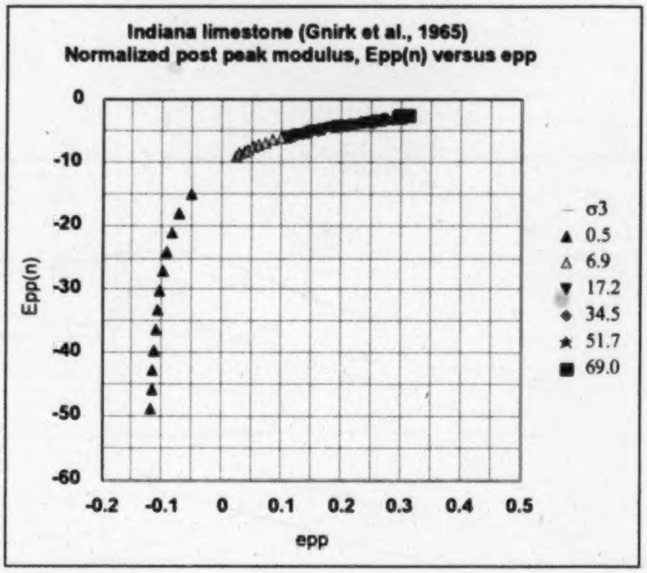

Criterion	Parameters			
Hoek-Brown peak strength	m	σ_c (MPa)	s	a
$\sigma_{1p} = \sigma_3 + \sigma_c\{m\sigma_3/\sigma_c + s\}^a$	9.7	19	1	0.5
Residual strength	D	F	σ_{cr} (MPa)	
$\sigma_{1r} = D\sigma_3^2 + F\sigma_3 + \sigma_{cr}$	-0.007	3.0	4	
Base strength & transition point	ϕ_b (deg.)	σ_{3t} (MPa)	σ_{1t} (MPa)	
$\sigma_{1b} = \{(1+\sin\phi_b)/(1-\sin\phi_b)\}\sigma_3$	24	101	241	
Friction-strain and base strain	R (deg.)	S	T	e_b
$\phi_e = R + Se_{pp} + Te_{pp}^2$	48	-111	127	0.44

Appendix K.18

Intact Virginia greenstone (Gnirk et al., 1965)

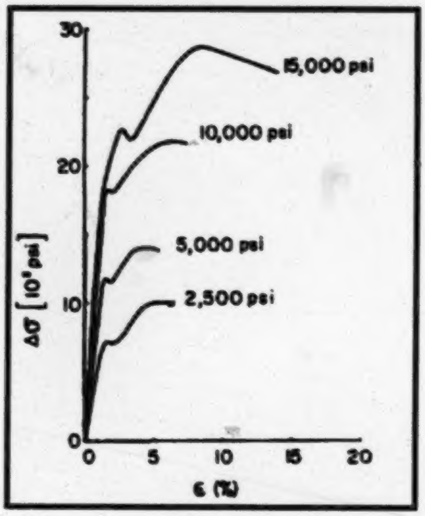

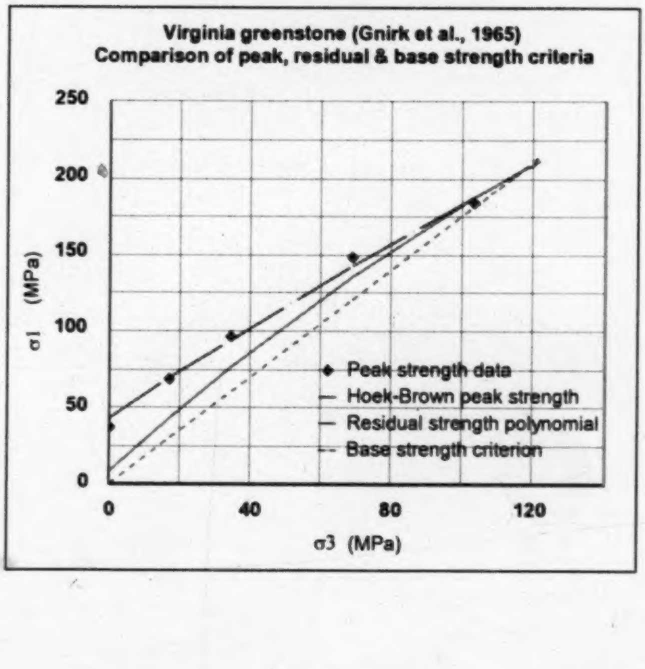

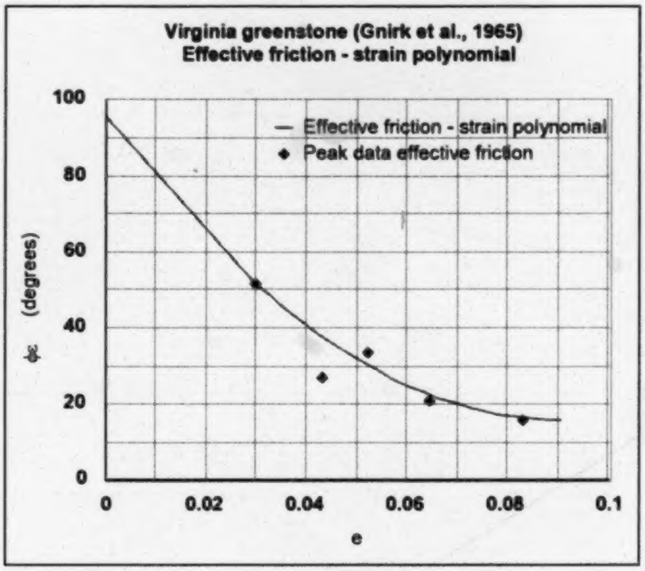
Virginia greenstone (Gnirk et al., 1965)
Effective friction - strain polynomial
φc (degrees)
100
80
60
40
20
0
0
0.02
0.04
0.06
0.08
0.1
e
Effective friction - strain polynomial
Peak data effective friction

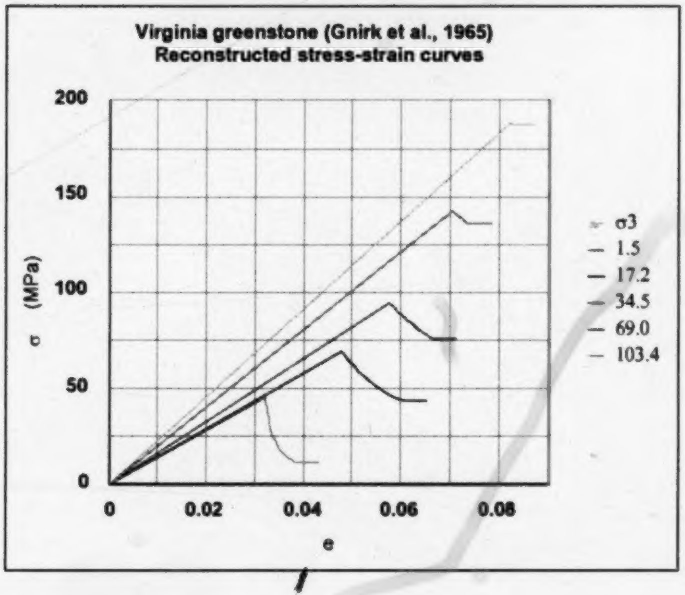
Virginia greenstone (Gnirk et al., 1965)
Reconstructed stress-strain curves
σ (MPa)
200
150
100
50
0
0
0.02
0.04
0.06
0.08
e
σ3
1.5
17.2
34.5
69.0
103.4

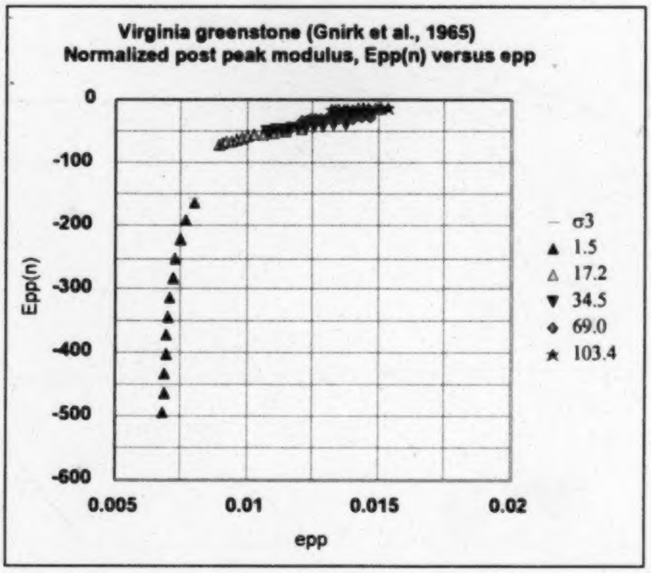

Criterion	Parameters			
Hoek-Brown peak strength	m	σ_c (MPa)	s	a
$\sigma_{1p} = \sigma_3 + \sigma_c\{m\sigma_3/\sigma_c + s\}^a$	1.2	43	1	0.5
Residual strength	D	F	σ_{cr} (MPa)	
$\sigma_{1r} = D\sigma_3^2 + F\sigma_3 + \sigma_{cr}$	-0.003	2.1	9	
Base strength & transition point	ϕ_b (deg.)	σ_{3t} (MPa)	σ_{1t} (MPa)	
$\sigma_{1b} = \{(1+\sin\phi_b)/(1-\sin\phi_b)\}\sigma_3$	16	117	206	
Friction-strain and base strain	R (deg.)	S	T	e_b
$\phi_c = R + Se_{pp} + Te_{pp}^2$	96	-1760	9710	0.09

Appendix K.19

Intact Jastrzebie sandstone (Kwasniewski, 1983)

σ_3 data	σ_{1p} data	e_p data
(MPa)	(MPa)	(strain)
0	92	0.004
12	140	0.007
18	183	0.010
24	218	0.010
29	223	0.014
35	230	0.012
47	269	0.019
53	283	0.019
60	290	0.021

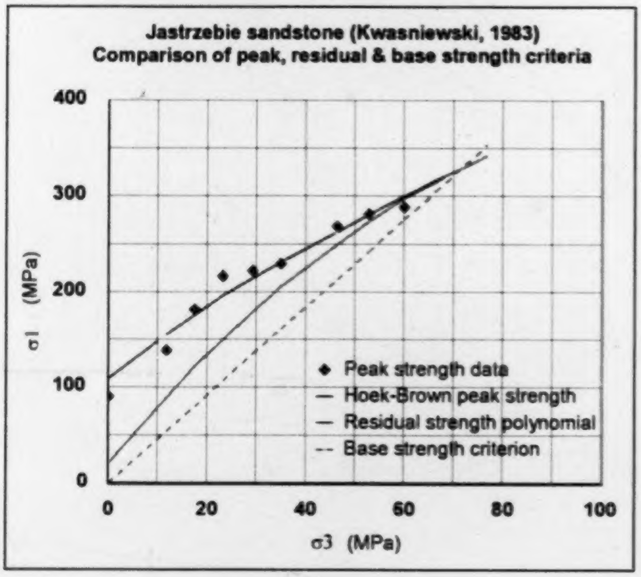

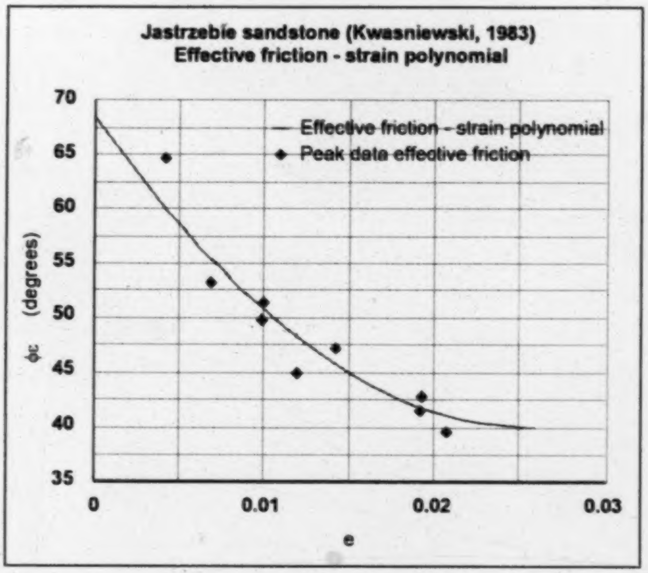
Jastrzebie sandstone (Kwasniewski, 1983)
Effective friction - strain polynomial

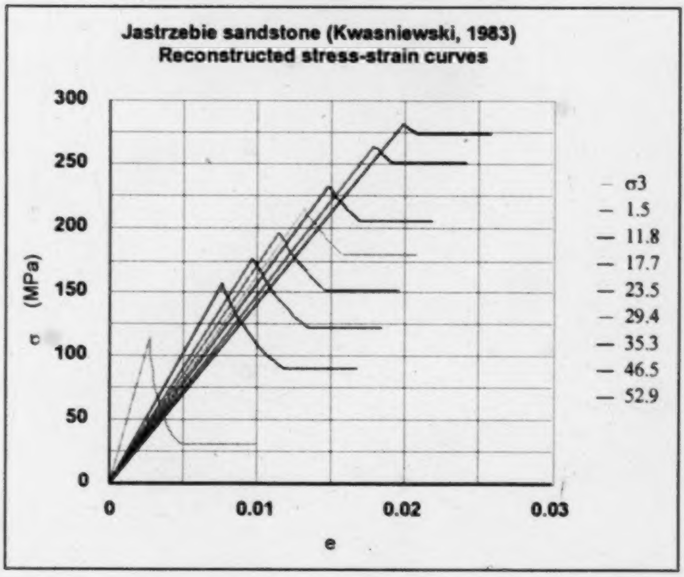
Jastrzebie sandstone (Kwasniewski, 1983)
Reconstructed stress-strain curves

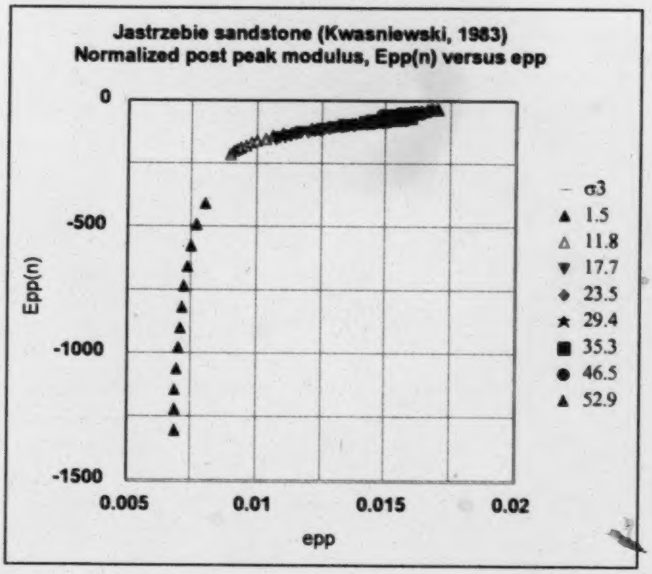

Criterion	Parameters			
Hoek-Brown peak strength	m	σ_c (MPa)	s	a
$\sigma_{1p} = \sigma_3 + \sigma_c\{m\sigma_3/\sigma_c + s\}^a$	7.0	110	1	0.5
Residual strength	D	F	σ_{cr} (MPa)	
$\sigma_{1r} = D\sigma_3^2 + F\sigma_3 + \sigma_{cr}$	-0.03	6.1	22	
Base strength & transition point	ϕ_b (deg.)	σ_{3t} (MPa)	σ_{1t} (MPa)	
$\sigma_{1b} = \{(1+\sin\phi_b)/(1-\sin\phi_b)\}\sigma_3$	40	72	331	
Friction-strain and base strain	R (deg.)	S	T	e_b
$\phi_c = R + Se_{pp} + Te_{pp}^2$	68.5	-2200	42500	0.03

Appendix K.20

Intact medium grained Pinowek sandstone (Kwasniewski, 1983)

σ_3 data (MPa)	σ_{1p} data (MPa)	e_p data (strain)
0	84	0.005
11	163	0.010
21	243	0.009
31	249	0.013
32	206	0.013
41	243	0.013
52	309	0.015
60	328	0.015

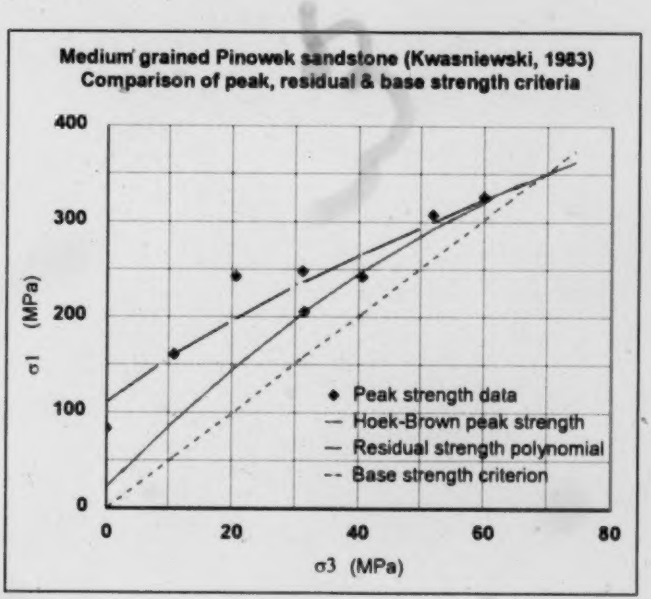

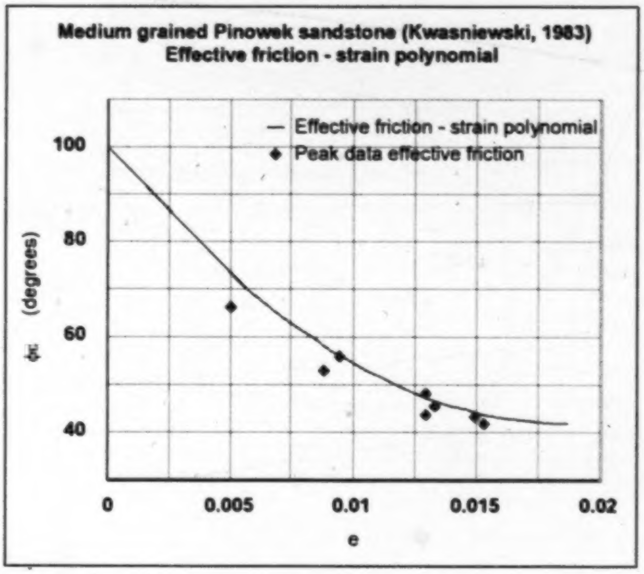

Medium grained Pinowek sandstone (Kwasniewski, 1983)
Effective friction - strain polynomial

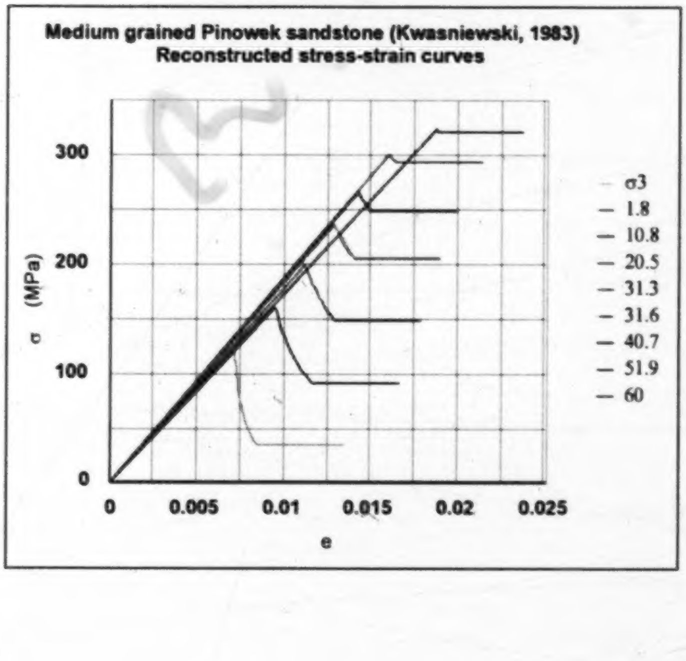

Medium grained Pinowek sandstone (Kwasniewski, 1983)
Reconstructed stress-strain curves

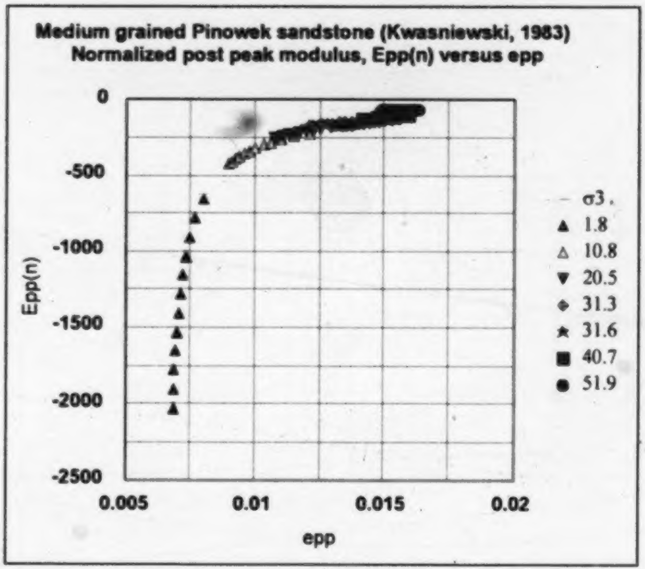

Criterion	Parameters			
Hoek-Brown peak strength	m	σ_c (MPa)	s	a
$\sigma_{1p} = \sigma_3 + \sigma_c\{m\sigma_3/\sigma_c + s\}^a$	8.6	111	1	0.5
Residual strength	D	F	σ_{cr} (MPa)	
$\sigma_{1r} = D\sigma_3^2 + F\sigma_3 + \sigma_{cr}$	-0.03	6.7	22	
Base strength & transition point	ϕ_b (deg.)	σ_{3t} (MPa)	σ_{1t} (MPa)	
$\sigma_{1b} = \{(1+\sin\phi_b)/(1-\sin\phi_b)\}\sigma_3$	42	69	350	
Friction-strain and base strain	R (deg.)	S	T	e_b
$\phi_c = R + Se_{pp} + Te_{pp}^2$	100	-6210	166000	0.02

Appendix K.21

Intact fine grained Pinowek sandstone (Kwasniewski, 1983)

σ_3 data (MPa)	σ_{1p} data (MPa)	e_p data (strain)
0	81	0.006
11	161	0.009
20	211	0.011
30	258	0.010
41	258	0.014
44	306	0.016
50	322	0.015
61	339	0.019

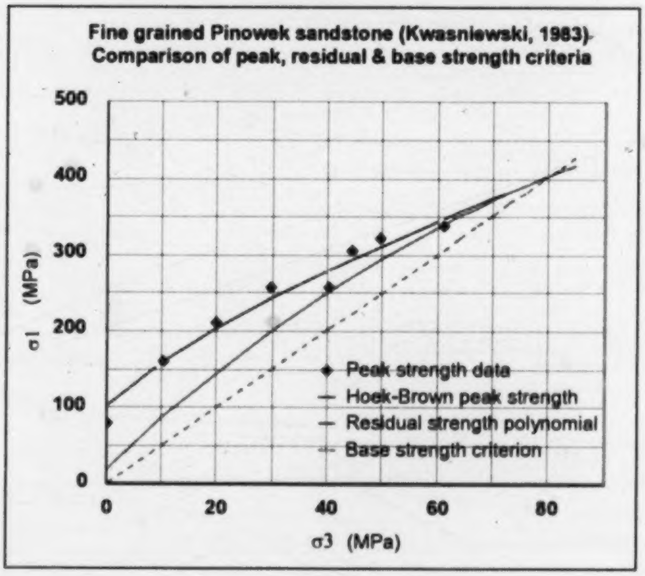

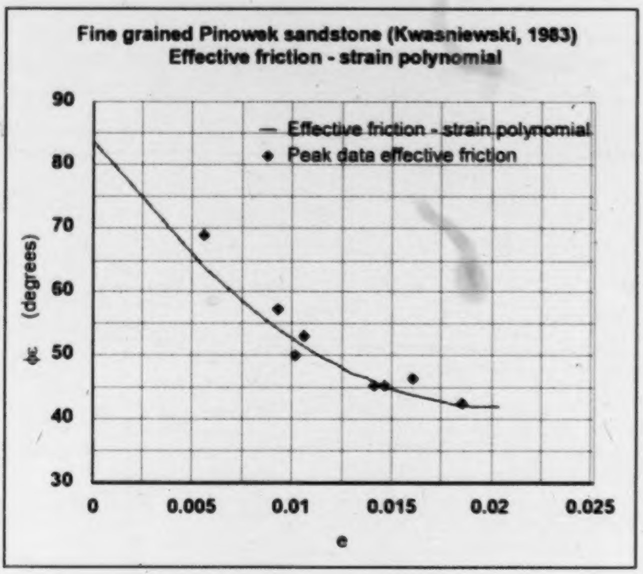
Fine grained Pinowek sandstone (Kwasniewski, 1983)
Effective friction - strain polynomial
Effective friction - strain polynomial
Peak data effective friction
φc (degrees)
90
80
70
60
50
40
30
0
0.005
0.01
0.015
0.02
0.025
e

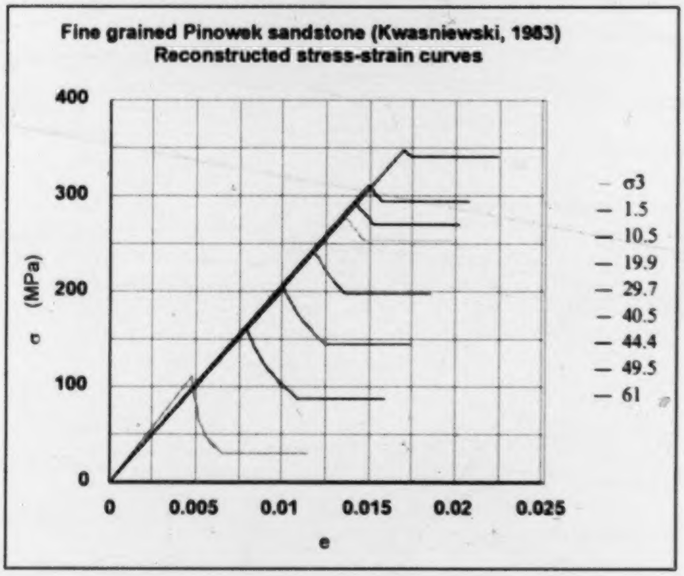
Fine grained Pinowek sandstone (Kwasniewski, 1983)
Reconstructed stress-strain curves
σ (MPa)
400
300
200
100
0
0
0.005
0.01
0.015
0.02
0.025
e
σ3
1.5
10.5
19.9
29.7
40.5
44.4
49.5
61

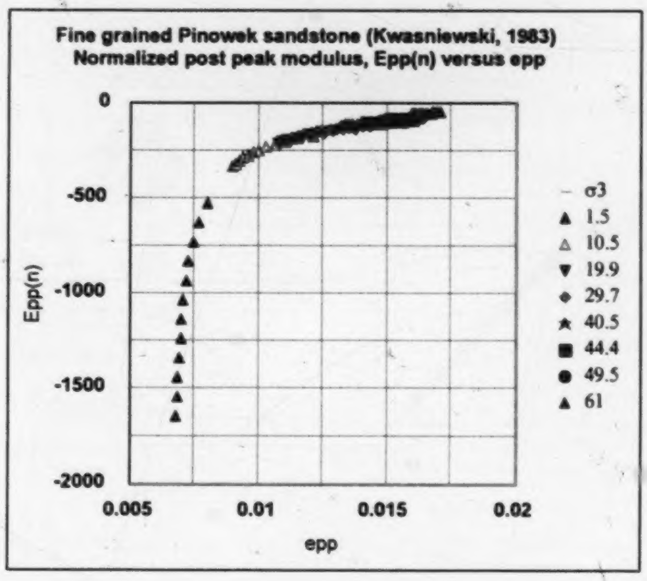

Criterion	Parameters			
Hoek-Brown peak strength	m	σ_c (MPa)	s	a
$\sigma_{1p} = \sigma_3 + \sigma_c\{m\sigma_3/\sigma_c + s\}^a$	11.5	102	1	0.5
Residual strength	D	F	σ_{cr} (MPa)	
$\sigma_{1r} = D\sigma_3^2 + F\sigma_3 + \sigma_{cr}$	-0.03	6.8	20	
Base strength & transition point	ϕ_b (deg.)	σ_{3t} (MPa)	σ_{1t} (MPa)	
$\sigma_{1b} = \{(1+\sin\phi_b)/(1-\sin\phi_b)\}\sigma_3$	42	80	404	
Friction-strain and base strain	R (deg.)	S	T	e_b
$\phi_e = R + Se_{pp} + Te_{pp}^2$	84	-4080	99900	0.02

Appendix K.22

Intact Inada granite (Mogi, 1964)

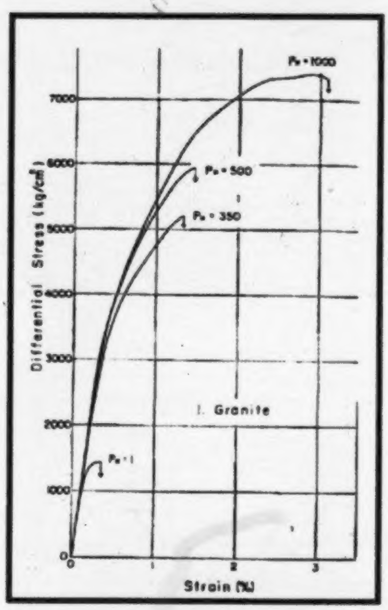

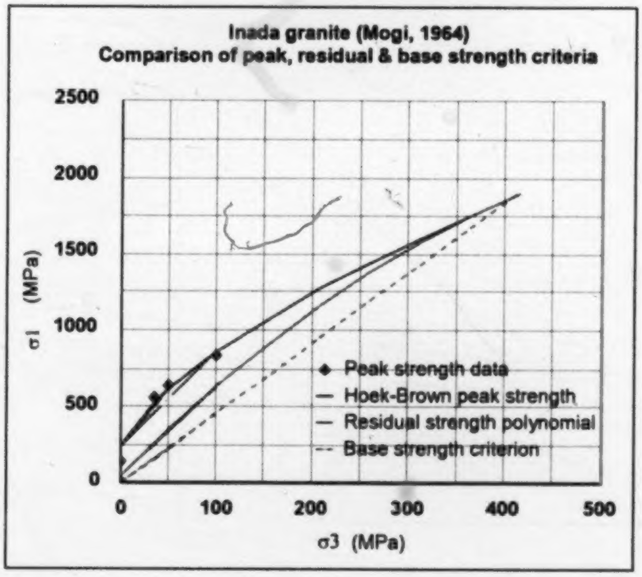

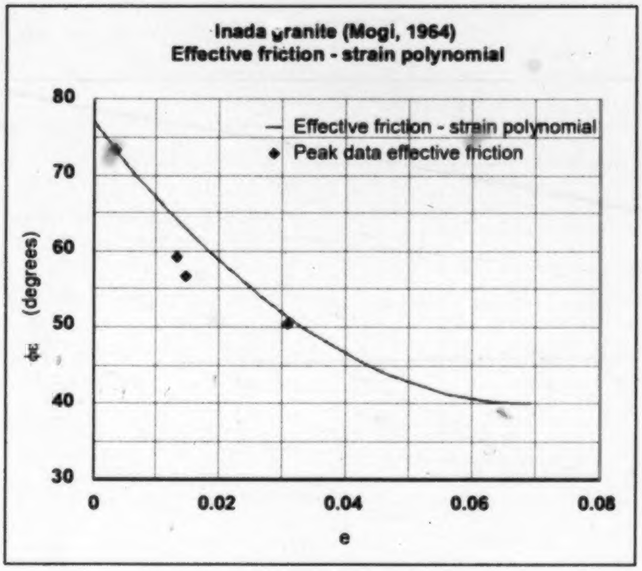
Inada granite (Mogi, 1964)
Effective friction - strain polynomial
Effective friction - strain polynomial
Peak data effective friction
φc (degrees)
80
70
60
50
40
30
0
0.02
0.04
0.06
0.08
e

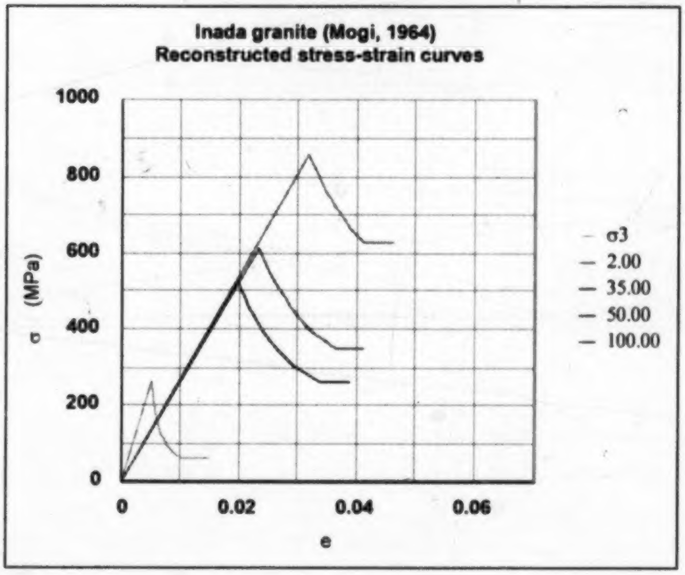
Inada granite (Mogi, 1964)
Reconstructed stress-strain curves
σ (MPa)
1000
800
600
400
200
0
0
0.02
0.04
0.06
e
σ3
2.00
35.00
50.00
100.00

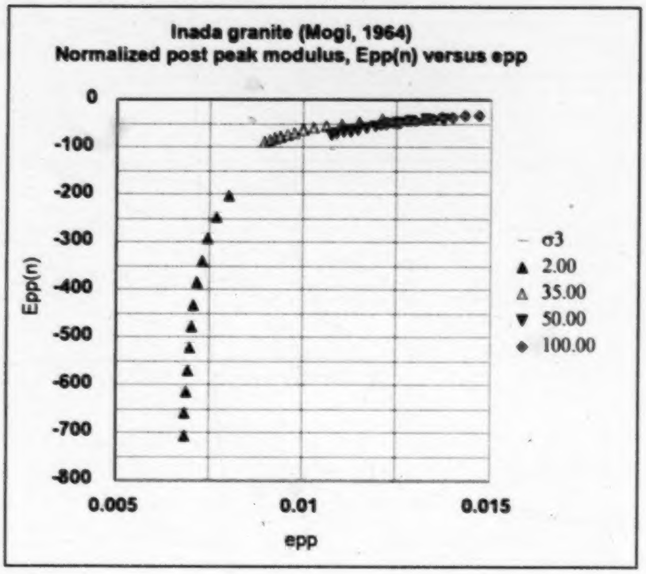

Criterion	Parameters			
Hoek-Brown peak strength	m	σ_c (MPa)	s	a
$\sigma_{1p} = \sigma_3 + \sigma_c\{m\sigma_3/\sigma_c + s\}^a$	21.3	244	1	0.5
Residual strength	D	F	σ_{cr} (MPa)	
$\sigma_{1r} = D\sigma_3^2 + F\sigma_3 + \sigma_{cr}$	-0.004	6.2	49	
Base strength & transition point	ϕ_b (deg.)	σ_{3t} (MPa)	σ_{1t} (MPa)	
$\sigma_{1b} = \{(1+\sin\phi_b)/(1-\sin\phi_b)\}\sigma_3$	40	411	1890	
Friction-strain and base strain	R (deg.)	S	T	e_b
$\phi_e = R + Se_{pp} + Te_{pp}^2$	77	-1070	7740	0.07

Appendix K.23

Intact Nabe-ishi peridotite (Mogi, 1965)

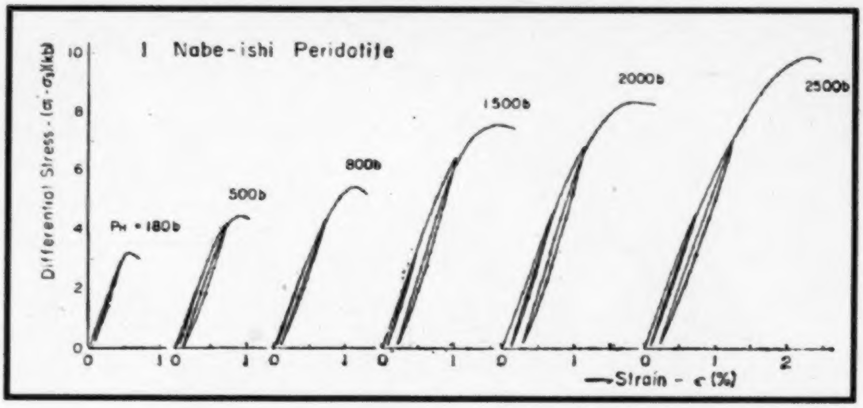

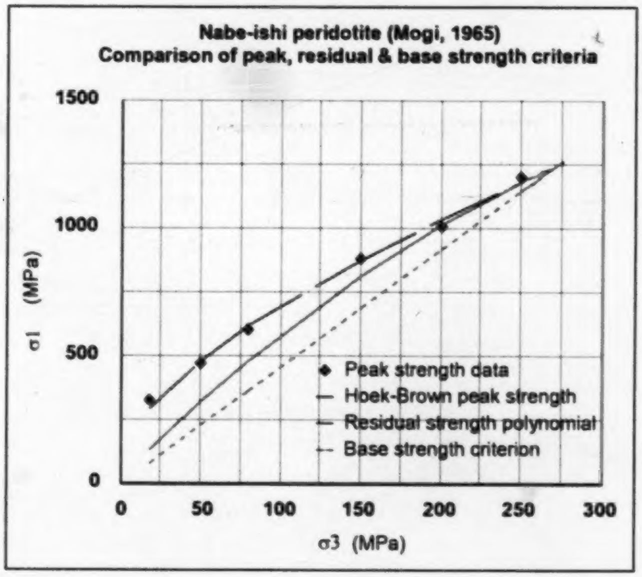

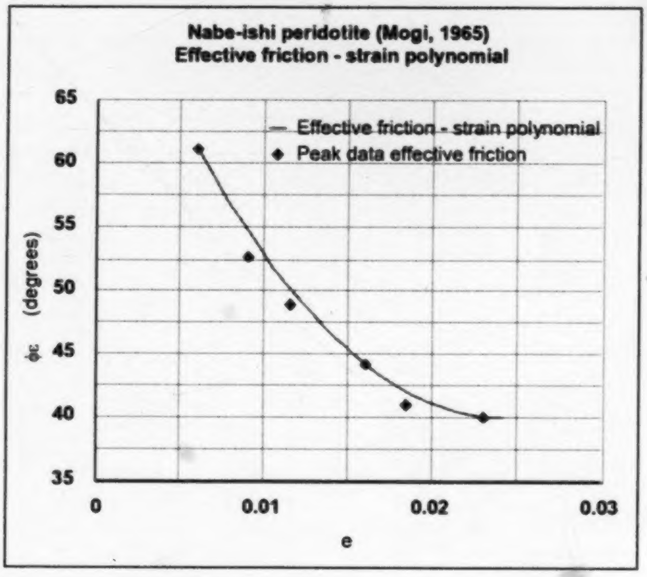
Nabe-ishi peridotite (Mogi, 1965)
Effective friction - strain polynomial
Effective friction - strain polynomial
Peak data effective friction
φc (degrees)
65
60
55
50
45
40
35
0
0.01
0.02
0.03
e

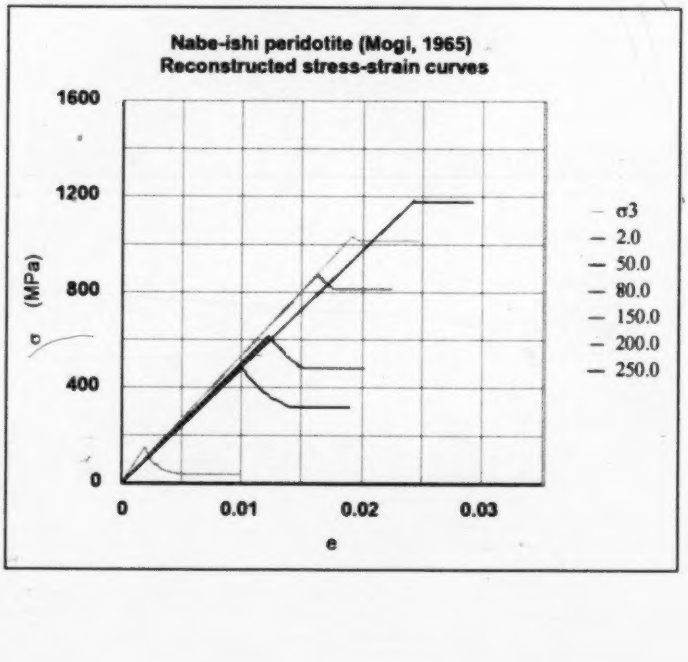
Nabe-ishi peridotite (Mogi, 1965)
Reconstructed stress-strain curves
σ (MPa)
1600
1200
800
400
0
0
0.01
0.02
0.03
e
σ3
2.0
50.0
80.0
150.0
200.0
250.0

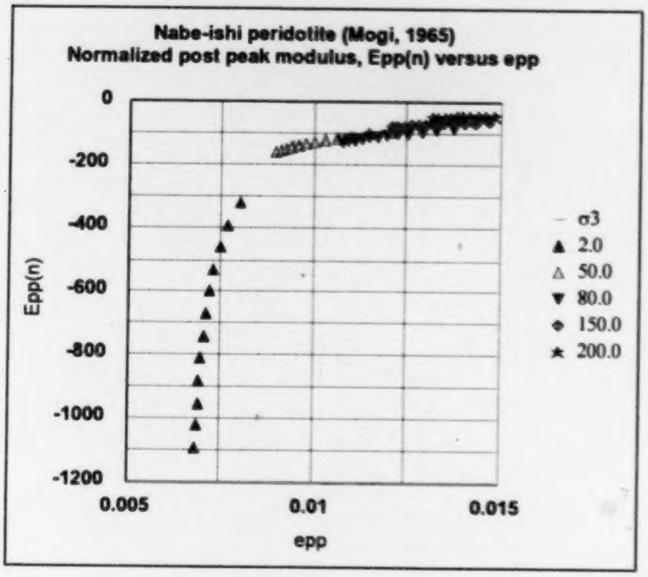

Criterion	Parameters			
Hoek-Brown peak strength	m	σ_c (MPa)	s	a
$\sigma_{1p} = \sigma_3 + \sigma_c\{m\sigma_3/\sigma_c + s\}^a$	27.4	126	1	0.5
Residual strength	D	F	σ_{cr} (MPa)	
$\sigma_{1r} = D\sigma_3^2 + F\sigma_3 + \sigma_{cr}$	-0.006	6.2	25	
Base strength & transition point	ϕ_b (deg.)	σ_{3t} (MPa)	σ_{1t} (MPa)	
$\sigma_{1b} = \{(1+\sin\phi_b)/(1-\sin\phi_b)\}\sigma_3$	40	271	1250	
Friction-strain and base strain	R (deg.)	S	T	e_b
$\phi_c = R + Se_{pp} + Te_{pp}^2$	77.5	-3100	63900	0.024

Appendix K.24

Intact Orikabe diorite (Mogi, 1965)

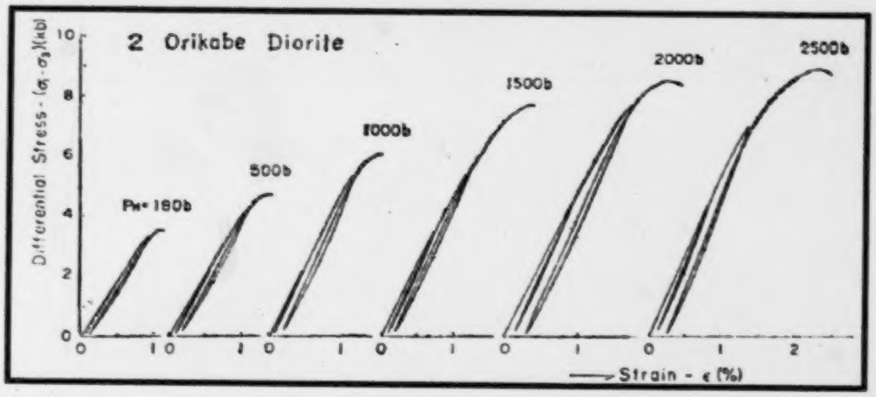

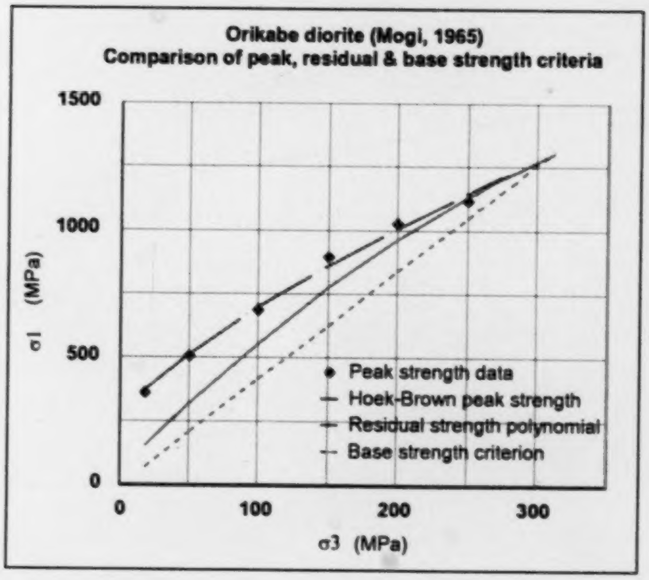

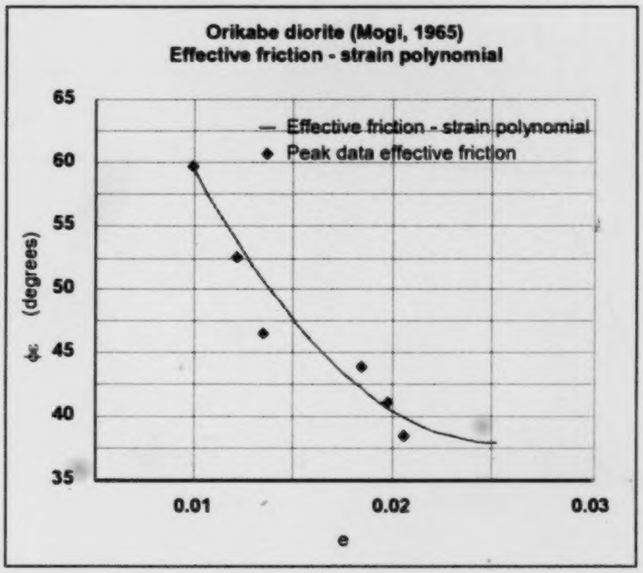
Orikabe diorite (Mogi, 1965)
Effective friction - strain polynomial
65
60
55
50
45
40
35
ϕc (degrees)
0.01
0.02
0.03
e
Effective friction - strain polynomial
Peak data effective friction

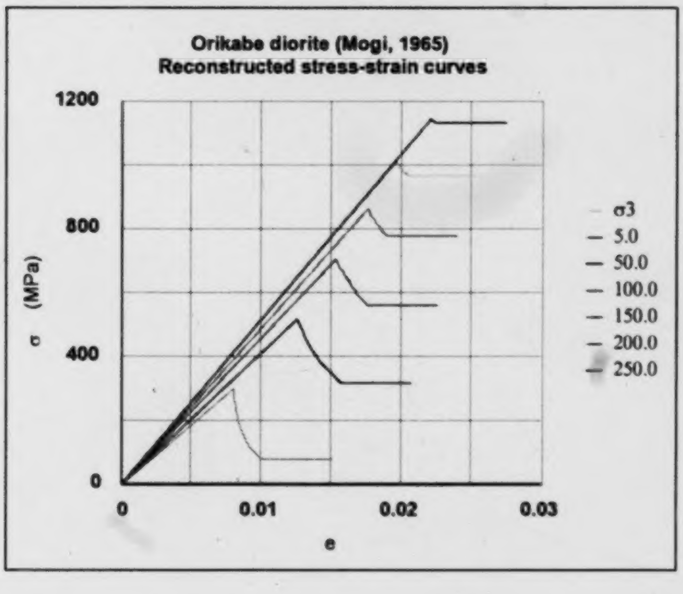
Orikabe diorite (Mogi, 1965)
Reconstructed stress-strain curves
1200
800
400
0
σ (MPa)
0
0.01
0.02
0.03
e
σ3
5.0
50.0
100.0
150.0
200.0
250.0

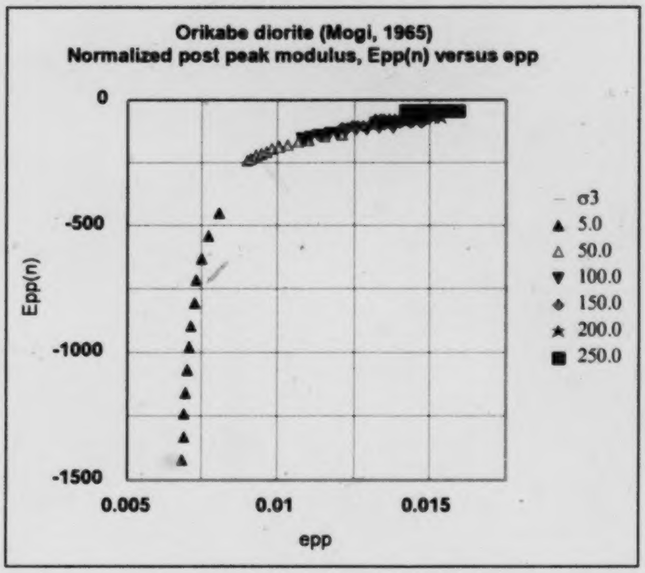

Criterion	Parameters			
Hoek-Brown peak strength	m	σ_c (MPa)	s	a
$\sigma_{1p} = \sigma_3 + \sigma_c\{m\sigma_3/\sigma_c + s\}^a$	10.7	274	1	0.5
Residual strength	D	F	σ_{cr} (MPa)	
$\sigma_{1r} = D\sigma_3^2 + F\sigma_3 + \sigma_{cr}$	-0.005	5.6	55	
Base strength & transition point	ϕ_b (deg.)	σ_{3t} (MPa)	σ_{1t} (MPa)	
$\sigma_{1b} = \{(1+\sin\phi_b)/(1-\sin\phi_b)\}\sigma_3$	38	308	1300	
Friction-strain and base strain	R (deg.)	S	T	e_b
$\phi_e = R + Se_{pp} + Te_{pp}^2$	97	-4670	92700	0.025

Appendix K.25

Intact Shirochoba andesite (Mogi, 1964)

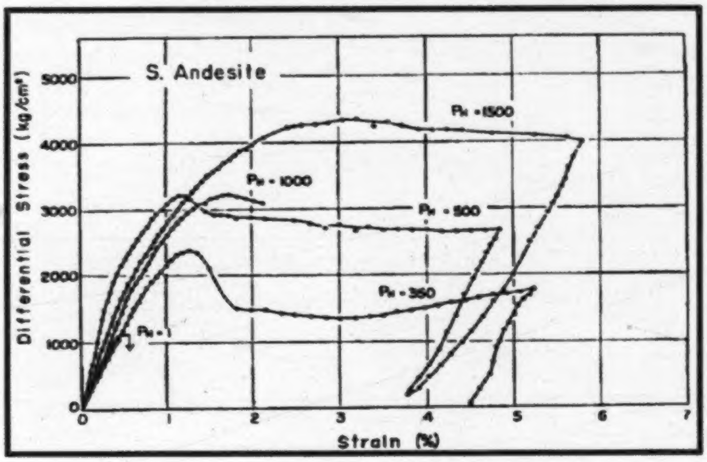

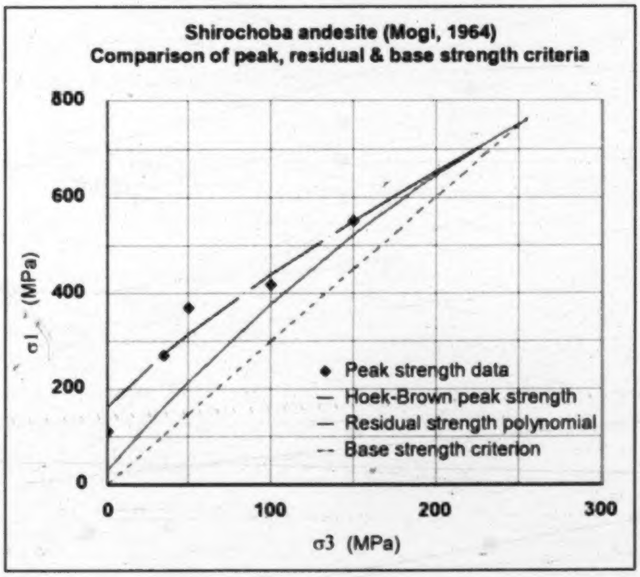

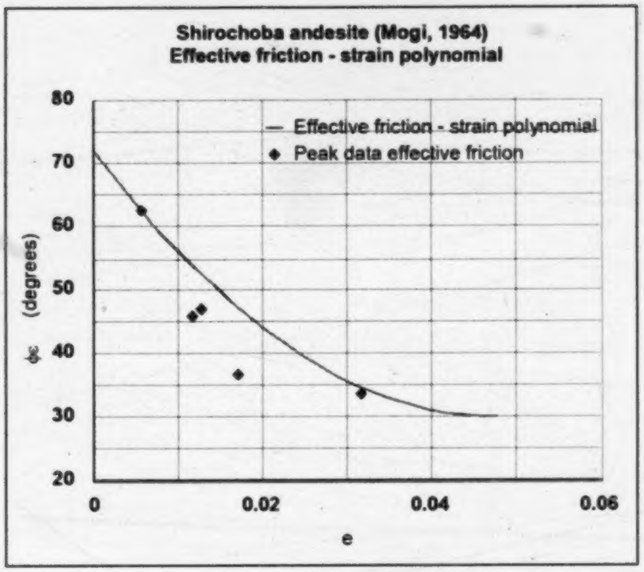

Shirochoba andesite (Mogi, 1964)
Effective friction - strain polynomial

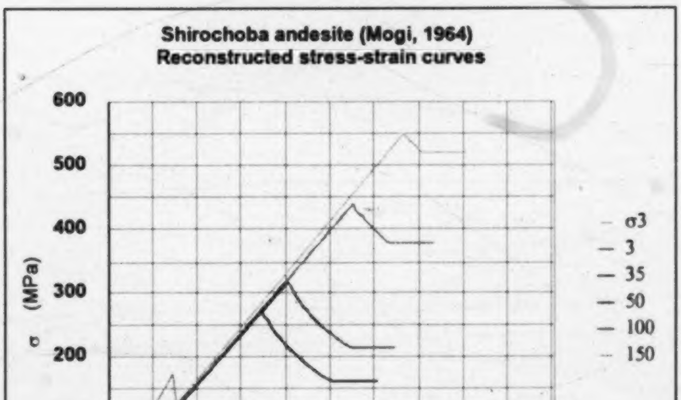

Shirochoba andesite (Mogi, 1964)
Reconstructed stress-strain curves

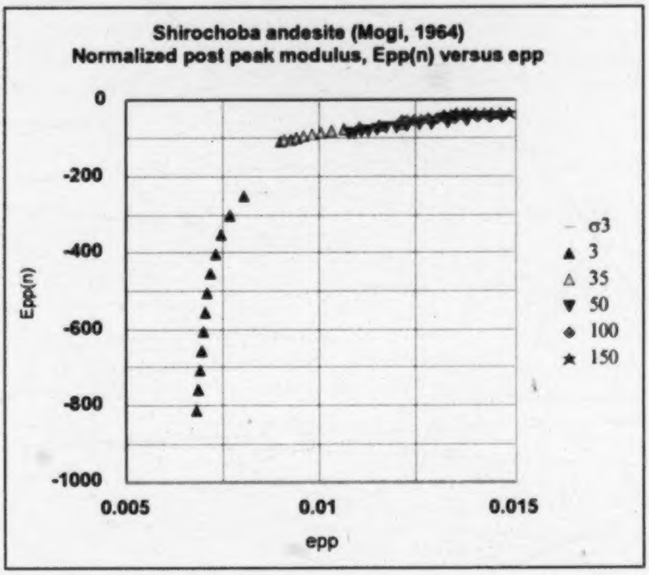

Criterion	Parameters			
Hoek-Brown peak strength	m	σ_c (MPa)	s	a
$\sigma_{1p} = \sigma_3 + \sigma_c\{m\sigma_3/\sigma_c + s\}^a$	5.5	163	1	0.5
Residual strength	D	F	σ_{cr} (MPa)	
$\sigma_{1r} = D\sigma_3^2 + F\sigma_3 + \sigma_{cr}$	-0.004	3.8	33	
Base strength & transition point	ϕ_b (deg.)	σ_{3t} (MPa)	σ_{1t} (MPa)	
$\sigma_{1b} = \{(1+\sin\phi_b)/(1-\sin\phi_b)\}\sigma_3$	30	250	751	
Friction-strain and base strain	R (deg.)	S	T	e_b
$\phi_e = R + Se_{pp} + Te_{pp}^2$	72	-1760	18500	0.05

Appendix K.26

Intact Ukigane diorite (Mogi, 1964)

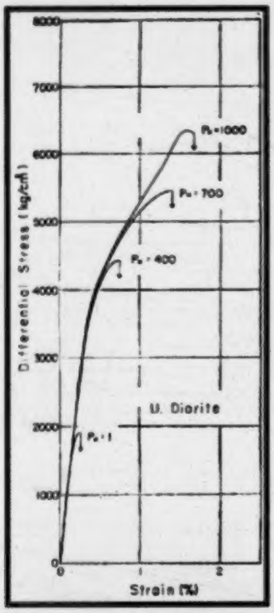

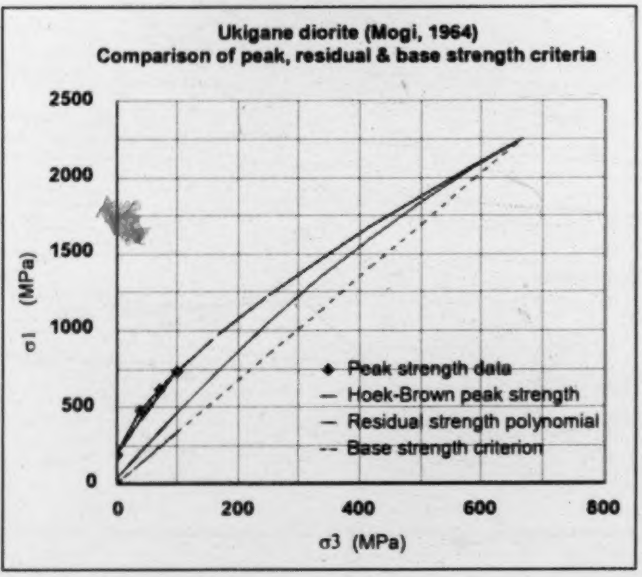

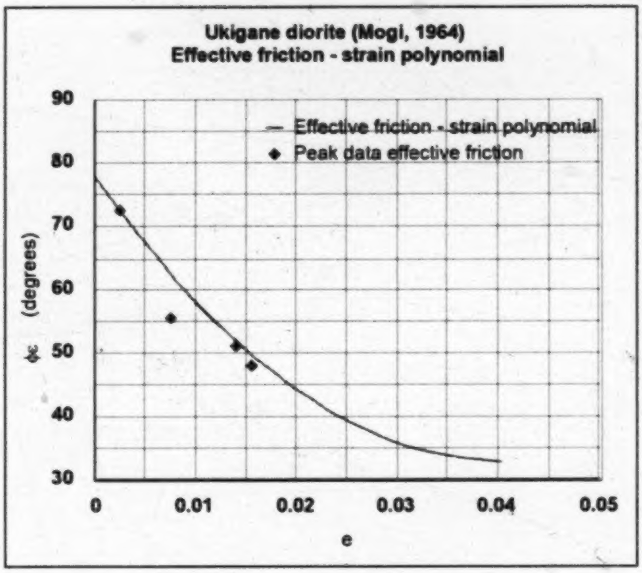
Ukigane diorite (Mogi, 1964)
Effective friction - strain polynomial
— Effective friction - strain polynomial
◆ Peak data effective friction
ϕc (degrees)
90
80
70
60
50
40
30
0
0.01
0.02
0.03
0.04
0.05
e

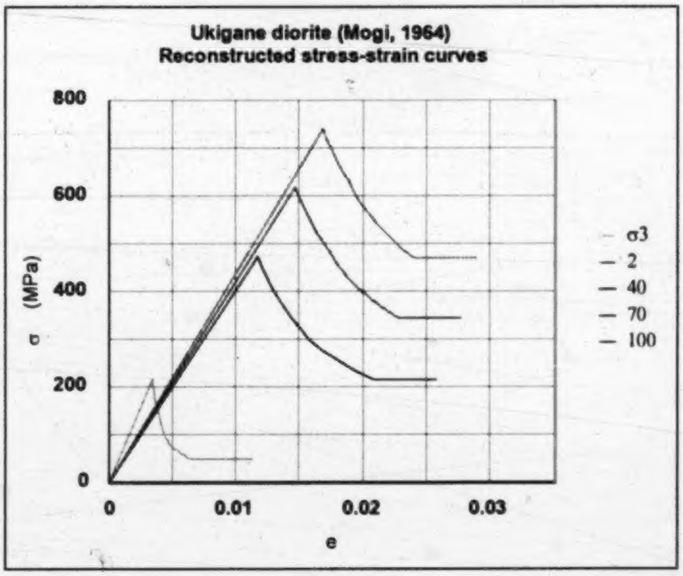
Ukigane diorite (Mogi, 1964)
Reconstructed stress-strain curves
σ (MPa)
800
600
400
200
0
0
0.01
0.02
0.03
e
σ3
2
40
70
100

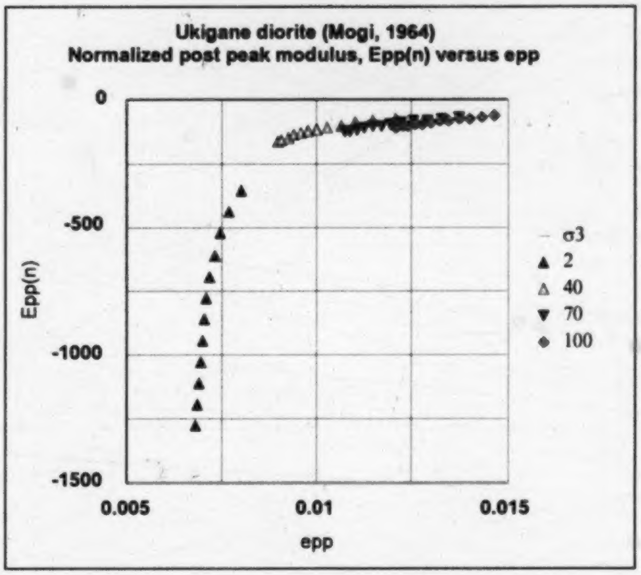

Criterion	Parameters			
Hoek-Brown peak strength	m	σ_c (MPa)	s	a
$\sigma_{1p} = \sigma_3 + \sigma_c\{m\sigma_3/\sigma_c + s\}^a$	18.6	201	1	0.5
Residual strength	D	F	σ_{cr} (MPa)	
$\sigma_{1r} = D\sigma_3^2 + F\sigma_3 + \sigma_{cr}$	-0.002	4.5	40	
Base strength & transition point	ϕ_b (deg.)	σ_{3t} (MPa)	σ_{1t} (MPa)	
$\sigma_{1b} = \{(1+\sin\phi_b)/(1-\sin\phi_b)\}\sigma_3$	33	662	2250	
Friction-strain and base strain	R (deg.)	S	T	e_b
$\phi_e = R + Se_{pp} + Te_{pp}^2$	78	-2230	27600	0.04

Appendix K.27

Intact carboniferous sandstone (Santarelli et al., 1989)

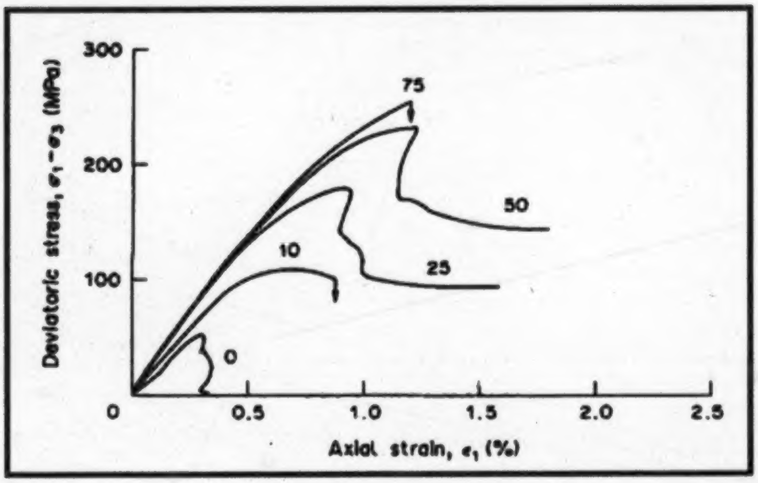

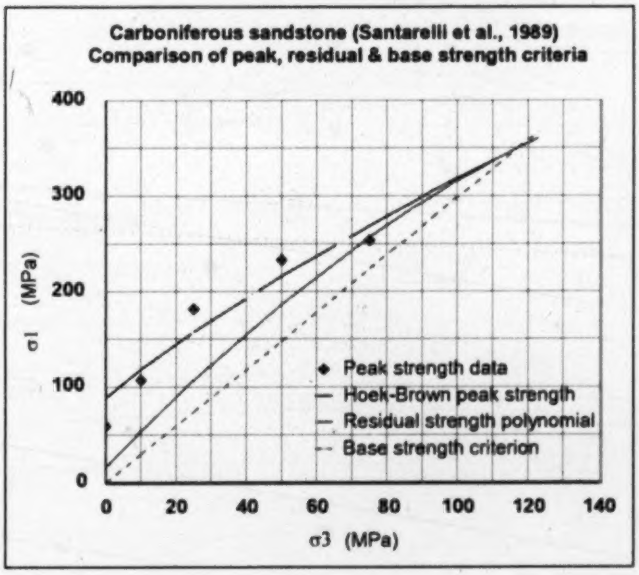

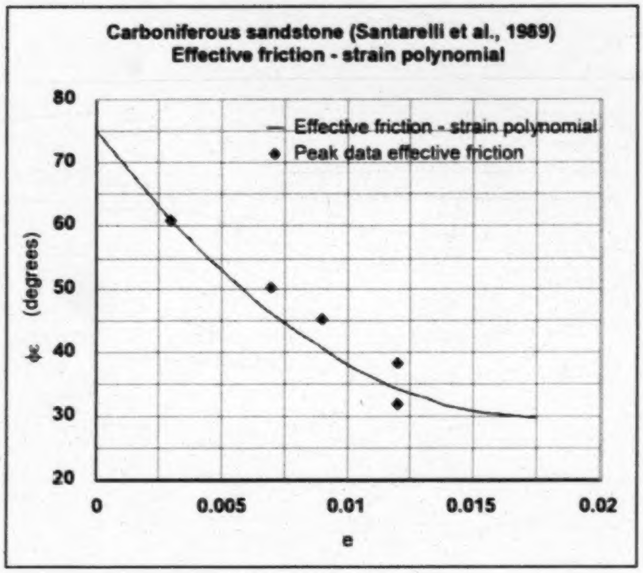

Carboniferous sandstone (Santarelli et al., 1989)
Effective friction - strain polynomial

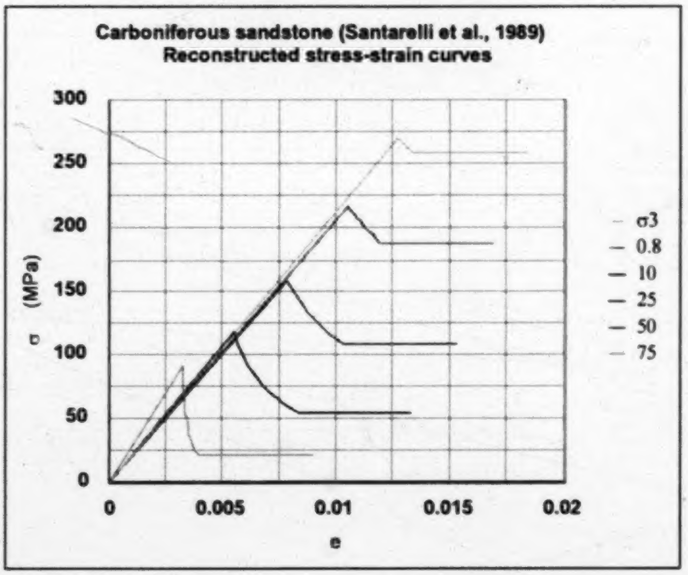

Carboniferous sandstone (Santarelli et al., 1989)
Reconstructed stress-strain curves

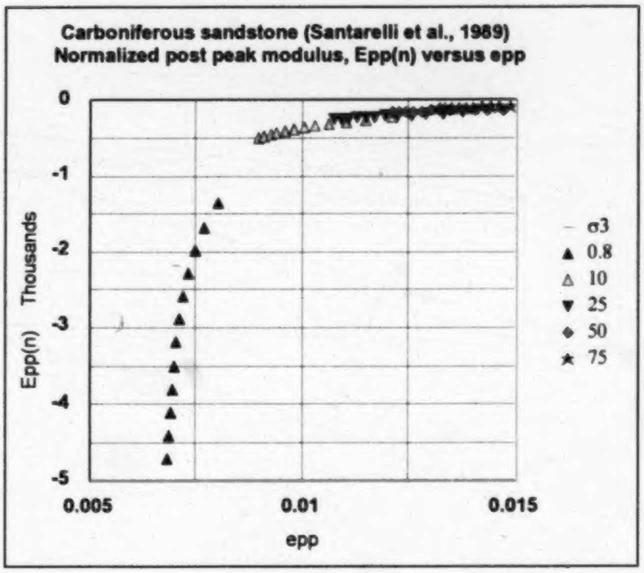

Criterion	Parameters			
Hoek-Brown peak strength	m	σ_c (MPa)	s	a
$\sigma_{1p} = \sigma_3 + \sigma_c\{m\sigma_3/\sigma_c + s\}^a$	4.5	89	1	0.5
Residual strength	D	F	σ_{cr} (MPa)	
$\sigma_{1r} = D\sigma_3^2 + F\sigma_3 + \sigma_{cr}$	-0.008	3.8	18	
Base strength & transition point	ϕ_b (deg.)	σ_{3t} (MPa)	σ_{1t} (MPa)	
$\sigma_{1b} = \{(1+\sin\phi_b)/(1-\sin\phi_b)\}\sigma_3$	30	118	353	
Friction-strain and base strain	R (deg.)	S	T	e_b
$\phi_c = R + Se_{pp} + Te_{pp}^2$	75	-5150	147000	0.02

Appendix K.28

Intact Tennessee marble (Wawersik et al., 1970)

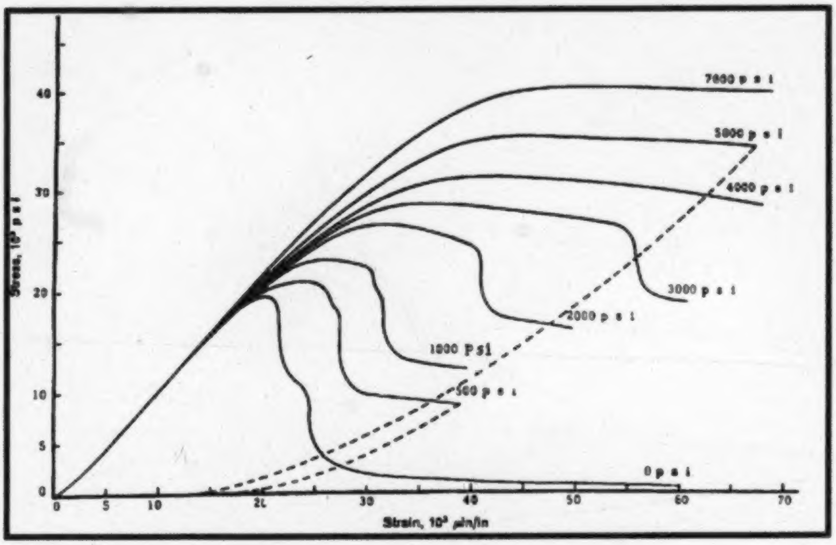

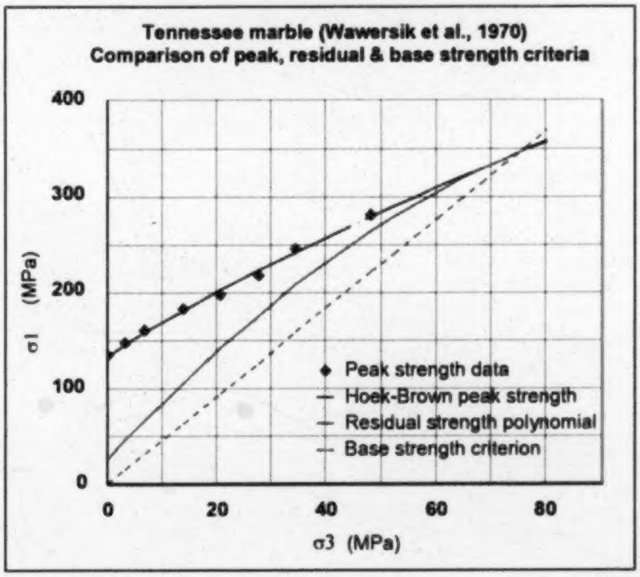
Tennessee marble (Wawersik et al., 1970)
Comparison of peak, residual & base strength criteria

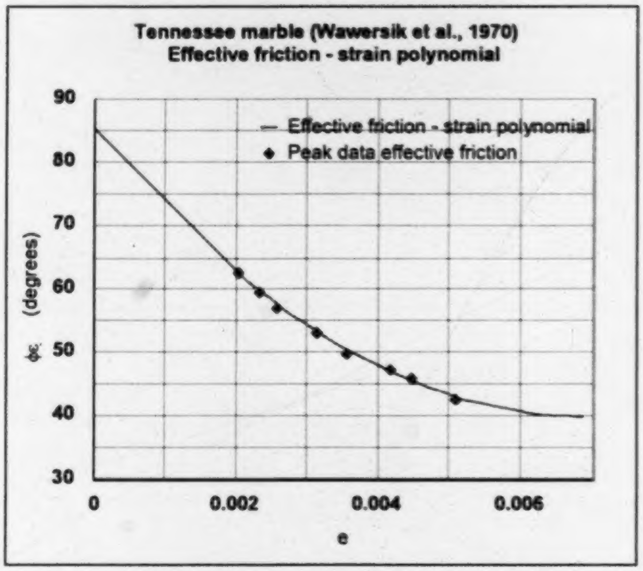

Tennessee marble (Wawersik et al., 1970)
Effective friction - strain polynomial

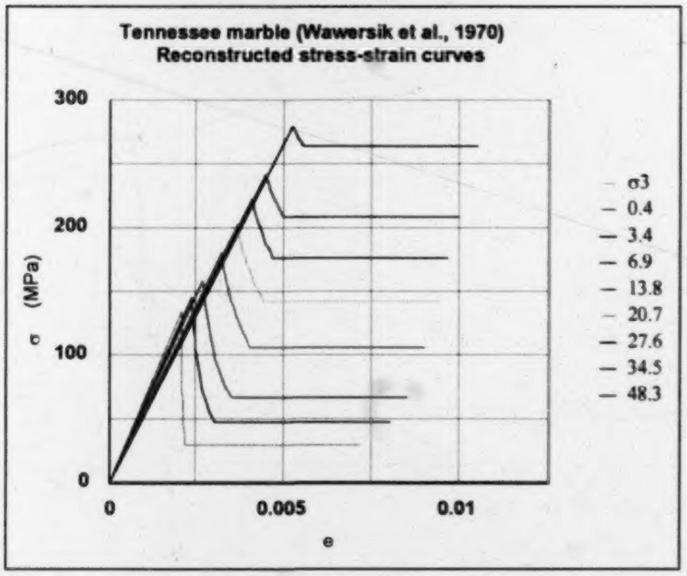

Tennessee marble (Wawersik et al., 1970)
Reconstructed stress-strain curves

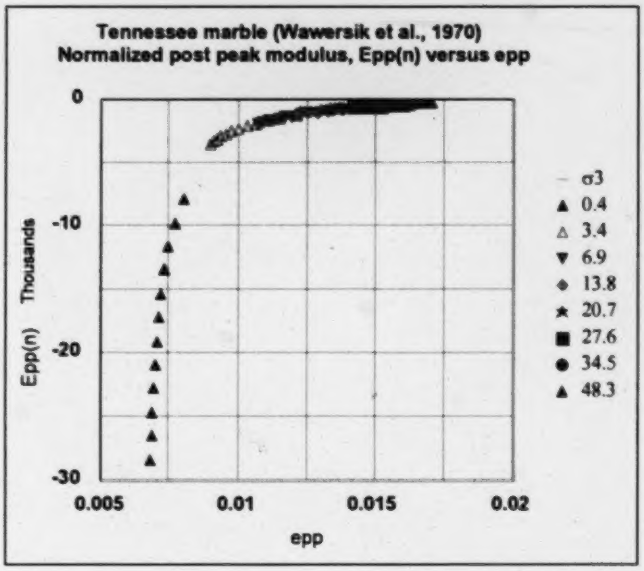

Criterion	Parameters			
Hoek-Brown peak strength	m	σ_c (MPa)	s	a
$\sigma_{1p} = \sigma_3 + \sigma_c\{m\sigma_3/\sigma_c + s\}^a$	5.5	134	1	0.5
Residual strength	D	F	σ_{cr} (MPa)	
$\sigma_{1r} = D\sigma_3^2 + F\sigma_3 + \sigma_{cr}$	-0.03	6.1	27	
Base strength & transition point	ϕ_b (deg.)	σ_{3t} (MPa)	σ_{1t} (MPa)	
$\sigma_{1b} = \{(1+\sin\phi_b)/(1-\sin\phi_b)\}\sigma_3$	40	75	346	
Friction-strain and base strain	R (deg.)	S	T	e_b
$\phi_e = R + Se_{pp} + Te_{pp}^2$	85	-13100	952000	0.007

Appendix K.29

Intact concrete type A (Xie et al., 1995)

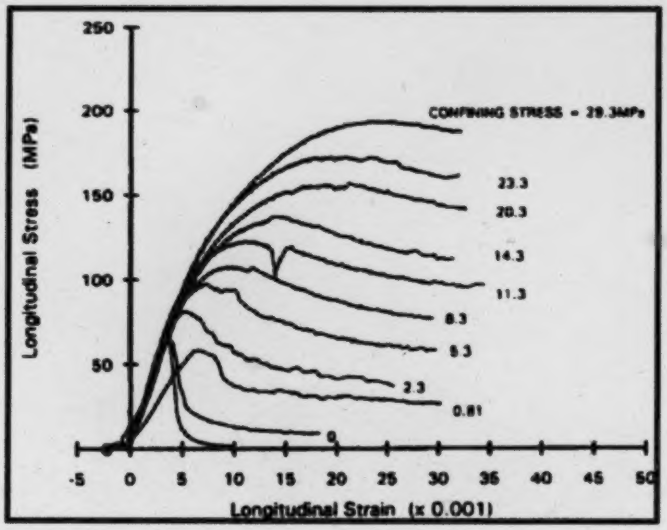

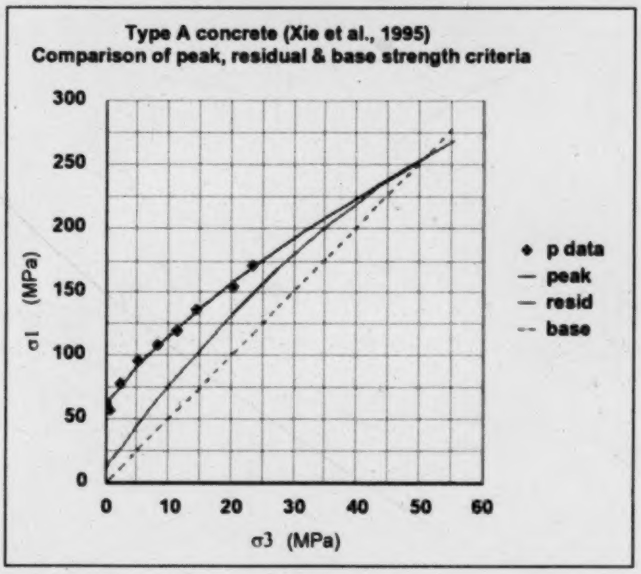

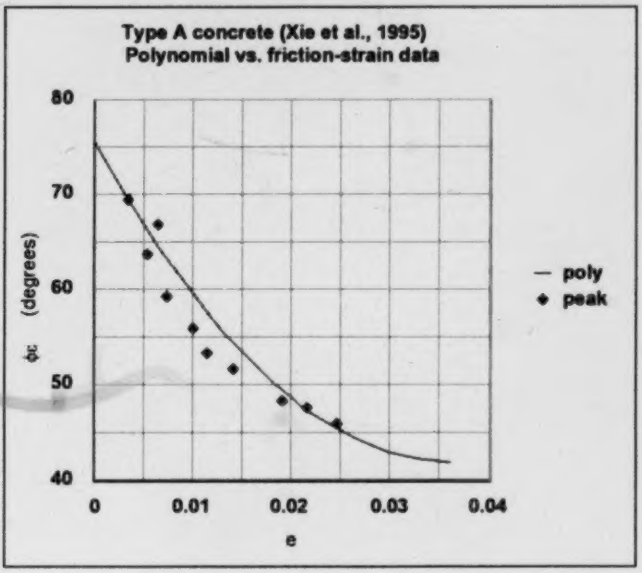
Type A concrete (Xie et al., 1995)
Polynomial vs. friction-strain data
80
70
60
50
40
φc (degrees)
0
0.01
0.02
0.03
0.04
e
— poly
◆ peak

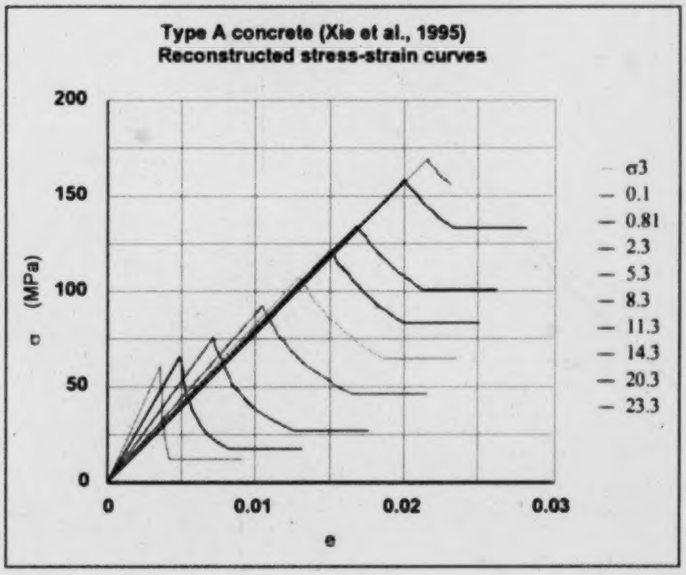
Type A concrete (Xie et al., 1995)
Reconstructed stress-strain curves
200
150
100
50
0
σ (MPa)
0
0.01
0.02
0.03
e
σ3
— 0.1
— 0.81
— 2.3
— 5.3
— 8.3
— 11.3
— 14.3
— 20.3
— 23.3

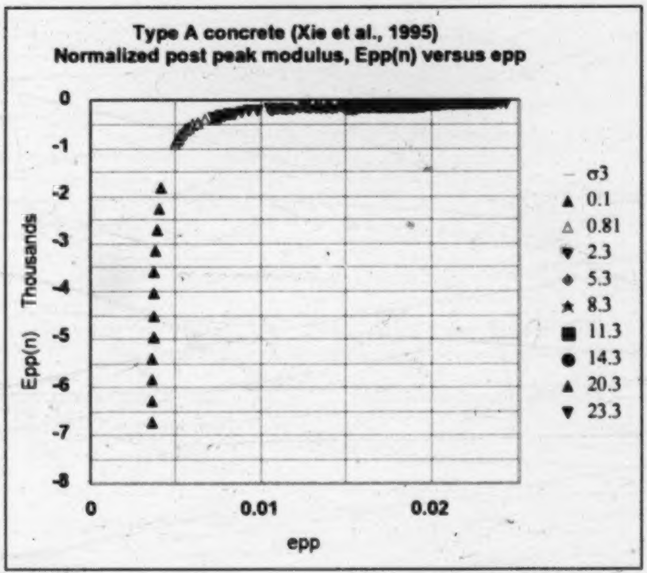

Criterion	Parameters			
Hoek-Brown peak strength	m	σ_c (MPa)	s	a
$\sigma_{1p} = \sigma_3 + \sigma_c\{m\sigma_3/\sigma_c + s\}^a$	12.5	61	1	0.5
Residual strength	D	F	σ_{cr} (MPa)	
$\sigma_{1r} = D\sigma_3^2 + F\sigma_3 + \sigma_{cr}$	-0.04	6.8	12	
Base strength & transition point	ϕ_b (deg.)	σ_{3t} (MPa)	σ_{1t} (MPa)	
$\sigma_{1b} = \{(1+\sin\phi_b)/(1-\sin\phi_b)\}\sigma_3$	42	51	256	
Friction-strain and base strain	R (deg.)	S	T	e_b
$\phi_e = R + Se_{pp} + Te_{pp}^2$	77	-1860	25600	0.04

Appendix K.30

Intact concrete type B (Xie et al., 1995)

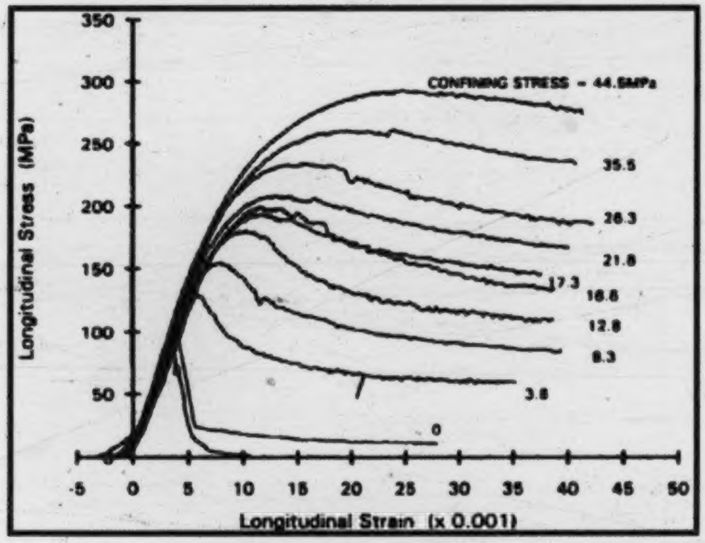

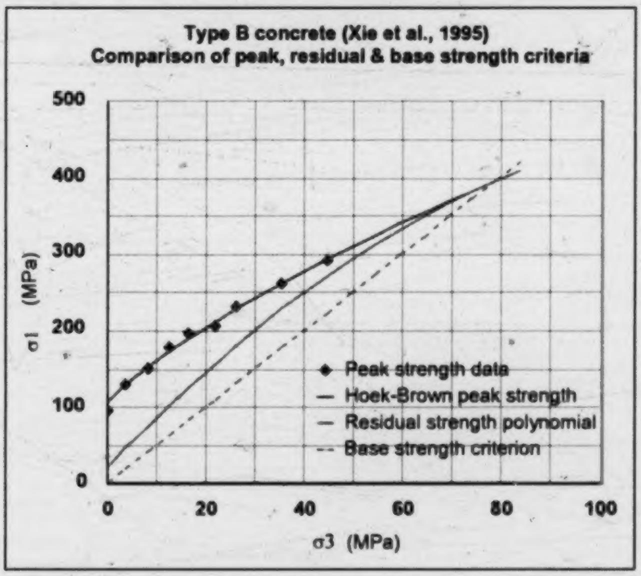
Type B concrete (Xie et al., 1995)
Comparison of peak, residual & base strength criteria

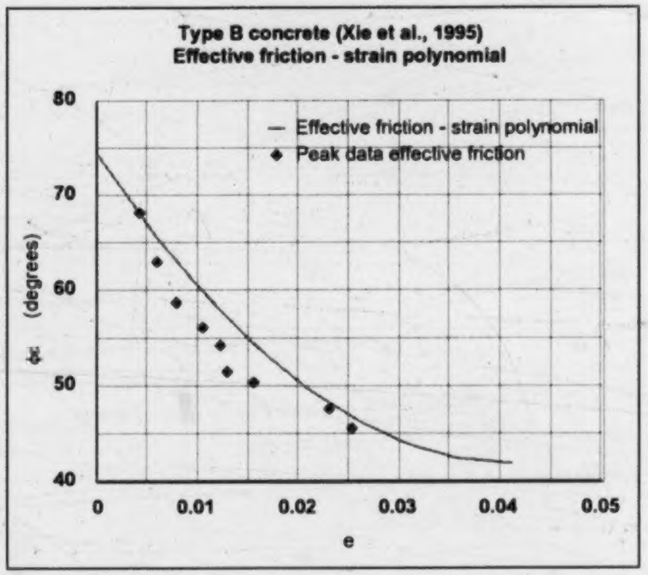
Type B concrete (Xie et al., 1995)
Effective friction - strain polynomial
80
70
60
50
40
φ (degrees)
0
0.01
0.02
0.03
0.04
0.05
e
— Effective friction - strain polynomial
◆ Peak data effective friction

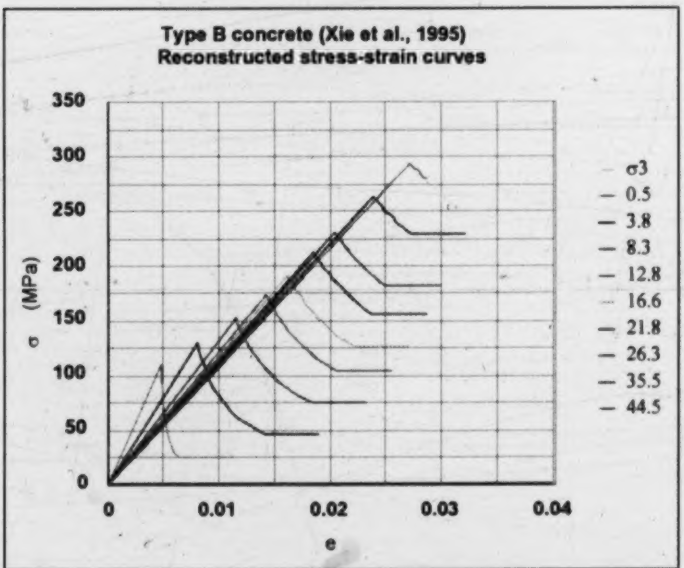
Type B concrete (Xie et al., 1995)
Reconstructed stress-strain curves
350
300
250
200
150
100
50
0
σ (MPa)
0
0.01
0.02
0.03
0.04
e
σ3
— 0.5
— 3.8
— 8.3
— 12.8
— 16.6
— 21.8
— 26.3
— 35.5
— 44.5

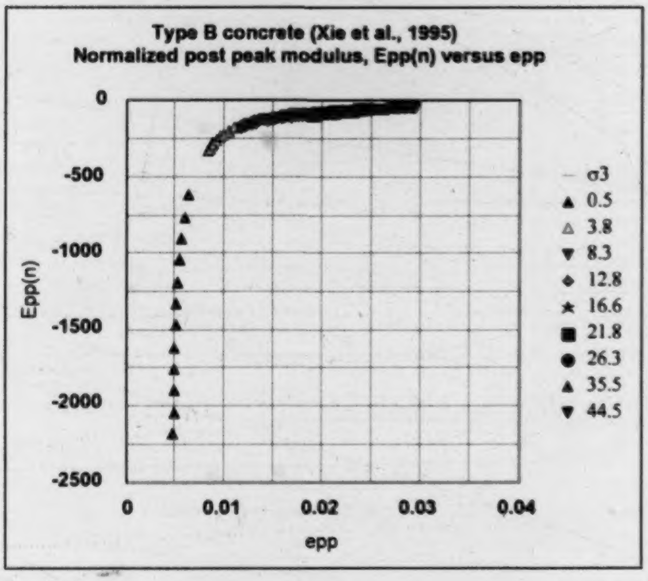

Criterion	Parameters			
Hoek-Brown peak strength $\sigma_{1p} = \sigma_3 + \sigma_c\{m\sigma_3/\sigma_c + s\}^a$	m 10.6	σ_c (MPa) 108	s 1	a 0.5
Residual strength $\sigma_{1r} = D\sigma_3^2 + F\sigma_3 + \sigma_{cr}$	D -0.03	F 6.8	σ_{cr} (MPa) 22	
Base strength & transition point $\sigma_{1b} = \{(1+\sin\phi_b)/(1-\sin\phi_b)\}\sigma_3$	ϕ_b (deg.) 42	σ_{3t} (MPa) 79	σ_{1t} (MPa) 397	
Friction-strain and base strain $\phi_e = R + Se_{pp} + Te_{pp}^2$	R (deg.) 74.5	S -1580	T 19100	e_b 0.04

Appendix K.31

Intact concrete type C (Xie et al., 1995)

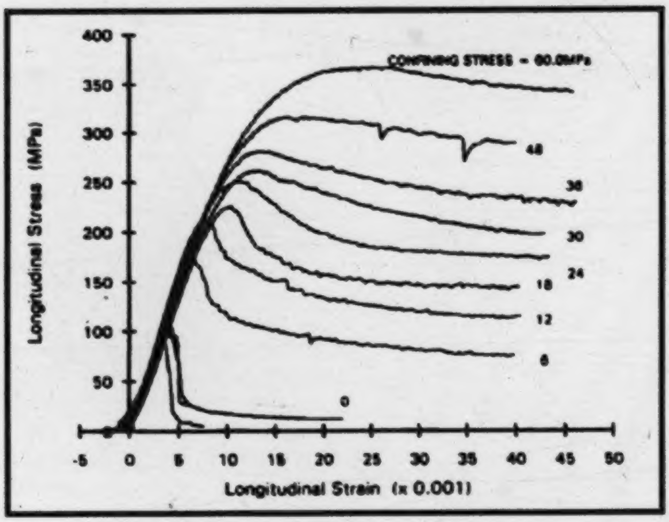

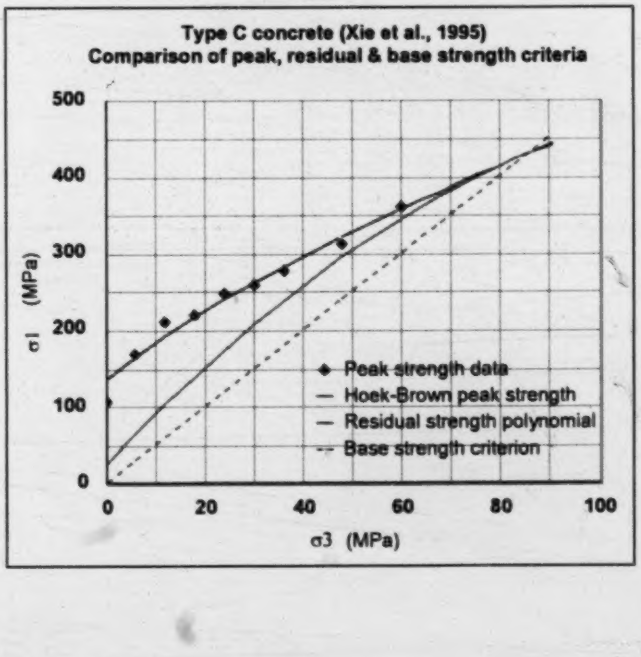

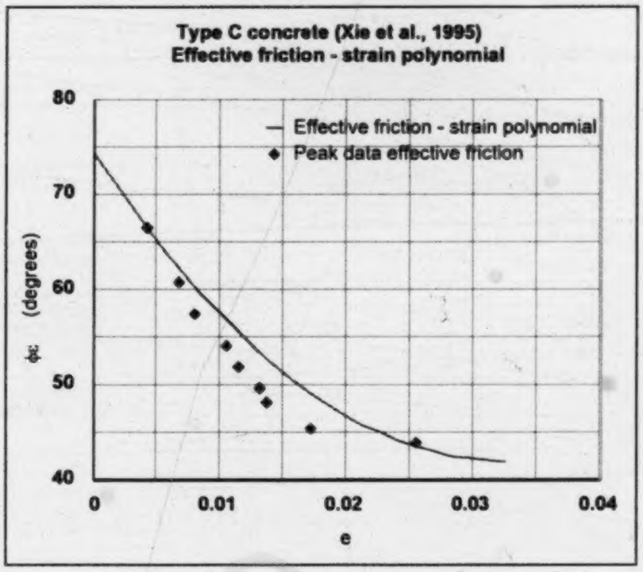

Type C concrete (Xie et al., 1995)
Effective friction - strain polynomial

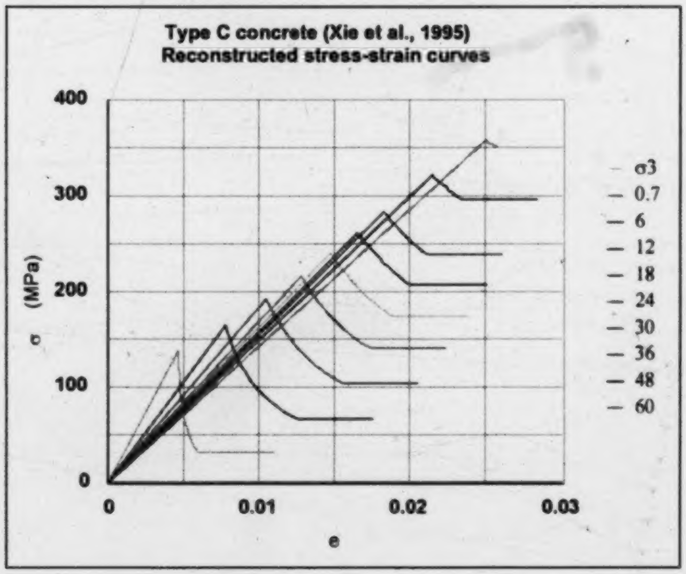

Type C concrete (Xie et al., 1995)
Reconstructed stress-strain curves

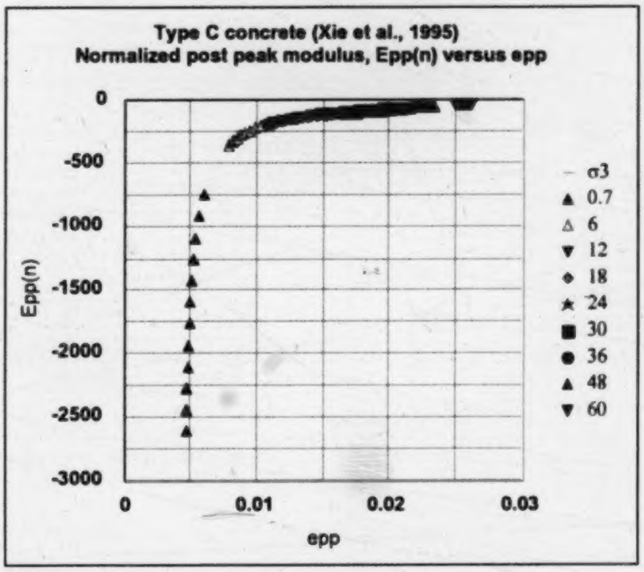

Criterion	Parameters			
Hoek-Brown peak strength	m	σ_c (MPa)	s	a
$\sigma_{1p} = \sigma_3 + \sigma_c\{m\sigma_3/\sigma_c + s\}^a$	8.6	137	1	0.5
Residual strength	D	F	σ_{cr} (MPa)	
$\sigma_{1r} = D\sigma_3^2 + F\sigma_3 + \sigma_{cr}$	-0.02	6.7	27	
Base strength & transition point	ϕ_b (deg.)	σ_{3t} (MPa)	σ_{1t} (MPa)	
$\sigma_{1b} = \{(1+\sin\phi_b)/(1-\sin\phi_b)\}\sigma_3$	42	85.5	431	
Friction-strain and base strain	R (deg.)	S	T	e_b
$\phi_e = R + Se_{pp} + Te_{pp}^2$	74	-1980	30200	0.03

Appendix K.32

Intact tuffaceous sandstone (Yoshinaka et al., 1980)

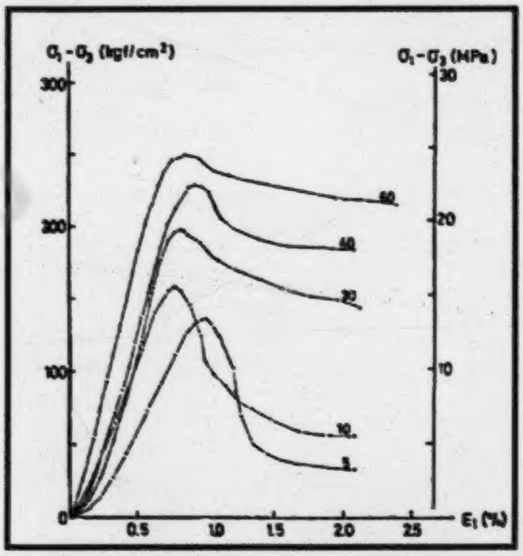

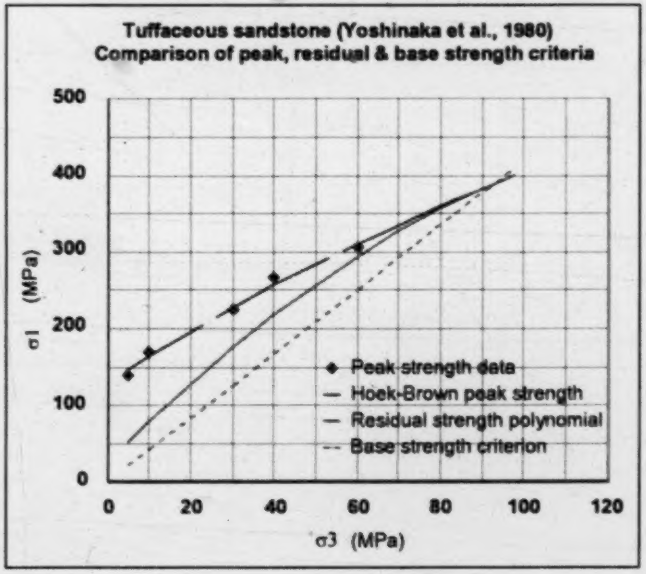

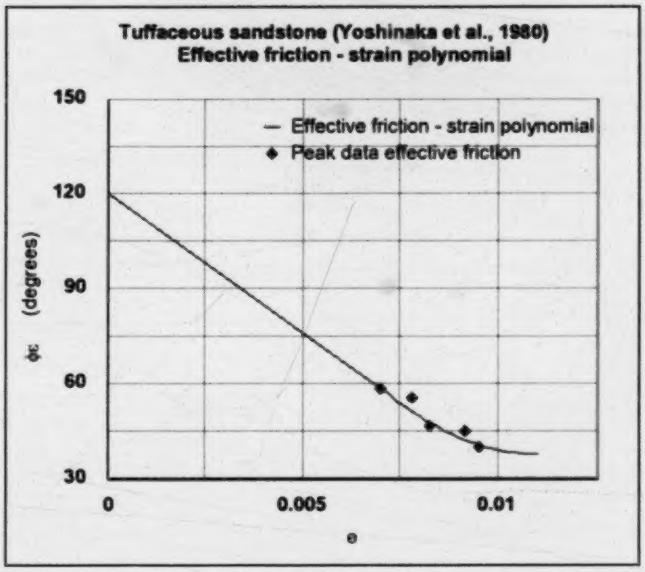

Tuffaceous sandstone (Yoshinaka et al., 1980)
Effective friction - strain polynomial

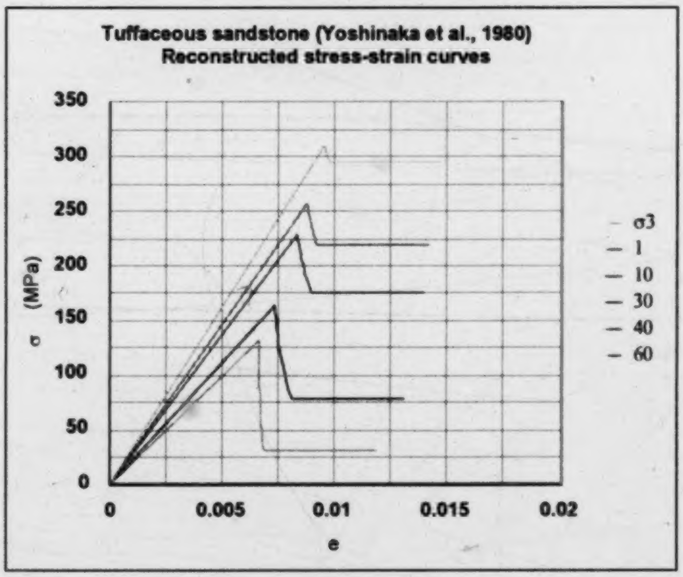

Tuffaceous sandstone (Yoshinaka et al., 1980)
Reconstructed stress-strain curves

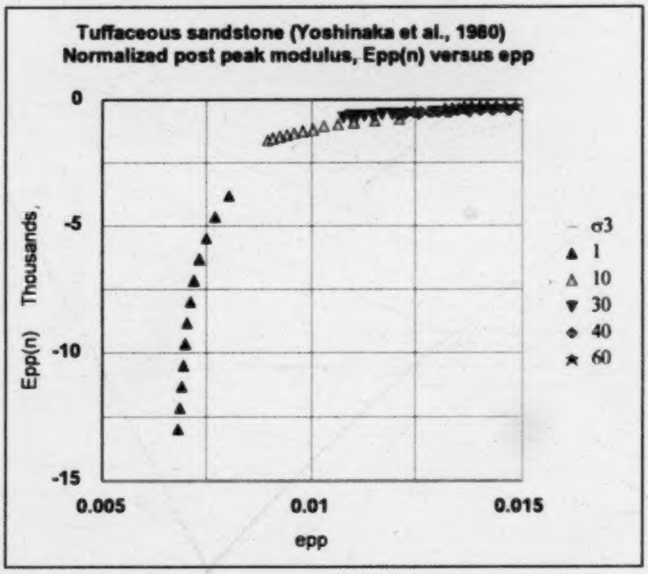

Criterion	Parameters			
Hoek-Brown peak strength	m	σ_c (MPa)	s	a
$\sigma_{1p} = \sigma_3 + \sigma_c\{m\sigma_3/\sigma_c + s\}^a$	6.1	128	1	0.5
Residual strength	D	F	σ_{cr} (MPa)	
$\sigma_{1r} = D\sigma_3^2 + F\sigma_3 + \sigma_{cr}$	-0.02	5.6	26	
Base strength & transition point	ϕ_b (deg.)	σ_{3t} (MPa)	σ_{1t} (MPa)	
$\sigma_{1b} = \{(1+\sin\phi_b)/(1-\sin\phi_b)\}\sigma_3$	38	93	390	
Friction-strain and base strain	R (deg.)	S	T	e_b
$\phi_c = R + Se_{pp} + Te_{pp}^2$	93	-28100	1270000	0.01

Appendix L

Evaluation of a residual strength 2nd order polynomial for broken rock

If the brittle-ductile transition point is known and it is assumed that the residual strength and the peak strength command the same value, σ_{1t} at σ_{3t} then for a 2nd order residual polynomial

$$\sigma_{1r}=D\sigma_3^2+F\sigma_3+\sigma_{cr}$$

$$\sigma_{1p}=\sigma_3+\sigma_c[m_b\frac{\sigma_3}{\sigma_c}+s]^a$$

$$\sigma_{1t}=\sigma_{1p}=\sigma_{3t}+\sigma_c[m_b\frac{\sigma_{3t}}{\sigma_c}+s]^a=\sigma_{1r}=D\sigma_{3t}^2+F\sigma_{3t}+\sigma_{cr}$$

Where D and F are the unknown constants. σ_{cr} is determined via assumption 12, equation 6.9, such that by equating equations 6.1 and 2.7 when $\sigma_3 = 0$, equation 6.11 is defined:

$$\sigma_{cr}=\sigma_c s^a \qquad 6.11$$

Re-arranging in terms of F

$$F=1+\frac{[[m_b\frac{\sigma_{3t}}{\sigma_c}+s]^a-\sigma_{cr}]}{\sigma_{3t}}-D\sigma_{3t} \qquad \text{L-1}$$

It is also assumed that the slopes of both the peak and residual strength criteria at the brittle-ductile transition point are the same:

$$\frac{\delta\sigma_{1p}}{\delta\sigma_{3t}}=1+am_b[m_b\frac{\sigma_{3t}}{\sigma_c}+s]^{a-1}=\frac{\delta\sigma_{1r}}{\delta\sigma_{3t}}=2D\sigma_{3t}+F$$

Re-arranging in terms of F

$$F=1+am_b[m_b\frac{\sigma_{3t}}{\sigma_c}+s]^{a-1}-2D\sigma_{3t} \qquad \text{L-2}$$

Equating L-1 and L-2 and solving for D

$$D=\frac{1}{\sigma_{3t}^2}[\sigma_{cr}-[m_b\frac{\sigma_{3t}}{\sigma_c}+s]^a+am_b\sigma_{3t}[m_b\frac{\sigma_{3t}}{\sigma_c}+s]^{a-1}] \qquad 6.12$$

Substituting 6.12 back into L-2 to solve for F:

$$F=1-am_b[m_b\frac{\sigma_{3t}}{\sigma_c}+s]^{a-1}-\frac{2}{\sigma_{3t}}[\sigma_{cr}-[m_b\frac{\sigma_{3t}}{\sigma_c}+s]^a] \qquad 6.13$$

Appendix M

Worked rock mass data sets

Appendix M.1

Average quality rock mass (Hoek et al., 1997)

GSI	m	σ_c	ϕ_b	$E_{m(broken)}$
		(MPa)	(degrees)	(MPa)
50	12	80	33	9000

The information tabulated above was provided in the literature. The value for ϕ_b was assumed from the Mohr-Coulomb value of effective friction, ϕ' provided. The intact pre-peak modulus, $E_{m(intact)}$ was determined using the empirical relation devised by the author, equation 6.8, with the intact rock RMR value, RMR_{intact} based on the uniaxial compressive strength of the rock, σ_c. Strain data was then generated from the Hoek-Brown intact and rock mass peak strengths and the respective appropriate pre-peak moduli.

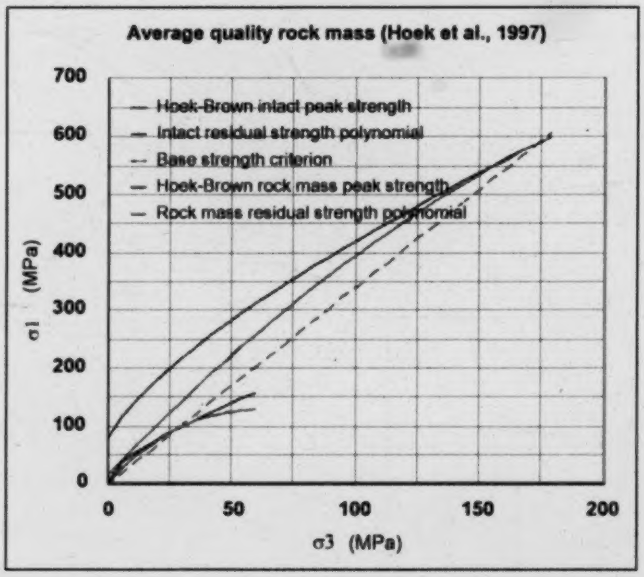

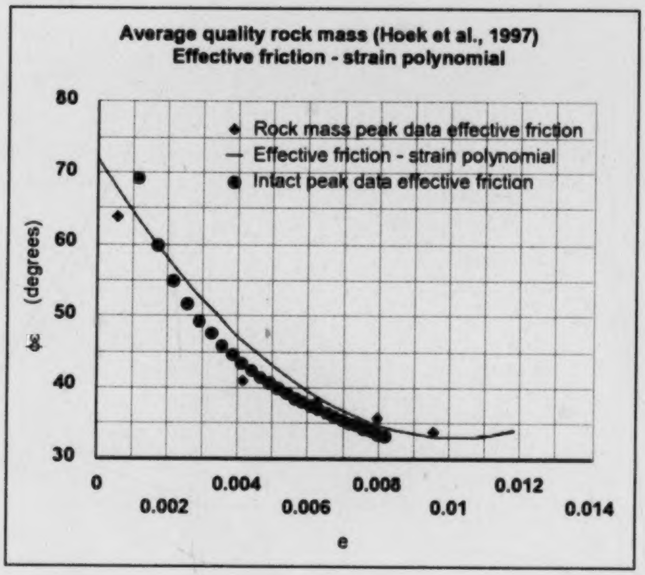
Average quality rock mass (Hoek et al., 1997)
Effective friction - strain polynomial
φc (degrees)
80
70
60
50
40
30
Rock mass peak data effective friction
Effective friction - strain polynomial
Intact peak data effective friction
0
0.002
0.004
0.006
0.008
0.01
0.012
0.014
e

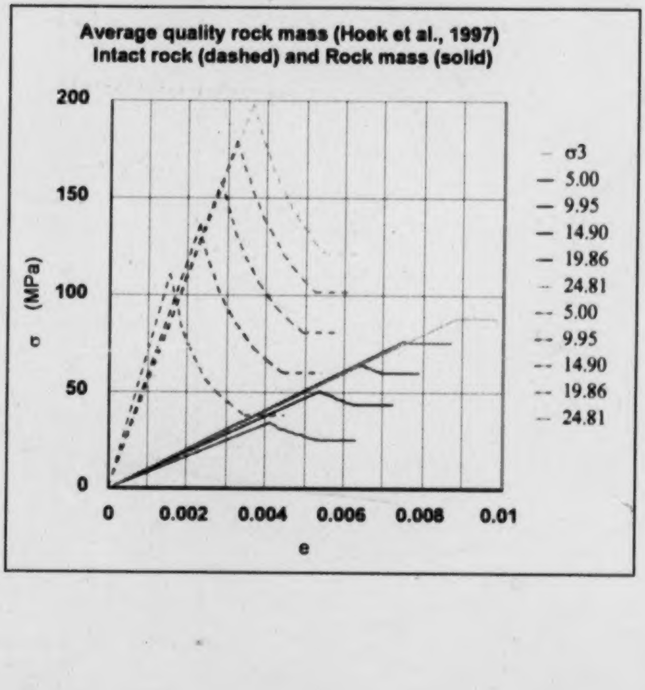
Average quality rock mass (Hoek et al., 1997)
Intact rock (dashed) and Rock mass (solid)
σ (MPa)
200
150
100
50
0
σ3
5.00
9.95
14.90
19.86
24.81
5.00
9.95
14.90
19.86
24.81
0
0.002
0.004
0.006
0.008
0.01
e

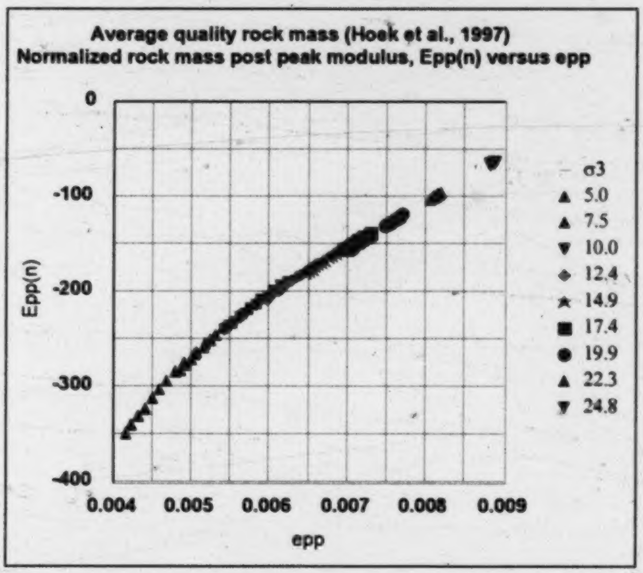

Criterion	Parameters			
Hoek-Brown intact peak strength	m	σ_c (MPa)	s	a
$\sigma_{1p} = \sigma_3 + \sigma_c\{m\sigma_3/\sigma_c + s\}^a$	12.0	80	1	0.5
Hoek-Brown rock mass peak strength	m	σ_c (MPa)	s	a
$\sigma_{1p} = \sigma_3 + \sigma_c\{m\sigma_3/\sigma_c + s\}^a$	2.0	80	0.004	0.5
Intact rock residual strength	D	F	σ_{cr} (MPa)	
$\sigma_{1r} = D\sigma_3^2 + F\sigma_3 + \sigma_{cr}$	-0.007	4.5	16	
Rock mass residual strength	D	F	σ_{cr} (MPa)	
$\sigma_{1r} = D\sigma_3^2 + F\sigma_3 + \sigma_{cr}$	-0.04	4.2	5	
Base strength & transition point	ϕ_b (deg.)	$\sigma_{3t\,(\mathrm{intact})}$	$\sigma_{3t\,(\mathrm{rk.mass})}$	
$\sigma_{1b} = \{(1+\sin\phi_b)/(1-\sin\phi_b)\}\sigma_3$	33	174	28	
Effective friction-strain & base strain	R (deg.)	S	T	e_b
$\phi_e = R + Se_{pp} + Te_{pp}^2$	72	-7700	380000	0.01

Appendix M.2

Very good hard quality rock mass (Hoek et al., 1997)

GSI	m	σ_c	ϕ_b	$E_{m(broken)}$
		(MPa)	(degrees)	(MPa)
75	25	150	42	42000

The information tabulated above was provided in the literature. The value for ϕ_b was assumed from the Mohr-Coulomb value of effective friction, ϕ' provided. The intact pre-peak modulus, $E_{m(intact)}$ was determined using the empirical relation devised by the author, equation 6.8, with the intact rock RMR value, RMR_{intact} based on the uniaxial compressive strength of the rock, σ_c. Strain data was then generated from the Hoek-Brown intact and rock mass peak strengths and the respective appropriate pre-peak moduli.

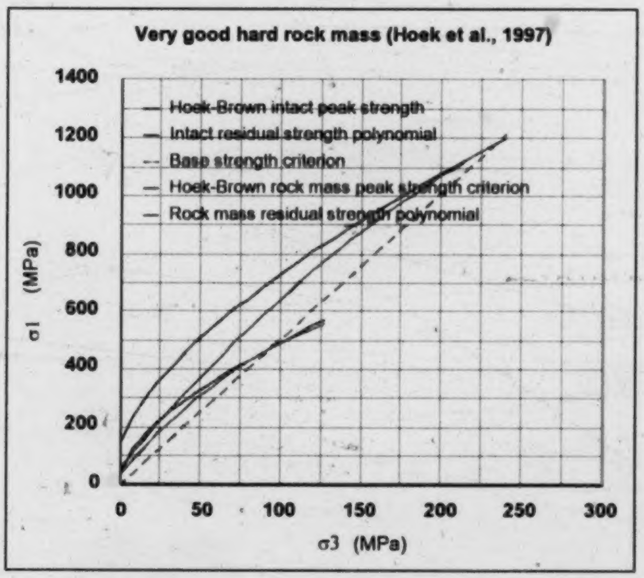

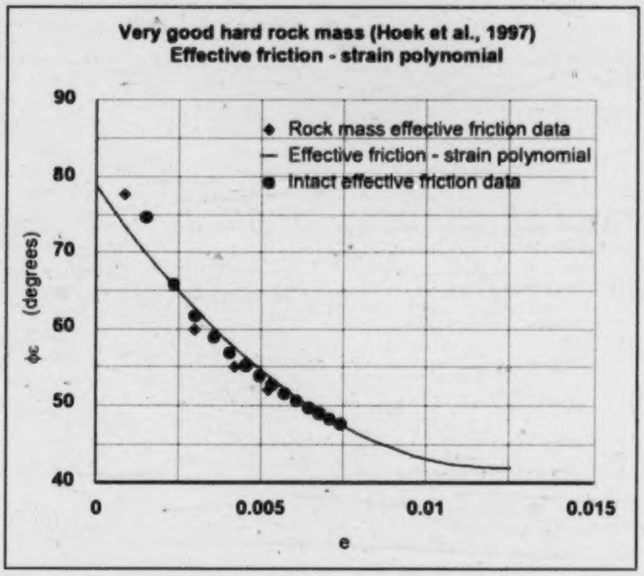
Very good hard rock mass (Hoek et al., 1997)
Effective friction - strain polynomial
90
80
70
60
50
40
φc (degrees)
0
0.005
0.01
0.015
e
◆ Rock mass effective friction data
— Effective friction - strain polynomial
● Intact effective friction data

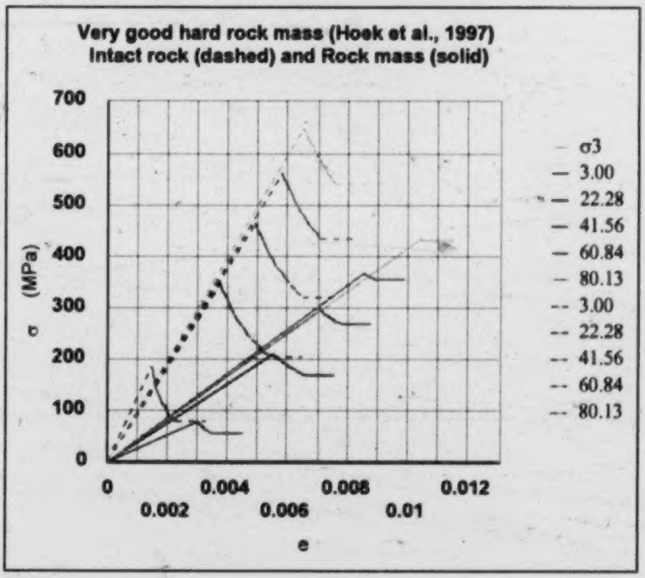
Very good hard rock mass (Hoek et al., 1997)
Intact rock (dashed) and Rock mass (solid)
700
600
500
400
300
200
100
0
σ (MPa)
0
0.002
0.004
0.006
0.008
0.01
0.012
e
σ3
— 3.00
— 22.28
— 41.56
— 60.84
— 80.13
-- 3.00
-- 22.28
-- 41.56
-- 60.84
-- 80.13

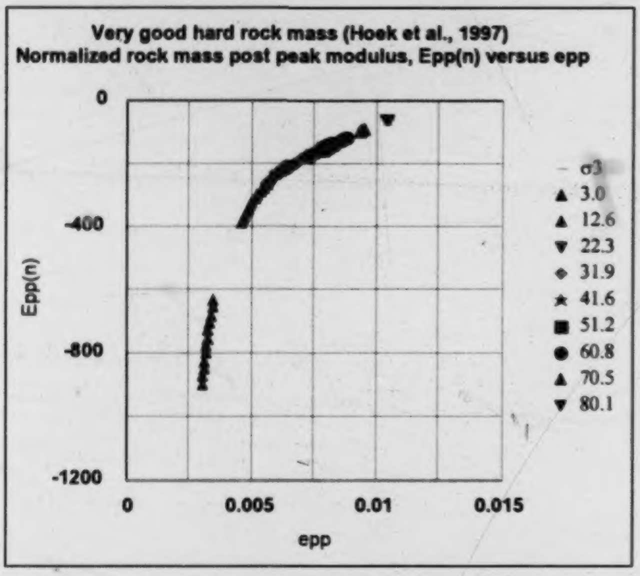

Criterion	Parameters			
Hoek-Brown intact peak strength	m	σ_c (MPa)	s	a
$\sigma_{1p} = \sigma_3 + \sigma_c\{m\sigma_3/\sigma_c + s\}^a$	25.0	150	1	0.5
Hoek-Brown rock mass peak strength	m	σ_c (MPa)	s	a
$\sigma_{1p} = \sigma_3 + \sigma_c\{m\sigma_3/\sigma_c + s\}^a$	10.2	150	0.06	0.5
Intact rock residual strength	D	F	σ_{cr} (MPa)	
$\sigma_{1r} = D\sigma_3^2 + F\sigma_3 + \sigma_{cr}$	-0.008	6.6	60	
Rock mass residual strength	D	F	σ_{cr} (MPa)	
$\sigma_{1r} = D\sigma_3^2 + F\sigma_3 + \sigma_{cr}$	-0.02	6.3	34	
Base strength & transition point	ϕ_b (deg.)	$\sigma_{3t\,(intact)}$	$\sigma_{3t\,(rk.mass)}$	
$\sigma_{1b} = \{(1+\sin\phi_b)/(1-\sin\phi_b)\}\sigma_3$	42	235	95	
Effective friction-strain & base strain	R (deg.)	S	T	e_b
$\phi_e = R + Se_{pp} + Te_{pp}^2$	79	-6040	249000	0.01

Appendix M.3

Poor quality rock mass (Hoek et al., 1997)

GSI	m	σ_c	ϕ_b	$E_{m(broken)}$
		(MPa)	(degrees)	(MPa)
30	8	20	15	1400

The information tabulated above was provided in the literature. The value for ϕ_b was assumed from the Mohr-Coulomb value of effective friction, ϕ' provided. The intact pre-peak modulus, $E_{m(intact)}$ was determined using the empirical relation devised by the author, equation 6.8, with the intact rock RMR value, RMR_{intact} based on the uniaxial compressive strength of the rock, σ_c. Strain data was then generated from the Hoek-Brown intact and rock mass peak strengths and the respective appropriate pre-peak moduli.

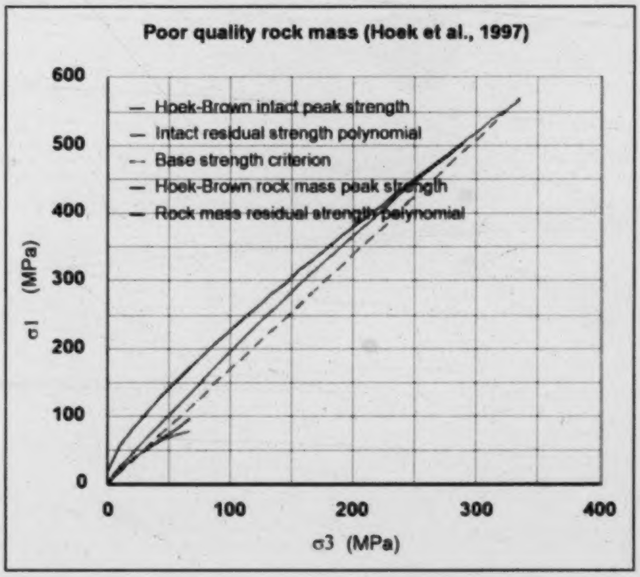

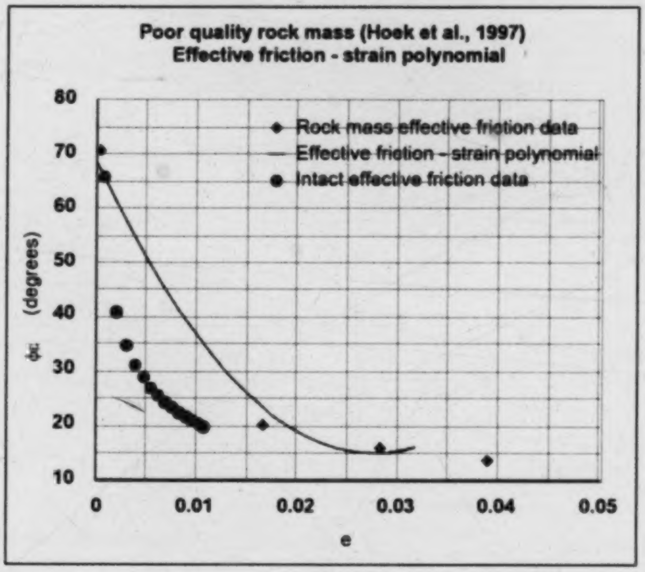
Poor quality rock mass (Hoek et al., 1997)
Effective friction - strain polynomial
80
70
60
50
40
30
20
10
φc (degrees)
0
0.01
0.02
0.03
0.04
0.05
e
Rock mass effective friction data
Effective friction - strain polynomial
Intact effective friction data

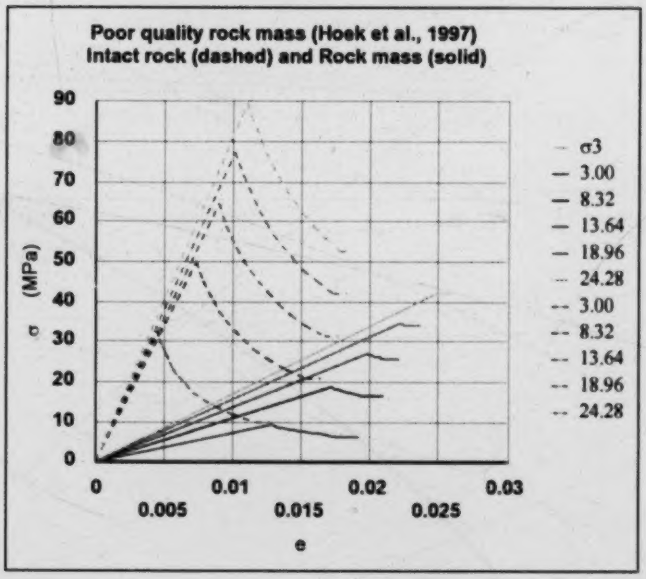
Poor quality rock mass (Hoek et al., 1997)
Intact rock (dashed) and Rock mass (solid)
90
80
70
60
50
40
30
20
10
0
σ (MPa)
0
0.005
0.01
0.015
0.02
0.025
0.03
e
σ3
3.00
8.32
13.64
18.96
24.28
3.00
8.32
13.64
18.96
24.28

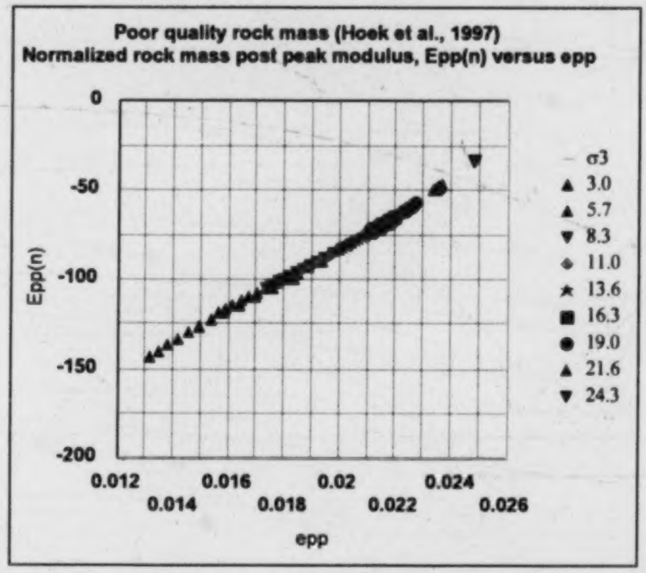

Poor quality rock mass (Hoek et al., 1997)
Normalized rock mass post peak modulus, Epp(n) versus epp

Criterion	Parameters			
Hoek-Brown intact peak strength	m	σ_c (MPa)	s	a
$\sigma_{1p} = \sigma_3 + \sigma_c\{m\sigma_3/\sigma_c + s\}^a$	8.0	20	1	0.5
Hoek-Brown rock mass peak strength	m_b	σ_c (MPa)	s	a
$\sigma_{1p} = \sigma_3 + \sigma_c\{m_b\sigma_3/\sigma_c + s\}^a$	0.7	20	0.0004	0.5
Intact rock residual strength	D	F	σ_{cr} (MPa)	
$\sigma_{1r} = D\sigma_3^2 + F\sigma_3 + \sigma_{cr}$	-0.001	2.0	4	
Rock mass residual strength	D	F	σ_{cr} (MPa)	
$\sigma_{1r} = D\sigma_3^2 + F\sigma_3 + \sigma_{cr}$	-0.01	2.0	0.4	
Base strength & transition point	ϕ_b (deg.)	$\sigma_{3t\,(\text{intact})}$	$\sigma_{3t\,(\text{rk.mass})}$	
$\sigma_{1b} = \{(1+\sin\phi_b)/(1-\sin\phi_b)\}\sigma_3$	15	331	27	
Effcetive friction-strain & base strain	R (deg.)	S	T	e_b
$\phi_e = R + Se_{pp} + Te_{pp}^2$	69	-3890	70700	0.03

Appendix M.4

Bilsthorpe mudstone (Hobbs, 1970)

Rock mass			Intact rock		
σ_3	σ_{1p}	e_p	σ_3	σ_{1p}	e_p
(MPa)	(MPa)	(strain)	(MPa)	(MPa)	(strain)
0.34	4	0.002	0	29	0.002
0.69	6	0.003	3.4	37	0.003
1.72	12	0.005	13.8	69	0.005
3.4	17	0.005	27.6	107	0.007
6.9	29	0.006			
13.8	52	0.007			
27.6	89	0.010			

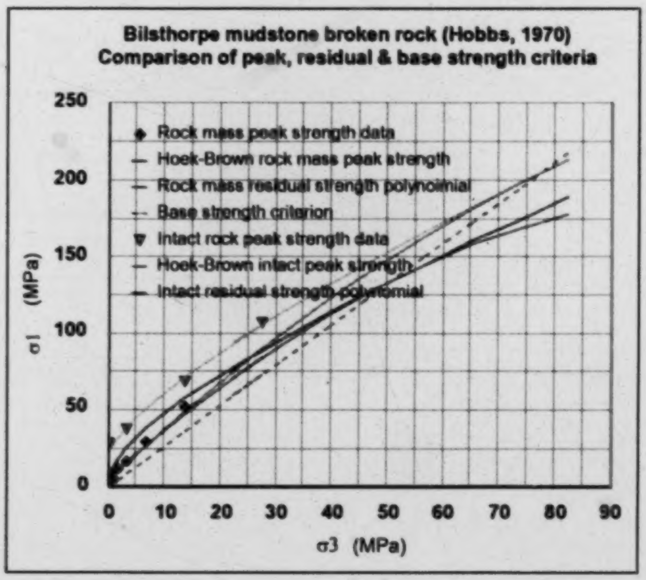

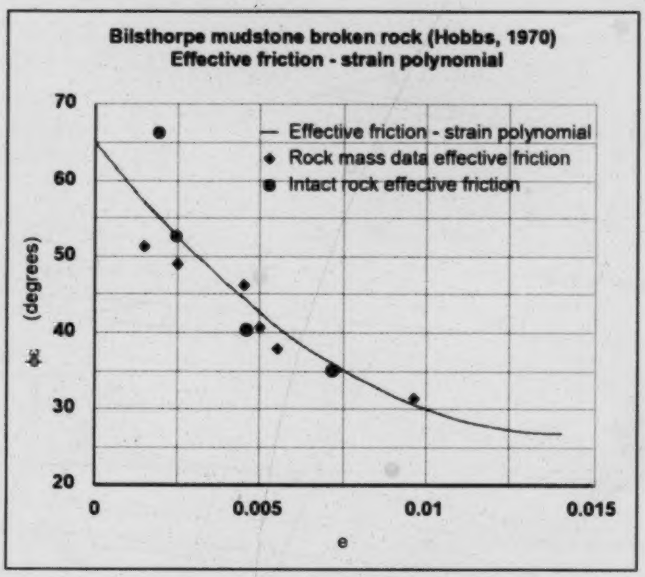
Bilsthorpe mudstone broken rock (Hobbs, 1970)
Effective friction - strain polynomial
Effective friction - strain polynomial
Rock mass data effective friction
Intact rock effective friction
φc (degrees)
70
60
50
40
30
20
0
0.005
0.01
0.015
e

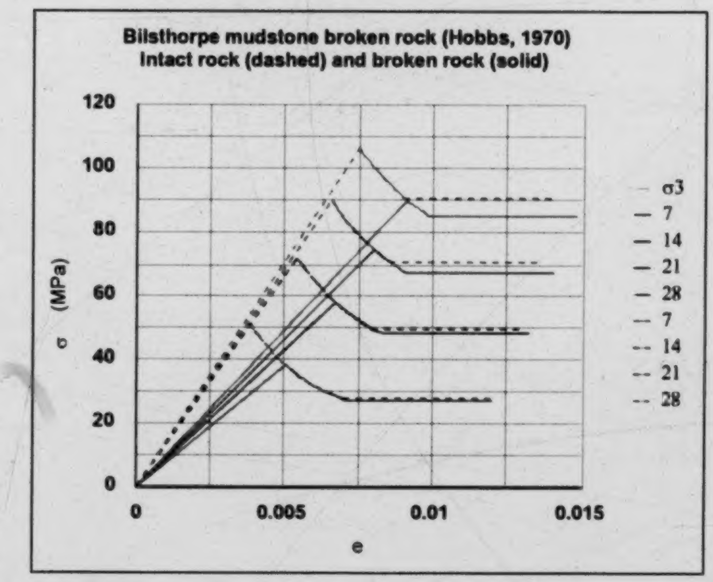
Bilsthorpe mudstone broken rock (Hobbs, 1970)
Intact rock (dashed) and broken rock (solid)
σ (MPa)
120
100
80
60
40
20
0
0
0.005
0.01
0.015
e
σ3
— 7
— 14
— 21
— 28
-- 7
-- 14
-- 21
-- 28

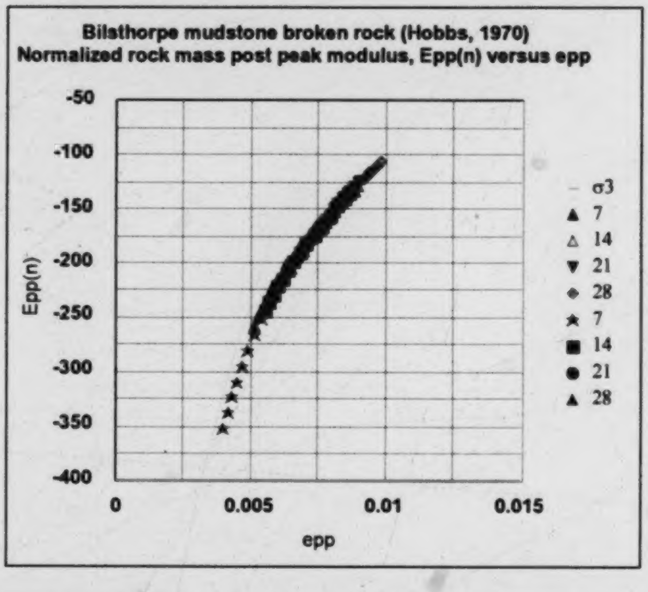

Criterion	Parameters			
Hoek-Brown intact peak strength	m	σ_c (MPa)	s	a
$\sigma_{1p} = \sigma_3 + \sigma_c\{m\sigma_3/\sigma_c + s\}^a$	8.6	24	1	0.5
Hoek-Brown rock mass peak strength	m_b	σ_c (MPa)	s	a
$\sigma_{1p} = \sigma_3 + \sigma_c\{m_b\sigma_3/\sigma_c + s\}^a$	5.8	24	0.06	0.5
Intact rock residual strength	D	F	σ_{cr} (MPa)	
$\sigma_{1r} = D\sigma_3^2 + F\sigma_3 + \sigma_{cr}$	-0.01	3.4	5	
Rock mass residual strength	D	F	σ_{cr} (MPa)	
$\sigma_{1r} = D\sigma_3^2 + F\sigma_3 + \sigma_{cr}$	-0.01	3.3	6	
Base strength & transition point	ϕ_b (deg.)	$\sigma_{3t\,(intact)}$	$\sigma_{3t\,(rk.mass)}$	
$\sigma_{1b} = \{(1+\sin\phi_b)/(1-\sin\phi_b)\}\sigma_3$	27	78	51	
Rock mass ϕ_c - e and base strain	R (deg.)	S	T	e_b
$\phi_c = R + Se_{pp} + Te_{pp}^2$	65	-5400	192000	0.014

Appendix M.5

Bilsthorpe silty mudstone (Hobbs, 1970)

Rock mass			Intact rock		
σ_3 (MPa)	σ_{1p} (MPa)	e_p (strain)	σ_3 (MPa)	σ_{1p} (MPa)	e_p (strain)
0.3	7	0.004	0	39	0.003
0.7	10	0.005	3.4	74	0.006
1.7	17	0.007	6.9	109	0.009
3.4	25	0.009	13.8	110	0.009
6.9	39	0.009	20.7	121	0.010
13.8	61	0.010			
27.6	100	0.014			

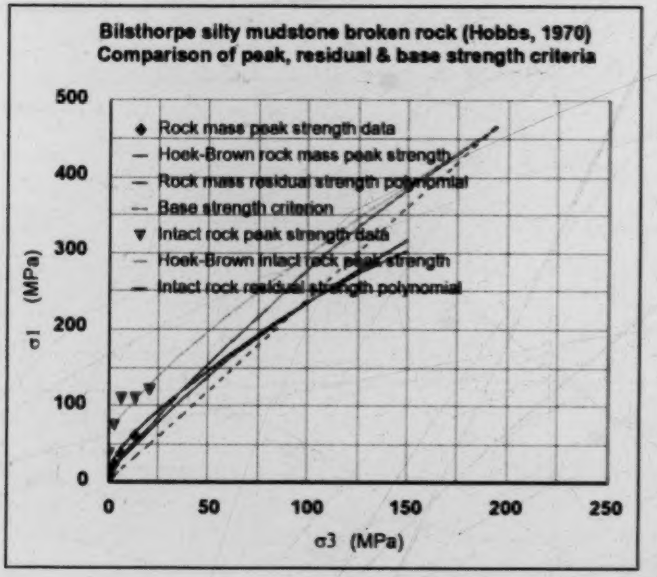

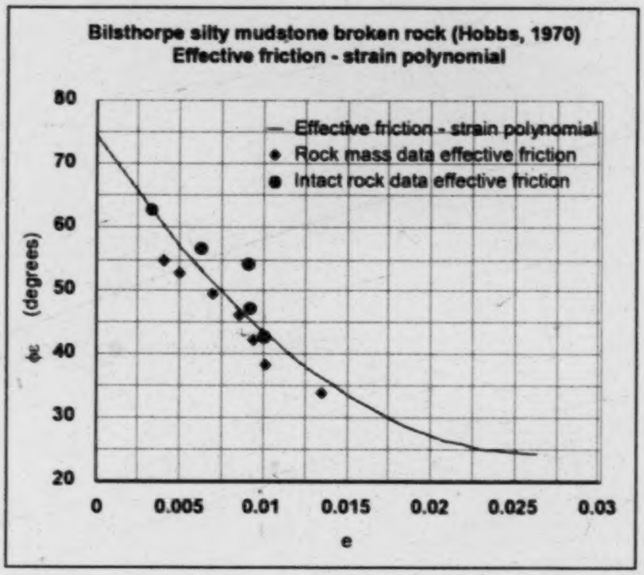
Bilsthorpe silty mudstone broken rock (Hobbs, 1970)
Effective friction - strain polynomial
80
70
60
50
40
30
20
φc (degrees)
0
0.005
0.01
0.015
0.02
0.025
0.03
e
Effective friction - strain polynomial
Rock mass data effective friction
Intact rock data effective friction

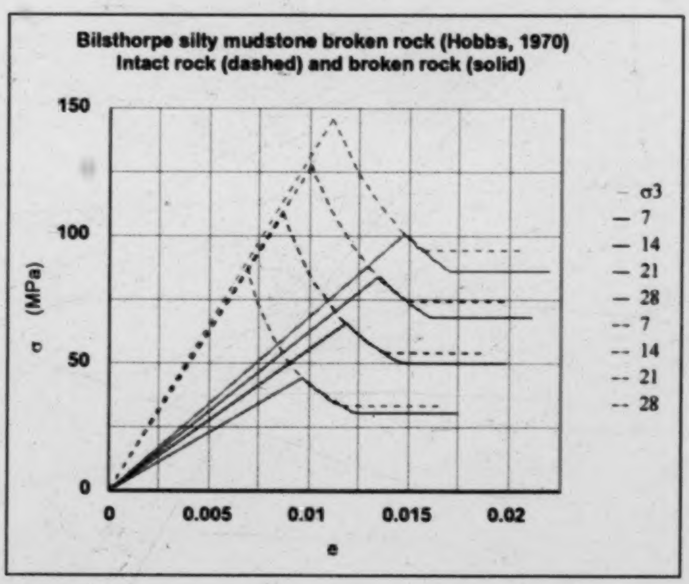
Bilsthorpe silty mudstone broken rock (Hobbs, 1970)
Intact rock (dashed) and broken rock (solid)
150
100
50
0
σ (MPa)
0
0.005
0.01
0.015
0.02
e
σ3
7
14
21
28
7
14
21
28

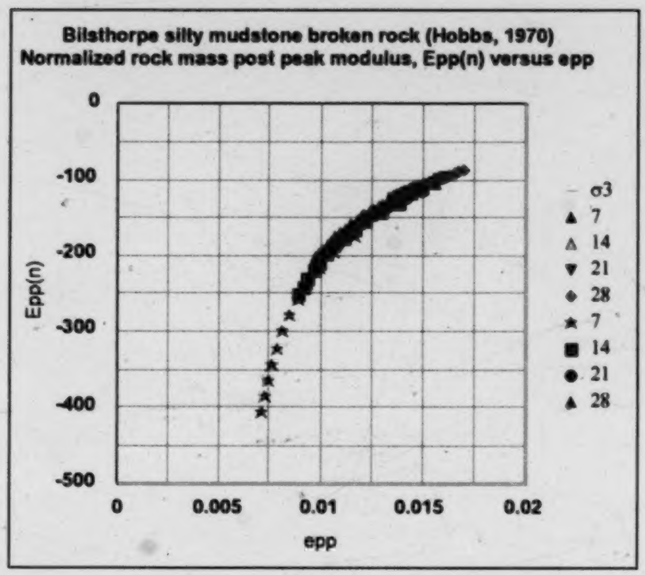

Criterion	Parameters			
Hoek-Brown intact peak strength	m	σ_c (MPa)	s	a
$\sigma_{1p} = \sigma_3 + \sigma_c\{m\sigma_3/\sigma_c + s\}^a$	5.6	64	1	0.5
Hoek-Brown rock mass peak strength	m_b	σ_c (MPa)	s	a
$\sigma_{1p} = \sigma_3 + \sigma_c\{m_b\sigma_3/\sigma_c + s\}^a$	2.9	64	0.03	0.5
Intact rock residual strength	D	F	σ_{cr} (MPa)	
$\sigma_{1r} = D\sigma_3^2 + F\sigma_3 + \sigma_{cr}$	-0.004	3.0	13	
Rock mass residual strength	D	F	σ_{cr} (MPa)	
$\sigma_{1r} = D\sigma_3^2 + F\sigma_3 + \sigma_{cr}$	-0.006	2.9	11	
Base strength & transition point	ϕ_b (deg.)	$\sigma_{3t\,(intact)}$	$\sigma_{3t\,(rk.mass)}$	
$\sigma_{1b} = \{(1+\sin\phi_b)/(1-\sin\phi_b)\}\sigma_3$	24	190	95	
Rock mass ϕ_e -'e and base strain	R (deg.)	S	T	e_b
$\phi_e = R + Se_{pp} + Te_{pp}^2$	74.5	-3800	72000	0.03

Appendix M.6

Hucknall shale (Hobbs, 1970)

Rock mass			Intact rock		
σ_3	σ_{1p}	e_p	σ_3	σ_{1p}	e_p
(MPa)	(MPa)	(strain)	(MPa)	(MPa)	(strain)
0.3	5	0.003	0	59	0.003
0.7	8	0.004	3.4	73	0.004
1.7	14	0.005	6.9	82	0.004
3.4	24	0.005	13.8	107	0.005
6.9	38	0.006			
13.8	64	0.008			
27.6	109	0.010			

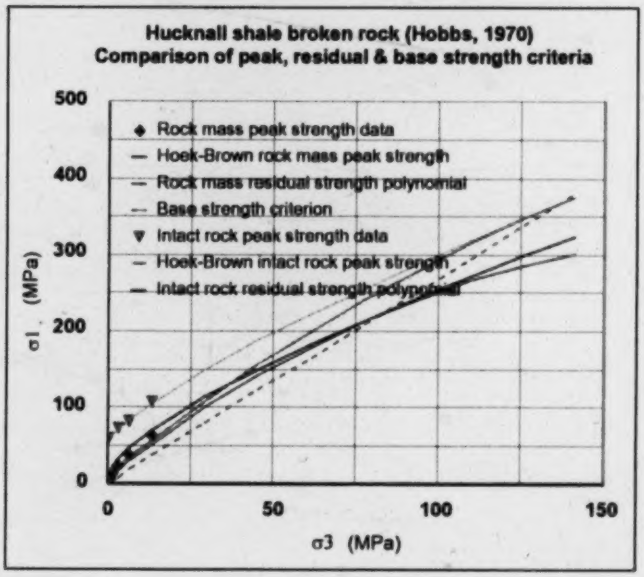

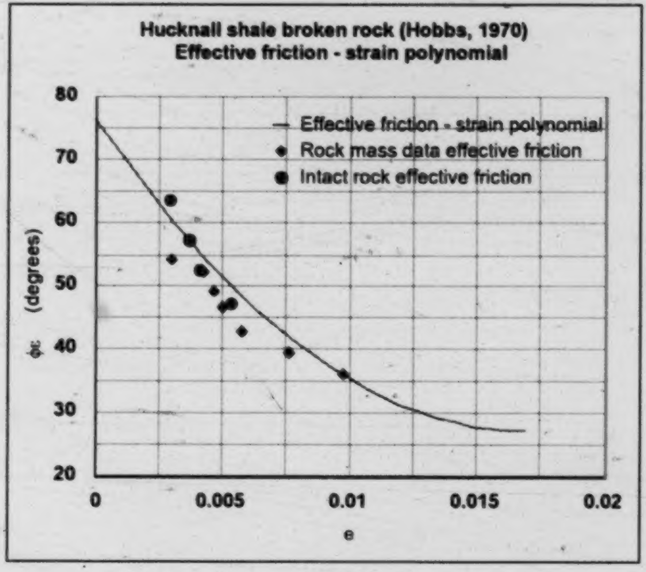
Hucknall shale broken rock (Hobbs, 1970)
Effective friction - strain polynomial
Effective friction - strain polynomial
Rock mass data effective friction
Intact rock effective friction
φc (degrees)
80
70
60
50
40
30
20
0
0.005
0.01
0.015
0.02
e

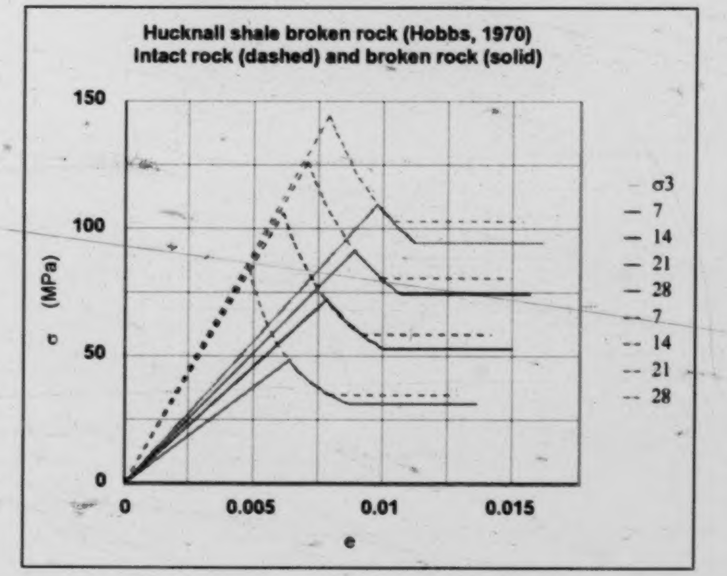
Hucknall shale broken rock (Hobbs, 1970)
Intact rock (dashed) and broken rock (solid)
σ (MPa)
150
100
50
0
0
0.005
0.01
0.015
e
σ3
— 7
— 14
— 21
— 28
-- 7
-- 14
-- 21
-- 28

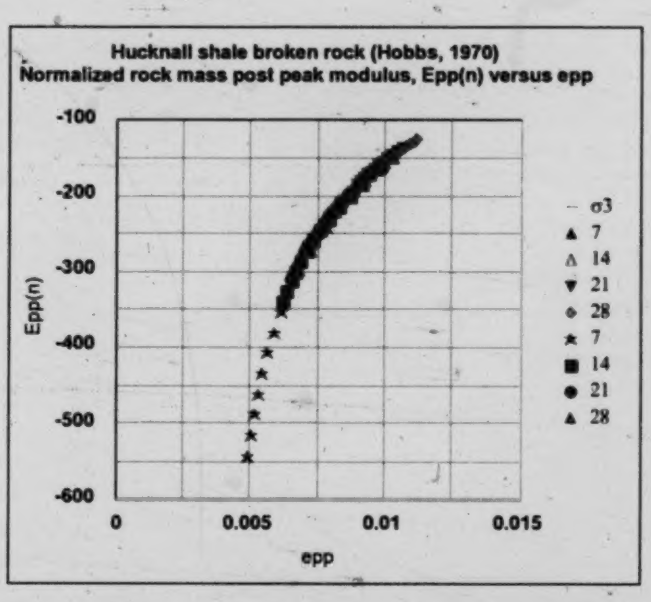

Criterion	Parameters			
Hoek-Brown intact peak strength $\sigma_{1p} = \sigma_3 + \sigma_c\{m\sigma_3/\sigma_c + s\}^a$	m 6.3	σ_c (MPa) 58	s 1	a 0.5
Hoek-Brown rock mass peak strength $\sigma_{1p} = \sigma_3 + \sigma_c\{m_b\sigma_3/\sigma_c + s\}^a$	m_b 4.1	σ_c (MPa) 58	s 0.02	a 0.5
Intact rock residual strength $\sigma_{1r} = D\sigma_3^2 + F\sigma_3 + \sigma_{cr}$	D -0.006	F 3.4	σ_{cr} (MPa) 12	
Rock mass residual strength $\sigma_{1r} = D\sigma_3^2 + F\sigma_3 + \sigma_{cr}$	D -0.009	F 3.3	σ_{cr} (MPa) 8	
Base strength & transition point $\sigma_{1b} = \{(1+\sin\phi_b)/(1-\sin\phi_b)\}\sigma_3$	ϕ_b (deg.) 27	$\sigma_{3t\,(intact)}$ 137	$\sigma_{3t\,(rk.mass)}$ 83	
Rock mass ϕ_e - e and base strain $\phi_e = R + Se_{pp} + Te_{pp}^2$	R (deg.) 76	S -5790	T 171000	e_b 0.02

Appendix M.7

Ormonde siltstone (Hobbs, 1970)

Rock mass			Intact rock		
σ_3 (MPa)	σ_{1p} (MPa)	e_p (strain)	σ_3 (MPa)	σ_{1p} (MPa)	e_p (strain)
0.3	6	0.004	0	56	0.002
0.7	8	0.004	3.4	83	0.003
1.7	16	0.005	6.9	107	0.004
3.4	26	0.006	13.8	131	0.005
6.9	43	0.008	20.7	148	0.005
13.8	68	0.010			
27.6	115	0.012			

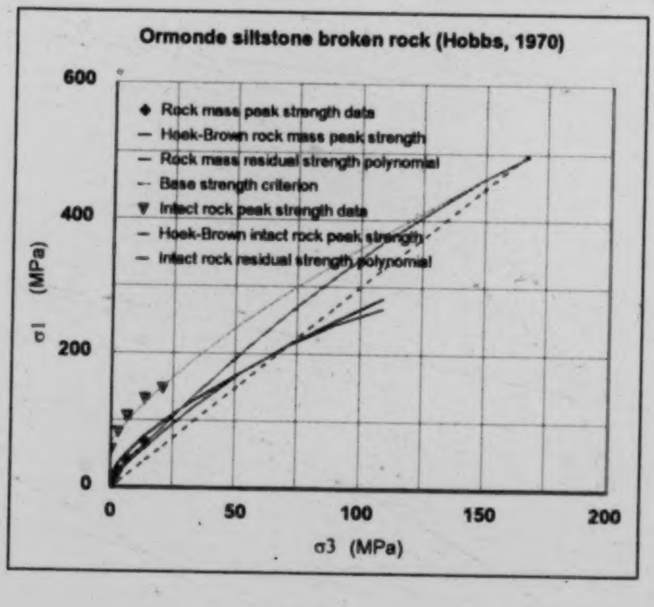

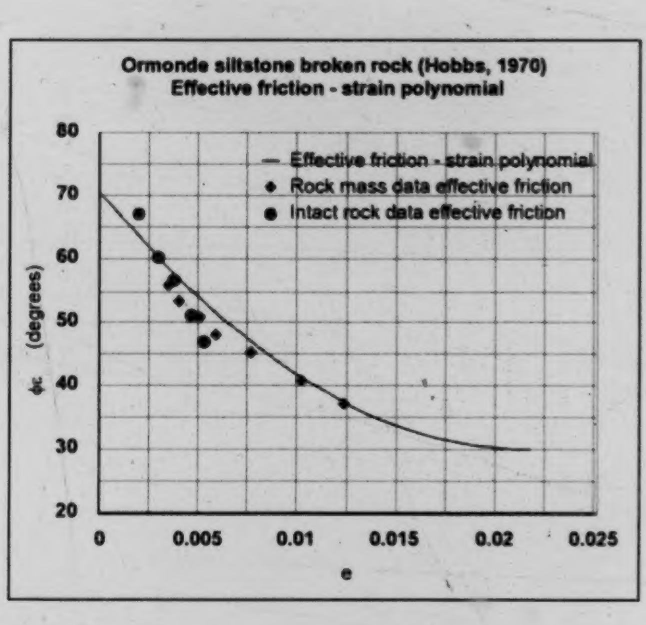
Ormonde siltstone broken rock (Hobbs, 1970)
Effective friction - strain polynomial
— Effective friction - strain polynomial
◆ Rock mass data effective friction
● Intact rock data effective friction
80
70
60
50
40
30
20
ϕ_c (degrees)
0
0.005
0.01
0.015
0.02
0.025
e

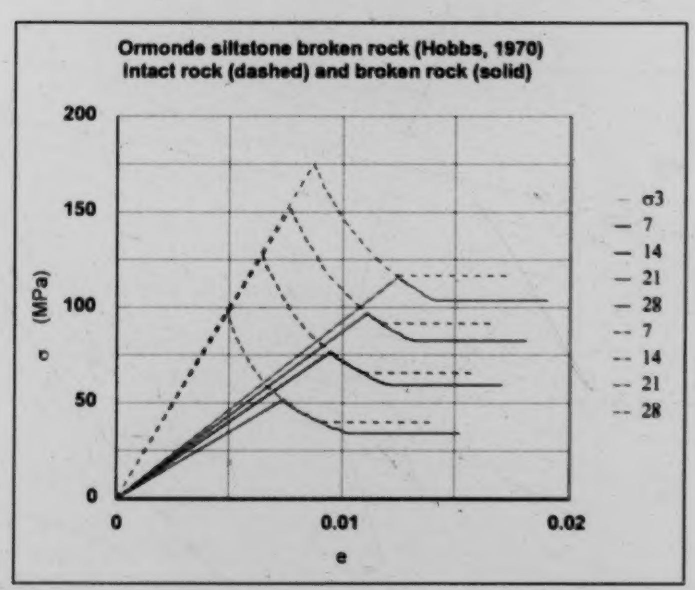
Ormonde siltstone broken rock (Hobbs, 1970)
Intact rock (dashed) and broken rock (solid)
200
150
100
50
0
σ (MPa)
0
0.01
0.02
e
$\sigma 3$
— 7
— 14
— 21
— 28
-- 7
-- 14
-- 21
-- 28

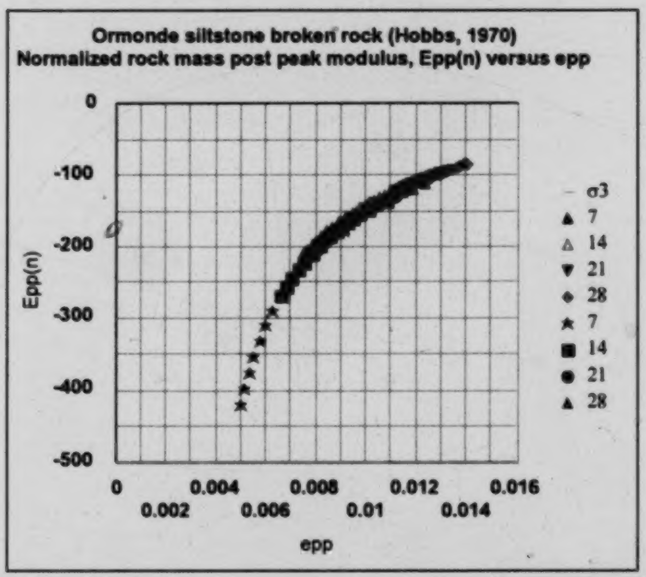

Ormonde siltstone broken rock (Hobbs, 1970)
Normalized rock mass post peak modulus, Epp(n) versus epp

Criterion	Parameters			
Hoek-Brown intact peak strength	m	σ_c (MPa)	s	a
$\sigma_{1p} = \sigma_3 + \sigma_c\{m\sigma_3/\sigma_c + s\}^a$	9.6	65	1	0.5
Hoek-Brown rock mass peak strength	m_b	σ_c (MPa)	s	a
$\sigma_{1p} = \sigma_3 + \sigma_c\{m_b\sigma_3/\sigma_c + s\}^a$	4.3	65	0.02	0.5
Intact rock residual strength	D	F	σ_{cr} (MPa)	
$\sigma_{1r} = D\sigma_3^2 + F\sigma_3 + \sigma_{cr}$	-0.006	3.9	13	
Rock mass residual strength	D	F	σ_{cr} (MPa)	
$\sigma_{1r} = D\sigma_3^2 + F\sigma_3 + \sigma_{cr}$	-0.01	3.7	10	
Base strength & transition point	ϕ_b (deg.)	$\sigma_{3t\,(intact)}$	$\sigma_{3t\,(rk.mass)}$	
$\sigma'_{1b} = \{(1+\sin\phi_b)/(1-\sin\phi_b)\}\sigma_3$	30	163	70	
Rock mass ϕ_c - e and base strain	R (deg.)	S	T	e_b
$\phi_c = R + Se_{pp} + Te_{pp}^2$	71	-3750	86300	0.02

Appendix N

Dense crushed basalt (Hussaini, 1991)

Data

	6.3 mm crush		12.7 mm crush		25.4 mm crush		50.8 mm crush		76.2 mm crush	
σ_3	σ_{1p}	e_p	σ_{1p}	e_p	σ_{1p}	e_p	σ_{1p}	e_p	σ_{1p}	e_p
(MPa)	(MPa)	(strain)	(MPa)	(strain)	(MPa)	(strain)	(MPa)	(strain)	(MPa)	(strain)
0.4	2.4	0.09	2.6	0.08	3.0	0.07	3.2	0.06	3.4	0.05
0.9	4.3	0.14	4.6	0.12	5.2	0.10	5.4	0.08	5.7	0.07
2.1	8.4	0.19	8.9	0.16	9.7	0.14	10.0	0.12	10.5	0.12
3.1	11.9	0.20	12.6	0.18	13.1	0.16	13.7	0.15	14.5	0.14

According to Hoek et al. (1997), the crushed basalt described by Hussaini (1991) would be very good (very rough, fresh unweathered surfaces). It would also be described as disintegrated, indicative of a poorly interlocking heavily broken rock mass, comprising of a mixture of angular and rounded rock pieces. Following the GSI descriptive charts (Hoek et al., 1997) a value for the GSI = 45 is estimated. Since the GSI value is greater than 25 then the Hoek-Brown exponent, a = 0.5.

Analysis of the peak strength data to determine m_b and s

Since broken rock triaxial data is available in this case, the procedure outlined in section 6.4.1 is appropriate. The first step is the evaluation of the broken rock peak strength criterion as described in section 6.4.1a. Hussaini (1991) provided a value for the uniaxial compressive strength, σ_c = 172.2 MPa.

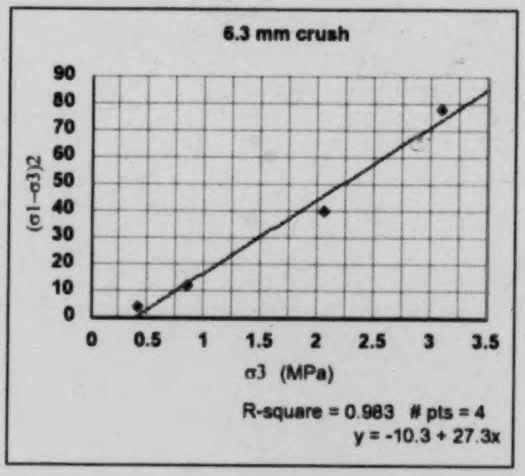

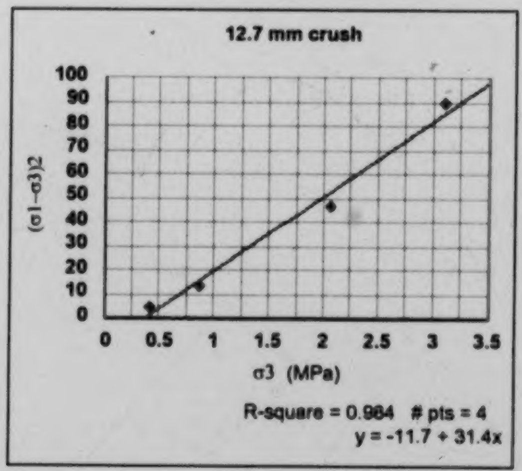

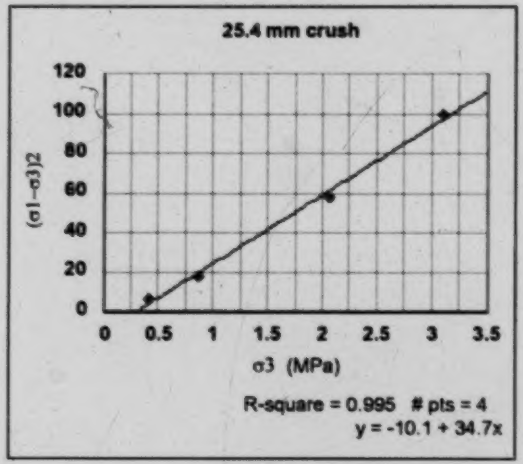
25.4 mm crush

R-square = 0.995 # pts = 4
y = -10.1 + 34.7x

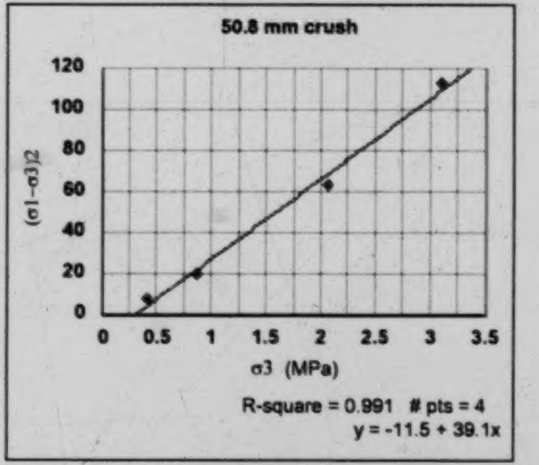
50.8 mm crush

R-square = 0.991 # pts = 4
y = -11.5 + 39.1x

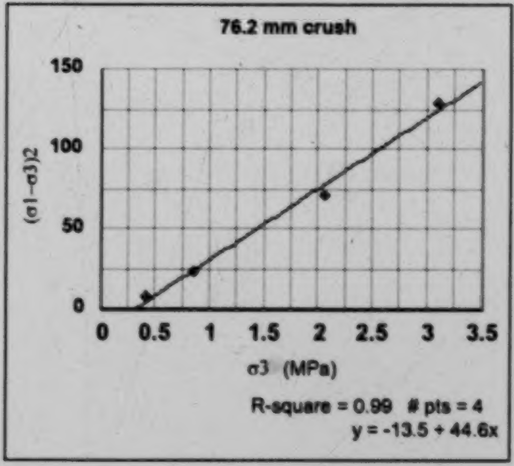
76.2 mm crush

R-square = 0.99 # pts = 4
y = -13.5 + 44.6x

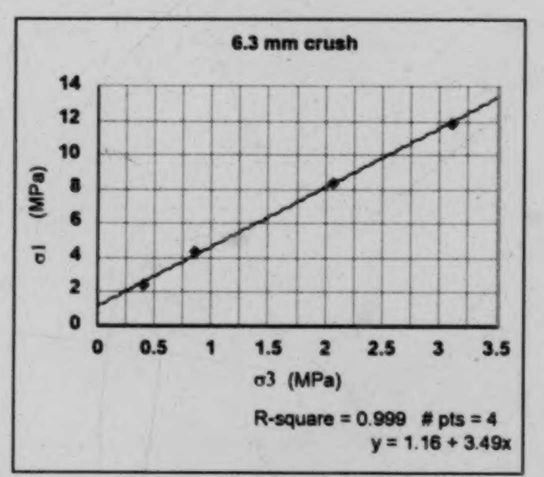

6.3 mm crush

R-square = 0.999 # pts = 4
y = 1.16 + 3.49x

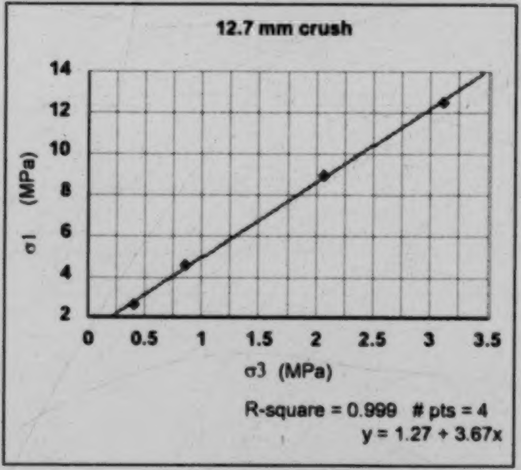

12.7 mm crush

R-square = 0.999 # pts = 4
y = 1.27 + 3.67x

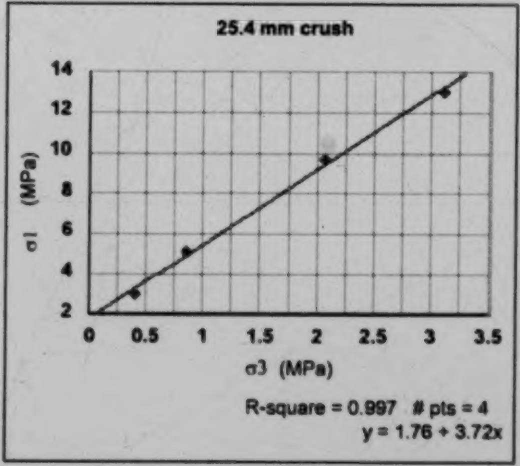

25.4 mm crush

R-square = 0.997 # pts = 4
y = 1.76 + 3.72x

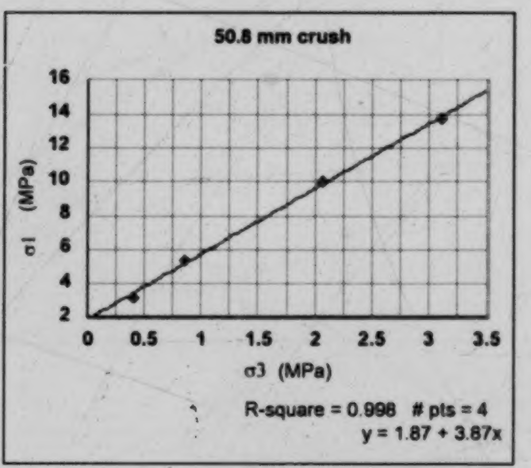
50.8 mm crush

R-square = 0.998 # pts = 4
y = 1.87 + 3.87x

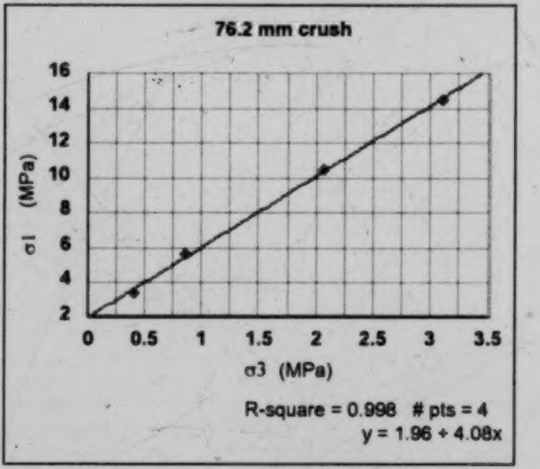
76.2 mm crush

R-square = 0.998 # pts = 4
y = 1.96 + 4.08x

Analysis summary of the above plots to determine m_b and s

	6.3 mm crush	12.7 mm crush	25.4 mm crush	50.8 mm crush	76.2 mm crush
σ_c (MPa)	172	172	172	172	172
m_b	0.16	0.18	0.20	0.23	0.26
s	0.00005	0.00005	0.00010	0.00012	0.00013

Determination of the brittle-ductile confinement and residual strength polynomial for each crush size

A value of $\phi_b = 33°$ was assumed by the author since no value was reported by Hussaini (1991). This enabled the base strength criterion to be determined as given below, and the brittle ductile-transition point confinement for each crush size. The residual strength polynomial for each crush size was determined as per section 6.4.1d. A summary of the brittle-ductile confinement and the residual strength polynomial parameters is given below by crush size.

$$\sigma_{1b} = 3.4\, \sigma_3$$

	6.3 mm crush	12.7 mm crush	25.4 mm crush	50.8 mm crush	76.2 mm crush
σ_{3t} (MPa)	4.8	5.5	6.2	6.9	7.9
σ_{cr} (MPa)	1.2	1.3	1.8	1.9	2.0
D	-0.20	-0.18	-0.15	-0.14	-0.12
F	4.12	4.14	4.03	4.06	4.10

Comparison of the peak, residual and base strength criteria

The peak, residual and base strength criteria are plotted with respect to crush size together with the original strength data in each case reported. The last plot in the series shows all curves together to give a global comparison of how crush size affects the strength criteria behaviour.

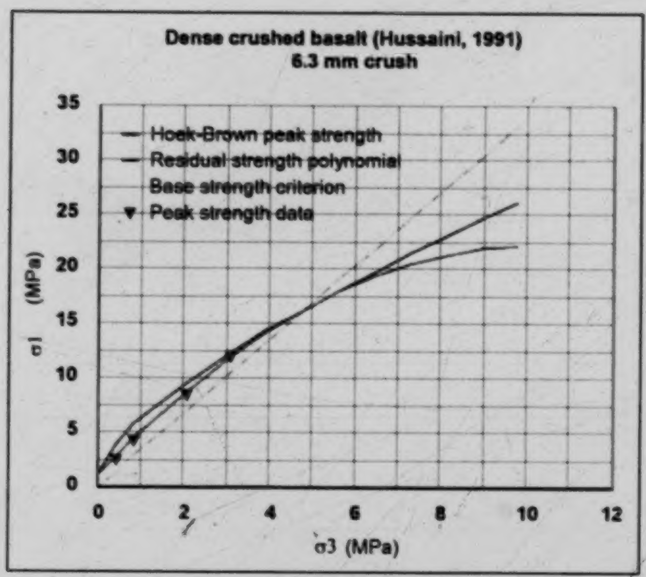
Dense crushed basalt (Hussaini, 1991)
6.3 mm crush
Hoek-Brown peak strength
Residual strength polynomial
Base strength criterion
▼ Peak strength data
σ1 (MPa)
σ3 (MPa)
0
5
10
15
20
25
30
35
0
2
4
6
8
10
12

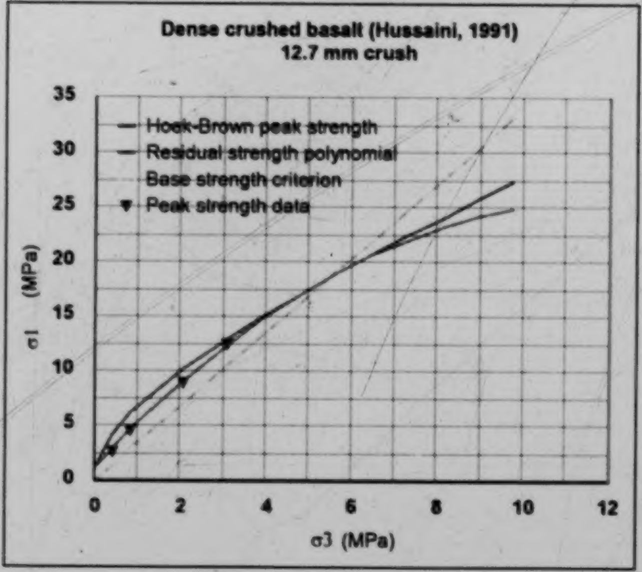
Dense crushed basalt (Hussaini, 1991)
12.7 mm crush
Hoek-Brown peak strength
Residual strength polynomial
Base strength criterion
▼ Peak strength data
σ1 (MPa)
σ3 (MPa)
0
5
10
15
20
25
30
35
0
2
4
6
8
10
12

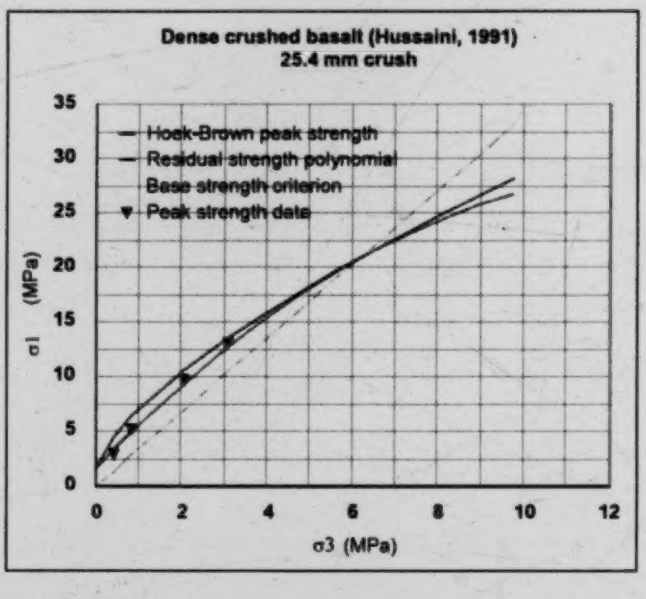
Dense crushed basalt (Hussaini, 1991)
25.4 mm crush
Hoek-Brown peak strength
Residual strength polynomial
Base strength criterion
Peak strength data
σ1 (MPa)
σ3 (MPa)
0
5
10
15
20
25
30
35
0
2
4
6
8
10
12

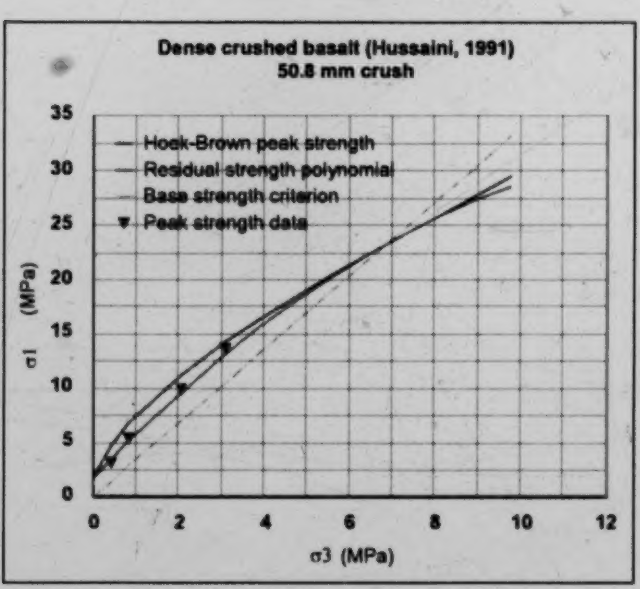
Dense crushed basalt (Hussaini, 1991)
50.8 mm crush
Hoek-Brown peak strength
Residual strength polynomial
Base strength criterion
Peak strength data
σ1 (MPa)
σ3 (MPa)
0
5
10
15
20
25
30
35
0
2
4
6
8
10
12

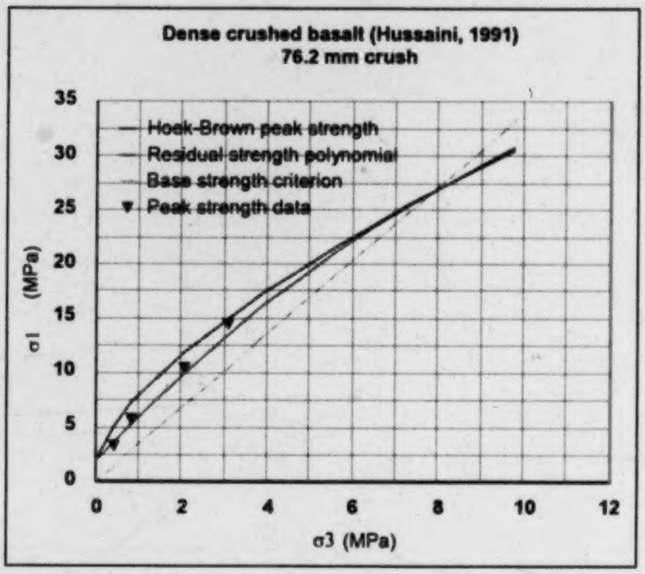
Dense crushed basalt (Hussaini, 1991)
76.2 mm crush
Hoek-Brown peak strength
Residual strength polynomial
Base strength criterion
▼ Peak strength data
σ1 (MPa)
σ3 (MPa)
0
5
10
15
20
25
30
35
0
2
4
6
8
10
12

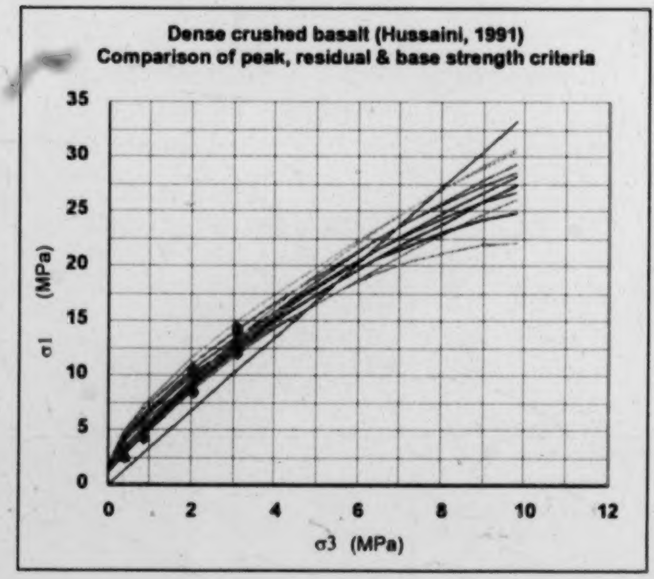
Dense crushed basalt (Hussaini, 1991)
Comparison of peak, residual & base strength criteria
σ1 (MPa)
σ3 (MPa)
0
5
10
15
20
25
30
35
0
2
4
6
8
10
12

Determination of e_b and the solution to the effective friction - strain polynomial

The procedure outlined in section 6.4.1f was used to determine the base strain, e_b and the values of R, S and T for an solution of the effective friction - strain polynomial. All data regardless of crush size was used in the Y versus e plot, as shown in the figure below, illustrating that all the data conformed to the same relationship.

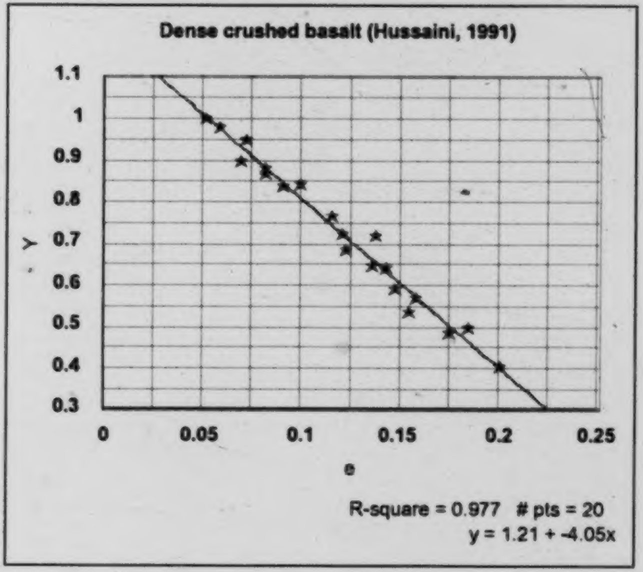

e_b	0.3
R	57.5
S	-164
T	275

The effective friction - strain polynomial compared to the crush data

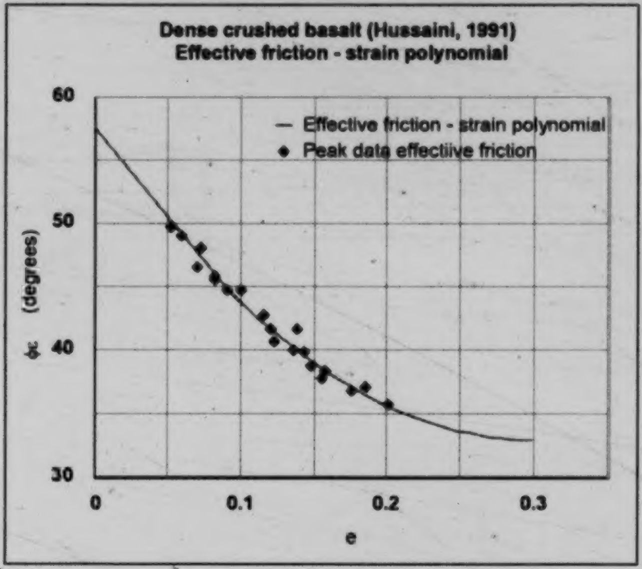

Reconstruction of the crushed rock stress-strain curves

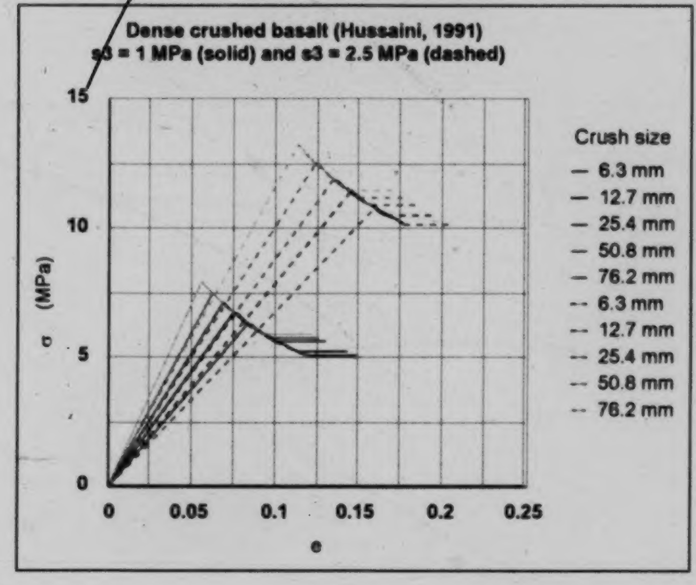

Normalized post peak modulus

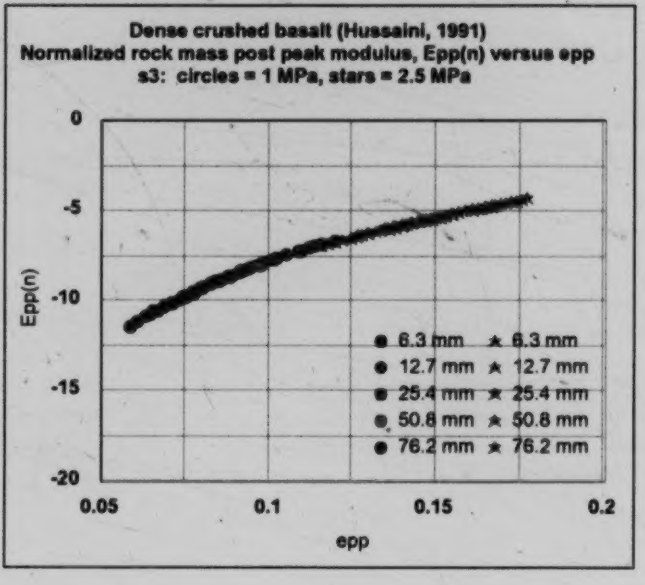

Appendix P

Panguna andesite (Hoek et al., 1980)

Data and initial calculations

			Degree of weathering			
	Undisturbed	Recompacted	Fresh/sl.	Moderate	High	Intact
RMR_{broken}	46	28	26	18	8	97
GSI	41	23	21	13	3	92
σ_c (MPa)	265	265	265	265	265	265
ϕ_b (deg.)	22	22	18	18	10	45
m_b	0.27	0.12	0.04	0.03	0.01	18.9
s	0.015	0.006	0.002	0.002	0.0006	1
a	0.5	0.54	0.55	0.59	0.64	0.5
$E_{m(broken)}$	7940	2820	2510	1590	891	94000

The Panguna andesite data reported by Hoek et al. (1980) comprised values for $RMR_{(broken)}$, m (intact) and σ_c. An adjustment of the RMR_{intact} value was made to compensate for the value of σ_c. Note that the values of s were determined using equation 6.3, and differ from those reported by Hoek et al., (1980).

Determination of the brittle-ductile confinement and residual strength polynomial for each data set

The base strength criterion was determined using the respective values for ϕ_b depending on the degree of weathering. The residual strength polynomial in each case was determined as per section 6.4.1d. A summary of the brittle-ductile confinement and the residual strength polynomial parameters are given below by degree of weathering.

			degree of weathering			
	Undisturbed	Recompacted	Fresh/slight	Moderate	High	Intact
σ_{3t} (MPa)	62.5	25	15	9	7.5	226
σ_{cr} (MPa)	32	17	9	6	2	53
D	-0.003	-0.004	-0.003	-0.002	-0.0009	-0.01
F	1.9	1.6	1.3	1.3	1.1	8.0

Comparison of the peak, residual and base strength criteria

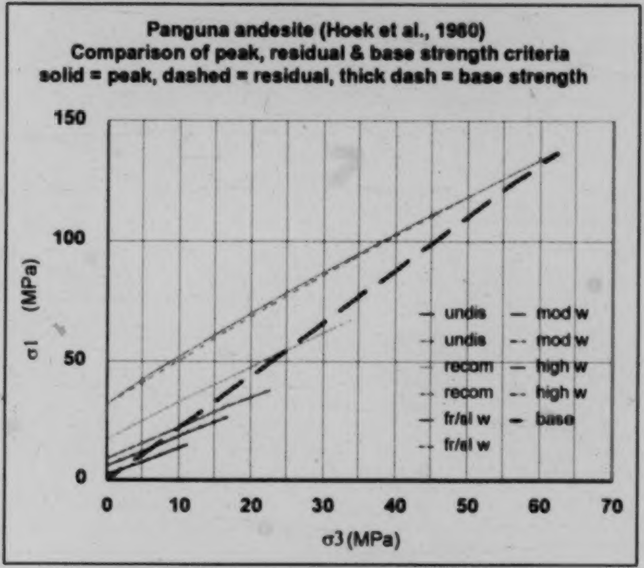

Determination of e_b and the solution to the effective friction - strain polynomial

The procedure outlined in section 6.4.2f was used to determine the base strain, e_b and the values of R, S and T for an exact solution of the effective friction - strain polynomial. All data irrespective of degree of weathering was used in the Y versus e plot, as shown in the figure below.

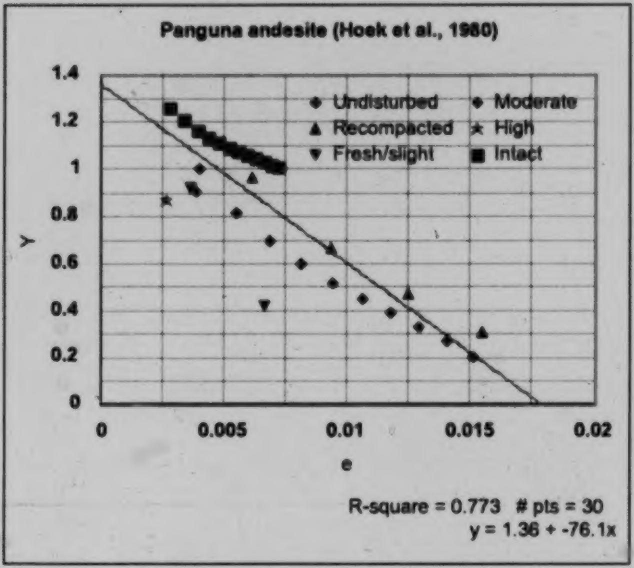

e_b	0.015
R	82
S	-8130
T	274000

The effective friction - strain polynomial compared to the available data

The effective friction - strain plot shows that the initial indication from the Y versus e plot, that the data was more spread out than previously experienced is verified. The plot indicates that there may be different values for the base angle of friction dependent on the degree of weathering. Also the intact data indicates a higher value for ϕ_b than assumed for the undisturbed and recompacted data.

The data was re-worked using values for ϕ_b assumed from the initial effective friction - strain plot for each set of data, resulting in a new effective friction - strain plot for each data set, as illustrated below.

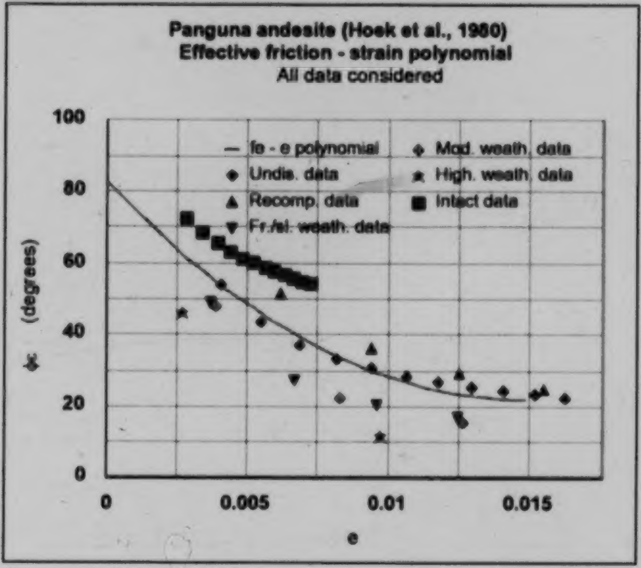

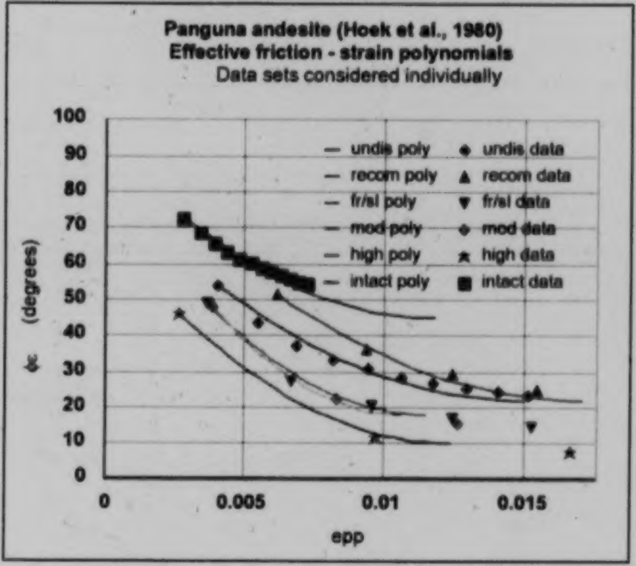

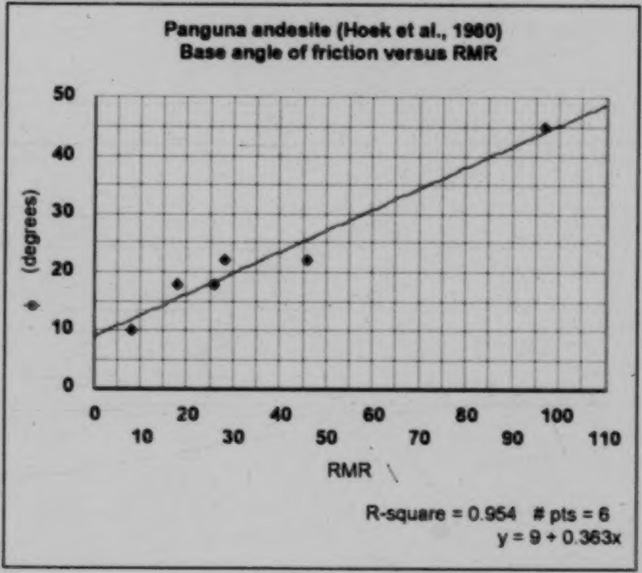

This new effective-friction - strain plot confirmed that there seemed to be different base friction values, dependent on the degree of weathering. Hoek et al. (1980) expressed the degree of weathering in terms of RMR, which when plotted by the author against ϕ_b showed a correlation between degree of weathering and the base angle of friction for the Panguna andesite rock mass, as shown above.

Reconstruction of the crushed rock stress-strain curves

Stress-strain curves were reconstructed for a randomly chosen level of confinement for the weathered and unweathered rock masses. In this case there is no agreement in post peak behaviour for a given confinement. This indicates that for a variable base angle of friction, the common post peak relationship previous seen for a given confinement with other rock masses does not hold. This is also reflected in the normalized post peak modulus curve as shown below.

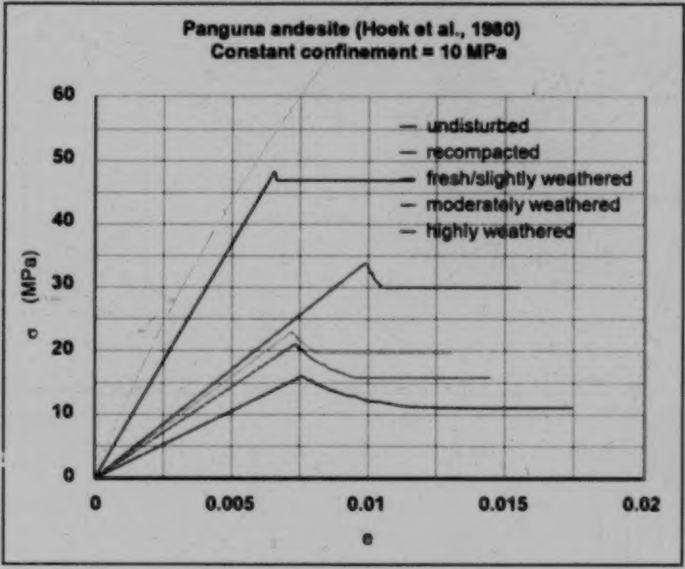

Normalized post peak modulus

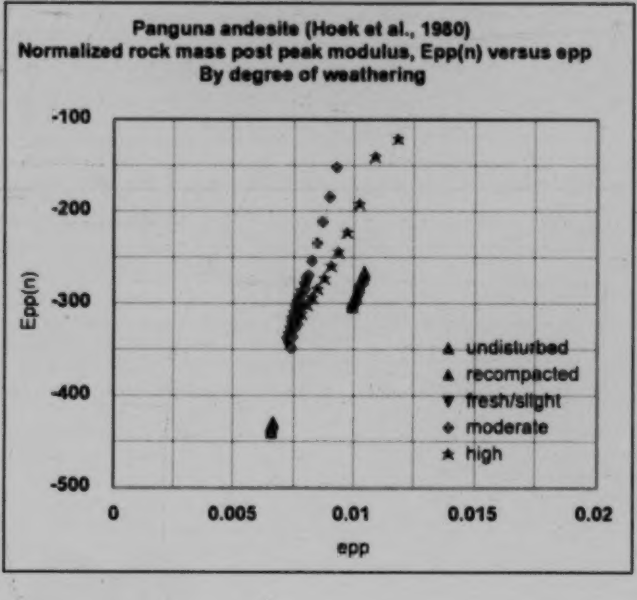

Appendix R

Worked coal data sets

Appendix R.1

Pittsburgh coal (Kripakov, 1981)

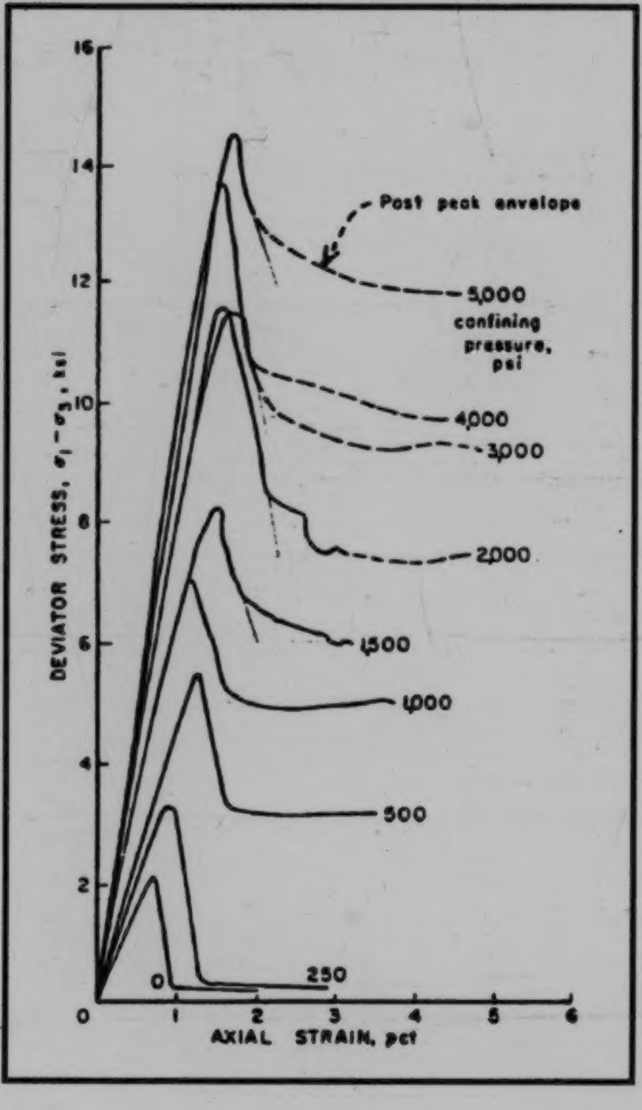

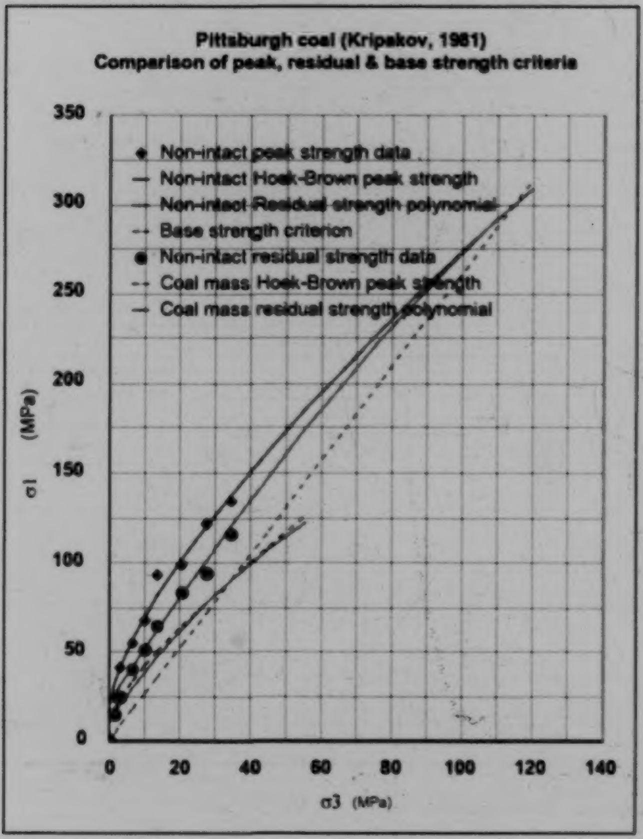
Pittsburgh coal (Kripakov, 1981)
Comparison of peak, residual & base strength criteria
Non-intact peak strength data
Non-intact Hoek-Brown peak strength
Non-intact Residual strength polynomial
Base strength criterion
Non-intact residual strength data
Coal mass Hoek-Brown peak strength
Coal mass residual strength polynomial
σ1 (MPa)
σ3 (MPa)
0
50
100
150
200
250
300
350
0
20
40
60
80
100
120
140

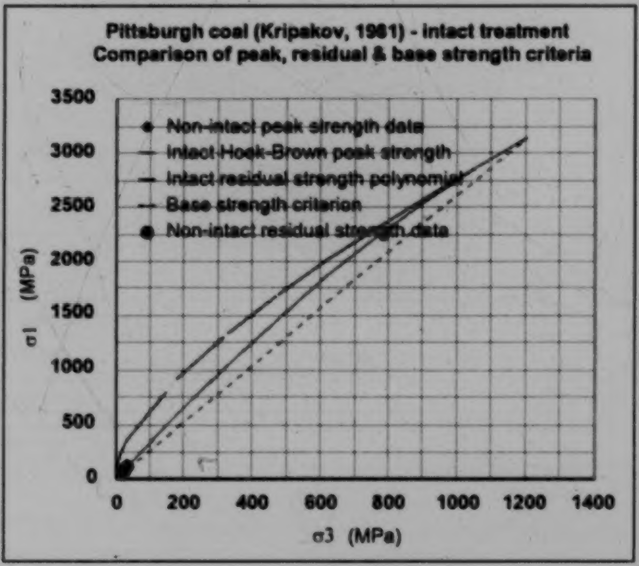
Pittsburgh coal (Kripakov, 1981) - intact treatment
Comparison of peak, residual & base strength criteria
Non-intact peak strength data
Intact Hoek-Brown peak strength
Intact residual strength polynomial
Base strength criterion
Non-intact residual strength data
σ1 (MPa)
3500
3000
2500
2000
1500
1000
500
0
0
200
400
600
800
1000
1200
1400
σ3 (MPa)

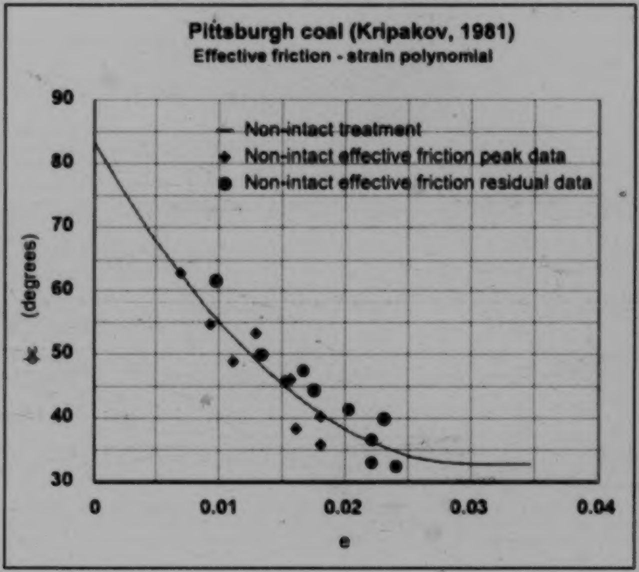
Pittsburgh coal (Kripakov, 1981)
Effective friction - strain polynomial
Non-intact treatment
Non-intact effective friction peak data
Non-intact effective friction residual data
φc (degrees)
90
80
70
60
50
40
30
0
0.01
0.02
0.03
0.04
e

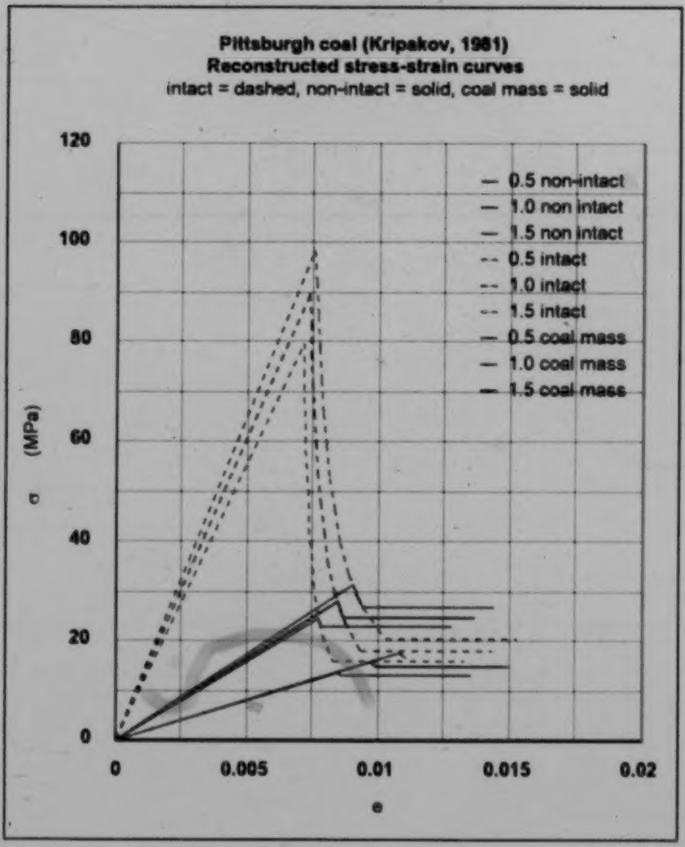
Pittsburgh coal (Kripakov, 1981)
Reconstructed stress-strain curves
intact = dashed, non-intact = solid, coal mass = solid
σ (MPa)
120
100
80
60
40
20
0
0
0.005
0.01
0.015
0.02
e
0.5 non-intact
1.0 non intact
1.5 non intact
0.5 intact
1.0 intact
1.5 intact
0.5 coal mass
1.0 coal mass
1.5 coal mass

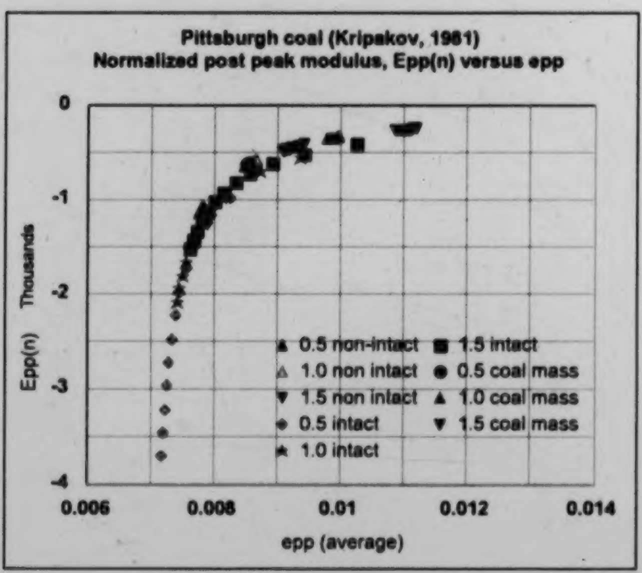

		Treatment		
Criterion	**Parameter**	**Non-intact**	**Coal mass**	**Intact**
Hoek-Brown	m	4.3	1.3	45.7
	σ_c (MPa)	69	69	69
	s *	0.095	0.028	1
Residual	D	-0.02	-0.04	-0.002
	F	3.8	3.3	4.5
	σ_{cr} (MPa)	21	11.5	14
Base strength	ϕ_b (degrees)	33	33	33
Brittle-ductile	σ_{3t} (MPa)	54	17	556
ϕ_c - e	R (degrees)	83.5		
	S	-3390		
	T	56900		
	e_b	0.03		

* Note: Kripakov (1981) did not report his specimen dimensions. It has therefore been assumed that b = 0.055 m and h = 0.11 m.

Appendix R.2

Barnsley brights coal (Hobbs, 1964)

σ_3 (psi)	σ_{1p} (psi)	E_m x 10^5 (psi)
10	3460	3.27
100	6250	3.59
250	6900	4.15
500	7340	4.21
1000	10460	5.77
3000	15710	4.59
5000	19280	5.01

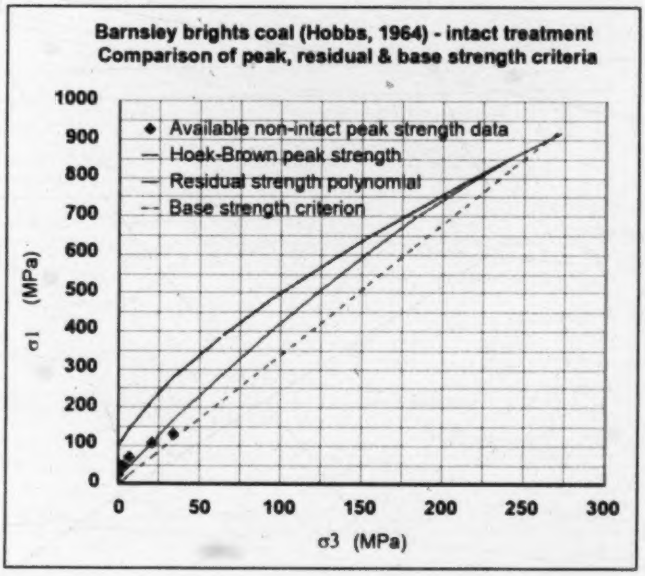

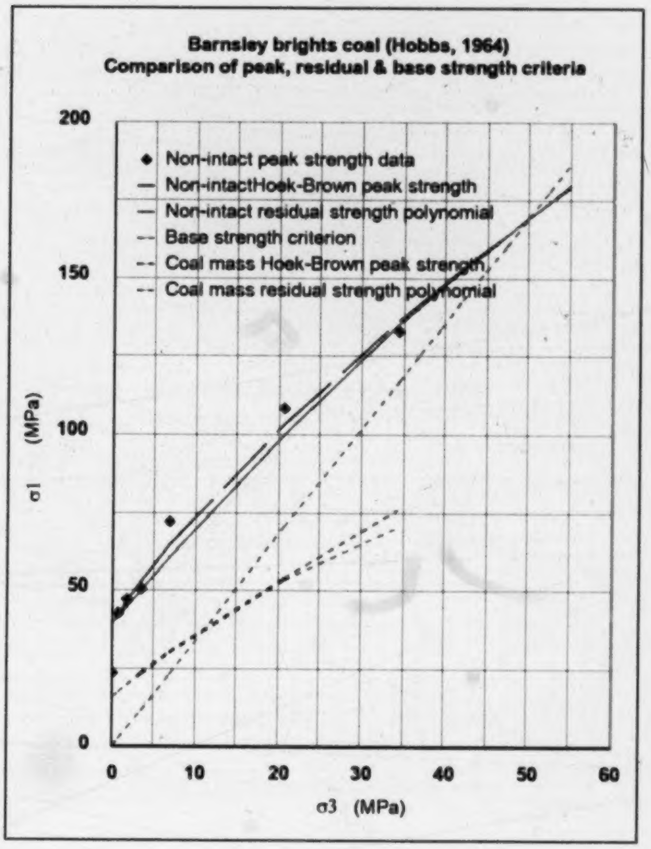
Barnsley brights coal (Hobbs, 1964)
Comparison of peak, residual & base strength criteria
Non-intact peak strength data
Non-intactHoek-Brown peak strength
Non-intact residual strength polynomial
Base strength criterion
Coal mass Hoek-Brown peak strength
Coal mass residual strength polynomial
200
150
100
50
0
σ1 (MPa)
0
10
20
30
40
50
60
σ3 (MPa)

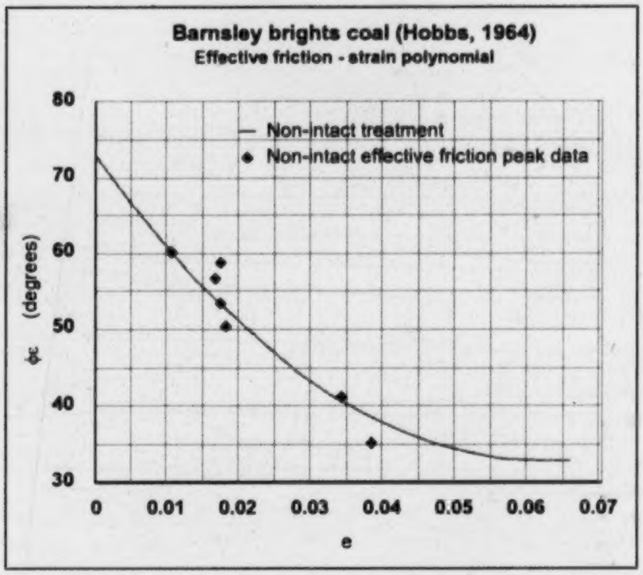

		Treatment		
Criterion	**Parameter**	**Non-intact**	**Coal mass**	**Intact**
Hoek-Brown	m	2.7	0.4	15.6
	σ_c (MPa)	96	96	96
	s	0.17	0.028	1
Residual	D	-0.01	-0.02	-0.004
	F	3.1	2.2	4.5
	σ_{cr} (MPa)	40	16	19
Base strength	ϕ_b (degrees)	33	33	33
Brittle-ductile	σ_{3t} (MPa)	50	11	268
ϕ_e - e	R (degrees)	73		
	S	-1310		
	T	10700		
	e_b	0.06		

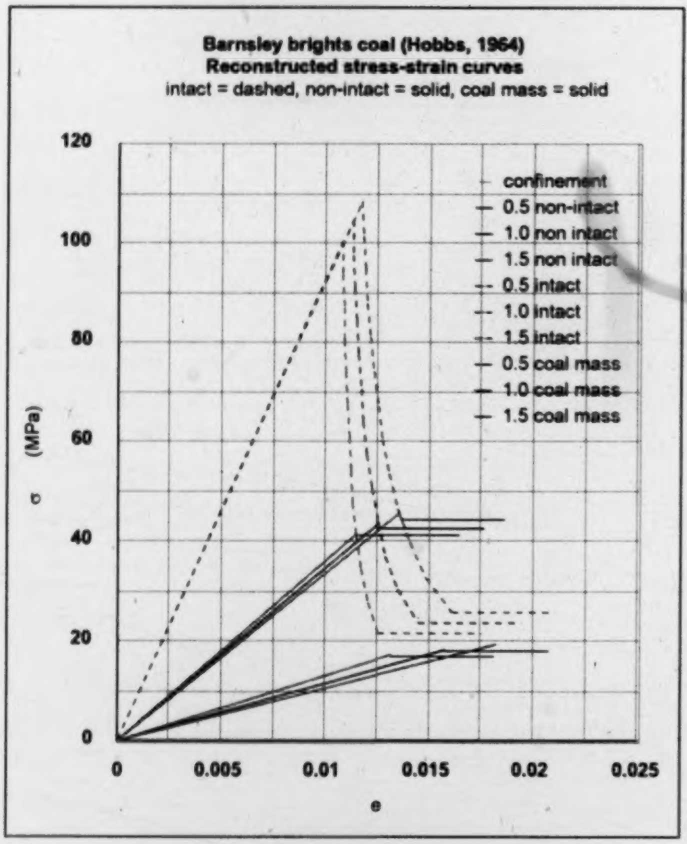

Barnsley brights coal (Hobbs, 1964)
Reconstructed stress-strain curves
intact = dashed, non-intact = solid, coal mass = solid

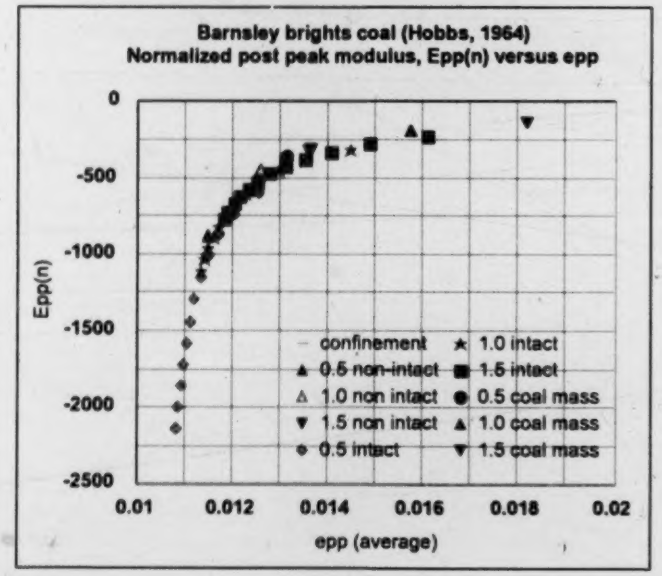

Barnsley brights coal (Hobbs, 1964)
Normalized post peak modulus, Epp(n) versus epp

Appendix R.3

Barnsley hards coal (Hobbs, 1964)

σ_3	σ_{1p}	E_m
(psi)	(psi)	x 10^5 (psi)
10	7450	4.17
100	8050	4.61
250	8410	4.55
500	9320	4.36
1000	14020	4.89
2000	14930	5.21
3000	16430	4.55
4000	17930	4.69
5000	20030	4.62

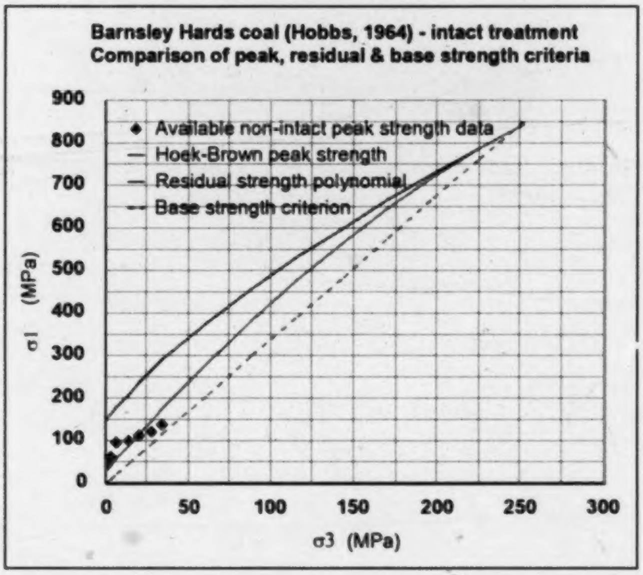

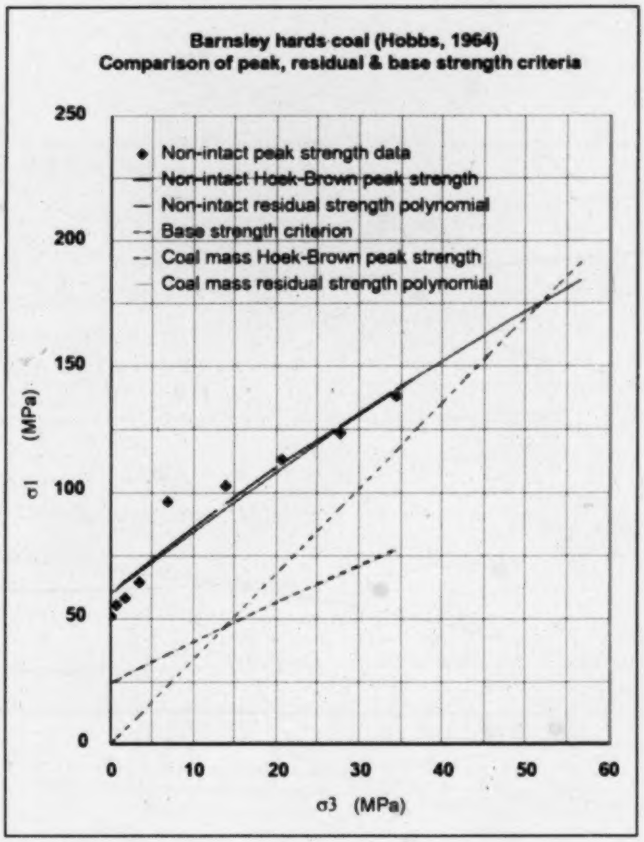
Barnsley hards coal (Hobbs, 1964)
Comparison of peak, residual & base strength criteria
250
200
150
100
50
0
σ1 (MPa)
0
10
20
30
40
50
60
σ3 (MPa)
Non-intact peak strength data
Non-intact Hoek-Brown peak strength
Non-intact residual strength polynomial
Base strength criterion
Coal mass Hoek-Brown peak strength
Coal mass residual strength polynomial

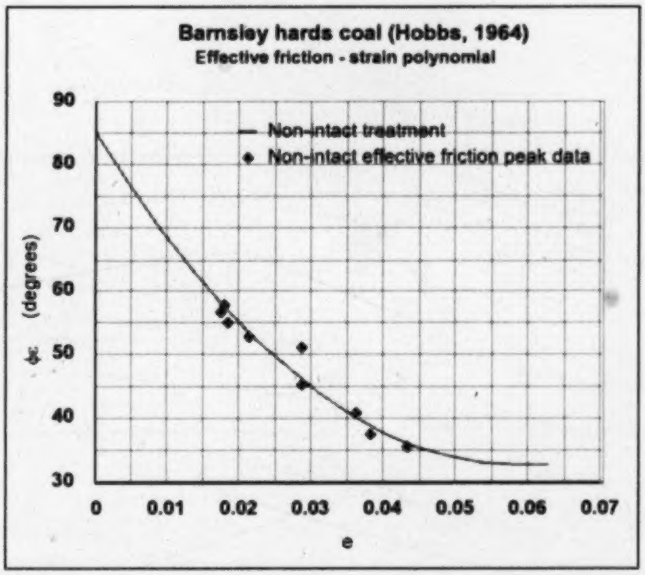

		Treatment		
Criterion	**Parameter**	**Non-intact**	**Coal mass**	**Intact**
Hoek-Brown	m	1.6	0.3	9.2
	σ_c (MPa)	145	145	145
	s	0.17	0.028	1
Residual	D	-0.006	-0.006	-0.005
	F	2.6	1.7	4.4
	σ_{cr} (MPa)	60	24	29
Base strength	ϕ_b (degrees)	33	33	33
Brittle-ductile	σ_{3t} (MPa)	52	14	247
ϕ_e - e	R (degrees)	85		
	S	-1800		
	T	15600		
	e_b	0.06		

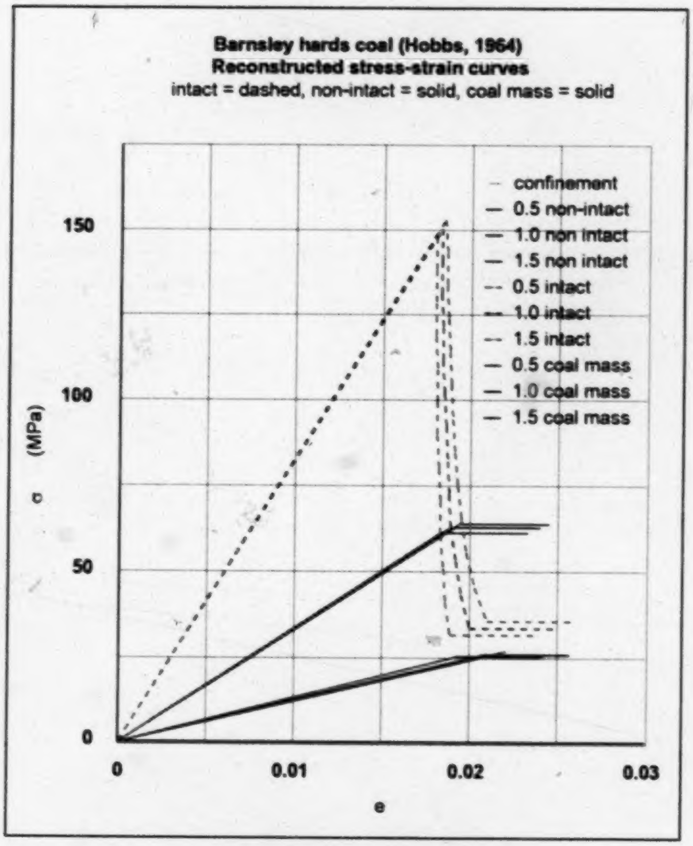
Barnsley hards coal (Hobbs, 1964)
Reconstructed stress-strain curves
intact = dashed, non-intact = solid, coal mass = solid
confinement
0.5 non-intact
1.0 non intact
1.5 non intact
0.5 intact
1.0 intact
1.5 intact
0.5 coal mass
1.0 coal mass
1.5 coal mass
σ (MPa)
150
100
50
0
0
0.01
0.02
0.03
e

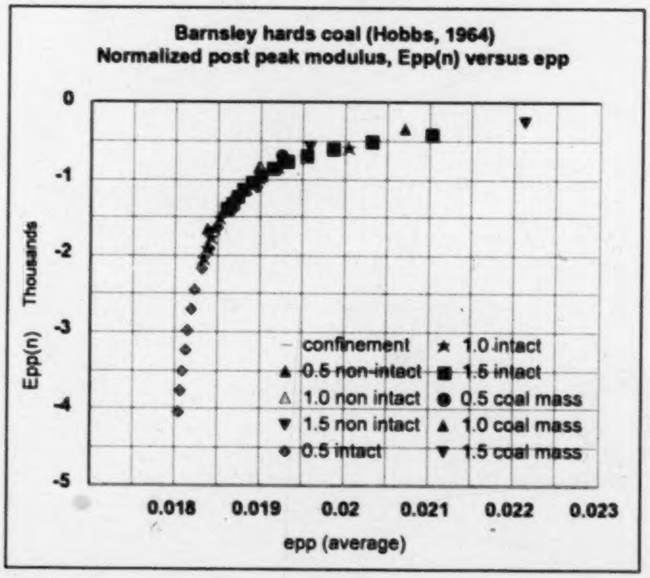
Barnsley hards coal (Hobbs, 1964)
Normalized post peak modulus, Epp(n) versus epp
Epp(n) Thousands
0
-1
-2
-3
-4
-5
0.018
0.019
0.02
0.021
0.022
0.023
epp (average)
confinement
0.5 non-intact
1.0 non intact
1.5 non intact
0.5 intact
1.0 intact
1.5 intact
0.5 coal mass
1.0 coal mass
1.5 coal mass

Appendix R.4

Cwmtillery coal (Hobbs, 1964)

σ_3 (psi)	σ_{1p} (psi)	E_m x 10^5 (psi)
10	1920	3.47
100	4310	4.81
250	4350	3.76
500	6210	4.43
1000	8520	5.94
3000	13690	5.14
5000	18160	6.02

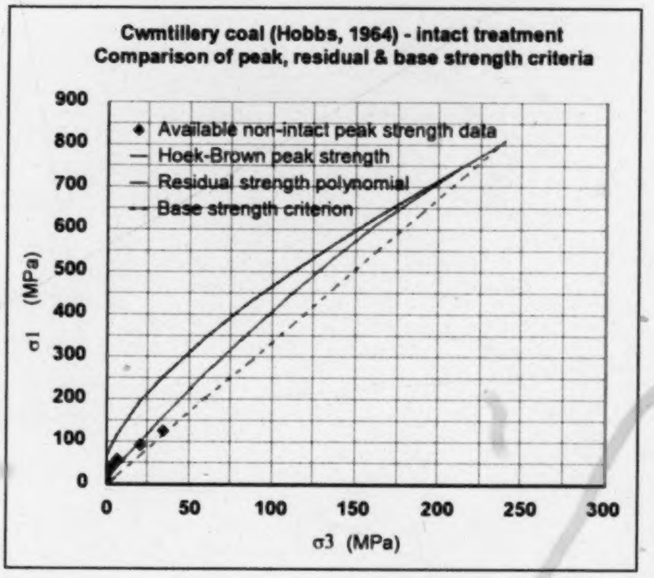

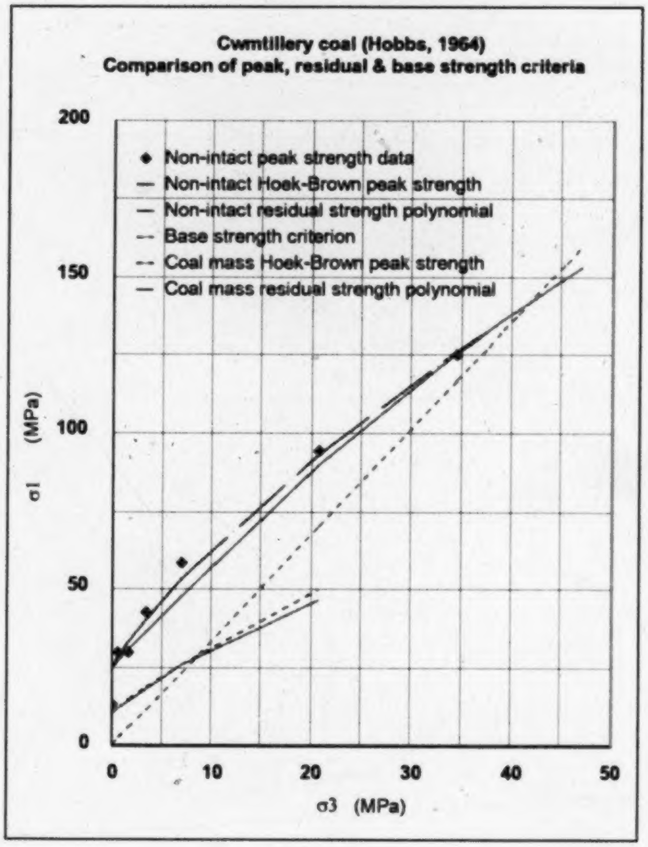
Cwmtillery coal (Hobbs, 1964)
Comparison of peak, residual & base strength criteria
◆ Non-intact peak strength data
— Non-intact Hoek-Brown peak strength
— Non-intact residual strength polynomial
-- Base strength criterion
-- Coal mass Hoek-Brown peak strength
— Coal mass residual strength polynomial
200
150
100
50
0
σ1 (MPa)
0
10
20
30
40
50
σ3 (MPa)

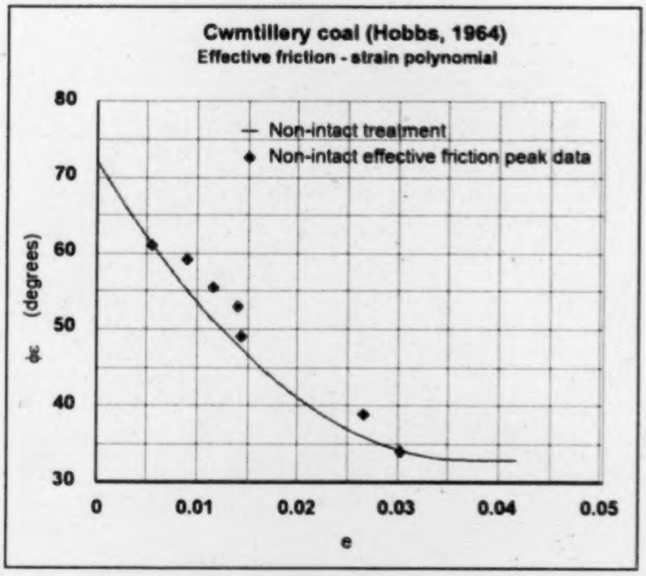

		Treatment		
Criterion	**Parameter**	**Non-intact**	**Coal mass**	**Intact**
Hoek-Brown	m	3.7	0.6	22.0
	σ_c (MPa)	60	60	60
	s	0.17	0.028	1
Residual	D	-0.02	-0.04	-0.005
	F	3.5	2.5	4.5
	σ_{cr} (MPa)	25	10	12
Base strength	ϕ_b (degrees)	33	33	33
Brittle-ductile	σ_{3t} (MPa)	42	9	235
ϕ_e - e	R (degrees)	72		
	S	-2130		
	T	28900		
	e_b	0.04		

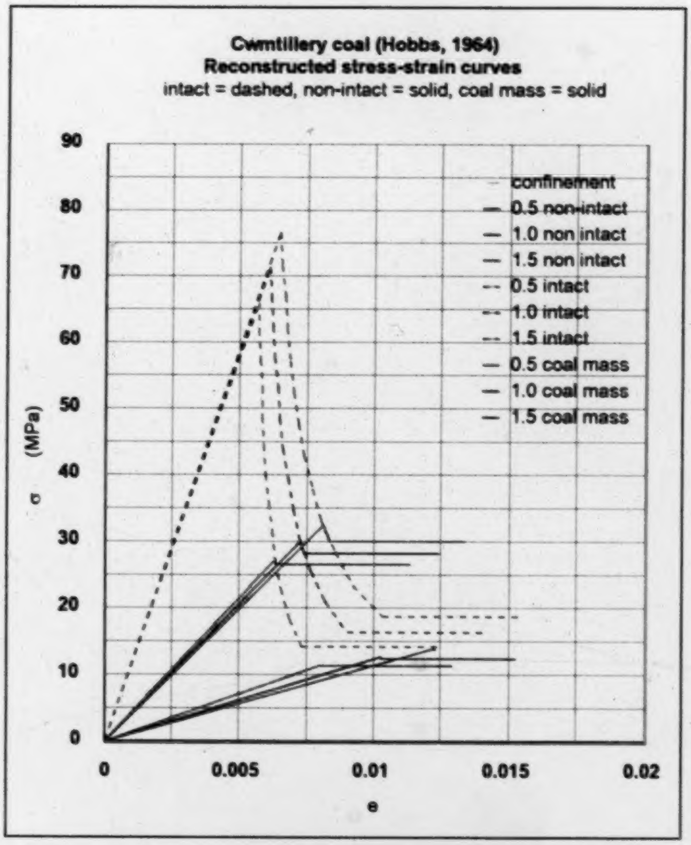
Cwmtillery coal (Hobbs, 1964)
Reconstructed stress-strain curves
intact = dashed, non-intact = solid, coal mass = solid
σ (MPa)
e
0
10
20
30
40
50
60
70
80
90
0
0.005
0.01
0.015
0.02
confinement
0.5 non-intact
1.0 non intact
1.5 non intact
0.5 intact
1.0 intact
1.5 intact
0.5 coal mass
1.0 coal mass
1.5 coal mass

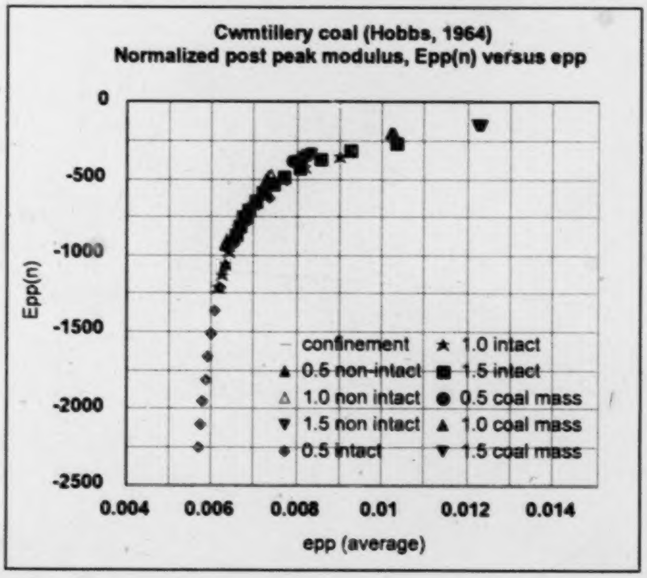
Cwmtillery coal (Hobbs, 1964)
Normalized post peak modulus, Epp(n) versus epp
Epp(n)
epp (average)
0
-500
-1000
-1500
-2000
-2500
0.004
0.006
0.008
0.01
0.012
0.014
confinement
0.5 non-intact
1.0 non intact
1.5 non intact
0.5 intact
1.0 intact
1.5 intact
0.5 coal mass
1.0 coal mass
1.5 coal mass

Appendix R.5

Deep Duffryn coal (Hobbs, 1964)

σ_3	σ_{1p}	E_m
(psi)	(psi)	x 10^5 (psi)
10	1000	2.53
100	2760	3.72
250	3780	3.29
500	5010	3.85
1000	7350	5.15
2000	9970	4.29
3000	11620	4.67
4000	14460	5.6
5000	16040	5.66

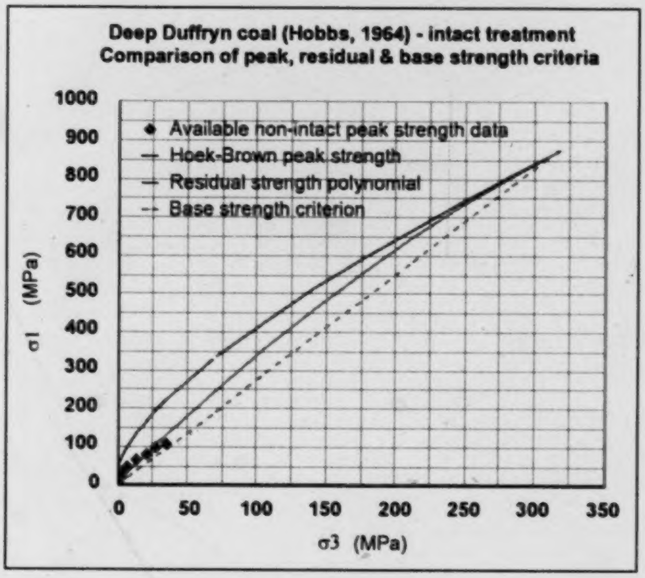

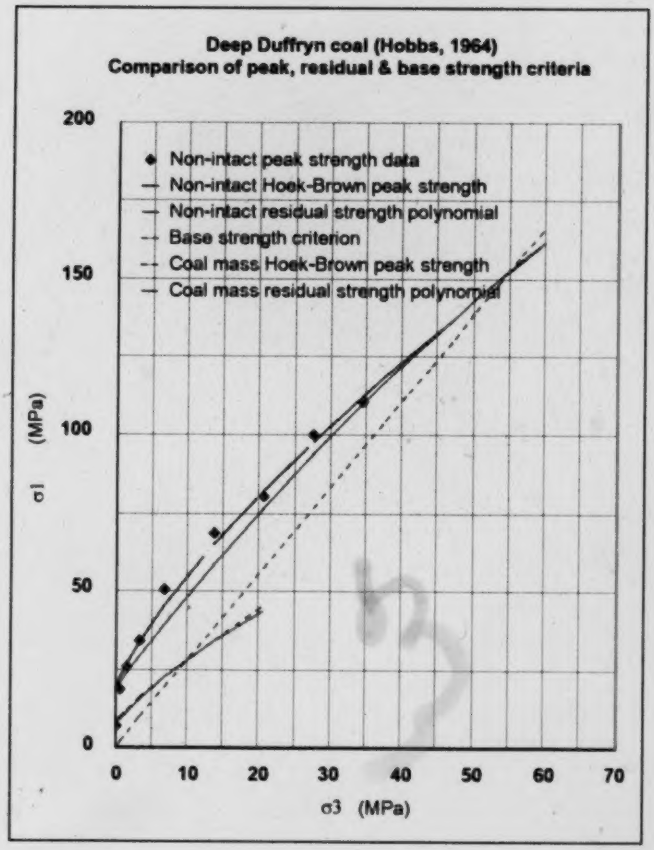

Deep Duffryn coal (Hobbs, 1964)
Comparison of peak, residual & base strength criteria

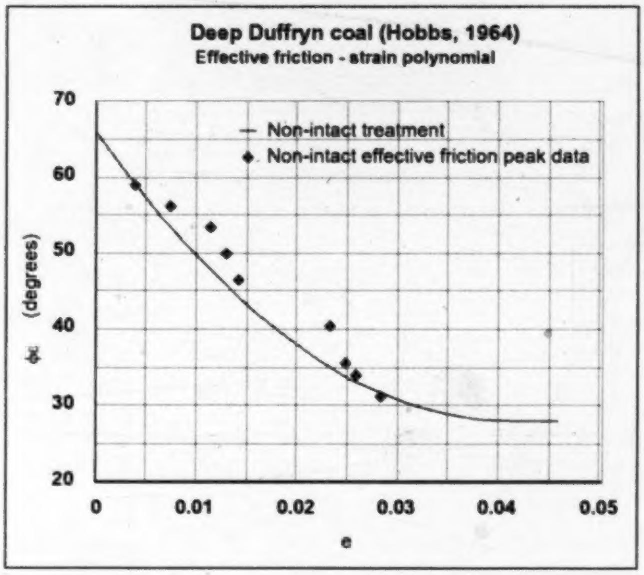

		Treatment		
Criterion	**Parameter**	**Non-intact**	**Coal mass**	**Intact**
Hoek-Brown	m	3.6	0.6	21.0
	σ_c (MPa)	46	46	46
	s	0.17	0.028	1
Residual	D	-0.01	-0.03	-0.003
	F	3.0	2.3	3.6
	σ_{cr} (MPa)	19	8	9
Base strength	ϕ_b (degrees)	28	28	28
Brittle-ductile	σ_{3t} (MPa)	55	11.5	313.5
ϕ_e - e	R (degrees)	66		
	S	-1850		
	T	22600		
	e_b	0.04		

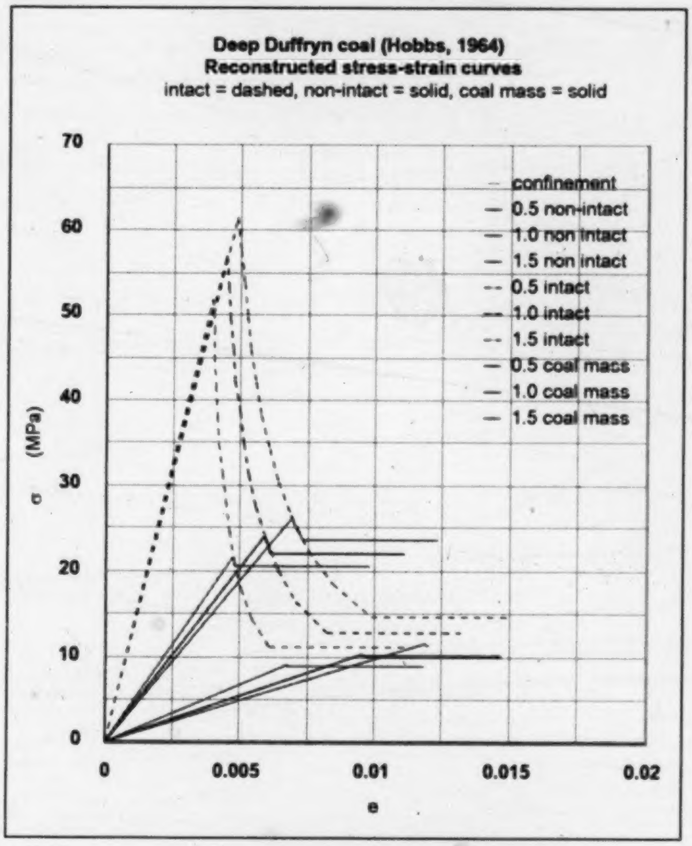
Deep Duffryn coal (Hobbs, 1964)
Reconstructed stress-strain curves
intact = dashed, non-intact = solid, coal mass = solid
σ (MPa)
0
10
20
30
40
50
60
70
0
0.005
0.01
0.015
0.02
e
confinement
0.5 non-intact
1.0 non intact
1.5 non intact
0.5 intact
1.0 intact
1.5 intact
0.5 coal mass
1.0 coal mass
1.5 coal mass

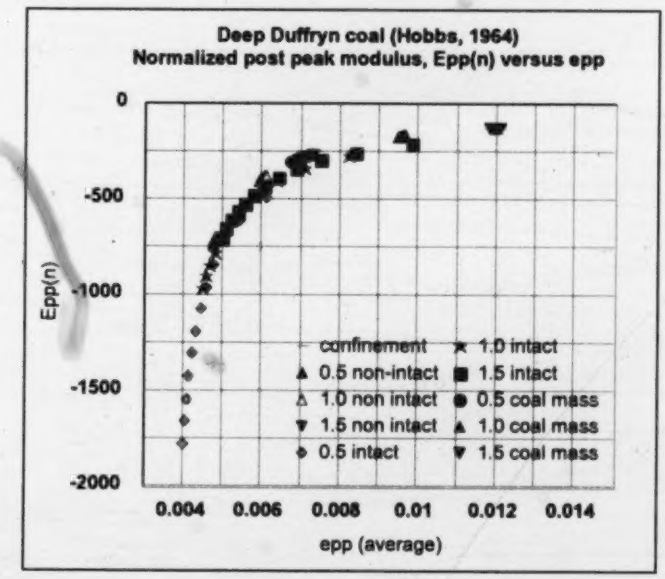
Deep Duffryn coal (Hobbs, 1964)
Normalized post peak modulus, Epp(n) versus epp
Epp(n)
0
-500
-1000
-1500
-2000
0.004
0.006
0.008
0.01
0.012
0.014
epp (average)
confinement
0.5 non-intact
1.0 non intact
1.5 non intact
0.5 intact
1.0 intact
1.5 intact
0.5 coal mass
1.0 coal mass
1.5 coal mass

Appendix R.6

Linby coal (Hobbs, 1964)

σ_3	σ_{1n}	E_m
(psi)	(psi)	x 10^5 (psi)
10	3150	4.71
100	5470	3.48
250	8370	4.14
500	8780	3.66
1000	11600	3.75
3000	17140	3.87
5000	21230	3.81

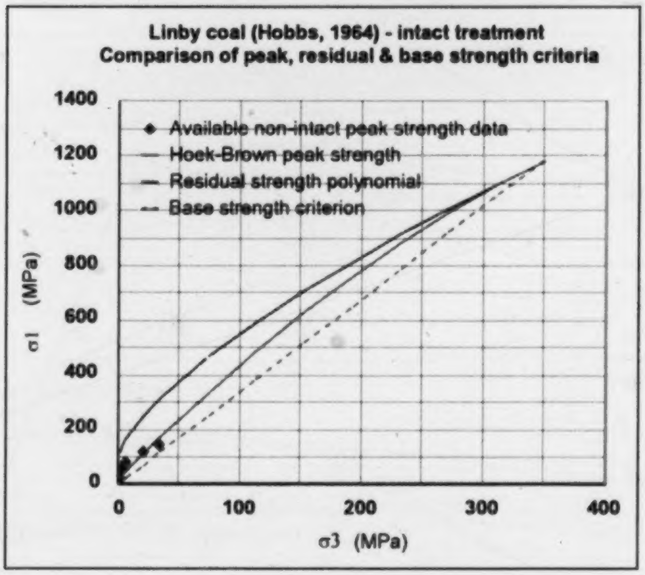

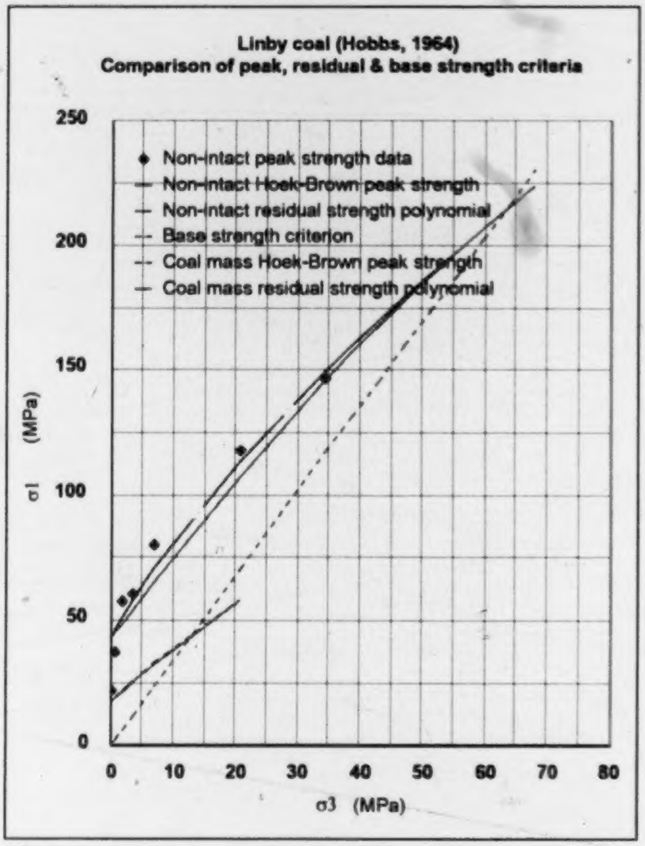
Linby coal (Hobbs, 1964)
Comparison of peak, residual & base strength criteria
Non-intact peak strength data
Non-intact Hoek-Brown peak strength
Non-intact residual strength polynomial
Base strength criterion
Coal mass Hoek-Brown peak strength
Coal mass residual strength polynomial
σ1 (MPa)
σ3 (MPa)
0
50
100
150
200
250
0
10
20
30
40
50
60
70
80

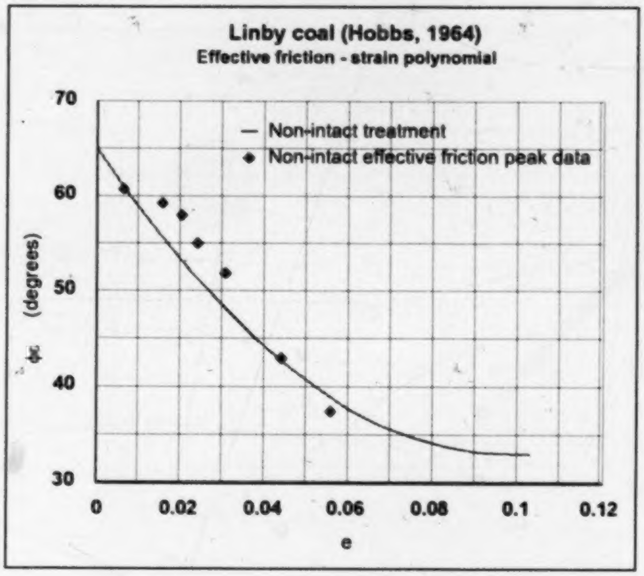

		Treatment		
Criterion	**Parameter**	**Non-intact**	**Coal mass**	**Intact**
Hoek-Brown	m	3.2	0.5	18.6
	σ_c (MPa)	105	105	105
	s	0.17	0.028	1
Residual	D	-0.01	-0.019	-0.003
	F	3.3	2.3	4.5
	σ_{cr} (MPa)	43	18	21
Base strength	ϕ_b (degrees)	33	33	33
Brittle-ductile	σ_{3t} (MPa)	63	13.5	346
ϕ_c - e	R (degrees)	65		
	S	-652		
	T	3310		
	e_b	0.1		

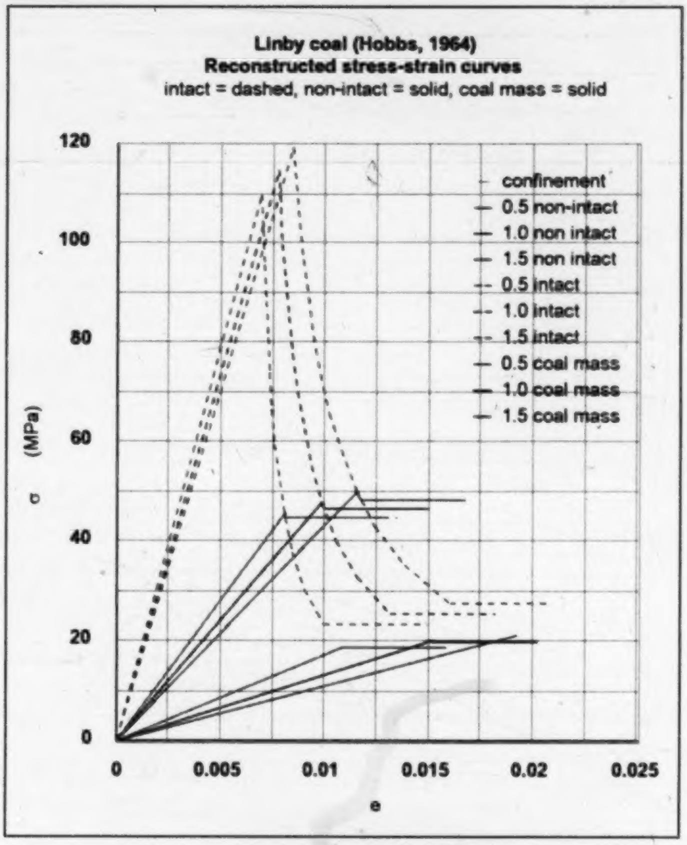
Linby coal (Hobbs, 1964)
Reconstructed stress-strain curves
intact = dashed, non-intact = solid, coal mass = solid
120
100
80
60
40
20
0
σ (MPa)
0
0.005
0.01
0.015
0.02
0.025
e
confinement
0.5 non-intact
1.0 non intact
1.5 non intact
0.5 intact
1.0 intact
1.5 intact
0.5 coal mass
1.0 coal mass
1.5 coal mass

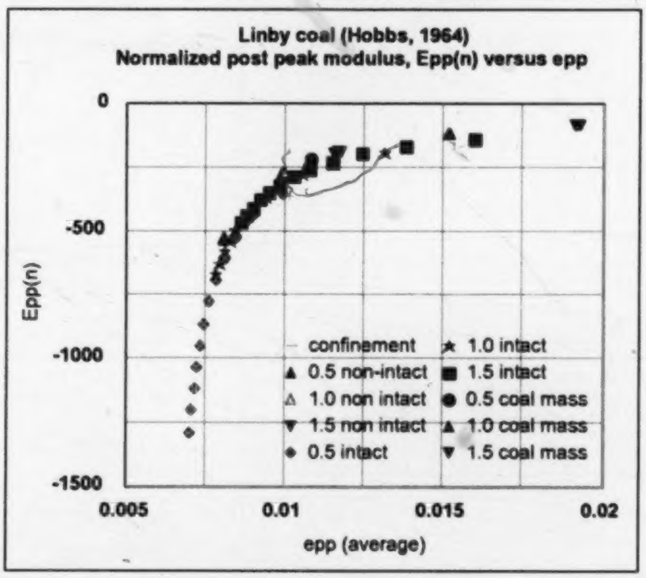
Linby coal (Hobbs, 1964)
Normalized post peak modulus, Epp(n) versus epp
0
-500
-1000
-1500
Epp(n)
0.005
0.01
0.015
0.02
epp (average)
confinement
0.5 non-intact
1.0 non intact
1.5 non intact
0.5 intact
1.0 intact
1.5 intact
0.5 coal mass
1.0 coal mass
1.5 coal mass

Appendix R.7

Markham coal (Hobbs, 1964)

σ_3	σ_{1p}	E_m
(psi)	(psi)	x 10^5 (psi)
10	3160	3.51
100	3550	3.39
250	6670	4.8
500	7560	5.04
1000	8350	4.54
2000	12060	5.34
3000	14350	5.09
4000	15300	5.53
5000	17900	5.16

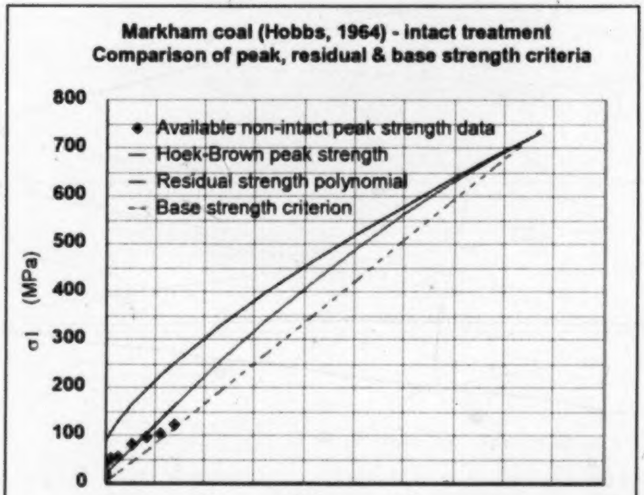

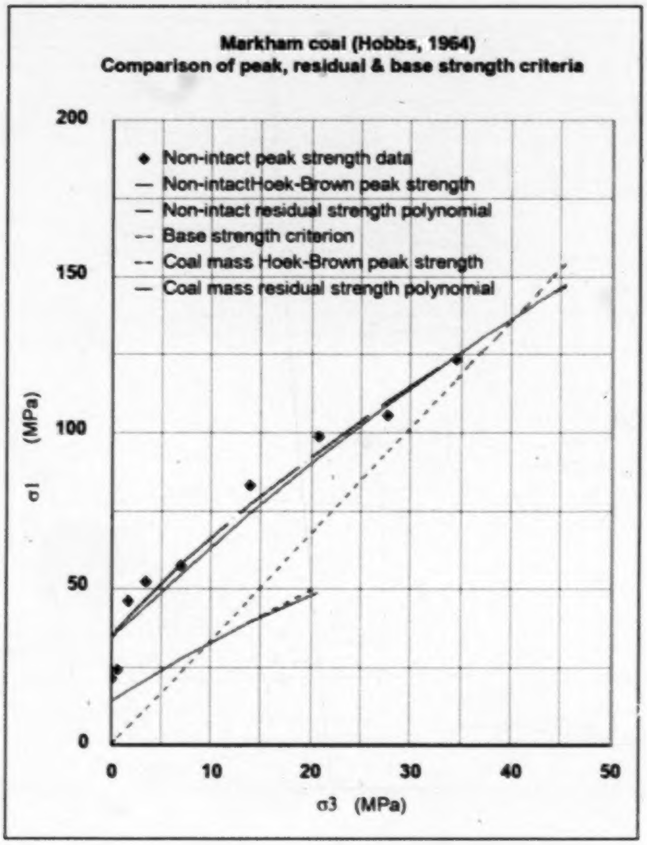
Markham coal (Hobbs, 1964)
Comparison of peak, residual & base strength criteria
◆ Non-intact peak strength data
— Non-intactHoek-Brown peak strength
— Non-intact residual strength polynomial
-- Base strength criterion
-- Coal mass Hoek-Brown peak strength
— Coal mass residual strength polynomial
σ1 (MPa)
σ3 (MPa)
0
50
100
150
200
0
10
20
30
40
50

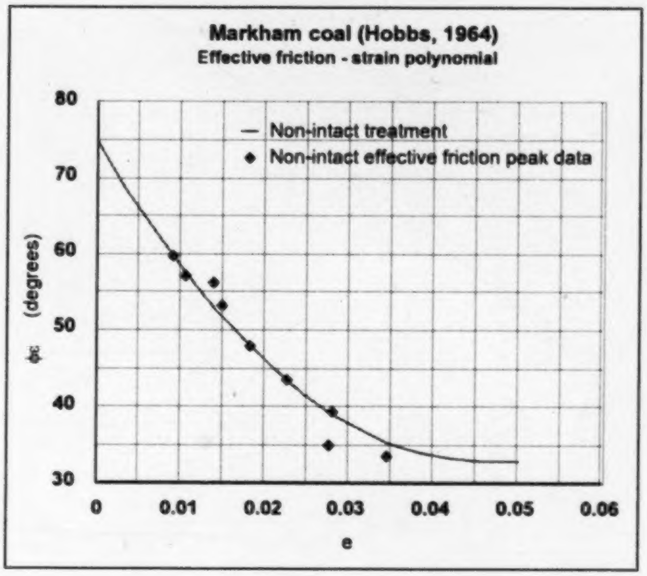

		Treatment		
Criterion	**Parameter**	**Non-intact**	**Coal mass**	**Intact**
Hoek-Brown	m	2.4	0.4	14.2
	σ_c (MPa)	84	84	84
	s	0.17	0.028	1
Residual	D	-0.01	-0.02	-0.005
	F	3.0	2.1	4.5
	σ_{cr} (MPa)	34.5	14	17
Base strength	ϕ_b (degrees)	33	33	33
Brittle-ductile	σ_{3l} (MPa)	40	9	214
ϕ_c - e	R (degrees)	75		
	S	-1840		
	T	20300		
	e_b	0.045		

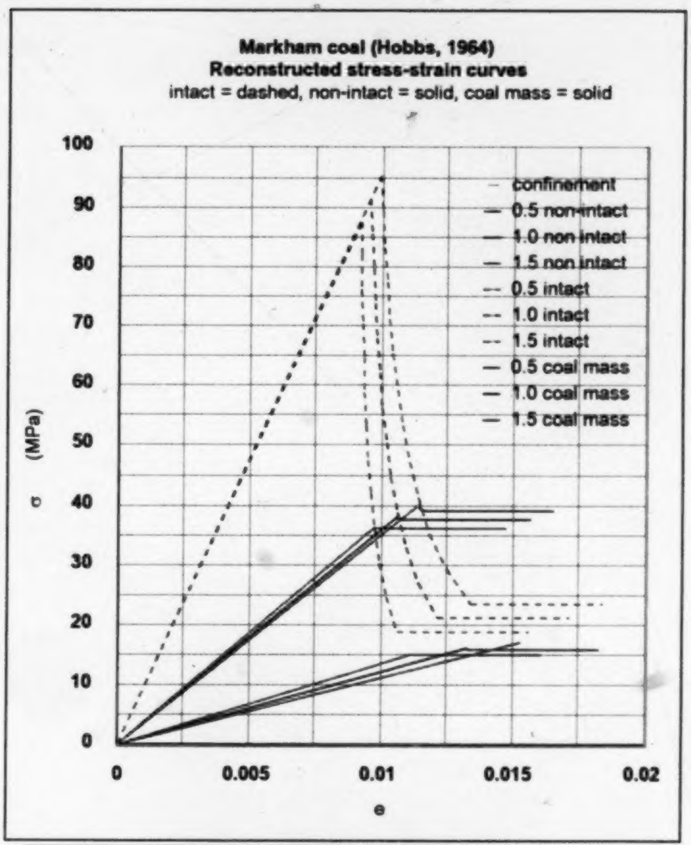

Markham coal (Hobbs, 1964)
Reconstructed stress-strain curves
intact = dashed, non-intact = solid, coal mass = solid

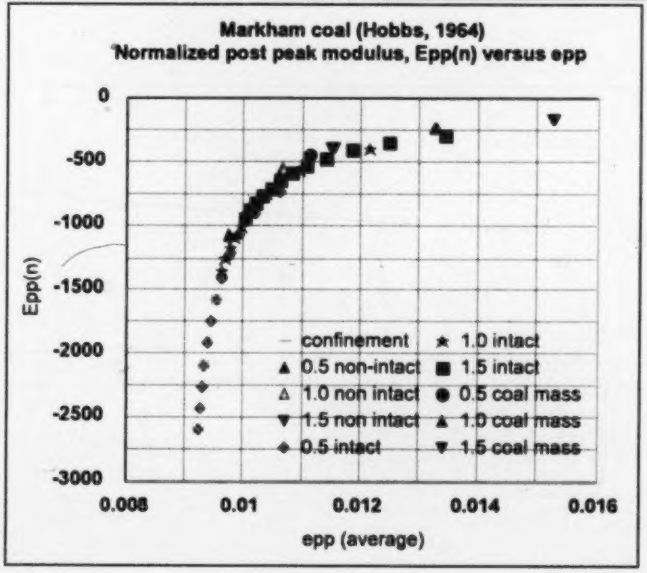

Markham coal (Hobbs, 1964)
Normalized post peak modulus, Epp(n) versus epp

Appendix R.8

Oakdale coal (Hobbs, 1964)

σ_3	σ_{1p}	E_m
(psi)	(psi)	x 10^5 (psi)
10	770	1.72
100	2890	2.87
250	3510	3.55
500	5990	5.31
1000	6160	4.21
2000	8160	4.58
3000	11110	5.04
4000	12670	5.02
5000	17000	6.46

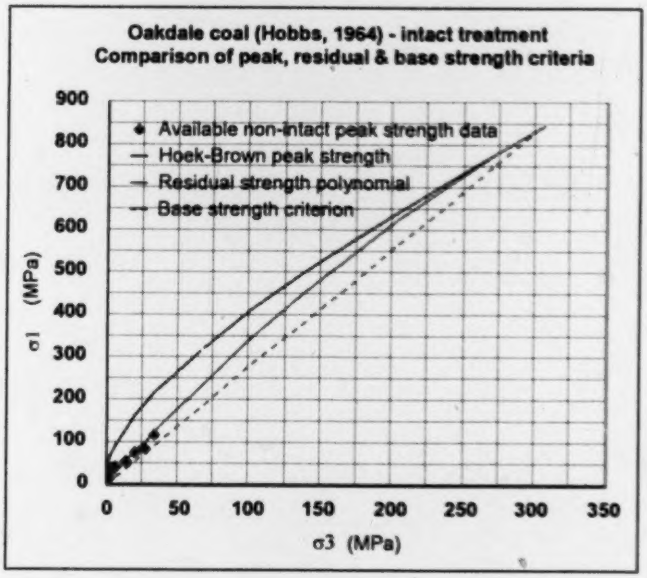

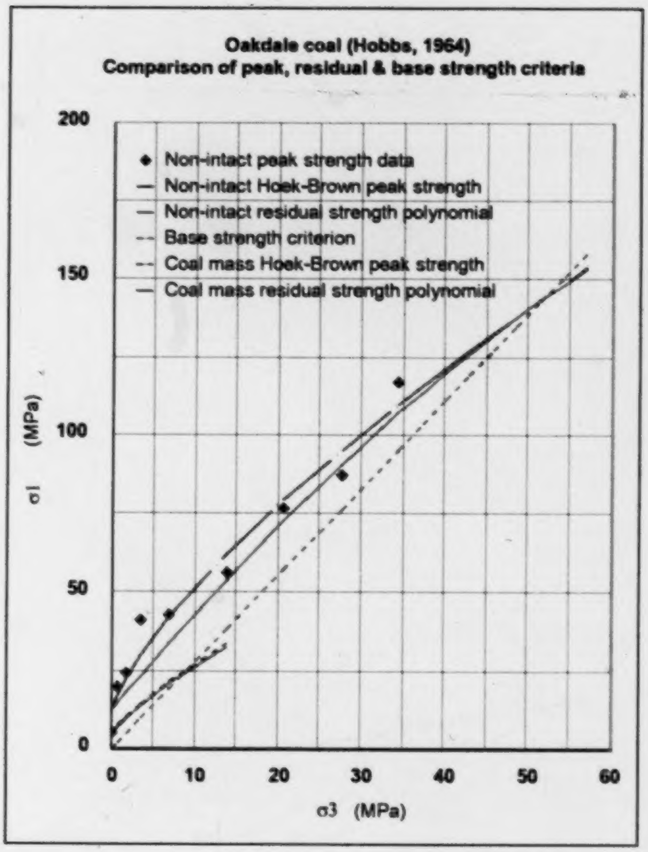
Oakdale coal (Hobbs, 1964)
Comparison of peak, residual & base strength criteria
Non-intact peak strength data
Non-intact Hoek-Brown peak strength
Non-intact residual strength polynomial
Base strength criterion
Coal mass Hoek-Brown peak strength
Coal mass residual strength polynomial
σ1 (MPa)
σ3 (MPa)
0
50
100
150
200
0
10
20
30
40
50
60

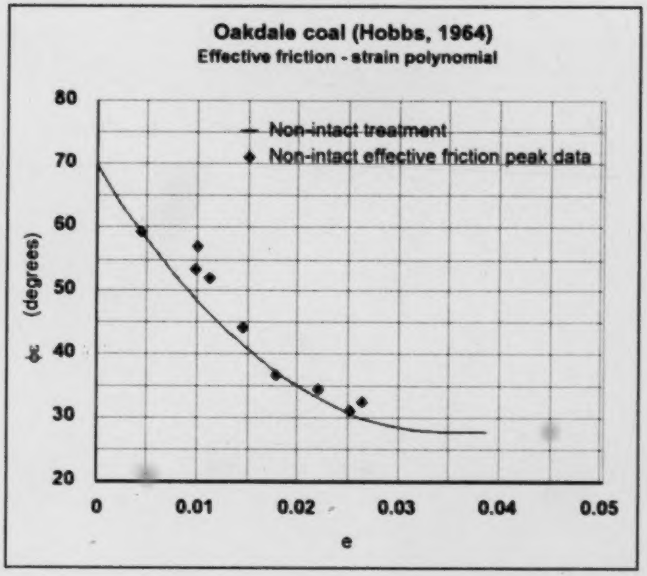

		Treatment		
Criterion	**Parameter**	**Non-intact**	**Coal mass**	**Intact**
Hoek-Brown	m	5.3	0.9	31.0
	σ_c (MPa)	30.5	30.5	30.5
	s	0.17	0.028	1
Residual	D	-0.01	-0.05	-0.003
	F	3.2	2.7	3.6
	σ_{cr} (MPa)	13	5	6
Base strength	ϕ_b (degrees)	28	28	28
Brittle-ductile	σ_{3t} (MPa)	52	9	302
ϕ_e - e	R (degrees)	70		
	S	-2470		
	T	36500		
	e_h	0.03		

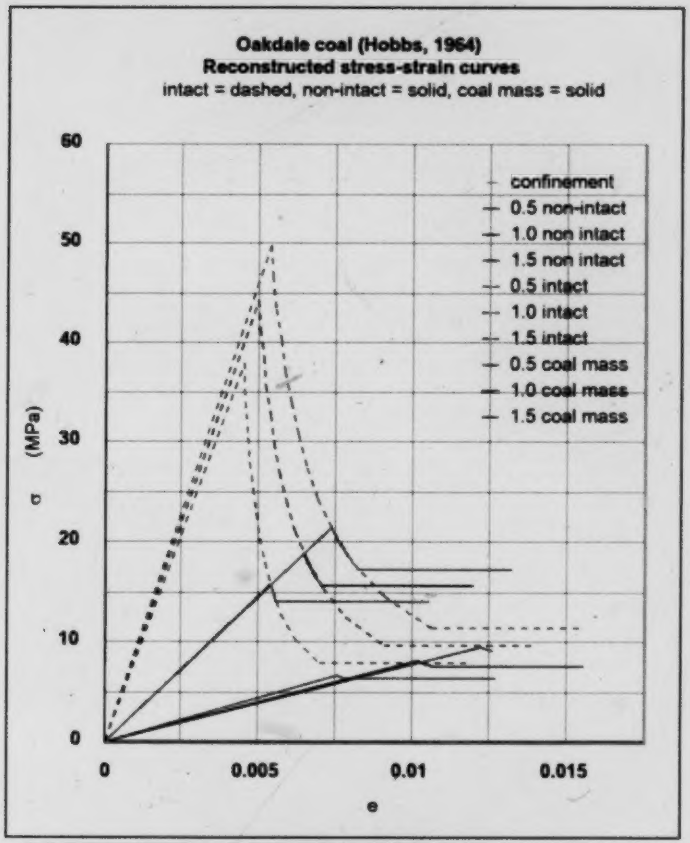

Oakdale coal (Hobbs, 1964)
Reconstructed stress-strain curves
intact = dashed, non-intact = solid, coal mass = solid

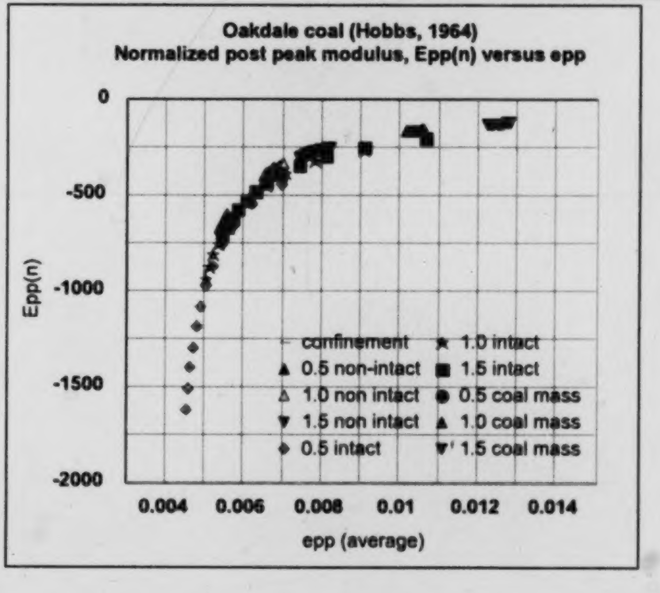

Oakdale coal (Hobbs, 1964)
Normalized post peak modulus, Epp(n) versus epp

Appendix R.9

Pentremawr coal (Hobbs, 1964)

σ_3	σ_{1p}	E_m
(psi)	(psi)	x 10^5 (psi)
10	4580	3.91
1000	11100	5.94
2000	14200	5.16
3000	18630	5.56
4000	22920	6.15

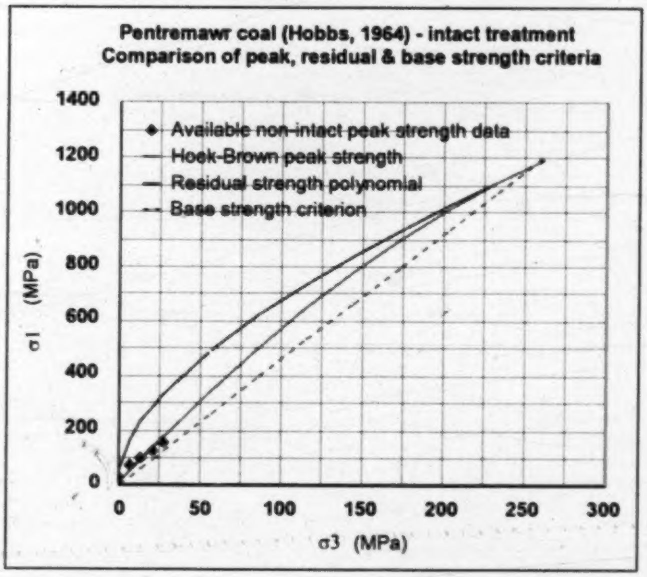

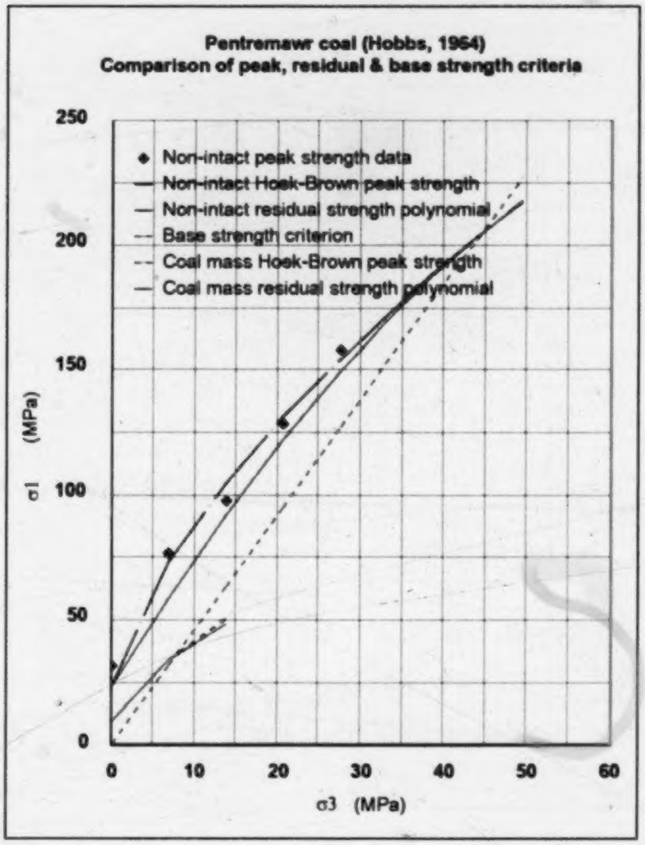
Pentremawr coal (Hobbs, 1964)
Comparison of peak, residual & base strength criteria
◆ Non-intact peak strength data
Non-intact Hoek-Brown peak strength
Non-intact residual strength polynomial
Base strength criterion
Coal mass Hoek-Brown peak strength
Coal mass residual strength polynomial
σ1 (MPa)
σ3 (MPa)
0
50
100
150
200
250
0
10
20
30
40
50
60

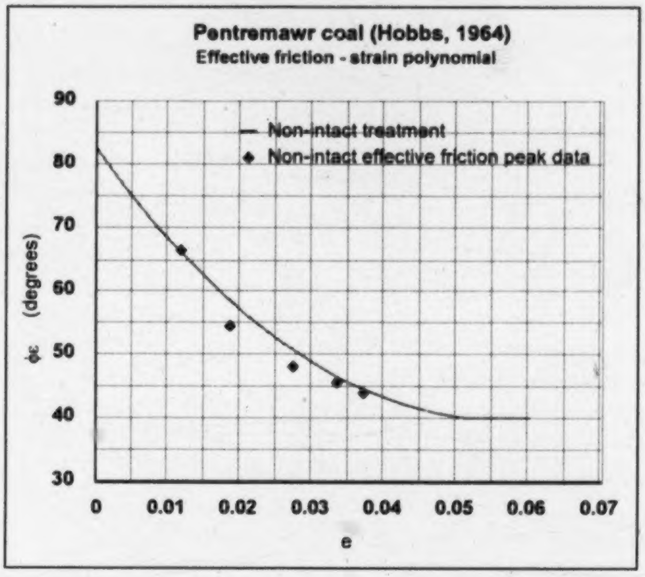

		Treatment		
Criterion	**Parameter**	**Non-intact**	**Coal mass**	**Intact**
Hoek-Brown	m	10.2	1.7	59.8
	σ_c (MPa)	55.5	55.5	55.5
	s	0.17	0.028	1
Residual	D	-0.03	-0.1	-0.007
	F	5.4	4.3	6.3
	σ_{cr} (MPa)	23	9	11
Base strength	ϕ_b (degrees)	40	40	40
Brittle-ductile	σ_{3t} (MPa)	44.5	8	257
ϕ_c - e	R (degrees)	82.5		
	S	-1540		
	T	13900		
	e_b	0.055		

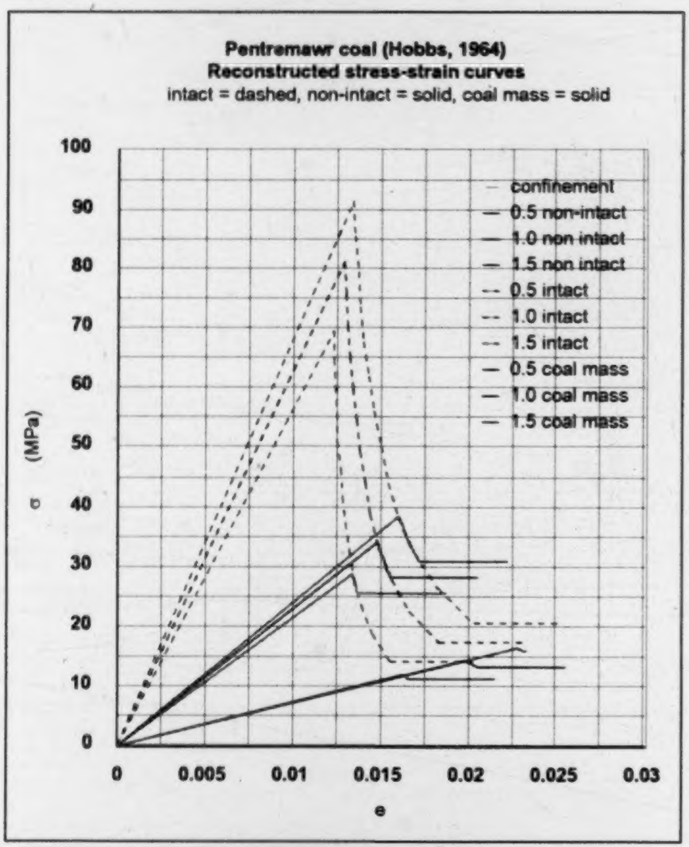

Pentremawr coal (Hobbs, 1964)
Reconstructed stress-strain curves
intact = dashed, non-intact = solid, coal mass = solid

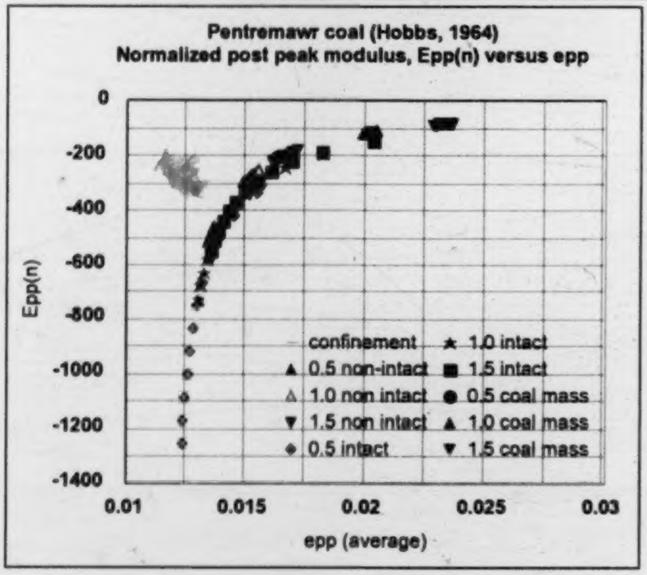

Pentremawr coal (Hobbs, 1964)
Normalized post peak modulus, Epp(n) versus epp

Appendix R.10

Teversal coal (Hobbs, 1964)

σ_3 (psi)	σ_{1p} (psi)	E_m x 10^5 (psi)
10	2280	1.66
500	6730	3.19
1000	9220	3.79
3000	15420	3.55
5000	18910	3.74

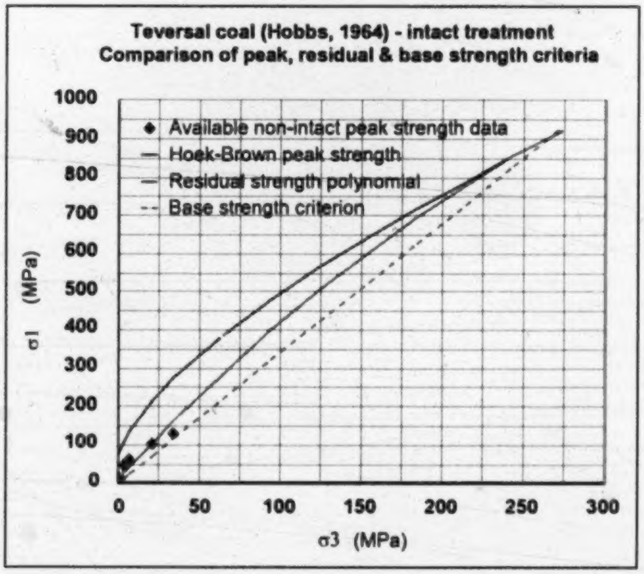

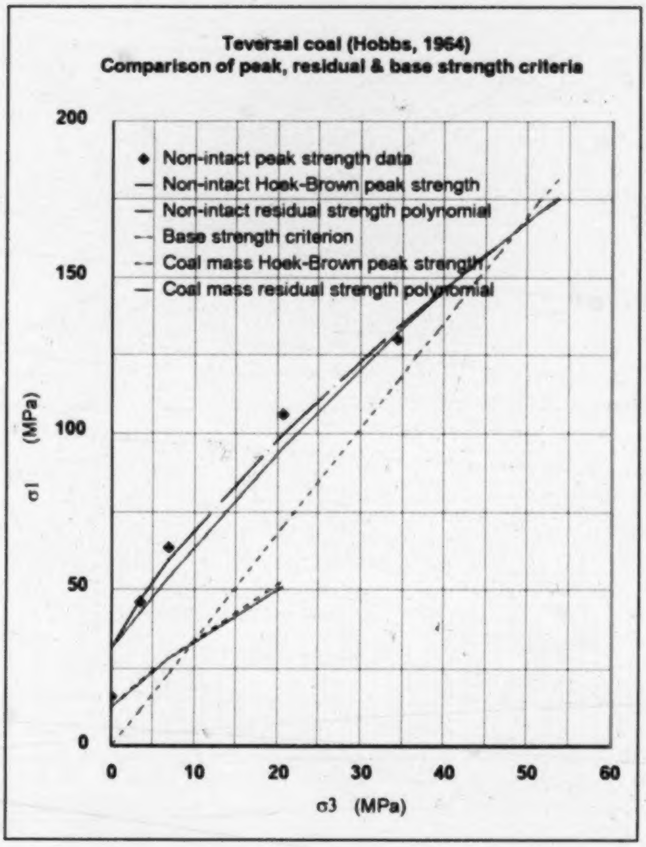
Teversal coal (Hobbs, 1964)
Comparison of peak, residual & base strength criteria
Non-intact peak strength data
Non-intact Hoek-Brown peak strength
Non-intact residual strength polynomial
Base strength criterion
Coal mass Hoek-Brown peak strength
Coal mass residual strength polynomial
200
150
100
50
0
σ1 (MPa)
0
10
20
30
40
50
60
σ3 (MPa)

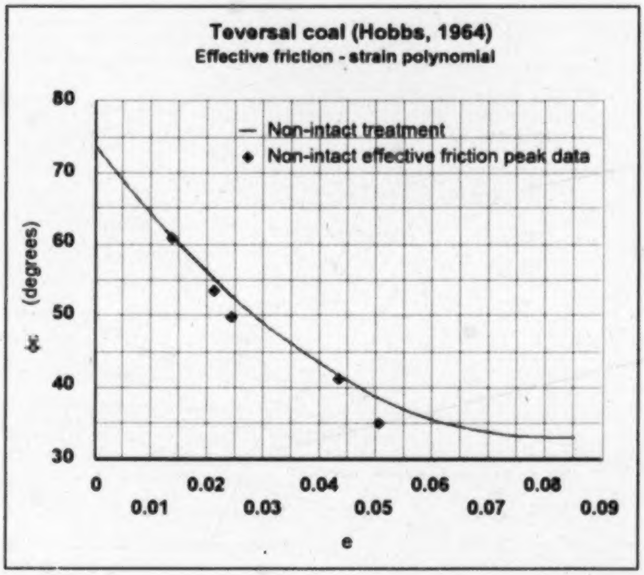

		Treatment		
Criterion	**Parameter**	**Non-intact**	**Coal mass**	**Intact**
Hoek-Brown	m	3.4	0.6	20.1
	σ_c (MPa)	76	76	76
	s	0.17	0.028	1
Residual	D	-0.01	-0.03	-0.004
	F	3.4	2.4	4.5
	σ_{cr} (MPa)	31	13	15
Base strength	ϕ_b (degrees)	33	33	33
Brittle-ductile	σ_{3t} (MPa)	49	10	269
ϕ_c - e	R (degrees)	74		
	S	-1010		
	T	6310		
	e_b	0.08		

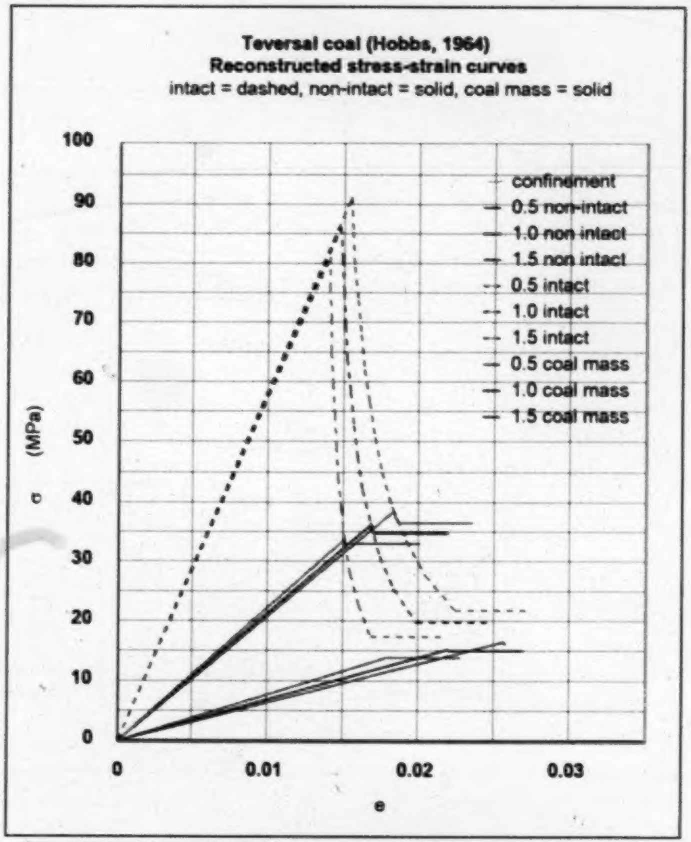

Teversal coal (Hobbs, 1964)
Reconstructed stress-strain curves
intact = dashed, non-intact = solid, coal mass = solid

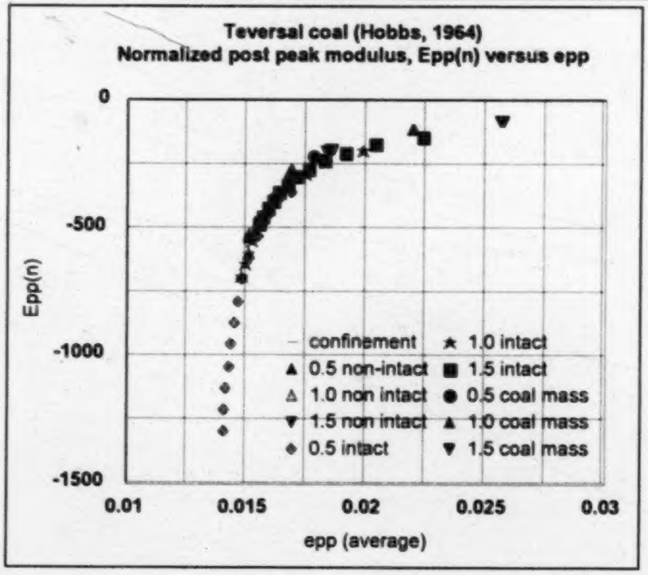

Teversal coal (Hobbs, 1964)
Normalized post peak modulus, Epp(n) versus epp

Appendix S

Flac 2d code for triaxial test and pillar models

Appendix S.1

Flac 2d input code file for a triaxial test at σ_3 = 14 MPa (after Itasca 1995)

```
; ************************
; Triaxial test of intact rock
; Intact rock sample: mudstone
; ************************
config axi
g 5 20

mod ss
call servo.fis

fix y j 1
fix y j 21

ini yvel -2.5e-6 j 21
ini yvel 2.5e-6 j 1

prop s=3.394e9 b=5.656e9 d=2283
prop ftab=1 ctab=2
prop fric=20.998 coh=19.191e6 ten=17.5e6

table 1 0,20.998 .002,5.456 1 5.456
table 2 0,19.191e6 .02,4.776e6 1 4.776e6

his nste=20

def sigmav
  sum=0.0
  loop i (1,igp)
    sum=sum+yforce(i,jgp)
  end_loop
  sigmav=sum/(x(igp,jgp)-x(1,jgp))
end

def ev
```

```
  ev=(ydisp(3,1)-ydisp(3,21))/(y(3,21)-y(3,1))
end

;averaging major and minor principal stress in pillar
def pillar1
 sum1=0.0
 sum3=0.0
  loop i (1,5)
   loop j (1,20)
    temp1=-0.5*(sxx(i,j)+syy(i,j))
    temp2=sqrt(sxy(i,j)*sxy(i,j)+0.25*((sxx(i,j)-syy(i,j))*(sxx(i,j)-syy(i,j))))
    s1=max(temp1+temp2,-szz(i,j))
    s3=min(temp1-temp2,-szz(i,j))
    sum1=sum1+s1
    sum3=sum3+s3
   end_loop
  end_loop
 pillar1=sum1/100.0 ;since 100 zones in the pillar
 pillar3=sum3/100.0 ;since 100 zones in the pillar
end

his nste=20            ;0
his unbal              ;1
hist sigmav            ;2
hist ev                ;3
hist pillar1           ;4
hist pillar3           ;5

set high_unbal=5e7
set low_unbal=2e4
set high_vel=1e-4
set his trx_wh14.out

step 12000
save trx_wh14.sav
plot h 2 vs 3 hold
plot h 4 vs 3 hold
plot h 5 vs 3 hold
his write 2 vs 3
his write 4 vs 5
ret
```

Appendix S.2

Flac 2d input code file for a pillar of W/H = 6.0 (after Itasca, 1995)

```
;************************
; Single strain softening pillar in elastic strata
; Strata=mudstone
; Pillar=mudstone  M-C ss model
;************************
gr 30,25
m e

prop s=3.394e9 b=5.656e9 d=2283.0
mod null i=1,3 j=11,14
mod null i=28,30 j=11,14

;M-C internal strain softening model
mod ss i=4,27 j=11,14

prop s=3.394e9 b=5.656e9 d=2283.0 i=4,27 j=11,14
prop ftab=1 ctab=2 i=4,27 j=11,14
prop fric=20.998 coh=19.191e6 ten=17.5e6 dil=11.5 i=4,27 j=11,14
table 1 0,20.998 .002,5.456 1 5.456
table 2 0,19.191e6 .002,4.776e6 1 4.776e6

fix x y j=1
fix x i=1
fix x i=31

his nste=80
set large
set his pill6.out

; vertical strain
def deforpil
 while_stepping
  deforpil=(ydisp(16,11)-ydisp(16,15))/(y(16,15)-y(16,11))
end

; averaging of pillar stress
```

```
def sigp
 while_stepping
  s=0.0
  loop i (4,27)
   s=s-syy(i,13)
  end_loop
 sigp=s/24.0 ;since 24 zones at width of pillar
end

;averaging of reaction stress at lower boundary
def avers
 force=0.0
  loop i (1,igp)
   force=force-yforce(i,1)
  end_loop
 avers=force/30.0 ;since 30 zones in the lower boundary of j=1
end

;averaging major and minor principal stress in pillar
def pillar1
 sum1=0.0
 sum3=0.0
  loop i (4,27)
   loop j (11,14)
    temp1=-0.5*(sxx(i,j)+syy(i,j))
    temp2=sqrt(sxy(i,j)*sxy(i,j)+0.25*((sxx(i,j)-syy(i,j))*(sxx(i,j)-syy(i,j))))
    s1=max(temp1+temp2,-szz(i,j))
    s3=min(temp1-temp2,-szz(i,j))
    sum1=sum1+s1
    sum3=sum3+s3
   end_loop
  end_loop
 pillar1=sum1/96.0 ;since 96 zones in the pillar
 pillar3=sum3/96.0 ;since 96 zones in the pillar
end

his nste=80          ;0
his unbal            ;1
history sigp         ;2
history deforpil     ;3
history pillar1      ;4
history pillar3         ;5
history avers           ;6
history yvel i=1 j=26   ;7

;let interfaces settle down under gravity before applying loads
set grav 10
step 500
ini xvel=0.0 yvel=0.0
;apply y-oriented velocities to compress pillar
ini yvel=-1e-3 j=26
ini yvel=1e-3 j=1
fix x y j=1
fix x y j=26
fix x i=1
fix x i=31

;servo to control y-velocity
def servo
while_stepping
 if unbal > 1e6 then
  loop i (1,31)
   yvel(i,26)=yvel(i,26)*.975
   yvel(i,1)=yvel(i,1)*.975
  end_loop
 end_if
 if unbal < 1e5 then
  loop i (1,31)
   yvel(i,26)=yvel(i,26)*1.025
   yvel(i,1)=yvel(i,1)*1.025
  end_loop
 end_if
end

step 40000
;output
save pill6.sav
his write 2 vs 3
his write 4 vs 5
ret
```

Appendix T

Manipulation of the post peak relationships to evaluate a new pseudo elastic modulus, E_{ps} for input into Phase 2, for a known previous post peak iteration

The post peak modulus, E_{pp}, is the change in stress for a given change in strain that follows the post peak stress-strain relationship, according to equation 2.14.

$$E_{pp}=\frac{\Delta\sigma_{pp}}{\Delta e_{pp}} \qquad 2.14$$

This has been derived in appendix B as equation 3.19:

$$E_{pp}=\frac{\sin 2\theta}{\sin^{2}\phi_{e}}\,\frac{(\sigma_{pp}-\sigma_{3})^{2}}{\sigma_{3}}\,\frac{(\phi_{e}-\phi_{b})}{(e_{pp}-e_{b})} \qquad 3.19$$

Equation 3.16 can be re-arranged by substitution using the double angle trigonometric identities, resulting in equation 8.4.

$$\tan\phi_{e}=\frac{(\sigma_{pp}-\sigma_{3})\sin 2\theta}{(\sigma_{pp}+\sigma_{3})+(\sigma_{pp}-\sigma_{3})\cos 2\theta} \qquad 3.16$$

$$\sin 2\theta=2\sin\theta\cos\theta=\frac{2\tan\theta}{1+\tan^{2}\theta} \qquad \cos 2\theta=\cos^{2}\theta-\sin^{2}\theta=\frac{1-\tan^{2}\theta}{1+\tan^{2}\theta}$$

$$\sigma_{pp}=\sigma_{3}\tan\theta\frac{(1+\tan\phi_{e}\tan\theta)}{(\tan\theta-\tan\phi_{e})} \qquad 8.4$$

Substituting equations 2.14 and 8.4 into equation 3.19 and re-arranging results in equation 8.5:

$$\Delta\sigma_{pp}=2\Delta e_{pp}\sigma_3\frac{\tan\theta}{\cos^2\phi_e}\frac{(\phi_b-\phi_e)}{(e_b-e_{pp})}\frac{(\tan^2\theta+1)}{(\tan\theta-\tan\phi_e)^2} \qquad 8.5$$

But $\Delta\sigma_{pp} = \sigma_{1n} - \sigma_{1o}$, where σ_{1n} is the revised post peak strength for the next iteration given σ_{1o}, the post peak strength returned by Phase 2 for the previous iteration. Replacing σ_{pp} in equation 8.4 with σ_{1n}, results in equation T-1.

$$\Delta\sigma_{pp}=\sigma_3\tan\theta\frac{(1+\tan\phi_e\tan\theta)}{(\tan\theta-\tan\phi_e)}-\sigma_{1o} \qquad \text{T-1}$$

Substituting σ_3 with σ_{3n} in equation T-1, such that $\sigma_{3n} = \sigma_{3o} + \Delta\sigma_3$, where σ_{3o} is the confinement returned by Phase 2 for the previous iteration and σ_{3n} is given by equating equations T-1 and 8.5 to yield an expression for the new confining pressure, σ_{3n}, equation 8.6.

$$\sigma_{3n}=\sigma_{1o}\frac{1-\dfrac{\tan\phi_e}{\tan\theta}}{[1+\tan\theta\tan\phi_e-2\dfrac{\Delta e_{pp}}{\cos^2\phi_e}\dfrac{(\phi_b-\phi_e)}{(e_b-e_{pp})}\dfrac{(\tan^2\theta+1)}{(\tan\theta-\tan\phi_e)}]} \qquad 8.6$$

σ_{1n} is then found by back substitution, replacing σ_3 by σ_{3n} in equation 8.4. The pseudo elastic post peak modulus is then given by equation 8.7:

$$E_{ps}=\frac{\sigma_{1n}}{e_{pp}}-2\nu\frac{\sigma_{3n}}{e_{pp}} \qquad 8.7$$

Appendix U

Modification of rib pillar strength to equivalent square pillar strength

From tributary area theory it can be shown that the average pillar stress on square and rectangular pillars are given by equations U.1 and U.2 respectively:

$$\sigma_S = \frac{(W+w_B)(W+w_L)}{W^2}\sigma_v \qquad \text{U.1}$$

$$\sigma_R = \frac{(W+w_B)(L+w_L)}{LW}\sigma_v \qquad \text{U.2}$$

Using U.1 and U.2, the ratio of the two is given by:

$$\frac{\sigma_S}{\sigma_R} = \frac{(W+w_L)}{(L+w_L)}\frac{L}{W}$$

Let L = nW, hence:

$$\frac{\sigma_S}{\sigma_R} = \frac{(W+w_L)}{(W+\frac{w_L}{n})}$$

For a square pillar $n = 1$, and for a rib pillar n = infinity. Thus, equation 8.14 is given by:

$$\sigma_S = \sigma_{rib}\frac{(W+w_L)}{W} = \psi\sigma_{rib} \qquad 8.14$$

It follows that to resist the same stress as that subjected to a rib pillar, the strength of a square pillar must be increased by a factor of ψ.

Appendix W

Modeling a pillar using Phase 2 and the Joseph-Barron post-peak criterion

This appendix describes the procedure employed to provide updated material properties for the pillar elements used in modeling an example pillar of W/H = 4 using the Phase 2 finite element software package. The calculation of new material properties in the form of pseudo-elastic moduli were performed using a spreadsheet and the Joseph-Barron post peak criterion, allowing a new pseudo-elastic modulus to be returned to Phase 2 manually for each element at each iterative step.

Pillars were modeled in plane-strain mode, allowing them to be interpreted as rib pillars. Only half a pillar was modeled due to symmetry, allowing the restricted number of material properties and pillar elements to be maximized.

The pillar model set up is illustrated in figure 8.3 and described below:

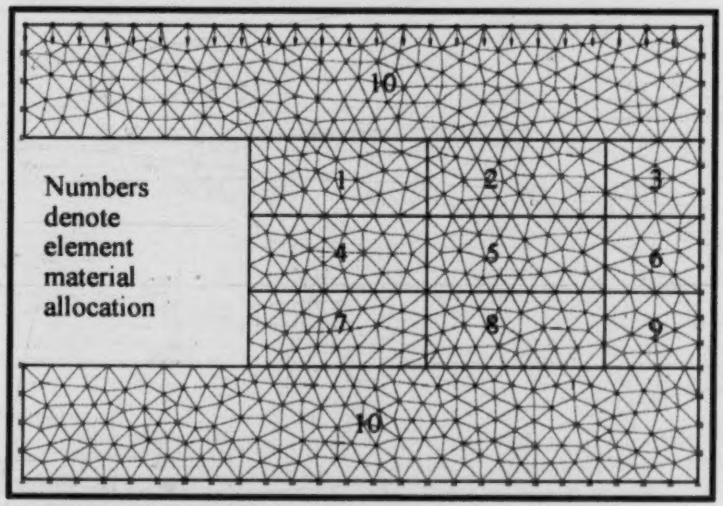

Figure 8.3: Phase 2 pillar model elements, discretization and boundary conditions.

i The Phase 2 job control was set to plane strain mode.

ii An external boundary was defined for a half pillar plus roof and floor material. For all pillars modeled, the pillar height was kept constant at 2.4 m, with an appropriate half pillar width commensurate with the width to height ratio of interest. The roof and floor material elements were given heights of 1.2 m respectively in each case.

iii A pillar of 9 elements was defined, with each element allocated a set of material properties. The roof and floor elements were defined by the 10th set of available material properties. For the purposes of the analysis, Poisson's ratio was held constant (0.3 for coal, and 0.25 for mudstone) and the pseudo-elastic modulus varied as the analysis proceeded.

iv The elements were discretized, allocating a finer set of constant strain triangle finite elements throughout the structure. However, the coarse nature of the structure defined the finite elements to behave in accordance with the 10 sets of material properties. A better system would be the ability to allocate each finite element constant strain triangle its own set of material properties. This would in turn necessitate a dynamic internal updating of material properties, since manual updating of hundreds of material properties is unrealistic.

v The boundary conditions were defined such that the base of the floor material was fixed in both the x and y directions (bottom of figure 8.3), the horizontal x direction was fixed at the pillar centreline (right hand side of figure 8.3), and the roof and floor material above the opening (far left hand side of figure 8.3) was fixed in the horizontal x direction.

All elements were initially allocated the same set of material properties defined by Young's modulus for the material, E, as given by the linear portion of the pre-peak stress-strain relation under unconfined uniaxial compression conditions.

The incremental step was defined as an increase in deformation applied uniformly across the top of the roof material element as illustrated in figure 8.3. A small incremental deformation step was selected and used accumulatively during the course of the modeling process. For the most part, the incremental pillar deformation steps were set at 0.02 m. Where some confusion arose, due to the coarse nature of the model elements and the degree of deformation, as to the value of the peak pillar strength in the analysis, the incremental deformation was reduced in the peak strength region to either 0.005 m or 0.01 m.

Once Phase 2 had computed the resulting major and minor principal stresses, σ_1 and σ_3 and the vertical deformation, u_y throughout the structure with respect to the constant strain triangle finite elements for a given increment of pillar deformation, interpretation of those values across each of the 9 material elements were measured using a Phase 2 'query line'. The query line values for σ_1, σ_3 and u_y were copied into a Joseph-Barron post-peak calculation spreadsheet, where average values for σ_1, σ_3 and vertical strain, e_1 were determined for each of the 9 pillar material elements. It was these average values that were employed in the evaluation of a new material modulus to be returned to Phase 2 for each material element.

The calculation procedure and decision process regarding pre-peak, post-peak and post e_r conditions in defining the pseudo-elastic modulus, E_{pe} is provided in detail in section 8.4.1. This procedure is summarized in the flow chart illustrated below.

It is assumed that triaxial strength tests and a tilt test have been conducted on the pillar material. These tests revealed values for the base angle of friction ϕ_b, the Hoek-Brown peak strength parameters m, s, and σ_c, the residual strength parameters D, F and σ_{cr}, and the effective friction - strain polynomial parameters R, S, T and e_b. Poisson's ratio, ν is held constant, and Young's modulus, E is known from unconfined uniaxial compression.

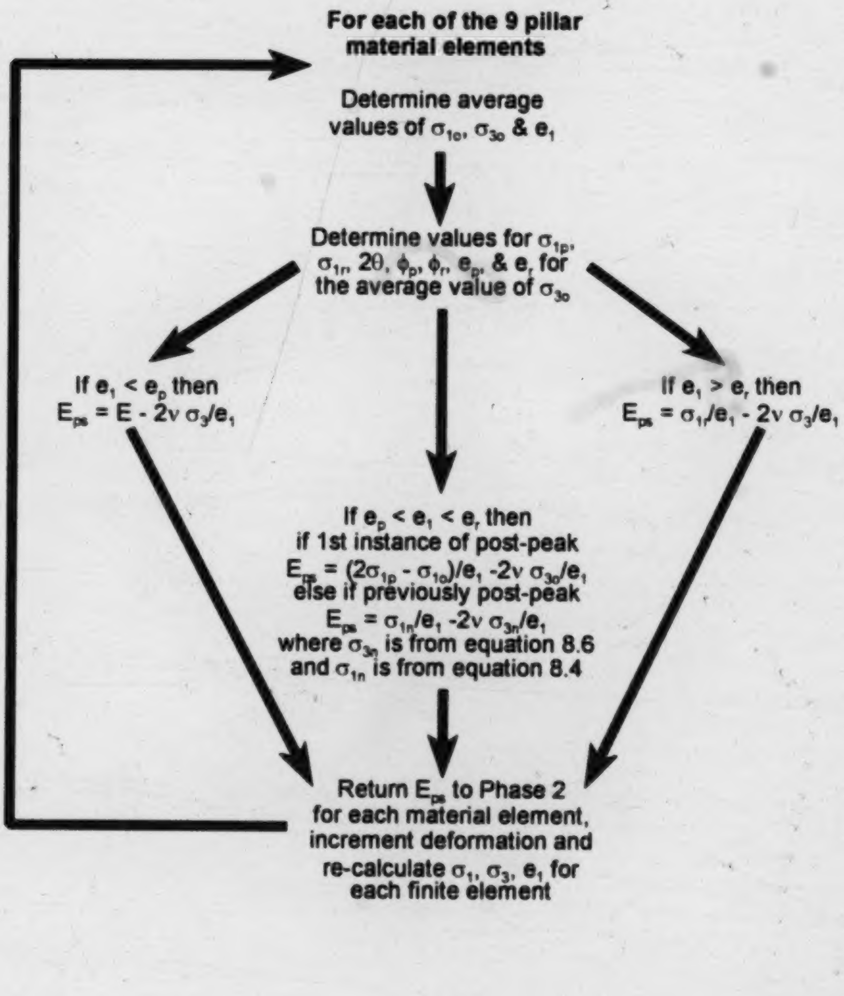
For each of the 9 pillar material elements
Determine average values of σ_{1o}, σ_{3o} & e_1
Determine values for σ_{1p}, σ_{1r}, 2θ, ϕ_p, ϕ_r, e_p, & e_r for the average value of σ_{3o}
If $e_1 < e_p$ then $E_{ps} = E - 2\nu\,\sigma_3/e_1$
If $e_1 > e_r$ then $E_{ps} = \sigma_{1r}/e_1 - 2\nu\,\sigma_3/e_1$
If $e_p < e_1 < e_r$ then
if 1st instance of post-peak
$E_{ps} = (2\sigma_{1p} - \sigma_{1o})/e_1 - 2\nu\,\sigma_{3o}/e_1$
else if previously post-peak
$E_{ps} = \sigma_{1n}/e_1 - 2\nu\,\sigma_{3n}/e_1$
where σ_{3n} is from equation 8.6
and σ_{1n} is from equation 8.4
Return E_{ps} to Phase 2 for each material element, increment deformation and re-calculate σ_1, σ_3, e_1 for each finite element